Reflow Soldering Processes and Troubleshooting: SMT, BGA, CSP and Flip Chip Technologies

VISIT…

To my mother, Shu-shuen Chang, for her care and encouragement

To my wife, Shen-chwen Lee, for her understanding and full support

Reflow Soldering Processes and Troubleshooting: SMT, BGA, CSP and Flip Chip Technologies

Ning-Cheng Lee

NEWNES

BOSTON OXFORD AUCKLAND JOHANNESBURG
MELBOURNE NEW DELHI

Copyright © 2002 by Newnes, an imprint of Butterworth-Heinemann

A member of the Reed Elsevier plc group

All rights reserved.

No part of this publication may be reproduced, stored in a retrieval system, or transmitted in any form or by any means, electronic, mechanical, photocopying, recording, or otherwise, without the prior written permission of the publisher.

Recognizing the importance of preserving what has been written, Butterworth-Heinemann prints its books on acid-free paper whenever possible.

Butterworth-Heinemann supports the efforts of American Forests and the Global ReLeaf program in its compaign for the betterment of trees, forests, and our environment.

Library of Congress Cataloging-in-Publication Data
A catalog record for this book is available from the Library of Congress

British Library Cataloguing-in-Publication Data
A catalog record for this book is available from the British Library

The Publisher offers special discounts on bulk orders of this book.

For information, please contact:
Manager of Special Sales
Butterworth-Heinemann
225 Wildwood Avenue
Woburn, MA 01801 – 2041
Tel: 781-904-2500
Fax: 781-904-2620

For information on all Newnes publications available, contact our World Wide Web home page at: http://www.newnespress.com

10 9 8 7 6 5 4 3 2 1

Typeset by Laser Words Private Limited, Chennai, India
Printed in the United States of America

PLANT A TREE
BTCV
British Trust for Conservation Volunteers
FOR EVERY TITLE THAT WE PUBLISH, BUTTERWORTH-HEINEMANN WILL PAY FOR BTCV TO PLANT AND CARE FOR A TREE.

Preface

1 Introduction to Surface Mount Technology

1.1 Surface mount technology

1.1.1 History and benefits

1.1.2 Surface mount components

1.1.3 Types of surface mount assembly technology

1.1.4 Surface mount soldering process

1.1.5 Advantages of solder paste technology in SMT

1.2 Surface mount technology trends

1.2.1 Technology driving force

1.2.2 Area array packages

1.3 Conclusion

2 Fundamentals of Solders and Soldering

2.1 Soldering theory

2.1.1 Spreading

2.1.2 Fluid flow

2.1.3 Dissolution of base metal

2.1.4 Intermetallics

2.2 Effect of elemental constituents on wetting

2.3 Phase diagram and soldering

2.4 Microstructure and soldering

2.4.1 Deformation mechanisms

2.4.2 Desirable solders and the soldering process

2.4.3 Effect of impurities on soldering

2.5 Conclusion

Appendix 2.1 Effect of flux surface tension on the spread of molten solder

3 Solder Paste Technology

3.1 Fluxing reactions

3.1.1 Acid–base reactions

3.1.2 Oxidation–reduction reactions

3.1.3 Fluxes for reflow soldering

3.2 Flux chemistry

3.2.1 Resins

3.2.2 Activators

3.2.3 Solvents

3.2.4 Rheological additives

3.3 Solder powder

3.3.1 Atomization

3.3.2 Particle size and shape

3.4 Solder paste composition and manufacturing

3.5 Solder paste rheology

3.5.1 Rheology basics

3.5.2 Solder paste viscosity measurement

3.6 Solder paste rheology requirement

3.6.1 Effect of composition on rheology

3.7 Conclusion

4 Surface Mount Assembly Processes

4.1 Solder paste materials

4.1.1 Paste handling and storage
4.1.2. Paste deposition
4.2 Printer level consideration
4.2.1 Stencil
4.2.2. Squeegee
4.2.3 Printing and inspection process
4.3. Pick-and-place
4.4 Reflow
4.4.1 Infrared reflow
4.4.2. Vapor phase reflow
4.4.3 Forced convection reflow
4.4.4 In-line conduction reflow
4.4.5. Hot-bar reflow
4.4.6. Laser reflow
4.5 Effect of reflow atmosphere on soldering
4.6 Special soldering considerations
4.6.1 Step soldering
4.6.2. Reflow-alloying
4.6.3 Paste-in-hole
4.7. Solder joint inspection
4.8. Cleaning
4.9 In-circuit-testing
4.10 Principle of troubleshooting reflow soldering
4.11. Conclusion

5 SMT Problems Prior to Reflow
5.1. Flux separation
5.2 Crusting
5.3. Paste hardening
5.4. Poor stencil life
5.5. Poor paste release from squeegee
5.6. Poor print thickness
5.7 Smear
5.8. Insufficiency
5.9. Needle clogging
5.10 Slump
5.11. Low tack
5.12. Short tack time
5.13. Conclusion

6 SMT Problems During Reflow
6.1. Cold joints
6.2. Nonwetting
6.3. Dewetting
6.4. Leaching
6.5. Intermetallics
6.5.1 General
6.5.2 Gold
6.6. Tombstoning
6.7. Skewing

6.8 Wicking
6.9 Bridging
6.10 Voiding
6.11 Opening
6.11.1 Pillowing
6.11.2 Other openings
6.11.3 Fillet lifting
6.11.4 Projected solder
6.12 Solder balling
6.13 Solder beading
6.14 Spattering
6.15 Conclusion

7 SMT Problems At the Post-reflow Stage

7.1 White residue
7.2 Charred residue
7.3 Poor probing contact
7.3.1 Flux residue content
7.3.2 Top-side flux spread
7.3.3 Bottom-side flux spread
7.3.4 Residue hardness
7.3.5 Reflow atmosphere
7.3.6 Metal content
7.3.7 Soft-residue versus low-residue
7.3.8 Soft-residue versus RMA residue
7.3.9 Multiple cycles probing testability
7.4 Surface insulation resistance or electrochemical migration failure
7.4.1 Surface insulation resistance (SIR)
7.4.2 Electrochemical migration (EM)
7.4.3 Effect of flux chemistry on IR values
7.4.4 Effect of soldering temperature
7.4.5 Effect of cleanliness of incoming parts
7.4.6 Effect of conformal coating/encapsulation
7.4.7 Effect of interaction between flux and solder mask
7.4.8 Effect of interaction between solder paste flux residue and wave flux
7.5 Delamination/voiding/non-curing of conformal coating/ encapsulants
7.5.1 Voiding
7.5.2 Delamination
7.5.3 Incomplete curing
7.6 Conclusion

8 Solder Bumping for Area Array Packages

8.1 Solder criteria
8.1.1 Alloys used in flip chip solder bumping and soldering
8.1.2 Alloys used in BGA and CSP solder bumping and soldering
8.1.3 Lead-free solders
8.2 Solder bumping and challenges
8.2.1 Build-up process
8.2.2 Liquid solder transfer process
8.2.3 Solid solder transfer processes
8.2.4 Solder paste bumping
8.3 Conclusion

9 BGA and CSP Assembly and Rework
9.1 Assembly process
9.1.1 General stencil design guideline
9.1.2 BGA/CSP placement
9.1.3 Reflow
9.1.4 Inspection
9.2 Rework
9.2.1 Process flow
9.2.2 Pre-baking
9.2.3 Component removal
9.2.4 Reflow equipment
9.2.5 Site preparation
9.2.6 Solder replenishment
9.2.7 Placement of component
9.2.8 Reflow of BGA and CSP
9.3 Challenges at assembly and rework stages
9.3.1 Starved solder joint
9.3.2 Poor self-alignment
9.3.3 Poor wetting
9.3.4 Voiding
9.3.5 Bridging
9.3.6 Open
9.3.7 Uneven joint height
9.3.8 Solder webbing
9.3.9 Solder balling
9.3.10 Popcorn and delamination
9.4 Conclusion

10 Flip Chip Reflow Attachment
10.1 Flip chip attachment
10.1.1 Conventional flip chip attachment
10.1.2 Snap cure
10.1.3 Epoxy flux
10.1.4 No-flow
10.1.5 SMT
10.1.6 Fluxless soldering
10.1.7 Wafer-applied underfill 10.1.8 Wafer level compressive-flow underfill (WLCFU)
10.2 Problems during flip chip reflow attachment
10.2.1 Misalignment
10.2.2 Poor wetting
10.2.3 Solder voiding
10.2.4 Underfill voiding
10.2.5 Bridging
10.2.6 Open
10.2.7 Underfill crack
10.2.8 Delamination
10.2.9 Filler segregation
10.2.10 Insufficient underfilling
10.3 Conclusion

11 Optimizing a Reflow Profile Via Defect Mechanisms Analysis
11.1 Flux reaction
11.1.1 Time/temperature requirement for the fluxing reaction
11.1.2 Fluxing contribution below the melting temperature

11.2 Peak temperature
11.2.1 Cold joint and poor wetting
11.2.2 Charring, delamination, and intermetallics
11.2.3 Leaching
11.3 Cooling stage
11.3.1 Intermetallics
11.3.2 Grain size
11.3.3 Internal stress-component cracking
11.3.4 Deformation of joints
11.3.5 Internal stress solder or pad detachment
11.4 Heating stage
11.4.1 Slumping and bridging
11.4.2 Solder beading
11.4.3 Wicking
11.4.4 Tombstoning and skewing
11.4.5 Solder balling
11.4.6 Poor wetting
11.4.7 Voiding
11.4.8 Opens
11.5 Timing considerations
11.5.1 Ramp-up stage
11.5.2 Soaking zone
11.5.3 Onset temperature of spike zone
11.6 Optimization of profile
11.6.1 Summary of desired profile feature
11.6.2 Engineering the optimized profile
11.7 Comparison with conventional profiles
11.7.1 Conventional profiles
11.7.2 Background of conventional profiles
11.7.3 Approach of conventional profiles
11.7.4 Compromise of conventional profiles
11.7.5 Earlier mass reflow technologies
11.7.6 Forced air convection reflow technology
11.7.7 Defect potential associated with conventional profiles
11.8 Discussion
11.8.1 Profiles for low temperature solder pastes
11.8.2 Profiles for high temperature solder pastes
11.8.3 Limited oxidation tolerance
11.8.4 Unevenly distributed high thermal mass systems
11.8.5 Nitrogen reflow atmosphere
11.8.6 Air flow rate
11.8.7 Adjustment of optimal profile
11.9 Implementing linear ramp-up profile
11.10 Conclusion

12 Lead-free Soldering
12.1 Initial activities
12.2 Recent activities
12.3 Impact of Japanese activities
12.4 US reactions
12.5 What is lead-free interconnect?
12.6 Criteria of lead-free solder
12.7 Viable lead-free alloys
12.7.1 Sn96.5/Ag3.5

12.7.2 Sn99.3/Cu0.7
12.7.3 Sn/Ag/Cu
12.7.4 Sn/Ag/Cu/X
12.7.5 Sn/Ag/Bi/X
12.7.6 Sn/Sb
12.7.7 Sn/Zn/X
12.7.8 Sn/Bi
12.8 Cost
12.9 PCB finishes
12.10 Components
12.11 Thermal damage
12.12 Other problems
12.13 Consortia activity
12.14 Opinions of consortia
12.15 The selections of pioneers
12.16 Possible path
12.17 Is lead-free safe?
12.18 Summary of lead-free adoption
12.19 Troubleshooting lead-free soldering
12.19.1 Compatibility with reflow process
12.19.2 Fillet lifting
12.19.3 Conductive anode filament
12.19.4 Grainy surface
12.19.5 Sn/Pb/Bi ternary low melting eutectic phase
12.20 Conclusion
Index

Preface

Reflow soldering is the primary method for interconnecting surface mount technology (SMT) applications. Successful implementation of this process depends on whether a low defect rate can be achieved. In general, defects often can be attributed to causes rooted in all three aspects, including materials, processes, and designs. Troubleshooting of reflow soldering requires identification and elimination of root causes. Where correcting these causes may be beyond the reach of manufacturers, further optimizing the other relevant factors becomes the next best option in order to minimize the defect rate.

Chapter 1 introduces the general design background and trends of electronic packaging and surface mount technology. Chapters 2 and 3 provide the fundamentals of soldering and solder materials. Chapter 4 describes the basics of reflow processes. These four chapters serve as the fundamentals needed for analyzing soldering defects. Chapters 5 through 7 discuss the defect types, defect mechanisms, and solutions for eliminating the defects encountered in the SMT process, while Chapters 8 through 10 address area array packages, including BGA, CSP and flip chips. Chapter 11 focuses on reflow profile optimization, since the profile is vital to reflow performance and often is easily controllable by manufacturers. Chapter 12 summarizes the background and options of lead-free soldering. It also discusses the defect types and mechanism of lead-free reflow processes.

This book emphasizes reflow process description and troubleshooting. The solutions for troubleshooting described should be regarded merely as examples. With defect mechanisms identified and the impact of relevant factors understood, only creativity can determine the limits of approaches possible for solutions.

Ning-Cheng Lee

1 Introduction to Surface Mount Technology

1.1 Surface mount technology

1.1.1 History and benefits

Surface mount technology (SMT) is a revolutionary change in the electronics industries. During the mid-1960s, the early stages of SMT emerged due to the advantage of being able to place components on both sides of the PCBs. However, SMT did not prevail until about 15 years later. During the late 1970s, through-hole technology (THT) ran into increasing difficulty in meeting the constant need for higher densities, primarily due to the increasing cost for drilling more holes for an increasing number of leads, and to the difficulty of drilling smaller holes for pitch dimensions smaller than 0.1 inch. It was then that interest in SMT increased rapidly and its potential became recognized by industries. On the other hand, the commercial availability of various plastic surface mount devices (SMDs), such as PLCC, SOIC, and SOT23, further ensured SMT to be a practical option. Since then, SMT started its rapid development and quickly became the major assembly technology.

By mounting flat leaded or leadless components and electronic packages on the surface of printed circuit boards (PCBs) (Figure 1.1(a)), as opposed to the conventional THT (Figure 1.1(b)), SMT allows a higher degree of automation, higher circuitry density, smaller volume, lower cost, and better performance. An example of the lower weights and smaller volumes offered by the surface mount components (SMCs) versus the equivalent through-hole components (THCs) is shown in Figure 1.2, where it is demonstrated that SMCs deliver up to 90 percent reduction in both weight and volume.

This is of particular interest in aerospace and portable device applications. The benefit of higher circuitry density is a natural result of the reduced components' size, and can be illustrated by Figure 1.3. In reality, at high lead density level, conventional THT is not only more expensive, it is also unmanufacturable. Additional benefits of SMT include a lower cost in the shipping and warehousing of components, and in the requirements of manufacturing space and equipment.

1.1.2 Surface mount components

SMCs are available for almost any type of application, such as capacitors, resistors, transistors, diodes, inductors, ICs, and connectors. However, due to the physical size restriction imposed by the surface mounting process, most SMCs are designed for power dissipation no higher than 1 to 2 W. Given below is a brief illustration of some commonly used components.

1.1.2.1 Chip resistors

A chip resistor is the simplest SMC, as shown in Figure 1.4. It consists of a rectangular ceramic substrate body with a metallized termination, usually palladium–silver (Pd–Ag), on both ends. A thick film

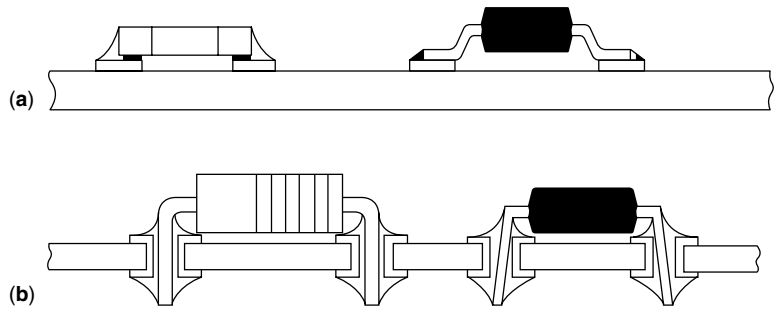

Figure 1.1 Schematic of printed circuit board technologies: (**a**) SMT, (**b**) THT

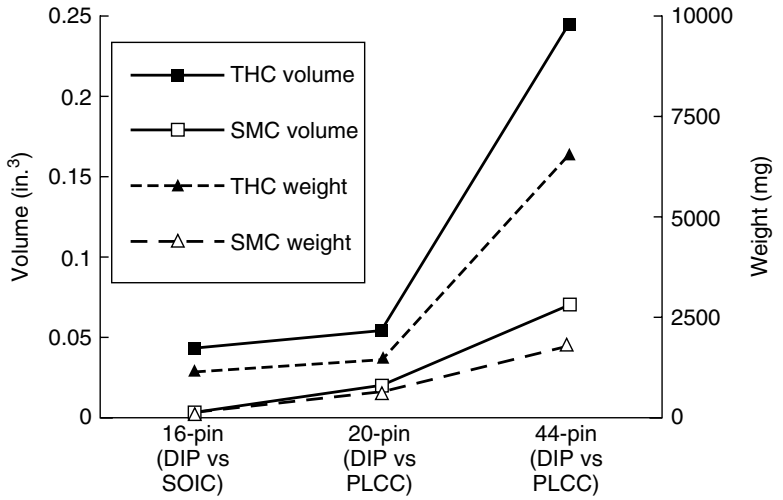

Figure 1.2 Comparison of weight and volume of SMCs and THCs [1]

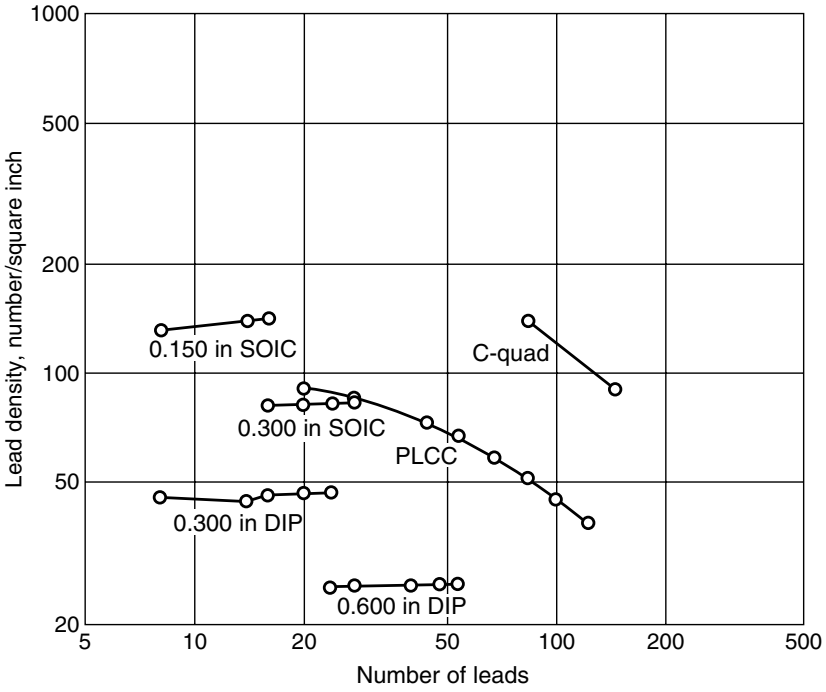

Figure 1.3 Lead density comparison of some SMCs and THCs [2]

resistor paste, generally based on ruthenium dioxide (RuO_2), is screened between the terminations and fired. The resistive film is then covered by a protective lead borosilicate glass film. A nickel barrier is usually applied over the Pd–Ag terminations to prevent silver leaching, and a final tin–lead or tin–lead–silver solder coating is applied over the nickel to preserve its solderability. The 1206 (0.120(L) × 0.060(W)-in.) and 0805 are the dominant sizes, with a trend toward increasing use of 0603. Currently the smallest size available is 0201, which has found use in hearing aids, and mobile phones.

1.1.2.2 Metal electrode face resistors

Metal electrode face resistors (MELFs) are similar to leaded cylindrical resistors except that the leaded electrodes are replaced by headed dumets, as shown in Figure 1.5. The manufacturing process is cheaper than

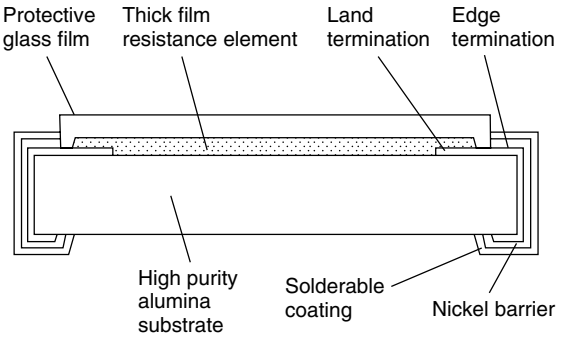

Figure 1.4 Chip resistor [3]

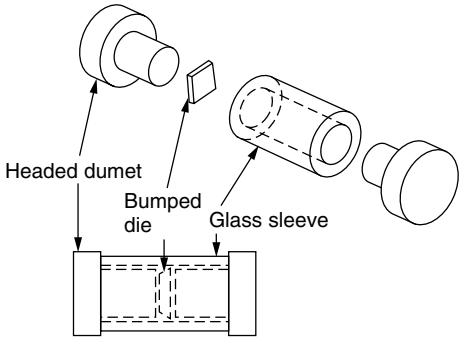

Figure 1.5 Metal electrode face resistor [4]

that for the thick film chip resistor. For this reason, they are widely used in the consumer-electronics orientated Asian SMT industry. However, since they tend to roll off the boards during the reflow process, their popularity is gradually diminishing.

1.1.2.3 Chip capacitors

The most commonly used SMT chip capacitor is the multilayer ceramic chip, also called a chip cap or ceramic cap. It consists of multiple layers of precious metal electrodes separated by layers of ceramic dielectric (Figure 1.6).

Each layer's electrode extends from one terminal to almost the other terminal, and each neighboring pair of electrodes forms a single capacitive layer. The required capacitance is obtained by the stacked layers. The construction of terminations are similar to that of chip resistors. Commonly used dielectric materials include (a) temperature-stable, low capacitance, primarily composed of titanium oxide (TiO_2), (b) semi-temperature stable, medium capacitance, typically composed of barium titanate ($BaTiO_3$) and other types of ferroelectric additives, and (c) general purpose, least thermally stable, high capacitance materials.

1.1.2.4 Chip inductors

Chip inductors employ a ceramic or ferrite core material wrapped around, either vertically or horizontally, by a polyurethane enamelled fine copper wire (Figure 1.7).

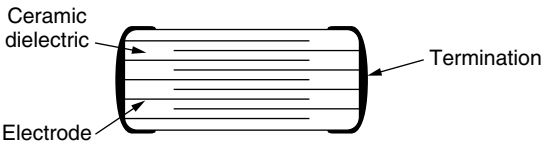

Figure 1.6 Construction of multilayer ceramic chip capacitor

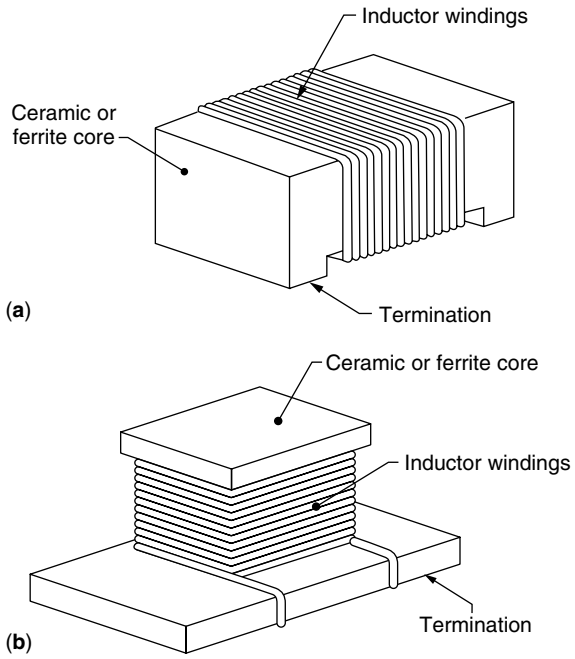

Figure 1.7 Chip inductors. (**a**) Vertical windings; (**b**) horizontal windings [2]

The chip is usually potted in an epoxy resin to facilitate automated handling.

1.1.2.5 Discrete semiconductors

Surface-mounted discrete semiconductors, such as diodes or transistors, often utilize similar types of packages. Typically, the SOT-23 (Figure 1.8(a)) and SOT-143 are used for low-power single diode and dual diode, respectively. The SOT-89 (Figure 1.8(b)) is used for high current devices. Here the center lead is extended across the bottom of the die to help dissipate the heat.

1.1.2.6 Integrated circuits

Surface mount integrated circuits (ICs) are supplied in a variety of packages. Some commonly used types include small-outline integrated circuit (SOIC), thin small-outline package (TSOP), plastic leaded chip carrier (PLCC), leadless ceramic chip carrier (LCCC), quad flat pack (QFP), and the more recently introduced ball grid array (BGA). The solder joint configurations of the IC packages can be represented by five major categories, as shown in Figure 1.9.

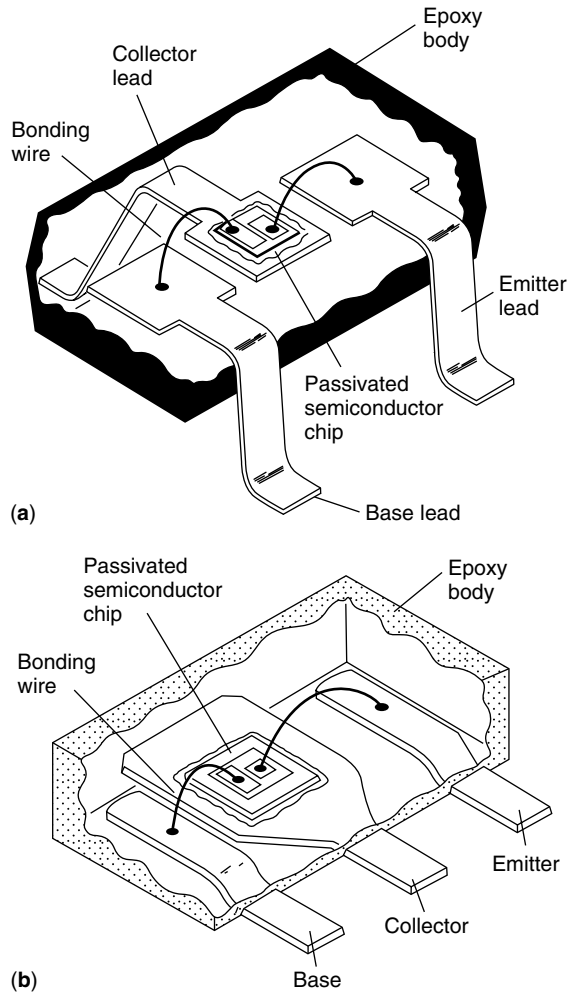

Figure 1.8 Discrete semiconductor packages. (**a**) SOT-23; (**b**) SOT-89

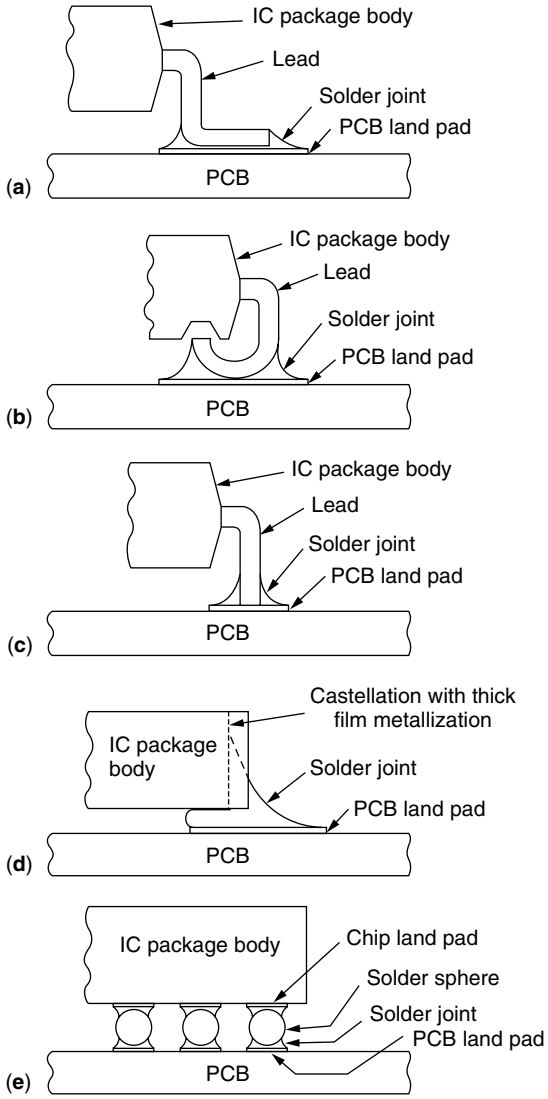

Figure 1.9 IC package lead configurations. (**a**) Gullwing; (**b**) J-lead; (**c**) Butt-lead; (**d**) Leadless metallization; (**e**) Ball-lead

Gullwing leads (Figure 1.9(a)) are the most popular lead configuration, particularly in the case of fine-pitch and ultra-fine-pitch applications. However, these leads are also susceptible to damage, such as bend or sweep, in handling. The J-lead design (Figure 1.9(b)) offers better handlability. But this benefit is offset by the difficulties in rework, inspection, and lead-forming. Butt-leads (Figure 1.9(c)) are easier to manufacture than both gullwing and J-lead designs. They are not as popular as gullwing leads, due to controversial performance in solder joint reliability. Figure 1.9(d) shows the joint configuration of a leadless ceramic chip carrier. Again, the reliability of the joints often poses problems, primarily due to a mismatch in the thermal coefficients of expansion of the packages and the PCB materials. In addition, the cleanability of flux residue for areas underneath the components also is questionable owing to the low standoff of the packages. The solder joint of BGA can be demonstrated by Figure 1.9(e). Here the high melting point solder bump underneath the plastic package is soldered onto the PCB through the use of solder paste. In the case of ceramic BGAs developed by IBM, the solder bump comprises a high melting solder column soldered onto the component. The emergence of BGAs makes 0.3 mm pitch SMT virtually a dead issue in North America. Furthermore, BGA will also provide an alternative to 0.4 mm processing. BGA, CSP, and flip chip will be discussed in more detail in section 1.2.2.

1.1.3 Types of surface mount assembly technology

SMCs can be assembled onto PCBs with the use of solder paste reflow, wave soldering, or conductive adhesive curing processes. The use of conductive adhesive is not common, but can be found in some flexible circuit boards

or boards with heat sensitive components. The assembly technology to be chosen depends on the board layout and whether there are through-hole components to be attached. In general, the assembly processes can be categorized into three major types, as described below.

1.1.3.1 Type I

Type I surface mount boards have SMCs only for both sides of the boards, as shown in Figure 1.10.

The assembly processes are depicted in Figure 1.11. The first side typically uses solder paste for bonding. The second side often also uses solder paste (see Figure 1.11(a)), particularly if there are fine pitch components to be attached. At the second reflow, the pre-assembled underside solder joints will melt again. The surface tension of solder in general is sufficient to hold the suspended components in place during the second reflow. However, it may be preferable to use the wave soldering process if there are heavy components involved on the underside at the second reflow. When using wave soldering, adhesives have to be used to secure the components in place (see Figure 1.11(b)). This requirement results in a total of process steps more than that of using solder paste only.

Depending on the flux chemistry, cleaning may or may not be needed. In the former case, cleaning can be done after the first pass or after the second pass. As a rule of thumb, the more heating excursions the fluxes have been through, the more difficult the cleaning will be. Many manufacturers have successfully implemented a single cleaning process for their products.

1.1.3.2 Type II

Type II boards have both SMCs and THCs on one side of the board and chip components on the other side, as shown in Figure 1.12. Normally the SMCs are attached via reflow soldering, then followed by wave soldering the THCs and chip components, as depicted in Figure 1.13. The THCs can also be inserted after the adhesive has been cured. Type II boards allow flexibility in using THCs for some features for which the supplies of SMCs may not be readily available. On the other hand, type II design requires the use of both wave soldering and reflow soldering. This complicates the assembly, test, and rework processes, and results in a need for more floor space.

1.1.3.3 Type III

Type III SMT have THCs on one side of the board and chip components on the other side, as shown in Figure 1.14. Similar to type II, the THCs can be inserted either before or after the attachment of chip components, as indicated in Figure 1.15. Type III requires only wave soldering for the bonding process, and represents the initial stage of converting from conventional through-hole technology to surface mount technology.

1.1.4 Surface mount soldering process

1.1.4.1 Wave soldering

As mentioned above, the two major soldering processes involved in surface mount technology are wave soldering and reflow soldering. Wave soldering, a type of flow soldering, has long been used in the through-hole technology era. Typically, the PCBs with THCs inserted are prefluxed via a foam fluxer, then passed over a single laminar solder wave for soldering. However, this process is not adequate for soldering SMCs. The presence of SMCs on the bottom side of a PCB interferes with the laminar solder flow, and consequently results in a "shadowing effect". As a common symptom, the leads at the trailing edge of a component usually exhibit insufficient solder volume. In addition, direct contact of SMCs on the bottom side with the hot solder wave also causes potential damage due to thermal shock. To minimize the shadowing effect, a dual-wave, with a turbulent wave preceding the laminar wave, is then used (Figure 1.16).

The turbulent wave ensures the wetting of all leads, while the subsequent laminar wave removes excessive solder in order to minimize solder bridging between the leads. Thermal shock potential is addressed by implementing sufficient preheating prior to wave-soldering. A typical wave-soldering thermal profile for SMCs soldering is shown in Figure 1.17. Use of dual-wave and proper

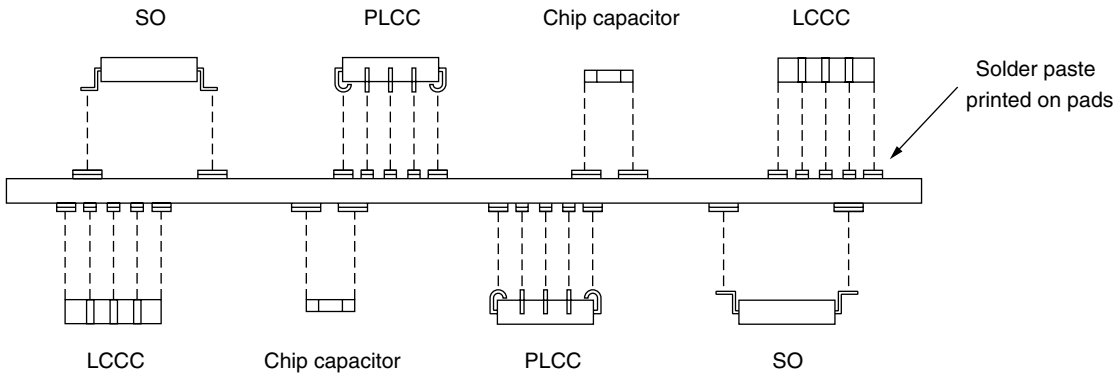

Figure 1.10 Schematic of type I surface mount boards

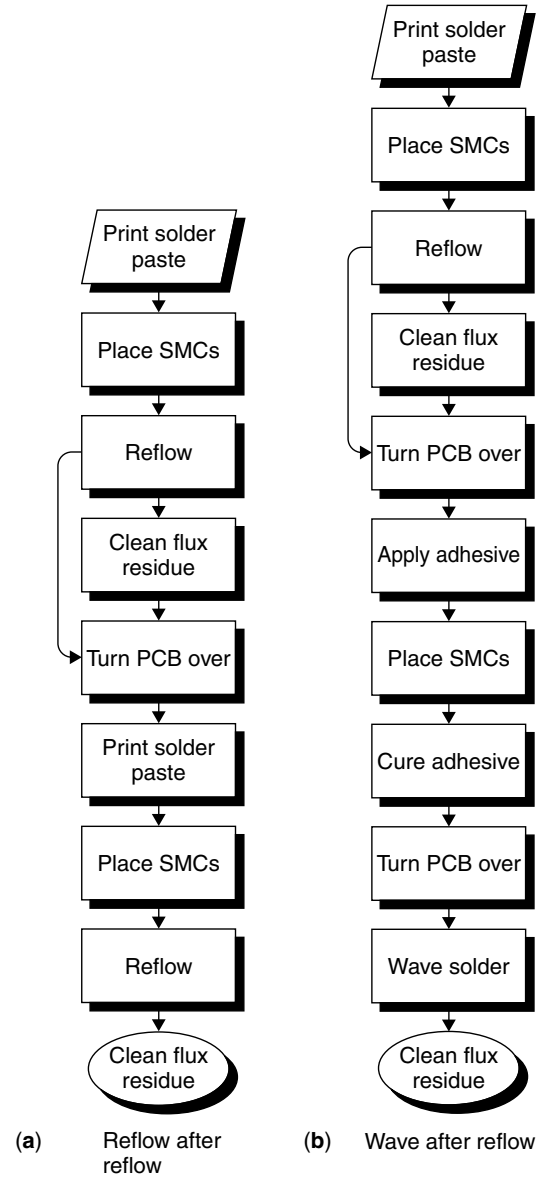

Figure 1.11 Assembly processes for type I surface mount boards

preheating allows small SMCs to be processed by wave soldering. However, for large SMCs and fine-pitch components, starved solder joints or bridgings are still a problem.

1.1.4.2 Reflow soldering

In order to eliminate the problems encountered in wave soldering SMCs, reflow soldering technology is introduced to SMT. Here the solder powder and flux are preblended to form a solder paste. The rheology of the paste usually is formulated to be thixotropic to facilitate the deposition process. This material is then deposited, usually through stencil printing or dispensing, onto the PCB pads where the SMCs are subsequently placed. This tacky solder paste serves as a temporary glue and holds the SMCs in place prior to the soldering process. The populated boards are then heated to above the liquidus temperature of the solder to reflow the solder powder. At this temperature, the flux reacts and accordingly removes the oxide of both solder powder and metallization of leads and pads, and consequently allows the solder to form solder joints. Some commonly used reflow methods include infrared reflow, vapor phase reflow, convection reflow, conduction reflow, and laser soldering.

1.1.5 Advantages of solder paste technology in SMT

As mentioned above, solder paste is the primary solder material used in the SMT reflow soldering process. Use of solder paste technology provides several major advantages over wave soldering technology. First, solder paste serves not only as a solder material, but also as a glue. The latter function allows the elimination of glue deposition and the curing process needed by wave soldering. Second, the deposition of solder paste is usually conducted by the stencil or screen printing, dispensing, or pin-transferring processes. The premetered deposition of solder material onto the sites to be soldered ensures a consistent solder volume for the joints, and accordingly eliminates the insufficient solder volume problems due to the shadowing effect encountered by wave soldering. In addition, this premetered solder deposition also reduces the incidence of bridging. This is particularly true in the case of fine pitch applications. Third, the use of mass

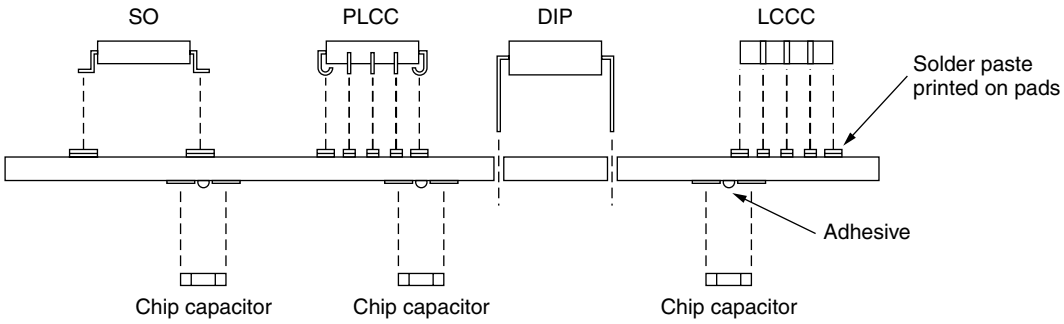

Figure 1.12 Schematic of type II surface mount boards

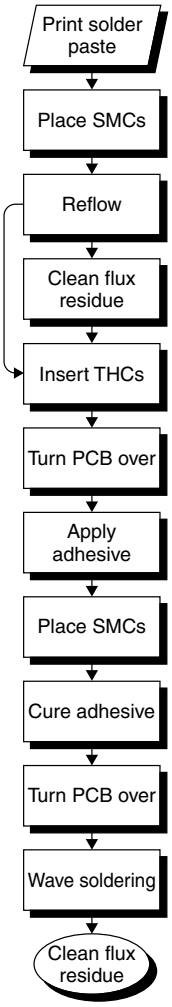

Figure 1.13 Assembly processes for type II surface mount boards

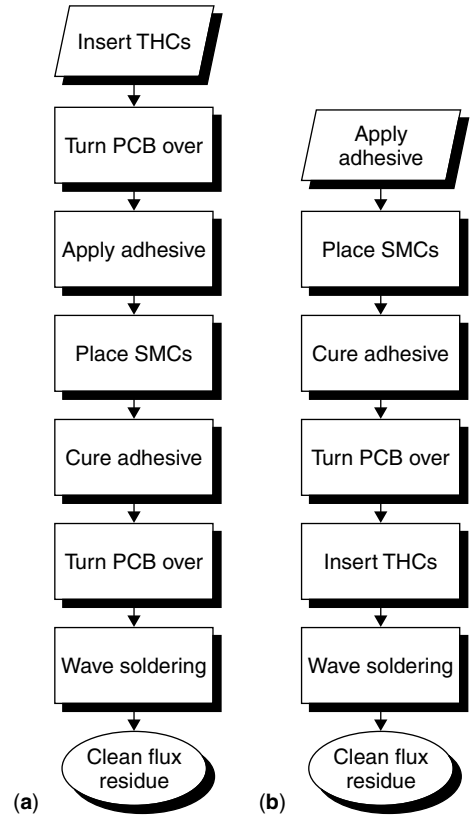

Figure 1.15 Assembly processes for type III surface mount boards, (**a**) THC inserted before SMC placement, (**b**) THCs inserted after the attachment of chip components

reflow process allows a well-controlled graduate heating profile, thus eliminating potential damage of the SMCs due to the thermal shock caused by the wave soldering. Fourth, the use of solder paste allows the possibility of step soldering. After the first step reflow, a solder paste with a lower solder melting point can be dispensed onto the sites to be soldered. This dispensed solder material can be reflowed later at a lower temperature without remelting the solder joints formed during the first step reflow. Fifth, the soldering performance of solder paste is not sensitive to the type of solder mask used on the PCBs. For the wave soldering process, a solder mask with a smooth finish is found to cause solder ball and bridging problems [1]. In addition, solder skip increases with increasing solder mask thickness [2].

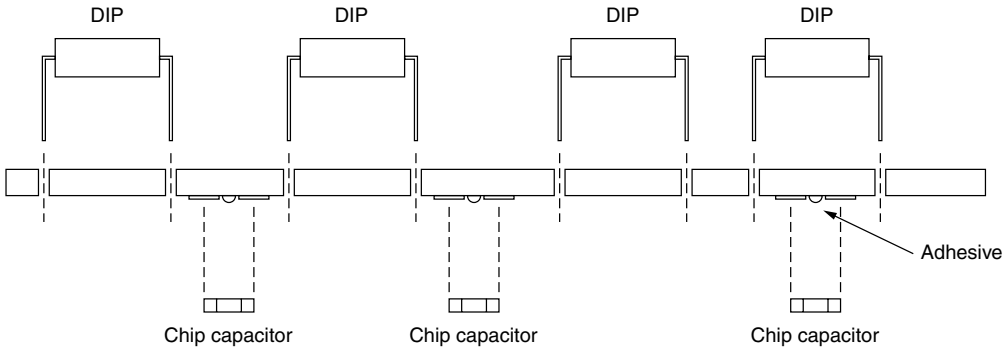

Figure 1.14 Schematic of type III surface mount boards

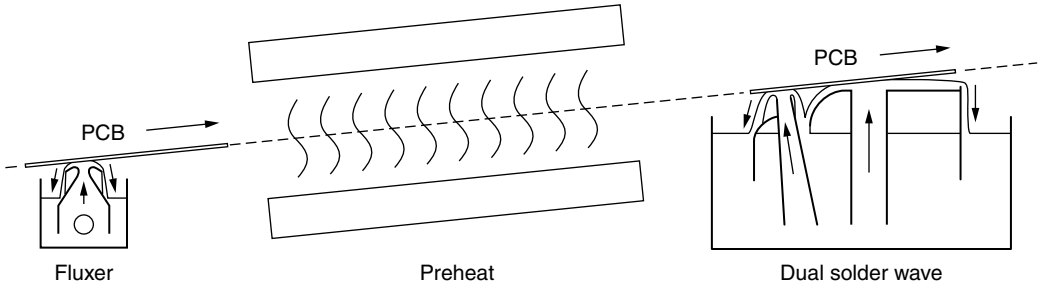

Figure 1.16 Schematic of the wave-soldering process

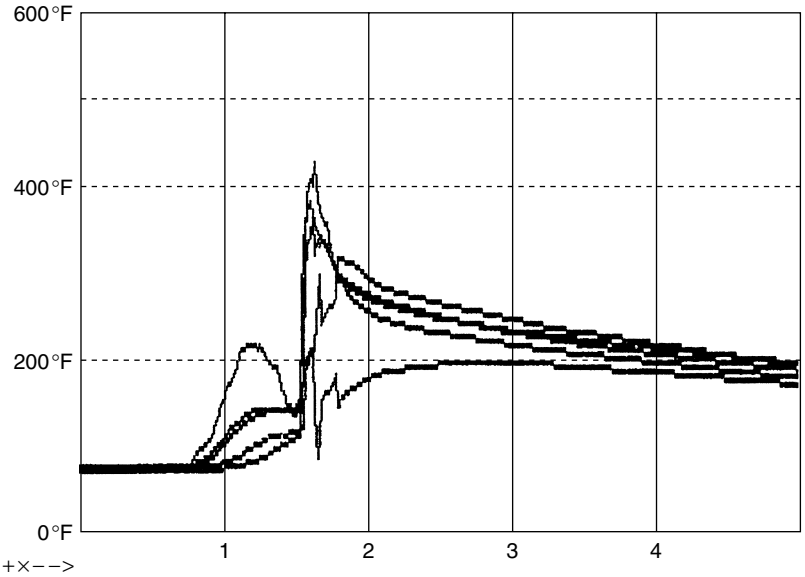

Figure 1.17 A typical wave-soldering thermal profile for SMCs soldering

The electronics industries are evolving constantly toward higher functional density, further miniaturization, and higher yield. Wave soldering technology failed to satisfy the constant need since the mid-1980s. It is the advantages of solder paste technology mentioned above that have enabled it to become the major board level bonding technology in SMT since the late 1980s. Recent studies [3–5] indicate that solder paste technology should be able to support the needs of solder bonding down to 12-mil pitch level applications.

1.2 Surface mount technology trends

1.2.1 Technology driving force

The electronics industry is mainly driven by the demand for "smaller, faster, higher complexity, lower power consumption, and cheaper". The Japanese industry, being strongly oriented toward consumer electronics products, places great emphasis on miniaturization and the cost factor. For instance, ultrathin packages, as thin as 0.4 mm, are prevailing in Japan [6], partly due to mature TAB infrastructure. In the USA the demand for ultrathin packages is low. The low limit of thickness is 1 mm. On the other hand, the computer oriented American industry appears to be more conscious of the speed and complexity issue. The trends of those factors on the SMT industry will be demonstrated in the following paragraphs. In fact, it may not be easy to distinguish the impact of those driving forces since improvement in one feature often results in improvement in other aspects.

1.2.1.1 Speed

The trend of increasing speed can be best described by the evolution of computer systems. Figure 1.18 [7] shows the processing performance in million instructions per second for computer systems. Low-end applications include consumer products, notebooks, personal computers and workstations. High-end applications include super, mainframe,

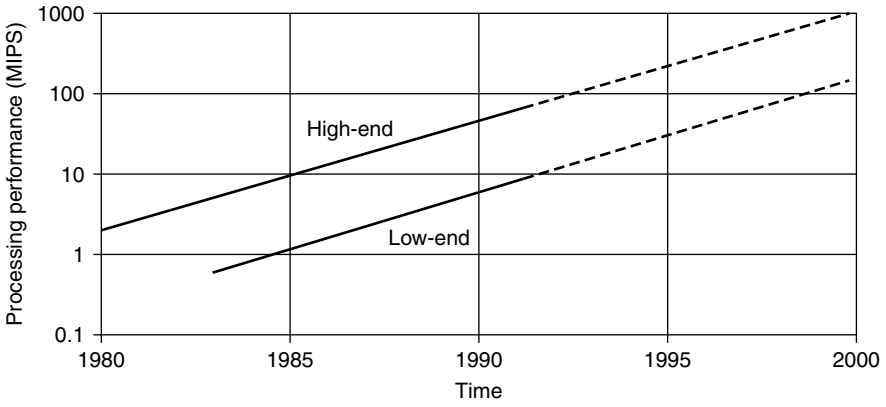

Figure 1.18 Processing performance of computer systems [6]. Performance (MIPS) = 1000/(cycle time × cycles per instruction) where the cycle time is in nanoseconds

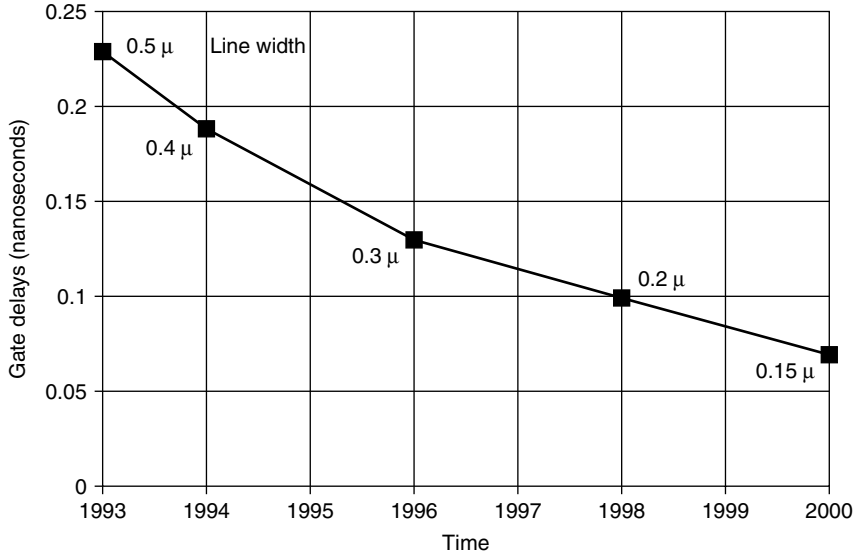

Figure 1.19 Gate delay of application-specific integrated circuits as a function of line width (μ)

mid-range computers, and possibly some advanced workstations as well [8]. In both instances, processing speed increases approximately five times in every 5 years. This increase in speed results from reduction in both on-chip delay in semiconductors and packaging delay. Figure 1.19 shows the trend of reduction in gate delay of application-specific integrated circuits (ASICs) from 1993 to 2000 [9]. The trend of increasing speed can also be demonstrated by the maximum performance (MHz) on chip reported by the Semiconductor Industry Association Roadmap [10], as indicated in Figure 1.20. The maximum performance on chip is projected to increase four to five times from 1997 to 2012.

Obviously this improvement in speed is closely associated with miniaturization of IC components, as demonstrated by the simultaneous reduction in line widths. Due to rapid advances in IC technology, packages have now become the slowing factor in computer systems. Proper choice, design, and manufacturing of a packaging system become crucial in order to reduce cycle time and improve performance.

1.2.1.2 Complexity

1.2.1.2.1 IC transistor integration Perhaps the trend of the electronics industry toward complexity can be best described by the evolution of computers. The complexity of semiconductor chips can be measured by transistor integration. Based on the "X86" CPU, the number of transistors on Intel's X86 microprocessors has increased by a factor of about 190 since the 8086's debut in 1978. Furthermore, microprocessor integration has increased by 2000× since its introduction in 1970, as shown in Figure 1.21 [11,12]. This increase in complexity of

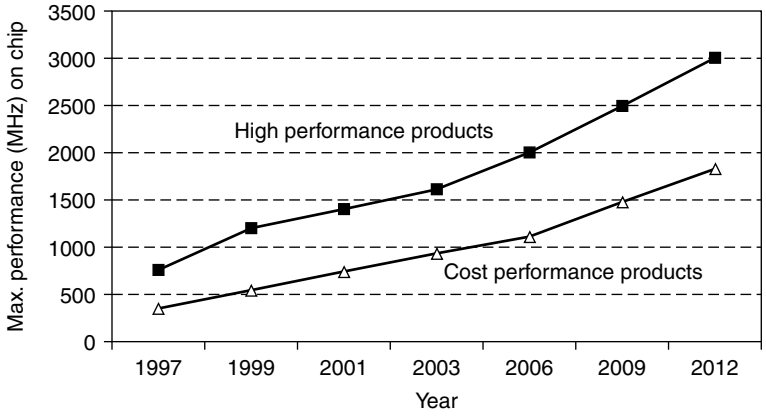

Figure 1.20 SIA technology roadmap for maximum performance of chip for high performance and cost performance products [10]

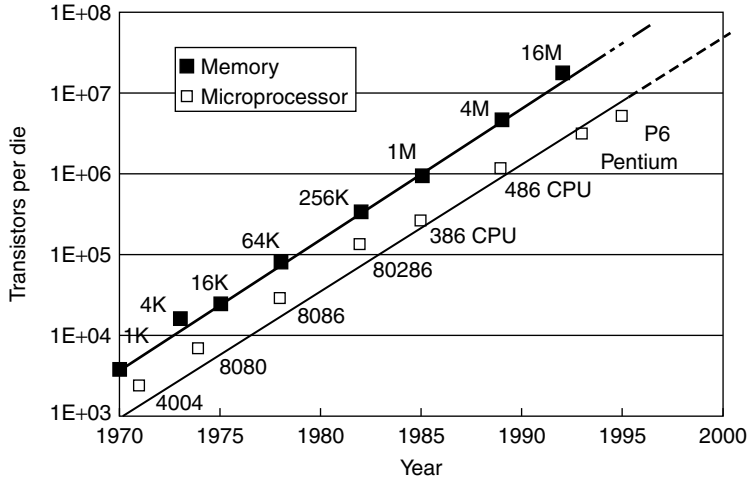

Figure 1.21 Increasing complexity as measured by transistor integration predicted by Moore's Law [11,12]

semiconductor chips essentially drives the evolution of corresponding packaging and assembly technology, as will be described later.

1.2.1.2.2 Pin count number A natural result of increasing IC complexity is an increase in the pin count number. Figure 1.22 [13] is a packaging technology roadmap covering the period from 1980 to 2000 published by National Semiconductor. In this roadmap, the pin count number will increase almost 100× from the through-hole technology in the early 1980s to modules/system packaging in the late 1990s. This increase in pin count number not only directly drives the evolution of packaging types, but also indirectly drives the trend toward miniaturization.

1.2.1.3 Miniaturization

Overall, due to the desire to make components smaller and lighter, miniaturization is the general trend in the electronics industries, particularly for consumer electronic products. Examples include camcorders, portable personal computers, cameras and portable phones. In fact, miniaturization is not only an independent driver but is also a logical result of the increasing complexity of functions. When increasing number of functions are to be built into increasingly smaller devices the only choice is to miniaturize component size and to increase packaging density.

IC feature size A typical example which best exemplifies the fact that miniaturization is a logical result of increasing complexity of functions is the IC feature size. Figure 1.23 shows the road to 5-million gate ASICs, as depicted by the Toshiba Corporation [14]. As the number of usable gates is to increase in ASICs, power consumption, gate delays, and line widths have to decrease in order to achieve a reasonable performance.

Discrete component size The miniaturization of discrete components can be exemplified by the size evolution of multilayer ceramic chip capacitors [15], as shown in

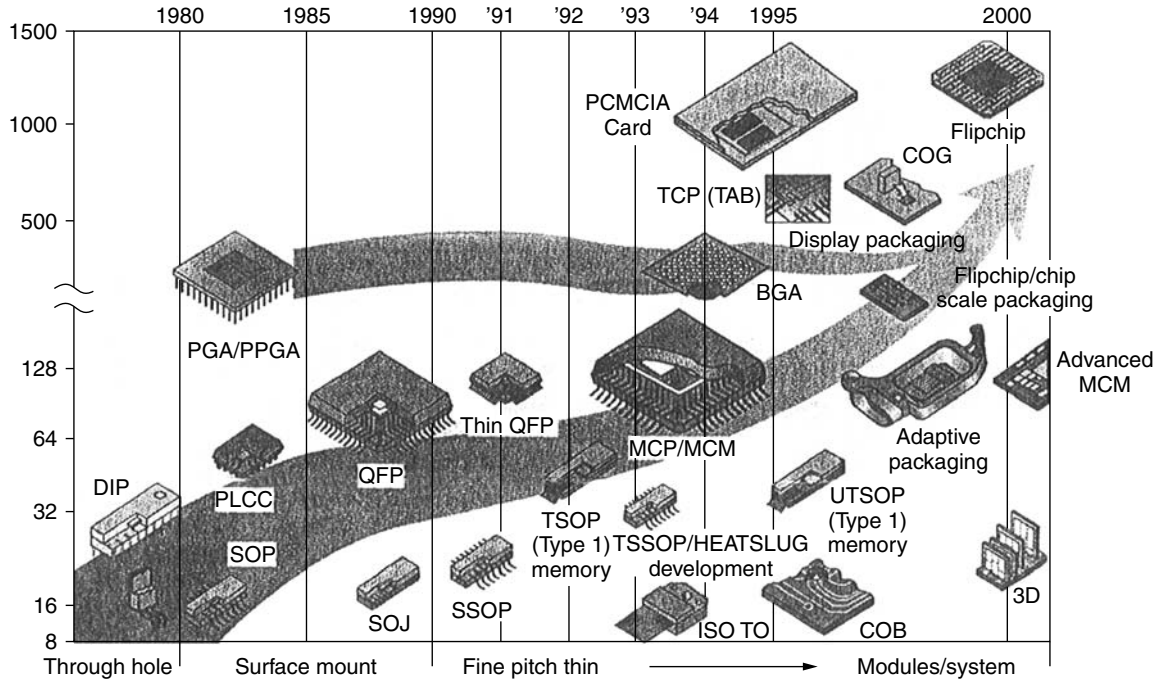

Figure 1.22 The ''Package Technology Roadmap'', published by National Semiconductor, depicts the evolution of package technology and pin count number [13]

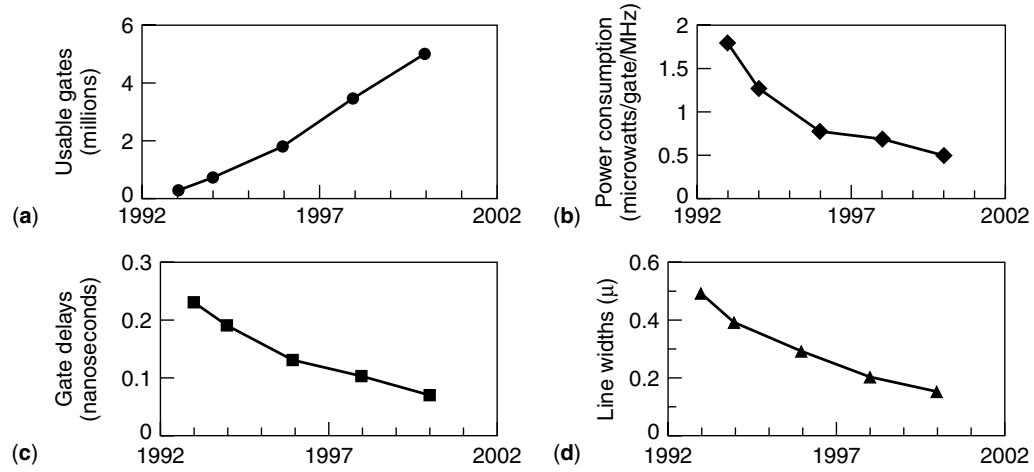

Figure 1.23 The road to five-million gate ASICs, developed by Toshiba Corporation [14]. (**a**) Usable gate, (**b**) power consumption, (**c**) gate delays, (**d**) line widths

Figure 1.24. Apparently, chip size is gradually reducing from 1206, with 0805 being the most popular size in 1989, 0603 in 1998, and 0402 projected to be the most popular size in 2003. 0201 emerged in 1998, and is rapidly gaining market acceptance, as shown in Figure 1.24. Difficulty in handling the small chips such as 0201 may result in a change in technology toward further miniaturization. A potential candidate technology may include integrated passives.

1.2.2 Area array packages

Area array packages are devices with I/Os interconnection distributed across the bottom side of components in an area array pattern. The interconnections often are composed of metal or polymer bumps, and the area array packages are mounted onto substrates through soldering or adhesives. Families of area array packages include BGA, CSP, and FC, as will be briefly described below.

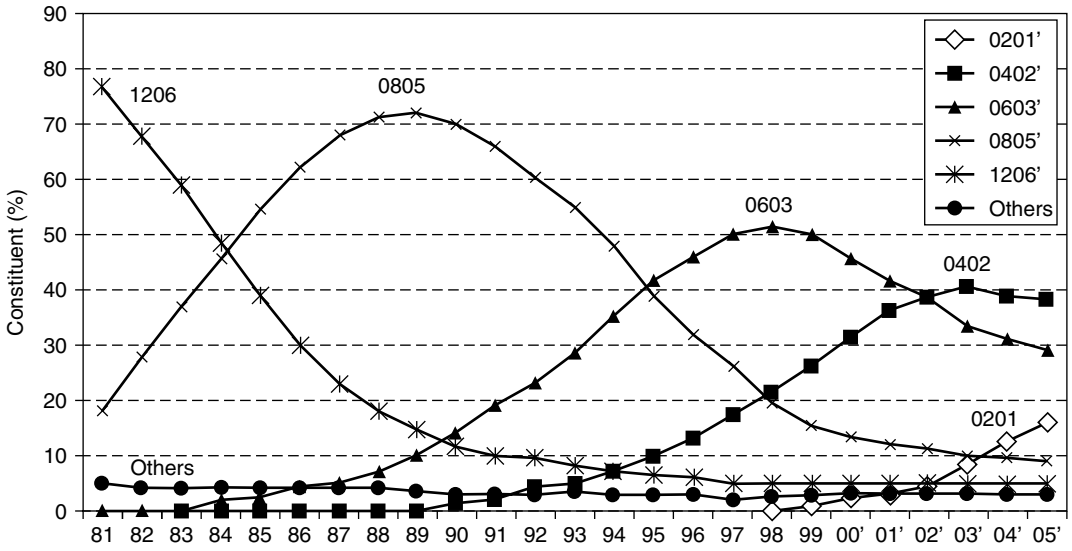

Figure 1.24 Size trends and life cycles for ceramic chip capacitors [15]

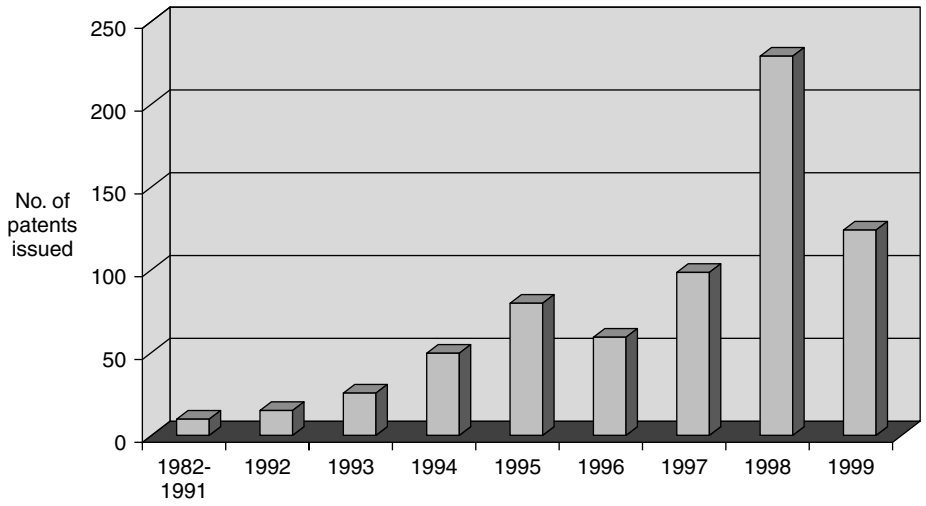

Figure 1.25 Number of patents issued for BGA, CSP, and WLP, according to International Interconnection Intelligence [16]

Area array packages are a new breed of surface mount devices, and clearly represent the direction of surface mount technology for the coming decades. This trend can also be reflected by the patents issued for area array packages. According to International Interconnection Intelligence, the number of patents issued for CSP, BGA, and WLP increases rapidly, as shown in Figure 1.25 [16].

1.2.2.1 BGA

Pressure of speed, complexity, and miniaturization have driven the peripheral package design down to 0.3 mm (16 mil) pitch for QFP [17], as shown in Figure 1.26. However, the rapidly increasing defect rate associated with miniaturization of peripheral design was recognized very quickly as the bottleneck in further improvements in performance. It is reported [17] that the assembly defect rate (ppm) of QFP is a strong function of the pitch size. The defect rate is 25 to 40 ppm for 50 mil pitch, and gradually increases to 25 to 100 ppm for 30 mil pitch and 40 to 233 ppm (5 sigma control) for 25 mil pitch. The defect rate becomes prohibitively high, 100 to 2300 ppm, for 20 mil pitch. This high defect rate is primarily associated with the vulnerability of the slim, thin gullwing leads of QFP toward handling. The high precision required for the ultra-fine-pitch component placement as well as solder paste deposition further aggrevates the problem.

To address this challenge, ball grid array (BGA) design emerges as a smart and logical answer. The BGA components are represented in Figure 1.27 [18].

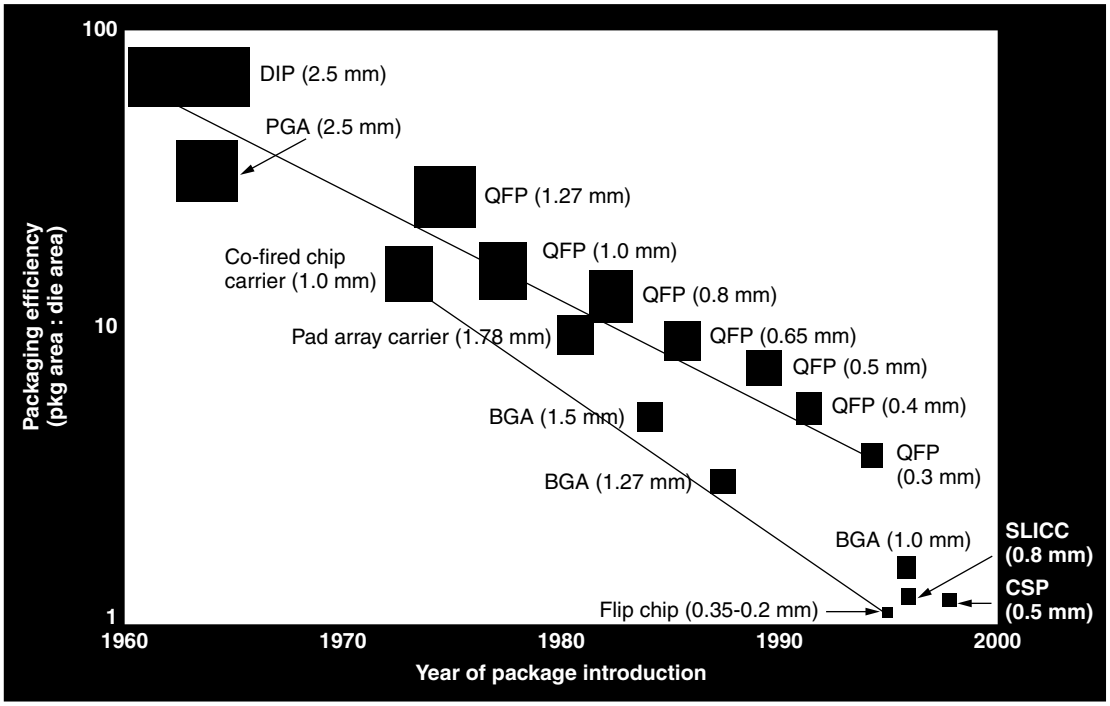

Figure 1.26 IC package time line [17]

In Figure 1.27(a), a Plastic BGA (PBGA) is illustrated. The I/O from a silicon die fans out to BT/glass substrate via wire bonding, and is then redistributed through the substrate to an area array pattern at the bottom side of component which is bumped with solder balls, such as Sn62/Pb36/Ag2 balls or Sn63/Pb37 balls. In Figure 1.27(b), ceramic column grid array (CCGA) and ceramic ball grid array (CBGA) are illustrated. In both cases, the IC is mounted onto a ceramic carrier through a flip chip interconnection, which will be described in the following section. The I/Os from the flip chip further fan out and are redistributed through the ceramic carrier. The ceramic carrier is bumped with high melting temperature solder spacers, such as 90Pb/10Sn solder columns or 90Pb/10Sn solder balls, in order to provide sufficient standoff so that the mismatch in coefficient of thermal expansion(CTE) between the ceramic substrate and the polymer PCB can be tolerated during service. Both CCGA and CBGA are typically soldered onto PCBs through the use of 63Sn/37Pb solder paste.

A change of I/O distribution from QFP peripheral pattern to BGA area array pattern provides a quantum leap in I/O density, as shown in Figure 1.25. This increase in I/O density allows a larger pitch, such as 60 mil pitch BGA, to be used to deliver the same I/O density of a fine-pitch QFP, hence effectively reducing the pressure of implementing a more accurate pick and placement equipment as well as a more precise solder paste deposition mechanism. Other advantages include better control of coplanarity, better space tolerance, design robustness, higher yield, and lower inductance (noise). A study [16] has reported that the PBGA assembly yield is 3.4 ppm (6 sigma control) for 60 and 50 mil pitch. This defect rate is several orders of magnitude lower than that of fine-pitch QFPs. However, the disadvantages of BGA should also be recognized. These include higher cost (molding, BT, ceramics, polyimide), solder ball control-size, missing, void, possibly a lower solder joint reliability, moisture sensitivity ("popcorn" effect), excessive PWB warpage during reflow, and CTE variation due to higher density of vias, difficulty in inspection, rework and cleaning (flux residue).

BGA technologies have been very rapidly accepted by the industry, as shown in Figure 1.28 [19]. Other reports [20] also indicate a strong growth in the BGA market. In 1996, the semiconductor package volume was 300 billion, with 66 billion in IC, and 234 billion in discretes. Within the IC packages, less than 1 percent is packaged in BGA. In 2001, 85 billion IC packages will be produced, and 4.5 percent will be packaged in BGA, and PBGA/LGA/CSP will account for 15 billion IC packages. TechSearch has reported [21] that an optimistic estimate of the BGA market is 500 million units in 1997, and 920 million units in 2000. The conservative estimate is about 60 percent of optimistic value.

Perhaps the greatest challenge affecting BGA technology is the overall cost [22] of the package. The cost per lead by package family is shown in Figure 1.29 [23]. For BGA, the cost per lead is somewhat higher than of most other packages, such as DIP, SO, CC, and QFP. Only PGA is considerably higher than BGA. However, for BGA, the cost per lead is reducing at a rate of -6.01 percent for CAGR, which is faster than -5.49 percent

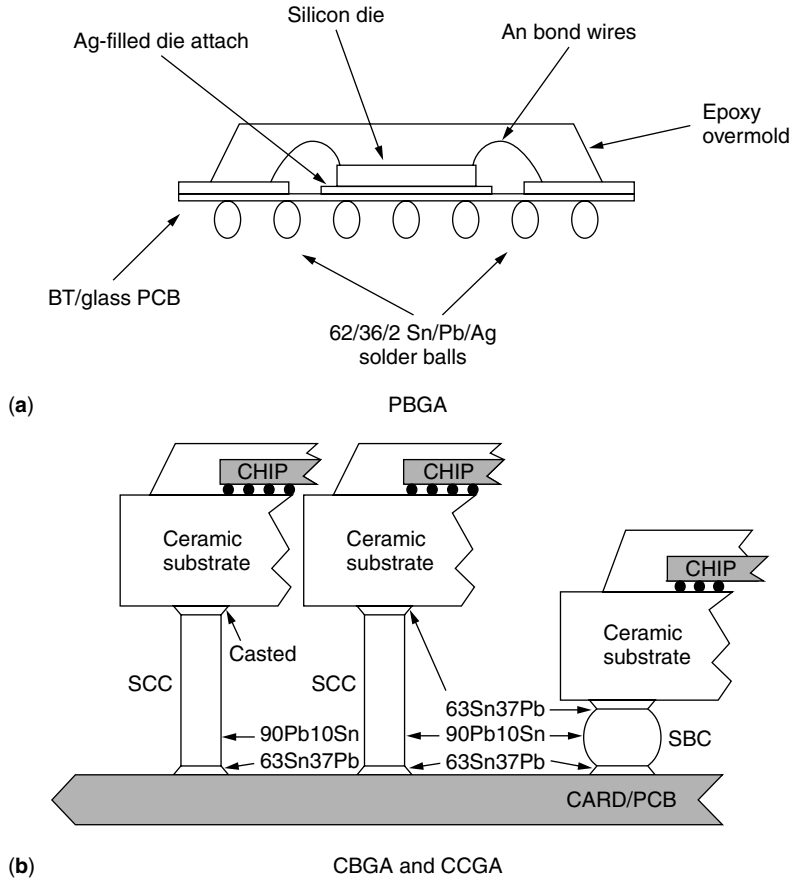

Figure 1.27 Schematic of various types of BGAs, (**a**) PBGA, (**b**) CBGA and CCGA

for DIP, −5.51 percent for CC, −2.39 percent for QFP, and −4.71 percent for PGA. As a result, the cost disadvantage of BGA is gradually diminishing. At present, the cost parity of the BGA to the QFP is above 200 I/O. The design methodology used to date has been cost effective for BGAs at or above 200 I/O but fails to be cost competitive below this pin count.

1.2.2.2 CSP

As indicated in Figure 1.26, the emergence of BGA satisfies the need for higher I/O density, but slows the drive toward finer pitch. However, with increasing demand toward further miniaturization, the packaging technology of BGA also reduces over time and consequently results in chip scale packages (CSP). A CSP is an IC area array package with size no larger than 1.2× of IC in the linear dimension, or no larger than 1.5× of IC in area. The package may use an interposer/carrier, and the interposer may be ceramic, plastic, or flex-film [24]. Depending on the CSP design, the interconnection [25] between IC and carrier may be wire bonding, TAB, Au-stud, soldering, or conductive adhesives. Currently, the minimum CSP array pitch is 0.5 mm, and will be 0.4 mm in 2000, and 0.3 mm in 2002 for the telecommunication market [26]. For the mobile systems market, the reduction rate of minimum CSP array pitch is even faster, with 0.5 mm in 1998, 0.3 mm in 2000, and 0.2–0.25 mm in 2004, according to the roadmap published by NETPACK (European Network in Microelectronic System Integration Technologies-Packaging). The options of alloys [24] and liquidus temperature used for CSP ball and attachment may include: 63Sn37Pb (183°C), 62Sn36Pb2Ag (179°C), 96.5Sn3.5Ag (221°C), 95Sn3.5Ag1.5In (218°C), 25In75Pb (264°C), and 10Sn90Pb (325°C).

For cellular phone applications, the most common I/Os in use at this stage are 32, 48, 64, 80, and 100. The ball size varies from 0.3 mm (12 mil) to 0.5 mm (20 mil), and size variation tolerance ranges from 0.03 mm (0.2 mil) to 0.075 mm (0.5 mil) [27]. It should be noted that the ball size changes for most of these devices depending on the manufacturer. The preference is to use as large a ball size as possible to assure the best reliability. The design of the CSP package also plays an important role in selection of ball size. For instance, Tessera's μ BGA® CSP uses a compliant layer making it possible to use smaller balls which reduces the chance of shorting, lowers weight and allows wider trace routing channels [28].

For the automotive industry, the maximum chip I/Os are 150 in 1998, and 200 in 2002, with CSP minimum

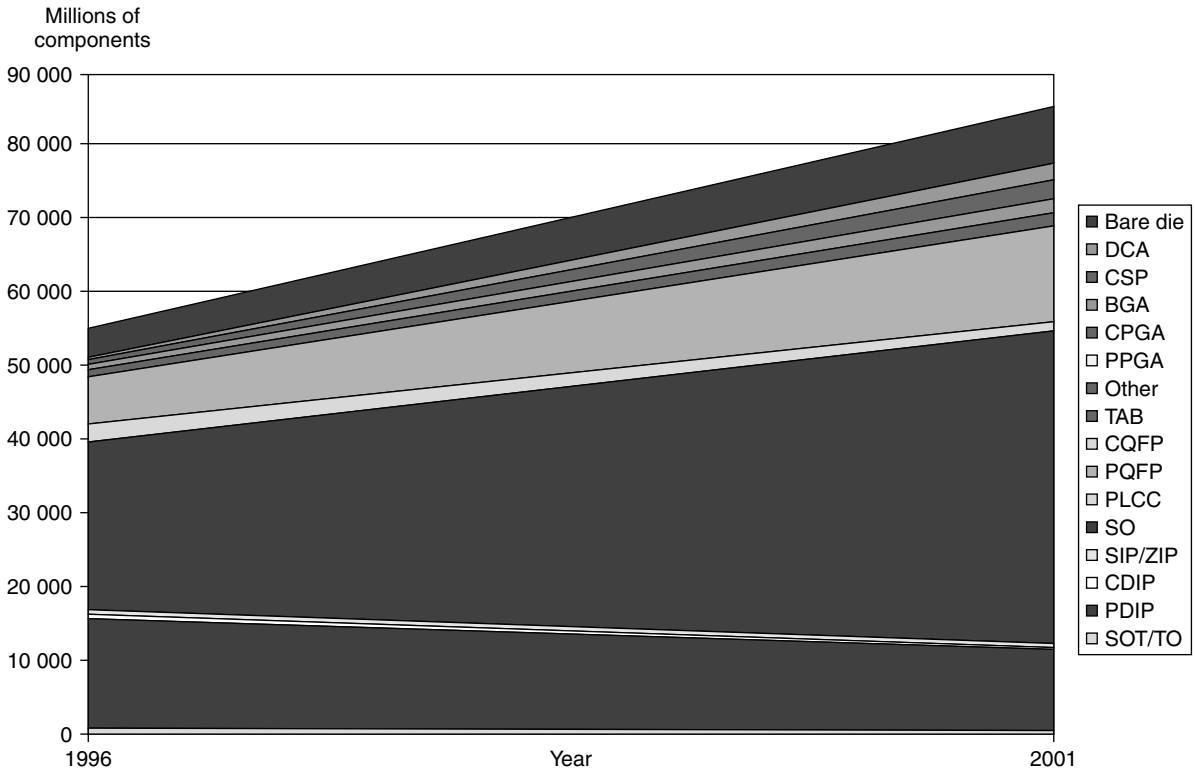

Figure 1.28 BGA market forecast [19]

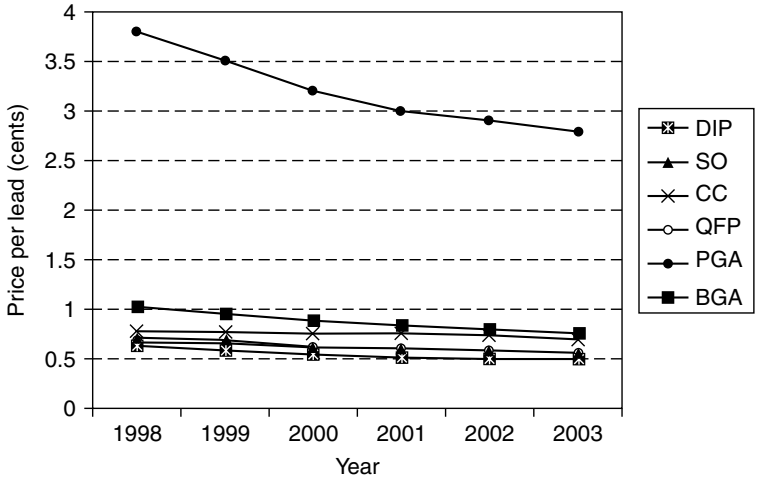

Figure 1.29 Cost per lead by family of packages [22]

pitch being maintained at 0.8 mm from 1998 throughout 2004. CSP can also deliver performance for very high I/O applications. The maximum chip I/Os for mobile systems are 500 in 1998, 600 in 1999, and are projected to be 700 in 2000, 800 in 2002, 900 in 2003, and 1000 in 2004 [25]. The current assembly yield [17] of CSP is estimated to be 3.4 ppm for 0.75 mm (30 mil) and 0.5 mm (20 mil) pitch, about the same level as a typical PBGA assembly yield.

1.2.2.3 Flip chip

Flip chip is a chip connection technology which interconnects an IC chip to its next level of packaging in such

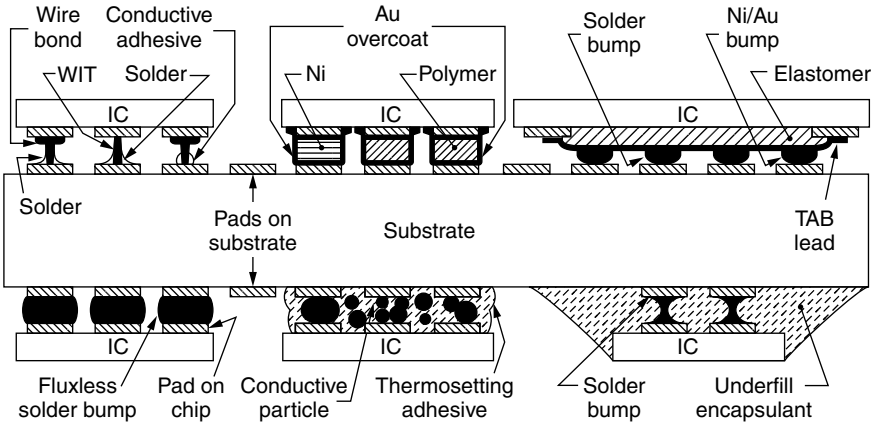

Figure 1.30 Various flip chip technology (courtesy of John H. Lau [29])

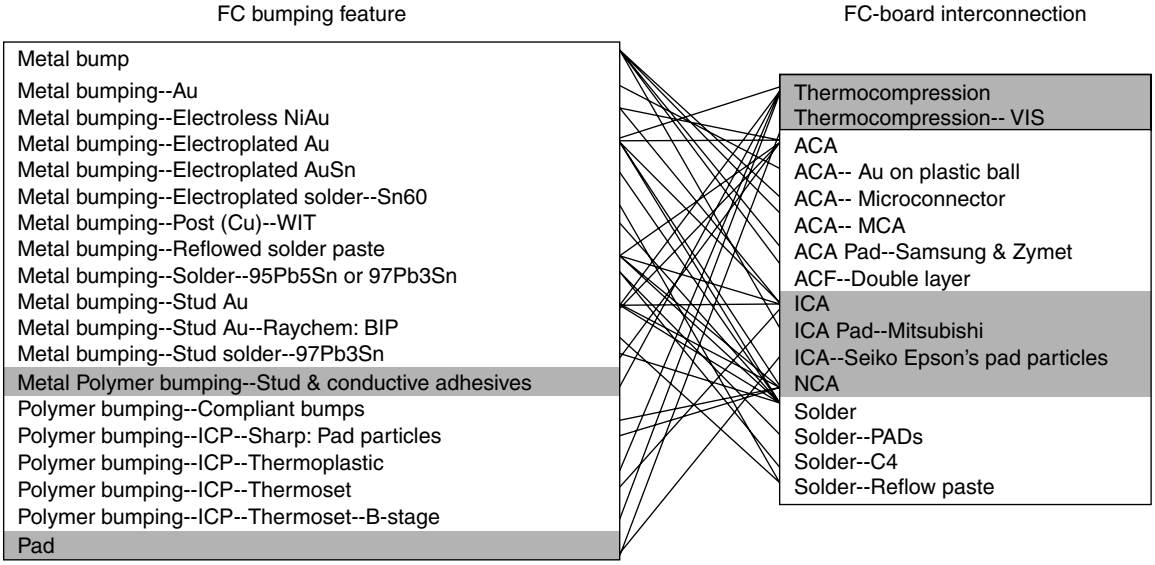

Figure 1.31 Flip chip interconnections [25]

a manner that the IC's active side faces the substrate. In terms of packaging efficiency (package area versus die area), flip chip technology reaches the ultimate goal of reducing chip size, as shown in Figure 1.26. Interconnection of flip chip with the substrate is shown in Figure 1.30 [29]. The bumping technologies used by flip chips are summarized in Figure 1.31 [24], and include plated metal bump, Au stud, metal stud plus polymer, Cu post, solder bump, and polymer bump. The bonding processes for flip chip attachment are also shown in Figure 1.28, and involve thermocompression, anisotropic conductive adhesives (ACA), isotropic conductive adhesives (ICA), non-conductive adhesives (NCA), and soldering.

Flip chip technologies are gaining market acceptance very rapidly. According to Electronic Trend Publications [29], the flip chip market was 568.7 million units in 1997, and will be 2.514 billion units in 2002, with an expected calculated annual growth rate (CAGR) 34.62 percent, as shown in Figure 1.32 [30]. The Die Attachment segment, including FCOB and FCOO (flip chip on other), has increased from 558.6 million units in 1997 to an estimated 1.334 billion units in 2002, with a CAGR of 19.02 percent. On the other hand, the Flip Chip In Package (FCIP) segment, including BGA FC, CSP FC, and MCM FC, has grown most rapidly from 10.1 million units in 1997 to an estimated 1.180 billion units in 2002, with a CAGR of 159.15 percent.

Prismark estimates flip chip die increased by 40 percent to 899 million units in 1998, which is 1.5 percent of the 60 billion ICs produced in 1998. This 40 percent annual growth rate is also expected for flip chip over the next five years [31]. The 899 M units were mostly DCA and 50 million units of these were FCIP. The majority of these FCIP will be delivered in BGA and CSP configurations.

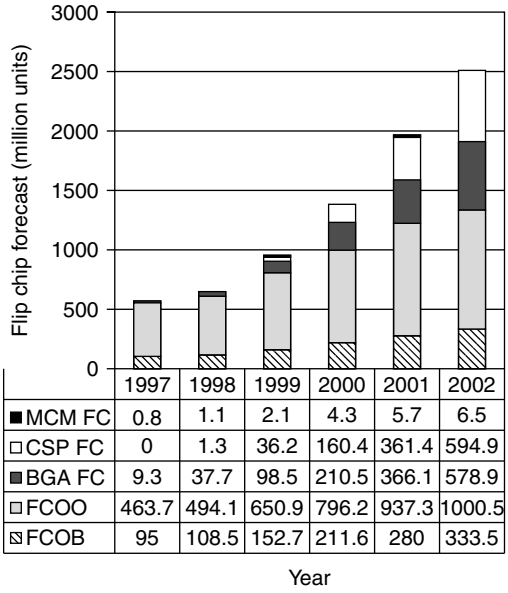

	1997	1998	1999	2000	2001	2002
MCM FC	0.8	1.1	2.1	4.3	5.7	6.5
CSP FC	0	1.3	36.2	160.4	361.4	594.9
BGA FC	9.3	37.7	98.5	210.5	366.1	578.9
FCOO	463.7	494.1	650.9	796.2	937.3	1000.5
FCOB	95	108.5	152.7	211.6	280	333.5

Figure 1.32 Flip chip forecast [30]

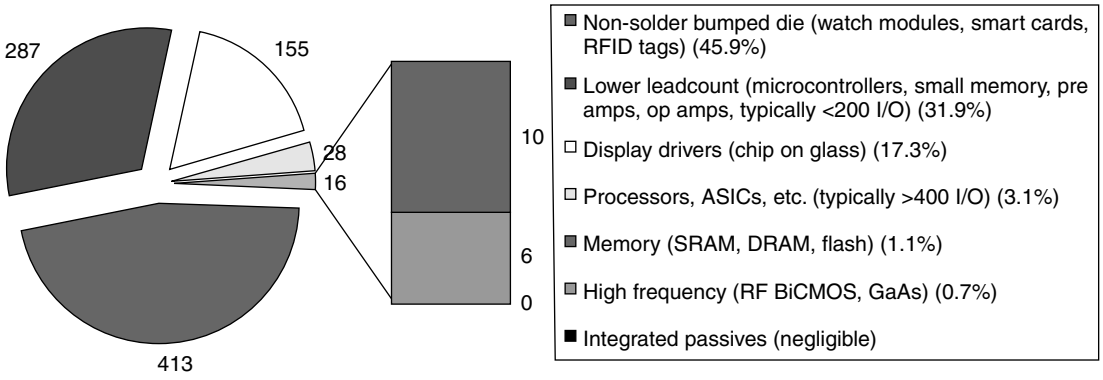

Figure 1.33 Breakdown of flip chip global production (million units) in 1998 [31]

Growth in FCIP brings that share of total FC devices up to an estimated 30 percent by 2004. A breakdown of global flip chip production in 1998 (total 899 million units) is shown in Figure 1.33.

A slightly more conservative forecast was released by TechSearch. In that study, the flip chip market was 760 million units in 1999, and is estimated to be 1.130 billion units in 2000, 1.450 billion units in 2001, 1.750 billion units in 2002, 2.000 billion units in 2003, and 2.400 billion units in 2004 [21]. The FCIP of overall FC will increase from 15 percent in 1999 to 27 percent in 2004. The balance is FCOB. Automotive electronics and watches, the two largest consumers of flip chip today, are expected to grow, but will account for a progressively smaller share of total flip chip consumed. Flip chip mounted driver ICs, while expected to see growth, will continue to represent about 10 percent of the total market. Telecom's share of the flip chip pie will grow. The growth of flip chip in switching and network applications will be overshadowed by the very large increase in the use of flip chip devices for portable telecom such as portable handsets and PDAs. The computer industry, representing portables all the way through high-end systems, is expected to see considerable growth. Its share of the total flip chip market is expected to expand to 40 percent by 2004. This will be driven by the growing consumption of flip chip-mounted processors and ASICs for home and portable personal computers.

1.3 Conclusion

Surface mount technology enables the progressing of the electronic industry toward the trends of becoming smaller, lighter, denser, faster, and cheaper. Competing with wave soldering, reflow soldering has quickly become the main stream interconnect technology, due to higher yield, throughput, and reliability. Area array packages alleviate pressure on peripheral packages toward finer

pitch, and provide higher I/O density together with easier manufacturability, smaller package size, and higher speed. BGA was the first array family to demonstrate the robustness of the surface mountable-area array package concept and now prevails in the industry. As a logical consequence of need for miniaturization, and based on the success of BGA, CSP and Flip Chip have both evolved rapidly and have become the new stars on the stage of advanced packaging technology. With the ultimate goal of having package reduction down to die size being within reach, the next challenge may be 3D packaging integration design.

References

1. D. Feryance and F. Shubert, ''Matte-surface Solder Masks Reduce Solder Ball Defects'', *EP&P*, pp. 58–60 (June 1993).
2. C. Hemens-Davis and R. Sunstrum, ''No-clean: Material Compatibility Issues'', *Circuits Assembly*, Vol. 4, No. 3, pp. 47–55 (March 1993).
3. M. Xiao, K. Lawless, and N.-C. Lee, ''Prospects of Solder Paste in UFPT Era'', in *Proc. of Surface Mount International 93*, San Jose, CA 29 (August–2 September 1993).
4. B.-T. Ma, A. Sarkhel, and C Woychik, ''Evaluation Solder Paste Printing and Reflow for Ultra Fine Pitch Surface Mount Process'', in *Proc. of Nepcon West*, Anaheim, CA, pp. 506–517 (1993).
5. ''Packaging Materials: Ball Grids Are Pinless PGAs'', *Electronic Materials Report*, Vol. 10, No. 1, pp. 8 (January 1994).
6. R. Iscoff, ''Ultrathin Packages: Are They Ahead of Their Time?'' *Semiconductor International*, pp. 48–52 (May 1994).
7. H. Wessely, O. Fritz, P. Klimke, W. Koschnick, and K. H. Schmidt, ''Electronic Packaging in the 90s – A Perspective from Europe,'' *Proceedings of the 40th IEEE Electronic Components and Technology conference*, pp. 16–33 (May 1991).
8. J. Lau and S. Erasmus, ''Review of Packaging Methods to Complement IC Performance'', *EP&P*, pp. 50–56 (June 1993).
9. R. Ristelhueber, ''Monster ASICs Emerge from 'Deep Submicron Silicon' '', *Electronic Business Buyer*, pp. 39–42 (February 1995).
10. C. Vaucher, ''Electrical test of Bare Printed Circuit Board: Requirements on the 'System Houses' Side'', *Future EMS International*, Issue 1, p. 46, (1999).
11. B. Siu and J. McMahon, ''Evolution and Trends for Microprocessors'', *Circuits Assembly Market Supplement*, S10–13 (September 1993).
12. T. R. Halfhill, ''Intel's P6'', *BYTE*, pp. 42–58 (April 1995).
13. R. Iscoff, ''Ultrathin Packages: Are They Ahead of Their Time?'' *Semiconductor International*, pp. 48–52 (May 1994).
14. R. Ristelhueber, ''Monster ASICs Emerge from 'Deep Submicron Silicon' '', *Electronic Business Buyer*, pp. 39–42 (February 1995).
15. M. Durkan, ''Integrating Technologies to Bring Speed to Market'', *Future EMS International*, Issue 1, pp. 69, (1999).
16. ''Area Array Packaging Options Continue to Blossom'', *EP&P*, p. 14 (November 1999).
17. I. Turlik, ''Chip-Scale Packaging Technology Trends'', *Chip Scale Review*, Vol. 1, No. 2, pp. 30–35 (July 1997).
18. J. H. Lau,(ed.), *'Ball Grid Array Technology'*, McGraw-Hill, New York (1995).
19. R. Lasky, ''Electronics: This is Only the Beginning'', *EP&P*, pp. 48–52, (November 1997).
20. G. Olachea, ''IC Packaging for the 21st Century'', *EP&P*, Vol. 37, No. 15, pp. 57–62, (November 1997).
21. T. Goodman, ''Flip Chip: Key Technologies and Applications Worldwide'', in *Proc. ISEPT'98*, Beijing, China, 17–21, August, pp. 435–439, (1998).
22. J. Miks and D. Daniels, ''Cost Effective Approach to Fine Pitch BGAs'', in *Proc. MCM'97*, Denver, CO (April 1997).
23. S. Winkler, ''Packaging Industry Outlook'', *HDI*, Vol. 2, No. 6, pp. 16–17 (June 1999).
24. V. Solberg, ''Assembly Process Development for Chip-Scale and Chip-Size uBGA®'', in *Proc. SMTA/IPC Electronics Assembly Expo*, Providence, RI, 24–29, October pp. S12–S14,(1998).
25. N. C. Lee, ''Interconnections for SMT, BGA, and Flip Chip Technologies'', Keynote Lecture, Nepcon Penang, 17, June 1996.
26. S. Berry, ''The Future of Leadcounts'', *HDI*, pp. 14–16, (April 1999).
27. Private communication from Jessie Buenaventura, Amkor-Manila, Philippines, 20, December, 1999.
28. Private communication from Joseph Fjelstad, Teserra, San Jose, CA, 21, December 1999.
29. John H. Lau, (ed.), *Flip Chip Technologies*, McGraw-Hill, New York, (1996).
30. Steve Berry and Sandra Winkler, ''Flip Chip Market Expanding to Meet Speed, Performance Demands'', *Chip Scale Review*, 11/12, p. 6 (1999).
31. L. Smith, C. Scanlan, and P. O'Brien, ''FCIP Delivers Flip Chip Benefits without DCA Complications'', *Advanced Packaging*, pp. 32–35, (August 1999).

2 Fundamentals of Solders and Soldering

Soldering uses molten filler metal to wet the surfaces of a joint and form metallurgical bonds between two metal parts. The melting temperature of the filler metal is lower than 450 °C. For filler materials that melt at a higher temperature, the joining process is classified as brazing [1]. Soldering is a vital interconnect technology involved in both level 1 (IC packaging) and level 2 (mounting of electronic components onto printed circuit boards) processes of the modern electronics industry. Therefore, to achieve a high quality and high yield soldering process, it is essential to understand the fundamentals of solder and soldering.

2.1 Soldering theory

Although soldering has been carried out by humans for more than several thousand years, an understanding of this process was minimal until recently. The soldering process can be depicted in Figure 2.1, and can be roughly divided into three stages: (1) spreading, (2) base metal dissolution, and (3) formation of an intermetallic compound layer [2]. In this figure, fluid stands for either flux or soldering atmosphere, and the base metal is the substrate.

2.1.1 Spreading

In order to solder, the solder material first has to be heated to a molten state. This molten solder is then allowed to wet to the surface of the base metal. Like any other wetting phenomenon, wetting of liquid solder on a base metal, as shown in Figure 2.1(a), has to comply with the physical law of balance of interfacial tension, as expressed by

$$\gamma_{SF} = \gamma_{LS} + \gamma_{LF} \times \cos\theta \tag{2.1}$$

In this relation, γ_{SF} stands for the interfacial tension between the base metal substrate and the fluid, γ_{LS} is the interfacial tension between substrate and the liquid solder, γ_{LF} is the interfacial tension between liquid solder and the fluid, and θ represents the contact angle between liquid solder and the substrate.

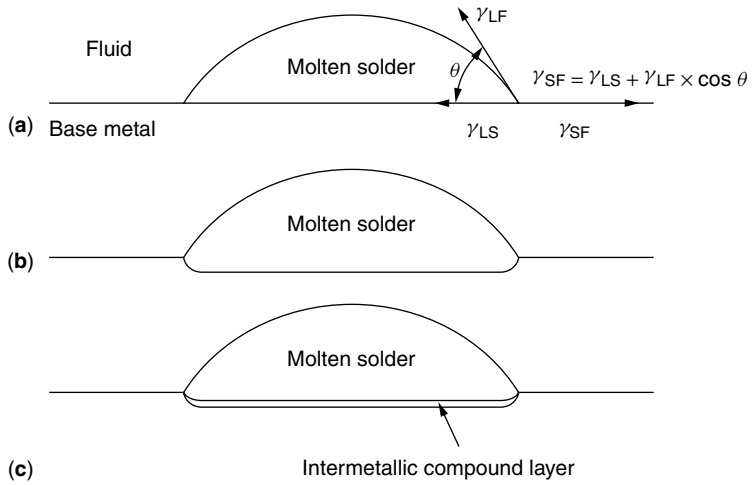

Figure 2.1 Solder wetting process involves (**a**) liquid solder spreading over base metal, with contact angle θ dictated by balance of interfacial tension forces, (**b**) base metal dissolving in liquid solder, (**c**) base metal reacting with liquid solder to form intermetallic compound layer

Equation (2.1) predicts that the spreading of a liquid on a solid surface reaches an equilibrium steady state when the contact angle achieves a θ value where the two opposite vector forces γ_{SF} and $(\gamma_{LS} + \gamma_{LF} \times \cos\theta)$ are balanced.

For electronics industry soldering applications, a solder joint with a satisfactory fillet formation is desired for minimum stress concentration, as demonstrated in Figure 2.2. In order to achieve this, a solder spreading characteristic with low θ value is needed. In fact, a small θ value is not only desirable due to stress consideration, it must also assure that a good metallurgical wetting is achieved, as will be illustrated in the following sections.

A low θ value can be achieved with both chemistry and physics approaches. The chemistry approach will be discussed later. The physics approach includes manipulation of surface tension of materials involved in the soldering process. In principle, use of (1) a low surface tension flux, (2) a high surface tension, or high surface energy, substrate, and (3) a low surface tension solder will allow formation of a low contact angle θ. The first situation can be derived easily from the effect of surface tension on interfacial tension, as shown in Appendix 2.1. The second and third situations can also be derived similarly. However, they can also be easily demonstrated by some common phenomena. Thus, the second situation can be illustrated by the poor wetting of water on a Teflon (low surface energy) substrate but relatively good wetting on a metal (high surface energy) substrate. The third situation can be demonstrated by good wetting of alcohol (low surface tension) but poor wetting of mercury (high surface energy) on a glass slide.

However, it should be emphasized again that for the soldering process, the balance of interfacial tension is only one of the driving forces determining the wetting phenomenon. Since generally the base metal will dissolve in and react with the solder, and since soldering is a short, non-equilibrated process instead of an equilibrated one, factors such as fluid viscosity, metal dissolution, and chemical reaction between solder and base metals often play a more important role, as will be discussed in the following sections.

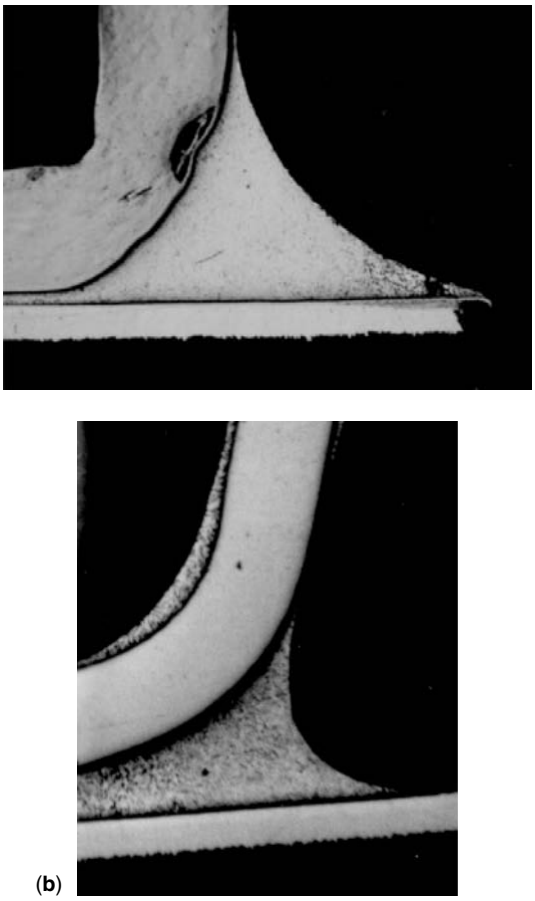

Figure 2.2 Example of SMT 62Sn/36Pb/2Ag solder joints with desired fillet formation, (**a**) melf on HAL pad, (**b**) IC gullwing lead on Cu pad

2.1.2 Fluid flow

In the previous section, we showed that the spreading of a fluid is determined by the balance in interfacial tension established at the equilibrium state. However, in the actual soldering process encountered in the electronics industry, only seconds or minutes are allowed, and the equilibrium condition virtually can never be met. Factors such as viscosity of the molten solder will affect the extent of solder flow, and thus can play an important role when time is a constraint.

Milner [3] has analyzed the fluid flow between two horizontal parallel plates with consideration of both surface tension and fluid viscosity factors. The conclusion on the rate of fluid flow through the parallel plates dl/dt drawn from his study can be expressed as

$$dl/dt = (\gamma_{LV} D \cos\theta)/(6\eta l) \tag{2.2}$$

Here l is the length of plates, η is the viscosity of the fluid, γ_{LV} is the interfacial tension between fluid and the surrounding vapor or atmosphere, D is the joint gap, and θ is the contact angle between fluid and the plate. Therefore, the rate of the liquid flow through the parallel plates dl/dt increases with increasing interfacial tension between liquid and vapor γ_{LV}, increasing joint gap D, but with decreasing contact angle θ, decreasing viscosity η, and decreasing plate length l.

By applying equation (2.2) to solder spreading, γ_{LV} can be rewritten as γ_{LF}, and represents the interfacial tension between liquid solder (L) and flux (F). Since $\gamma_{LF} = \gamma_L - \gamma_F$ according to Antonow's rule (see Appendix 2.1), for a given solder with surface tension γ_L, an increase in γ_{LF} would have to depend on a decrease in the surface tension of flux γ_F. Hence a flux with a low surface tension will not only increase the spread, as discussed in the previous section, but will also increase the liquid solder flow rate.

Humpston and Jacobson [1] have calculated the filling rate of molten solder in joints 50 μm wide with the use of this equation, and found the filling rate is typically 0.3 to 0.7 m/s. Thus a joint 5 mm (0.2 in.) in length will be filled in around 0.01 second. Considering that the surface energy

driving force is often opposed by viscosity and surface irregularity, as reported by De Gennes [4], a joint filling time of the order of 0.1 second may be more realistic.

2.1.3 Dissolution of base metal

Flow and spreading of liquid solder over a base metal substrate are not sufficient to form metallurgical bonds, which are required to form solder joints, as demonstrated by placing liquid solder on a glass surface. In order to form a metallurgical bond, the solder and base metal have to be mixed at the atomic level at the interface. This is typically accomplished through dissolution of base metal into the solder at the microscopic level ($<100\,\mu m$) [1], as shown in Figure 2.1(b).

For the electronics industry, the soldering process is often confined to a relatively low temperature, such as 220 °C, and a short cycle time, often no longer than several seconds or minutes, due to materials limitations and throughput consideration. Therefore, the dissolution of a base metal in solder needs to be reasonably easy and fast. For tin–lead systems, which have been the prevalent choice of solders for the past several decades, the acceptable base metals or metallization include, but are not limited to, Sn, Pb, Bi, Au, Ag, Cu, Pd, Pt, and Ni. The dissolution rate dC/dt of some of those metallization in 60Sn/40Pb as a function of temperature is shown in Figure 2.3 [1,5], and can be represented by the Arrhenius relationship, as shown in the following equation:

$$dC/dt \propto \exp[-E/(kT)] \tag{2.3}$$

where C is the concentration of the base metal, E is the activation energy, k is the Boltzmann constant, and T is temperature in degrees Kelvin. The dissolution rate of a base metal in solder is also a function of time [1,6,7], as expressed by

$$dC/dt = KA(C_S - C)/V \tag{2.4}$$

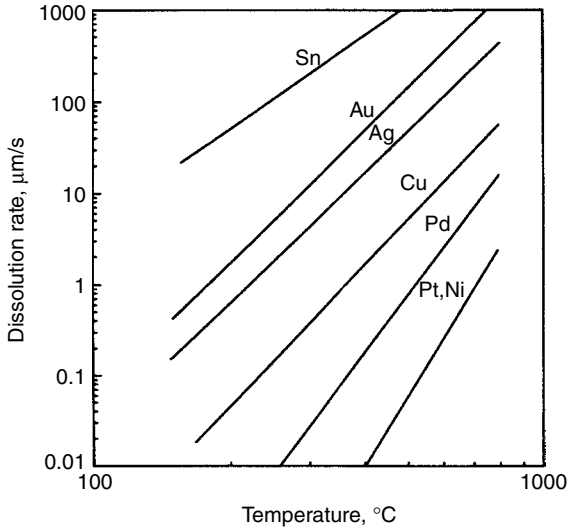

Figure 2.3 Dissolution rate of some commonly used metals and metallizations in 60Sn/40Pb as a function of temperature [32,36]

where C is the concentration of the base metal, C_S is the concentration limit of the dissolved metal in the molten solder at any given temperature, t is time, K is the dissolution rate constant, A is the wetted surface area, and V is the volume of the molten solder. By integrating equation (2.4), the relation between C and t can be expressed by Figure 2.4 [1], where C reaches an equilibrium concentration in an inverse exponential relationship with t. The dissolution of a base metal in solder as a function of time and temperature can be demonstrated by Figure 2.5, where the dissolution of base metal silver in molten tin increases with increasing time and temperature [8]. Humpston and Jacobson reported that the equilibrium condition can be reached within seconds at the process temperature according to their calculations, suggesting the feasibility of predicting solder joint composition with an equilibrium phase diagram.

The dissolution rate of a base metal in solder is a function not only of time, temperature, and base metal type but also of solder alloy type [5]. Therefore, for Ag, the dissolution rate in solders decreases in the following order: Sn > 99Sn/1Cu > 90Sn/10Pb > 80Sn/20Pb > 62Sn/38Pb. For Cu, the dissolution rate decreases as: Sn > 60Sn/40Pb > 35Sn/65Pb > 57Sn/38Pb/5Ag > 62Pb/33Sn/5Ag. The dissolution rate can be changed by shifting the initial concentration of the base metal in the solder by engineering the solder composition. Hence, by adding 2 percent Ag to tin–lead solder, the dissolution rate of base metal Ag can be reduced significantly, as exemplified by comparing the dissolution rate of Ag in the 40Pb/60Sn and 36Pb/62Sn/2Ag solder systems [9] (see Figure 2.6).

In general, the wettability of metallization appears to increase with increasing dissolution rate in the solder. Although this phenomenon may be related to chemical reactions, as will be discussed in Section 2.1.4, it may also be attributable to the entropy factor, since dissolution of a base metal in solder will result in an increase in

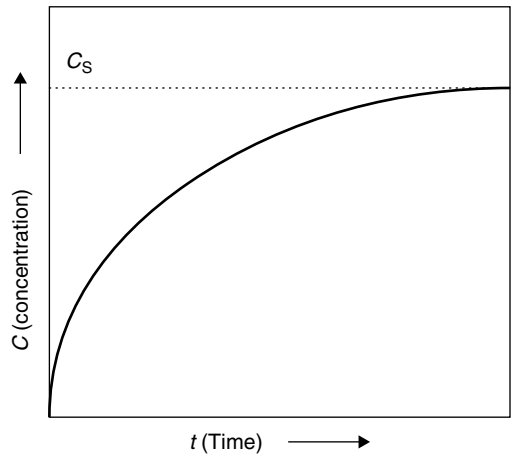

Figure 2.4 The concentration C of base metal increases in an inverse exponential relationship with time t, and approaches equilibrium concentration C_s quickly [32]

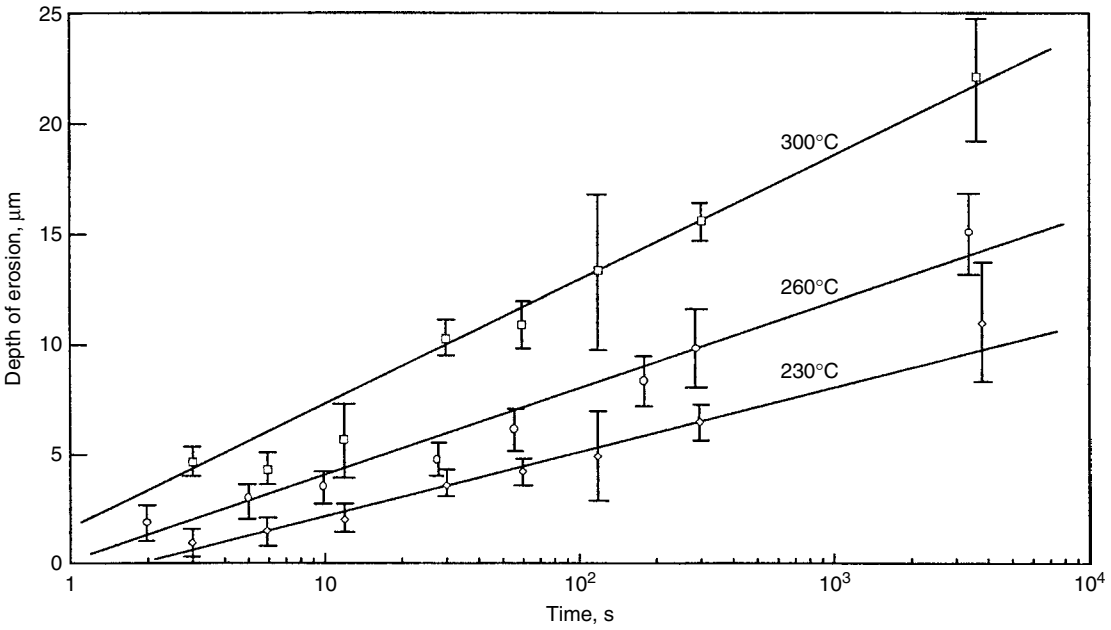

Figure 2.5 Dissolution of silver by molten tin as a function of time and temperature

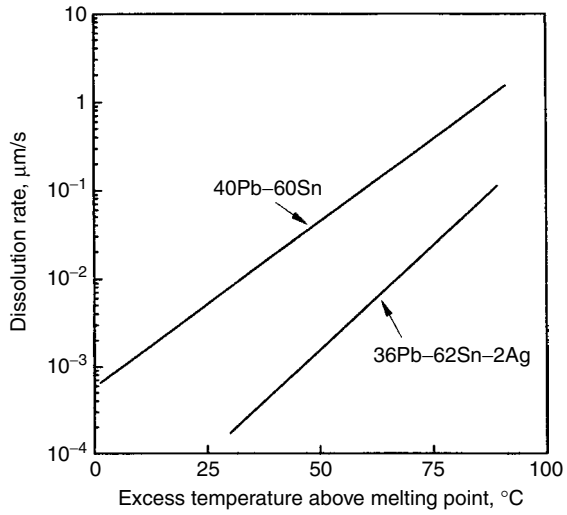

Figure 2.6 Dissolution rate of silver in tin–lead and tin–lead–silver solder systems [40]

entropy. Since the dissolution rate increases with increasing temperature and time, this allows control of dissolution rate with processing parameter. On the other hand, the strong influence of the base metal type and the solder type on dissolution rate indicates the importance of materials selection at the engineering design stage.

Although dissolution of a base metal is essential in forming metallurgical bonds, too fast a dissolution rate may result in a serious leaching problem hence loss of metallurgical bonds. In addition, it may also cause a significant change in solder composition, therefore causing deterioration of joint reliability. These situations are not desirable, and will be discussed later.

2.1.4 Intermetallics

Soldering often involves not only the physical dissolution of base metals in the molten solder but also the chemical reaction products between base metal and solder components. The reaction products formed typically are intermetallic compounds (IMC, or intermetallics) at the interface between solder and base metal, as shown in Figure 2.1(c). Intermetallic compounds are exact stoichiometric compounds which tend to form when one of the two elements is strongly metallic in character and the other significantly less so. For instance, intermetallics Cu_6Sn_5 and Cu_3Sn normally are formed between tin–lead solder and base metal Cu. Intermetallics tend to be hard and brittle because their crystal structure has low symmetry, and this limits the plastic flow.

The effect of intermetallics formation on soldering includes (1) enhancement of solder wetting on the base metal due to favorable thermodynamics, (2) slowing of the dissolution rate of the base metal in solder due to the diffusion barrier role of the intermetallics layer, and (3) deteriorating the wettability of a pretinned surface through oxidation of intermetallics. Those effects will be discussed in detail below.

2.1.4.1 Wetting enhancement

It has been reported by Yost and Romig [10] that even though the imbalance of surface energy will result in energy release thus favoring solder spreading, the free energy of formation of intermetallics between liquid antimony, cadmium, and tin with base metal copper was about

two orders of magnitude larger. Hence, it is no surprise to learn that the wetting behavior increases with increasing formation rate of intermetallics, and is dictated by the intermetallics formation rate.

The first intermetallic compound to be formed at the solder/substrate interface can be predicted by calculating metastable equilibria between the substrate and the liquid solder phases and by comparing the calculated driving forces of formation for individual phases. This feasibility of prediction was demonstrated for the interface reactions between Cu substrate and Sn–Pb, Sn–Bi and Sn–Zn binary eutectic solders [11].

Like the dissolution of a base metal in solder, the formation rate of intermetallics is also a function of time, temperature, type of substrate metallization, and solder type. Figure 2.7 shows the growth of copper–tin intermetallics on a copper substrate wetted by eutectic tin–lead solder. The intermetallics thickness decreases with decreasing time and temperature [1]. Growth in intermetallics continues even at temperatures below the melting point of solder, although at a much slower rate, as illustrated in Figure 2.8. Kay and Mackay [12] reported that the thickness of tin-base intermetallic phases developed at 170 °C via solid-phase diffusion is a function of substrate materials, and varies in the following order: Co > Ag > Cu > Ni > Fe. The effect of solder type on the intermetallics formation rate of several metallizations has been studied by Muckett *et al.* [13] and their findings are reported in Table 2.1. It is interesting to note that, compared with 63Sn/37Pb and 62Sn/36Pb/2Ag, 50Pb/50In produced a thicker intermetallics on Cu, but a thinner intermetallics on Au/Ni/W metallization.

The intermetallic layer thickness at any time during the soldering process can also be calculated with a numeric method, as reported by Schaefer *et al.* [14]. As input, the method requires the soldering temperature–time profile

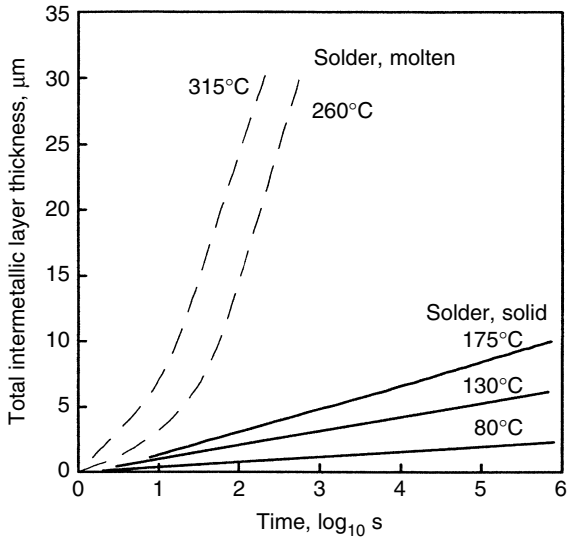

Figure 2.7 Formation of copper–tin intermetallic layer for copper substrate wetted by eutectic tin–lead solder [32]

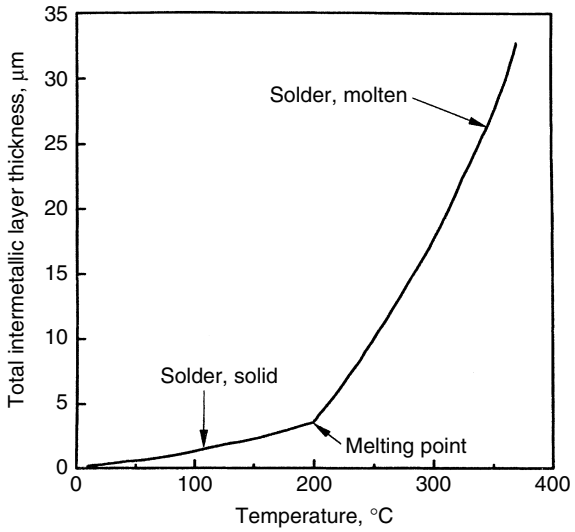

Figure 2.8 Growth of copper–tin intermetallic compound for copper substrate wetted by tin–lead solder for 100 seconds [32]

Table 2.1 Compound layer thickness immediately after reflow soldering of solder pastes

Solder	*Intermetallic thickness (μm) on*		
	Cu	*Au/Pt*	*Au/Ni/W*
63Sn/37Pb	2.4	2.0	2.0
62Sn/36Pb/2Ag	2.1	2.0	2.0
50Pb/50In	3.5	2.0	<1.0

and the isothermal liquid state growth rate parameters for the growth of the intermetallic layer, consisting of a growth constant and an activation energy. The validity of the method is demonstrated for intermetallic growth between copper and 62Sn/36Pb/2Ag solder.

2.1.4.2 Dissolution barrier

In general, the intermetallics formed has a higher melting point than the soldering temperature encountered in the electronics industry, and will remain as a solid during the soldering process. For many systems, the intermetallics forms a continuous layer between molten solder and the solid base metal, as demonstrated by the intermetallic Cu_3Sn in Figure 2.9 [15], and consequently slows the rate of base metal atoms diffusion through the intermetallics layer. This is attributed to the phenomenon that the solid-state diffusion process is roughly two orders of magnitude slower than solid–liquid reactions. As a result, the dissolution rate of the base metal in solder is greatly reduced.

However, not all intermetallic compounds form layered structures. For instance, the Cu_6Sn_5 intermetallics between the eutectic SnPb solder and Cu have grown as scallop-like grains into the molten solder. Between the

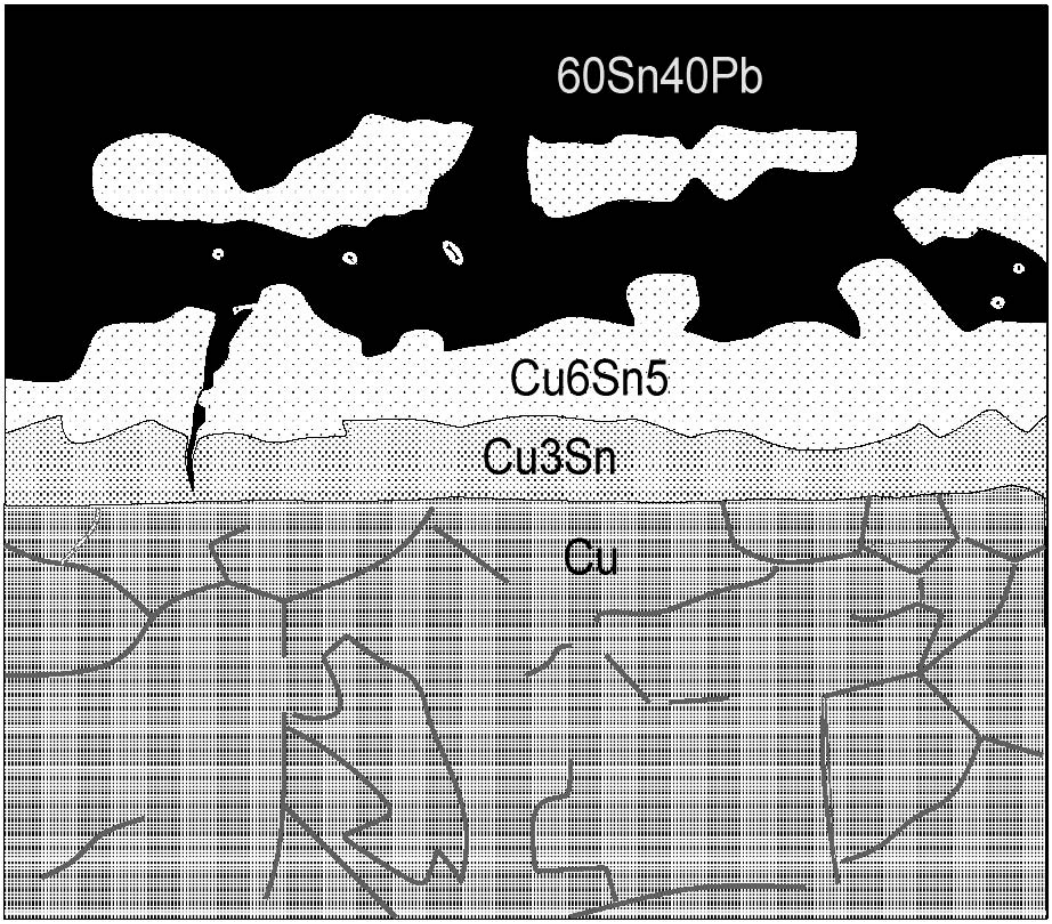

Figure 2.9 Cross-section of a coating 60Sn/40Pb on soft copper (marker = 20 μ). Two intermetallic compound layers Cu_3Sn and Cu_6Sn_5 are produced [46]

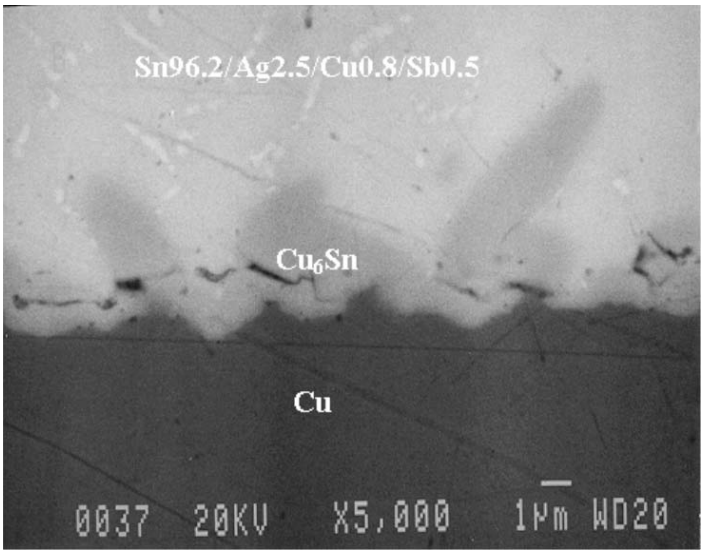

Figure 2.10 Formation of Cu_6Sn_5 intermetallics between Sn96.2/Ag2.5/Cu0.8/Sb0.5 and Cu substrate

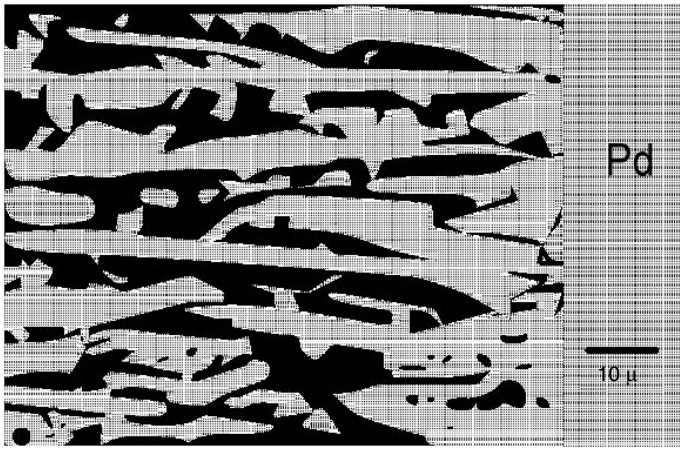

Figure 2.11 The $PdSn_3$ lamellae grow in a direction normal to the interface for Pd substrate wetted by eutectic SnPb [48]

scallop grains, there are molten solder channels extending almost all the way to the Cu interface. In aging, these channels serve as fast diffusion and dissolution paths of Cu in the solder to feed the reaction [16]. The Cu–Sn intermetallics formed between Cu and a lead-free solder Sn96.2/Ag2.5/Cu0.8/Sb0.5 shows a similar structure (Figure 2.10).

The structure of the intermetallic compound formed may not be easy to predict. Therefore, the intermetallic $PdSn_3$ formed between a molten 63Sn/37Pb solder grows as lamellae into the molten solder, instead of as a diffusion barrier layer (see Figure 2.11). The direction of growth is normal to the liquid/solid interface, and the molten solder between the lamellae serves as fast diffusion channels during soldering. However, if the Pd is in contact with molten Sn (Pb-free), the formation rate of intermetallics $PdSn_4$ is slower by one order of magnitude. No lamellar structure was observed and the intermetallics grows as a diffusion barrier between the Sn and Pd [17].

2.1.4.3 Susceptibility toward oxidation

Although formation of intermetallics enhances wetting during the soldering process, the solderability of intermetallics thus formed is actually poorer than the base metal itself. Yost *et al.* [18] evaluated the wettability of several solid samples including Cu, Cu_6Sn_5, and Cu_3Sn at 235 °C with the use of a wetting balance containing a 60Sn/40Pb solder bath. For the freshly etched solid samples, the wettability of Cu is much better than Cu_3Sn and Cu_6Sn_5 if a non-activated R flux is used for testing (see Figure 2.12). The difference in wettability diminishes if a mildly-activated RMA flux is used. However, if the solid samples were stored at room temperature for 3 days before testing, the wettability of all three samples degraded considerably if the R flux is used, with Cu being much better than Cu_6Sn_5, which in turn is slightly better than Cu_3Sn. The effect of storage on Cu is negligible when the RMA flux is used, while both intermetallic compounds suffer considerable degradation in wettability due to storage.

The results above indicate that the intermetallic compounds are wettable by solder, with Cu_6Sn_5 being slightly more wettable than Cu_3Sn. However, the wettability of both intermetallics degraded much more rapidly than Cu after storage. This vulnerability of intermetallics toward oxidation suggests potential shelf-life concerns associated with pretinned metallization and solderability problems associated with the rework process. It has been suggested that the intermetallics could be internally oxidized without having broken through to the pretinned surface. The wetting difficulty would arise once the pretinned surface is melted off during soldering [19,20]. In general, wettability decreases with decreasing initial solder coating thickness and increasing intermetallics thickness [21]. For immersion tin-coated printed wiring boards, a minimum thickness of approximately 60 μ-in. (1.5 μm) was determined to be critical for assembly operations involving multiple thermal excursions. The electroless copper substrate will cause significantly more intermetallic formation [22].

2.2 Effect of elemental constituents on wetting

Since wetting is greatly affected by the formation of intermetallics, and since the formation of intermetallics is dictated by the reaction between elements, it is reasonable to expect that the elemental constituents of solders should have a significant effect on the wetting of solder alloys. Humpston and Jacobson [23] studied the spreading characteristics of a series of eutectic binary alloys as a function of excess temperature above the melting point of solders. Results indicate there is a ranking order for the elements studied in their ability to promote spreading, as follows: tin > lead > silver > indium > bismuth. This ranking order is reported to be maintained even for ternary and quaternary solders.

It should also be pointed out that the effect of elemental constituents on wetting should be treated as a guideline only. Many other parameters, such as viscosity or the additive effect, may override the elemental effect and alter the relative order of spreading of solders. For

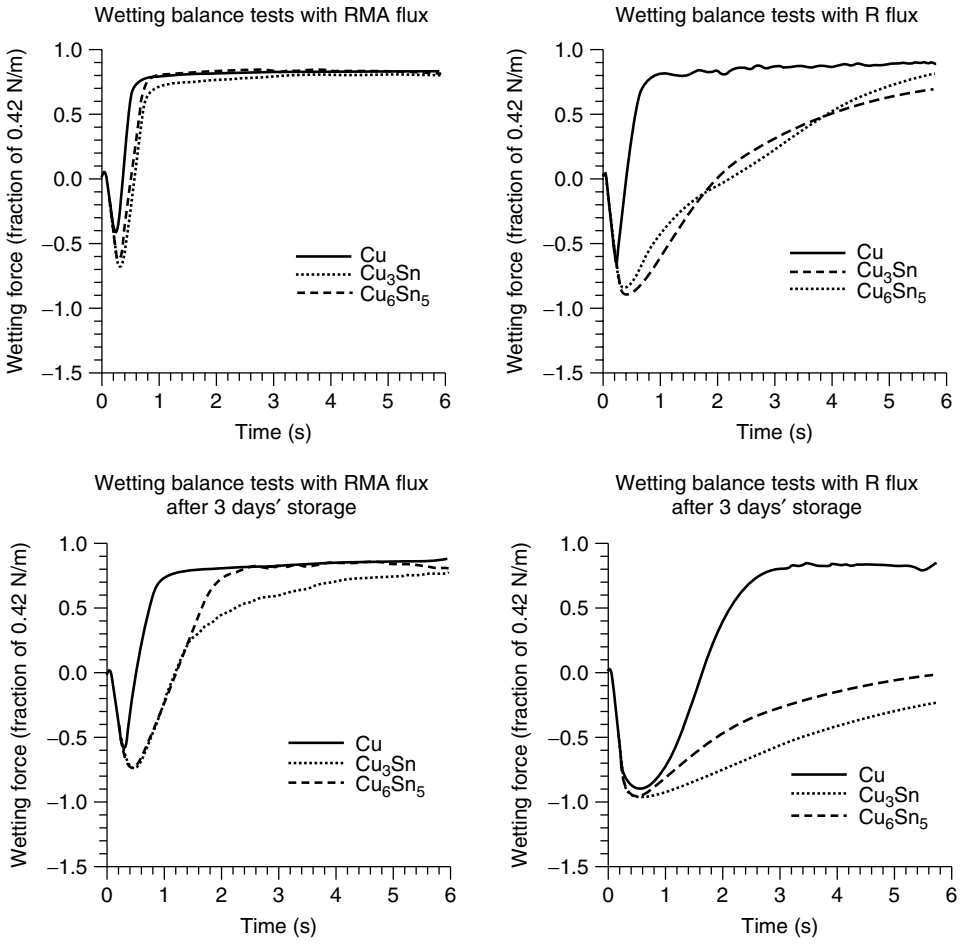
Wetting balance tests with RMA flux
Wetting balance tests with R flux
Wetting balance tests with RMA flux after 3 days' storage
Wetting balance tests with R flux after 3 days' storage
Wetting force (fraction of 0.42 N/m)
Time (s)
Cu
Cu3Sn
Cu6Sn5

Figure 2.12 Wetting balance results on the solderability of Cu, Cu_3Sn, and Cu_6Sn_5 using R and RMA fluxes and 60Sn/40Pb solder bath at 235 °C

instance, although pure Sn is superior in wetting compared with eutectic SnPb on Cu [24], SnAgBi alloys, such as 91.7Sn/3.5Ag/4.8Bi, wet better than eutectic SnAg [25], despite the addition of the less favored element Bi.

2.3 Phase diagram and soldering

A phase diagram is a description of a thermodynamically equilibrium state of phases as a function of composition and thermodynamic parameters such as temperature. It is helpful in providing the composition of probable phases as well as the melting temperature of those components. Being thermodynamic in nature, a phase diagram cannot predict kinetic properties, such as reaction rate between ingredients, and wetting characteristics, such as wetting speed on an oxidized base metal. In addition, it cannot predict the morphology of various phases in the solder joint.

Although soldering is typically a short process involving chemical reactions, hence being highly kinetic in nature, proper use of a phase diagram together with supplementary information does allow a deeper understanding and some prediction of soldering behavior. The application of a phase diagram to soldering can be illustrated by the following examples.

For a SnPb solder system, the binary eutectic phase diagram is shown in Figure 2.13. The soldering characteristics of various compositions can be exemplified by compositions A–C.

At composition B (70Pb/30Sn), the solder begins to melt at the solidus temperature of 183 °C, but will not turn completely to liquid before reaching the liquidus temperature of 257 °C. The solidus indicates that the upper limit of service temperature has to be considerably lower than 183 °C. The 257 °C liquidus indicates a sluggish flow of a pasty solder is to be expected if the soldering is processed at a temperature below this. This will inevitably result in a poor spread of solder for joint formation. However, if a proper flow is to be assured, a soldering temperature considerably higher than 257 °C will be needed. This high process temperature requirement will result in thermal damage to many of the electronic components, thus eliminating this solder composition as a viable candidate for mainstream electronic industry interconnect applications.

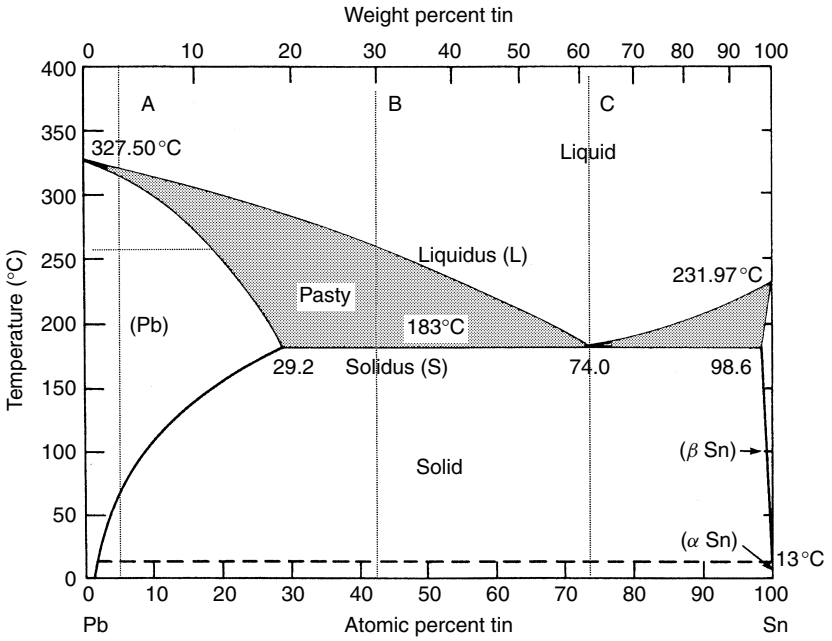

Figure 2.13 Phase diagram of binary Sn–Pb system

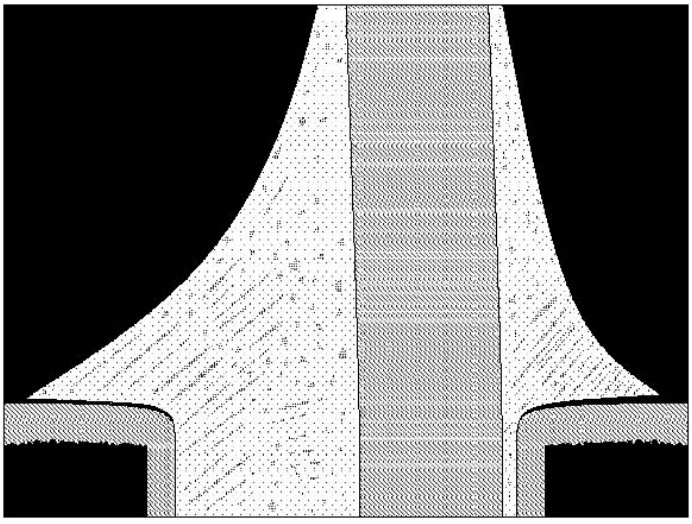

Figure 2.14 Fillet lifting of 91.8Sn/3.4Ag/4.8Bi with CDIP device leads [57]

Another disadvantage of solder with a wide pasty range is the tendency of having fillet lift. Fillet lift is a phenomenon observed during wave soldering, where the fillet is being lifted from the toe along the solder–substrate interface, as shown in Figure 2.14 [26]. The mechanism can be attributed to mismatch in thermal expansion coefficients between solder and the parts, which is further aggravated by solders with a large pasty range, as illustrated by Figure 2.15 [27]. Upon cooling, the excessive shrinkage of PCB on the z-axis and that of solder in the $x-y$ direction generates a lifting force on solder joints. Before the solder can be fully solidified, this lifting force may rupture the fillet from the toe where the stress is highly concentrated. Thus 96.5Sn/3.5Ag shows the lowest tendency and 91.9Sn/3.4Ag/4.7Bi a severe tendency toward fillet lift.

At composition A (63Sn/37Pb), the solder is eutectic and will turn into liquid from solid instantly at 183 °C. The viscosity of this solder is minimal when compared with adjacent composition [28], as shown in Figure 2.16. The low viscosity together with the interaction of molten solder with the base metal [29] drive the solder to spread

- Thermal expansion mismatch
- Cooling for stress-free state generates lifting forces
- Alloys with a larger pasty range are more susceptible to fillet lift

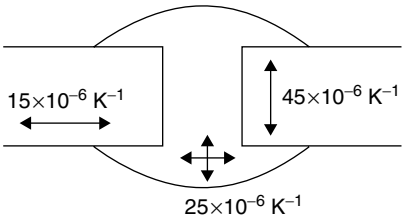

Figure 2.15 Basic mechanism of fillet lift during wave soldering [57]

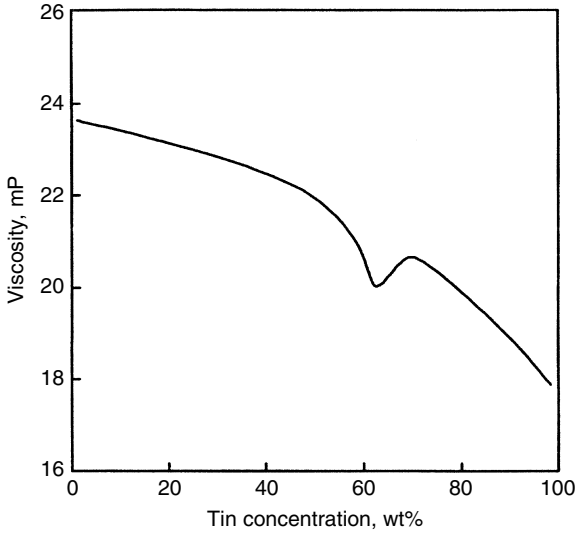

Figure 2.16 Viscosity of SnPb solder at 50 °C above the liquidus temperature [58]

readily during soldering. This superior spreading characteristic is often the reason that eutectic solders are the preferred choice over hypo- and hypereutectic compositions for soldering applications [1].

At composition A (97Pb/3Sn), the solder exhibits a pasty range with solidus 316 °C and liquidus 321 °C. This narrow pasty range allows the solder to be processed consistently for wetting at a high temperature around or above 340 °C. Hence it can be used for certain specific soldering applications, such as flip chip C4 (controlled collapse chip carrier) interconnect applications.

2.4 Microstructure and soldering

The mechanical properties and reliability of solder joints are greatly influenced by solder microstructures, including motion of dislocations and growth and reconfiguration of the grains. With the melting point being slightly above room temperature, the deformation mechanisms as well as failure modes of solders in general are high-temperature mechanisms, such as creep and recrystallization. Those mechanisms are not only affected by the composition, but are also strong functions of microstructure, which in turn is affected by both composition and the soldering process. Therefore understanding the structure–property and the structure–process relationship of a solder microstructure will allow the solder type and soldering process to be tailored to form the desired microstructure.

2.4.1 Deformation mechanisms

Creep is deformation of materials with time under a given tension or shear load and occurs by a thermally activated process. It is important when the service temperature exceeds half the melting temperature (in degrees kelvin) of solder. Creep is the most important deformation mechanism of solder [30]. The creep behavior can be represented by Figure 2.17, and can be roughly divided into three stages – primary, steady-state, and tertiary creep. In the primary state, the strain rate gradually decreases and reaches steady-state. The strain rate maintains the steady-state value for a while, until it reaches the tertiary state, where the strain increases rapidly and eventually leads to rupture. The strain rate at steady-state is most commonly used to characterize the creep behavior, and can be represented by

$$\dot{\gamma} = A\tau^n \exp\left(-\frac{E}{KT}\right) \tag{2.5}$$

where $\dot{\gamma}$ is the strain rate, τ is the stress, n is the stress exponent, and E is activation energy, K is the Boltzmann constant, and T is temperature in degrees Kelvin.

Depending on the stress level, the deformation mechanism can be represented by Figure 2.18 [31]. With increasing stress τ, the creep mechanisms shift from a dislocation climb-controlled bulk creep mechanism to a grain boundary slide-controlled intergranular creep mechanism to a dislocation glide-controlled creep mechanism.

At low stress, the solders creep by a mechanism dominated by the motion of dislocations through the bulk of the crystal grains (dislocation climb). The activation energy is

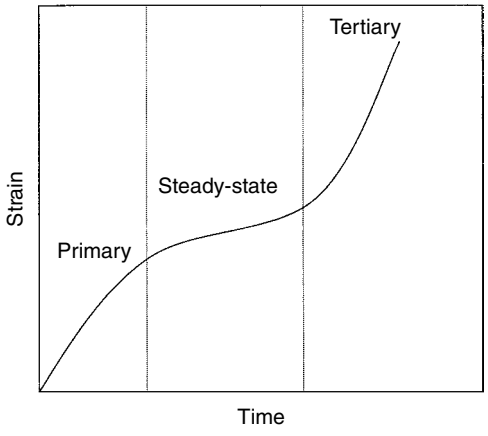

Figure 2.17 Typical creep response of solders

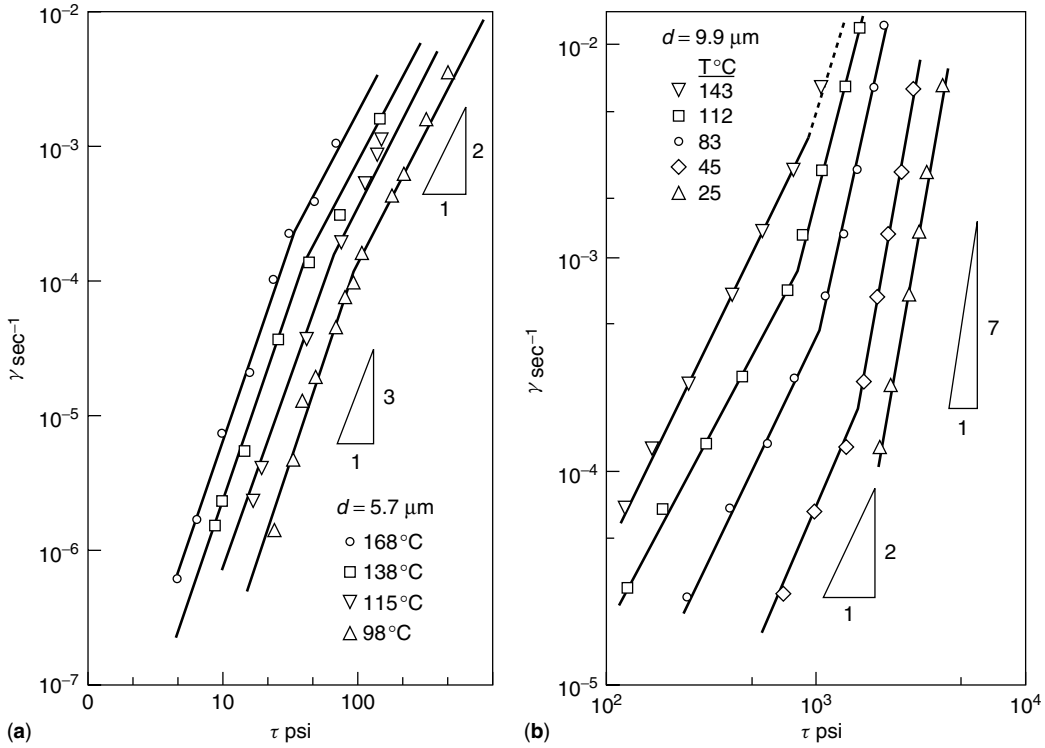

Figure 2.18 Creep data for eutectic Sn–Pb showing three phases of creep behavior, (1) dislocation climb-controlled creep ($n \sim 3$), (2) grain-boundary controlled creep ($n \sim 2$), and (3) dislocation glide-controlled creep ($n \sim 3$–7)

close to that for self-diffusion in the bulk (bulk diffusion), and is sensitive to composition, not to microstructure. This bulk deformation mechanism maintains contact along the boundaries, and along three grain-junction lines.

At intermediate stress, intergranular creep can occur, if the temperature is high enough and if the grain size is small and equiaxed. The intergranular creep is deformation of solder by grain boundary sliding, in which grains are displaced with respect to one another by slipping along the boundary between them. Grain boundary sliding is associated with boundary migration, and with rotations and reorientation of individual grains and grain clusters toward the direction of maximum shear stress which are required to maintain grain coherency. The traces of grain boundary migration are preferable sites for cavitation and microcracking [32].

Intergranular creep rate is proportional to the reciprocal of square of grain size, and is negligibly slow unless the mean grain size is less than a few microns. Intergranular creep has an activation energy close to that for grain boundary diffusion, and leads to a very stable and non-damaging plastic deformation. This creep mechanism leads to superplasticity, in which a material undergoes creep strains of several hundred percent prior to failure, hence providing exceptional creep ductility and excellent fatigue resistance. Furthermore, Mei and Morris [33,34] have reported that cyclic deformation by intergranular creep causes little or no microstructural damage. Although fine, equiaxed grain size favors the occurrence of intergranular creep, the fine grain size will grow and the growth rate will increase with increasing service temperature.

At high stress, the deformation mechanism undergoes a transition to tertiary creep and elongation to failure. The creep is sensitive to microstructure and the mechanisms include (1) onset of cavitation damage at grain boundaries and (2) plastic instability leading to inhomogeneous deformation. Morris *et al*. [34] have reported that cavitation is responsible for tertiary creep in bulk solder samples tested in tension. Cavities nucleate primarily at three- or four-grain junctions. They grow with strain, and merge to form larger voids to cause failure. This process is aggravated by (1) increase in grain size, which enhances the stress concentration at grain junctions, (2) irregular grain shapes, which introduce sites of unusual stress concentration, and (3) possibly intergranular precipitates, which constrain deformation at grain boundaries, which can result in uneven stress distribution. Plastic instability occurs mainly at shear bands which often follow planes of microstructural weakness, such as phase boundaries and colony boundaries in eutectic materials [35,36]. It does not necessarily lead to rapid failure. The development of shear bands is particularly pronounced in solders exhibiting unstable, eutectic microstructures that are easily recrystallizable, such as eutectic Sn–Pb. In these solders, the incipient shear bands cause development of the well-defined recrystallized bands for joints that have crept or fatigued in shear. Such a localized recrystallized material usually observed near an intermetallic layer

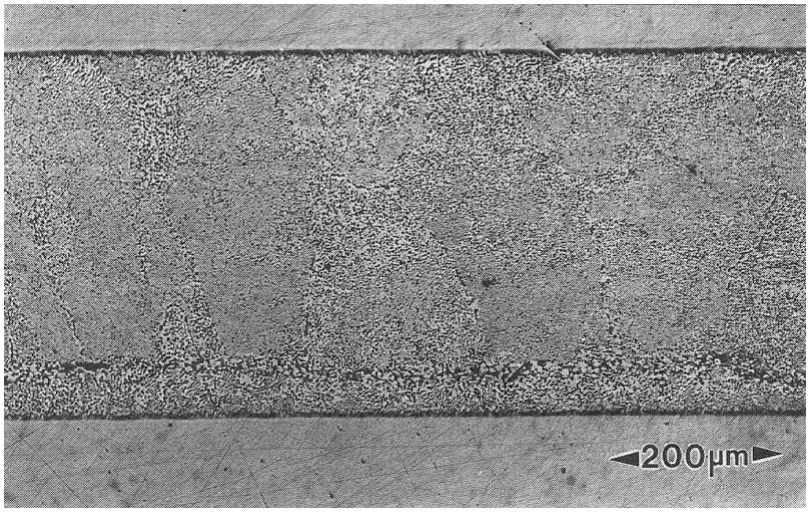

Figure 2.19 Optical micrograph of a deformed SnPb solder joint, showing the shear band of coarsened and recrystallized material [34]

accelerates damage processes and shortens the fatigue life of solder joints, as shown in Figure 2.19 [34]. The recrystallized Sn and Pb boundaries become well organized and aligned with the direction of maximum shear stress.

Formation of a thicker IMC layer results in a weaker tensile strength, as demonstrated by Figure 2.20 [1]. However, the effect of IMC on reliability is fairly complicated. In general, creep fatigue failure often is located within the bulk solder, unless the IMC layer is thick. During a tensile test for 60Sn/40Pb solder, if the joint is solidified slowly and forms a eutectic microstructure with double-layered IMC layers, a crack often propagates through a Cu_6Sn_5 layer [37]. Formation of a thicker IMC layer does not change the failure pattern, unless the long rods of Cu_6Sn_5 are allowed to be dispersed into the body of the solder, where the fracture may shift from the IMC layer into the solder due to the void nucleation effect of those IMC rods.

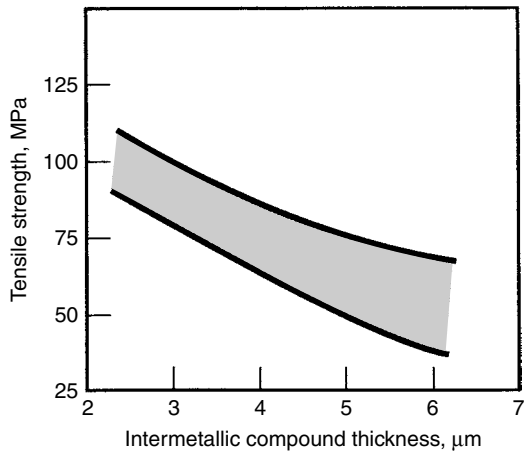

Figure 2.20 Effect of Cu–Sn intermetallic compound thickness on tensile strength of solder joint for 63Sn/3Pb at room temperature

2.4.2 Desirable solders and the soldering process

The eutectic lamellar structure exhibits high surface area, therefore it is not stable and tends to form coarser equiaxed grains with aging. The equiaxed grain structure is more stable than the lamellar microstructure, due to the fine mixture of two different phases for an equiaxed system. To form the equiaxed fine-grain structure which is desirable for achieving intergranular creep behavior, hence a better fatigue resistance, a soldering process with a rapid cooling rate will be preferable.

To minimize the IMC thickness formed during soldering, a lower soldering temperature and a shorter dwell time above the solder melting temperature will be desired, as suggested earlier by Figures 2.7 and 2.8.

The creep resistance in descending order for several alloys was reported to be 62Sn/36Pb/2Ag > 96.5Sn/3.5Ag > 63Sn/37Pb > 58Bi/42Sn > 60Sn/40Pb > 70Sn/30In > 60In/40Sn [38]. Addition of 2% Ag appears to be effective in refining and retaining the grain size of eutectic Sn–Pb solder, thereby imparting a better fatigue resistance. Also, addition of small amounts of In and Cd to eutectic Sn–Pb inhibits complete formation of a eutectic lamellar microstructure. This results in formation of featureless broad bands along the eutectic colony boundaries, and provides significant improvement in shear fatigue life [35,36]. Off-eutectic SnPb solders have better fatigue resistance than Sn63, due to the formation of a mixed microstructure that contains relatively large pro-eutectic grains.

2.4.3 Effect of impurities on soldering

Surface tension isotherms (250 °C) for 60Sn/40Pb with 0–4 percent Bi or 0–5 percent Sb show a non-linear fall with increasing ternary addition which may be explained

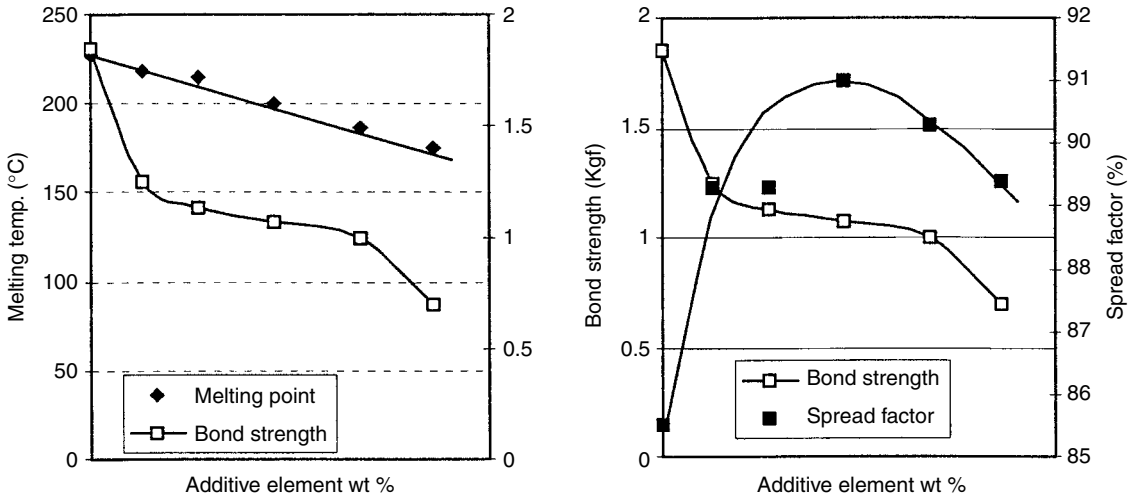

Figure 2.21 Effect of additive amount on solder melting point, joint bond strength, and wetting (spread factor)

Table 2.2 Lowest impurity levels producing detrimental effect on a 60Sn/40Pb solder

Impurity element	*Impurity, %*	*Effect*
Aluminum	0.0005	Oxide-promoting element, causes a lack of adhesion, grittiness, and dull solder surface. No dewetting on Cu or brass, 0.001% showed onset of dewetting on steel and nickel. Sb eliminate Al by promoting rapid drossing-out of AlSb compound.
Antimony	1	Area of spread decreases slightly with increase in Sb content. Prevent transformation of beta Sn to alpha Sn at sub-zero temperature. Drosses out Zn, Al, and Cd from solder.
Arsenic	0.2 0.005	25% decrease in area of spread. Dewetting and grittiness on brass, probably due to formation of As–Zn IMC.
Bismuth	0.5	Discoloration and oxidation of solder coating. Reduce the area of spread slightly. Increase the rate of spread.
Cadmium	0.15	25% decrease in area of spread. Dull surface due to oxide film.
Copper	0.29	Grittiness due to Cu–Sn IMC. Excessive solder increases the liquidus temperature of the solder making it more viscous or sluggish. Negligible effect on wetting.
Gold	0.1	Gritty joints and surfaces. Weaken solder dramatically at 4%.
Iron	0.02	Grittiness of solder coating.
Nickel	0.05	Grittiness at over 0.02%.
Phosphorus	0.01	Deoxidant. Dewetting at 0.012% on Cu and steel. Grittiness at 0.1% on Cu.
Silver	2	Increase spread and strength of solder, grittiness in excess of solubility. Ag_3Sn IMC is soft and ductile and non-embrittling.
Sulfur	0.0015	S additions up to 0.25% produced no dewetting effects, but give a severe gritty appearance of the solder coating due to the presence of discrete IMC particles of SnS and PbS. A powerful grain refiner.
Zinc	0.003	Oxide forming element. Dewetting at 0.001%. Loss of solder brightness at 0.005%.

by the lower surface tension of the third elements. Surface tension isotherms for 60Sn/40Pb with 0–2 percent Ag (215° and 250 °C) or 0–0.6 percent Cu (250 °C) indicated higher values with increasing ternary additions which may be explained by the higher surface tension of the third elements. However, the surface tension isotherm (250 °C) for 60Sn/40Pb with 0–0.013 P indicated higher values with increasing ternary additions. This result is not consistent with the low surface tension of P and requires further study [39].

The wetting process is favored by a low surface energy between solder and substrate. However, both interfacial energies γ_{SF} and γ_{LF}(see Figure 2.1) can be affected by impurities in the solder. The general rule is that a small amount of surface-active impurity can produce a marked decrease in surface energy, while similar amounts of a surface-inactive impurity do not produce more than a very small rise in surface energy. It follows that the effects of surface-inactive impurities on solder should be too small to have any significant effect on wetting behavior [40]. Furusawa *et al*. [41] reported that addition of small amounts of some additive elements will reduce the melting temperature and the bond strength, but increase initially, reaching a maximum, then decrease the wetting of solders, as shown in Figure 2.21 [41]. The wetting phenomenon observed in this case suggests the relation

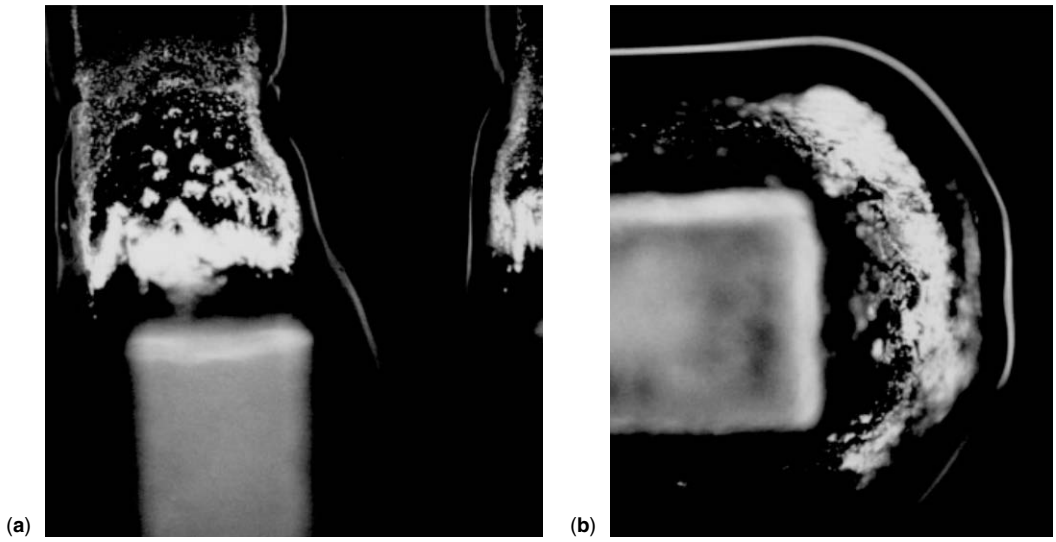

Figure 2.22 Gritty surface of solder joint for 62Sn/36Pb/2Ag on (**a**) Cu pads and (**b**) 1.5 μ Au pads

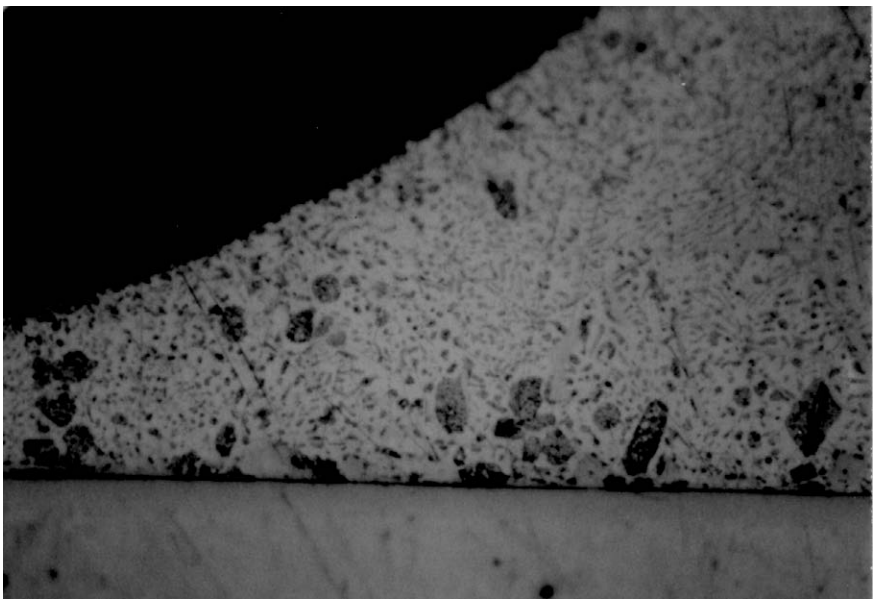

Figure 2.23 Optical micrograph

Table 2.3 QQ-S-571E solder alloy specifications, showing major composition and maximum impurities allowed

Element	*Sn63*	*Sn62*	*Sn60*
Sn	62.5–63.5	61.5 to 62.5	59.5 to 61.5
Pb	Remainder	Remainder	Remainder
Sb	0.20 to 0.50	0.20 to 0.50	0.20 to 0.50
Bi	0.25	0.25	0.25
Ag		1.75 to 2.25	
Cu	0.08	0.08	0.08
Fe	0.02	0.02	0.02
Zn	0.005	0.005	0.005
Al	0.005	0.005	0.005
As	0.03	0.03	0.03
Total of others	0.08	0.08	0.08

between wetting and surface energy may only be a secondary effect.

Some impurity elements have a significantly adverse impact on soldering performance. Table 2.2 shows the lowest impurity levels producing a detrimental effect for 60Sn/40Pb solder [42]. Grittiness is a common symptom of undesirable impurities. Figure 2.22 shows an example of gritty solder fillet surface due to the formation of Sn-containing IMC for a 62Sn/36Pb/2Ag solder joint on both Cu pads and Au pads. The gritty surface appearance originates from Au–Sn IMC particulate formation in the later case, as shown in Figure 2.23. Table 2.3 shows QQ-S-571E solder alloy specifications for several commonly used SnPb solders, with major composition and maximum impurities allowed.

2.5 Conclusion

The soldering process involves both physical spreading of molten solder, dissolution of base metal, and chemical interaction between solder and base metal, and is governed by the chemical reaction factor due to thermodynamic considerations. Both dissolution and IMC formation are influenced by time, temperature, type of solder, and type of metallization of substrate. Although formation of IMC is desired to achieve solder wetting, its presence reduces the solderability of a base metal for a subsequent soldering process. Deformation of solder involves grain boundary sliding, migration, grain rotation, and cavitation. Formation of a solder joint with fine grains is desired for better creep and fatigue resistance, and can be achieved by a rapid cooling process as well as use of grain-refining additives. A thinner IMC layer is preferred for higher mechanical strength and better fatigue performance, and is favored with a lower soldering temperature and a shorter time. Impurities may affect surface tension, wetting, oxidation resistance, and solder appearance. Overall, soldering is a process delivering low cost, high throughput, and high quality interconnects. However, due to the chemical reactions involved during soldering and the evolving nature of the solder joints once formed, care should be taken in the soldering process and in selecting the material systems involved in soldering.

References

1. G. Humpston and D. Jacobson, *Principles of Soldering and Brazing*, ASM International, Materials Park, OH (1993).
2. C. Lea, *A Scientific Guide to Surface Mount Technology*, Electrochemical Publications Ltd, (1988).
3. R. D. Milner, ''A Survey of the Scientific Principles Related to Wetting and Spreading'', *Br. Weld. J.*, Vol. 5, pp. 90–105 (1958).
4. P. G. de Gennes, ''Wetting: Statistics and Dynamics'', *Review of Modern Physics*, Vol. 57(3), pp. 827–863 (1985).
5. R. J. Klein Wassink, *Soldering in Electronics*, Electrochemical Publications Ltd, (1984).
6. J. R. Weeks and D. H. Gurinsky, *Liquid Metals and Solidification*, American Society for Metals, pp. 106–161 (1958).
7. N. Tunca, G. W. Delamore, and R. W. Smith, ''Corrosion of Mo, Nb, Cr, and Y in Molten Aluminum'', *Metall. Trans. A*, Vol. 21A (No. 11), pp. 2919–2928 (1990).
8. D. S. Evans and S. G. Denner, ''An Apparatus for the Determination of Solid/Liquid Metal Interactions Under Controlled Conditions'', *Pract. Metallogr.*, Vol. 15, pp. 486–493 (1978).
9. R. A. Bulwith and C. A. Mackay, ''Silver Scavenging Inhibition of Some Silver Loaded Solders'', *Weld. J.*, Vol. 64 (No. 3), pp. 86s–90s (1985).
10. F. G. Yost and A. D. Romig, ''Thermodynamics of Wetting by Liquid Metals'', *Mater. Res. Soc. Symp. Proc.*, Vol. 108, pp. 385–390 (1988).
11. B. J Lee, N. M. Hwang, and H. M. Lee, ''Prediction of Interface Reaction Products Between Cu and Various Solder Alloys by Thermodynamic Calculation'', *Acta Materialia*, Vol. 45, No. 5, pp. 1867–1874 (1997).
12. P. J. Kay and C. A. Mackay, ''Barrier Layers Against Diffusion'', Paper 4, Proc. 3rd Int. Brazing Soldering Conf., London, 1979.
13. S. J. Muckett, M. E. Warwick, and P. E. Davis, *Plating and Surface Finishing*, p. 44 (January 1986).
14. M. Schaefer, W. Laub, J. M. Sabee, R. A. Fournelle, and P. S. Lee, A Numerical Method for Predicting Intermetallic Layer Thickness Developed During the Formation Of Solder Joints'', *Journal of Electronic Materials*, Vol. 25, No. 6, pp. 992–1003 (June 1996).
15. M. E. Warwick and S. J. Muckett, ''Observations on the Growth and Impact of Intermetallic Compounds on Tin-coated Substrates'', *Circuit World*, Vol. 9, No. 4, pp. 5–11 (1983).
16. H. K. Kim and K. N. Tu, ''Kinetic Analysis of the Soldering Reaction between Eutectic SnPb Alloy and Cu Accompanied by Ripening'', *Physical Review B (Condensed Matter)*, Vol. 53, No. 23, pp. 16027–16034 (1996).
17. Y. Wang and K. N. Tu, ''Ultrafast Intermetallic Compound Formation between Eutectic SnPb and Pd Where the Intermetallic is not a Diffusion Barrier'', *Applied Physics Letters*, Vol. 67, No. 8, pp. 1069–71 (August 1995).
18. F. G. Yost, F. M. Hosking, and D. R. Frear (eds), *The Mechanics of Solder Alloy – Wetting & Spreading*, Van Nostrand Reinhold, New York (1993).
19. H. Geist and M. Kottke, *IEEE Trans. On Components, Hybrids, and Manufacturing Tech.*, Vol. 11, p. 270 (1988).
20. G. Lucey, J. Marshall, C. A. Handwerker, D. Tench, and A. Sunwoo, NEPCON'91 West Proc. Des Plaines, IL: Cahners Exposition Group, pp. 3–10, 1991.
21. P. E. Davis, M. E. Warwick, and P. J. Kay, ''Intermetallic Compound Growth and Solderability'', *Plating and Surface Finishing*, Vol. 69, pp. 72–76 (September 1982).
22. U. Ray, I. Artaki, and P. T. Vianco, ''Influence of Temperature and Humidity on the Wettability of Immersion Tin Coated Printed Wiring Boards'', *IEEE Transactions on Components, Packaging, and Manufacturing Technology*, Part A, Vol. 18, No. 1, pp. 153–162 (March 1995).
23. G. Humpston and D. M. Jacobson, ''Solder Spread: a Criterion for Evaluation of Soldering'', *Gold Bull.*, Vol. 23, No. 3, pp. 83–95 (1990).
24. P. T. Vianco, F. M. Hosking, and J. A. Rejent, *''Wettability Analysis of Tin-based, Lead-free Solders''*, *Proc. of Nepcon West'92*, Vol. 3, pp. 1730–1738 (1992).
25. B. Huang and N. C. Lee, ''Prospects of Lead-free Alternatives for Reflow Soldering'', in *Proc. of IPC Works'99*, S-03-10, Minneapolis, MN, 23–28, October 1999.

26. ''Lead-free Solder Project Final Report'', NCMS Report 0401RE96 (August 1997).
27. C. Handwerker, ''NCMS Lead Free Solder Project: A National Program'', NEMI Lead Free Solder Meeting, Chicago, 25, May 1999.
28. H. J. Fisher and A. Pillips, ''Viscosity and Density of Liquid Lead–tin and Antimony–cadmium Alloys'', *J. Inst. Met.*, Vol. 11, pp. 1060–1070 (1954).
29. J. C. Ambrose, M. G. Nicholas, and A. M. Stoneham, *''Kinetics of Brazing Spreading'', Proc. Conf. British Association for Brazing and Soldering*, 1992 Autumn Conference, Coventry, UK.
30. J. Glazer, ''Metallurgy of Low Temperature Pb-free Solders for Electronic Assembly'', *International Materials Reviews*, Vol. 40, No. 2, pp. 65–93 (1995).
31. D. Grivas, MS Thesis, University of California at Berkeley, January, 1974.
32. A. Zubelewicz and B. Sammakia, ''Physically Based Reliability Models for BGA Assemblies'', in *Proc. of Nepcon West 1998*, Anaheim, CA, 1–5, March 1998.
33. Z. Mei and J. W. Morris, Jr, *Trans. ASME, J. Electronic Packaging*, Vol. 114, p. 104 (1992).
34. J. W. Morris, Jr, J. L. Freer Goldstein, and Z. Mei, ''Microstructural Influences on the Mechanical Properties of Solder'', in *The Mechanics of Solder Alloy Interconnects*, edited by D. Frear, H. Morgan, S. Burchett, and J. Lau, Van Nostrand Reinhold, New York (1994).
35. D. Tribula, PhD Thesis, University of California at Berkeley, June 1990.
36. D. Tribula and J. W. Morris, Jr, *ASME Journal of Electronic Packaging*, Vol. 112, p. 87 (1990).
37. L. Quan, D. R. Frear, D. Grivas, and J. W. Morris, Jr, *J. Electronic Mater.*, Vol. 16, p. 203 (1987).
38. J. S. Hwang and R. M. Vargas, *Solder. Surface Mount Technol.*, Vol. 5, pp. 38–45 (1990).
39. M. A. Carroll and M. E. Warwick, ''Surface Tension of Some Sn–Pb Alloys: Part 1 – Effect of Bi, Sb, P, Ag and Cu on 60Sn–40Pb Solder'', *Materials Science and Technology*, Vol. 3, pp. 1040–1045 (December 1987).
40. H. A. H. Steen and G. Becker, ''The Effect of Impurity Elements on the Soldering Properties of Eutectic and Near-eutectic Tin–lead Solder'', *Brazing & Soldering*, Vol. 11, pp. 4–11, (Autumn 1986).
41. A. Furusawa, K. Suetsugu, A. Yamaguchi, and H. Taketomo, ''Thermoset Pb-free Solder Using Heat-resistant Sn–Ag Paste'', National Technical Report, Vol. 43, No. 1, Feb. 1997.
42. M. L. Ackroyd, C. A. MacKay, and C. J. Thwaites, ''Effect of Certain Impurity Elements on the Wetting Properties of 60%tin–40% Lead Solders'', *Metals Technology*, pp. 73–85 (February 1975).

Appendix 2.1 Effect of flux surface tension on the spread of molten solder

At reflow, a quasi-equilibrium state is established after the solder is melted. The profile of this system can be schematically expressed by the figure below, and the relation expressed in equation (2A.1)

$$\gamma_{SF} = \gamma_{LS} + \gamma_{LF} \times \cos\theta \tag{2A.1}$$

In this relation, γ_{SF} stands for the interfacial tension between the substrate and the flux, γ_{LS} is the interfacial tension between substrate and the liquid solder, γ_{LF} is the interfacial tension between liquid solder and the flux, and θ represents the contact angle between liquid solder and the substrate.

The interfacial tension can be approximated, according to Antonow's rule, by the following relations:

$$\gamma_{SF} = \gamma_S - \gamma_F \tag{2A.2}$$

$$\gamma_{LF} = \gamma_L - \gamma_F \tag{2A.3}$$

where γ_S is the surface tension of substrate, γ_L is the surface tension of liquid solder, and γ_F is the surface tension of flux.

If the flux is replaced with another flux with lower surface tension, γ'_F, the equilibrium described above will be disrupted until a new equilibrium with a new contact angle θ is established again. The effect of flux surface tension on contact angle can be derived through the following relations.

Let $\gamma'_F = \gamma_F - K$ (2A.4)

Since $\gamma'_{SF} = \gamma_S - \gamma'_F$ (2A.5)

And $\gamma'_{LF} = \gamma_L - \gamma'_F$ (2A.6)

We have

$$\begin{aligned}
&\gamma'_{SF} - (\gamma_{LS} + \gamma'_{LF} \times \cos\theta) \\
&= (\gamma_S - \gamma'_F) - [\gamma_{LS} + (\gamma_L - \gamma'_F) \times \cos\theta] \\
&\quad \text{from (2A.5) and (2A.6)} \\
&= [\gamma_S - (\gamma_F - K)] - \{\gamma_{LS} + [\gamma_L - (\gamma_F - K)] \\
&\quad \times \cos\theta\} \text{ from (2A.4)} \\
&= [(\gamma_S - \gamma_F) + K)] - \{\gamma_{LS} + [(\gamma_L - \gamma_F) \\
&\quad + K)] \times \cos\theta\} \\
&= [\gamma_{SF} + K] - \{\gamma_{LS} + [\gamma_{LF} + K] \times \cos\theta\} \\
&\quad \text{from (2A.2) and (2A.3)} \\
&= [\gamma_{SF} + K] - \{(\gamma_{LS} + \gamma_{LF} \times \cos\theta) + K \times \cos\theta\} \\
&= [\gamma_{SF} + K] - \{\gamma_{SF} + K \times \cos\theta\} \text{ from (2A.1)} \\
&= K - K \times \cos\theta
\end{aligned}$$

In the case of $\theta > 0$, K is larger than $K \times \cos\theta$. Accordingly, we have the result

$$\gamma'_{SF} > (\gamma_{LS} + \gamma'_{LF} \times \cos\theta) \tag{2A.7}$$

In other words, the liquid solder will tend to spread further until a new equilibrium condition with contact angle θ' is reached. Here the angle θ' will be smaller than θ. Physically speaking, the driving force for this spreading after change of flux originates from an unequal increase

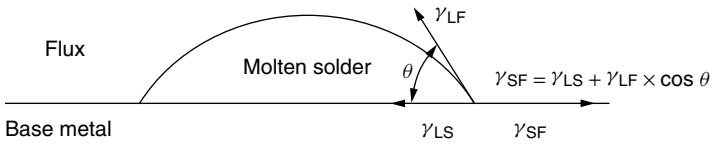

Figure A2-1

of tension in spreading and anti-spreading. Based on the derivation shown above, the increase of tension is K and $K \times \cos\theta$ for spreading and anti-spreading, respectively. Since K is always no less than $K \times \cos\theta$, a new equilibrium can only be obtained through spreading. This concludes that a flux system with a higher surface tension will result in less spreading for molten solder flow when other parameters remain equal.

The relative magnitude of θ and θ' can also be obtained from the following derivation.

At equilibrium, $\gamma_{SF} = \gamma_{LS} + \gamma_{LF} \times \cos\theta$ from equation (2A.1)

and $\gamma'_{SF} = \gamma_{LS} + \gamma'_{LF} \times \cos\theta'$ (2A.8)

Therefore, $\cos\theta = (\gamma_{SF} - \gamma_{LS})/\gamma_{LF}$

Also $\gamma'_{SF} = \gamma_{LS} + K$ from (2A.2), (2A.4) and (2A.5)

$\gamma'_{LF} = \gamma_{LV} + K$ from (2A.3), (2A.4) and (2A.6)

Hence $\cos\theta' = (\gamma'_{SF} - \gamma_{LS})/\gamma'_{LF}$ from (2A.8)

$= [(\gamma_{LS} + K)] - \gamma_{LS})/(\gamma_{LV} + K)$

$= (\gamma_{LS} - \gamma_{LS} + K)/(\gamma_{LV} + K)$

Accordingly,

$$\begin{aligned}\cos\theta - \cos\theta' &= [(\gamma_{SF} - \gamma_{LS})/\gamma_{LF}] - (\gamma_{LS} - \gamma_{LS} + K)/ \\ &\quad (\gamma_{LV} + K) \\ &= (\gamma_{SF}\gamma_{LF} - \gamma_{LS}\gamma_{LF} + K \times \gamma_{LF} - \gamma_{LF}\gamma_{SF} \\ &\quad -K \times \gamma_{SF} + \gamma_{LF}\gamma_{SL} + K \times \gamma_{LS})/ \\ &\quad [(\gamma_{LF} + K)/\gamma_{LV}] \\ &= K(\gamma_{LF} + \gamma_{LS} - \gamma_{SF})/[(\gamma_{LF} - +K) \times \gamma_{LF}] \\ &\geq K(\gamma_{LF} \times \cos\theta + \gamma_{LS} - \gamma_{SF})/ \\ &\quad [(\gamma_{LF} - +K) \times \gamma_{LF}] \text{ where } 0 \geq \theta \geq \pi \\ &= 0\end{aligned}$$

Hence $\cos\theta \geq \cos\theta'$, or $\theta \leq 0$

$\theta' = \theta$ when $\theta = 0$,

$\theta' < \theta$ when $\theta = 0$

Therefore, the flux with a lower surface tension γ'_F will have a smaller contact angle θ' or a wider spread.

3 Solder Paste Technology

Solder paste is a creamy mixture of solder powder and flux. This creamy nature of solder paste allows it to be maneuvered by automated deposition equipment, such as stencil printer or dispenser, thus enabling the implementation of high-speed, high-volume throughput production practice. The particle size of solder is dictated by the end application, with smaller particle sizes used for smaller deposition. As to the flux, it serves two functions in solder paste. The first and also the primary function of flux is a soldering aid. During soldering, the flux removes metal oxides as well as other surface tarnishes such as grease or metal carbonates, hence allowing the coalescence of solder powder and the wetting of parts by the molten solder. The second function of flux is serving as a vehicle for solder powder. The rheology of the flux vehicle is required to provide not only a stable suspension of solder powder in this vehicle during storage and handling, but also a solder paste which can be easily handled by paste deposition equipment. In addition, the rheology of solder paste needs to sustain the subsequent reflow process without slumping and bridging issue. With properly formulated solder paste, the material can be fairly homogeneous thus allowing the composition of the mixture to be consistent from dot to dot during paste deposition.

3.1 Fluxing reactions

A solder flux needs to perform a number of important functions at the same time. It must promote thermal transfer to the area of the solder joint, enhance wetting of the solder on the base metal, and prevent oxidation of the metal surfaces at soldering temperatures. Among those, the primary task is to remove the tarnish layer from the metal joint that is about to be soldered. Although the process of soldering electronic devices involves a multi-billion-dollar industry, the actual chemical reactions that occur during this fluxing process are not well understood. For most of the fluxes used, the flux reactions can be simulated with the interactions at the metal/metal oxide/electrolyte solution interface. The fluxing reactions that can occur at the oxide/solution interface include acid–base reactions and oxidation–reduction reactions. Variables such as the structure of the metal oxide, temperature, pH, concentration of the electrolyte, and the chemical nature of the solute and solvent all affect the reaction rates and mechanisms [1].

3.1.1 Acid–base reactions

As mentioned above, the primary role of flux is elimination of metal oxides. The most common type of flux reaction is acid–base reaction. In general, this can be accomplished with the use of organic acids, such as carboxylic acids, or inorganic acids, such as halogen acids, as fluxes. The reactions between flux and metal oxides can be exemplified by the simplified equations as shown below:

$$MO_n + 2n\text{RCOOH} \longrightarrow M(\text{RCOO})_n + nH_2O$$

$$MO_n + 2n\text{HX} \longrightarrow MX_n + nH_2O$$

where M stands for metal, O represents oxygen, RCOOH represents carboxylic acids, and X stands for halides, such as F, Cl or Br.

The fluxing reaction is favored in terms of free energy of reaction, as exemplified by the negative values of ΔG calculated by Ludwig [2]. Table 3.1 shows the enthalpy of fluxing reaction between MO_n and HX, Table 3.2 the entropy of reaction between MO_n and HX, and Table 3.3 the free energy of reaction calculated accordingly [2].

Although the reactions shown in Tables 3.1–3.3 are fairly illustrative for fluxing reaction, the detailed reaction can be more complicated. For instance, the reaction between flux HCl and copper during soldering with eutectic tin–lead can be expressed as follows:

$$Cu_2O + 2HCl \longrightarrow CuCl_2 + Cu + H_2O$$

$$CuCl_2 + Sn \longrightarrow SnCl_2 + Cu$$

$$2CuCl_2 + Sn \longrightarrow SnCl_4 + 2Cu$$

$$CuCl_2 + Pb \longrightarrow PbCl_2 + Cu$$

On the other hand, the fluxing reaction between H_2SO_4 and cuprous oxide can be shown as

$$Cu_2O + H_2SO_4 \longrightarrow CuSO_4 + Cu + H_2O$$

Since a fluxing reaction typically occurs at soldering temperature, usually above 200 °C, for systems involving multiple chemicals, study of the reaction mechanism

Table 3.1 Enthalpy of reaction between MO_n and HX [2]

Reaction kJ/mole										ΔH kJ/mole
I	PbO	+	$2H^+$	+	$2Cl^-$	$\longleftrightarrow$	$PbCl_2$	+	H_2O	
	−217		0		2 (−167)		−359		−285	−93
II	SnO_2	+	$4H^+$	+	$4Br^-$	$\longleftrightarrow$	$SnBr_4$	+	$2H_2O$	
	−577		0		4 (−121)		−377		2 (−285)	−114
III	PbO	+	$2H^+$	+	$2Br^-$	$\longleftrightarrow$	$PbBr_2$	+	H_2O	
	−217		0		2 (−121)		−287		−285	−104

* Solvation effect of MX_m is not considered. All MO_n and MX_m are in crystalline form, and all ionics are aqueous 1 M in concentration.

Table 3.2 Entropy of reaction between MO_n and HX [2]

Reaction J/K.mole										ΔS J/K.mole
I	PbO	+	$2H^+$	+	$2Cl^-$	$\longleftrightarrow$	$PbCl_2$	+	H_2O	
	68.6		0		2 (57)		136		70	25
II	SnO_2	+	$4H^+$	+	$4Br^-$	$\longleftrightarrow$	$SnBr_4$	+	$2H_2O$	
	49		0		4 (82)		264		2 (70)	27
III	PbO	+	$2H^+$	+	$2Br^-$	$\longleftrightarrow$	$PbBr_2$	+	H_2O	
	68.6		0		2 (82)		161		70	0

* Solvation effect of MX_m is not considered. All MO_n and MX_m are in crystalline form, and all ionics are aqueous 1 M in concentration.

Table 3.3 Gibbs free energy for reaction between MO_n and HX at 210 °C [2]

Reaction	ΔH kJ/mole	ΔS J/K.mole	$-T\Delta S$ kJ/mole	ΔG kJ/mole
I	−93	25	−12	−105
II	−114	29	−13	−127
III	−104	0	0	−104

often is difficult. This constraint may be overcome by examining the chemical reaction between flux chemicals and the metal oxide under a simplified condition. For instance, by studying the reaction of SnO in aqueous solution of HX, with $X = F^-$, Cl^-, or Br^-, the reaction mechanism shown below is expected to reflect the reaction of fluxing during the soldering process.

$$SnO + 3HX \longrightarrow [SnX_3]^- + H_2O$$

where $[SnX_3]^-$ represents the predominant species formed [3], with X^- serving as a ligand for this complex ion species.

Organic acids also form this type of three-coordinated complex, such as $[Sn(RCOO)_3]^-$. For acetate in organic solvent systems, polynuclear complexes such as $[Sn_2(CH_3COO)_5]^-$ and $[Sn_3(CH_3COO)_7]^-$ are less stable, but may also exist. In the case of insufficient X or RCOO being present to complex all the tin to $[SnX_3]^-$ or $[Sn(RCOO)_3]^-$, the reaction may form $[Sn(OH)X_2]^-$ or $[Sn(OH)(RCOO)_2]^-$ instead.

When SnO_2 dissolves in aqueous solution of HX, the predominant product formed is 6-coordinated $[SnX_6]^{2-}$ with an octahedral structure. Unlike the common occurrence of tin(II) carboxylate compounds, tin(IV) carboxylate compounds are not well known, and only a few, such as $Sn(CH_3COO)_4$, have been synthesized via the following process:

$$Sn(CH{=}CH_2)_4 + (CH_3CO)_2O \longrightarrow Sn(CH_3COO)_4$$

$SnCl_2$ and $SnBr_2$ are readily soluble in acetone, glycol, alcohols, and THF, while $SnCl_4$ and $SnBr_4$ are soluble in a wide range of organic solvents.

3.1.2 Oxidation–reduction reactions

The second type of flux reaction is oxidation–reduction. Examples include the following:

$$N_2H_4 + 2Cu_2O \longrightarrow 4Cu + 2H_2O + N_2$$

Another example of oxidation–reduction involves the use of formic acid HCOOH. One wave soldering process designed introduces the formic acid into the wave soldering chamber by bubbling nitrogen through a tank containing liquid formic acid [4]. The concentration of formic acid in nitrogen is less than 1 percent by volume. In this vaporized form and at temperatures just below 150 °C, formic acid is an effective stripper/eliminator of metal oxides, as shown below:

$$MO + 2HCOOH \longrightarrow M(COOH)_2 + H_2O$$

The products of this reaction are not stable at soldering temperature, and break down further as follows:

$$M(COOH)_2 \longrightarrow M + 2CO_2 + H_2$$

The reducing power of the hydrogen generated is expected to enhance the reducing process of the formic acid. It is speculated that the reaction here involves a number of partial reactions, such as initial loosening of the oxide layers, thermal breakdown of the resultant chemicals, and final reduction of the oxides. It is interesting to note that a white powder reaction product is found in the system's tunnel. The powder attaches itself to the interior of the glass plates in the area of the solder pot. The composition of this powder is almost entirely tin oxides, and no lead oxide is present.

There is another oxidation–reduction fluxing reaction, reduced oxide soldering activation (ROSA), introduced to the industry in 1994. In this case, oxides of Sn, Sn–Pb, and Cu are reduced to metallic surface in an aqueous solution containing highly reducing vanadous ions that can be continuously regenerated via an electrochemical process in a closed-loop system [5,6]:

$$4V^{+2} \longrightarrow 4V^{+3} + 4e$$

$$SnO_2 + 4H^+ + 4e \longrightarrow Sn + 2H_2O$$

Regeneration of V^{+2} at cathode:

$$4V^{+3} + 4e \longrightarrow 4V^{+2}$$

Regeneration reaction at anode:

$$2H_2O \longrightarrow 4H^+ + O_2 + 4e$$

Net reaction of ROSA:

$$SnO_2 \longrightarrow Sn + O_2$$

The recently developed ROSA method is shown to be compatible with long-term use with mass soldering processes. The operating window for the process is reported to be wide and component degradation caused by exposure to the fully charged solution is minimal. The ROSA treatment is claimed to provide soldering performance comparable to that attainable with a fully activated rosin flux and offers the promise of providing low soldering defect rates without the use of CFC solvents [7].

Instead of using a wet process, such as ROSA, a dry oxidation–reduction treatment called plasma assisted dry soldering (PADS) was developed by MCNC in 1995 that converts the surface oxide to oxyfluorides. This conversion film passivates the solder surface and breaks down when the solder melts in an inert oven or even in air [5,8,9].

$$SF_6 \longrightarrow 4F\cdot + SF_2 + e$$

$$yF\cdot + SnO_x \longrightarrow SnO_xF_y$$

SnO_xF_y (on top of molten solder) $\rightarrow$ Sn (wetted with solder) + oxyfluoride residues.

The PADS method is attracting significant attention in the marketplace. Considerable progress has been made with the first domestic PADS technology licenses granted in 1995. International licensing began in 1996.

3.1.3 Fluxes for reflow soldering

All the reactions described above can be considered as fluxing reactions in a broad sense. Among those, only a few of the systems are adequate for reflow applications. In general, the chemicals to be used as flux for solder paste have to be sufficiently non-reactive toward metals at room temperature so that proper shelf life of the solder paste can be obtained. In addition, the chemicals also have to be retainable in the solder paste during the handling of materials. Therefore chemicals that are either too reactive or too volatile are not suitable as ingredient for the fluxes used in solder pastes. The most commonly used fluxes for solder pastes include organic acids, organic bases, organic halogen compounds, and organic halide salts, as will be discussed in the next section.

3.2 Flux chemistry

Since flux serves multiple functions for reflow applications, the ingredients in flux are often also fairly complicated. In general, fluxes used for solder paste comprise resins, activators, solvents, and rheological additives. For certain special systems, additives such as tackifiers, surfactants, or corrosion inhibitors may also be used.

3.2.1 Resins

Resin refers to organic materials with medium to high molecular weight. It may include natural products, such as rosin, or synthetic materials, such as polymers. Often it is used to provide fluxing activity, tackiness, and an oxygen barrier. Sometimes it may also serve as a rheological aid. The most commonly used resins are water-white rosin or chemically modified rosins. The latter type is sometimes referred to as synthetic rosin or synthetic resin by the soldering industry. The major components of water-white rosin are 80–90 percent abietic acid ($C_{20}H_{30}O_2$), 10–15 percent dehydroabietic acid ($C_{20}H_{28}O_2$) and dihydroabietic ($C_{20}H_{32}O_2$), and 5–10 percent neutral matter [10]. Figure 3.1 shows some common isomers of rosin. Rosin is a distillation product from the pine tree. Depending on the species, regions, and environment, the composition of rosin may vary, and therefore it may introduce some inconsistency, such as viscosity, color, and fluxing activity. Although rosin is relatively thermally stable, it does undergo isomeric transformations [11,12], as shown in Figure 3.2. Most of the rosin isomers are sensitive not only to heat but also to air and light [13,14]. Therefore, abietic acid will turn yellow upon exposure to air. At higher temperatures, disproportionation of abietic acid results in mixtures of dehydroabietic acid and di- and tetra-hydroabeitic acid. Among those isomers, dehydroabietic acid exhibits the highest oxidative stability. Rosin may also undergo thermal dimerization at elevated temperatures, such as 200 °C [15]. It was postulated by Parkin *et al*. [15] that these heat induced products are largely ester in nature, probably resulting from addition of the

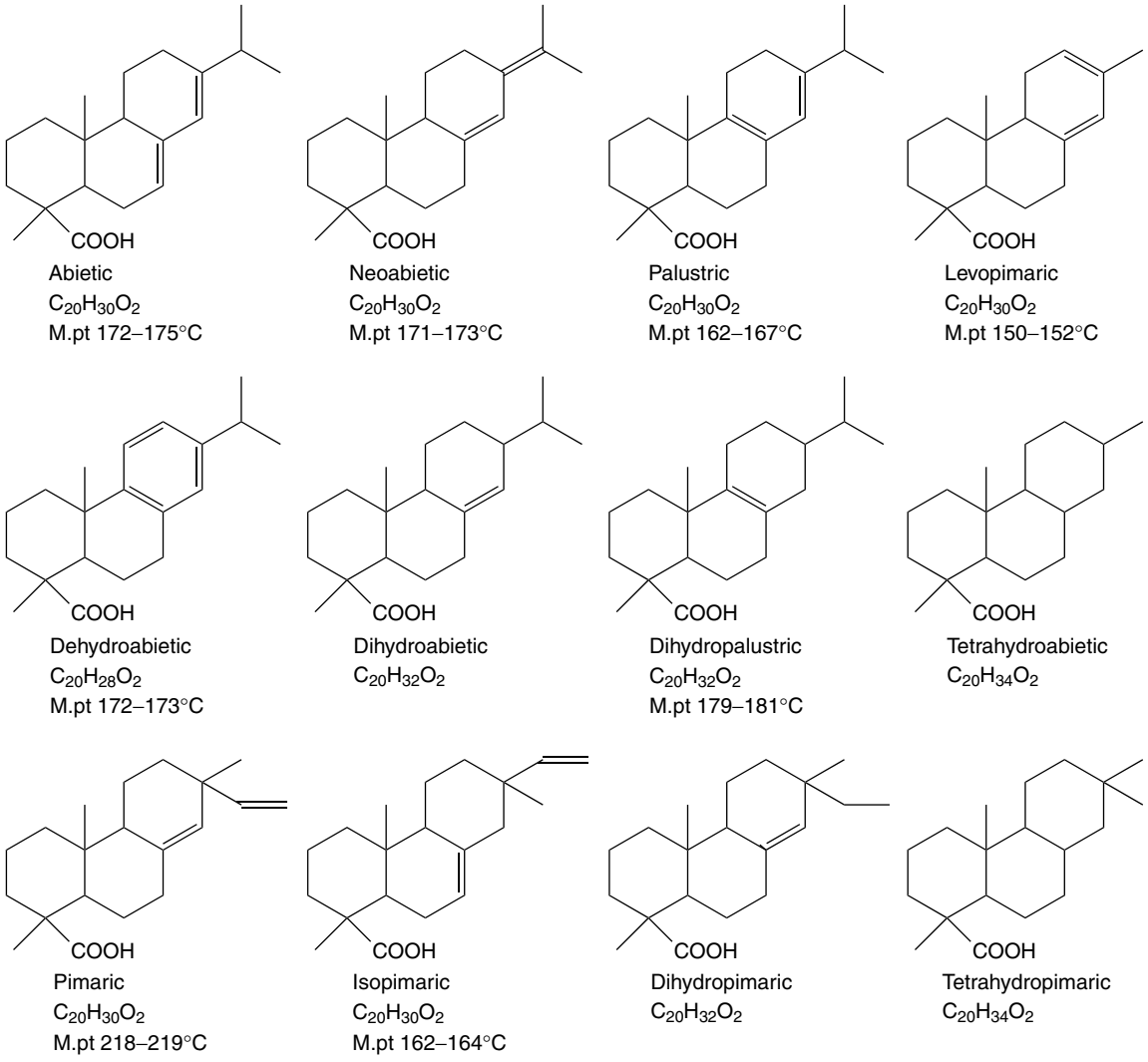

Figure 3.1 Some common isomers of rosin [10]

abietic acid carboxylic group across one of the double bonds of another abietic acid molecule. In addition, a further auto-oxidation reaction may occur in air [16,17,18], and result in the formation of glycols, ketones and ethers of varying molecular weights. The auto-oxidative polymerization mechanism can be schematically shown below:

$$2R{-}C{=}C{-}CH2{-}R' \xrightarrow{\text{oxygen}} 2R{-}C{=}C{-}C(-OOH){-}R'$$

$$\xrightarrow{-\text{water}} (R{-}C{=}C{-}CR'{-})_2O$$

Some rosins used in the soldering industry are chemically modified, such as polymerization, hydrogenation, or functional group modification, to impart additional features such as higher tackiness, better thermal stability, or greater fluxing activity. Due to its non-polar nature, rosin is rarely used in water washable applications, and is typically used in no-clean applications or RMA type of fluxes. However, rosin may also be cleaned by an aqueous system with the aid of saponifiers, which is a mixture of alkali amines, alcohols, and surfactants usually applied in a 2–10% solution in water. The saponification reaction converts the hydrophobic rosin $C_{19}H_{29}COOH$, which is insoluble in water, into water soluble hydrophilic reaction products $CH_{19}H_{29}COOCH_2CH_2NH_2$, as shown below:

$$C_{19}H_{29}COOH + HOCH_2CH_2NH_2 \rightarrow CH_{19}H_{29}COOCH_2 \times CH_2NH_2 + H_2O$$

Rosin	ethanolamine (saponifier)	water-soluble rosin soap

3.2.2 Activators

Although resin may provide certain fluxing activity, the soldering performance of resin alone is rarely good

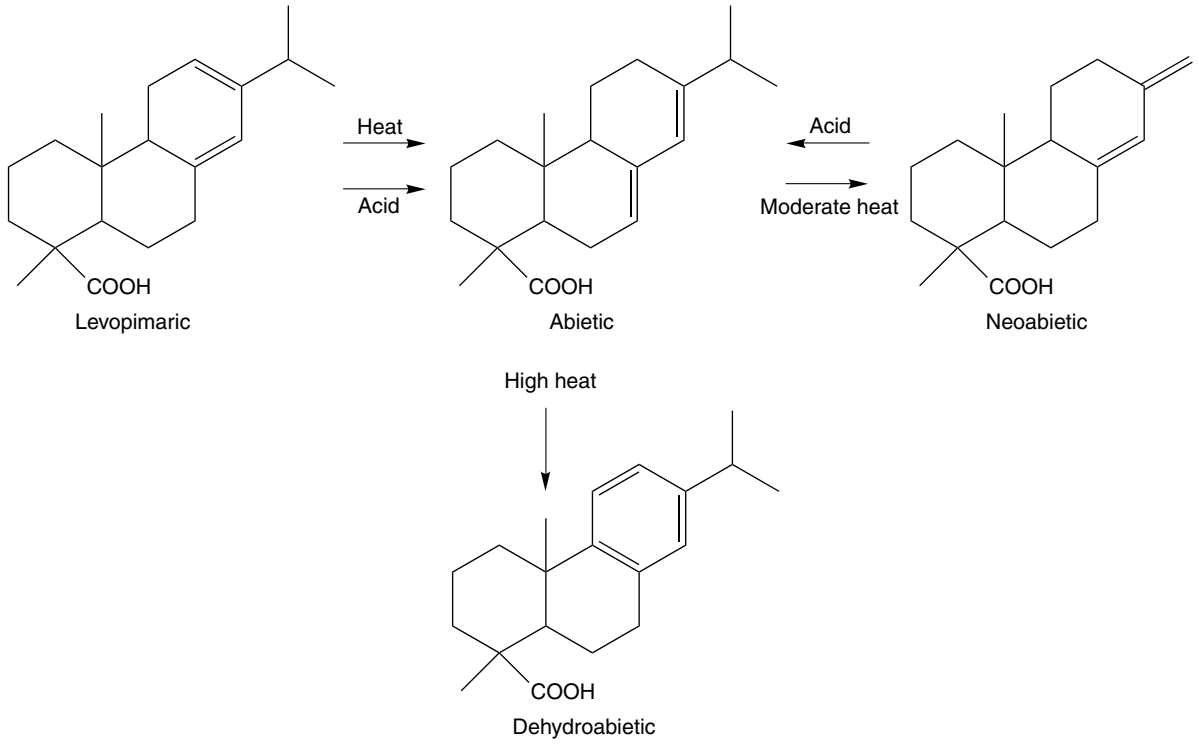

Figure 3.2 Some isomeric transformations of abietic acid [10]

Table 3.4 Linear dicarboxylic acid activators [19]

Name	*Structure*	*Melting point (°C)*	*pK1*	*pK2*	*Solubility in 100 parts water*
Oxalic acid	HOOCCOOH	189d	1.271	4.272	9.5
Malonic acid	$HOOCCH_2COOH$	135d	2.826	5.696	154
Succinic acid	$HOOC(CH_2)_2COOH$	187	4.207	5.635	7.7
Glutaric acid	$HOOC(CH_2)_3COOH$	97.5	3.77	6.08	64
Adipic acid	$HOOC(CH_2)_4COOH$	152	4.418	5.412	1.4
Pimelic acid	$HOOC(CH_2)_5COOH$	105.8	4.484	5.424	5
Suberic acid	$HOOC(CH_2)_6COOH$	140	4.512	5.404	0.16
Azelaic acid	$HOOC(CH_2)_7COOH$	106.5	4.53	5.4	0.24
Sebacid acid	$HOOC(CH_2)_8COOH$	134.5	4.59	5.59	0.1

enough for the electronics industry. Often some activator chemicals have to be added to the flux in order to boost fluxing activity. The most commonly used activators include linear dicarboxylic acids (see Table 3.4), special carboxylic acids (Table 3.5), and organic halide salts (Table 3.6). Linear dicarboxylic acids are more effective than mono-carboxylic acids as activators, and are most effective at relatively low molecular weight. Activators with a greater solubility in water, such as glutaric acid and citric acid, generally are more adequate for water washable flux systems, while those with a lower solubility, such as adipic acid, are better for no-clean applications.

Halide salts often provide more effective fluxing activity than organic acids. However, halide salts also are more reactive at ambient temperature, therefore causing some concern on shelf life and open life of solder paste. Instead of using halide salts, some solder paste utilizes covalent halides R−X as activator. At soldering temperature, this covalent halogen dissociates and presumably forms a halide salt which in turn undergoes fluxing reaction. Since covalent halides typically are fairly stable at ambient temperature, use of covalent halides effectively lessens concerns on shelf life and open life.

In addition to the use of organic acids or halides, organic bases such as amines are also often used as activators. It is a common practice of the electronics industry to use a combination of some or all of those groups of activators in fluxes used for solder pastes in

Table 3.5 Special carboxylic acid activators [19]

Name	*Structure*	*Melting point (°C)*	*pK1*	*pK2*	*Solubility in 100 parts water*
Citric acid	$HOOCCH_2C(OH)(COOH)CH_2COOH$	152	3.128	4.761	59
Fumaric acid	$HOOCCH{=}CHCOOH$	299d	3.1	4.6	0.6
Tartaric acid	$HOOCCH(OH)CH(OH)COOH$	210	3.22	4.81	139
Glutamic acid	$HOOCCH_2CH_2CH(NH)_2COOH$	200s	2.162(+1)	4.272(0)	0.8
Malic acid	$HOOCCH_2CH(OH)COOH$	131			55.8
Phthalic acid	C_6H_4-1,2-$(COOH)_2$	210d	2.95	5.408	0.6
Levulinic acid	$CH_3COCH_2CH_2COOH$	30			∞
Stearic acid	$CH_3(CH_2)_{16}COOH$	67			Slightly
Benzoic acid	C_6H_5COOH	122	4.204		0.29

Table 3.6 Organic halide salt activators [19]

Name	*Structure*	*Melting point (°C)*
Dimethylamine hydrochloride	$(CH_3)_2NH{\cdot}HCl$	170
Diethylamine hydrochloride	$(C_2H_5)_2NH{\cdot}HCl$	227
Diethylamine hydrobromide	$(C_2H_5)_2NH{\cdot}HBr$	218
Aniline hydrochloride	$C_6H_5NH_2{\cdot}HCl$	196
Pyridine hydrobromide	$C_5H_5N{\cdot}HBr$	200d
Pyridine hydrochloride	$C_5H_5N{\cdot}HCl$	145
Ethanolamine hydrochloride	$H_2NCH_2CH_2OH{\cdot}HCl$	84
Diethanolamine hydrochloride	$(HOCH_2CH_2)_2NH{\cdot}HCl$	liquid
Triethanolamine hydrochloride	$(HOCH_2CH_2)_3N{\cdot}HCl$	177

Table 3.7 Commonly used solvents in fluxes of solder paste

Solvent family	*Example*
Alcohols	Isopropanol, *n*-butanol, isobutanol, ethanol, terpineol
Amines	Aliphatic amines
Esters	Aliphatic esters
Ethers	Aliphatic ethers
Glycols	Ethylene glycol, propylene glycol, triethylene glycol, tetraethylene glycol
Glycol ethers	Aliphatic ethylene glycol ethers, aliphatic propylene glycol ethers
Glycol esters	Aliphatic ethylene glycol esters, aliphatic propylene glycol esters
Hydrocarbons	Aliphatic hydrocarbons, aromatic hydrocarbons, terpenes
Ketones	Aliphatic ketones
Pyrols	M-pyrol, V-pyrol

order to maximize soldering performance (see Tables 3.4 to 3.6).

3.2.3 Solvents

Virtually all the resins and activators discussed above, together with solder powder, are solids. It is obvious that a mixture of those materials still cannot be processed with automated high volume, high throughput deposition equipment such as printers or dispensers. In order to convert the soldering materials into a more maneuverable homogeneous fluid form, use of solvents thus becomes indispensable.

Commonly used solvents are referred to in Table 3.7. Among those, glycol systems appear to be the most prevailing solvent chemistry used in the industry, primarily due to balanced solvency power, soldering aid performance, and viscosity. Also commonly used are alcohols, particularly terpineol solvent, due to its superior solvency for rosins. The selection of a solvent chemistry for a flux system is primarily determined by the flux chemistry. For instance, for a water washable activator system, such as citric acid, use of polar solvents such as glycols is often necessary in order to dissolve the activator. Other factors to be considered include the odor of solder paste as well as the target stencil life and tack time of solder paste. Obviously selection of a volatile solvent will not be adequate if a long stencil life and long tack time is desired.

It should be mentioned that health and environmental concerns are also very important factors to be considered. For instance, the first five or six of the glycol solvents shown in Table 3.8 have been cited as chemicals to be banned by certain users or governments [20–22], primarily due to environmental considerations. However, the remaining chemicals in the same table, although cited, are virtually regarded as regular chemicals and are handled with general precautions [23].

Being a very large chemical family involving several hundred possible structures, the glycol family should not be over-simplified and treated as one single chemical. Since the glycol family typically provides superior features for flux applications as discussed earlier, a simple elimination of the use of all glycol chemicals in the fluxes can easily result in an unnecessary compromise in soldering performance.

3.2.4 Rheological additives

Although soldering materials in fluid form allow the possibility of automating the deposition process, a simple

Table 3.8 Glycol chemicals which have been cited as health concerns

Chemicals	*CAS #*	*References*
Ethylene glycol monomethyl ether	109-86-4	20–22
Ethylene glycol monomethyl ether acetate	110-49-6	20–22
Ethylene glycol monoethyl ether	110-80-5	20, 22
Ethylene glycol monoethyl ether acetate	111-15-9	20, 22
Diethylene glycol dimethyl ether	111-96-6	20, 21
2-Ethoxyethyl acetate	110-11-9	21
Ethylene glycol	107-21-1	23
Ethylene glycol diformate	629-15-2	23
Ethylene glycol dinitrate	628-96-6	23
Ethylene glycol isopropyl ether	109-59-1	23
Ethylene glycol monobenzyl ether	622-08-2	23
Ethylene glycol monobutyl ether	111-76-2	23
Ethylene glycol monoethyl ether acrylate	106-74-1	23
Ethylene glycol monophenyl ether	122-99-6	23
1,2-Propylene glycol	57-55-6	23
1,2-Propylene glycol dinitrate	6423-43-4	23
Propylene glycol monomethyl ether	107-98-2	23

mixture of flux chemicals, solvents, and solder powder is usually the most acceptable to be used directly in surface mount applications. For instance, during the solder paste printing process, the paste is required to flow easily during printing, but not to flow at all after. On the other hand, a paste is required to be sufficiently non-tacky to be released from the stencil aperture, but tacky enough to hold onto the substrate and the components to be placed subsequently onto the paste after printing. In order to meet the requirement of a variety of processes, the rheology of solder paste has to be tailored to each specific application. This can normally be accomplished with the use of adequate rheological additives in the flux systems. Table 3.9 shows some commonly used rheological additives.

Perhaps the most commonly used rheological additives are castor oil derivatives. This family is highly hydrocarbon in nature, and is typically used in no-clean or RMA flux applications. For water-wash fluxes, polyethylene glycols or derivatives of polyethylene glycols are the prevailing choices due to their high solubility in water.

3.3 Solder powder

Generally, the solder metal in powder form has to be used if a fluidized solder material is desired for an automated deposition process. Solder powder is made by the atomization process, as discussed below. The powder as atomized needs to be sized to a proper dimension, then mixed with flux to form a solder paste.

3.3.1 Atomization

Atomization is a process converting metal into very fine particles. Commonly used methods are shown in Table 3.10. Although potentially all those methods can be used for solder materials, the preferred methods, such as gas, centrifugal, or ultrasonic atomization, have to be able to produce a low oxide, small, and highly spherical powder required for surface mount applications.

Figure 3.3 shows a schematic detailed design of a gas atomization nozzle [24]. The molten solder leaving the reservoir orifice is bombarded with an inert gas stream and blasted into many molten solder droplets which quickly solidify before hitting the chamber wall. Figure 3.4 shows the system design of a pilot-scale inert gas atomization facility [24]. In this case, the powder collected is sent to a cyclone collector for subsequent sizing. Figure 3.5 shows a schematic design of rotating disk atomization [24]. The molten solder stream from a melt pot impinges a rapidly spinning disk, and disintegrates into millions of molten solder droplets at the periphery of disk. Again, these droplets solidify quickly in the cold inert gas jet environment and are collected for further sizing.

Table 3.9 Some commonly used rheological additives [19]

Rheological additives	*Example*	*Note*
Castor oil derivatives	Castor oil is triglyceride of fatty acids. Fatty acid composition is approximately 87% ricinoleic, 7% oleic, 3% linoleic, 2% palmitic, 1% stearic, and trace amounts of dihydroxystearic. Modification of castor oil may be hydrogenation, etc. The nature of modification is very proprietary.	No-clean/RMA fluxes
Petroleum-based waxes	Petrolatum	No-clean/RMA fluxes
Synthetic polymers	Polyethylene glycols (water soluble)	Water-wash fluxes
	Derivatives of polyethylene glycols	No-clean/RMA fluxes
	Polyethylene	
Natural waxes	Vegetable wax	No-clean/RMA fluxes
Inorganic thixotropic additives	Activated silicate powders	No-clean/RMA fluxes
	Activated clays	

Table 3.10 Methods of atomization [24]

Commercial methods	*Near-commercial methods*	*Other methods*
Water atomization	Ultrasonic gas atomization	Centrifugal shot casting process
Oil atomization	Rotating disk atomization	Spinning cup atomization
Gas atomization	Electron beam rotating disk process	Centrifugal impact atomization
Vacuum atomization	Roller atomization	Laser spin atomization
Rotating electrode atomization		Durarc process
		Vibrating electrode atomization

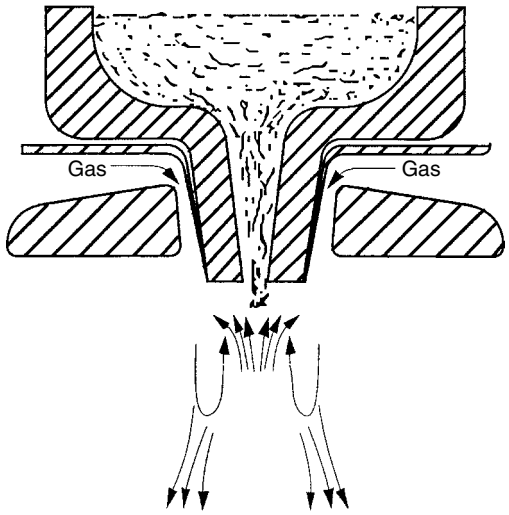

Figure 3.3 Schematic of a confined gas atomization nozzle

3.3.2 Particle size and shape

For the electronics industry, the solder powder used can be categorized into the dimensions shown in Table 3.11 [25]. Due to the miniaturization trend of the surface mount industry, the prevailing solder powder size also reduces with time, as shown in Figure 3.6 [26]. Type 2 solder powder was used prior to the early 1990s. Currently type 3 is mainly used with the need for type 4 beginning to emerge in 1998–1999. Although powder sizes of type 5 and type 6 are not common, there is already a demand for those powders. These fine powders are primarily intended for use in either ultra-fine pitch applications or wafer solder paste bumping.

Since sieving is commonly used for powder classification, solder powder particle size is often also expressed in sieve number as shown in Table 3.12. For instance, type 2 powder is designated as −200 mesh/+325 mesh, indicating that the particle size is smaller than 200 mesh, but larger than 325 mesh. Similarly, type 3 powder is expressed as −325 mesh/+500 mesh, and type 4 powder as −400 mesh/+500 mesh.

The solder powder not only has to be consistent in particle size distribution, as specified in Table 3.11, but also has to be highly spherical in order to facilitate a good flow of paste during the deposition stage. Spherical powder with a smooth surface also reflects the surface of solder powder being very low in oxide during the atomization process. This allows the surface tension of molten solder to serve as the dominant force which converts the solder droplet into a spherical ball. Figure 3.7 shows an example of type 3 62Sn/36Pb/2Ag solder powder with a consistent spherical shape.

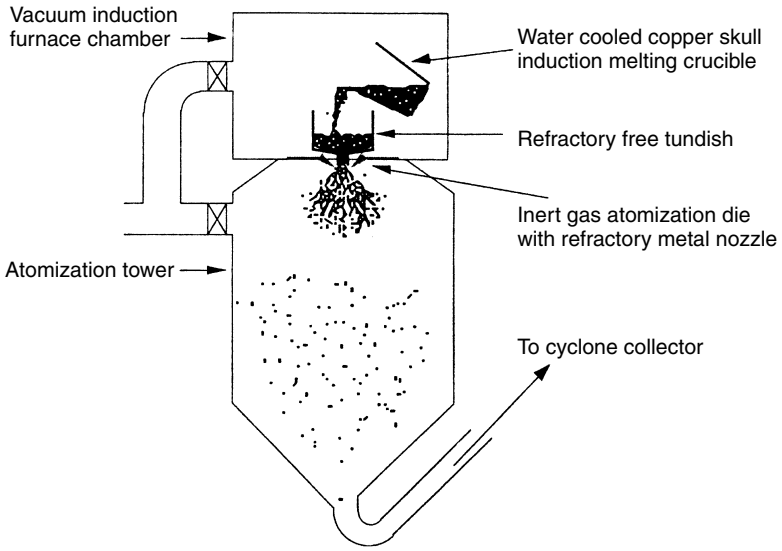
Vacuum induction furnace chamber
Water cooled copper skull induction melting crucible
Refractory free tundish
Inert gas atomization die with refractory metal nozzle
Atomization tower
To cyclone collector

Figure 3.4 Schematic of a pilot-scale inert gas atomization facility

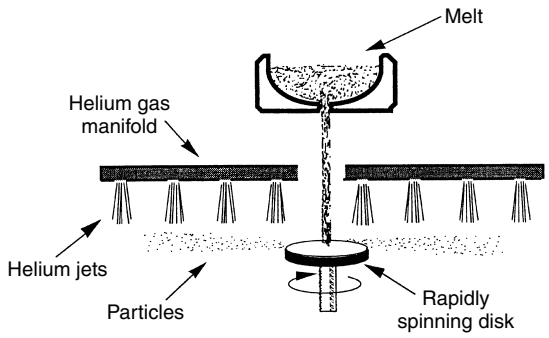

Figure 3.5 Schematic of a rotating disk atomization system

Table 3.11 Classification of solder powder size, expressed as percent of sample by weight – nominal sizes [25]

Category	*None larger than*	*Less than 1% larger than*	*80% minimum between*	*10% maximum less than*
Type 1	160 µ	150 µ	150–75 µ	20 µ
Type 2	80 µ	75 µ	75–45 µ	20 µ
Type 3	50 µ	45 µ	45–25 µ	20 µ
Type 4	40 µ	38 µ	38–20 µ	20 µ
Type 5	30 µ	25 µ	25–15 µ	15 µ
Type 6	20 µ	15 µ	15–5 µ	5 µ

Besides the oxidation factor, the type of processes used in solder atomization may also affect the shape of the solder powder. Certain processes may have greater potential to promote formation of irregular shapes than other methods, regardless of the oxygen content of the atomization atmosphere. Since an irregular shape represents a larger surface area per unit solder volume compared with a spherical shape, an undesirable higher solder oxide content is accordingly expected for those particles. Physical defects in solder powder quality may include (1) fines, (2) satellites, (3) elongated irregular particles, (4) flattened particles, (5) loose conglomerates, (6) welded conglomerates, (7) angled surface, and (8) wrapped particles, as demonstrated in Figure 3.8.

Table 3.12 Specifications for USA standard testing sieves, ASTM-E-11

Sieve number	*Microns*	*Inches*
50	300	0.0117
60	250	0.0098
70	212	0.0083
80	180	0.007
100	150	0.0059
120	125	0.0049
140	106	0.0041
170	90	0.0035
200	75	0.0029
230	63	0.0025
270	53	0.0021
325	45	0.0017
400	38	0.0015
450	32	0.0012
500	25	0.001
635	20	0.0008

Solder powder with a size finer than type 3 or type 4 is not yet common. In general, finer solder powders with a low oxide content are more difficult to produce and classify. Figure 3.9 shows an example of a type 6 solder powder.

3.4 Solder paste composition and manufacturing

Solder paste is manufactured by making flux and solder powder individually first. The two components are then blended together to form a solder paste. Depending on the applications, the solder paste composition can be roughly represented by Table 3.13. As a rule of thumb, the powder size used should be no larger than 1/7 of aperture size for printing applications, or no larger than 1/10 of needle inner diameter for dispensing applications. The deposition performance often is compromised if a powder coarser than the size mentioned above is used.

The metal content shown in Table 3.13 is typical for eutectic tin–lead solder paste. For solder alloys other than

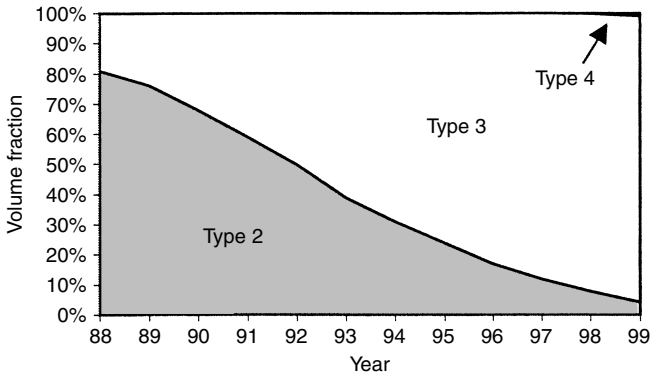

Figure 3.6 Evolution of powder size for solder paste used in SMT industry

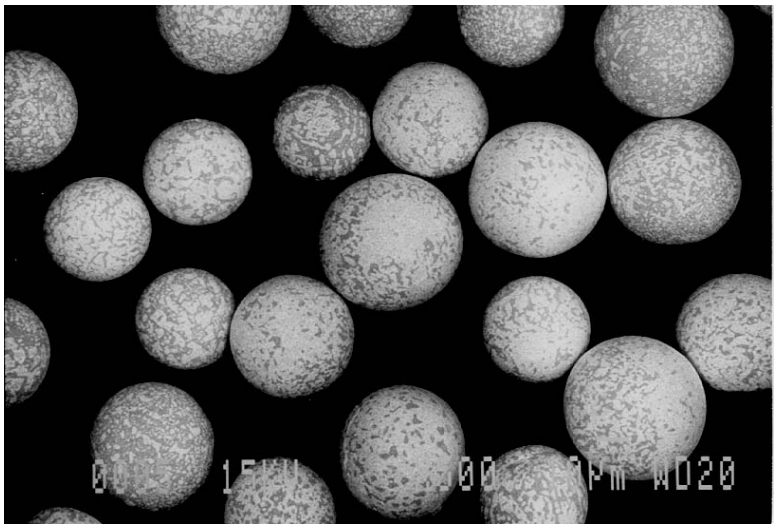

Figure 3.7 SEM picture of type 3, spherical, high quality 62Sn/36Pb/2Ag solder powder

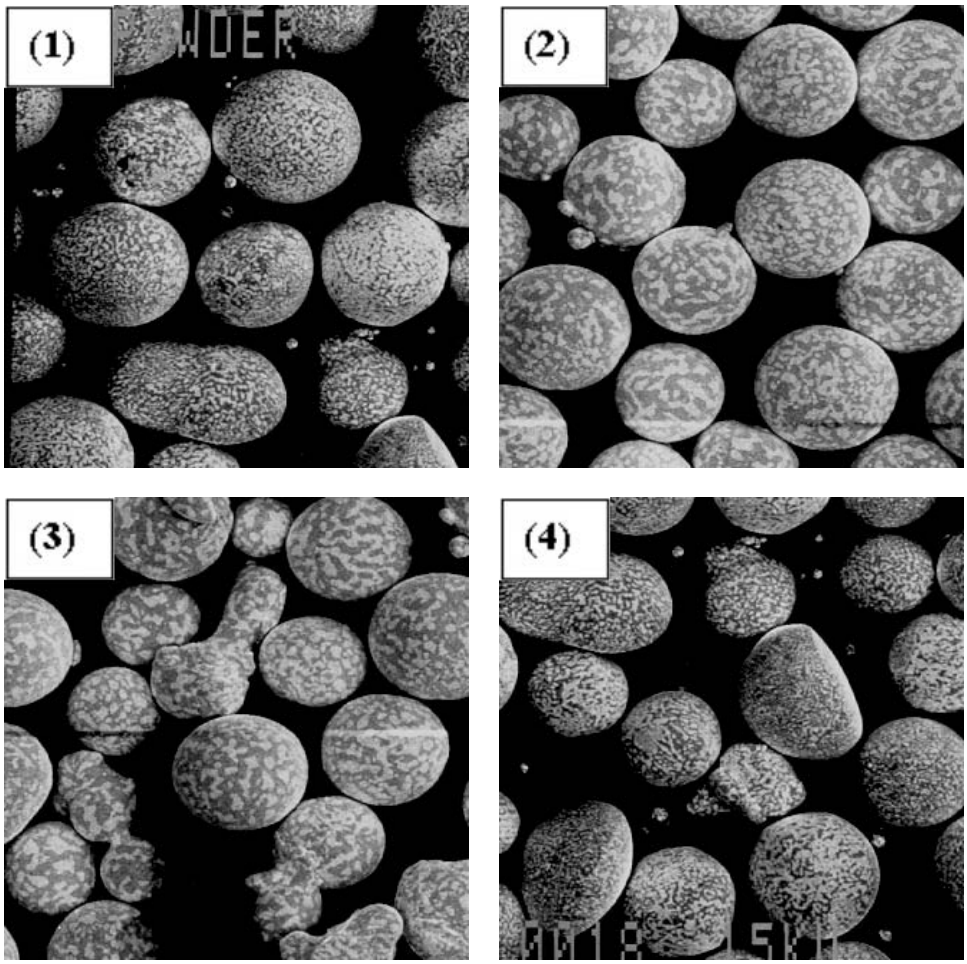

Figure 3.8 SEM pictures of defects in solder powder, including (**1**) fines, (**2**) satellites, (**3**) elongated irregular particles, (**4**) flattened particles, (**5**) loose conglomerates, (**6**) welded conglomerates, (**7**) angled surface, and (**8**) wrapped particles

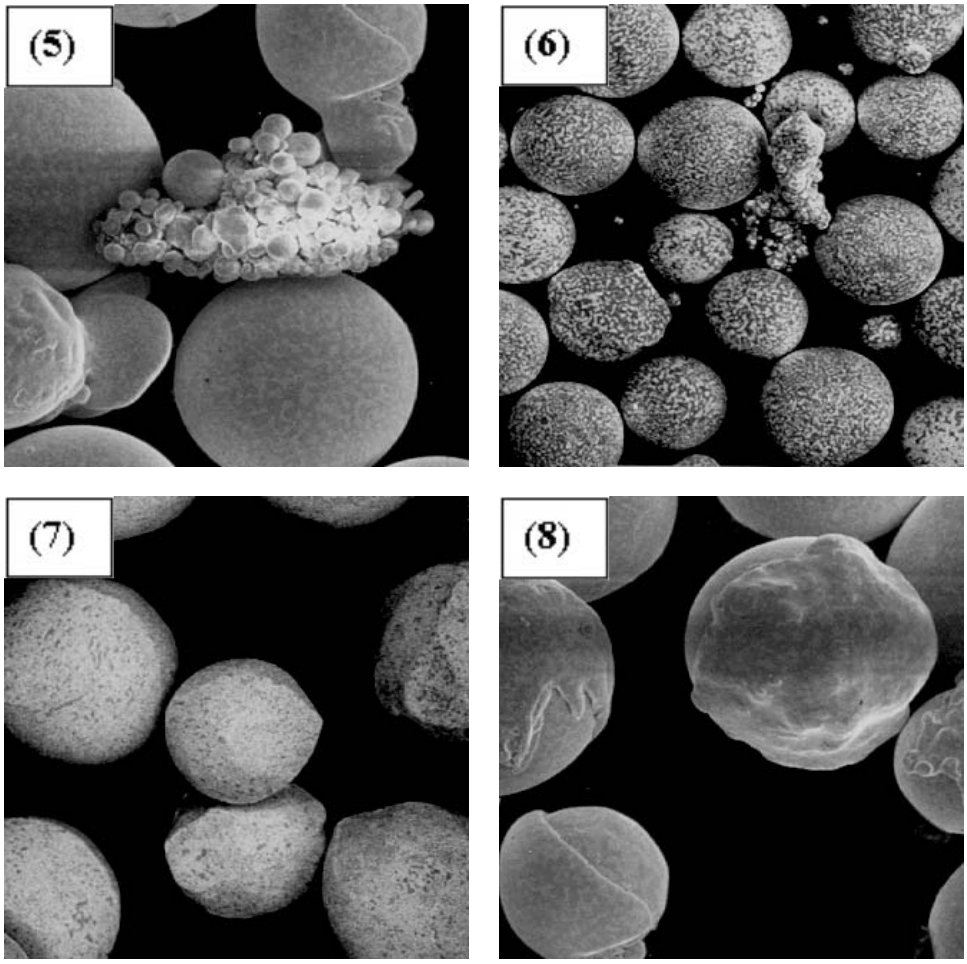

Figure 3.8 (*Continued*)

Table 3.13 Composition of solder paste

Powder size	*Metal content (%)*	*Applications*
Type 2	88–90	Printing, 50 mil pitch
Type 3	85–88	Dispensing, down to 20 mil pitch, possible with 16 mil
Type 3	88–91	Printing, down to 20 mil pitch, possible with 16 mil pitch
Type 4 or 5	85–88	Dispensing, down to 16 mil pitch, possible with 12 mil
Type 4 or 5	88–91	Printing, down to 16 mil pitch, possible with 12 mil pitch
Type 5 or 6	89–91	Printing, wafer level solder bumping using solder paste

eutectic tin–lead, the solder density, and accordingly the solder volume fraction of solder paste, will be different. Since deposition performance is largely affected by the solder volume fraction [27], the solder content should be adjusted in order to maintain proper volume fraction of solder in solder paste.

The solder volume fraction of solder paste can be calculated as follows:

$$V = \frac{\dfrac{x}{ds}}{\dfrac{x}{ds} + \dfrac{100 - x}{df}}$$

where V represents the volume fraction of solder in solder paste, x metal content (% w/w) of solder paste, ds the density of solder alloy, and df the density of flux. For instance, for 63Sn/37Pb solder paste with 90 percent w/w metal content and using a flux with density 1 gm/cm^3, the volume fraction of solder is calculated to be 51.7 percent, as shown below. Here the solder density of 63Sn/37Pb is 8.4 gm/cm^3.

$$V = \frac{\dfrac{90}{8.4}}{\dfrac{90}{8.4} + \dfrac{100 - 90}{1.0}} = 0.517 \text{ (or } 51.7\%)$$

Figure 3.10 shows the relation between metal volume percent and metal weight percent of 63Sn/37Pb solder

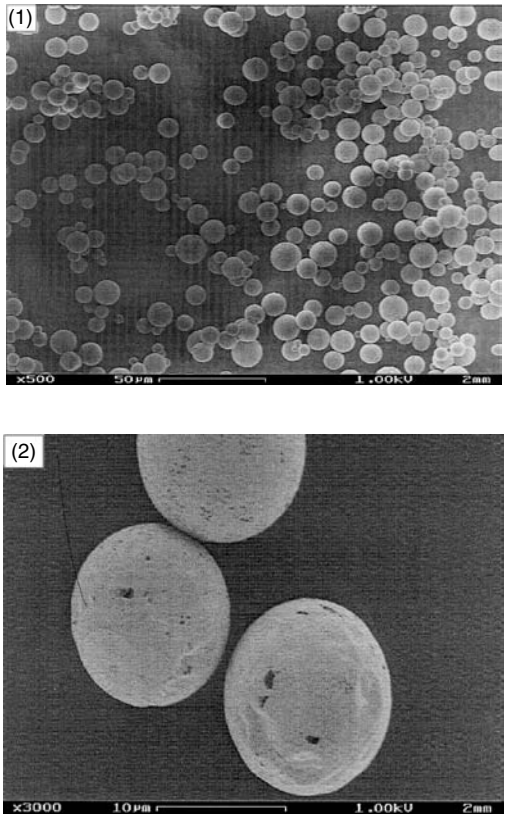

Figure 3.9 SEM picture of type 6 63Sn/37Pb solder powder

paste (sp.gr.: 63Sn/37Pb 8.40, flux 1.00). The volume fraction of solder increases rapidly with increasing metal content (w/w) at a metal load beyond 90 percent w/w, suggesting a potentially high sensitivity of deposition performance toward metal content. This stipulation is verified

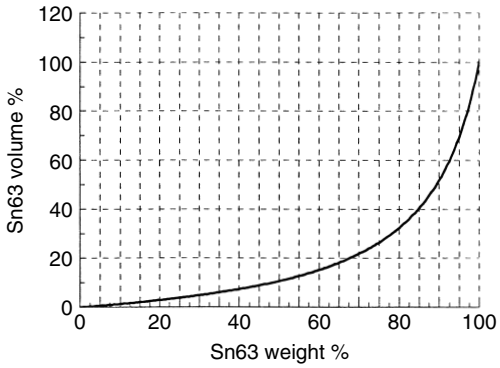

Figure 3.10 Relation between metal volume percent and metal weight percent of Sn63 solder paste (sp.gr.: Sn63 8.40, flux/vehicle 1.00)

by the earlier work of Xiao *et al.* [27] which shows a high sensitivity of viscosity, thixotropic index, tack, slump, printing defects, and solder balling toward metal volume fraction. The high sensitivity of solder paste performance toward solder volume fraction validates the importance of maintaining the solder volume fraction if the solder alloy is to be changed for a given flux system. Figure 3.11 shows the calculated solder content (percent w/w) for alloy X with various densities if a solder volume fraction equivalent to 89, 90, and 91 percent w/w of eutectic tin–lead solder paste is desired. Here a value of 1 gm/cm^3 is used to represent the flux density.

Mixing of solder powder with flux has to be carried out with caution. Due to the soft nature of solder powder, high speed, high shear mixing should be avoided. In addition, humidity and air-entrapment in the solder paste due to mixing should also be avoided in order to assure consistency in both viscosity and stability. Hence, a slow thorough mixing under vacuum and/or an inert atmosphere at a controlled temperature is most desirable. Since

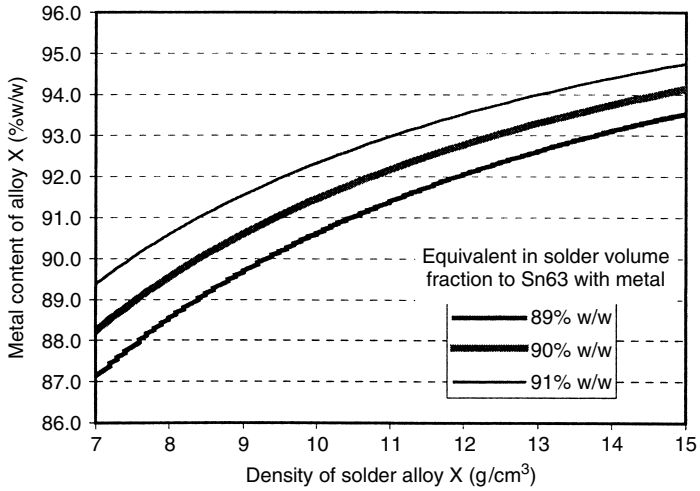

Figure 3.11 The calculated solder content for alloy X with various density if a solder volume fraction equivalent to designated content (% w/w) of eutectic tin–lead solder paste is desired. In this calculation, a flux density of 1.0 g/cm^3 is used

Figure 3.12 A Ross double planetary mixing equipment used for solder paste mixing

solder paste is not quite flowable, the mixing mechanism should cover each space mechanically with the mixer stirrer blades. Figure 3.12 shows a commercial double planetary mixing equipment used for solder paste mixing [28]. During the mix cycle, two rectangularly shaped stirrer blades revolve around the tank on a central axis. Simultaneously, each blade revolves on its own axis at approximately the speed of the central rotation. With each revolution on its own axis, each stirrer blade advances along the tank wall. Figure 3.13 shows the mixing pattern of this equipment [28]. After mixing, the paste is then transferred to packing equipment which loads the material into individual containers.

3.5 Solder paste rheology

Successful implementation of solder paste deposition and reflow processes relies on a very well-engineered paste rheology. The viscosity of solder paste needs to be high enough to maintain a stable suspension of the heavy metal powder in the flux fluid system during storage and handling. It needs to be sufficiently low during the paste deposition stage so that the paste can flow readily through the stencil aperture or the dispensing needle. Then again, the paste needs to be high enough in viscosity after deposition in order to hold the shape of the deposited paste and avoid slumping and bridging, either before or during the reflow process. To make things more complicated, the solder paste needs to be non-tacky enough to be released from a squeegee and stencil aperture, but sufficiently tacky to stick to the substrate and also to hold the components placed on top of the paste deposits. Therefore, a thorough understanding of rheology is essential in order to achieve a high yield solder paste deposition and reflow process.

3.5.1 Rheology basics

One of the most commonly encountered rheological properties is viscosity. Viscosity is the internal friction of a fluid, caused by molecular or atomic attraction, which makes it resist a tendency to flow [29]. Newton defined viscosity with the use of the model shown in Figure 3.14 [30] where V_1 is speed of the top plane, and V_2 is the bottom plane of a fluid. In this model, the force F required to maintain the speed difference, $\mathrm{d}v$, of the two parallel planes with surface area A is considered to be proportional to the velocity gradient $\mathrm{d}v/\mathrm{d}x$. The relation can be expressed as

$$\frac{F}{A} = \eta \frac{\mathrm{d}v}{\mathrm{d}x}$$

where η is a constant called viscosity. Hence, viscosity may also be interpreted as the perturbation (shear stress) needed in order to achieve certain flow (shear rate), as shown below:

$$\eta \text{ (viscosity)} = F' \text{ (shear stress)}/S \text{ (shear rate)}$$

where $F' = F/A$, and $S = \mathrm{d}v/\mathrm{d}x$.

Depending on the material's property, the flow behavior may vary over a wide range. Newtonian fluid, as shown in Figure 3.15, exhibits a constant viscosity regardless of the shear rate. For pseudoplastic fluid, the viscosity decreases with increasing shear rate (see Figure 3.16). In contrast to pseudoplastic fluid, dilatant fluid exhibits an increasing viscosity with increasing shear rate, as shown

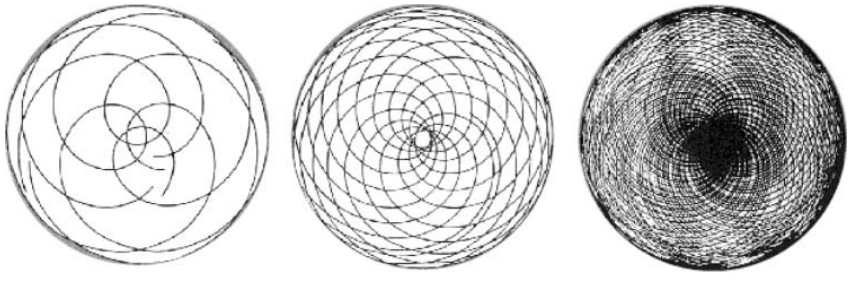

Figure 3.13 Mixing pattern of double planetary mixer

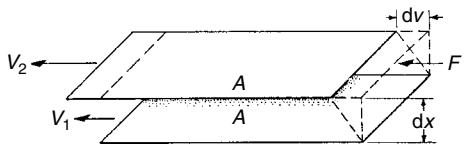

Figure 3.14 Definition of viscosity

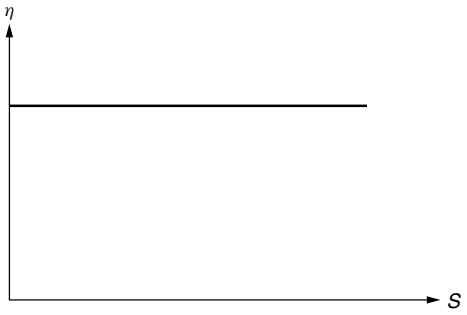

Figure 3.15 Flow behavior of Newtonian fluid

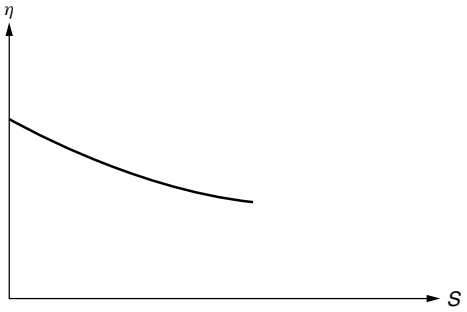

Figure 3.16 Flow behavior of a pseudoplastic fluid

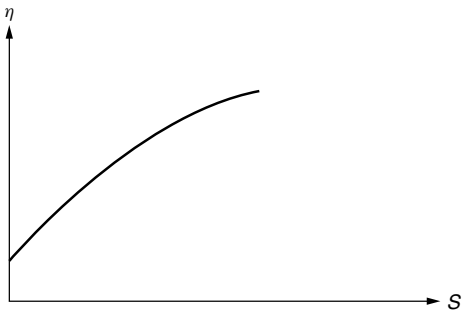

Figure 3.17 Flow behavior of a dilatant fluid

in Figure 3.17. Plastic fluid remains solid-like when the shear stress is less than the yield value, as shown in Figure 3.18. Once the yield value is exceeded and flow begins, the fluid may display any patterns such as that of Newtonian, pseudoplastic, or dilatant fluids. Thixotropic fluid exhibits a decrease in viscosity with time when subjected to constant shear rate, as shown in Figure 3.19.

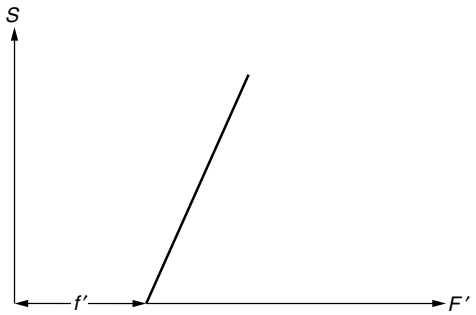

Figure 3.18 Flow behavior of plastic fluid

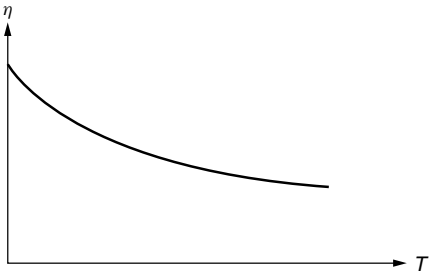

Figure 3.19 Flow behavior of thixotropic fluid

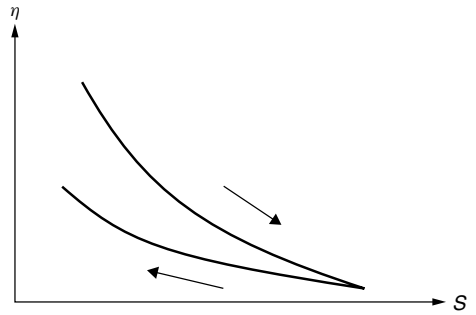

Figure 3.20 Flow behavior of thixotropic fluid under varying rates of shear

When subjected to varying rates of shear, thixotropic fluid will exhibit flow behavior as shown in Figure 3.20. On the other hand, rheopectic fluid exhibits an increase in viscosity with time when subjected to a constant shear rate, as shown in Figure 3.21. The flow behavior of rheopectic fluid under varying shear rate is shown in Figure 3.22. The "hysteresis loop" enclosed by the "up" and "down" curves in Figures 3.20 and 3.22 reflects the effect of time on viscosity for those two types of fluids.

3.5.2 Solder paste viscosity measurement

There are two major types of viscometer commonly used for solder paste viscosity measurement. The most commonly used is the Brookfield viscometer, as shown in Figure 3.23. Here a spindle with a cross-bar is immersed

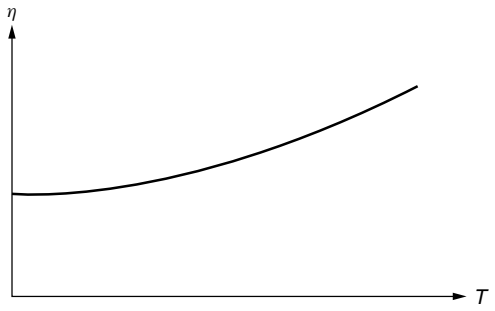

Figure 3.21 Flow behavior of rheopectic fluid

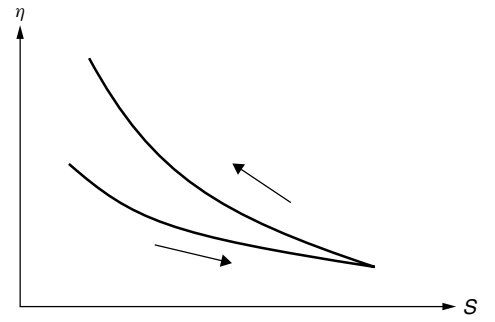

Figure 3.22 Flow behavior of rheopectic fluid under varying rates of shear

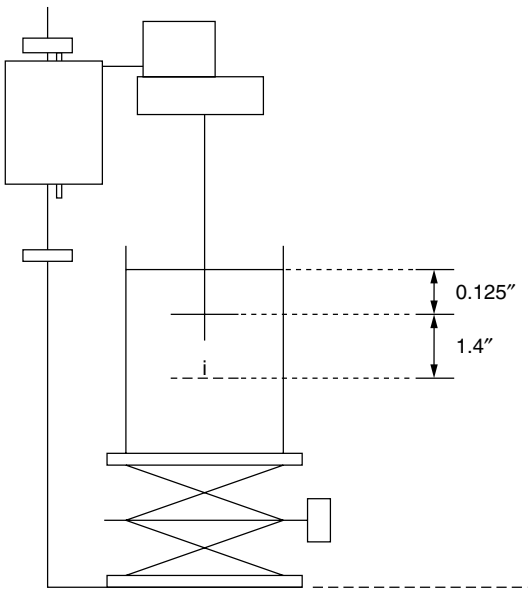

Figure 3.23 Schematic of Brookfield viscometer used for solder paste viscosity measurement

in the solder paste, and the viscosity is measured while the spindle is travelling up and down within the solder paste. The immersion depth, spindle travelling distance, and number of vertical travelling cycles have to be specified if the data is to be cross-compared.

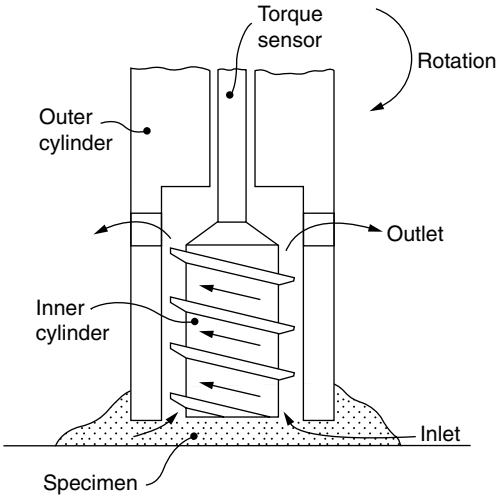

Figure 3.24 Schematic of a spiral pump viscometer used for solder paste viscosity measurement

Another type of viscometer also commonly used for solder paste applications is the spiral pump viscometer, as shown in Figure 3.24. Rotation of inner cylinder/sensor pumps the solder paste through the probe. The solder paste exits from the upper opening and falls back to the paste container.

Since the solder paste is often thixotropic in nature and has memory of paste handling, the viscosity reading is affected by the detailed measurement procedure, and is sensitive to the paste handling as well. The spiral viscometer appears to be less sensitive, and is considered to be more reproducible in viscosity measurement.

Measurement of viscosity should be conducted at a controlled temperature, since the viscosity of solder paste decreases with increasing temperature, as exemplified in Figure 3.25. Some solder pastes exhibit a fairly high sensitivity toward temperature, such as paste B, while other pastes may be less sensitive, such as pastes A and C.

3.6 Solder paste rheology requirement

The rheology of solder paste desired is application dependent. Bao and Lee [31] have reported that the rheology of a solder paste has a significant effect on its stencil printing, tack, and slump performance. Their work describes a series of tests designed to investigate the rheological properties of a series of solder pastes and fluxes, and correlation with the solder paste performance prior to reflow. Data indicate that (1) print defect is proportional to the compliance (J1 and J2) and inversely proportional to the elastic properties (G'/G'' and Recovery) and meta-rigidity (Yield Stress); (2) slump resistance is proportional to elastic properties (Recovery), solid characteristics (Stress $[G' = G'']$), and rigidity ($|G^*|$); (3) high elastic properties (Recovery), low compliance (J1 and J2), and low solid characteristics (Stress $[G' = G'']$) are required in order to achieve high tack value. Good correlation between fluxes and solder

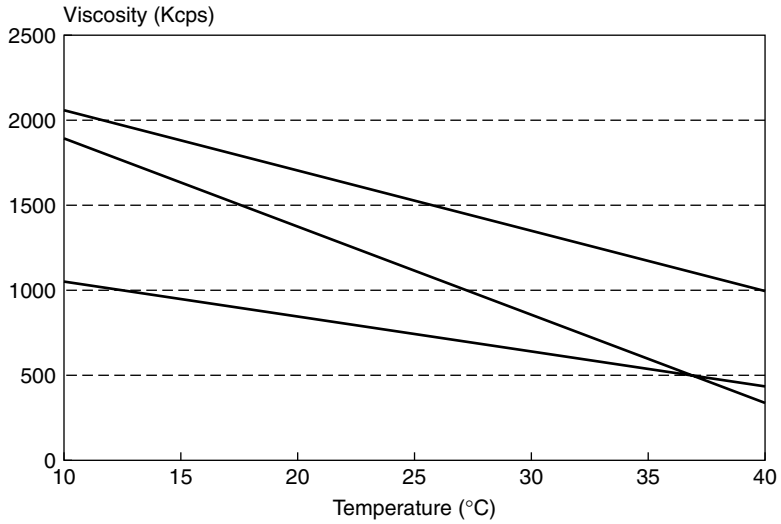

Figure 3.25 Viscosity of solder pastes as a function of temperature when measured with a Brookfield viscometer at 5 rpm

pastes are observed for Yield Stress and Recovery only, suggesting those two properties are primarily dictated by fluxes.

Trend 1 dictates that solder pastes with lower compliance (J1 and J2), higher elastic properties (G'/G'' and Recovery), and higher meta-rigidity (Yield Stress) are desired in order to minimize the print defect. Materials with lower compliance and higher meta-rigidity will have less tendency to ooze out underneath the stencil during printing, and therefore are less likely to be smeared. Higher elastic properties will help the material to pull together during stencil release, and hence will reduce the chance of clogging.

Trend 2 indicates that higher elastic properties (Recovery), higher solid characteristics (Stress [$G' = G''$]), and higher rigidity ($|G^*|$) will help in reducing slump. It is self-evident that an elastic material will be slump resistant. An elastic material may slump slightly but an equilibrium should be established very quickly and no further slump should occur. Higher solid characteristics and higher rigidity (high G' and high G'') will provide slump resistance via both high storage modulus and high loss modulus. Similar to the case of elastic properties, the high storage modulus contributes to slump resistance via its elastic nature. The high loss modulus will contribute to slump resistance via the kinetic mechanism, i.e. by slowing down the slumping process via high viscosity.

Trend 3 prescribes that high elastic properties (Recovery), low compliance (J1 and J2), and low solid characteristics (Stress [$G' = G''$]) are required in order to achieve high tack value. In general, tack is considered to be a function of both cohesion and adhesion. A high cohesion of material is required in order to prevent tack failure due to rupture through the material itself. On the other hand, a high adhesion is needed in order to avoid interfacial failure. Both high elastic properties and low compliance will contribute to high cohesion properties. A low solid characteristic could enhance the wetting between the solder paste and the devices, and accordingly improve adhesion.

The work of Bao and Lee indicates that a material with a high yield stress and a high elastic property is favored for stencil printing and dispensing applications. Since the solder paste needs to be low in viscosity during deposition but high in viscosity before and after deposition, a pseudoplastic material appears to be a better fit. However, the rheology of commercial solder pastes available is primarily thixotropic in nature, due to the difficulty in eliminating the effect of time on viscosity. Accordingly, the emphasis of this book in the field of solder paste rheology will be on thixotropic materials.

The thixotropy of solder paste can be quantitatively expressed as thixotropic index (TI), as shown in Figure 3.26 [19]. Here the log value of viscosity is plotted against the log value of shear rate, with the slope being defined as TI. It should be noted that the definition used here is widely accepted by the industry, but is not the only way to define TI. For instance, Harada has arbitrarily defined TI as the ratio of log viscosity at shear rate $1.8\,s^{-1}$ to the viscosity at $18\,s^{-1}$ [32]. By plotting the

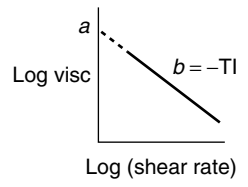

$Y = a + b * X$

Where Y = log value of viscosity
a = material constant
b = slope of the linear regression line for X and Y relation, equals (–TI)
X = log value of shear rate of viscometer

Figure 3.26 Definition of thixotropic index (TI) [19]

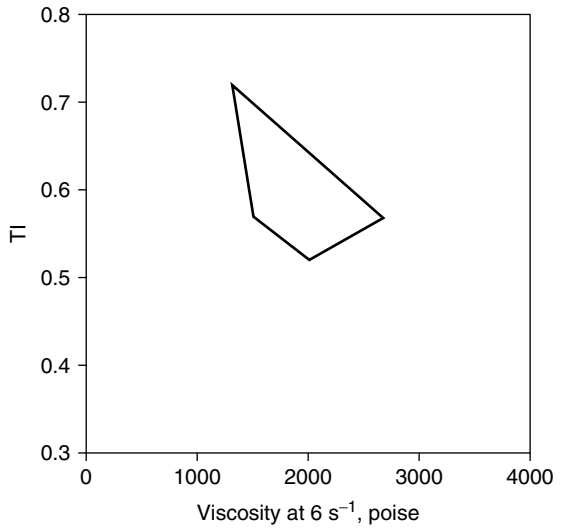

Figure 3.27 Harada operating window for good printing performance

TI value versus viscosity value determined at $6\,s^{-1}$ for a series of solder pastes, Harada observed that there is a "window" for good printing performance, as shown in Figure 3.27. Therefore, a solder paste with parameters that fit within the window generally performs well on printing. Since the optimum window is highly empirical and may vary with flux chemistry, solder powder size and content, stencil aperture design, as well as printing parameters, care should be taken before adopting any criteria for the purpose of solder paste selection. Harada also noticed that pastes with too much hysteresis are poorer in tolerating continuous working in production. This observation supports that a pseudoplastic material is considered a better fit for solder paste applications, as discussed earlier.

The flow of fluids is affected not only by the rheology of fluids but also by the physical environment of the fluid. For instance, the flow rate of fluid through a circular tube, such as solder paste being dispensed through a needle, can be expressed by the Hagen and Poiseuillie relation, as shown in Figure 3.28 [19]. This relation indicates that the dispensing rate is a strong function of the tube inner-diameter (ID). Hence by reducing the tube ID to $\frac{1}{2}$ in dimension, the volume flow rate will be drastically reduced to $\frac{1}{16}$ although the cross-sectional area of the tube opening is reduced only to $\frac{1}{4}$. In order to compensate for the decrease in volume flow rate, a low viscosity material, particularly a thixotroic material, is generally preferred.

3.6.1 Effect of composition on rheology

The rheological properties of solder paste are primarily determined by the flux chemistry. However, solder powder size and metal content also contribute to the rheological behavior, as discussed below.

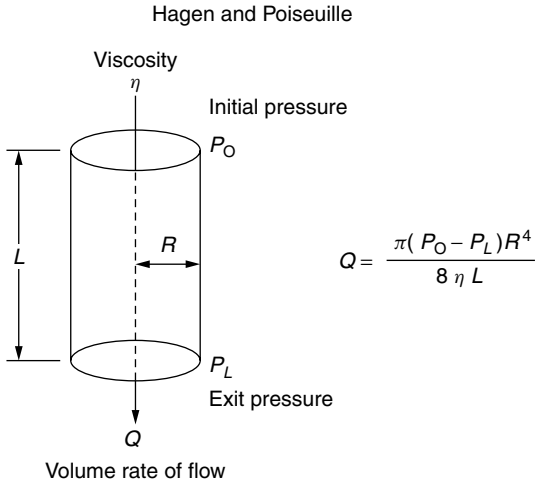

Figure 3.28 Flow through a circular tube

3.6.1.1 Effect of metal load

Generally, solder paste can be regarded as a composite system. Since the volume content of filler, or solder powder, appears to be more meaningful for a structure–property correlation study of a composite system, all the relations will be based on the volume content parameter. Figure 3.10 shows the relation between metal weight content and metal volume content for the Sn63-containing solder pastes. The volume content of solder first increases slowly, then rises rapidly with increasing solder weight content. The rapid rise of volume content results in an even more rapid rise in viscosity of paste, as shown in Figure 3.29 [27].

Theoretically, the maximum powder volume content is 74 percent for a monodispersed sphere system with a face centered cubic packing structure, or 68 percent for a body centered cubic packing structure. Solder powder, although it exhibits a broader size distribution, displays a considerably lower packing density. The tap density of Sn63 solder powders typically is about 4.9 gm/cm^3, and is not sensitive to powder size distribution. This tap density is equivalent to 59 percent solder volume occupancy. For the solder paste used here, a 59 percent solder volume content is equivalent to 92.5 percent metal content. In other

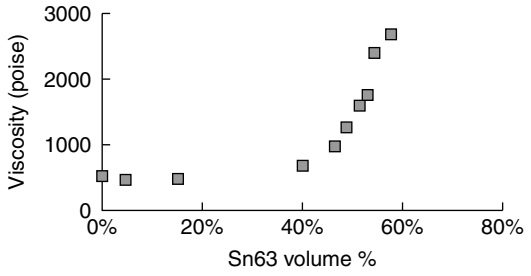

Figure 3.29 Relation between viscosity and metal volume content of Sn63 solder paste

words, 92.5 percent (w/w) is the maximum metal load allowed for pastes. Therefore, this rapid increase in viscosity for solder content beyond 50 percent (v/v), or 89.5 percent (w/w), can most likely be attributed to the onset of formation of powder clusters. As a result, the viscosity of a high metal load paste starts being dictated by the solder powder continuity, and variation in the flux/vehicle viscosity will have a relatively minor effect on the paste viscosity.

Figure 3.30 shows the effect of solder volume content on TI. It is interesting to note that the TI decreases first, then increases with increasing solder volume content. The turning point occurs at around 50 percent solder volume. The initial decrease in TI can be attributed to the dilution effect of the thixotropic flux/vehicle by the powder. The increase of TI with increasing metal content can be attributed to the pseudo-thixotropic-additive effect of the powder cluster network [27]. It indicates that the TI value can be regulated through metal content adjustment for further improvement in printability.

3.6.1.2 Effect of powder size

The size of solder powder also plays a significant role in paste rheology. Figure 3.31 shows that the viscosity increases with decreasing powder size [27]. This can be explained by the increasing particle surface area associated with finer powder. It results in an increasing interaction force between flux and powder, and consequently a higher viscosity. In the case of thixotropic property, the finer powder results in a lower TI value, as indicated by Figure 3.32 [27] Again, this can be attributed to the greater interaction force between flux and the finer particles. This interaction force, being primarily a surface adsorption phenomenon, is believed to be non-thixotropic in nature. Since it contributes to the paste's viscosity, the material is accordingly expected to be less thixotropic. Hence, the finer powder needed for ultra-fine-pitch printing will increase the paste's viscosity and decrease the thixotropic property. Assuming that the "Harada Operating Window" is also applicable to ultra-fine-pitch printing, both influences would require more from the flux/vehicle rheology development to compensate for the changes caused by using finer powder.

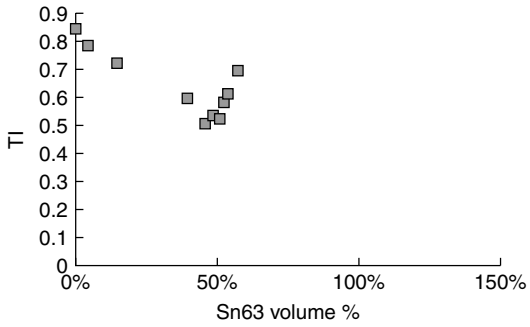

Figure 3.30 Relation between metal volume content and TI of Sn63 solder paste

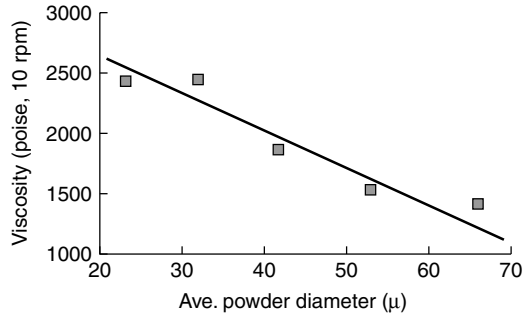

Figure 3.31 Relation between powder size and viscosity of Sn63 solder paste

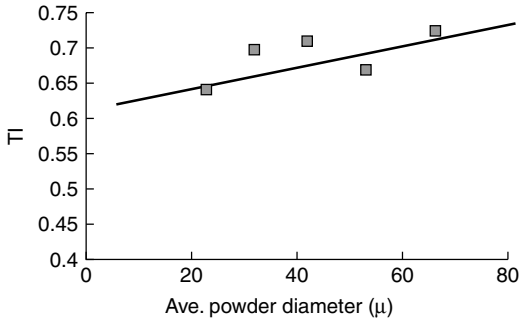

Figure 3.32 Relation between powder size and TI of Sn63 solder pastes with 90.5 percent metal content

Overall, paste rheology can be further optimized by varying the metal load and flux rheology for better printability in an ultra-fine-pitch application. The fine powder size required for good printability, in contrast, places a burden on the rheology improvement effort.

3.7 Conclusion

Solder paste is the vital element in surface mount technology. Its creamy characteristics enable the use of an automated deposition process. Solder paste serves as a temporary glue during component placement and forms a permanent electrical and mechanical interconnect after the soldering process. The fluxing chemistry employed includes acid–base reaction as well as oxidation–reduction, with the former being the primary system used for SMT applications. Thixotropic rheology prevails, although the hysteresis caused by the memory of paste shearing may result in too low a viscosity and accordingly limited production working time. Evolution of solder paste technology not only supports the continuous miniaturization of surface mount industry, but also promises the implementation of low cost solder bumping processes.

References

1. M. Nasta and H. C. Peebles, "A Model of the Solder Flux Reaction: Reactions at the Metal/metal oxide/electrolyte Solution Interface", *Circuit World*, Vol. 21, No. 4, pp. 10–13 (July 1995).
2. R. T. Ludwig, Indium Corporation of America internal technical report, 2 December 1999.
3. P. G. Harrison, *Chemistry of Tin*, Blackie (1989).

4. P. Fodor and P. J. Lensch, ''Cover Gas Soldering Leaves Nothing to Clean Off PCB Assembly'', *EP&P*, pp. 64–66 (April 1990).
5. J. S. Hwang, ''Have You Heard of ROSA or PADS?'' *SMT*, pp. 14–16 (June, 1994).
6. D. M. Tench, D. P. Anderson, P. Jambazian, P. Kim, J. White, D. Hillman, G. K. Lucey, T. Gher, and B. Piekarski, ''A New Reduced-Oxide Soldering Activation Method'', *JOM*, pp. 36–41 (June 1995).
7. D. M. Tench, D. P. Anderson, P. Jambazian, P. Kim, J. White, D. Hillman, D. Frommelt, G. K. Lucey, T. Gher, and B. Piekarski, ''Reduced Oxide Soldering Activation (ROSA) Production Compatibility Evaluation'', *Soldering & Surface Mount Technology*, No. 19, pp. 18–25 (February 1995).
8. J. H. Lau (ed.), *Flip Chip Technologies*, McGraw-Hill, New York, (1996).
9. K. Koopman, ''Fluxless Soldering Gaining Followers'', *Circuits Assembly*, Vol. No. 7, pp. 48, 50 (July 1996).
10. Merck Index, 11th edn, Merck & Co., Rahway, NJ (1989).
11. C. Lea, *After CFCs?* Electrochemical Publications, Isle of Man, UK (1992).
12. I. Artake, U. Ray, H. M. Gordon, and M. S. Gervasio, ''Thermal Degradation of Rosin During High Temperature Solder Reflow'', AT&T Bell Laboratories report, 1992.
13. L. F. Feiser and M. Feiser in *Natural Products Related to Phenanthrene*, Chapter 2, Reinhold Publishing Corp., New York (1949).
14. J. Simonsen and D. H. R Barton, in *The Terpenes*, Vol III, Chapter V, Cambridge University Press, New York (1961).
15. B. A. Parkin Jr, W. H. Schuller, and R. V. Lawrence, *I&EC Product Research and Development*, Vol. 8, p. 304 (1969).
16. J. March in *Advanced Organic Chemistry*, 3rd edn, John Wiley, New York (1985).
17. R. Stewart, *Oxidation Mechanisms*, p. 14, Benjamin, New York (1964).
18. C. R. Martens (ed.) in *Technology of Paints, Varnishes and Lacquers*, p. 390, R. E. Kreigler Publishing Inc., New York (1974).
19. N. C. Lee, ''How to Make Solder Paste Work in Ultra-fine-pitch and Non-CFC Era'', short course at Surface Mount International, San Jose, CA (September 1994).
20. Chemicals banned by IBM, according to IBM Engineering Specification ''Environmental Specification for Vendor-Supplied Parts and Materials'' PN 99F6961 (10 November 1993).
21. Banned chemicals at Hewlett-Packard Bolingon, Germany (1995).
22. Chemicals listed as ''Developmental Toxicity'' and ''Male Reproductive Toxicity'' per California law ''Proposition 65'', 1986.
23. Controlled substances required to be reported at concentration greater than 1 percent wt/wt, per Canada SOR/DORS/88–66.
24. A. Lawley, *Atomization – The Production of Metal Powders*, Metal Powder Industries Federation, Princeton, New Jersey (1992).
25. J-STD-006, ''General Requirements and Test Methods for Electronic Grade Solder Alloys and Fluxed and Non-Fluxed Solid Solders for electronic Soldering Applications'' (1994).
26. N. C. Lee, Market study of Indium Corporation of America (1999).
27. M. Xiao, K. J. Lawless, and N. C. Lee, ''Prospects of Solder Paste Applications in Ultra-fine Pitch Era'', in *Proc. of Surface Mount International*, San Jose, CA (August 1993).
28. Product data sheet of Ross Corporation.
29. *Webster's New World Dictionary of the American Language*, 2nd college edn (1971).
30. ''More Solutions to Sticky Problems – A Guide to Getting More from your Brookfield Viscometer'', Literature of Brookfield Engineering Laboratories, Inc., AG6000, 20 M, 5/85.
31. X. Bao and N. C. Lee, ''Engineering Solder Paste Performance Via Controlled Stress Rheology Analysis'', in *Proc. of Surface Mount International*, San Jose, CA, September 1996.
32. W. Rubin and M. Warwick, ''Some Developments in Solder Cream Technology'', *Journal of SMT*, pp. 17–24 (April 1990).

4 Surface Mount Assembly Processes

Surface mount assembly is primarily a process of reflow soldering, as shown in Section 1.1.3 of Chapter 1. It involves deposition of solder paste, component placement, reflow, and possibly wave soldering and cleaning. Although detailed SMT processes may involve more processes such as surface mount adhesive dispensing and curing, the emphasis of this chapter will be on the processes and equipment involving solder paste.

4.1 Solder paste materials

4.1.1 Paste handling and storage

In general, solder paste is relatively sensitive to exposure to heat, air, or humidity. Heat may not only cause reaction between flux and solder powder, but may also result in a separation of flux and solder powder. Exposure to air and humidity will result in drying, oxidation, and moisture pickup. Typically, solder paste is recommended to be stored in a freezer or refrigerator. For storage of solder paste in a cartridge, a vertical orientation with the nozzle pointing downward is preferred to minimize the impact of any flux separation. Prior to exposing the paste to open air, the temperature of the paste should be brought to ambient temperature to avoid moisture condensation. Depending on the container size and the storage temperature, the time needed for the thawing process may range from one to several hours. Jaeger [1] showed that, for refrigerated solder paste, one hour is sufficient for 500 gram paste in a jar or 700 gram paste in a cartridge to be thawed properly when placed on a table under ambient temperature, as shown in Figure 4.1.

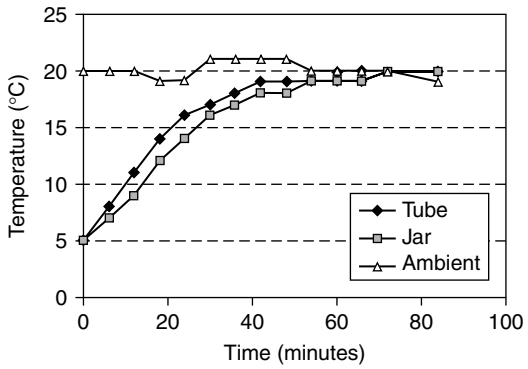

Figure 4.1 Time for refrigerated solder pastes to reach room temperature [1]

4.1.2 Paste deposition

The most commonly used solder paste deposition process is stencil printing, although other technologies are also used, including dispensing, pin-transferring, and roller-coating.

4.1.2.1 Stencil printing

Stencil printing evolves from the screen printing process. Compared with the screen (see Figure 4.2) use of a stencil allows more precise control of the solder paste volume deposited, therefore a finer pitch application. The stencil printing process can be schematically illustrated by Figure 4.3. A stencil is typically formed of metal foil with a pattern of aperture matching the footprint on the PCB where deposition of solder paste is desired. This stencil is placed on top of the PCB with patterns registered properly. The solder paste is then deposited onto one side of the stencil, followed by being wiped across the stencil with the use of a squeegee. The PCB is then detached from the stencil, with solder paste deposited on top of the corresponding pads.

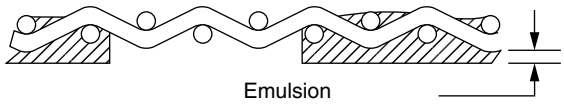

Figure 4.2 Schematic of a screen used in the solder paste printing process

The printing process is the most commonly used solder paste deposition technology. Compared with many other technologies, it promises a higher speed, higher throughput, better pattern registration, and better solder paste volume control. More details on stencil printing technology will be discussed in a later section. The constraint of using the stencil printing process is the requirement of a flat substrate surface for the stencil to be laid on.

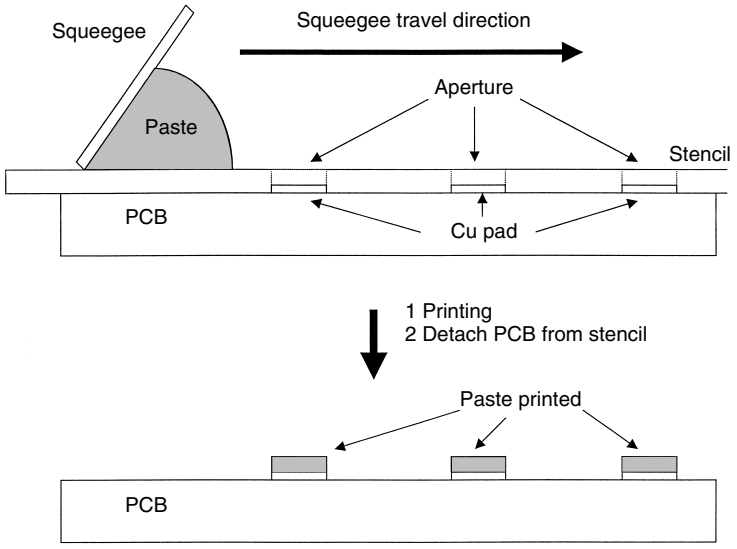

Figure 4.3 Schematic of the stencil printing process

This limits the potential of using the printing process for rework purpose or for a soldering task on a non-flat surface.

Depending on the flux chemistry, solder paste used for stencil printing often ranges from 800 to 1000 Kcps in viscosity, with a metal load 88–91 percent for a eutectic Sn–Pb alloy. The powder size employed typically is no larger than 1/7 of the aperture size if a low printing defect is desired [2]. Solder pastes used for screen printing are typically slightly lower in both viscosity and metal content than those for stencil printing. Screen printing does not provide as precise paste volume control as stencil printing, hence it is rarely used for fine-pitch applications.

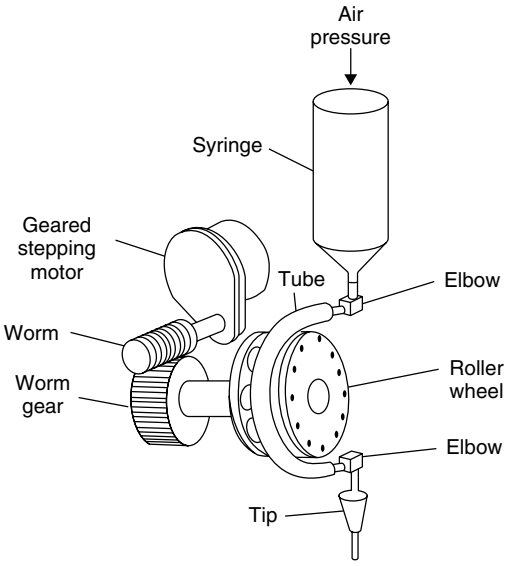

Figure 4.4 Schematic of pneumatic roller wheel dispenser [3]

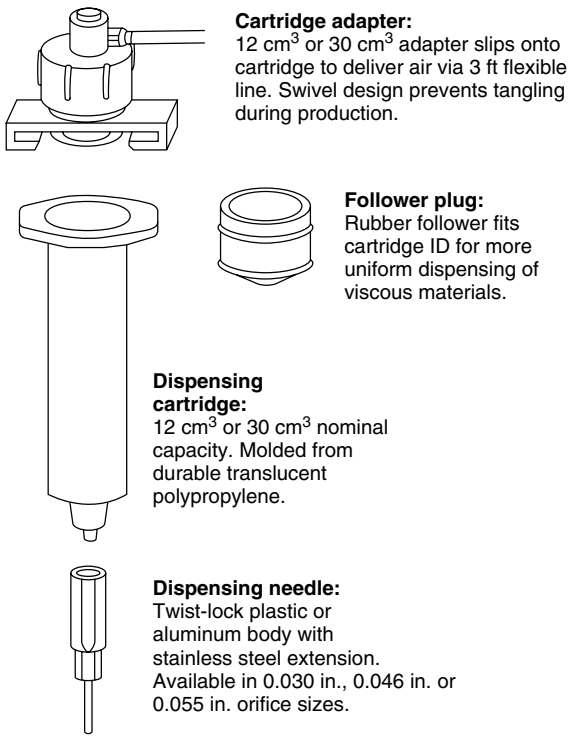
Cartridge adapter:
12 cm3 or 30 cm3 adapter slips onto cartridge to deliver air via 3 ft flexible line. Swivel design prevents tangling during production.
Follower plug:
Rubber follower fits cartridge ID for more uniform dispensing of viscous materials.
Dispensing cartridge:
12 cm3 or 30 cm3 nominal capacity. Molded from durable translucent polypropylene.
Dispensing needle:
Twist-lock plastic or aluminum body with stainless steel extension. Available in 0.030 in., 0.046 in. or 0.055 in. orifice sizes.

Figure 4.5 Schematic of time/pressure pneumatic dispenser [4]

4.1.2.2 Dispensing

The dispensing process deposits solder paste by forcing the paste through a needle for paste registration and volume control. Some commonly used dispensing mechanisms include a pneumatic roller wheel dispenser (see Figure 4.4 [3]), a time/pressure pneumatic dispenser

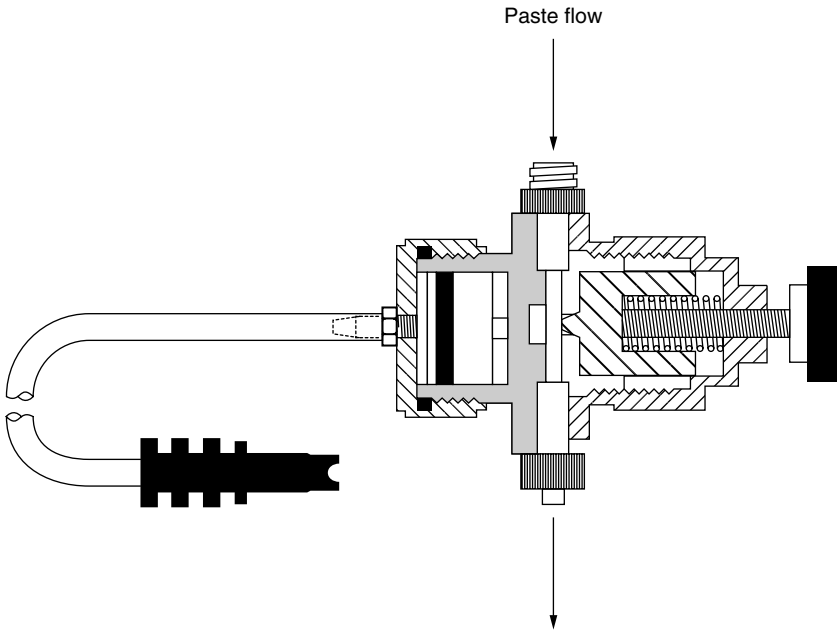

Figure 4.6 Schematic of time/pressure pinch valve pneumatic dispenser [5]

(see Figure 4.5 [4]), a time/pressure pinch valve pneumatic dispenser (see Figure 4.6 [5]), an Auger type with an Archimedes screw dispenser (see Figure 4.7 [6,7]), a tubing-squeezing positive displacement dispenser (see Figure 4.8 [8]), and a piston positive displacement dispenser (see Figure 4.9 [6,7]).

The pneumatic roller wheel dispenser is good for handling large volume of continuous solder paste deposition applications, but falls short in handling small volume deposition. Both types of time/pressure pneumatic dispenser provide some flexibility in controlling solder paste volume to be dispensed, with the pinch valve version being more precise in control. The precision level provided by these time/pressure dispensers may be acceptable for coarse pitch SMT applications. An Archimedes Metering Valve type offers even higher precision than that of pinch valve, and is acceptable for fine-pitch applications. Tubing-squeezing and piston positive displacement systems offer the highest precision in small volume control, and are considered more adequate for fine-pitch applications.

The dispensing process is a very versatile tool for addressing the need of reflow soldering on a non-flat surface. Often it is used for component manufacturing or rework. It may also be used for reflow soldering some manually placed components, such as edge connectors.

Solder paste used for the dispensing process typically exhibits a viscosity of 300–600 Kcps, with a particle size no larger than 1/10 of needle ID. The metal load employed ranges from 85–88 percent w/w for eutectic Sn–Pb, depending on the needle ID and particle size. For high Pb solder alloys, the metal content may be higher due to the greater density of solder alloys. On the other hand, for indium-containing alloys, the metal content is often lower, due to the tendency of cold welding of the soft solder powder during dispensing.

4.1.2.3 Pin-transferring

For small objects with a relatively coarse pitch pattern, pin-transfer (see Figure 4.10 [9]) solder paste deposition may be a better choice in terms of speed. In this process, a matrix of pins is mounted on a base-holder with a pattern of pins matching that of the footprint of pads to be soldered. On the other hand, a solder paste is spread and leveled on a flat bed with a controlled paste thickness. This matrix of pins is then dipped into the solder paste, followed by lifting the pins, with the solder paste wrapped around the tip of the pins. These pins with solder paste are then stamped onto the footprint of the pads, with the solder paste transferred from the pin tip to the pads, followed by lifting the pins for the next cycle.

As in dispensing, the solder paste used for the pin-transfer process is typically low in both metal content and viscosity. The paste also has to be fairly non-hygroscopic and drying resistant in order to be consistent in viscosity upon constant exposure to ambient environment.

4.1.2.4 Roller coating

Roller-coating is a special type of solder paste deposition, mainly used for component manufacturing, such as leaded chip capacitors. As shown in Figure 4.11 [9], a 2-in. cylindrical roller is mounted with a solder paste reservoir, with a spacing of approximately 0.030–0.040-in. between the reservoir wall and the roller surface. Upon rotation, the roller drags the solder paste out of the reservoir and forms an even paste film on the surface of the

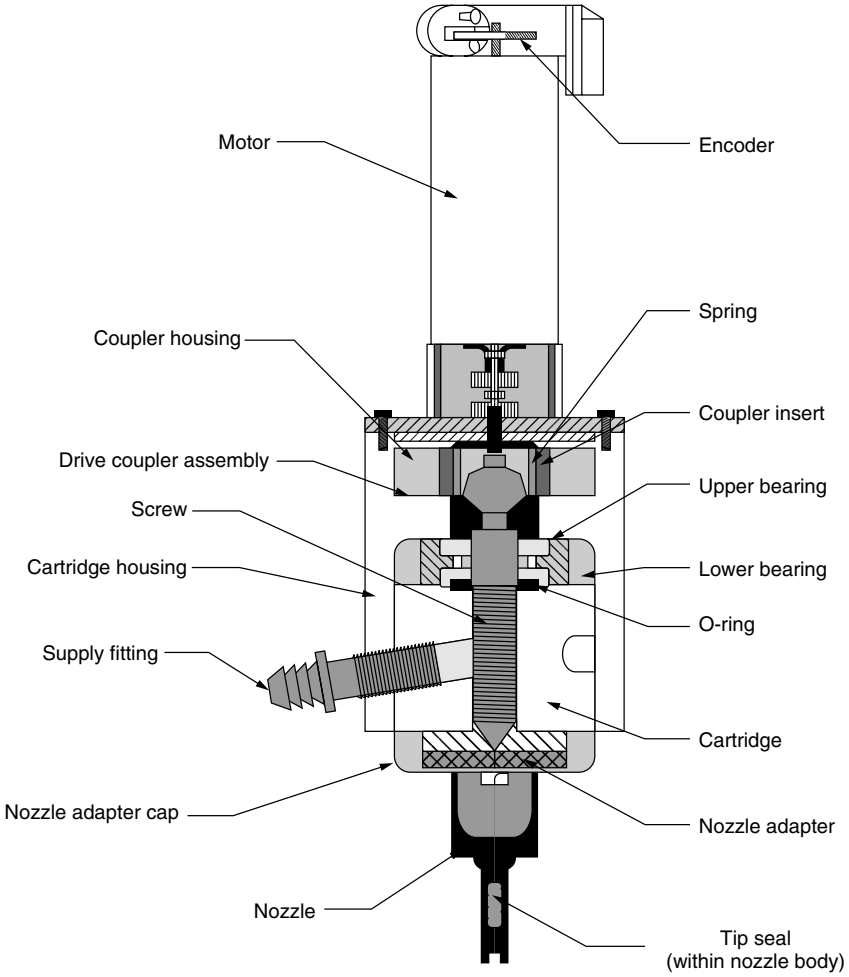

Figure 4.7 Auger type with Archimedes screw dispenser [6,7]

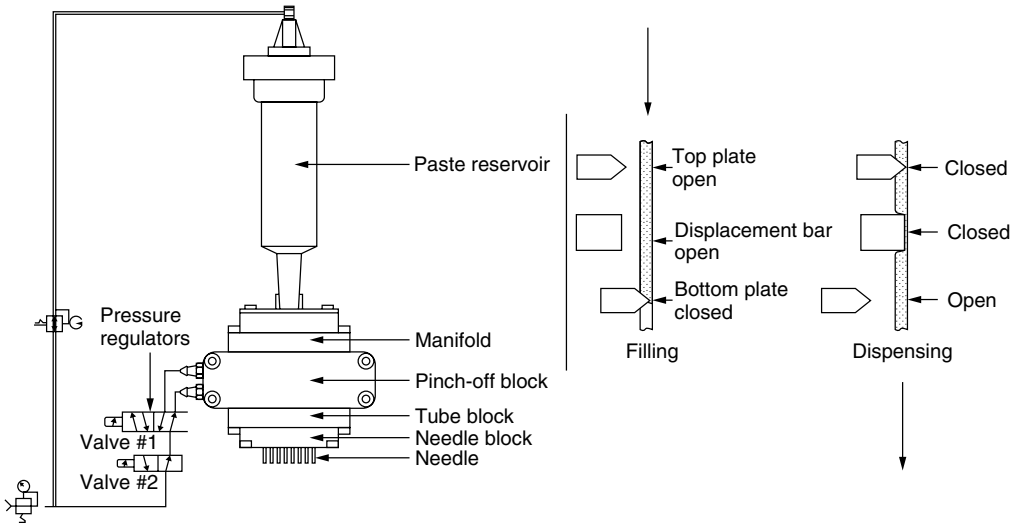

Figure 4.8 Schematic of tubing-squeezing positive displacement dispenser diagram [8]

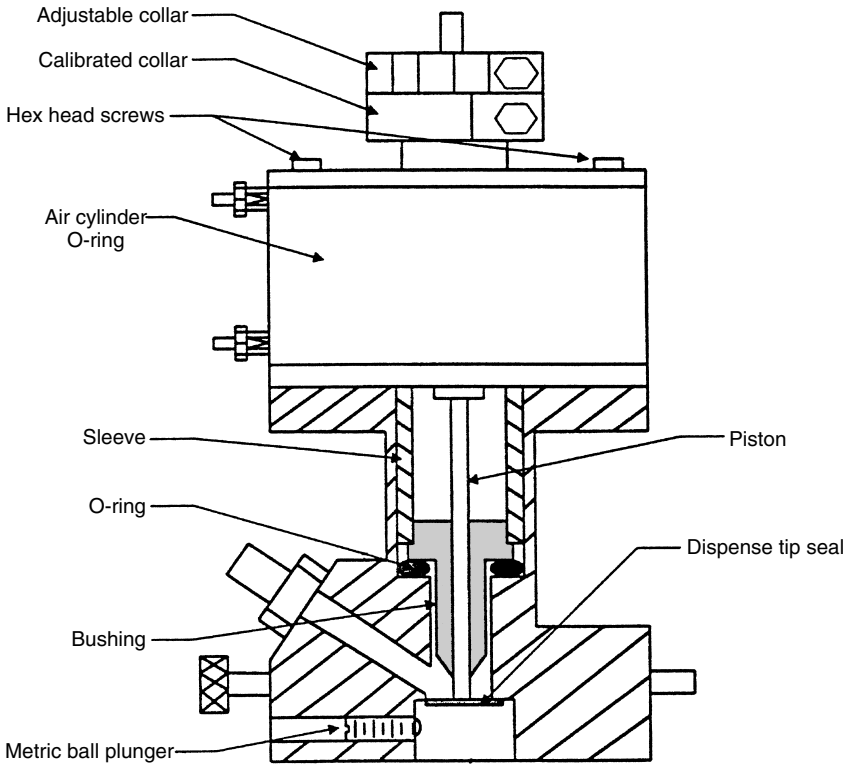

Figure 4.9 Piston positive displacement dispenser [6,7]

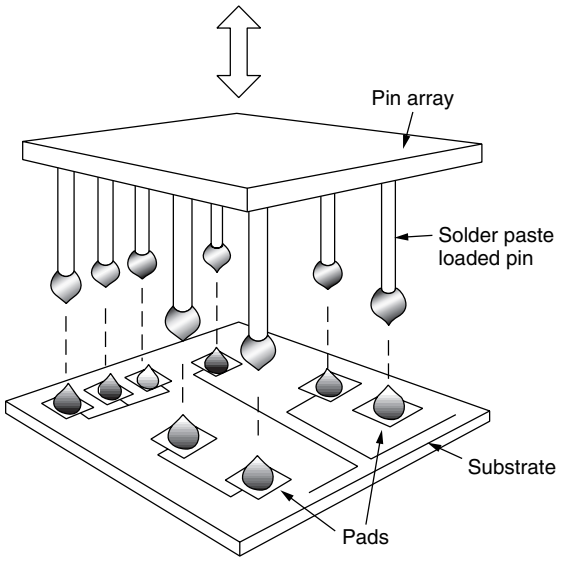

Figure 4.10 Pin-transfer process [9]

roller, with the film thickness being governed by the adjustable spacing. An array of nail-head leads on a carrier is conveyed across the bottom of the roller at a speed synchronized with the roller rotation speed. The conveyor is set at a height so that the nail-head tip almost reaches the roller surface. As a result, the nail-head immerses in the solder paste film as it is passing through the bottom of the roller, then detaches from the paste film with some paste being picked up by the nail-head. Two nail-head leads with paste coated on the tips are then aligned and assembled onto both ends of the capacitor, followed by the reflow soldering process.

Other versions of the roller coating process have also been developed. For instance, one design deposits solder paste onto the tops of pins which have been inserted into a PGA ceramic substrate. The paste film formed on the roller is about 2–3 mils in thickness. After paste deposition, the paste is then reflowed so that the pins are solder-bonded onto the Cu thick film on the PGA substrate.

Solder paste used for the roller coating process has to be fairly low in both metal content and viscosity. The viscosity typically is lower than 200 Kcps in order to allow reasonable paste pick-up. Since the paste is constantly being well exposed to ambient atmosphere during the deposition stage, it has to be non-hygroscopic, drying-resistant, and stable against oxidation.

4.2 Printer level consideration

At printer level, the most important factors affecting solder paste printing performance include stencil materials, stencil forming technology, pattern design, squeegee type,

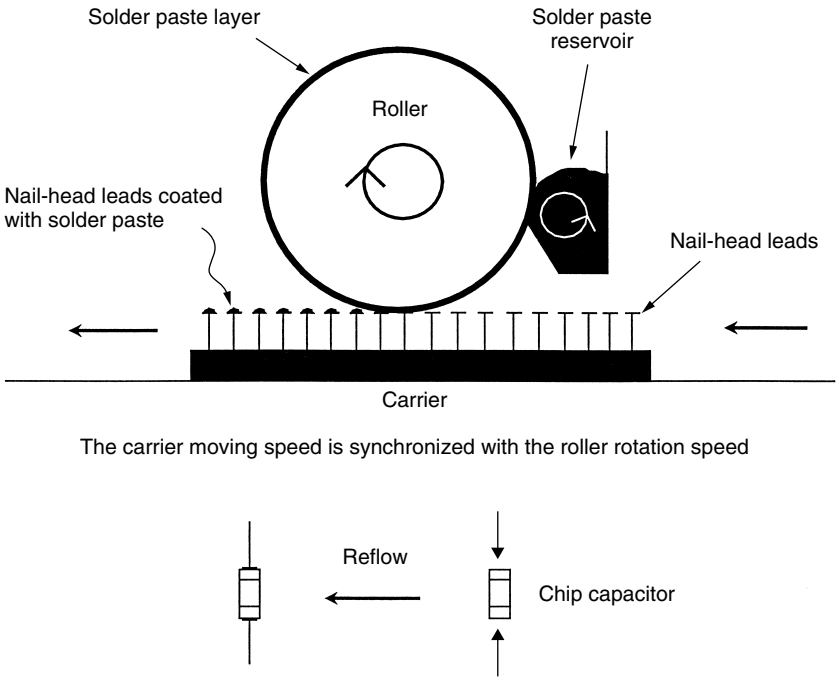

Figure 4.11 Schematic of roller coating process [9]

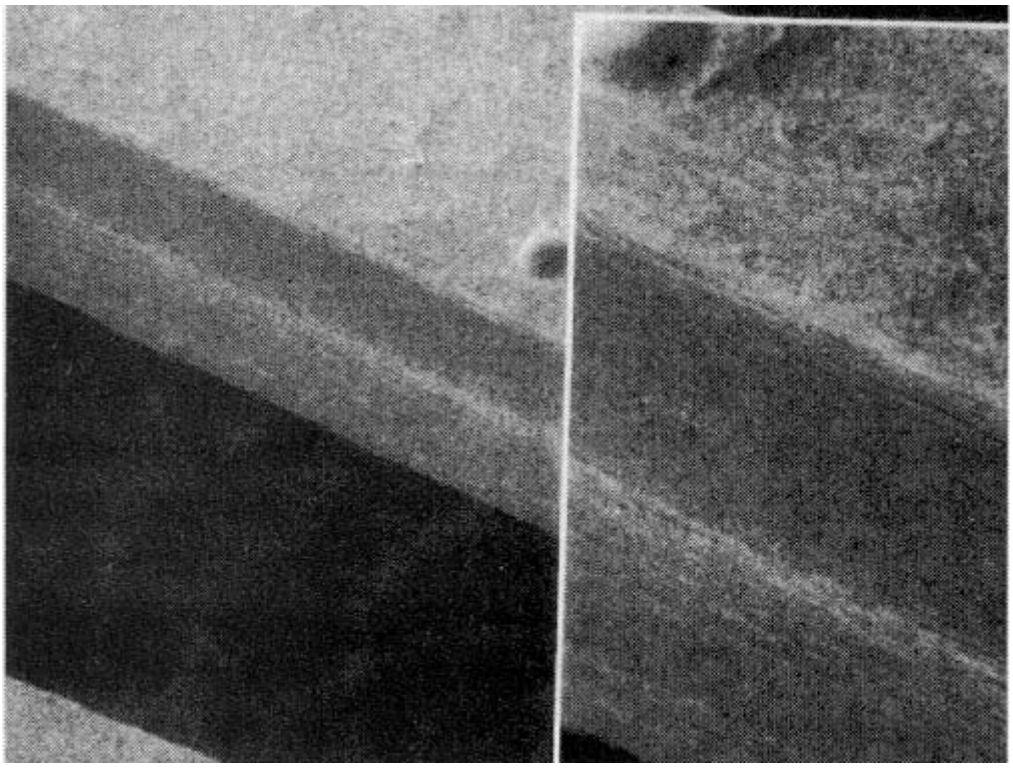

Figure 4.12 Molybdenum stencil [10–12]. (From M. D. Herbst, ''Metal Mask Stencils for Ultra Fine Pitch Printing'', in *Proc. of Surface Mount Technology*, San Jose, CA, pp. 101–109 (29 August–2 September 1993): reprinted by permission.)

and printing setting, as will be discussed in the following sections.

4.2.1 Stencil

4.2.1.1 Stencil materials

Depending on cost considerations and the stencil forming technology chosen, the materials used for stencil include brass, stainless steel, molybdenum, nickel, and plastics, as shown in Table 4.1. Stainless steel and brass are the most commonly used materials for the chemical etching process. Molybdenum stencil (see Figure 4.12) is produced by similar processes to chemically etched brass and stainless steel with a different and more hazardous etchant solution. Molybdenum has been promoted as an alternative metal to stainless steel or brass due to its denser grain structure which reportedly will improve solder paste release from the stencil [10–12]. Nickel is the material of choice for electroforming technology, due to chemistry requirements. For laser cut technology, stainless steel is the primary choice. Recently a plastics material, KEPOCH, has been introduced [13] for the laser cut process, as shown in Figure 4.13. The primary advantages claimed for the KEPOCH stencil system are low cost, 6 hours' turn around time, easy stencil cleanability, better stencil release, and better resistance against stencil deformation or denting.

Table 4.1 Comparison of stencil manufacturing technology and cost [9]

Manufacturing technology	*Type*	*Material*	*Cost ($)*
Chemical etch	Conventional	Stainless steel	325
		Brass	325
		Molybdenum	475
	Band-etch	Stainless steel	370
Electroform		Nickel (only)	1500
Laser cut		Stainless steel	1500
		Plastics	450
Extra treatment	Electropolish	Stainless steel (only)	60
	Nickel plating	Brass (only)	75
	Step down	Stainless steel	100
		Brass	100

4.2.1.2 Stencil forming technology

The most commonly used method is chemical etch technology [10,14]. The process includes (1) cleaning metal, (2) applying photoresist, (3) imaging photo tool, (4) developing, (5) etching, and (6) removing photoresist, as shown in Figure 4.14. However, a 50 : 50 chemically etched opening often suffers the hourglass profile problem, as shown in Figure 4.15 [15]. The presence of the hourglass profile hinders the release of solder paste. The typical hourglass taper will measure less than 0.0005 in. The smallest opening size achievable versus stencil thickness is a ratio of 1.3 to 1.5, although some stencil manufacturers claim to have a capability up to a ratio of 1.1–1.2. During the dual-sided etching process, the etchant etches not only in a vertical direction but also laterally, therefore the original artwork must be compensated to account for lateral etching. Normal etch compensation calls for reducing pad

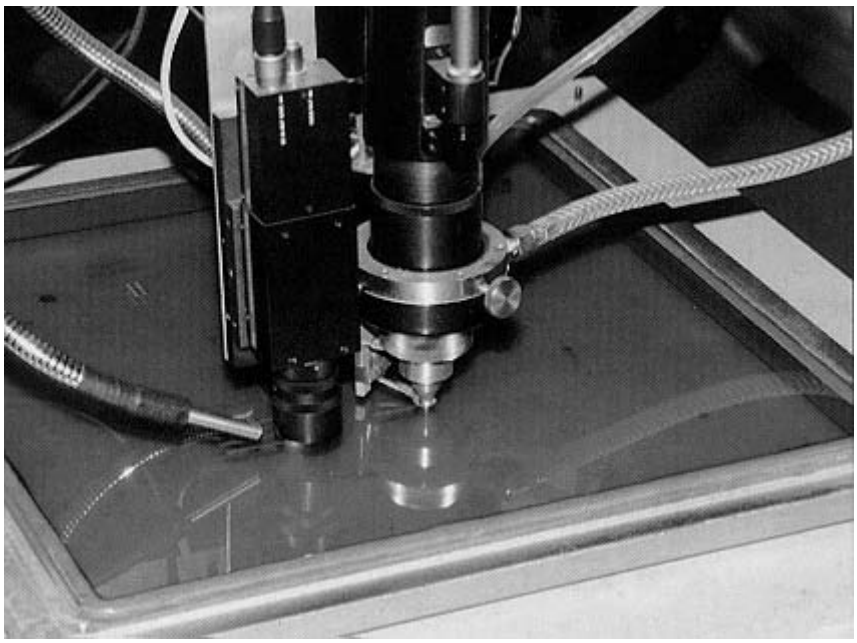

Figure 4.13 KEPOCH plastics laser cut stencil. (From Technical Data Sheet of K. J. Marketing Services, 1999: reprinted by permission.)

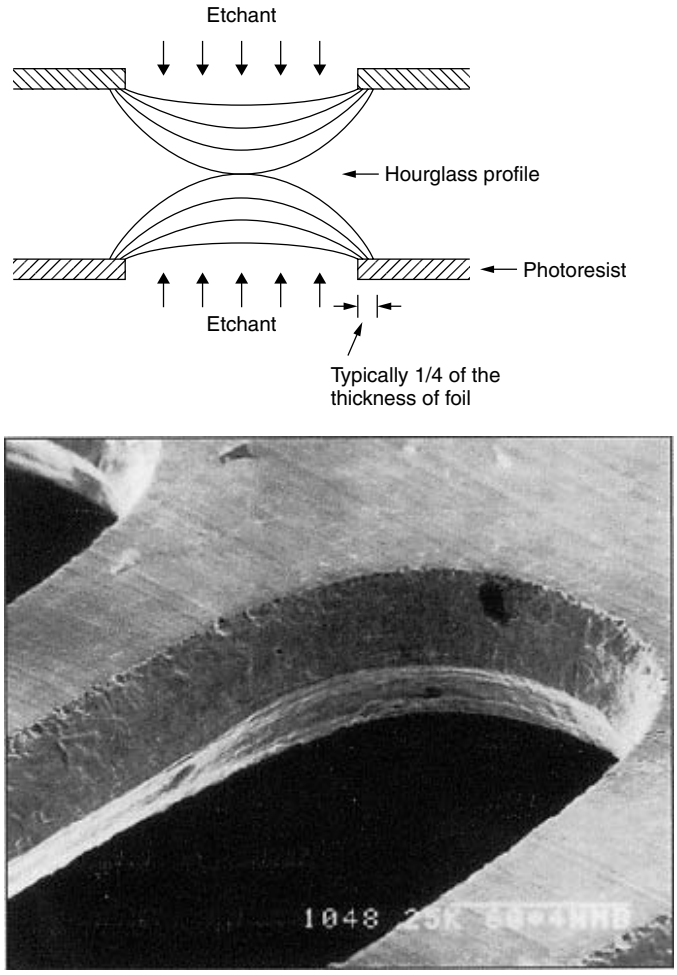

Figure 4.14 Chemical etch process and aperture [10,14]

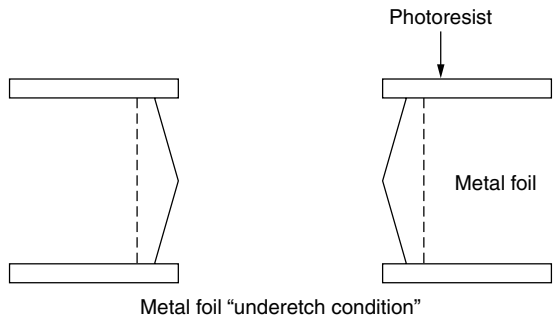

Figure 4.15 Metal foil with underetched aperture [15]

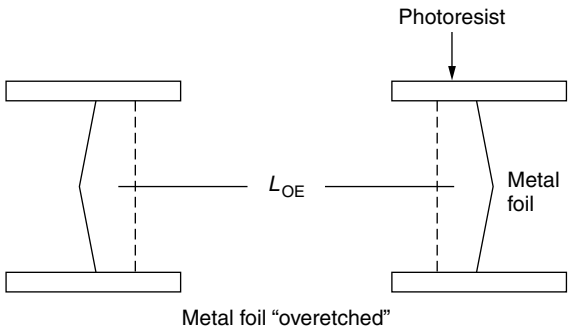

Figure 4.16 Metal foil with overetched aperture [15]

opening by half the thickness of the stencil foil. Besides the hourglass profile caused by underetching, there are other problems encountered during the chemical etch. These include overetching, rounded pad opening, and misregistered phototool, as shown in Figures 4.16–4.18, respectively [15]. All these stencil defects will result in a poor release of solder paste from the aperture.

Phototools are a key component in the chemical etching process. However, the film will shrink or expand with fluctuations of temperature and humidity, and this will affect the accuracy of registration. Etching tolerance can vary from +/−0.0005 to 0.002 in., depending on the stencil thickness, and can create a fairly large overall variation.

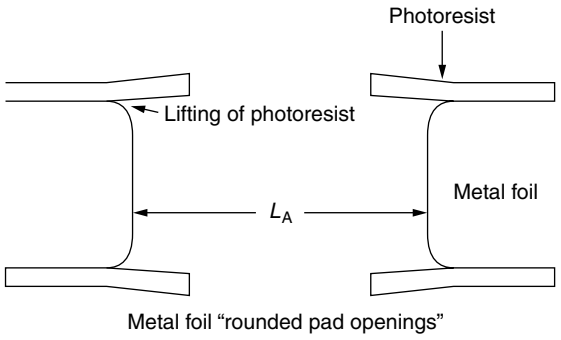

Figure 4.17 Metal foil with rounded pad openings [15]

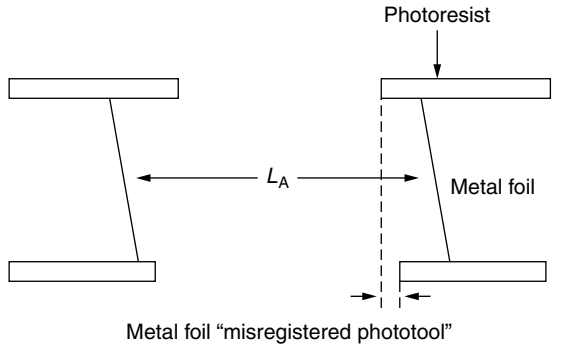

Figure 4.18 Metal foil with misregistered phototools [15]

The chemical etch process is cheap and adequate, hence preferred, for non-fine-pitch applications. When the pitch becomes finer, the quality of aperture gradually declines. To address this limitation, band etch stencil technology has been developed to extend the potential of chemical etch technology toward finer pitch applications. Figure 4.19 shows the characteristics of band etching technology [16], where a thin sharply etched band is formed around each aperture. A band width of 5–6 mil is typical for 25 mil pitch or higher. Narrower band width is possible for finer pitch.

The laser cut stencil process involves (1) processing Gerber data, and (2) cutting image [10,17]. Typically stainless steel or other low zinc content materials are used. Common problems exhibited are a saw-toothed edge or dross buildup on the stencil surface. Post-cutting processing such as electropolishing is able to remove the dross buildup. The minimum feature size and tolerances for laser are a function of the beam configuration and machine parameters. Typical minimum aperture size is 0.002 to 0.004 in., with a tolerance of +/−0.00025 to 0.0003 in. Both straight and tapered (0.001-in.) apertures are easily achievable. Figure 4.20 shows a laser cut stencil aperture [17]. Being sequential in processing, the cost of laser cut stencil increases with increasing number of apertures. When a pattern with mixed pitches is desired, the stencil is often made by using chemical-etch for the non-fine-pitch area, followed by laser cut for the fine-pitch area in order to minimize the cost and maximize stencil quality.

Electropolishing is a secondary micro etching procedure applied to the stainless steel after the primary aperture forming process has been completed [10]. The process for electropolishing is placing the chemical etched or laser cut stencil in a tank containing alkaline or acidic solution and introducing an electric current into the solution. Electropolishing will remove the high points and rough points from the stencil surface hence creating a shiny surface. The process has been promoted as being able to improve on the solder paste release from the fine pitch openings. However, too shiny a surface may result in skipping, hence improper rolling of the solder paste during printing. This problem is resolved by selectively polishing the aperture walls without polishing the surface of the stencil. Typically, electropolishing increases the aperture size by about 1 mil which must be included when performing etch compensation. A comparison of

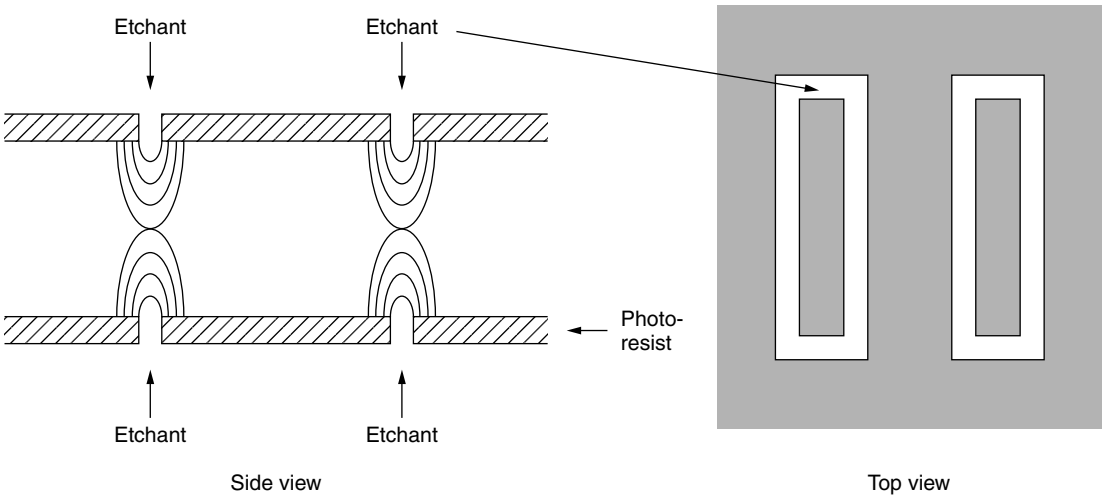

Figure 4.19 Schematic of band etch stencil technology [16]

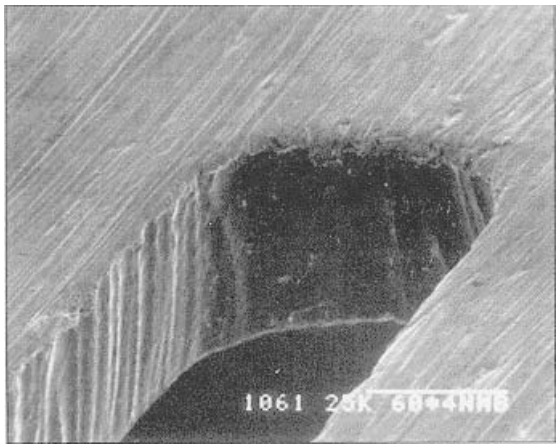

Figure 4.20 Laser cut stencil aperture [17]

aperture walls before and after electropolishing is shown in Figure 4.21 [18].

Electroforming is an additive process [10,17]. A mandrel is used as a base for the photoresist application and for resolution of the image. The mandrel is then placed in a bath where Ni is plated. The opening will be formed around the photoresist until the desired thickness of the stencil has been achieved. The definition and tolerances of electroforming are better than the chemical etching process. However, it should be noted that nickel is soft and more prone to damage. A smooth wall, presumably plus low surface tension of Ni may favor paste release from the aperture. The surface tension effect may be questionable in the paste release process. The surface may also be too smooth to allow for a proper paste rolling action. The permanent gasket formed is expected to reduce paste bleedout. The stencil thickness ranges from 0.001 to 0.012 inch, with minimum aperture width being 1.1 × thickness. Tapered side walls are also possible. An example of an electroformed stencil is shown in Figure 4.22.

As in electroforming, another additive process, but mainly used as a surface finishing technology, is nickel plated stencil [10,14,18]. The electroless nickel is plated onto the finished stencil in a thickness range of 0.0003–0.0005 in., as shown in Figure 4.23. This increase in the stencil thickness and decrease in the hole size should be compensated at the primary etch phase. Surface passivation of brass is necessary with caustic aqueous/saponifier cleaning. Ni-plating does not actually increase tensile strength. It will neither improve on the dimensional tolerances nor eliminate any defects or imperfections created during the chemical etching process. The reason for nickel plating is that by adding a smooth coating onto the stencil, it will improve the solder paste release from the fine pitch openings. Also, a nickel coated surface exhibits low surface tension which is expected to reduce the wear of the squeegee and extend the service life of both squeegee and stencil. However, as noted earlier, too smooth a surface may result in skip or slide across the surface hence preventing the paste from rolling properly.

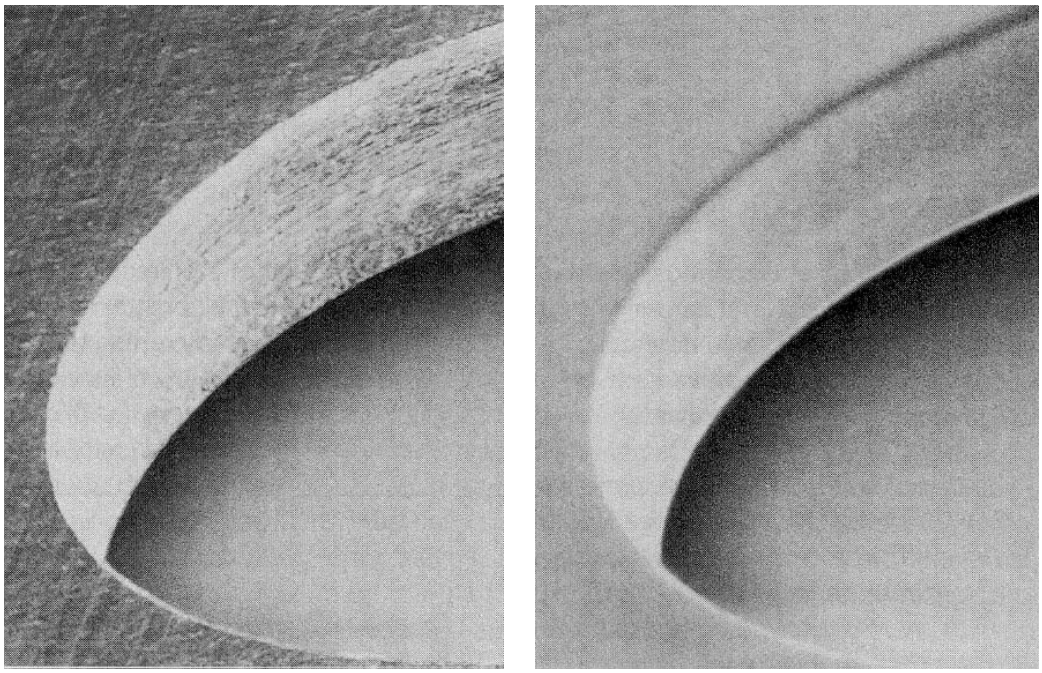

Figure 4.21 Photomicrographs of hole wall geometry shown after etching (*left*) and after electropolishing (*right*). Such ''substractive'' coating is one of the preferred methods for stencil plates since the dimensions experience little change. (From T. R. Jillings, ''Stencils: Understanding the Basic Components'', *Surface Mount Technology*, pp. 38–40 (February 1993): reproduced with permission.)

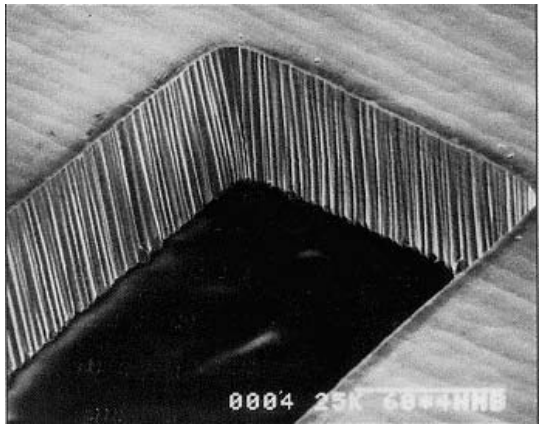

Figure 4.22 Electroformed stencil aperture. (From Metal Etching Technology, Technical Information (1993): reprinted with permission.)

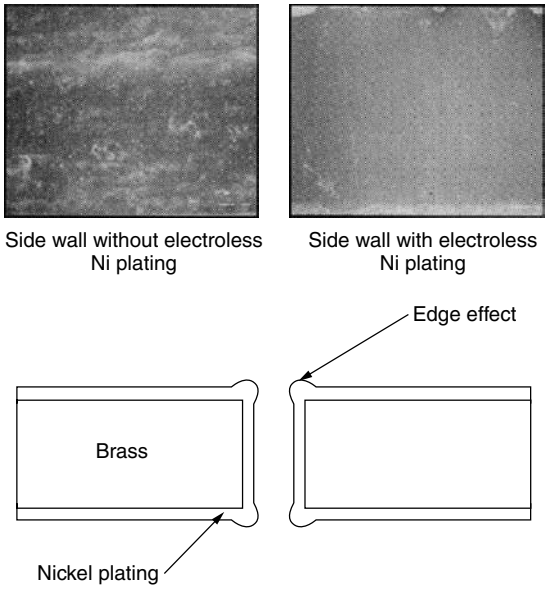

Figure 4.23 Electroless nickel plated stencil [19]

Some coatings may also be prone to delamination. This is particularly true of nickel on stainless steel, which does not adhere to laminations of any kind. Nickel will adhere better to brass and Alloy 42. An alternative to the plain Ni-plating process is the PTFE/nickel impregnation process. This can be performed at a cost in the range of $200 to $250. Like electroforming technology, nickel plating technologies also tend to form a rim or lip around the apertures of stencil, as shown in Figure 4.24 [19]. The presence of this lip around the aperture has been reported to enhance the gasketing effect during printing, accordingly reducing the possibility of paste leaking or bleeding.

4.2.1.3 Pattern design for fine-pitch applications

Although printing is the dominant technology for solder paste deposition, fine pitch applications still face

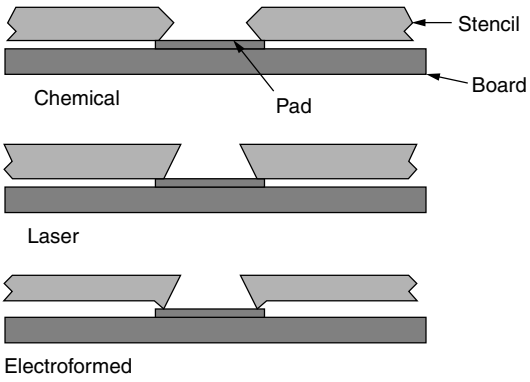

Figure 4.24 Aperture profile of various stencil forming technologies [20]

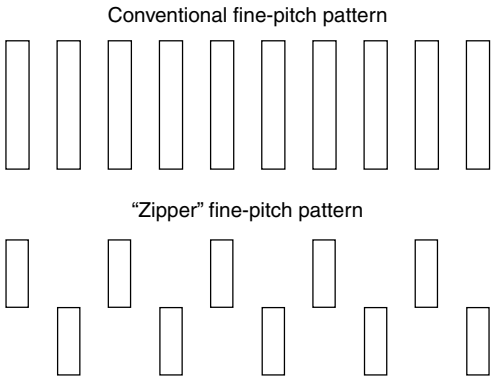

Figure 4.25 Conventional versus zipper of staggered fine-pitch pattern

challenges of delivering a high quality paste deposition. Several approaches in pattern design such as zipper pattern, micromodification, step-down, and taper treatment have been employed in order to address these challenges.

The conventional design of aperture pattern is almost a carbon copy of the pad footprint design, as shown in Figure 4.25. For fine pitch applications, particularly in the case of QFP components, the small spacing between neighboring paste deposits often results in bridging either before or after reflow. To avoid this problem, the aperture pattern can be modified to a zipper or staggered pattern, where the spacing between neighboring deposits is virtually tripled.

In the previous section, micromodification has been noted as a technique for correcting the impact of lateral etching or electropolishing processes. The same technique can also be used for improving fine-pitch solder paste deposition, as shown in Figure 4.26. In this case, the aperture for fine-pitch pads is reduced to a slightly smaller scale. A commonly used guideline is about 1 mil recession for each side. This reduced paste volume deposition effectively reduces paste smearing, slumping, and bridging problems.

A tapered aperture exhibits a wider bottom-side than the top-side, as shown in Figure 4.27, thus supposedly

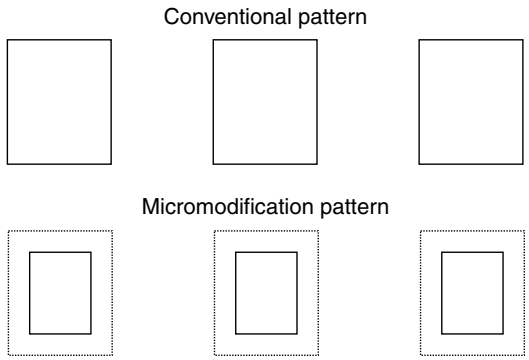

Figure 4.26 Conventional versus micromodification pattern

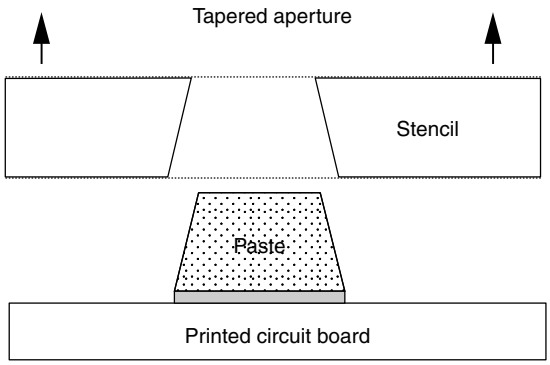

Figure 4.27 Schematic of tapered aperture

favoring a better release of solder paste. A tapered aperture is a natural result of the stencil forming process of laser cut and electroforming technologies, as demonstrated by the cross-section of a laser cut aperture (see Figure 4.28 [20]). Table 4.2 compares the defect rate of tapered patterns versus that of non-tapered patterns. The data are the averaged performance of all pastes and all stencils. It is interesting to note that the tapered pattern shows a considerably higher smear rate than the non-tapered pattern. Presumably this can be attributed to the wider opening of the bottom side of the tapered aperture, which allows the paste to flow more readily under printing pressure. In general, the tapering treatment reduces the overall defect rate slightly, primarily due to the reduction of insufficiency rate. Apparently this can be related to the better release of the tapered shape.

Table 4.2 Effect of tapering treatment on defect rate [2]

Aperture feature	*Smear defect rate*	*Insufficiency defect rate*	*Overall defect rate*
Non-tapered	0.86%	20.95%	21.81%
Tapered	1.97%	19.19%	21.16%
Tapered/non-tapered	2.29	0.92	0.97

However, as shown in Figure 4.29, the tapering treatment gradually shows an adverse effect on the

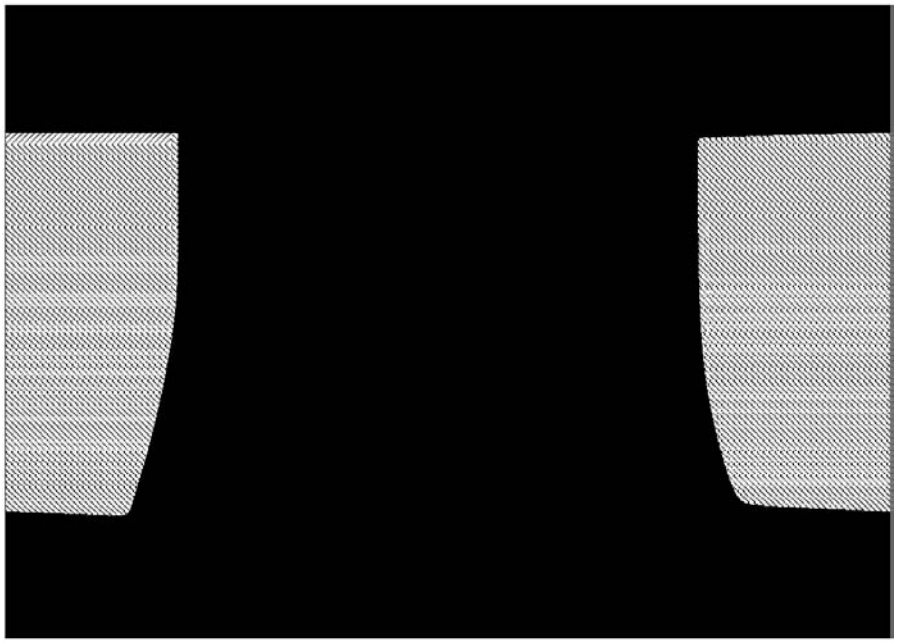

Figure 4.28 Cross-section of a laser cut stencil with a tapered aperture [21]

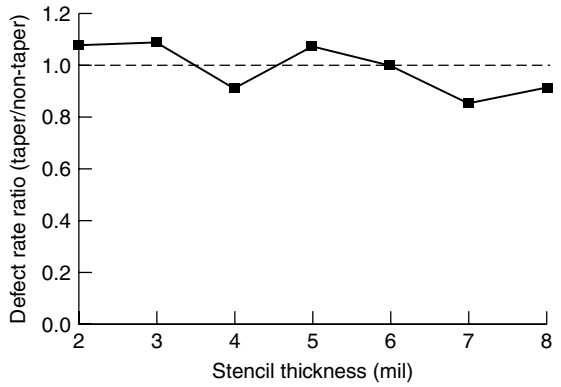

Figure 4.29 Effect of stencil thickness on defect rate ratio (tapered/non-tapered) [2]

Table 4.3 Commonly used stencil configuration [10]

Single-level stencil configuration			*Multi-level stencil configuration*		
Stencil thickness (in.)	*Pitch (in.)*	*Opening reduction (%)*	*Stencil thickness (in.)*	*Step-down (in.)*	*Pitch (in.)*
0.008	0.025	15	0.008	0.007	0.025
0.007	0.025	10	0.008	0.006	0.020
0.007	0.020	20	0.008	0.006	0.025
0.007	0.015	25	0.008	0.005	0.020
0.006	0.020	10	0.008	0.005	0.015
0.006	0.015	20	0.008	0.004	0.015
0.005	0.015	10	0.008	0.004	0.012
0.005	0.012	20			

overall defect rate with decreasing stencil thickness. This is mainly due to the increasing contribution of smear to the overall defect rate, as demonstrated in Figure 4.1. For the ultra-fine-pitch printing process, since the stencil thickness is expected to become smaller, it is very questionable whether the tapering treatment is still desirable [2].

The step-down pattern is also a commonly used approach for fine-pitch applications, as shown in Figure 4.30. This approach employs a thinner stencil block for the fine-pitch area, and a thicker stencil block for the coarser pitch area on the same stencil. In general, the gap for step-down should not be greater than 4 mils, and the spacing between the step-down pattern and the regular pattern should not be less than 75 mils [17]. Table 4.3 shows the commonly used stencil configuration [10].

The advantage of the step-stencil is its capability to deliver various paste deposition thickness. It can be used not only for systems containing both regular pitch and fine pitch components, but also for mixed technology systems containing both surface mount and through-hole components. The process of utilizing reflow soldering for through-hole applications is called the paste-in-hole process or intrusive reflow process. The trend of moving toward paste-in-hole applications is driven by both cost reduction and environmental considerations. By employing the solder paste reflow process for soldering both surface mount components and through-hole components, the wave soldering step can be eliminated. This accordingly will result in a reduced process step as well as reduced VOC emission.

However, since through-hole solder joints require a large amount of solder to form an adequate solder joint, the volume of solder paste to be printed at the through-hole spot has to be much more than that for surface mount solder joints. For mixed technology boards, this great variation in solder paste volume deposited on the same board can be addressed with either a step-stencil approach or a double-print process [12]. The step-stencil is 0.020 in. thick in the through-hole components area and 0.006 to 0.008 in. in the surface mount components area, as shown in Figure 4.31. This approach is less favorable, due to (1) difficulty in manufacturing stencil with a large step, (2) large clearance between through-hole and SMD areas,

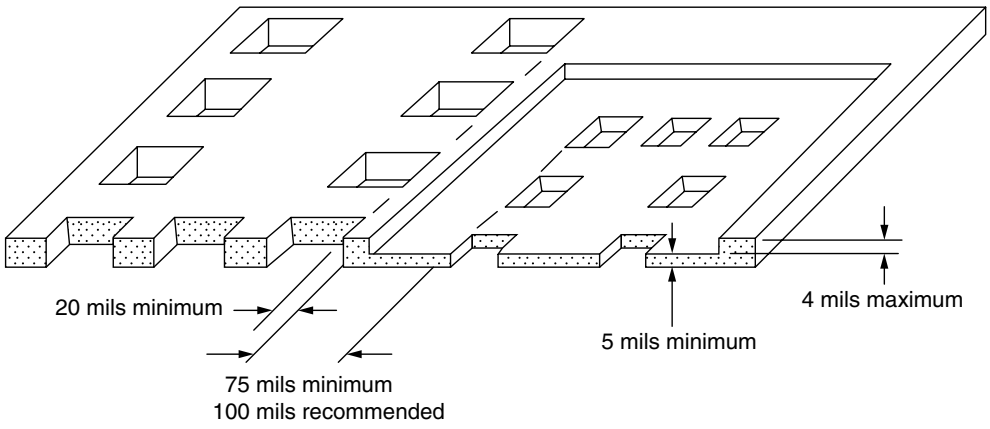

Figure 4.30 Guideline for design of step-down stencil pattern [17]

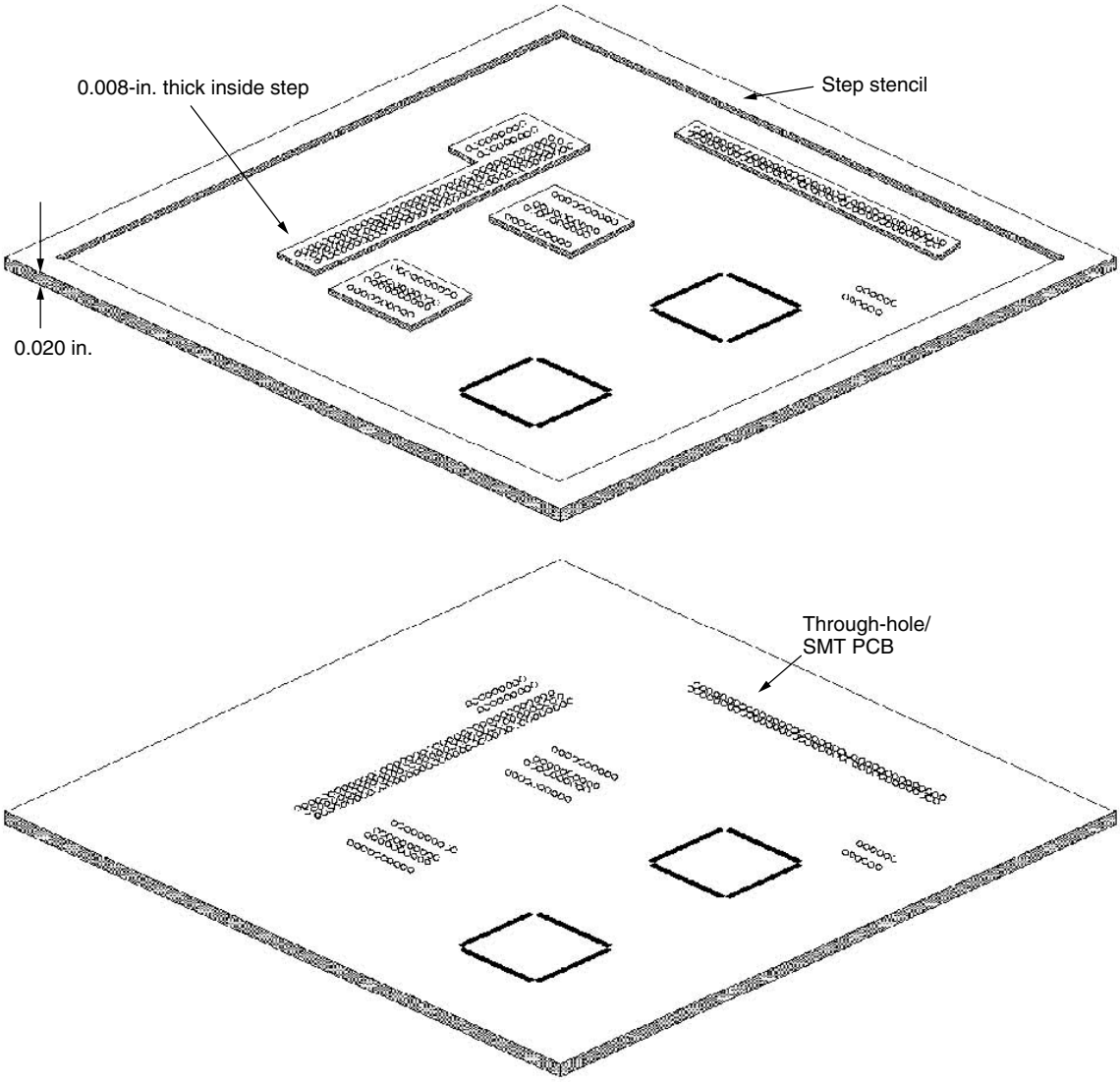

Figure 4.31 Step-stencil for mixed technology [12]

and (3) difficulty in printing a large step. The more favorable approach is the double-print process, as shown in Figure 4.32. In this process, the paste for SMDs is printed first with a stencil 0.006 to 0.008 in. thick. The board is then printed for through-hole components with a stencil 0.020 in. thick. The latter has a relief-etch area on the contact side half into the foil (0.010 in. deep). Solder paste from the first print is protected by the relief-etch area, hence it is not disturbed or smeared by the second print. Parts are placed and reflowed after the second print. The double-print process is the more favorable option than the paste-in-hole process. Although it requires one more step in paste deposition, it does eliminate the drawback encountered by the step-stencil approach and provides optimum paste volume deposition.

4.2.2 Squeegee

The squeegee is a plate-like applicator which forces solder paste through the aperture while pushing it across the stencil surface. The sharp edge of the plate wipes the solder paste cleanly from the stencil surface, and leaves a well-defined solder paste brick on the PCB pad upon lifting of the stencil, as shown in Figure 4.3. There are two major types of squeegee materials in use. The first type is polyurethane rubber. Depending on the squeegee fixture design, as demonstrated by Figure 4.33 [19], the shape of the polyurethane squeegee may vary from model to model. Examples include standard rectangular, diamond, wedge end, double-wedge end, and double knife, as exemplified by Figure 4.34. The square-shaped rectangular and

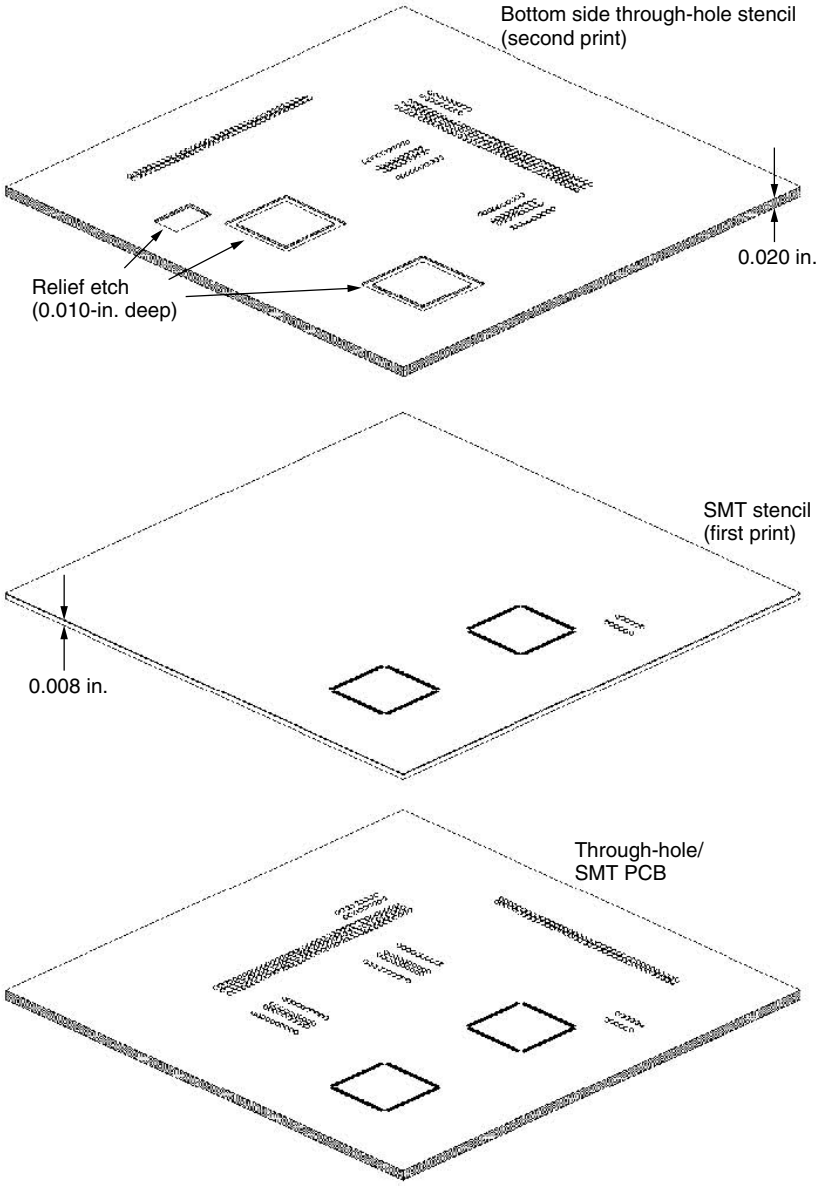

Figure 4.32 Double-print stencil for mixed technology [12]

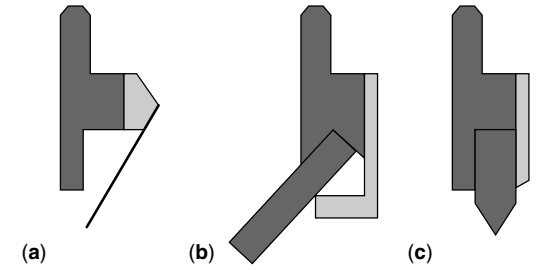

Figure 4.33 Examples of side view of squeegee fixture design: (**a**) metal squeegee, (**b**) polyurethane trailing edge, (**c**) polyurethane D-cut [20]

diamond types are designed for being used at all four printable edges. The hardness of the polyurethane usually ranges from Shore A hardness 55 to 95, with hardness 90 perhaps being the most popular choice [21]. Table 4.4 shows examples of rubber squeegee materials and their applications [22].

The second type of squeegee material is metal [23]. The Permalex approach (see Figure 4.35) is based upon a polymer which is metallurgically infused into a noble, hard, porous edge layer of metal. The substrate is made of a special spring alloy. The result is a composite design with the lubricity and smoothness of a polymer, the hardness and stiffness and smoothness of noble metal, and the

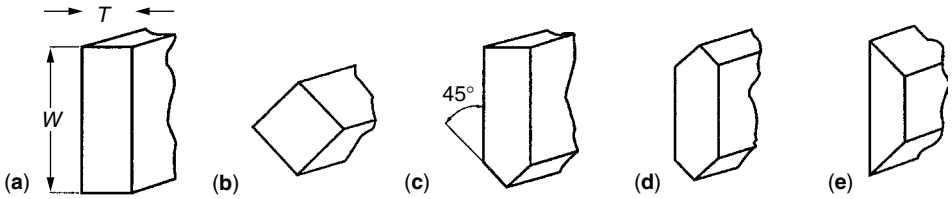

Figure 4.34 Type of polyurethane squeegee; (**a**) standard, (**b**) diamond, (**c**) wedge end, (**d**) double-wedge ends, and (**e**) double knife [22]

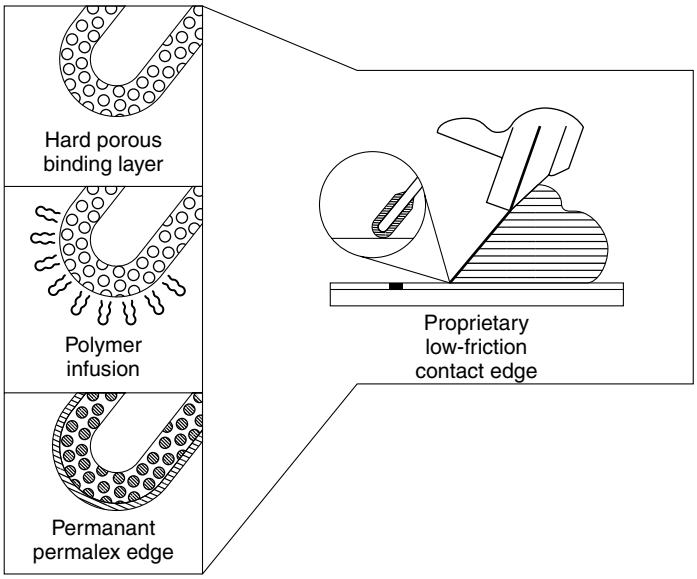

Figure 4.35 Permalex edge coating technology for metal squeegee [24]

Table 4.4 Examples of rubber squeegee materials and applications [22]

Hardness grade	*Material*	*Remarks*	*Applications*
60	Polyurethane	Soft	General screen printing, some thick film printing
70	Polyurethane	Medium	Widely used for most thick film printing
80	Polyurethane	Medium hard	Thick film printing, SMT, solder paste
90	Polyurethane	Hard	Solder paste, SMT applications
100	Polyurethane	Harder	Fine-pitch solder paste, SMT applications
110	Polyurethane	Very hard	Fine-pitch solder paste, SMT applications
120	Polyurethane	Exceptionally hard	Fine-pitch solder paste, SMT applications
180	Hi-density polymer	Hardest	Fine-pitch solder paste, SMT applications

compliance of spring steel. This polymer coating material yields a low friction contact edge, thus preventing scratching of the stencil upon printing. It is solvent and heat resistant. The hard metal blade edge prevents the scooping effect. The polyurethane rubber squeegee tends to dig into the aperture and scoop solder paste due to the softness of rubber, as shown in Figure 4.36. In contrast, the metal blade maintains a flat cut when wiping through the aperture. Figure 4.37 shows a comparison of the solder paste printed using these two types of squeegee.

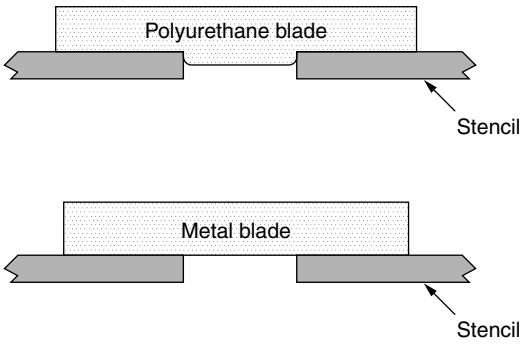

Figure 4.36 Polyurethane squeegee tends to scoop solder paste, while the metal blade maintains a flat cut

Table 4.5 Print thickness reduction rate (μm/kg) versus squeegee hardness. (Trailing edge polyurethane squeegee, 8.25 in. × 1.20 in. × 0.275 in.) [24]

Squeegee type	*Fine-pitch pads*	*Capacitor pads*
Metal	0.9	0.9
94 shore	4.5	5.9
94 shore tip /85 shore body	4.2	6.6
85 shore	13	16.3
85 Shore tip /94 Shore body	12	17.4

Table 4.5 shows the print thickness reduction rate as a function of squeegee hardness [24]. Obviously, the hardness of the squeegee tip dictates the extent of scooping, with a greater hardness producing less scooping.

The metal blade maintains the compliance desired due to the use of a thin blade. By combining an adequate squeegee angle and squeegee pressure, this allows the metal squeegee to be used not only on a flat surface, but also on a step-stencil, as illustrated in Figure 4.38. According to Transition Automation, the bending mechanics of a metal blade is such that given a 1/16-in. clearance between the step and the pad opening, a metal blade can bend to accommodate a 2 mil step. However, it has been reported that 0.20-in. clearance is required for every 2 mil step.

The conventional printing process leaves the solder paste exposed in front of the squeegee blade. This inevitably results in the deterioration of solder paste due to solvent loss, oxidation, and moisture pick-up. Recently, a new printing head design retains the solder paste in a closed chamber during printing [25], as shown in Figure 4.39. Today, there are two major chamber-print designs on the market, one is ProFlow from DEK, and the other is RheoPump from MPM. The elimination of paste exposure avoids problems associated with drying, oxidation, and moisture absorption. In addition, the pressurized paste in the chamber ensures a better aperture filling, thus reportedly yielding a better print quality. However, there are also side effects observed for some solder paste systems which function properly on conventional printers. Some of those solder pastes tend to thicken up in the chamber with an increasing number of printings, while some others tend to turn soupy and leak out of the chamber. Both symptoms are caused by the excessive internal shearing of paste in the chamber, as will be discussed in the following chapters.

4.2.3 Printing and inspection process

At the printing stage, the solder paste is loaded onto the stencil by either manually transferring the paste from a jar or automatically dispensing it from a cartridge. The quantity of paste to be loaded depends on the type of paste used. In general, the preferred diameter of the paste doll formed in front of the squeegee ranges from about 0.25 in. to 0.75 in.

The printer can be set in off-contact mode or on-contact mode. For off-contact mode, the maximum snap-off should not be greater than 10 × stencil thickness. The commonly used snap-off value ranges from 30 to 50 mil. During printing, the separation between stencil and printed paste should be 1–2 in. behind the squeegee. Off-contact mode could reduce smear for a poorly registered

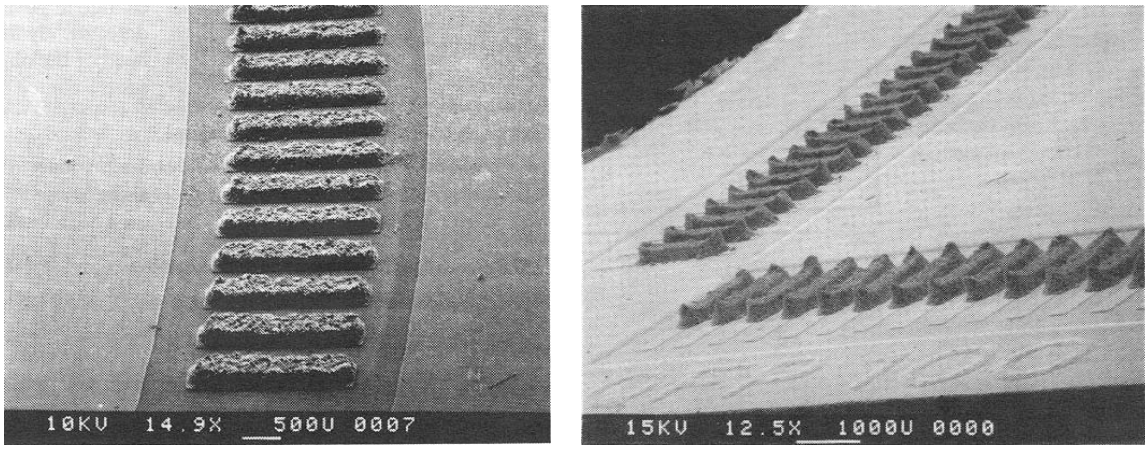

Figure 4.37 (*Left*) Flat cut solder paste bricks from metal squeegee, (*right*) scooped paste bricks from a polyurethane squeegee [24]

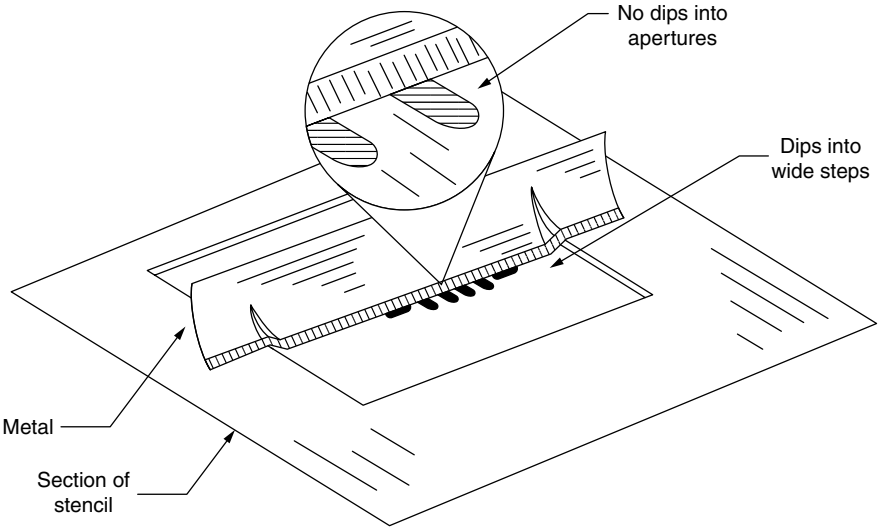

Figure 4.38 Metal squeegee flexing mechanics [24]

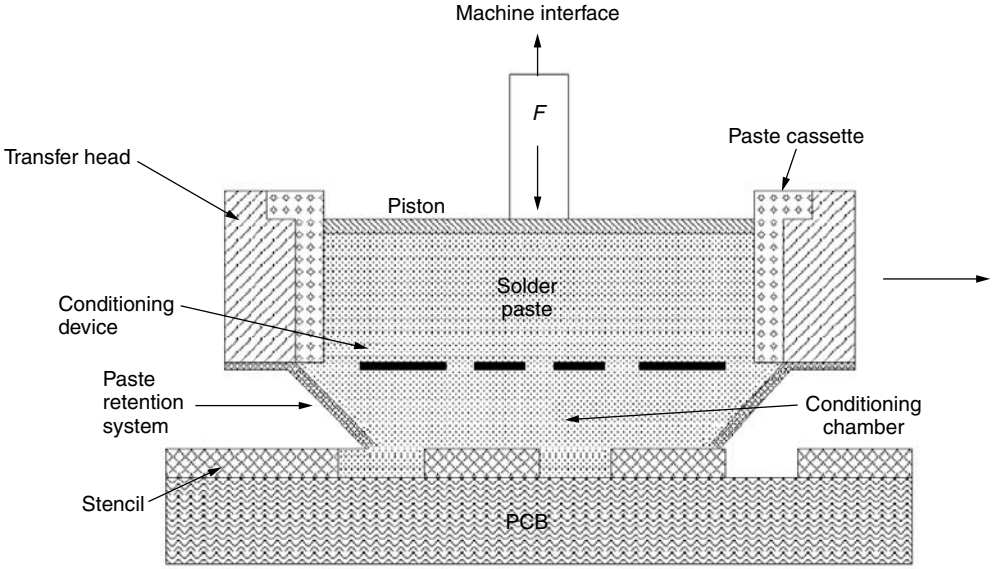

Figure 4.39 Schematic of chamber print mechanism [25]

system. A clam-shell opening mechanism is acceptable. The on-contact mode generally provides a more accurate print. This mode requires a pure vertical motion opening mechanism. In general, a slow snap-out speed, such as 0.04 in./sec, is more desirable in order to achieve good print quality [24,26].

A commonly used squeegee speed ranges from 0.75 to 4 in./sec. In general, the finer the pitch, the slower the squeegee speed desired. 3 in./sec is typically used for 50 mil pitch, and 0.75–1.0 in./sec for 20 mil pitch. However, at too slow a squeegee speed, the paste will not roll and hence will not flow evenly into openings. When the squeegee speed is too high, the paste will slide and skip the apertures. As a result, insufficiency and shadowing will occur. Currently the industry is gradually shifting toward a faster squeegee speed, due to the demand for a higher throughput. 5 in./sec print speed has been reported, and 10 in./sec print condition is being included as a desired feature in some solder paste evaluations for future applications.

For the off-contact mode, the squeegee pressure commonly used is 1–1.5 lb/inch squeegee blade. For the on-contact mode, a squeegee pressure of 0.75 lb/inch squeegee blade is preferred for a trailing edge blade using 90+ Shore A rubber.

After the printing process, the paste deposited should be sampled for inspection. A laser-based sensor can be scanned over the circuit board to measure solder paste

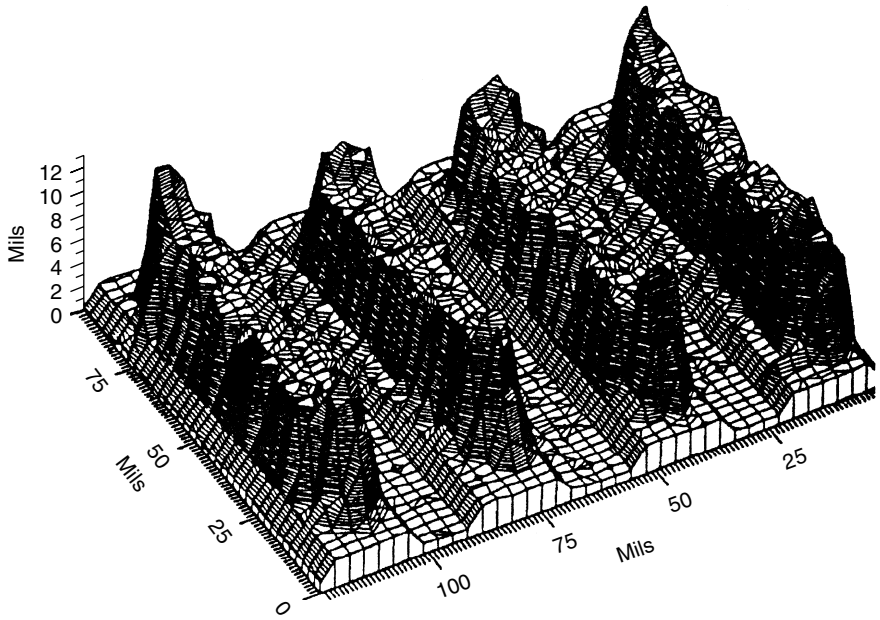

Figure 4.40 Process control for solder paste deposition with the use of laser-based sensor [29]

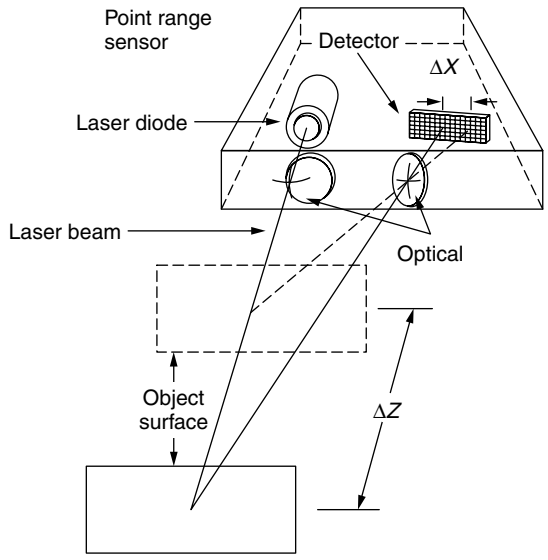

Figure 4.41 Laser sensor technology [30]

characteristics [27], as shown in Figure 4.40. The sensing principle most widely used for height measurement is called triangulation, as shown in Figure 4.41. Light from a laser diode is reflected from the object surface (represented by the solid "object surface" rectangle) and imaged onto a detector array. If the object surface was closer to the sensor (dashed "object surface" rectangle), the reflected light would be imaged to a different location on the detector. The height measurement can have a resolution of 0.38 μm [28]. A manually operated optical inspection device can also be used, as shown in Figure 4.42. To measure solder paste height, operators position the horizontal video measurement lines on the laser stripe over the solder paste and over the circuit board surface. The height value displayed on the monitor indicates the solder paste height [27].

4.3 Pick-and-place

After the solder paste has been printed, the PCB is then transported to the next station for component pick-and-place. In terms of placement timing, there are four major types of pick-and-place machines [29]. The first type is In-line Placement. This machine configuration has individual placement stations where its respective components are placed as the board moves past that station. The second type is Sequential Placement. Components are individually placed in a specific order. This sequence is determined by either a pre-programmed moving placement head or a moving X–Y table. The third type is Sequential/simultaneous Placement. Using a moving X–Y table and multiple placement heads, this machine places individual components in succession. The last type is Simultaneous Placement. All the components are positioned and placed on the board in a single operation.

For very small and simple chip placement, a high speed chip shooter is used, and can be categorized according to the movement of parts [30]. The first type is a stationary placement head and movable PCB and movable feeder table, as shown in Figure 4.43. The advantage is high placement performance (theoretically up to approx. 25 000 components/hour). The disadvantages include: (1) considerable drop in performance when a batch is changed, (2) replenishing of components is not possible during the

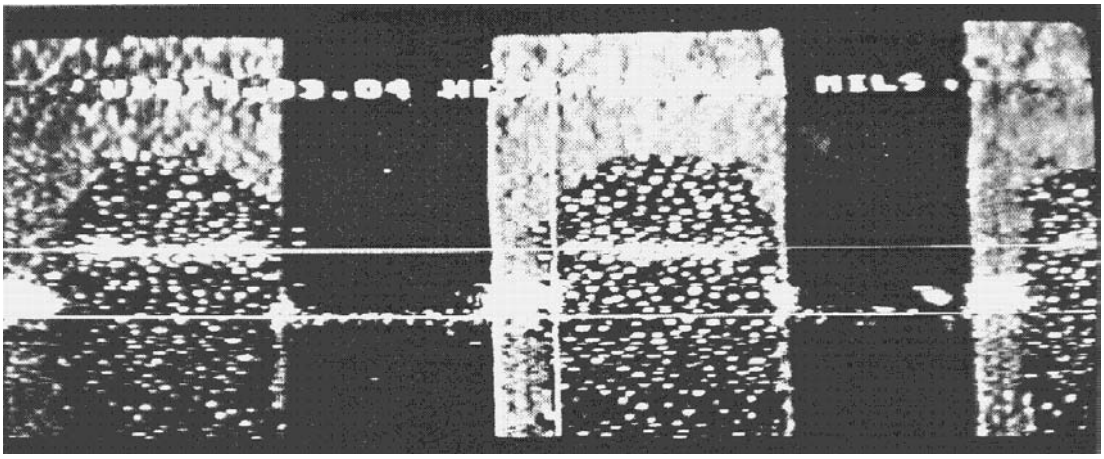

Figure 4.42 Measurement of solder paste deposition height with an optical device. (From T. L. Hodson, ''Selecting pick-and-place Equipment'', *EP&P*, pp. 32–37 (June 1993): reprinted by permission.)

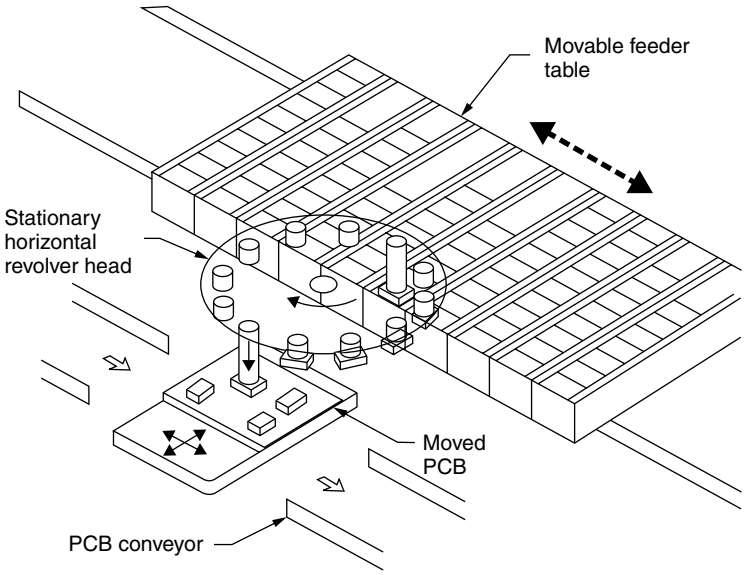

Figure 4.43 Classical chip shooter principle, with a movable feeder table and PCB but a stationary revolver head [32]

placement process, (3) the constant accelerating and decelerating may cause components which have already been placed to slip, (4) placement of 0402 components is possible but very difficult due to the fixed relationship between the pickup position of the vacuum nozzle on the revolver head and the position of the feeder modules at right angles to the transport movement, and (5) bulk component processing is impossible. The second type involves a fixed PCB and feeder bank, but a movable revolver head, as shown in Figure 4.44. The principle is combining the advantages of the flexible pick-and-place systems with those of the high-performance shooter. The major difference compared to the pick-and-place systems is that, instead of a simple head, an X/Y gantry system carries a revolver head with up to 12 vacuum nozzles and a horizontal axis of rotation. Advantages over the classical shooters include: (1) lower drops in performance when a batch is changed and thus better suitability for JIT philosophy, (2) the stationary component feeder permits components to be replenished during operation, and (3) it is impossible for components already placed to slip, since the PCB is stationary.

Placement equipment is one source of capacitor cracking. After picking the component from the tape and reel with its vacuum head, jaws grip the capacitors to align them with the pads on the board. This gripping force can damage the parts even if the normal force is adjusted to a "reasonable" level. The reason is that the jaws' speed can still cause impact damage similar to a blow of a hammer [31].

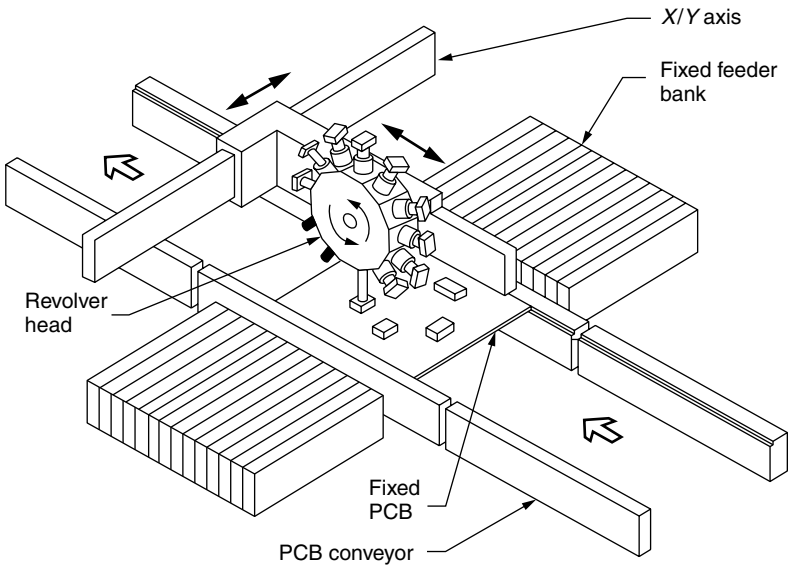

Figure 4.44 Collect and place chip shooter principle, with a movable revolver head and fixed PCB and feeder bank [32]

Table 4.6 Summary of reflow methods characteristics [32]

Features	*Infrared*	*Vapor phase*	*Convection*	*In-line-conduction*
Advantages	Rapid heat transfer. Rapid heat recovery. Wide range of temperatures available.	Rapid uniform heating on a wide variation of assembly thermal masses. Temperature is constrained to a known maximum. Rapid heat recovery.	Low equipment and low production use cost. All objects heat uniformly. The slow heat transfer minimizes component cracking. The heat transfer provides adequate flux preheat.	Even heat transfer to board. Yield is not sensitive to thermal mass of components. Easy maintenance.
Disadvantages	Different surface features and body colors cause nonlinear heating. Source temperatures higher than the Tm of solder. Source temperature difficult to monitor. Each assembly requires a unique thermal profile.	Heat flow is too rapid, damaging some components and materials.	Slow heat transfer. Slow recovery rate. Equipment may be large.	Not easy for double-sided PCBs. Limited throughput.
Relative cost of equipment	Medium to expensive	Medium	Medium	Low
Relative cost in production use	Medium to high depending on profile time.	Low to medium	Low	Low

4.4 Reflow

Once all the parts are placed onto the PCB, the loaded board is then ready for reflow. Commonly used massive reflow methods include infrared reflow, vapor phase reflow, forced convection reflow, and in-line-conduction reflow. Table 4.6 shows the characteristics of those reflow methods. Besides the methods listed in Table 4.6, other methods are also in use, such as laser reflow, soft beam reflow, hot-bar reflow, collet soldering, and resistance soldering. Those methods generally are not high volume throughput processes, and will not be addressed in detail in this chapter.

The heating rate of several major reflow methods are shown in Table 4.7. Compared with other methods, with vapor phase reflow it is more difficult to regulate the rapid

Table 4.7 Heating rate (Q) of major reflow methods [33]

Reflow methods	*Heating rate*	*Legend*
Vapor phase	$Q = H A_A (T_S - T_A)$	H = vapor heat transfer coeff. A_A = assembly area T_S = saturated vapor temp T_A = assembly temp
Infrared	$Q = \sigma A F \varepsilon F_a (T_S{}^4 - T_A{}^4)$	σ = Stefan–Boltzman constant A = area being heated $F\varepsilon$ = source and product emissivity factor F_a = configuration of the assembly T_S = temperature of the source T_A = temperature of the area being heated
Convection	$Q = H_C A_S (T_g - T_S)$	H_C = thermal convection conductance A_S = assembly surface area T_g = gas temp. near the surface T_S = assembly surface temp

heating rate, and accordingly is more vulnerable to many defects. Infrared is very efficient in heating. However, the sensitivity of heating rate towards variation in material type and color results in a great challenge in maintaining an even temperature distribution across the boards. Convection reflow is effective in heat transfer. In addition, it is not sensitive to material type as well as color of the parts, hence is the prevailing method of choice.

A commonly used profile is shown in Figure 4.45. Many component manufacturers specify a maximum rate of temperature rise of 2 to 4 °C/sec, as expressed by dT/dt. Too rapid a temperature rise will result in component cracking, mainly caused by thermal stress build-up due to temperature gradient formation, moisture-entrapment, and mismatch in thermal expansion coefficients of the component materials. This is particularly true for some ceramic components. In the case of solder paste, a rapid temperature rise may promote or aggravate slump behavior. This is primarily due to the rapid drop in viscosity before the solvent has a chance to dry out thoroughly. In addition, rapid outgassing of volatiles can contribute to the solder beading problem around low stand-off components, such as chip capacitors and chip resistors.

The purpose of soaking is to evaporate solvents and activate the flux. A typical temperature range recommended by the solder paste vendors is between 150° and 175 °C. Most fluxes are activated at temperatures above 150 °C. The solvent evaporation rate may vary significantly from paste to paste, depending on the solvent type used.

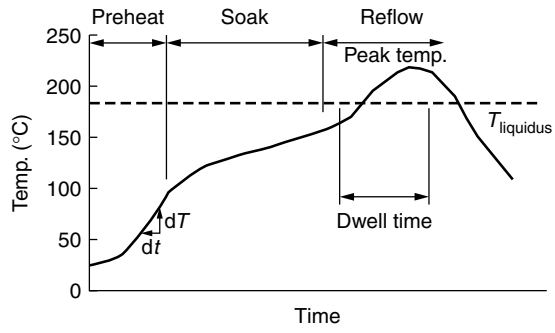

Figure 4.45 A commonly used reflow profile

The second reason for a soaking period is to equilibrate the temperature across the printed circuit board before entering the reflow zone. With a smaller temperature gap between components when entering the reflow zone, a smaller difference will result between the maximum temperature reached. If a significant temperature gradient is developed at reflow, the following problems can result: (1) cold solder joints coexist with charred boards or components, and (2) tombstoning or walking parts due to uneven wetting behavior at the two ends of chip capacitors or chip resistors. However, too long a soaking time will promote excessive powder oxidation and flux volatilization, and will result in solder balling, voiding, and poor wetting. This is especially true for the fine-pitch process. In addition, many low-residue no-clean and water washable solder pastes appear to be more sensitive to the use of a long soaking time. The most commonly used soaking time ranges from 30 seconds to 2.5 minutes.

As to the reflow zone, although Sn63 solder exhibits a liquidus temperature of 183 °C, a considerably higher temperature is needed for the solder to flow and to wet properly. A minimum peak temperature of 200 °C should be reached in order to obtain minimum acceptable joint quality. However, whenever possible, a minimum peak temperature of 210 °C is preferred. The maximum peak temperature allowed is dictated by solder paste chemistry, the characteristics of components and the PCB materials. In general, too high a peak temperature will cause discoloration or degradation of the PCB material, deterioration of electrical properties of board materials or components, a grainy or wrinkled solder joint surface, and a charred flux residue. The commonly used maximum peak temperature specification ranges from 230° to 250 °C. The dwell time above liquidus temperature is to be kept as short as possible. A longer time and a higher temperature lead to a more rapid growth in intermetallics. Since the mechanical and electrical properties are virtually affected by the thermal load, too long a dwell time has a similar effect to that

of too high a peak temperature. Typical dwell time used by industry ranges from 30 to 90 seconds, depending on the peak temperature.

However, it should be noted that the optimal reflow profile is dictated by the reflow technology. The profile shown in Figure 4.45 is primarily developed for infrared reflow method. For the convection reflow method, a linear ramp-up reflow profile is more adequate [34], as will be discussed in a later chapter. In the following sections, several major reflow methods will be discussed in further detail.

4.4.1 Infrared reflow

The wavelength of the infrared region is located between visible light and microwave region in the electromagnetic spectrum, with 0.72 to 1.5 μ being near-IR, 1.5 to 5.6 μ middle-IR, and 5.6 to 1000 μ far-IR. The wavelength of IR emitted is determined by the emitter type used, as shown in Table 4.8 [35].

One of the advantages of a near-IR reflow system is the penetrating energy exerted, thus allowing an even temperature rise throughout the paste along with controlled outgassing of volatiles [36], as shown in Figure 4.46. On the other hand, the far-IR has the advantage of avoiding shadowing effects and sensitivity toward the color of parts. In addition, the ability of far-IR to heat the air within the furnace also enhances the rate of heat transfer [37,38]. Figure 4.47 shows the tunnel end view of an area source IR furnace [39].

4.4.2 Vapor phase reflow

Vapor phase reflow was one of the prevailing reflow technologies in the 1980s. The equilibrium and maximum temperatures provided by vapor phase soldering is the boiling point of the primary fluorocarbon fluid. The reflow results are not affected by the configuration and location of components, and no overheating or cold joints will be developed as long as a sufficient dwell time is allowed at reflow. Since no tedious profiling work is required regardless of variation in the board design, this method is particularly useful for reflowing low volume and high mix type products. Since the air is expelled from the reflow zone by the inert fluorocarbon vapor, the soldering process basically is conducted under an oxygen-free environment. Accordingly the flux used in the solder paste can be fairly moderate and still accomplish a satisfactory reflow result. Although tombstoning and/or chip cracking could be a problem associated with rapid heating of the vapor phase soldering process, they can be prevented through addition of IR-preheat, proper pad design, improvement in the solderability of components and boards [40]. Figure 4.48 shows an in-line vapor phase reflow system with IR-preheat [42].

Table 4.8 Characteristics and suitability for SMT of infrared sources [35]

Emitter type	*Emission*	*Wattage*	*Suitability*
Focused tungsten tube filament lamp	Near-IR	300 W/cm	Shadowing by components. Thermal degradation: board delamination, board warping, charring. Color selectivity
Diffuse array of tungsten tube filament lamps	Near-IR	50–100 W/cm	Color selectivity
Diffuse array of nichrome tube filament lamps	Near-to middle-IR	15–50 W/cm	Greater component densities are possible. Little color selectivity problem.
Area source secondary emitter	Middle-to far-IR	1–4 W/cm2	No shadowing. No color selectivity

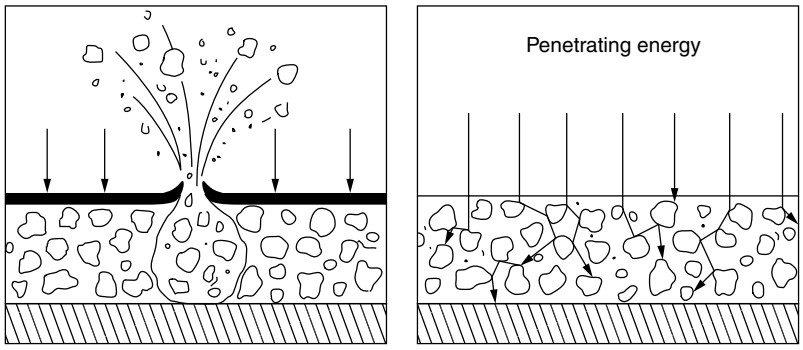

Figure 4.46 Advantage of lamp IR reflow system. Vapor phase and panel heater systems deliver all their energy to the surface of the solder paste. Volatiles trapped beneath the hardened surface erupt causing spattering and solder balling (*left*). The high energy infrared radiation from quartz lamps penetrates the solder paste and reflects throughout the suspended solder particles to achieve an even temperature rise throughout the paste along with controlled outgassing of volatiles (*right*) [38]

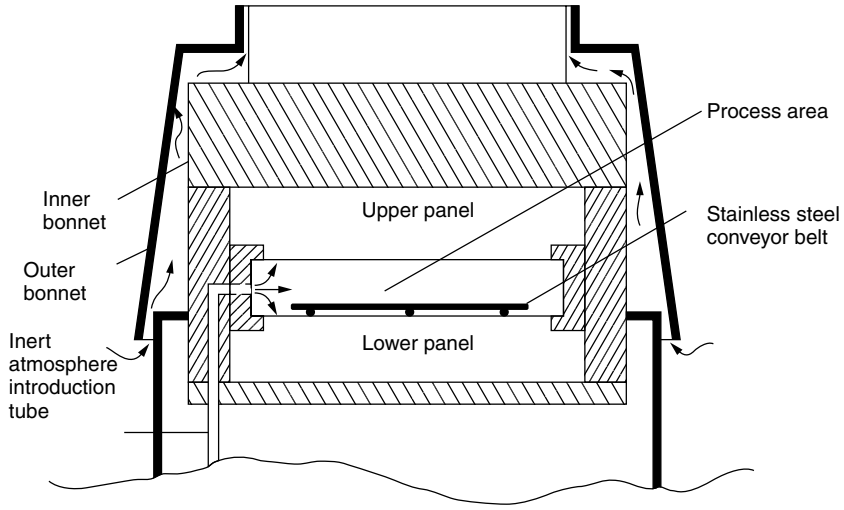

Figure 4.47 Area source IR furnace tunnel end view [41]

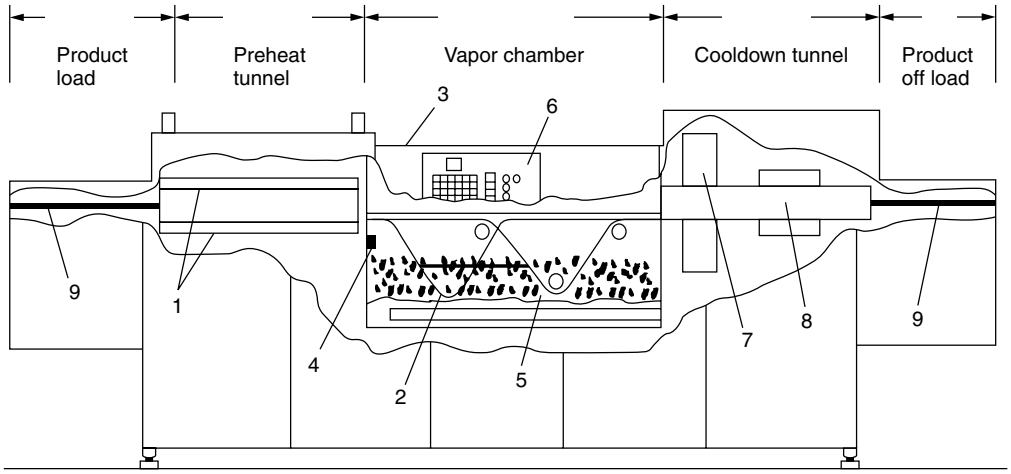

Figure 4.48 In-line vapor phase reflow system with IR-preheat [42]. Vapor phase reflow soldering system and compartmentalization diagram of functions. Ancillary systems include ceramic IR preheater (**1**), horizontal board (**2**), window (**3**), vapor containment (**4**), saturated vapor (**5**), control (**6**), cooldown and vapor reclaim (**7**), 2.5-in. product reflow tunnel (**8**), and exit pallet area (**9**)

4.4.3 Forced convection reflow

True forced convection systems utilize heated, forced convection in all zones (upper and lower) within the heating chamber. They are almost always multiple-zone systems, in which the convection is distinctly divided into individual temperature-controlled zones. The method of heating is convection-dominant, with very little IR component. However, there is always some IR contribution to PCB heating from the heated tunnel interior. A common method of delivery in these systems is a perforated panel-type heater with a plenum behind it. Air or gas is forced through the panel and heated in the process, and encounters the PCB. After heating the PCB, the gas is usually drawn off through ducts positioned between the perforated panels [41]. Some oven designs employ perpendicular gas flow, as shown in Figure 4.49 [42], in order to eliminate the stationary gas boundary layer on surface of the PCB hence promoting better heat transfer efficiency [43].

The disadvantages of forced convection reflow is the need for a high volume gas flow to provide efficient heating. Normally it is difficult to achieve low ppm oxygen inert atmospheres – especially at reasonable cost. At the same oxygen content levels, a forced convection system tends to have more solder balling and wetting problems than the IR reflow process, particularly in the case of low residue no-clean and water soluble solder pastes. This is due to a higher gas flow rate around devices, therefore more oxidation is required for heating [41].

4.4.4 In-line-conduction reflow

There are two types of conduction reflow system available, (1) belt-type, and (2) sweeping type. For a

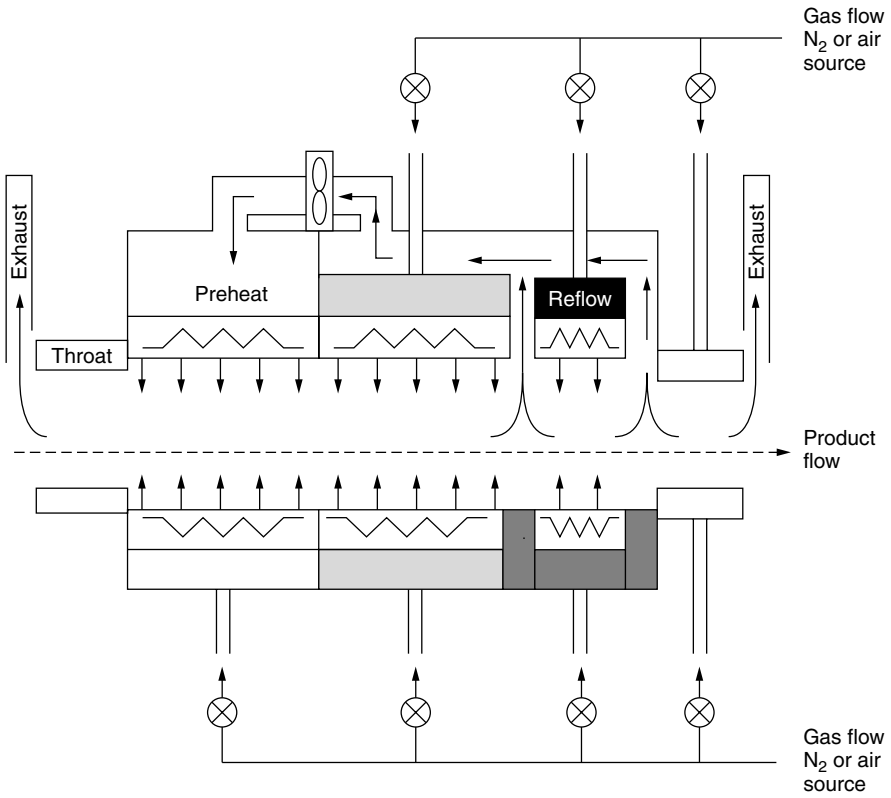

Figure 4.49 Convection oven design using perpendicular gas flow [44]

belt-type system, the conveyor belt is made of a fiberglass mesh impregnated with polytetrafluoroethylene (PTFE). All Teflon-impregnated belts have carbon added to make them electrically conductive, although all surfaces in contact with the belt are nonconductive. Belt conductivity allows the belt to be externally grounded with a tensile wiper brush [44]. The belt-type system may also be coupled with an IR system. The unit may employ bottom-side conductive heat while introducing IR heat energy from the top. The conductive heat passes through a thin Teflon and carbon impregnated fiberglass belt, introducing a sufficient amount of heat through the substrates into the solder, together with top-side IR units that offer independently controlled IR energy. The IR preheat unit is of a non-focused panel type. Diffused IR heating via a woven quartz cloth panel coated with black ceramic for high emissivity. The usual wavelength range is 2.5 to 6.0 μ.

For a sweeping system, the heat is transferred directly from the metal heating platen to the substrates to be reflowed. A series of evenly spaced sweeping bars push the parts across a series of heating platens at a pre-programmed temperature. The sweeping type may be combined with a convection reflow system, as shown in Figure 4.50 [45]. Here the hot air is being forced out of the through-holes distributed across the heating platen, thus providing additional means of heat transfer for the reflow process.

4.4.5 Hot-bar reflow

The hot-bar reflow system is primarily a resistance soldering device. The electrode is normally molybdenum through which the electric current is passed. The components can be placed on a printed solder paste, or solder dipped, in order to aid solder flow over the top surface of the lead. The heat is supplied to the head either continuously, maintaining a constant temperature, or by a short pulse. The impulse heating mode gives better results [46].

4.4.6 Laser reflow

The commonly used laser reflow systems include the 10.6 μ wavelength light emitted by the CO_2 laser and the 1.06 μ wavelength light emitted by the Nd:YAG laser. Laser reflow is an ideal process for attaching heat sensitive devices since the heat is applied only to the area of the joint. It is also ideal for dense packaging of devices on a board since it can reach closely spaced components without disturbing adjacent parts. It is one of the few techniques that will easily solder devices already attached to heat sinks, including those attached to heat pipes [38]. However, improper soldering conditions such as too high an energy or too short a time can cause inhomogeneous heat transfer and will result in a number of defects including solder balling and charring [46].

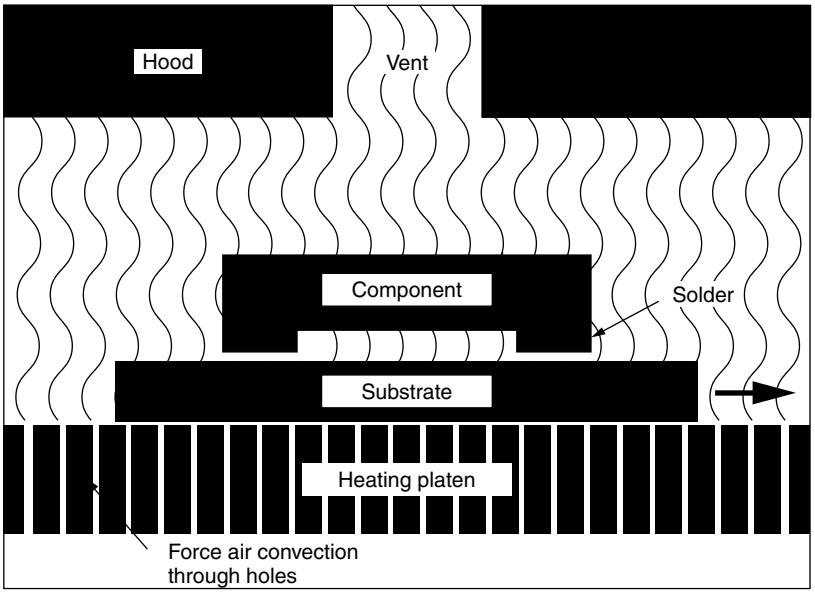

Figure 4.50 Diagram of conduction + convection reflow system [47]

4.5 Effect of reflow atmosphere on soldering

Since the fluxing reaction involves removal of metal oxides, any reflow atmosphere which minimizes the formation of metal oxide will help in reducing the work load of fluxes. This will result in a more satisfactory soldering performance [47], and will be discussed in more detail in a later chapter. Therefore, inert atmospheres, such as nitrogen or helium, and reducing atmospheres, such as hydrogen or carbon monoxide, will improve reflow soldering performance. However, the extent of this improvement is determined by flux chemistry. For some robust fluxes such as some RMA or water-washable solder pastes, the improvement may be negligible. For other fluxes such as low residue fluxes, it can be very significant.

4.6 Special soldering considerations

The reflow processes discussed above are typical SMT processes. There are also applications requiring some special soldering processes, such as step soldering, reflow alloying and paste-in-hole, as discussed below.

4.6.1 Step soldering

There are some applications where a series of soldering steps with a reduced soldering temperature for latter steps will be required; for instance, to solder thermally-sensitive components onto previously assembled board, or to reduce the thermal exposure of previously assembled components when reflow for the second-side assembly. For those processes, the requirements for the solder alloy melting temperature dictates that the liquidus temperature of the solder for second-step reflow is to be no less than 40 °C lower than the solidus temperature of the solder for first-step reflow. The maximum reflow temperature for the second-step soldering should be no less than 10 °C lower than the solidus temperature of the solder used in first-step soldering [9].

4.6.2 Reflow-alloying

In many instances, the assembly procedures involve multiple soldering processes, such as soldering some pre-assembled plastic packages onto a PCB. Very often, the final soldering process is dictated by the end users of the packages and often requires the use of typical solders, such as Sn62/Pb36/Ag2 or Sn63/Pb37 solder alloys. This requires the solder alloys used for the pre-assembly process to have a melting point higher than the peak temperature of the second reflow process, 220–230 °C, thus excluding the use of Sn96.5/Ag3.5 (melting point 221 °C). In the case of pre-assembled plastic packages, the options are fairly limited, due to the relatively poor thermal stability of plastic materials. Typically, the maximum soldering temperature allowed for manufacturing plastic components should not be higher than 250 °C. On the other hand, for the solder paste reflow process, the reflow temperature needs to be about 30 °C higher than the melting point of solder. Accordingly, the solder to be used for the pre-assembly component manufacturing process should have a melting point no higher than about 220 °C [9].

The answer to this special constraint can be provided by the reflow-alloying technique. Figure 4.51 illustrates the mechanism of the reflow-alloying process. A low melting alloy powder A is blended with a high melting alloy powder B in the solder paste. By reflowing the low melting alloy A, the melting point of alloy A will be gradually

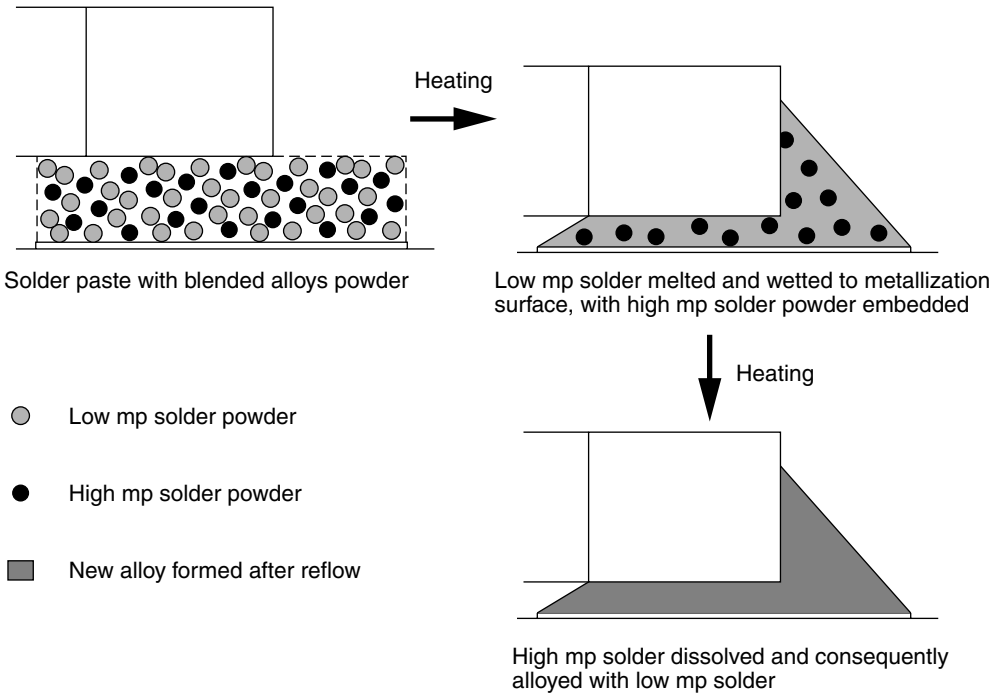
Heating
Solder paste with blended alloys powder
Low mp solder melted and wetted to metallization surface, with high mp solder powder embedded
Heating
Low mp solder powder
High mp solder powder
New alloy formed after reflow
High mp solder dissolved and consequently alloyed with low mp solder

Figure 4.51 Mechanism of reflow alloying process

raised due to the dissolution of the high melting alloy B at the reflow stage, and will eventually reach the melting point of a new alloy C. Here alloy C is the new composition formed by alloying A and B [9].

An example of an alloy system for reflow-alloying is the In–Pb system. Figure 4.52 shows the phase diagram of In–Pb alloys [9,48]. By employing a solder paste material composed of 70 percent of Pb60/In40 (solidus 197 °C, liquidus 231 °C) and 30 percent of Pb95/In5 (solidus 300 °C, liquidus 313 °C), the reflow process can be conducted at 250 °C. This reflow-alloying process results in a new alloy with composition Pb70.5/In29.5 (solidus 218 °C, liquidus 250 °C), as verified by the differential scanning calorimetry data shown in Figure 4.53 [49].

Some other alloy systems which may also be considered for the reflow-alloying process include alloys with a high content of Au, Ag, or Cu for a high melting alloy and

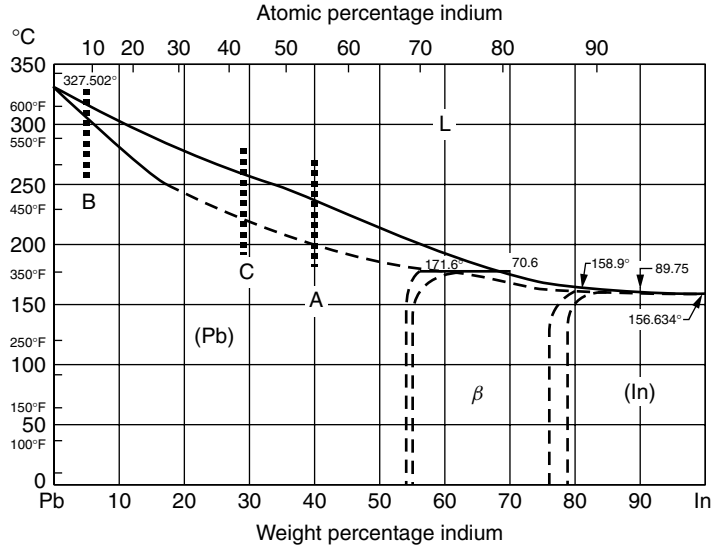

Figure 4.52 Indium–lead phase diagram [51], where A = Pb60/In40, B = Pb95/In5, C = 70 percent A + 30 percent B

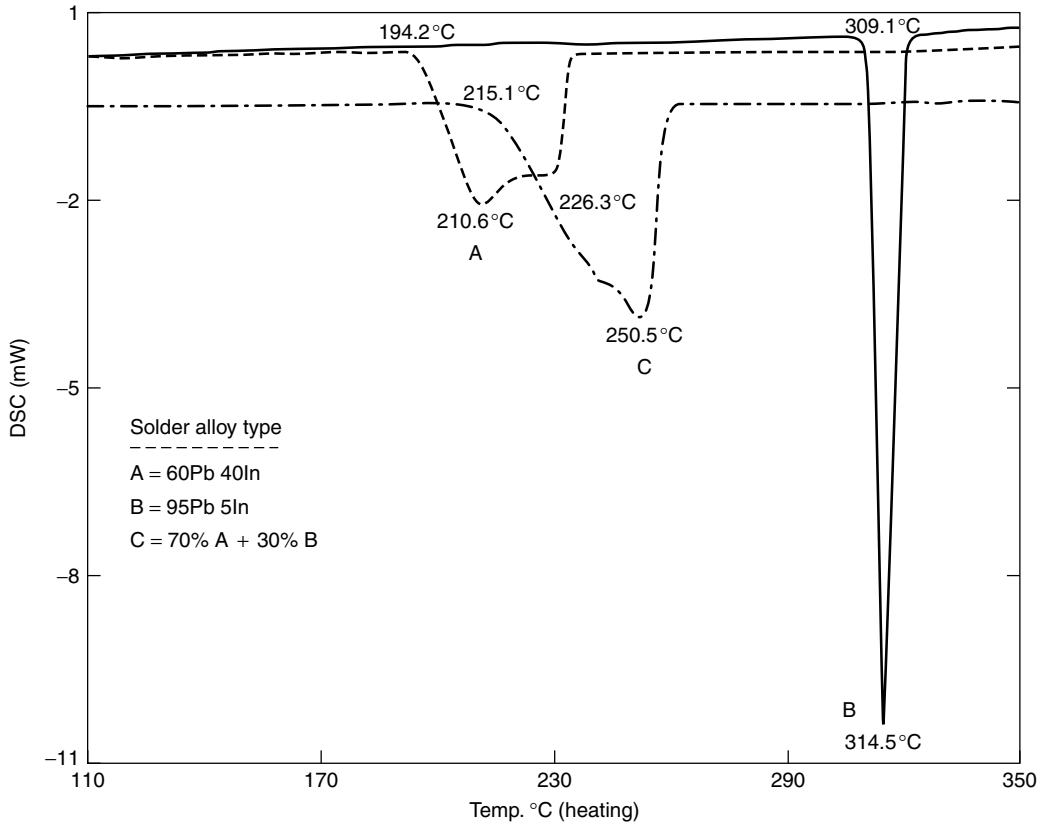

Figure 4.53 DSC data for In–Pb alloys and reflowed In–Pb alloys blend [52]. Sample A is Pb60/In40 solder power (−200/+35 mesh). Sample B is Pb95/In5 solder power (−200/+325 mesh). Sample C is a solder paste, with 10 percent RMA flux, 63 percent Pb60/40 and 27 percent Pb95/In5 solder powder. Sample A and Sample B are measured on DSC as is. Sample C has been reflowed at 250 °C for 30 seconds prior to DSC measurement. The DSC scanning rate is 10 °C/min

alloys with high content in In for a low melting alloy. The process is also called a modified solid-liquid-interdiffusion (SLID) process [50–53].

4.6.3 Paste-in-hole

With the electronics industry becoming more cost and environment conscious, elimination of the wave soldering process is on the agenda of many assembly houses. By eliminating the wave soldering process, the VOC emission rate on the assembly line, mostly due to wave fluxes, can be significantly reduced. In addition, wave soldering equipment, operating cost, and floor space occupied can also be eliminated. Unfortunately, many of the through-hole components such as some connectors are still needed due to either lack of availability of SMD or high mechanical strength requirement. A solution for soldering those through-hole components is by employing the paste-in-hole process. By printing solder paste at through-hole sites, followed by inserting the components, the device is then sent through a reflow furnace to complete the soldering process. Since the solder joint of a through-hole component typically takes much more solder than a SMT solder joint, the aperture size and stencil thickness have to be enlarged in order to deliver sufficient solder volume. Commonly used approaches include the step-stencil or the double-print process, as shown in Figures 4.31 and 4.32. For the no-clean process, the quantity of flux residue at through-hole joints often far exceeds that of SMT solder joints due to the use of a very large quantity of solder paste per through-hole joint.

4.7 Solder joint inspection

Inspection of solder joints can be done with (1) visual, (2) optical, (3) real-time X-ray, (4) laser-infrared, and (5) acoustic microscopy inspections. Visual inspection detects missing joints, solder bridging, wetting performance, part alignment, and solder balling, but not internal structure defects. On average, the accuracy of visual inspection is believed to be below 75–85 percent, with the limit of throughput about 10 joints per second. Visual inspection varies with the operator. However, simplifying the joint quality criteria may enhance consistency among operators [54,55]. Table 4.9 summarizes the applications of oblique and vertical viewing systems [56].

X-ray systems are good for inspecting voids, opens, hidden solder balls, hidden bridging, and skewed solder

Table 4.9 Optical inspection systems [56]

Defect	*Identification techniques*	*Inspection point*	*Corrective action*
Coplanarity	Oblique viewing	After reflow	Solder touch-up, replace package
Placement	Vertical viewing	Before/after reflow	Remove and resolder
Solderability	Oblique viewing	After reflow	Solder touch-up, or remove and resolder
Bridging	Oblique viewing	After reflow	Solder touch-up
Contamination	Oblique viewing	After reflow	Rework
Solder paste defects	Oblique viewing	Before placement	Rescreening or restenciling
Epoxy paste defects	Oblique viewing	Before reflow	Touch-up

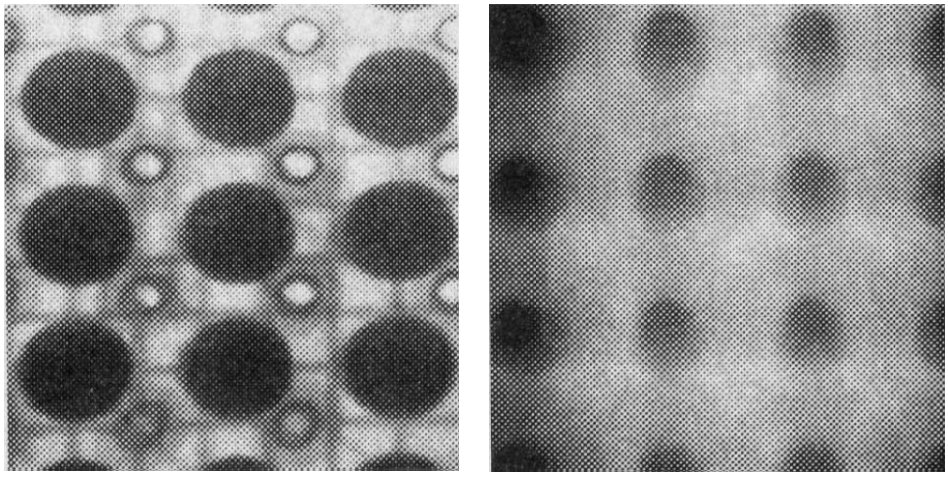

Figure 4.54 X-ray images of BGA solder joints inspected via a transmission (*left*) and a cross-sectional (*right*) X-ray system. (From S. Rooks, ''Controlling BGA Assembly using X-ray Laminography'', *EP&P*, pp. 24–30 (January 1997): reprinted by permission.)

joints. Commonly used systems include transmission X-ray and cross-section X-ray systems. Figure 4.54 shows the solder joints of a BGA assembly [57]. The cross-sectional X-ray image clearly identifies the open non-collapsible BGA joints (right). Transmission X-ray systems often cannot detect open solder joints (left). This constraint of transmission X-ray systems can be partially relieved by inspecting the solder joints at a tilted angle. However, this approach may not work for large boards, due to the limitation in tilting angle allowed within the chamber.

Laser IR inspection system uses a controlled pulse of laser energy to slightly heat the joint surface. The resultant rise and decay curve becomes the joint's "signature". It then compares the signature of a good joint for each location on the PCB, and reports the location and amount of deviation from predetermined standards. The operating speed is 10 solder joints per second with 0.1-in. spacing and 30 millisecond exposure. The laser types include heating (continuous ND: YAG, 15 watts min. at target) and spotting (HeNe visible light, 1 mW max. at target). The infrared detector used is cryogenically cooled indium antimonide InSb [58]. Figure 4.55 shows some thermal signatures correlated with some defects of solder joints. Laser IR inspection is not a commonly adopted method in production environment, presumably due to the complicated interpretation required for signature registered.

Acoustic microscopes produce very high resolution images with ultrasound ranging in frequency from 10 to 500 MHz or higher. There are three intrinsically different types of acoustic microscopes, as shown in Figure 4.56 [59]. The SLAM (scanning laser acoustic microscope) is a transmission mode instrument that produces real-time images of a material, detecting defects and discontinuities throughout the thickness of the sample. Ultrasound frequencies employed range from 10 to 100 MHz, and possibly to 500 MHz. The other two types are reflection mode instruments which use a single focused transducer to send and receive the ultrasound and create an image on a CRT in 8–10 seconds. These instruments are known as scanning acoustic microscope (SAM) and C-mode scanning acoustic microscope (C-SAM). The SAM utilizes 100–400 MHz frequencies of ultrasound to investigate the surface and near surface regions of a sample (a few microns deep), while the C-SAM utilizes 25–100 MHz frequencies to obtain penetration power for inspecting deeper lying features (several millimeters deep) [59].

4.8 Cleaning

Depending on the type of solder paste materials used, the boards assembled may or may not need to be cleaned.

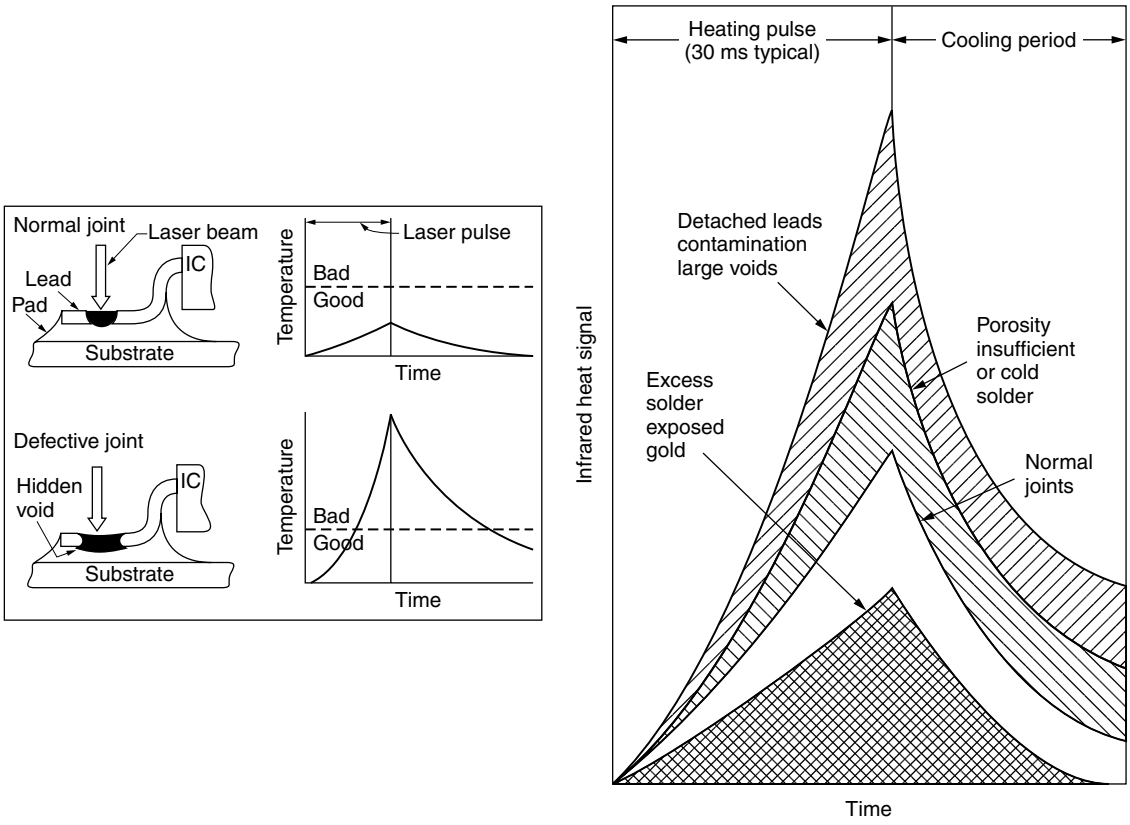

Figure 4.55 Thermal signatures vs defects of solder joints [61]

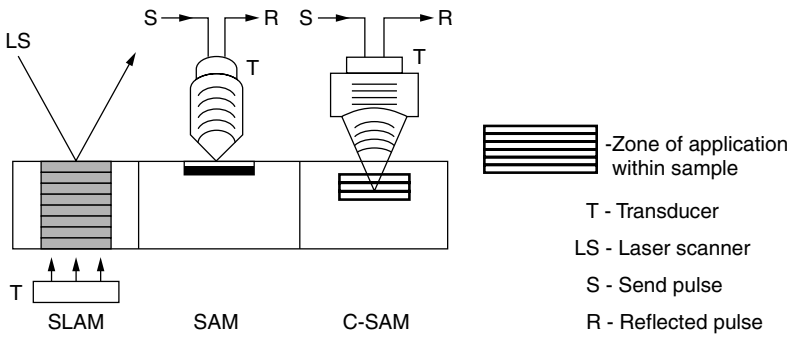

Figure 4.56 Schematic of acoustic microscopy techniques [62]

Although the trend of the industry is gradually shifting towards the no-clean process, a considerable part of the industry still applies cleaning to postsolder PCBs.

The contamination on the PCB can be categorized as particulates, ionics, and nonionics, shown in Table 4.10 [60]. Hymes [61] has stated that the reasons for cleaning include: (1) removal of residues which could contribute to electromigration and result in current leakage between circuitry, (2) eliminating the possibility of corrosion of circuitry and component packages as a result of flux residues themselves, or as a result of pick-up of harmful particulate contaminants by the flux residues, (3) providing for reliable adherence of correctly applied protective coatings by removal of materials which might result in porosity or reduce the bond strength between the coating and the substrate or components, (4) facilitating accurate, reliable, repeatable bed of nails testing and inspection using visual or infrared techniques, and (5) providing for cosmetically appealing solder joints.

Due to concern for ozone depletion, the primary cleaner chlorofluorocarbon (CFC) solvents used in the past have been replaced by other cleaner chemistries, including hydrochlorofluorocarbon (HCFC), non-halogenated organic solvents, aqueous, and semi-aqueous systems. The first

Table 4.10 Classification of the chief contamination types on PCB [60]

Particulate	*Polar, ionic, or inorganic*	*Nonpolar, nonionic, or organic*
Resin and fiberglass debris from drilling and/or punching operations	Flux activators	Flux resin
Metal and plastic chips from machining and/or trimming operations	Activator residues	Flux rosin
Dust	Soldering salts	Oils
Handling soils	Handling soils (sodium and potassium chlorides)	Grease
Lint	Residual plating salts	Waxes
Insulation	Neutralizers	Synthetic polymers
Hair/skin	Ethanolamines	Soldering oils
	Surfactants (ionic)	Metal oxides
		Handling soils
		Polyglycol degradation byproduct
		Hand creams
		Lubricants
		Silicones
		Surfactants (nonionic)

two systems are a moderate transition from CFC cleaning technology. While the cleaning efficiency is considered to be satisfactory, disposal of these waste solvents remains a problem. Aqueous cleaning is the most attractive cleaning system, due to the low cost and the recyclability of water. However, since most of the solder pastes used in the industry are either rosin or non-hydrophilic resin systems, aqueous cleaning will not be adequate and either semi-aqueous or saponified aqueous cleaning systems have to be employed to address the washability issue.

Once the cleaner chemistry is selected, the next decision is the choice of cleaning equipment. Board size and volume requirement are two major factors determining the equipment type for use. Cleanup of small boards produced in low volume is costly and inefficient within a large in-line system environment, while large boards may not fit in some of the smaller systems [62]. A benchtop cleaning system is good for small volume manufacturers. It can also be used for cleanup after manual operations. A floor-standing batch cleaning system is pertinent for handling large boards and medium volumes. For very high throughput and large PCBs, high-volume in-line systems are needed. Heat, spray, and ultrasonic agitation improve cleaning efficiency. However, the use of ultrasonics may accelerate the failure of faulty wire-bonding. On the other hand, it is argued that ultrasonic agitation can be used as a good environmental "screen" for poor quality in component design and assembly. Figure 4.57 shows an example of in-line defluxer with liquid seals [63], and Figure 4.58 illustrates an in-line water cleaning system [64,65].

4.9 In-circuit-testing

For some assembly lines in-circuit-testing will be needed at the post-soldering or post-cleaning stage. In the no-clean process, false opens may become an issue if the presence of flux residue interferes with establishment of electrical contact. The problem may be aggravated if the flux accumulates at the probe head. Although a higher probing pressure may help in lessening the problem, constant brushing of the probe head may still be required in order to reduce the rate of false opens. This problem can also be resolved by utilizing an adequate solder paste, as will be discussed in a later chapter.

4.10 Principle of troubleshooting reflow soldering

The potential problems associated with using solder pastes for SMT applications can be categorized into prior-to-reflow and post-reflow stages. In general, virtually all problems can be traced back to all three major contributing factors–material, process, and design–although sometimes one factor may contribute more than the others. To troubleshoot the reflow soldering processing, the first step is to identify the root causes of problems, ideally followed by correcting these causes.

However, sometimes the root causes may not be within the reach of the manufacturer. For situations like this, it should be pointed out that the problems still might be eliminated or lessened by examining and further optimizing the remaining contributing factors which are within the capability of the manufacturer. Although possibly less obvious, this approach often can be effective enough to alleviate the problem completely. For instance, unbalanced pad dimension design may be the root cause of tombstoning of chip capacitors in some assembly processes. For assembly contract manufacturers, requesting the OEM to change the pad design may be either out of the question or too time consuming. Fortunately, problems like this could still be solved by taking the processing approach of employing a reflow profile with a slow ramp-up rate when crossing over the melting point of solders. It may also be solved by taking the material approach by employing a solder paste with a pasty range. Both approaches are not considered root causes, but could be

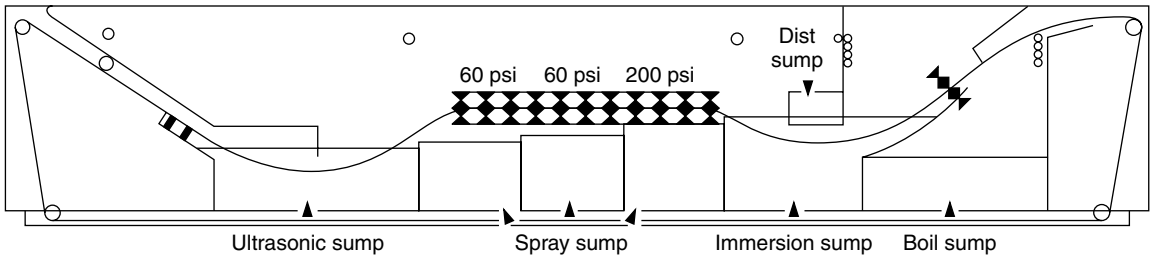

Figure 4.57 Scheme of conveyorized defluxed with liquid seals [66]

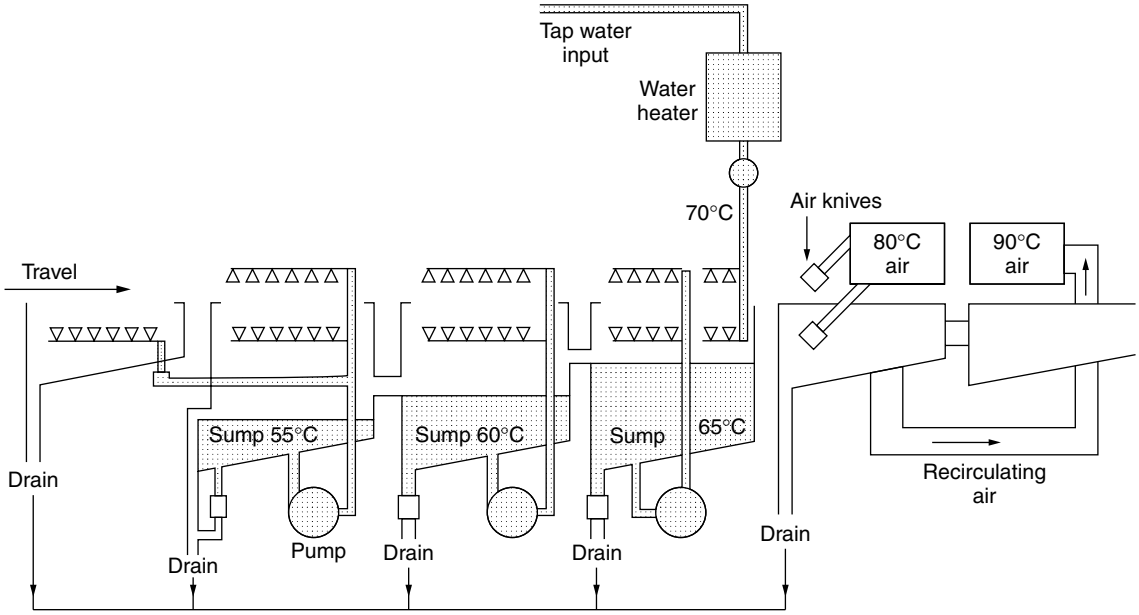

Figure 4.58 Example of in-line water cleaning system [67,68]. The stage on the left is the prewash. This is followed by three recirculating washes connected in cascade, each with its own pump. As the PCBs progress the water becomes hotter and cleaner

effective enough to eliminate the tombstoning problem. Details of this as well as other examples will be discussed in subsequent chapters.

4.11 Conclusion

Surface mount assembly utilizes solder paste as the primary bonding material. Successful implementation of the assembly process involves a good understanding of solder paste properties, an adequate stencil design as well as printer setting, components placement, proper reflow, inspection, and testing. Besides the trend toward miniaturization, cost reduction and environment-friendly considerations also drive the evolution of processing technology.

References

1. P. Jaeger, private communication, 26 April 2000.
2. M. Xiao, K. J. Lawless, and N. C. Lee, ''Prospects of Solder Paste Applications in Ultra-fine Pitch Era'', in *Proc. of Surface Mount International*, San Jose, CA, August 1993.
3. N. Peterson, ''A Solder Paste Dispenser for SMD assembly'', *Surface Mount Technology*, International Electronic Packaging Society, 3–2 (1989).
4. Fusion product data sheet.
5. TSI product data sheet.
6. Universal Instrument Inc. product data sheet.
7. R. Ludwig, N. C. Lee, S. R. Marongelli, S. Porcari, and S. Chhabra, ''Achieving Ultra-fine Dot Solder Paste Dispensing'', in *Proceedings of Advanced Electronic Assembly Conference*, Providence, RI, October 1998.
8. SCM-Dispensit product data sheet.
9. N. C. Lee, ''How to Make Solder Paste Work in Ultra-fine-pitch and Non-CFC Era'', short course at Surface Mount International, San Jose, CA, September 1994.
10. M. D. Herbst, ''Metal Mask Stencils for Ultra Fine Pitch Printing'', in *Proc. of Surface Mount International*, San Jose, CA, pp. 101–109 (29 August–2 September 1993).
11. Elcon Inc.: Technical information.
12. W. E. Coleman, 'Photochemically Etched Stencils for Ultra-fine-pitch Printing', *Surface Mount Technology* (June 1993).
13. Technical Data Sheet of KJ Marketing Services (1999).
14. Micro-Screen: Technical information (November 1993).
15. W. E. Coleman, ''Stencils for Ultra Fine Pitch Solder Paste Printing'', in *Proc. of Nepcon West*, Anaheim, CA, pp. 1219–1231 (7–11 February 1993).
16. K. Jenczewski and R. Venkat, ''Band Etch Technology: An Overview'', Beam On Technology Corp., San Jose, CA (1993).

17. Metal Etching Technology: Technical information (November 1993).
18. T. R. Jillings, ''Stencils: Understanding the Basic Components'', *Surface Mount Technology*, pp. 38–40 (February 1993).
19. A. Johnson, short course on ''Fine Pitch Stencil Printing and Applications Class'' (1999).
20. Photo Stencil Inc. technical data sheet (1993).
21. UNIPUR Co. technical data sheet (1994).
22. Microcircuit Engineering Corporation: Technical Information on Precision Machined Polyurethane Squeegee Blades.
23. Transition Automation, ''Everything You Wanted to Know about Fine-pitch Printing (but were afraid to ask)'', technical literature (1992).
24. C. P. Brown, ''Process Solutions for Ultra Fine Pitch Production'', in *Proc. of Surface Mount International*, San Jose, CA, pp. 119–126 (29 August–2 September 1993).
25. DEK ProFlow technical data sheet.
26. Y. Guo, ''A Study of Solder Paste Printing Process'', in *Proc. of Nepcon West*, Anaheim, CA, pp. 1739–1754 (7–11 February 1993).
27. ''Measure It! Process Control for Solder Paste Deposition'', CyberOptics: Surface Mount Technology Technotes.
28. S. K. Case, ''Inspection of Solder Paste on the Board'', *EP&P* (May 1991).
29. T. L. Hodson, ''Selecting Pick-and-place Equipment'', *EP&P*, pp. 32–37 (June 1993).
30. H. Pawlischek, ''Major Requirements for Fine-pitch SMD Placement Systems'', in *Proc. of Surface Mount International*, San Jose, CA, pp. 127–138 (29 August–2 September 1993).
31. J. M. Anderton and M. Sweeney, ''Chip Cracking: A Study of Capacitor Failure Modes'', *Surface Mount Technology*, pp. 45–46 (March 1992).
32. P. Marcoux, *Fine Pitch Surface Mount Technology: Quality, Design and Manufacturing Techniques*, Van Nostrand Reinhold, New York, pp. 169–198 (1992).
33. N. M. Dytrych, ''Reviewing the Basics of Mass Reflow Soldering'', *EP&P*, pp. 34–40 (July 1993).
34. N. C. Lee, ''Optimizing Reflow Profile via Defect Mechanisms Analysis'', IPC Printed Circuits Expo '98.
35. S. J. Dow, ''Use of Radiant Infra-red in Soldering Surface Mounted Devices to PCBs'', *Brazing & Soldering*, No. 8, pp. 16–19 (1985).
36. Radiant Technology Corporation: ''The Better Way to Solder Attach Surface Mount Devices'' (1993).
37. D. Schoenthaler, ''Solder Joining and Fusing with Radiant Heating'', *Assembly & Joining Techniques*, IPC, Illinois (1978).
38. C. Lea, *A Scientific Guide to Surface Mount Technology*, Electrochemical Publications, Isle of Man, UK (1988).
39. S. J. Dow, ''Use of Radiant Infra-red in Soldering Surface Mounted Devices to PCBs'', *Brazing & Soldering*, No. 8, pp. 16–19 (1985).
40. S. Patel, ''Vapor Phase: A User's Point of View'', *Surface Mount Technology*, pp. 27–28 (March 1992).
41. D. Brammer, ''Reductions in Inert Gas Usage and No-clean Processes in Recirculating Forced Convection SMT Reflow Systems'', in *Proc. of NEPCON WEST*, Anaheim, CA, pp. 137–142 (1993).
42. Research Inc.: Technical Information on MICRO-FLO XG Forced Convection Reflow System (April 1993).
43. N. Cox, ''Optimizing Nitrogen Purity and Flow in a Convection Reflow Oven'', in *Proc. of NEPCON WEST*, Anaheim, CA, pp. 149–157 (1993).
44. MCT/BROWNE: Application Notes on MCT/BROWNE 6800IR Series Belt-Type Infra-red Reflow Soldering System.
45. Sikama International, Inc.: Technical Information on FALCON 8/C and FLACON 12/C (1993).
46. R. J. Klein-Wassink, *Soldering in Electronics*, 2nd edn, Electrochemical Publications, Ayr, Scotland (1989).
47. P. Jaeger and N.-C. Lee, ''A Model Study of Low Residue No-clean Solder Paste'', in *Proc. of Nepcon West*, Anaheim, CA (February 1992).
48. *Metal Handbook, Vol. 8: Metallography, Structures and Phase Diagrams*, 8th edn, American Society for Metals, Metals Park, OH (1973).
49. Indium Corporation of America Technical Data (October 1993)
50. C. M. Melton, A. Skipor, and W. M. Beckenbaugh, ''Low Temperature-wetting Tin-base Solder Pastes'', US Patent 5,229,070 (20 July 1993).
51. L. Bernstein, ''Semiconductor Joining by the Solid–Liquid-Interdiffusion (SLID) Process: I. The Systems Ag-In, Au-In, and Cu-In'', *Journal of the Electrochemical Society*, pp. 1282–1288 (December 1966).
52. L. Bernstein and H. Bartholomew, ''Applications of Solid–Liquid Interdiffusion (SLID) Bonding in Integrated-circuit Fabrication'', *Transactions of the Metallurgical Society of AIME*, Vol. 236, pp. 405–412 (March 1966).
53. J. W. Roman and T. W. Eagar, ''Low Stress Die Attach by Low Temperature Transient Liquid Phase Bonding'', in *Proc. of ISHM*, pp. 52–57 (1992).
54. AT&T-Federal Systems Division, Edward Barnes.
55. J. S. Hwang, *Solder Paste in Electronics Packaging*, Van Nostrand Reinhold, New York (1989).
56. P. E. Nothnagle, ''Surface Mount and Optical Inspection'', *Circuits Assembly*, pp. 38–39 (August 1993).
57. S. Rooks, ''Controlling BGA Assembly using X-ray Laminography'', *EP&P*, pp. 24–30 (January 1997).
58. Vanzetti Systems, Inc.: Technical Information on Laser Inspect (1985).
59. Sonoscan, Inc.: Technical Information on Applications in Acoustic Microscopy (1988).
60. ANSI/IPC-SC-60 1987.
61. L. Hymes (ed.), *Cleaning Printed Wiring Assembles in Today's Environment*, Van Norstrand Reinhold., New York (1991).
62. C. Hutchins, ''Equipping for the Cleanup'', *Surface Mount Technology*, p. 11 (November 1992).
63. Allied-Signal/Baron-Blakeslee.
64. C. Lea, *After CFCs?* Electrochemical Publications, Isle of Man, UK (1992).
65. *Post-solder Aqueous Cleaning Handbook*, Institute for Interconnecting and Packaging Electronic Circuits, IPC-AC-62 (1986).

5 SMT Problems Prior to Reflow

As described in Chapter 4, the processing of solder paste starts with paste handling and storage therefore there are associated problems. This chapter covers all the major problems related to solder paste applications in SMT prior to reflow, with a primary emphasis on storage, deposition, and component placement.

5.1 Flux separation

Ideally, solder paste should be a homogeneous mixture of flux and solder powder. However, sometimes it may display flux separation upon opening the container. The symptom typically is a yellow layer of flux on top of gray paste in either a jar or a syringe container. In the case of a syringe, if this is laid down on its side during storage, the separated flux may show up as a stripe along the top. Slight flux separation is acceptable but serious flux separation may result in smear and slump, as well as uneven solder volume deposit, therefore it has to be corrected.

The possible causes of flux separation include: (1) too high a shipping or storage temperature, (2) paste being left too long on the shelf, (3) paste being too low in viscosity, and (4) paste being too low in thixotropic property.

The solutions for eliminating flux separation can be categorized as process and material. Processwise, the solutions include: (1) using paste within its recommended shelf life, (2) storing the paste on a rotating rack, (3) storing the paste at a low temperature, usually -10° to 5°C will be considered adequate although a lower temperature often is more beneficial, and (4) stirring the paste prior to use, either manually or using equipment. However, it should be noted that excessive mixing of the solder paste may result in hardening of the paste due to cold welding, therefore this should be avoided. Materialwise, the solutions include: (1) using a paste with a sufficiently high viscosity and (2) using a paste with a sufficiently high thixotropic property. For printing and dispensing purposes, a thixotropic index of -0.5 to -0.8, as defined in Chapter 3, is considered adequate.

5.2 Crusting

Solder paste may also display a layer of crust on its surface. This can be observed in either a newly opened container or a container with used paste.

Materialwise, crusting can be caused by employing solder alloys with a very high lead content, such as 97Pb/3Sn, 97.5Pb/2.5Ag, 97.5Pb/1.5Ag/1Sn, or 98Pb/2Sb. Alloys with a high indium content also are prone to exhibiting crusting. It may also be caused by using a flux which is too corrosive or reactive in storage conditions. With the flux reacting with the solder, the metal salts formed are higher in molecular weight, therefore are higher in viscosity and appear as a skin or crust on the surface of solder paste. Processwise, the paste may have been extensively exposed to air or moisture, due to (1) trying to scavenge a used paste, (2) container being left open for too long a time, (3) inadequate paste packaging which allows moisture and air to penetrate through the container wall, and (4) too high a storage temperature.

Materialwise, the solutions include: (1) using a paste less corrosive or reactive in storage conditions and (2) using solder alloys with a lower Pb or In content. Processwise, the first solution is trying to avoid putting the used paste back in the container and reusing it later. One side benefit of using a cartridge as container is that solder paste dispensed can be assured of being unused. When using a jar as a container, the jar should be covered with a lid whenever feasible. An insert in contact with the paste is recommended. The paste packaging should be gas tight, and using materials which do not allow moisture and oxygen to permeate through the container wall. Unless specified by the solder paste supplier, all solder pastes are recommended to be stored at a low temperature. The lower the storage temperature, the longer the shelf life will be. It should be noted that, unlike liquid fluxes, solder pastes typically have no flux crystallization problems due to low storage temperature.

5.3 Paste hardening

The unused solder paste in a container may already turn out to be hard or very viscous at the user site. This can be observed for a well-packaged solder paste.

The causes of this problem can be due to the material factor. The flux may be too reactive in storage conditions. As discussed in Chapter 3, flux reacts with metal oxide and forms a metal salt which is higher in viscosity than the flux itself. This reaction may occur with or without the

presence of oxygen and moisture. Ideally, this flux reaction will occur at the soldering temperature. However, if the reaction occurs extensively at storage temperature, the solder paste may have too many metal salts hence may become very viscous. In addition, solder powder without the protection of an oxide layer tends to cold weld and form a hard powder cluster, thus further aggravating the problem. This cold welding problem could be more serious with soft alloys such as high indium-containing solders. The process factor may include a too high shipping or storage temperature.

Effective solutions include: (1) reduced shipping and storage temperature, and (2) employing fluxes with low activity at shipping and storage temperatures. Also, using solder powder with higher oxide content would help alleviate the problem. This is particularly true for soft alloys. However, the latter approach may compromise soldering performance, such as soldering balling, wetting, and voiding, as will be discussed later.

5.4 Poor stencil life

During stencil printing, the quality of print may initially be good. However, with increasing printing time, the print quality may start to degrade. The most commonly encountered symptom is a paste gradually thickening up, as shown in Figure 5.1, with resultant skipping, incomplete filling, poor release from the squeegee, and aperture clogging. For some type of pastes, the symptom may be the opposite. The paste may gradually thin with an increasing number of prints, and result in smearing and flux bleeding. Both cases result in a compromised stencil life.

For a conventional stencil printer, paste thickening on the stencil can be caused by (1) paste becoming crusted or solder powder cold-welded due to high flux activity at ambient temperature, (2) paste drying out too quickly due to the use of volatile solvents in the flux, (3) too low a paste consumption / replenishment rate, (4) too high an ambient temperature, (5) too high a humidity, and (6) too much air drift above the stencil.

The effect of humidity on the viscosity of paste on stencil can be twofold for no-clean or RMA solder pastes. The paste viscosity often increases with time under high humidity, such as 80%RH, due to the augmented chemical reaction between flux and metal in the presence of moisture. On the other hand, low humidity such as 20%RH or less may also cause problems. For no-clean and RMA solder pastes with a volatile solvent system, paste viscosity often increases with increasing exposure time under low humidity, mainly due to solvent loss.

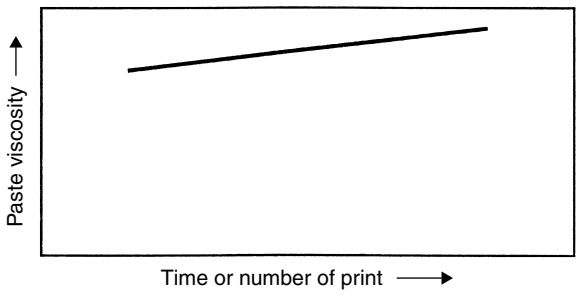

Figure 5.1 Solder paste thickens up with increasing number of prints

For water-washable solder pastes, paste viscosity often decreases with increasing time on stencil under high humidity conditions. Since water washable solder paste is hygroscopic in nature, the rapid viscosity decrease due to moisture-pick-up often overtakes the viscosity increase due to chemical reactions. It is fairly crucial to maintain a low humidity while running water washable solder pastes.

To troubleshoot the stencil life problem for conventional printer applications, materialwise, a non-corrosive paste with a low metal load and a non-volatile solvent system will be desirable. Processwise, minimizing the air drift above the stencil and maintaining a moderate humidity and temperature at the printer will be effective.

For closed chamber printing, such as RheoPump or ProFlow design, stencil life may also be an issue. As discussed in Chapter 4, the elimination of paste exposure avoids problems associated with drying, oxidation, and moisture absorption, and therefore should result in a longer stencil life. However, there are some side effects observed for some solder paste systems which function properly on conventional printers. Some solder pastes tend to thicken in the chamber with increasing numbers of printings, while others tend to thin and leak out of the chamber.

As illustrated in Figure 5.2 [1], a conventional printer shears solder paste through the contact of paste with a standard squeegee head and stencil. There is a substantial amount of solder paste doll free from surface shearing. However, for a closed chamber printer, such as the rheometric pump shown in Figure 5.2, the solder paste is sheared excessively all around through contact with the chamber and the stencil. Depending on the paste's chemistry, excessive shearing may cause either shear-thinning or shear-thickening. Although more data are needed to confirm the trend, solder pastes with low elastic properties or low recovery [2] are believed to be more prone to having the shear-thinning symptom. On the other hand, fluxes that are reactive or corrosive at ambient temperature will readily break down the solder oxide protective layer, and consequently result in cold-welding or paste-thickening under excessive shearing conditions [3]. The symptom may appear as early as 50–60 prints, or as late as about 1000 prints.

Materialwise, the solutions to achieve a better stencil life for closed chamber printing include: (1) lower flux reactivity and corrosivity at room temperature, (2) a higher elastic property or a higher recovery in rheology, (3) lower metal load, such as 89 percent or 88 percent, (4) coarser solder powder, and (5) a higher oxide content in the solder powder. Items (3), (4), and (5) compromise on slump, print definition, and solder balling/wetting performance respectively, as will be discussed later. Processwise, the solutions include (1) a slower print speed, (2) a lower pressure on the solder paste, and (3) a more frequent preventive maintenance schedule. Designwise,

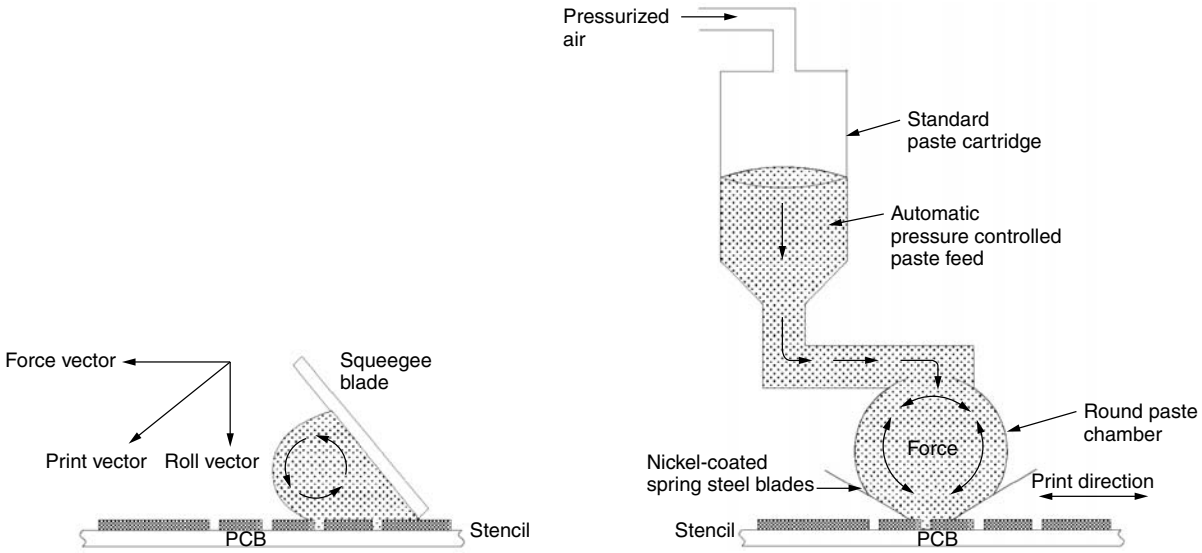

Figure 5.2 Comparison of paste shearing pattern for standard squeegee head (left) and rheometric pump print head (right) [1]

the chamber shape and paste feeding port might be further improved to eliminate the dead corner for solder paste flow.

5.5 Poor paste release from squeegee

Figure 5.3 shows an example of poor release of solder paste from the squeegee after one print for a single squeegee system which prints in one direction only. When the squeegee is moving back to the ready-to-print position, the excessive paste remaining on the squeegee is dragged across the stencil surface. During this some paste may be left on the top of some of the apertures and consequently contribute to smearing or clogging. Figure 5.4 shows an example of poor release for a dual squeegee system. At the end of one print in the right direction, the left squeegee is lifted, with a significant amount of paste adhering to the squeegee. The right squeegee is ready for the next print in the left direction. However, only a very small amount of paste is left in front of the squeegee for printing. A similar problem can also occur for a single squeegee system where the squeegee prints back and forth, and the squeegee moves to the other end of the paste pile at the end of one print, as shown in Figure 5.5.

The causes of poor paste release from a squeegee can be attributed to: (1) the paste being too tacky, (2) the paste being too stringy, (3) the paste gradually drying out on the stencil, (4) insufficient paste placed on the stencil, (5) the squeegee holder protruding too much together with a short squeegee height, (6) too small a contact angle between squeegee and stencil, and (7) too smooth a stencil surface.

During printing, the paste often creeps up along the squeegee, and results in a slightly greater contact area with squeegee than with the stencil, as illustrated in Figure 5.6. Upon squeegee lifting, the solder paste experiences two competing forces: (1) adhesion to both squeegee and stencil, and (2) gravity of solder paste; the distribution of solder paste is dependent on the balance of these two forces. For a properly formulated solder paste, the sum

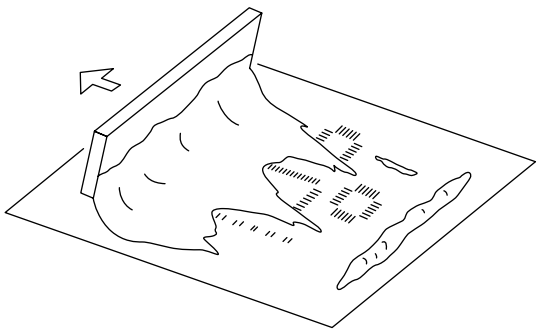

Figure 5.3 Schematic of poor release of solder paste from squeegee during printing

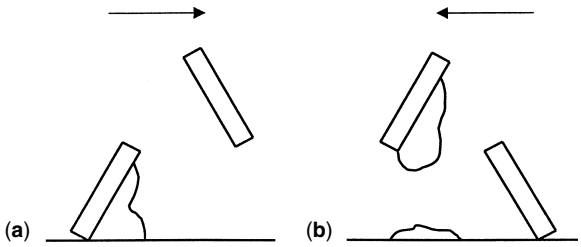

Figure 5.4 Schematic of poor squeegee release for dual squeegee system: (**a**) end of print toward right direction, (**b**) left squeegee lifted, with significant amount of paste hung onto the squeegee. Right squeegee is ready for next print toward left direction. However, there is not enough paste in front of the squeegee for printing

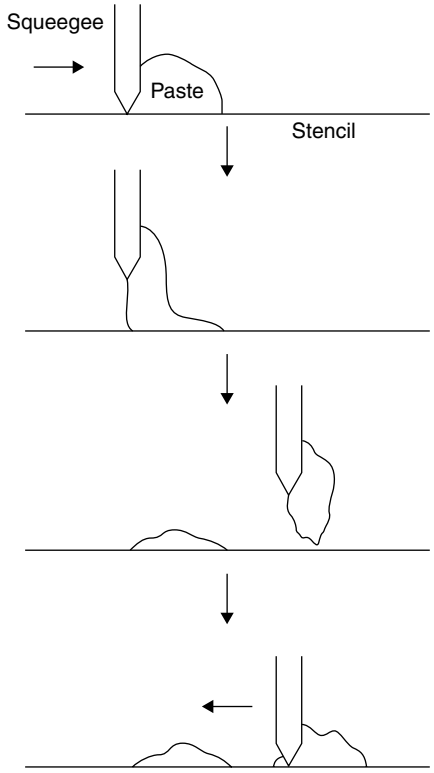

Figure 5.5 Poor release of paste from squeegee for single squeegee system where the squeegee prints back and forth, and the squeegee hops to the other end of the paste pile at the end of one print

of gravity and adhesion with a stencil overrides adhesion with a squeegee, and most of the paste stays on the stencil.

If the solder paste is very tacky or very stringy, the gravity factor will be negligible relative to adhesion, and the slightly larger contact surface area with the squeegee determines the distribution of solder paste. As a result, most of the paste will stick to the squeegee. A similar symptom will be observed if the solder paste gradually dries out, hence gradually gaining more tack. Although a low tack solder paste will result in easy release from the squeegee, the loss in ability to hold components during the pick and place process essentially rules out the acceptability of this approach. A desirable solder paste will be moderate in tack, with non-volatile solvents. Although a lower metal content will also help in improving squeegee release by reducing the tack value [4], this approach will result in a higher slump, therefore it can remain only as a supplementary option. In general, for fine-pitch SMT applications, the metal load preferred is around or higher than 90 percent w/w.

The effect of a larger contact surface area with the squeegee than with the stencil is augmented if the paste volume, hence the paste weight, is very small. Not surprisingly, this often results in poor squeegee release. Therefore, depending on the type of solder paste, the diameter of the paste doll is recommended to be greater than 0.5 in. For some solder pastes with a higher tack value, a doll diameter of no less than 0.75 in will be desired. At the end of one print, release of paste from the squeegee can also be facilitated by holding the squeegee in place for 10–20 seconds before starting the next print. Other means which can prevent the paste from drying out or thickening, as discussed in section 5.5, are also expected to help in maintaining squeegee release performance.

The design of the squeegee holder also has a strong influence on squeegee release. For some printers, the squeegee height is short and the squeegee holder protrudes considerably toward the stencil, as shown in Figure 5.7. Upon printing, the paste smudges the holder, and results in a much larger contact area between the paste and the squeegee system, hence inevitably causing squeegee release. Problems such as this can be corrected by employing a squeegee with a large height and/or a thin securing plate for the side facing the stencil, as shown in Figure 5.8. In addition, a larger contact angle between squeegee blade and stencil would help in reducing the creeping height of the solder paste, hence reducing poor squeegee release.

Since the squeegee release problem is a result of adhesion between paste and the surface of the squeegee and stencil, adjusting the surface properties may improve squeegee release. In principle, a smooth surface and a low surface energy are expected to result in low adhesion, and consequently satisfactory squeegee release. Generally, all squeegees, including those made of rubber or metal, exhibit a smooth surface finish.

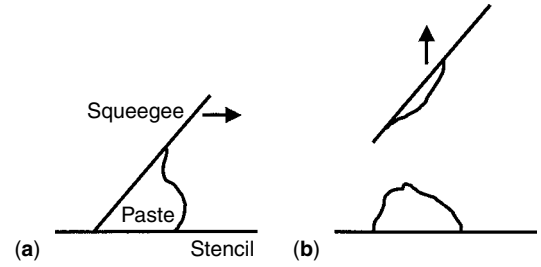

Figure 5.6 Typical solder paste distribution (**a**) during printing, and (**b**) upon squeegee lifting

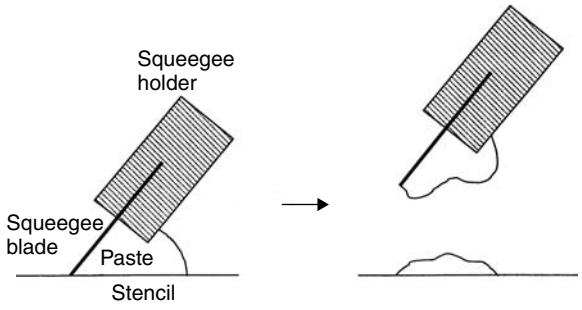

Figure 5.7 Schematic of poor solder paste release from squeegee due to protruding squeegee holder together with a short squeegee height

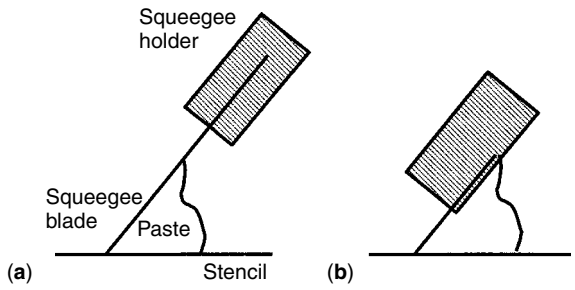

Figure 5.8 Modified squeegee system design for better solder paste release: (**a**) squeegee blade with a greater height, (**b**) squeegee holder with a thinner securing plate on the side facing stencil

Furthermore, altering the surface finish properties by applying Teflon coatings or plating with nickel has been found to have no effect on improving squeegee release [5]. However, on the other hand, it is feasible to manufacture a stencil with a rough surface, thus increasing adhesion between paste and stencil. This approach has been proved to be fairly effective.

5.6 Poor print thickness

One study of SMT defects showed that most are due to lead non-coplanarity (ASIC/bypass), missing parts, solder bridging, and opens such as tombstoning, misaligned parts and lack of solder [6]. Among the process-related defects on the 100 percent populated SMT boards [7], the causes were further categorized as solder paste printing process (63.8 percent), component placement (15.3 percent), reflow soldering and cleaning (15.2 percent), and incoming components (5.7 percent). Obviously, printing quality is the most critical performance of the SMT assembly process. Since the print thickness of solder paste reflects the solder volume deposited, which in turn governs defects such as opens, starved solder joints, joints with excessive solder volume, tombstoning, skewing, and bridging, as will be discussed later, it is extremely important to have a consistent and well-controlled print thickness at printing [3]. Unfortunately, the print thickness often deviates from the target thickness, being either too high, or too low, or inconsistent.

Factors affecting print thickness, besides stencil thickness, include: (1) solder powder size, (2) surface finish of pads, (3) thickness of solder mask, (4) proximity of labels, (5) debris on bottom of stencil or on top of PCB, (6) leveling of squeegee, (7) squeegee speed, (8) squeegee pressure and leveling, (9) squeegee hardness, (10) squeegee wear, (11) snap-off, (12) leveling of stencil versus PCB surface, (13) aperture warp, (14) aperture size, and (15) aperture orientation.

Solder powder size affects the homogeneity of solder paste. Apparently, too large a powder size is not going to provide a smooth print. For a consistent, high quality print, the powder size should not exceed 1/7 of the aperture size [4]. The surface finish of pads also affects print thickness. HASL often results in inconsistent print thickness, particularly for pads with high solder domes. This is due to solder scoop and skips caused by the dome of the pad entering the stencil opening [8]. Other surface finishes such as Ni/Au, immersion Sn, immersion Ag, and OSP have no adverse effect on print thickness.

If the thickness of the solder mask is greater than the height of the pad, paste thickness can be greater than the stencil thickness. An irregular solder mask thickness will directly contribute to inconsistent print thickness. Similarly, if the label or legend is very close to the aperture, the print thickness can also be greater. The presence of debris on either the bottom of the stencil or on the top of the PCB will result in an increase in print thickness.

Squeegee type and printer setting have a great impact on print thickness. Thus the print thickness increases with increasing snap-off, squeegee speed and decreasing squeegee pressure [9,10]. At a high squeegee speed, the print thickness can even be greater than the stencil thickness. This is caused by the high fluid pressure created at the squeegee tip forcing paste back under the squeegee [9]. At lower squeegee speed, increasing or decreasing the squeegee pressure produces a greater change in print thickness than at a higher squeegee speed [10]. This relationship is shown in Figure 5.9 [10]. This can probably be attributed to the flow time factor. At a lower squeegee speed, the paste has a longer flow time to allow it to comply with the pressure exerted by

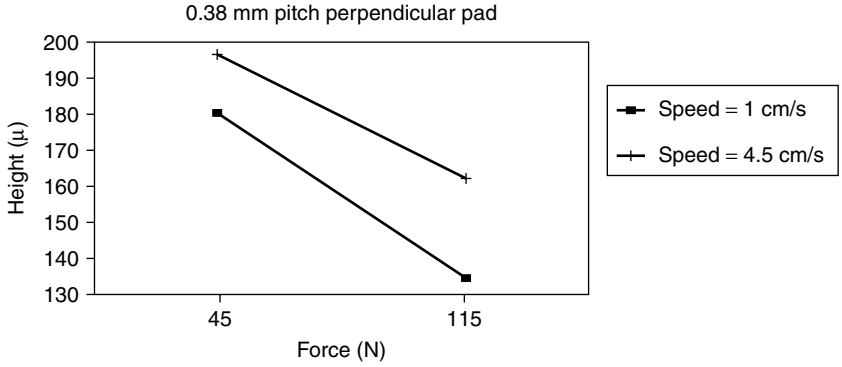

Figure 5.9 Effect of squeegee speed and squeegee pressure on print height for pads perpendicular to squeegee printing direction [10]

the squeegee. Thus the higher the squeegee pressure, the smaller the print thickness. On the other hand, at a higher squeegee speed, the paste does not have sufficient time to comply with the squeegee pressure. Hence, the print thickness becomes insensitive to squeegee pressure. As implied by the effect of the squeegee pressure, squeegee leveling also has a great influence on print thickness consistency.

The squeegee's hardness may have the most obvious effect on print thickness. A soft squeegee tends to deform readily under pressure and dig into the aperture during printing, as illustrated in Figure 5.10 [10]. This will inevitably result in scooping, hence a smaller print thickness. Table 4.5 in Chapter 4 demonstrated that the print thickness reduction rate increases with increasing softness [11]. Print thickness also increases with increasing squeegee wear because there is no sharp edge to dig into the openings, and also because the attack angle of the squeegee increases [12], as illustrated in Figure 5.11.

A greater snap-off will result in a larger print thickness. For the same reason, if the stencil is not leveled properly against the substrate's surface, the print thickness will also vary, with areas exhibiting larger snap-off, resulting in a larger print thickness.

Obviously, stencil aperture warp can result in a larger print thickness. The orientation of the aperture, as defined in Figure 5.12, has a complicated effect on print thickness. In general, perpendicular apertures result in a greater print thickness than parallel apertures, as reported by Mannan *et al*. [10] for a squeegee speed range of 10–60 mm/sec. The difference in print thickness is also supported by the data on paste volume using a polyurethane squeegee, as shown in Figure 5.13 [13]. Here the paste volume measured for parallel pads Nos. 1–40 and 81–120 is consistently less than that of perpendicular pads Nos. 41–80 and 121–160. A metal squeegee appears to be insensitive to aperture orientation, but, this is not always the case. When using a metal squeegee at very low speed such as 10 mm/sec, the print thickness for parallel orientation has been observed by Husman *et al*. [9] to be greater than that for perpendicular orientation. When the squeegee speed increases, the perpendicular orientation gradually exhibits a greater print thickness than the parallel orientation [9]. The difference in print thickness caused by aperture orientation can be eliminated by employing diagonal orientation.

A smaller aperture width also reduces the extent of digging of the squeegee's edge into the aperture, thus

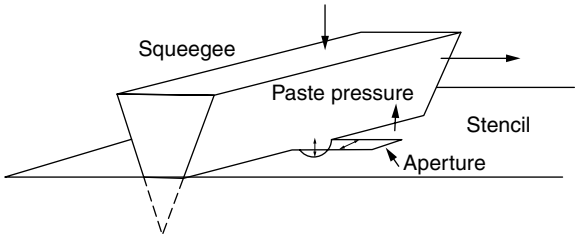

Figure 5.10 Deformation of squeegee under pressure while traveling across the stencil

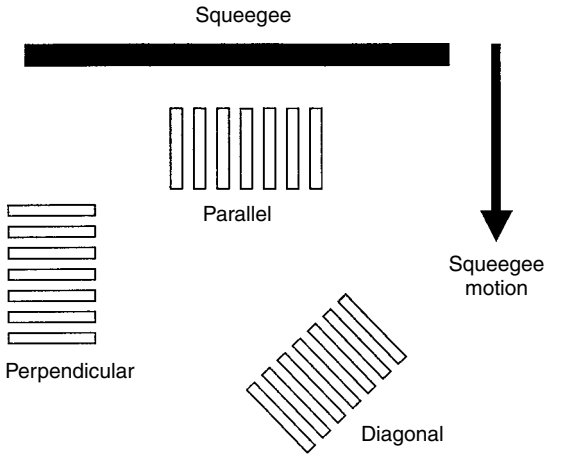

Figure 5.12 Orientation of perpendicular, parallel and diagonal apertures

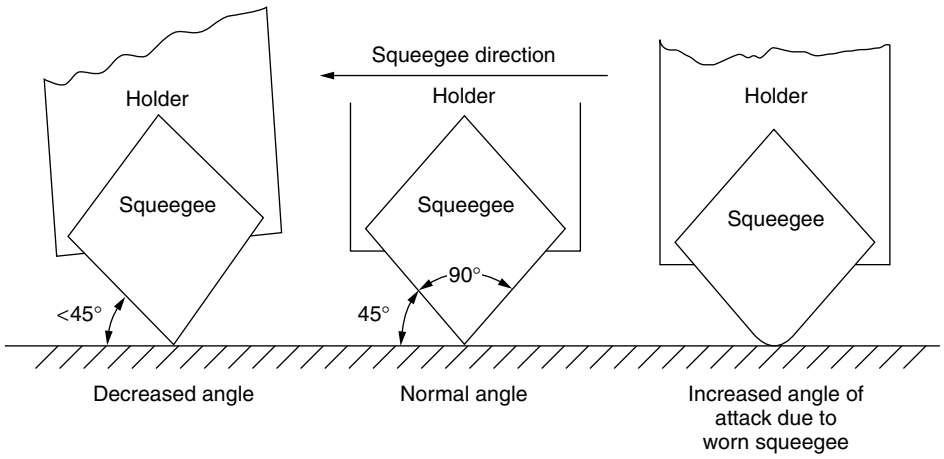

Figure 5.11 Squeegee wear reduces contact angle and scooping during printing [12]

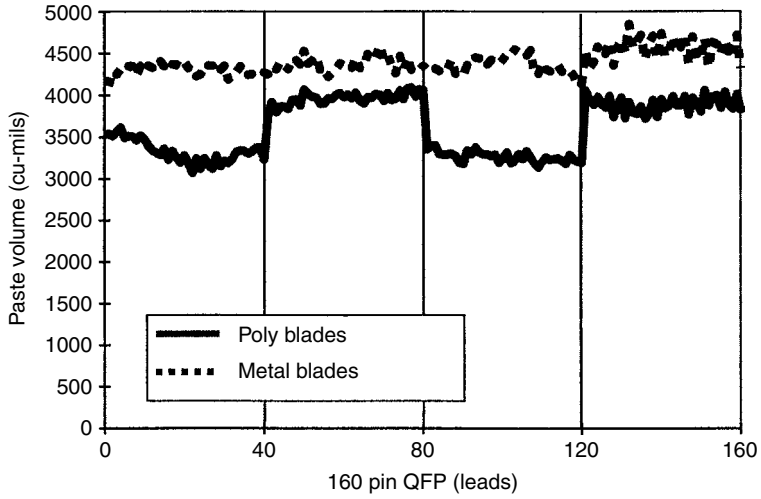

Figure 5.13 Effect of aperture orientation and squeegee material type on paste volume deposit [13]

resulting in a smaller print thickness [10]. The aperture width effect is measurable for a parallel aperture, but negligible for a perpendicular one.

Since the print thickness is affected by so many factors, it is crucial to maintain the consistency of each factor in order to have a consistent print thickness. These include proper leveling of stencil, board, consistent solder mask thickness, proper snap-off, squeegee pressure, and squeegee alignment, and proper wiping of the bottom of the stencil. Also, inconsistency caused by one factor may be compensated by another factor. For instance, if a diagonal orientation of aperture design is not possible, using a larger parallel aperture width than a perpendicular aperture would allow an equal paste volume to be deposited onto the footprint of a component.

5.7 Smear

Smear is the deposition of paste beyond the targeted deposition area upon lifting of the stencil during printing. It may appear as smudged paste around the pads, or as solder paste bridges between neighboring pads. Smear is often directly caused by the coating of solder paste around the aperture at the bottom of the stencil. Thus at the next print, the solder paste around the aperture is then transferred to the substrate and results in smear.

Factors contributing to smear include (1) stencil thickness, (2) taper treatment, (3) pitch dimension, (4) aperture orientation, (5) powder size, (6) squeegee pressure, (7) downstop, (8) poor gasketing of stencil on the PCB, (9) snap-off, (10) buildup of paste on the bottom of stencil, and (11) HASL quality.

Smear generally decreases with increasing stencil thickness, as shown in Figure 5.14 [4]. Presumably the printing pressure exerted onto the paste decreases gradually with increasing distance from the top of the aperture. As a result, the driving force for the paste to ooze into the space between the stencil and the board also becomes weaker when a thicker stencil is used.

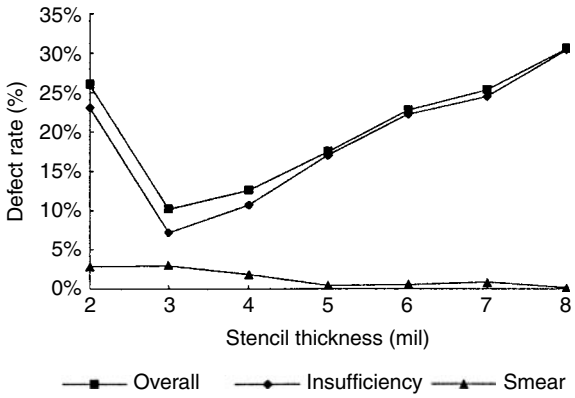

Figure 5.14 Effect of stencil thickness on print defect [4]

Table 5.1 Effect of tapering treatment on defect rate [4]

Aperture feature	*Smear defect rate(%)*	*Insufficiency defect rate(%)*	*Overall defect rate(%)*
Non-tapered	0.86	20.95	21.81
Tapered	1.97	19.19	21.16
Tapered/ non-tapered	2.29	0.92	0.97

Table 5.1 compares the defect rate of tapered patterns versus that of non-tapered patterns. The data are the averaged performance of all pastes and all stencils. It is interesting to note that the tapered pattern shows a considerably higher smear rate than the non-tapered pattern. Presumably this can be attributed to the wider opening of the bottom of the tapered aperture, which allows the paste to flow more readily under printing pressure.

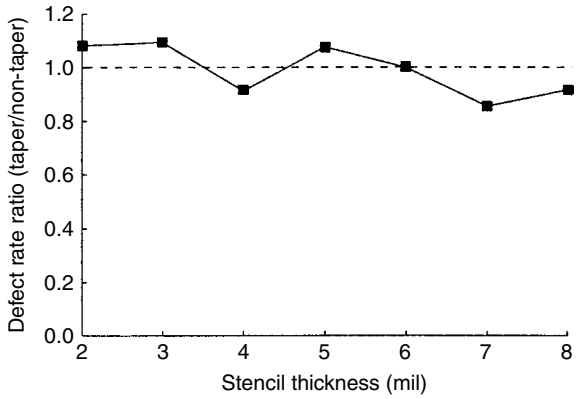

Figure 5.15 Effect of stencil thickness and taper treatment on the defect rate [4]

As shown in Figure 5.15, the adverse effect of tapering treatment on the overall defect rate gradually increases with decreasing stencil thickness. This is mainly due to the increasing contribution of smear to the overall defect rate, as demonstrated in Figure 5.14. For the ultra-fine-pitch printing process, since the stencil thickness is expected to become less, it is very questionable whether the tapering treatment is still desirable [4].

In Figure 5.16 the contribution of smear to the overall defect increases from virtually 0 percent to 8 percent when the pitch decreases from 50 to 8 mils [4]. This probably can be explained by the relative rate of paste leaked out versus spacing reduction. Hypothetically, the amount of paste leaked out should decrease with decreasing aperture size due to decreasing print pressure transmitted to the paste near the bottom of the aperture. On the other hand, a spacing reduction would enhance the probability of smear. It is possible that the spacing reduction effect overcompensates the paste leakage reduction effect, resulting in an increasing contribution of smear to the overall defect rate.

Parallel orientation of the aperture shows a higher defect rate than that of perpendicular orientation. The adverse effect of parallel orientation is particularly pronounced for smear type defect, as shown in Figure 5.17 [4]. This can be explained by the gasketing and restrained flow effects. In the case of perpendicular

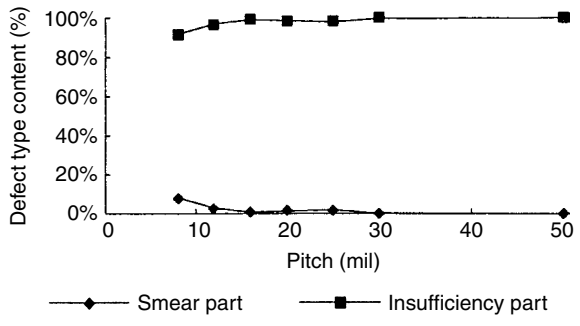

Figure 5.16 Effect of pitch dimension on distribution of various type of defect [4]

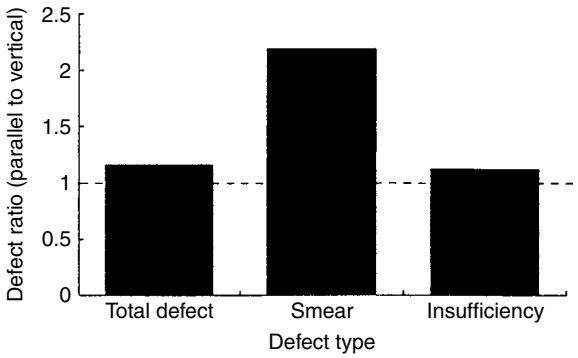

Figure 5.17 Effect of aperture orientation on defect rate [4]

orientation, the aperture axis is parallel to the squeegee axis. Hence the whole aperture is virtually pressed simultaneously by the squeegee during printing. This will not only create a very tight gasketing effect, but will also leave no free opening for the paste to flow out of the aperture. The former effect will result in a lower smear rate, while the latter will ensure a better filling of aperture with paste, and consequently a lower insufficiency rate.

The effect of aperture orientation on defect rate suggests that printability probably can be improved through redesigning the pattern orientation. Presumably this can be accomplished relatively easily through modifying the alignment of the printed circuit board on the printer by 45°.

To address the printability issue of ultra-fine-pitch, the use of fine powder is probably the most frequently adopted approach. Figure 5.18 shows the effect of solder powder size on defect type and defect rate. Here smear decreases with decreasing particle size. Presumably this can be accounted for by the restrained paste flow due to the higher viscosity and higher tack associated with finer powder [4].

Downstop is the downward distance the squeegee is allowed to travel beyond the board surface during the print stroke. Excessive squeegee pressure or downstop will force paste to ooze from the bottom of aperture and results in smear. Poor gasketing between stencil and board

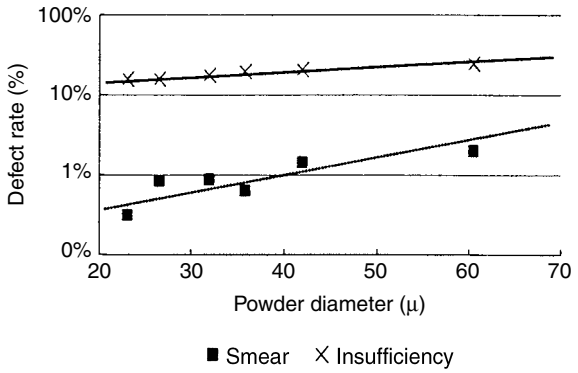

Figure 5.18 Effect of powder size on defect rate [4]

would allow the paste to leak out easily. This poor gasketing can be caused by (1) misregistration of the stencil on the board, (2) too high a solder mask thickness, (3) poor stencil leveling against the board, (4) too large a snap-off, and (5) buildup of solder paste at the bottom of the stencil around the aperture. Poor HASL quality, such as bridging or formation of an icicle, may also cause poor gasketing and result in smear.

In the event of having paste buildup at the bottom of the stencil, the easiest troubleshooting approach may be to employ stencil wiping. However, it should be noted that the solvent used for stencil wiping should be chosen properly. In general, a volatile and moderately polar solvent such as isopropanol will be adequate. If the solvent is not volatile enough, the remaining solvent may blend with the solder paste in the subsequent printing process, and consequently further aggravate the smearing problem.

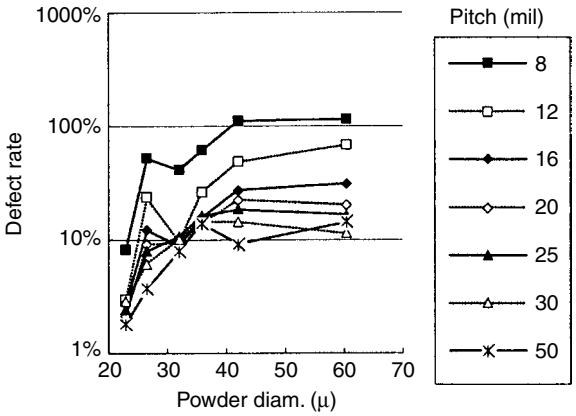

Figure 5.19 Results of printability test using 2 mil stencil. Both powder size and pitch dimension varied [4]

5.8 Insufficiency

A common problem at the stencil printing stage is insufficiency. Here the solder paste volume deposited onto the pads is less than the targeted volume, mainly due to aperture clogging. The symptoms presented include partial paste imprint or thinner print thickness.

Causes for insufficiency include (1) stencil thickness, (2) taper treatment, (3) pitch dimension, (4) aperture orientation, (5) powder size, (6) inadequate aperture design, (7) poor aperture quality, (8) insufficient squeegee pressure, and (9) inadequate paste rheology.

Figure 5.14 shows that, in general, the overall defect level rapidly increases with increasing stencil thickness. The print defect mainly constitutes insufficiency, which also increases rapidly with increasing stencil thickness. Apparently this is due to incomplete filling and clogging. However, at 2 mils stencil thickness, the insufficiency rate is substantially higher than the major trend. The unusually high defect rate associated with 2 mil stencil prints holds true not only for coarse powders but also for fine powders, as shown in Figure 5.19. Results indicate that in all incidents, the print defect rate using 2 mils stencil is always higher than 1 percent. This abnormity is attributed to scooping during printing [4].

The tapering treatment reduces the overall defect rate slightly, as shown in Table 5.1. This is primarily due to the reduction of insufficiency rate. Apparently this can be related to the better release of the tapered shape [4].

The print defect rate increases very rapidly with decreasing pitch at a pitch level below 30 mils (see Figure 5.20). As indicated in Figure 5.16, the primary defect type is insufficiency. This is quite understandable, since more and more clogging is expected to occur with decreasing aperture size.

The effect of aperture orientation on insufficiency is very small, as indicated in Figure 5.17. Here the parallel aperture shows a slightly higher insufficiency than the perpendicular aperture [4].

Figure 5.18 shows the effect of solder powder size on defect type and defect rate. Data represent the averaged performance of pastes with 90.5 percent metal load tested

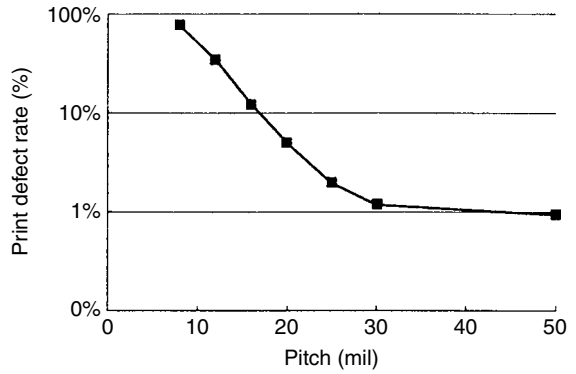

Figure 5.20 Effect of pitch dimension on defect rate [4]

on all stencils. The insufficiency is reduced with decreasing particle size. The relation observed for insufficiency appears to be self-evident, since the chance of clogging should be reduced with decreasing powder size, especially for very small apertures [4].

Aperture design is a crucial factor affecting paste release from the aperture. With an aspect ratio of opening versus stencil thickness of less than 1.5, it becomes very difficult to have a full paste release from the aperture. In addition, a smooth aperture wall is also a necessary condition for easy paste release. The laser cut stencil process [14,15] often suffers problems of a saw-toothed edge or dross buildup on the stencil surface, and post-cutting processing such as electropolishing is commonly used to remove dross buildup.

Clogging of the aperture can also be caused by a paste film left on the stencil's surface after the squeegee wiping process. This paste film may be a result of (1) too low a squeegee pressure, (2) too small a squeegee contact angle, or (3) too stringy in paste rheology. Paste rheology is a very important factor in governing paste release from the aperture. Even in the case of a clean stencil wipe, clogging can still be caused by a poor paste rheology resulting from (1) too low thixotropy, (2) too high viscosity, possibly

due to poor formulation, using expired paste, or using paste not thawed properly, (3) too much solvent loss due to drying, and (4) crusting caused by a reaction between flux and solder powder. The latter two cases can be the result of leaving the paste too long on the stencil, printing reused paste, or printing under high humidity conditions.

5.9 Needle clogging

As SMT advances toward further miniaturization, so too will the needle size for paste dispensing, but this is beset by clogging problems. Clogging occurs mainly due to a gradual separation of the solder powder from the flux/vehicle under a high shear force. This separation first causes a thickening of the paste as the metal percentage slowly rises due to excess flux being dispensed. Eventually the needle clogs due to high metal loading. The process of clogging is accelerated by rapid and repetitive dispensing cycles. The symptoms include (1) gradually decreasing paste volume dispensed with time, and (2) missing shots.

Causes of needle clogging include (1) large powder size, (2) high metal content, (3) inadequate viscosity, (4) too high an ambient temperature, (5) too large a metal load, (6) low thixotropy, (7) a soft and reactive alloy, (8) a reactive flux, (9) inadequate design of paste flow path in the dispensing headset, and (10) an inadequate dispensing mechanism.

Minimizing separation is a difficult problem due to the combined effects of the high shear forces during dispensing and the large density difference between the metal and flux/vehicle (typically a factor of 10). This problem can be minimized by using a smaller particle size, with adequate particle size distribution of the powder in the paste and by again ensuring that the proper viscosity paste is being used. Too low a viscosity will result in powder settlement and cause clogging. However, too high a viscosity will create difficulty for the paste to go through the needle. Too high an ambient temperature may reduce the paste viscosity, and also result in clogging.

A lower metal content can also help. This will reduce powder cluster formation, and accordingly clogging. However, the trade-off would be a greater slump as well as more flux/vehicle to be removed after reflow. In the formulation of the paste, the separation can be reduced by increasing the thixotropic property or by improving the paste's stability through careful design of a colloidal flux/vehicle system [16].

If the solder alloy is soft, such as solder alloys with a high indium content, repeated pressurizing can result in cold welding of the powder and causing clogging. Also, if the alloy is more prone to react with the flux, either due to reactive alloy or reactive flux, the metal oxide protective layer on the powder's surface can be removed prematurely and cold welding can be developed more easily. The reaction between solder powder and flux may also cause clogging when a very fine solder powder is used. This is because of the much greater surface area of powder available for reacting with the flux.

Needle clogging can also be improved by eliminating the dead corners of a dispensing device. The paste being dispensed is constantly under repeated pressure cycling. If there are dead corners along the paste's flow path, the accumulated effect of pressurizing can result in cold welding and a cluster of powder causing clogging. Stability increases with increasing flux activation temperature for a pneumatic dispensing system, as shown in Figure 5.21 [17], and is expected to be poor for low thixotropy and low viscosity. A large powder size may cause immediate clogging, while a small size may cold weld under repeated pressure cycling using pneumatic pump systems [17]. Positive displacement dispensing is less prone to clogging, since the paste is not under repeated pressure cycling. Solutions for eliminating

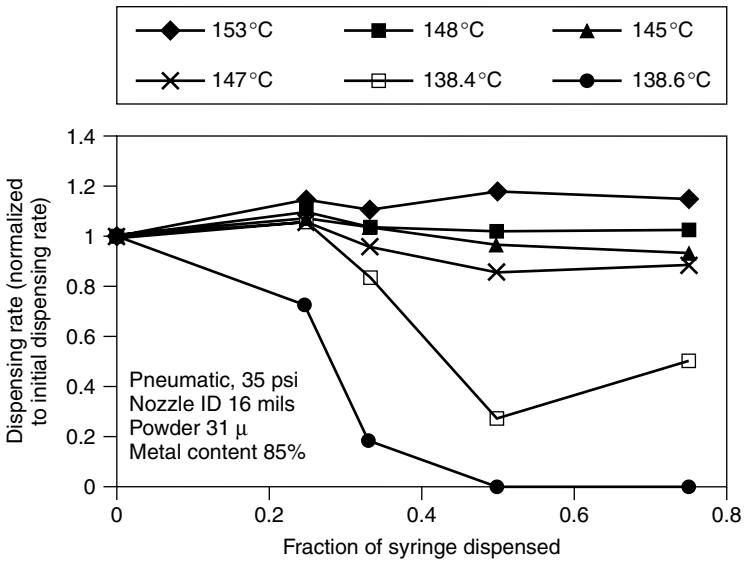

Figure 5.21 Effect of flux activation temperature on the dispensing consistency using a pneumatic dispensing device [17]

needle clogging include (1) adequate powder size, metal load, viscosity, thixotropy, and ambient temperature control, (2) non-reactive flux at ambient temperature, and (3) a proper dispensing system design.

5.10 Slump

Depending on the temperature, slump can be categorized into cold and hot slump. Cold slump refers to the slumping behavior occurring at ambient temperature. After the printing process, the solder paste gradually spreads out and the paste deposit slowly changes from a brick shape into a smooth dome-shaped deposit at ambient conditions (see Figure 5.22). Hot slump refers to the slumping during the reflow stage.

The causes of cold slump include: (1) low thixotropy, (2) low viscosity, (3) low metal or solid content, (4) small particle size, (5) wide particle size distribution, (6) low surface tension of flux, (7) high humidity, (8) hygroscopic paste, and (9) high component placement pressure. In addition, hot slump, is also affected by the ramp-up rate of the reflow profile.

Slump is a phenomenon where the paste viscosity is not high enough to resist the collapsing force exerted by gravity, and consequently results in spreading beyond the area to be deposited. The effect of thixotropy and viscosity on slump can be illustrated by Figure 5.23. Here *A* stands for the minimum viscosity needed to resist the gravity and have no slump after a print, *B* is the maximum viscosity allowed for the paste to roll and fill the aperture during printing. In Figure 5.23, both pastes have a viscosity no higher than *B* at a given print speed and both are acceptable for paste rolling and filling the aperture. However, for paste with low thixotropy, the viscosity at zero shear is lower than the *A* value, and consequently suffers slumping after printing. For paste with a high thixotropy, the viscosity at zero shear is higher than *A*, hence it shows no slump after printing. It should be pointed out that a paste with high thixotropy but too low a viscosity at zero shear is still not good enough to be slump-free.

The effect of metal load on slump has been studied by Xiao *et al.* [4] using Sn63 solder pastes with −325/+500 mesh powder, with results shown in Figure 5.24. Here the slump index reflects the tendency to slump. A higher slump index represents a greater tendency to slump. For a cold slump, the metal load has only a very slight positive effect on reducing slump. At 100°C, there is no bridging observed for 91 and 92 percent metal load. However, at a metal load below 90 percent, hot slump increases rapidly with decreasing metal load. The low slump of the high metal load paste can be attributed to high viscosity, since metal powder does not flow on its own before melting. At temperature above the melting point of solder, the flow of molten solder is further restrained by the high surface tension of solder and the powder coalescence process. For fine-pitch pattern design, the spacing to pad

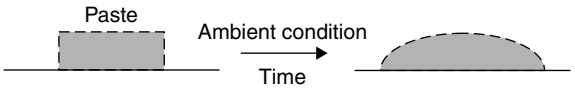

Figure 5.22 Schematic of cold slump. Hot slump shows a similar behavior at elevated temperatures

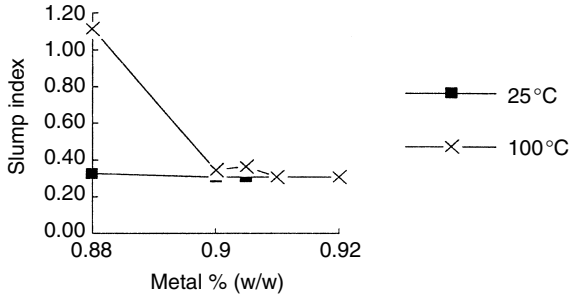

Figure 5.24 Effect of metal load on slump [4]

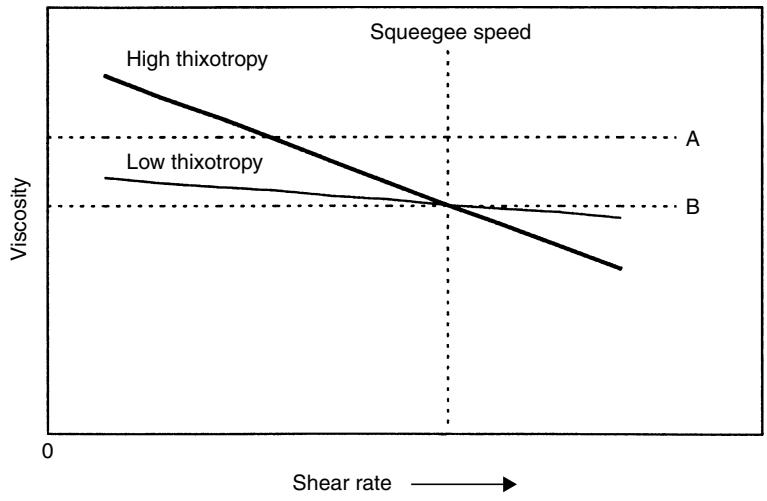

Figure 5.23 Effect of thixotropy and viscosity on slump

width ratio normally is around 1 or slightly less than 1. This suggests that a metal load of 90.5 percent or higher should satisfy the non-bridging needs of ultra-fine-pitch application.

Besides the metal load effect, slump typically also reduces with increasing flux solid content. A flux with a higher solid content usually exhibits a higher viscosity not only at room temperature but also at elevated temperature, and accordingly results in a greater slump resistance.

Solder powder particle size and particle size distribution also affect slump, as indicated by Figures 5.25 and 5.26. Since the solder powder remains solid at both room temperature and 100 °C, the greater slump observed in the 100 °C test suggests that the slump is caused by flux thinning, since the flux melts at 100 °C. This flux liquidizing effect can be offset by reducing the powder size which will result in an increase in paste viscosity. As a result, the slump is reduced with decreasing powder size, particularly at 100 °C. Also, it is found at both temperatures that a wide particle size distribution (PSD) aggravates the slump when compared with a narrow PSD. Upon heating, the flux between particles melts, and serves as a lubricant allowing the powders to pass each other and slump. The higher the frequency of point-to-point contact, the more the resistance against slippage, and the less the slump will be. Presumably the greater slump associated with a wide PSD can be attributed to the better packing of powder, which reduces the frequency of particle-to-particle contact, as shown in Figure 5.27.

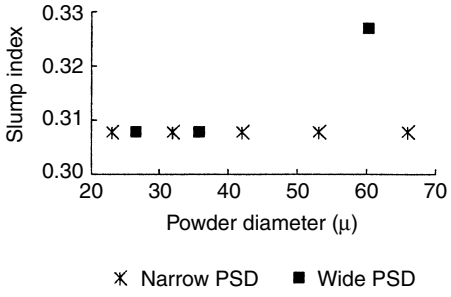

Figure 5.25 Effect of powder size and size distribution on slump at 25 °C [4]

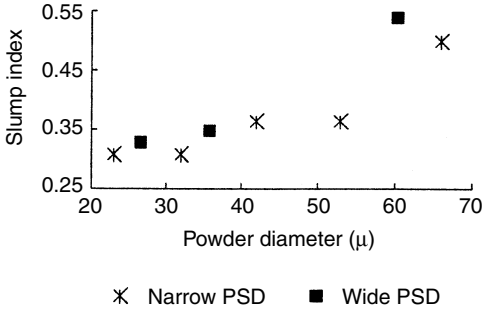

Figure 5.26 Effect of powder size and size distribution on slump at 100 °C [4]

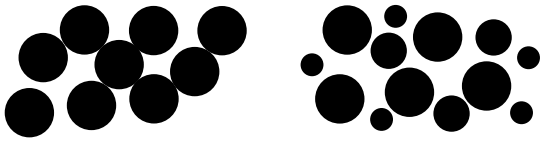

Narrow PSD, more point contacts, less lubrication, less slump

Wide PSD, better packing thus fewer point contacts, more lubrication, more slump

Figure 5.27 Effect of particle size distribution (PSD) on slump

The surface tension of the flux is another important factor affecting slump. Fluxes with a higher surface tension have a greater tendency to minimize surface area, thus having a greater resistance against spreading or slumping. This is true at both ambient and elevated temperatures. A high surface tension of flux not only reduces the slump of solder paste, but also reduces the spreading of molten solder, as discussed in Appendix 2.1.

If the humidity around the paste processing line is too high, the paste can pick up significant amounts of moisture which results in low viscosity and slump. This is particularly true for many water soluble solder pastes that are fairly hygroscopic. For most solder pastes, a relative humidity of 30–50 percent is considered adequate.

High component placement pressure squashes the paste, hence aggravating slump behavior. However, strictly speaking, paste squashing should be considered outside the category of slump behavior.

Slump can also be affected by ramp-up rate at reflow [18]. In general, the viscosity of materials with a fixed composition and chemical structure decreases with increasing temperature, due to increasing thermal agitation at the molecular level. This decrease in viscosity at a higher temperature will yield a greater slump. On the other hand, an increase in temperature usually dries out more solvent from the flux and results in an increase in solid content, thus an increase in viscosity. These two opposite effects, thermal agitation and solvent loss, are shown in Figure 5.28.

The thermal agitation effect is an intrinsic material property. It is a function of temperature only and is independent of time. Therefore, the ramp-up rate has no effect

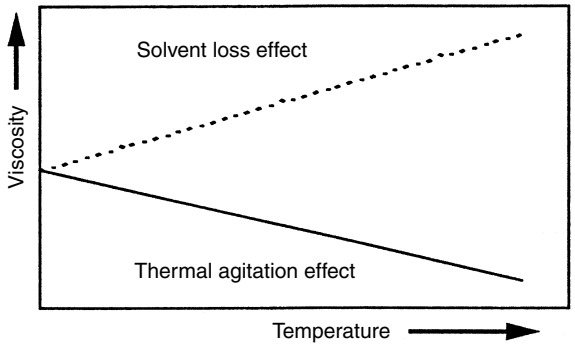

Figure 5.28 The effect of thermal agitation and solvent loss on viscosity as a function of temperature [18]

on it. However, the solvent loss effect is a kinetic phenomenon and will be affected by the ramp-up rate. The solvent vaporization rate is proportional to the thermal energy, or temperature, of the solvent. The solvent loss quantity is proportional to the product of the vaporization rate and the time allowed for vaporization. In other words, the total solvent loss is a function of both time and temperature, and hence can be regulated by varying the reflow ramp-up rate. At a slow ramp-up rate, the viscosity of solder paste is higher than that at the fast ramp-up rate at any given elevated temperature due to a greater amount of solvent loss, as shown in Figure 5.29.

Therefore, by applying a fairly slow ramp-up rate, the solvent loss effect can be enhanced and can override the thermal agitation effect. This will result in either a viscosity decrease or even a net viscosity increase with increasing temperature. Consequently, slump decreases with decreasing ramp-up rate, as shown in Figure 5.30. In general, a ramp-up rate of 0.5 to 1 °C/sec from room temperature to melting temperature is recommended.

Slump is primarily a characteristic of solder paste materials. Most of the solutions for reducing slump reside in material design. Processwise, humidity control and ramp-up rate control are effective approaches in minimizing slump.

5.11 Low tack

The symptom of low tack is that the components do not adhere to the paste during or after placement.

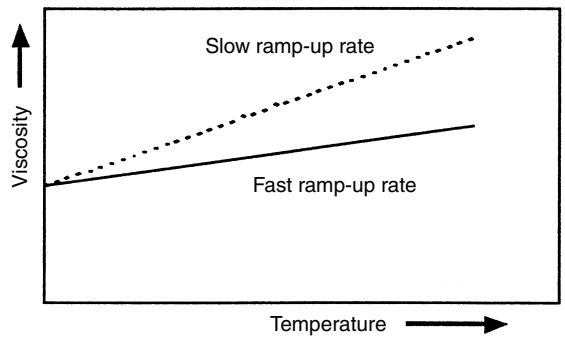

Figure 5.29 Relation between ramp-up rate and viscosity due to solvent loss effect [18]

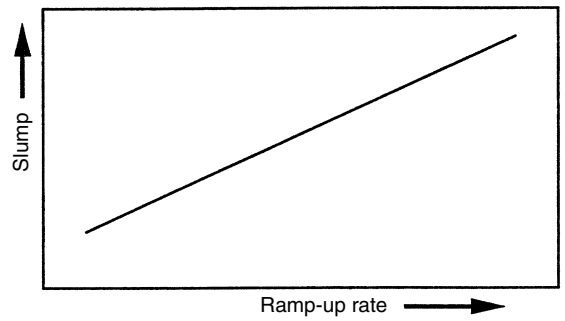

Figure 5.30 Relation between slump and ramp-up rate [18]

Causes of low tack include (1) insufficient solder paste deposited, (2) insufficient flux tackiness, (3) inadequate metal content, (4) too coarse a powder size, (5) rapid board movement at placement, (6) inadequate board supporting design during placement, and (7) humidity.

Obviously, if the solder paste printed is not sufficient, the paste will not be able to hold the components placed. Causes of insufficient paste deposition or low print thickness have been discussed in sections 5.6 and 5.8.

The tackiness of flux is the dictating factor for the tackiness of the solder paste. A flux with a low tackiness will result in a paste with a low tack value. Since powder offers no tack of its own, an excessive amount of powder is undesirable. However, the relation between metal content and tack is fairly complicated, as shown in Figure 5.31 [4]. With increasing metal load, the tack drops rapidly at first, then declines slowly until 40 percent volume content. This declining trend can most likely be related to the sample thickness at test. In general, the lower the powder content, the more the paste can be squashed during the tack test, and consequently the smaller the clearance between the test probe and substrate will be. Since a smaller clearance favors a better gasketing effect upon detachment, a higher tack is then expected. At metal loads beyond 40 percent, the tack shows an increase followed by a decrease with a further increase in the metal load. The increase in tack can be attributed to the increasing cohesive force due to the increasing filler reinforcement effect. The decrease in the tack at metal volume content beyond 53 percent presumably can be related to the gradually increasing insufficiency of the flux binder for the solder powder.

The effect of powder size on the tack of paste has been reported for 63Sn/37Pb solder pastes with 90.5 percent metal load, as shown in Figure 5.32 [4]. The tack increases with decreasing powder size and is believed to be proportional to the adhesive and cohesives forces of the paste. The adhesive force is governed by the flux/vehicle alone. However, the cohesive force increases with decreasing powder size due to the increase in the viscosity of the paste, and consequently results in an increase in the tack.

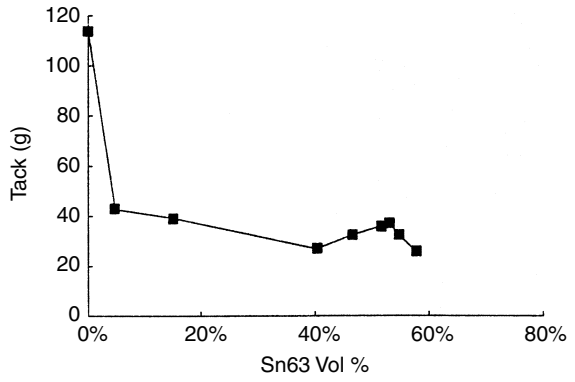

Figure 5.31 Relation between metal content and tack of 63Sn/37Pb solder paste with powder size 25–45 μ [4]

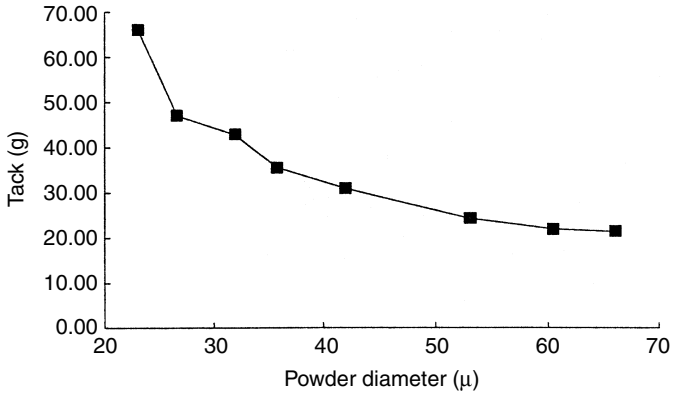

Figure 5.32 Relation between solder power size and tack of 63Sn/37Pb solder paste [4]

A component's holding power is determined not only by the tackiness of the solder paste, but also by the challenges presented by the pick-and-place equipment. A solder paste may perform very well for one placement machine but fail miserably for another. One of the factors affecting the component's holding capability is board movement. If the board moves very quickly at the placement stage, the inertia momentum of the components can override the tack force of the paste and result in the component falling off. Another factor is the steadiness of the board during placement. If the board is not supported firmly by the pellet and supporting rods, it may tremble significantly upon being hit by the placement arm hence throwing off the components. Adequate design should include reasonable layout of supporting rods plus a sturdy pellet for holding the board.

Since tack is a strong function of flux characteristics, and since some flux may pick up moisture fairly readily, it is no surprise that humidity will also affect the tack value. High humidity can often cause either crusting or paste thinning and result in low tack, and hence should be avoided.

5.12 Short tack time

A solder paste may have a proper or even a high tack when exposed. However, the tack of the paste may decrease very quickly with time after it is printed, thus resulting in a very short process window.

Causes of short tack time include (1) metal load too high, (2) solvent volatility too high, (3) powder size too coarse, (4) crusting developed over time for the printed paste, (5) the air drift around the printed paste too high, (6) the humidity too low or too high, (7) the ambient temperature too high, and (8) stencil used too thin.

The effect of metal content on tack time for a Sn63 solder paste with −325/+500 mesh powder has been reported, as shown in Figure 5.33 [4]. There is virtually no tack time observed at 92 percent metal load, and the tack time increases with decreasing metal load. Apparently the increasing tack time associated with increasing flux content can be easily attributed to an increase in solvent

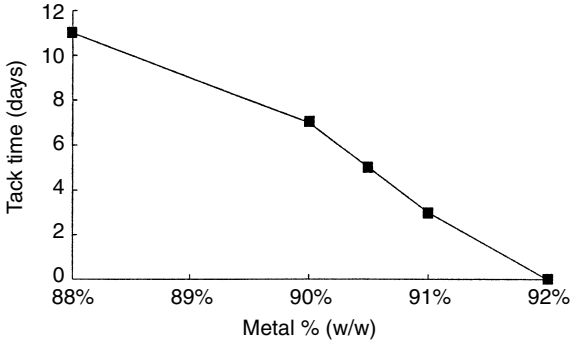

Figure 5.33 Relation between metal content and tack time of 63Sn/37Pb solder paste with 25–45 μ powder size [4]

content. Also a metal content of no more than 91 percent (w/w) seems to be desirable for achieving a reasonable tack time.

The effect of powder size on tack time is not a simple relationship, as reflected in Figure 5.34 [4]. The tack time increases first, then reaches the peak at approximately 35 μ powder diameter, then decreases with decreasing powder size. The initial increase can be explained by the increasing diffusion path length for the solvent to

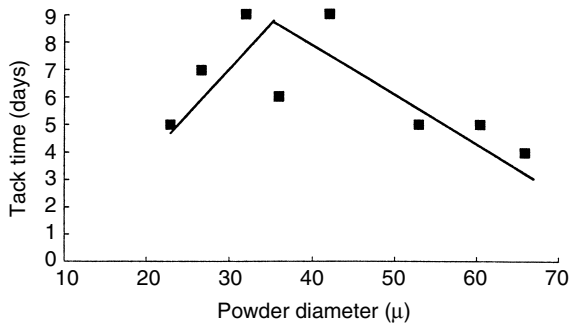

Figure 5.34 Relation between powder size and tack time of 63Sn/37Pb solder paste with 25–45 powder size and 90.5 percent metal content [4]

reach the paste surface before it dries out. In addition, the increase in powder surface area also helps to retain the solvent longer due to increasing powder-solvent surface adsorption. The declining trend beyond the peak can probably be attributed to the skin formation effect caused by excessive chemical reactions between flux and the fine powder. This dry skin formed consequently will reduce the adhesive force of the paste, and result in a short tack time.

5.13 Conclusion

Although the SMT solder paste reflow process is a mature technology, care should be taken in handling the paste at each stage in order to achieve a high yield, low cost process. This is particularly true in the printing process, since the majority of defects in the reflow process can be attributed to problems at this stage. Other symptoms prior to reflow also contribute directly or indirectly to the final defect level, and therefore should be prevented as much as possible.

References

1. Technical data sheet of MPM Technology Update, ''Rheometric Pump Print Head Technology'', October 1997.
2. X. Bao and N. C. Lee, ''Engineering Solder Paste Performance Via Controlled Stress Rheology Analysis'', in *Proc. of Surface Mount International*, San Jose, CA (September 1996).
3. N. C. Lee, ''How to Make Solder Paste Work in Ultra-fine-pitch and Non-CFC Era'', short course at Surface Mount International, San Jose, CA, September 1994.
4. M. Xiao, K. J. Lawless, and N. C. Lee, ''Prospects of Solder Paste Applications in Ultra-fine Pitch Era'', in *Proc. of Surface Mount International*, San Jose, CA (August 1993).
5. Private communication from Alden Johnson, MPM, at Nepcon East, Boston, MA, 13 June 2000.
6. H. Markstein, ''Inspecting Assembled PCBs'', *EP&P*, pp.70–74 (September 1993).
7. C.-H. Mangin, ''Where Quality is Lost on SMT Boards'', *Circuits Assembly* (February 1991).
8. B. Willis, P. Hunter, and J. Porter, ''Evaluation of Bare-Board finishes – A Study of Solderability'', *Printed Circuit Fabrication*, Vol.16, No.12, pp. 52–54 (December 1993).
9. M. S. Husman, J. P. Rukavina and Y. Guo, ''A Study of Solder Paste Volumes for Screen Printing'', in *Proc. of Nepcon West*, Anaheim, CA, pp.1771–1781 (7–11 February 1993).
10. S. H. Mannan, N. N. Ekere, E. K. Lo and I. Ismail, ''Predicting Scooping and Skipping in Solder Paste Printing for Reflow Soldering of SMT Devices'', *Soldering & Surface Mount Technology*, No.15, pp. 14–17 (October 1993).
11. C. P. Brown, ''Process Solutions for Ultra Fine Pitch Production'', in *Proc. of Surface Mount International*, San Jose, CA, pp. 119–126 (29 August–2 September 1993).
12. C. Missele, ''Screen Printing Primer – Part 3'', *Hybrid Circuit Technology* (May 1985).
13. Alden Johnson, short course on ''Fine Pitch Stencil Printing & Applications Class'', 1999.
14. M. D. Herbst, ''Metal Mask Stencils For Ultra Fine Pitch Printing'', in *Proc. of Surface Mount International*, San Jose, CA, pp.101–109 (29 August–2 September 1993).
15. Metal Etching Technology: Technical information (November 1993).
16. G. Evans and N. C. Lee, ''Solder Paste: Meeting the SMT Challenge'', *SITE Magazine*, 1987.
17. R. Ludwig, N. C. Lee, S. R. Marongelli, S. Porcari, and S. Chhabra, ''Achieving Ultra-Fine Dot Solder Paste Dispensing'', in *Proceedings of Advanced Electronic Assembly Conference*, Providence, RI, October 1998.
18. N. C. Lee, ''Optimizing Reflow Profile via Defect Mechanisms Analysis'', *IPC Printed Circuits Expo '98*.

6 SMT Problems During Reflow

Problems during reflow can be roughly categorized into two major groups. The first relates to metallurgical phenomena, including (1) cold joints, (2) nonwetting, (3) dewetting, (4) leaching, and (5) excessive intermetallics. The second group reflects abnormal solder joint conformation, including (1) tombstoning, (2) skewing, (3) wicking, (4) bridging, (5) voiding, (6) opening, (7) solder balling, (8) solder beading, and (9) spattering.

6.1 Cold joints

Cold joints refers to joints formed with signs of incomplete reflow, such as grainy joint appearance, irregular joint shape, or incomplete coalescence of solder powder, as shown in Figure 6.1.

Nominally, cold joints means an under-reflowed solder joint appearance. However, there are other factors which also contribute to the formation of such joints. Therefore, the causes of cold joints include (1) insufficient heat input at reflow, (2) disturbed joint at the cooling stage, (3) poisoning of flux due to surface contamination, (4) insufficient fluxing capacity, and (5) poor solder powder quality.

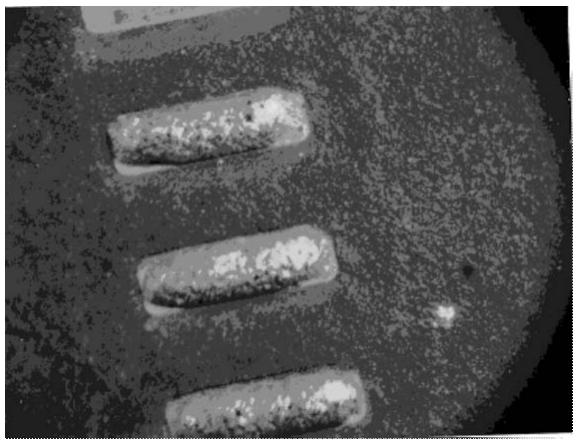

Figure 6.1 Example of cold joints

Insufficient heat input during reflow, either due to too low a temperature or too short a dwell time above liquidus temperature, will result in incomplete coalescence of the solder powder. For eutectic Sn/Pb solder, the recommended peak temperature is around 215 °C with a recommended dwell time above the liquidus temperature being 30–90 seconds.

At the cooling stage, if the solder joints are disturbed, a rugged appearance may be retained on the joint's surface. This is particularly true for a temperature at or slightly below the melting point where the solder is very soft. The disturbance may be caused by either a strong cooling air jet or a jerky conveyor belt movement.

Surface contamination on and around the pads or leads may cause poisoning of the fluxing reaction and result in incomplete reflow. In some instances, unreflowed solder powder can be observed on the joint surface. An example of such contamination is the remaining plating chemicals used for certain pad/lead metallization. Causes such as this should be addressed with a proper post-plating cleaning process.

Insufficient fluxing capacity will result in an incomplete removal of metal oxide, and consequently incomplete coalescence. Similar to the surface contamination case, the symptom often includes solder balls around the solder joints as well.

Poor solder powder quality can also cause a cold joint problem. Figure 6.2 shows a cold joint with a spherical inclusion, presumably caused by a highly oxidized powder or a "wrapped" solder powder, as shown in Figure 3.8(8) in Chapter 3.

6.2 Nonwetting

Nonwetting refers to the coverage of solder on substrate metallization or lead being less than the targeted solder wetting area, as shown in Figure 6.3. It is typically associated with a large contact angle between the solder and the base metal. Here the solder paste may have a larger coverage area prior to reflow than the final spread area. Figure 6.4 shows a solder spread where the solder fully wets where the solder paste was printed. Figure 6.5 gives an example of nonwetting where the solder paste retracts back upon reflow and leaves the base metal exposed.

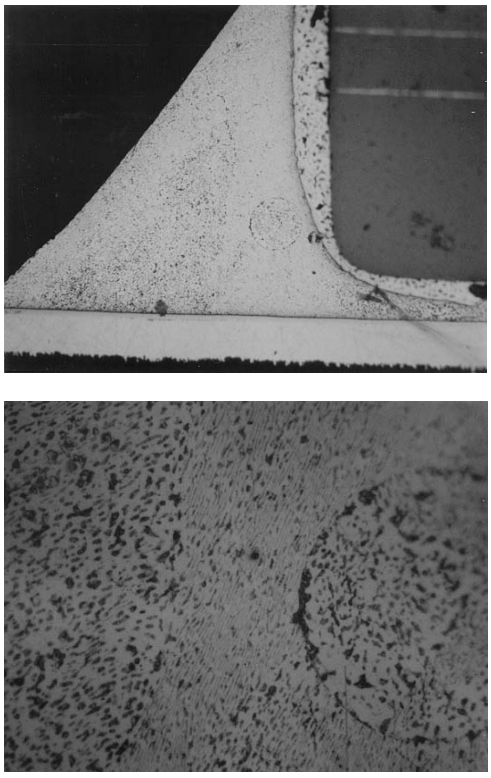

Figure 6.2 Cold joint with a spherical inclusion for a 62Sn/36Pb/2Ag solder joint using solder paste with 45–75 μ solder powder size on HAL surface, The spherical inclusion has a diameter 60 μ

Figure 6.3 Example of nonwetting shown by the exposed copper pads

Nonwetting also refers to the area where the solder may be in contact but does not form metallurgical bonding with the base metal, such as an unwetted spot within a solder joint. Causes of nonwetting include: (1) poor wettability of metallization, (2) poor solder alloy quality, (3) poor solder powder quality, (4) poor flux activity, and (5) inadequate reflow profile/atmosphere.

The poor wettability of metallization can be attributed to impurity or tarnishes or the nature of the metallization

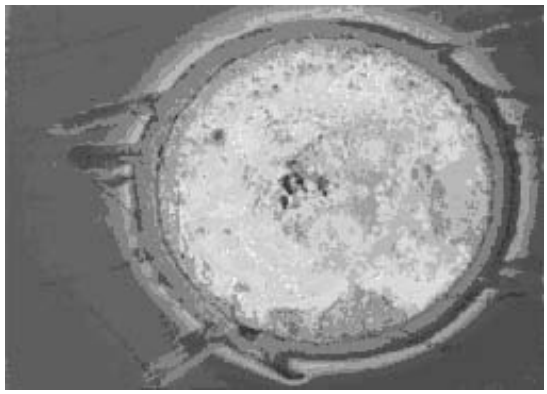

Figure 6.4 Example of solder spread where solder paste fully wets where the solder paste was printed

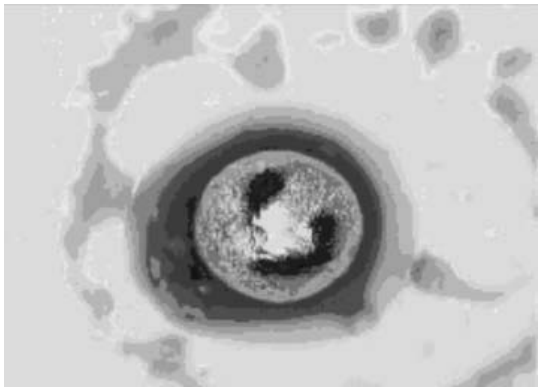

Figure 6.5 Example of nonwetting where solder paste coalesces and retracts back upon reflow

of pads or leads. For instance, the presence of phosphorus in a Ni/Au surface finish due to the plating process, nickel oxide formation due to pin-hole formation in the Au layer, oxidized copper pads, exposed alloy 42 at the ends of leads, or too thick a layer of OSP coating can all contribute to poor wetting.

The same comments are also applicable to solder alloys. Impurities such as Al, Cd or As in solder can all result in poor wetting, as shown in Table 2.2, Chapter 2. Poor solder powder quality can be demonstrated by Figure 3.8 of Chapter 3. The irregular solder powder shape reflects a greater oxide content, which in turn depletes more flux and results in a poorer wetting. Apparently, poor wetting is expected from poor flux activity.

Time, temperature, and reflow atmosphere have a great impact on wetting performance. Insufficient heat input, due either to too short a time or too low a temperature, will result in an incomplete fluxing reaction as well as incomplete metallurgical wetting and accordingly will result in poor wetting. On the other hand, an excessive heat input prior to solder melting will not only oxidize the metallization of pads and leads excessively, but also will burn off more fluxes. Both phenomena will result in poor wetting. This relation becomes more significant in an oxidative reflow atmosphere. A nitrogen reflow atmosphere

often results in a significant improvement in wetting, and will be discussed in more detail later.

In general, the solder can easily wet fully on the HASL pads, since the process of wetting is virtually a coalescence of molten solder from solder paste with that from HASL. For surface finishes other than HASL, such as OSP or Ni/Au, the pads often are not fully wetted around the pad perimeter although an adequate fillet formation may have been formed. Instead of being merely a coalescence process, the smaller amount of solder spreading experienced with non-HASL surface finishes is attributed to the energy and time needed for the solder to react and form a metallurgical bond with those finishes.

Nonwetting may or may not be an issue. It is an issue if the solder joint formed does not have sufficient bond strength and fatigue resistance. However, if a proper contact angle is established for the fillet, the joint is usually considered reliable even if an area on the pad is still not wetted by the solder. For fine-pitch applications, the aperture dimension is often smaller than the pad size in order to assure a satisfactory gasketing effect as well as minimizing bridging. As a result, nonwetting becomes common around the perimeter of pads for non-HASL surface finishes. Depending on the design, generally an area coverage of about 90 percent is considered acceptable.

6.3 Dewetting

Dewetting of a solder paste upon reflow has the appearance of water on a greasy surface, as shown in Figure 6.6. The surface is wetted initially but retracts after a time causing the solder to collect into discrete globules and ridges. Although the remainder of the base metal surface retains the gray color of solder, this solder layer is very thin and has poor solderability. This thin layer is mainly an intermetallic compound. Dewetting is a problem in a variety of substrates and compromises the quality of solder joints by reducing the size of the solder fillets [1,2].

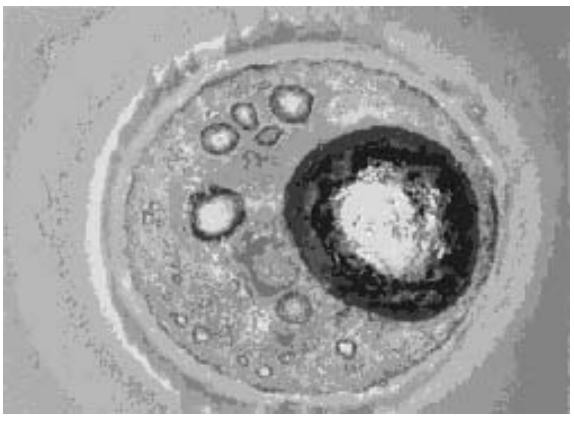

Figure 6.6 Example of dewetting where solder paste retracts back upon reflow and wets only part of the area covered by paste. A thin solder film formed on the area originally covered by the solder paste, with scattered solder domes in between

Causes of dewetting include (1) poor and uneven solderability of the base metal, (2) degeneration of solderability of the base metal, (3) outgassing, and (4) inadequate reflow profile and atmosphere.

A relatively poor and uneven solderability of the base metal can cause dewetting. Klein Wassink *et al.* [3] have proposed a metastability model to demonstrate mathematically the occurrence of dewetting through this mechanism, as shown in Figure 6.7. The small nonwettable spots cover a fractional area f. After dewetting the solder droplets have a base area A_1 and a dome area A_2 per dome. In the left of Figure 6.7 a wettable surface with some nonwettable spots is completely covered with a thick layer of solder. On the right the same base surface is partly covered with solder droplets, and partly with a very thin film of solder on the wettable surface and no solder on the nonwettable spots. If the fractional area of spots is f, then, in the first case the free surface of solder per unit substrate area (SS) is simply

$$SS(\text{left}) = 1 + f$$

Let the thickness of the solder coating be d. Then the volume per unit area is also d.

In the second case the surface is partially dewetted. The solder volume has been taken up into N domes per unit substrate area. The dome is assumed here to be of equal size, with base area A_1 and dome top surface area A_2 for each dome. The free surface of solder, per unit substrate area, is therefore the dome surface area ($NA_2 + fNA_1$) plus the film surface area $(1 - f)\ (1 - NA_1)$.

$$SS(\text{right}) = (NA_2 + fNA_1) + (1 - f)(1 - NA_1)$$

The difference between these two solder surface areas $\Delta SS = SS(\text{left}) - SS(\text{right})$ is a measure of the change in the total surface energy of the system because the wettable part of the substrate surface is completely wetted in both cases and so contributes nothing to the energy change. When ΔSS is positive, then the flat solder layer is merely metastable and dewetting can occur favorably. Its value is a function of the solder thickness d, the fractional area of nonwettable spots f, the number of droplets N and the contact angle of the droplets which defines the ratio $A_1{:}A_2$.

It should be noted that ΔSS is an approximation for estimating the potential of dewetting. The actual number and size of solder bumps formed during dewetting are affected not only by the total difference in surface area ΔSS, but also by the radius of curvature of the individual domes, as illustrated by Figure 6.8. For a curved surface, any point on the surface can be specified by two principal

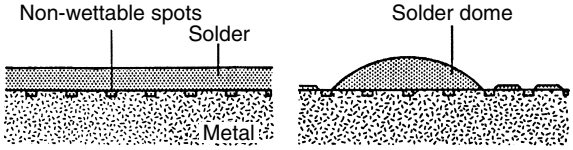

Figure 6.7 A model to demonstrate the dewetting mechanism. (Left) The base metal being covered by the molten solder in the beginning. (Right) The equilibrated solder distribution

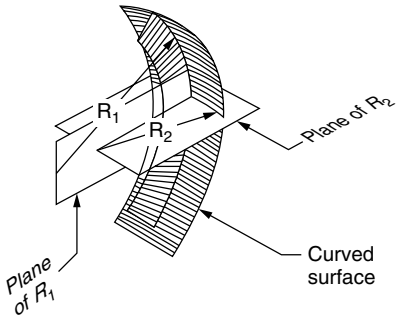

Figure 6.8 Relation between curvature and internal pressure for formation of molten solder [22,26,27]
Young and Laplace equation:

$$\Delta P = \gamma \left(\frac{1}{R_1} + \frac{1}{R_2} \right)$$

where

ΔP = pressure in the solder (with respect to ambient pressure)
R_1 and R_2 are the principal radii of curvature of the surface
γ = the surface tension of the molten solder

radii of curvature. R_1 is the radius of curvature in the plane of the paper and R_2 the radius of curvature perpendicular to the plane of the paper. The effect of radius of curvature on the dome stability can be revealed by

$$\Delta P = \gamma \left(\frac{1}{R_1} + \frac{1}{R_2} \right) \tag{6.1}$$

Equation (6.1) describes the pressure difference across a curved interface (ΔP) in terms of the surface tension of the interface (γ) and the two principal radii of curvature at a point on the surface [4]. Therefore, a smaller radius of curvature represents a greater hydraulic pressure within the molten solder, and accordingly results in a higher energy state that is less prone to form.

Even if the base metal is wettable initially, degeneration of the solderability over time can still result in dewetting. There may be contamination on a base metal under a coating of tin, tin–lead, silver or gold. During soldering the coating dissolves and the contamination is exposed. Alternatively the growth of the intermetallic compound at the interface might also cause dewetting, since generally intermetallics rapidly become unsolderable when exposed to air. In both cases, the solderability degenerates and small nonwettable areas result.

Dewetting may also result from gas evolution during exposure of the part to molten solder. Thermal breakdown of organics or the release of water of hydration from inorganics generates the gas. Water vapor can also be generated from a fluxing reaction, as discussed in Chapter 3. At soldering temperatures, water vapor is highly oxidizing and results in oxidation either of the surface of the molten solder film or of the intermetallic surface at the molten solder interface. Once the intermetallic is exposed, if oxidized, it will become a nonwetting surface. Gas released from heavy co-deposited organics in an alloyable coating can also result in passivation of the intermetallic surface. Degree of dewetting depends on the amount of gas released, the composition of the gas, and the location of the gas release. The greater the amount, the higher the water vapor content, and the deeper the location of the contamination causing the release, the more severe the dewetting.

Inadequate reflow profile and atmosphere can also cause dewetting. For a marginally wettable surface, insufficient heat input such as too low a reflow temperature or too short a dwell time will aggravate poor wetting, and result in more non-wetted spots at the solder–base metal interface. As discussed in the metastability model section, this will cause dewetting.

On the other hand, excessive heat input may also cause dewetting through degeneration or outgassing. It has often been observed that higher soldering temperatures and longer dwell times result in more severe dewetting. This often happens when the unwettable hidden contamination within the base metal is exposed after the wettable surface finishes dissolve into the solder. As discussed earlier, the degenerated solderability can result in dewetting. Dewetting can also happen if the source of the outgassing is in the base metal. The increased reaction rates at higher temperatures produce a more vigorous release, while the longer dwell time increases release time. Both result in an increased release volume which may result in the consequent dewetting.

An oxidative reflow atmosphere reduces the solderability of both solder and base metal. This will aggravate the dewetting due to metastability and degeneration mechanisms. Solutions for elimination of dewetting include (1) improving the solderability of the base metal, (2) eliminating impurities and outgassing sources in the base metal, (3) employing an inert or reducing reflow atmosphere, and (4) applying an adequate reflow profile.

6.4 Leaching

Leaching is a phenomenon where the base metal dissolves in the molten solder at reflow. As a result, the solder joint may be saturated with these alien metals and discretes which may contain significant amounts of particles of intermetallics derived from these metals. Very often, the surface of a solder joint may appear to be gritty, due to the surfacing of those particles. In the case of excessive leaching, the base metal, such as the surface metallization of a thick film, can be totally deprived and accordingly results in nonwetting. Leaching can be caused by (1) high dissolution rate of the base metal into the solder, (2) too thin a metallization, (3) high flux activity, (4) a high reflow temperature, and (5) a long dwell time at reflow.

Figure 6.9 shows the dissolution of metals and metallizations in 60Sn/40Pb [5]. The dissolution rate decreases in the following order: Sn > Au > Ag > Cu > Pd > Ni. Theoretically, the leaching problem caused by the high dissolution rate of some base metals can be regulated by either replacing with or introducing or combining with some metals with a lower dissolution rate. The extremely high dissolution rate of Sn plus its low melting temperature mandates that Sn can only be used as a surface finish, not as a base metal. Au may be used as a base metal, such as Au thick film. The leaching problem of Au supposedly

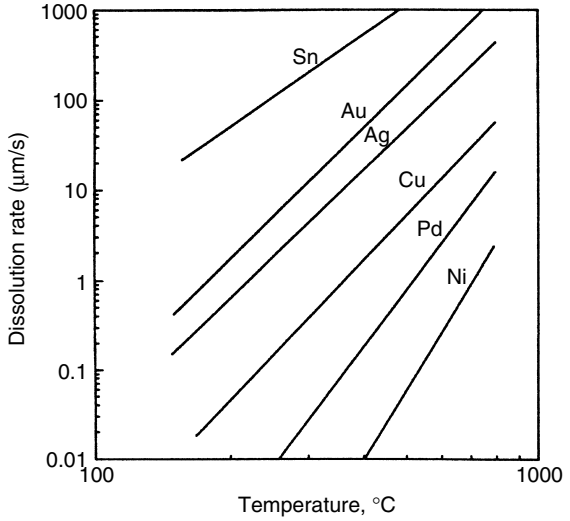

Figure 6.9 Dissolution of metals and metallizations in 60Sn/40Pb [5]

can be addressed by replacing it with Cu, Pd, or Ni to reduce the leaching rate. However, Cu is prone to oxidation, and has to be protected by some surface finishes, such as OSP. Pd is stable, but does not have very good solderability. Ni is also prone to oxidation, and has to be protected by some surface finishes. One practical solution is by taking composite material approach, such as immersion Au on top of electroless Ni. Here the Au is a 3–8 μ-in. thin film and serves as an oxidation protection layer, while the Ni is a 150–200 μ-in. layer, and serves as both dissolution barrier and diffusion barrier. When soldering on electroless Ni/immersion Au, the Au flash normally completely dissolves in the solder within a fraction of a second, thus allowing direct metallurgical bond formation between solder and the oxide-free Ni.

Other systems in use include electroless Au/electroless Ni and electrolytic Au/electrolytic Ni. In the case of Ag, often the Ag is alloyed with Pd in order to reduce the dissolution rate while still maintaining a satisfactory solderability.

Leaching can be a problem if the base metal is too thin, since a slight dissolution may completely eliminate it from the substrate, thus causing nonwetting problems. For hybrid applications, the thick film may also exhibit a high dissolution rate due to the high porosity in the thick film caused by a poor sintering process.

The high dissolution rate of base metal may also be addressed by predoping the solder with the base metal. For instance, the dissolution of Ag in the 60Sn/40Pb solder alloy is significantly reduced by the addition of a small amount of Ag to the solder, as shown in Figure 6.10 [6]. This is accomplished by shifting the equilibrium of Ag in the solder with Ag doping.

However, the same approach cannot be applied to soldering onto an Au surface. Doping Au into a Sn/Pb system will form too much $AuSn_4$ intermetallics. The excessive $AuSn_4$ intermetallics will convert the solder into a sluggish fluid and consequently result in a poor wetting.

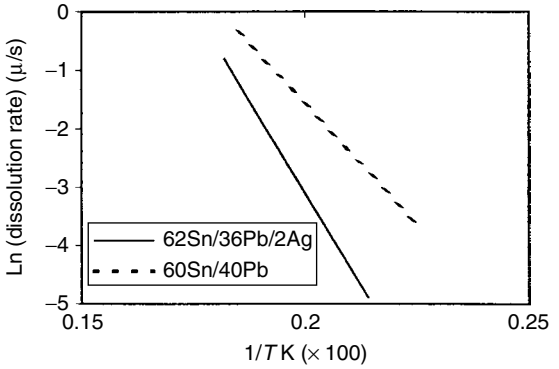

Figure 6.10 Effect of Ag addition to solder on Ag dissolution rate in 60Sn/40Pb [6]

Although leaching is a metallurgical phenomenon, it has been observed that the activity of flux may also play a role. Leaching often is aggravated by the use of a more active flux. It is stipulated that fluxes with a higher activity would remove metal oxide more readily, thus allowing intimate contact to be formed sooner and therefore longer between the molten solder and the base metal. With a fixed reflow profile, a longer contact time will mean a greater extent of leaching.

A high process temperature and long dwell time at reflow would have a dual impact on leaching. First, the dissolution of metallization into solder will increase, as indicated in Figure 6.9. Second, the flux activity will also increase with increasing temperature, as discussed above, thus allowing further increase in the extent of leaching. In general, the window allowed for most reflow processes can be approximated as "target peak temperature 220 ± 15 °C", and "target dwell time 75 ± 15 seconds". Within this window, variation in the reflow temperature will have a greater effect than the dwell time on leaching. For instance, the dissolution rate of Au in 60Sn/40Pb may increase 1.5× when the dwell time increases from 60 seconds to 90 seconds, but will increase about 3× when the soldering temperature increases from 205 °C to 235 °C, according to Figure 6.9.

Solutions for reducing leaching include (1) replacing the base metal with a metal with a lower dissolution rate, with or without the use of some surface finishes, (2) doping the base metal with an element with a lower dissolution rate, (3) doping the solder with the element of the base metal, (4) assuring the sintering quality of thick film, (5) using a flux with a lower activity, and (6) using a lower heat input.

6.5 Intermetallics

When two metal elements have a limited solubility toward each other, the alloys may form new phases when the alloy solution solidifies. These new phases are not solid solutions and are known as intermediate phases, or intermetallic compounds (IMCs), or simply as intermetallics.

6.5.1 General

The intermetallics can be categorized as stoichiometric and non-stoichiometric compounds [5]. The density of the free electrons that bind the atoms of the metal together characterizes the metallic property. Exact stoichiometric compounds tend to form when one of the two elements is strongly metallic and the other significantly less so. The crystal structures formed often are low in symmetry which restrains the direction of plastic flow and results in hard and brittle characteristics. The interfaces between these compounds and other phases also tend to be weak. Examples of such intermetallics include Cu_3P, Cu_3Sn, and Cu_6Sn_5.

Non-stoichiometric compounds refer to compounds that are stable over a range of compositions [5]. They tend to be moderately ductile and have crystal structures exhibiting high symmetry. Those compounds tend to have a negligible effect on joint properties. Examples include Ag_3Sn, which is stable over the composition range from 13% to 20% Ag at room temperature.

Stoichiometric IMC results in a lower tensile strength and shear strength [7]. For the latter case, Figure 6.11 shows the results obtained on plug-and-ring specimens with Cu soldered with 30Sn/70Pb. The initial shear strength level represents the strength of the solder material itself. As the intermetallic builds up to a thickness of about 1.3 μ, the shear strength increases by about 20 percent. On further buildup, the brittleness of the layer begins to manifest itself and the strength curve falls to below that of the bulk solder itself. IMC also results in a poor solder wetting. Davis *et al*. [8] have reported wetting balance results for 60Sn/40Pb coatings of 2, 4, and 8 μ in thickness on copper after reflowing and aging at 135 °C under vacuum. In general, wetting time increases with increasing IMC layer thickness and decreasing initial solder coating thickness. Wetting force displays the opposite trend. Since both weak interfaces and poor wetting are not desirable in a solder joint, the occurrence of intermetallics, particularly that of stoichiometric IMC, should be avoided.

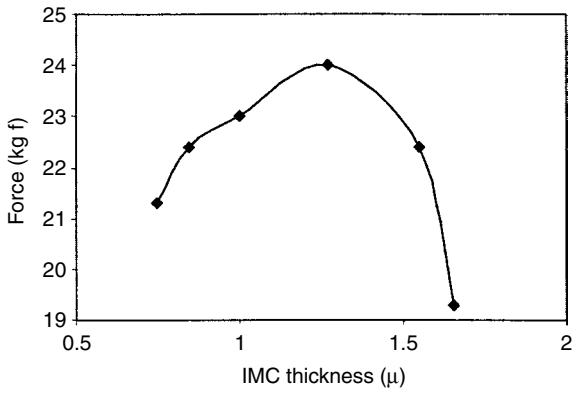

Figure 6.11 Effect of intermetallic layer thickness on shear strength [7]

The morphology of IMC depends strongly on the condition of formation. Steen [9] has reported that the shape and growth of IMC formed between the base metal and a liquid solder coating depends on the thickness and flow state of the liquid solder, as illustrated in Figure 6.12. Under a steady flow condition, as shown in Figure 6.12(a), the surface of the IMC layer is relatively planar, since any IMC texture protruding into the liquid flow will dissolve rapidly. On the other hand, during cooling, as shown in Figures 6.12(b) and 6.12(c), the exclusion of other species such as the Pb and other impurities in Sn/Pb solder results in a nodular or a dendritic structure, depending on the cooling rate and the ability of the liquid coating to minimize the concentration gradient at the interface. For Cu/Sn IMC formation, the above relationship is demonstrated by Schmitt-Thomas in Figure 6.13 [10]. When wave soldering or hot solder dipping, the IMC surface is swept by the liquid solder and accordingly evolves into a smooth "cobblestone" appearance (see Figure 6.13(a)). However, when reflow soldering, the solder volume is very small and the solder flow is highly restricted, thus a more fragile dendritic structure is formed, as shown in Figure 6.13(b). Perhaps the most commonly encountered IMCs in the electronics industry are Cu/Sn intermetallics, with compositions Cu_3Sn and Cu_6Sn_5. The Cu_6Sn_5 phase is formed at all temperatures and is relatively coarse in grain structure, as shown in Figure 6.13. At temperatures above 60 °C, the Cu_3Sn phase begins to grow at the $Cu-Cu_6Sn_5$ interface [11,12]. Factors affecting the IMC thickness include (1) time, (2) temperature, (3) type of metallization of the base metal, and (4) solder composition.

Since IMC is a reaction product between two metals, the formation rate is expected to be affected by the

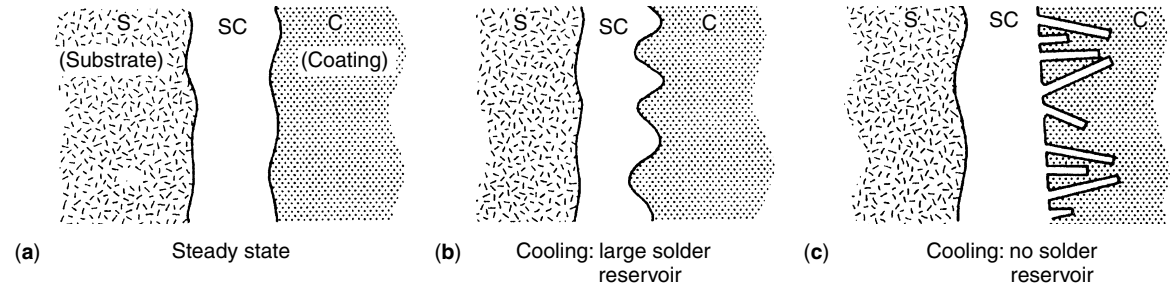

Figure 6.12 Schematic diagram showing the growth of IMC in contact with a liquid solder coating [9]

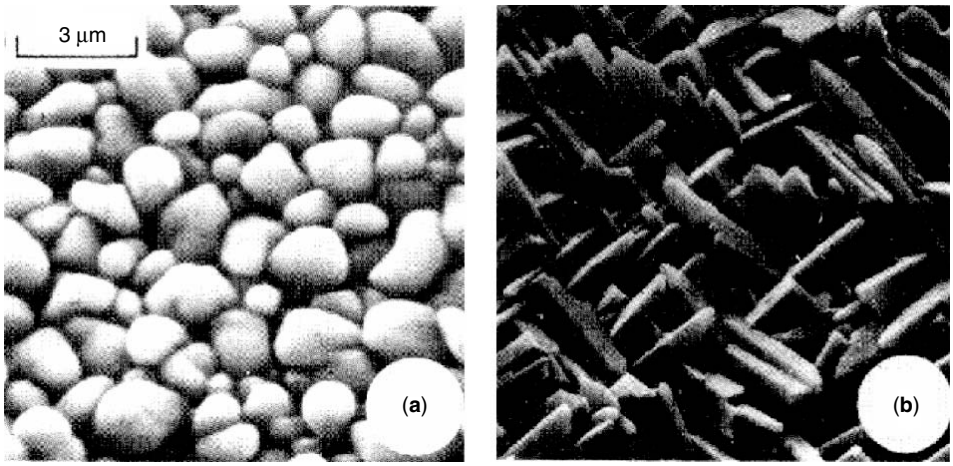

Figure 6.13 SEM of Cu/Sn intermetallics formed between Cu and eutectic Sn/Pb solder: (**a**) IMC developed from a wave soldering process, (**b**) IMC developed from a reflow soldering process [10]

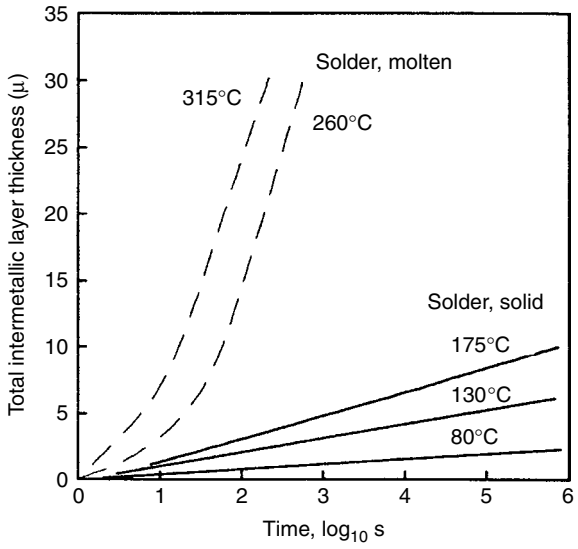

Figure 6.14 Growth rate of Cu/Sn IMC on Cu wetted by 63Sn/37Pb [7]

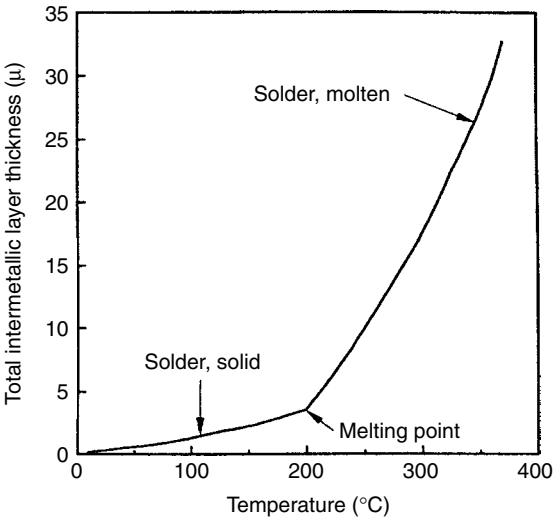

Figure 6.15 Growth rate of Cu/Sn IMC on Cu wetted by 63Sn/37Pb as a function of temperature [7]

temperature and time of reaction. Figure 6.14 shows the growth of Cu/Sn IMC on Cu wetted by 63Sn/37Pb increases with both increasing time and temperature [7]. The growth rate of IMC is a strong function of phase state. Thus, as shown in Figure 6.15, the growth rate increases smoothly initially with increasing temperature before reaching the melting temperature of solder. Beyond the melting temperature, the IMC growth rate increases much more rapidly. Effective means of reducing the amount of IMC formed during reflow include use of both a lower temperature and a shorter reflow time, particularly at temperatures above the melting temperature of solders.

Besides the processing time and temperature, the type of metallization of base metal also has a significant effect on the IMC formed, as reported by Kay *et al*. [13]. In that study, various surface metallizations including Co, Ni–Fe, Ag, Ni, and Fe with 5 μm thickness was electroplated onto Cu or brass, followed by a layer of electroplated tin of 25 μm thickness. The specimen was then aged at 170 °C, with the IMC thickness being monitored as a function of time, as shown in Figure 6.16 [13]. Results here indicate that iron has the least tendency to form IMC, $FeSn_2$, while cobalt has a strong tendency to form $CoSn_2$ IMC, with remaining metallizations falling in between. Cu is the prevailing choice of circuitry material, mainly due to its superior electrical conductivity and good solderability. Unfortunately, the IMC formation rate of Cu is still appreciable. Hence, use of a diffusion barrier on top of copper to slow the IMC formation rate between Cu and the solder appears to be a logical choice for enhancing the solder joint's reliability.

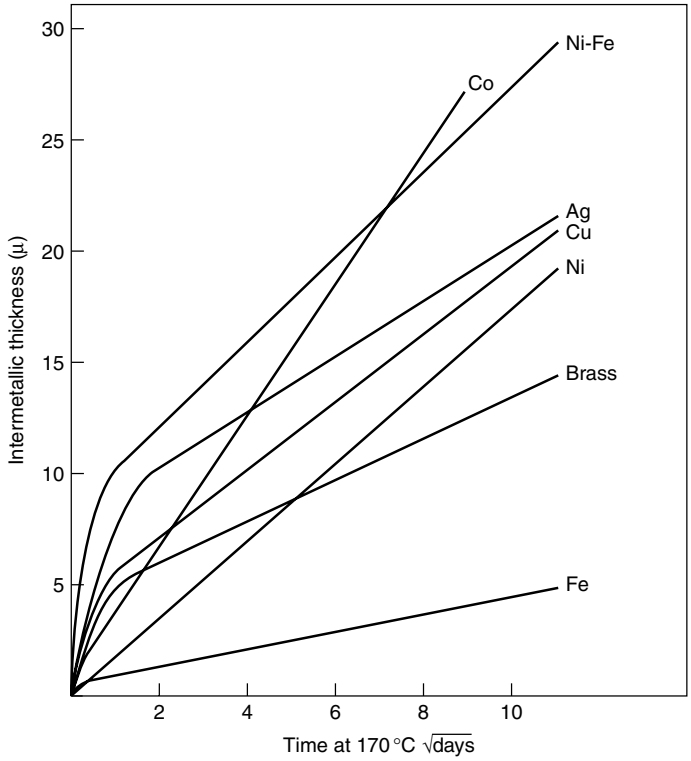

Figure 6.16 Effect of metallization type on intermetallics formation rate [13]

Figure 6.17 shows the growth of basis metal–tin compound at 170 °C under a layer of fully reacted barrier metal–tin compound, (a) copper–tin, and (b) brass–tin [13]. Here speculum is a single-phase electroplated coating with composition 38–42 percent Sn and 58–62 percent Cu, and with a structure similar to the equilibrium phase Cu_6Sn_5. A heat treatment for one hour at 135 °C converts it to the equilibrium phase Cu_3Sn for this composition. In general, Ni is considered a good choice of diffusion barrier meeting the requirements of (1) reasonably good solderability, (2) very low IMC formation rate of its own, and (3) satisfactory diffusion barrier capability. It is interesting to note that the presence of a Pb barrier layer appears to accelerate the copper–tin IMC growth rate, compared with unpreplated samples.

The intermetallic compound growth rate is also affected by the composition of Sn–Pb solders, as shown in Figure 6.18 [14]. The total IMC growth rate reduces with increasing tin composition initially, then increases again with a further increase in tin composition. This relation is further illustrated in Figure 6.19, where the activation energies derived from the Arrhenius plots for growth of total IMC from all coatings on both hard and soft copper is expressed as a function of tin composition [13]. There appears to be a trend toward a maximum activation energy for the lowest melting point alloy in this system. Although Kay *et al*. [13] have proposed that such a relationship implies a surface interaction between lead in the lead-rich interface zone and the Cu_6Sn_5, which has to be overcome by the incoming tin atoms, the exact mechanism has yet to be elucidated.

The high IMC formation rate for high tin composition suggests that the IMC may be a concern for Pb-free solder alternatives, since the choices are all high tin alloys, such as eutectic Sn–Ag–Cu or eutectic Sn–Ag systems, as will be discussed later. Solutions for minimizing the formation of IMC include (1) soldering at a lower temperature and for a shorter time, (2) employing barrier metals, such as Ni, and (3) employing solders with a proper Sn composition.

6.5.2 Gold

Au is one of the most commonly encountered surface metallizations used for solder joint formation in the electronics industry due to its superior stability and solderability. Gold, as an impurity in solder, is very detrimental to ductility because of the formation of brittle Sn–Au intermetallic compounds, mainly $AuSn_4$. Although a low concentration of $AuSn_4$ enhances the mechanical properties of many Sn-containing solders, including Sn–Pb [5], the tensile strength, elongation at failure, and the impact resistance of bulk 60Sn/40Pb drop quickly as the Au content in solder increases beyond 4 percent [1].

Pads with pure or alloyed Au up to 1.5 μ thickness can completely dissolve in molten solder during wave soldering. The amount of $AuSn_4$ formed is insufficient to impair its mechanical properties. For the surface mount solder paste process, the tolerable Au film thickness is much

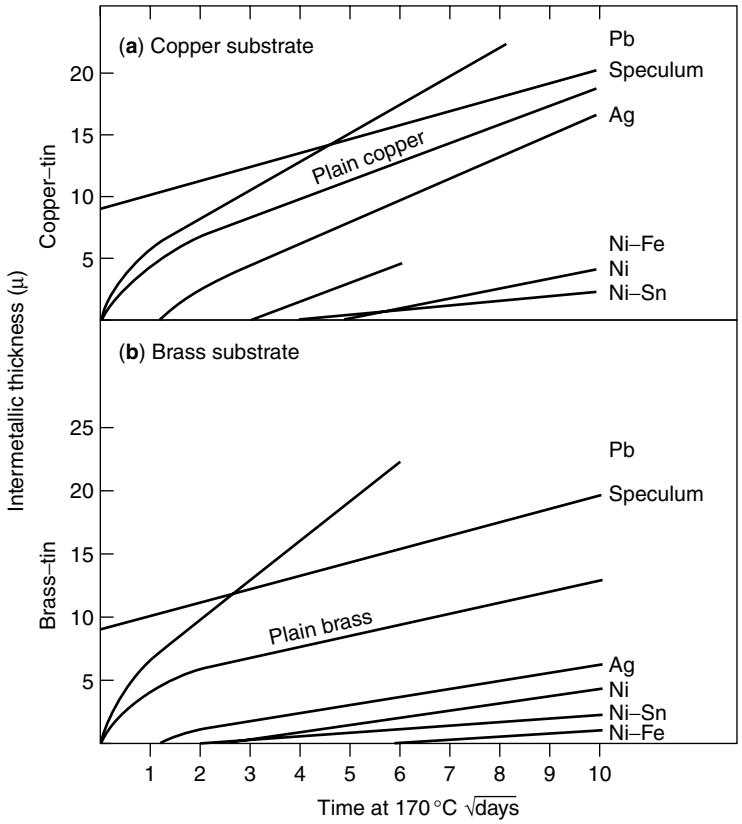

Figure 6.17 Development of base metal–tin intermetallic compound at 170 °C under layer of fully reacted barrier metal–tin compound: (**a**) copper–tin, (**b**) brass–tin [13]

lower and needs to be calculated [15]. Glazer *et al*. [16] have reported that the solder joints' reliability is not impaired as long as the Au concentration in solder joints between plastic quad flat packs and Cu–Ni–Au metallization on FR-4 PCBs does not exceed 3.0 w/o.

The presence of excessive IMC not only compromises the joint strength due to the brittle nature of IMC, but also affects the voiding performance of solder joints. Figure 6.20 shows the solder joints formed on a Cu–Ni–Au pad with 1.63 μ Au layer. The pads are reflowed with 7 mils (175 μ) 63Sn/37Pb no-clean solder paste with 91 percent metal content. Au–Sn intermetallics dispersed widely as particulates in the solder joint, as shown in Figure 6.20(a). The solder joints formed are highly voided, as shown in Figures 6.20(b) and 6.20(c), presumably caused by the sluggish solder flow due to the presence of excessive IMC particulates.

Unlike soldering on Ag surface metallization, where addition of Ag to Sn–Pb solder slows the leaching of Ag, addition of Ag to a Sn–Pb solder has a negligible effect on the Au–Sn IMC growth rate [17,18]. Moreover, it may interfere with the initial wetting [17]. Indium-rich solders, such as In–Pb or In–Sn alloys, may be used to greatly reduce embrittlement, since Au is less soluble in these alloys [19]. Other alloys such as Sn–Cd and Sn–Pb–Cd also give a combination of high heel strength with a low rate of dissolution of Au.

Although erosion of Au by molten In increases with increasing temperature, it levels off rapidly and is independent of time within a short time frame, as shown in Figure 6.21 [5]. The low level of Au erosion is a result of both the steep slope of the liquidus line on the In–Au phase diagram and the formation of a thin, continuous intermetallic compound ($AuIn_2$) between the molten solder and the Au metallization.

However, the solid-state diffusion still continues slowly with time. Therefore, the Au–In IMC layer thickness increases with temperature and time in a long time frame [19], as shown in Figure 6.22 [20], and eventually results in failure of solder joints if a thick layer of Au surface metallization is involved. Figure 6.23 shows peeling In/Pb solder joints on Au pads after temperature cycling. The thickness of Au is 2.5 μ (100 μ-in.), and is intended for both soldering and wire bonding purpose. EDX of surface L shows the presence of Au, In and Pb. Surface M is mostly Au with some In. Results here demonstrate that the Au–In IMC can still grow with time and cause failure, even with the use of preferred In/Pb solder alloys.

For applications involving both reflow soldering and wire bonding on the same substrate plane, the conflicting requirement in optimal Au layer thickness dictates that the Au surface finish has to be prepared separately according to applications. Thus, a thin Au layer will be advised for

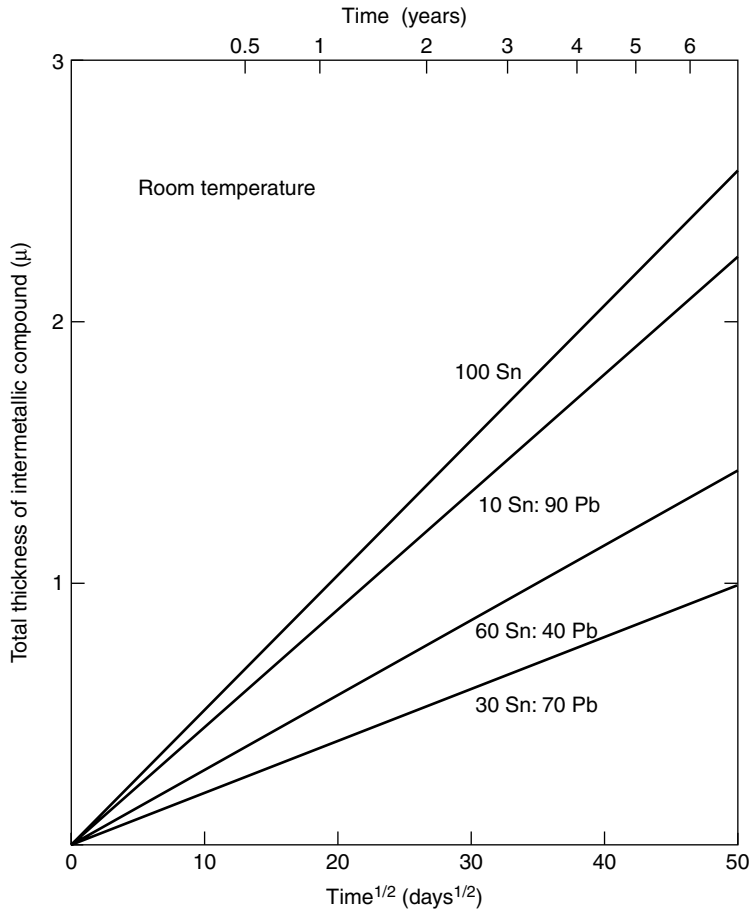

Figure 6.18 Effect of tin–lead composition on total Cu–Sn intermetallic compound thickness on copper when stored at room temperature [14]

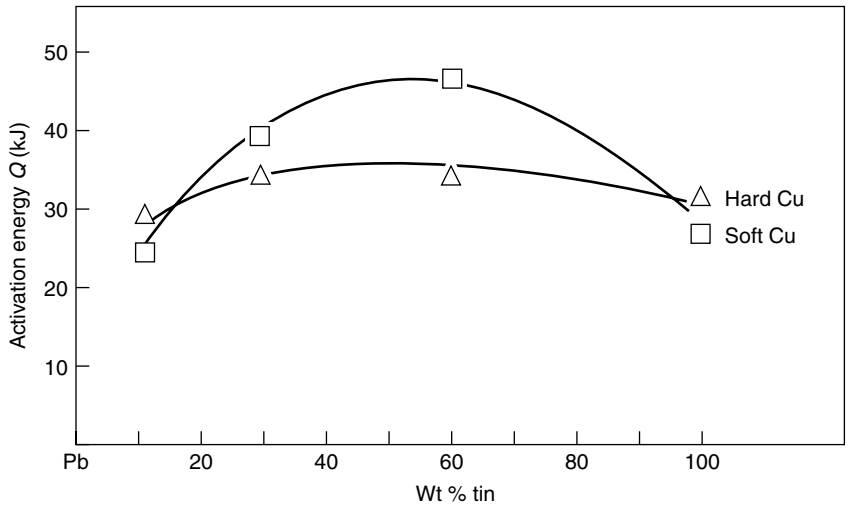

Figure 6.19 Effect of Sn content on the activation energies for growth of total intermetallic compound for Sn–Pb solder system on both hard and soft copper [14]

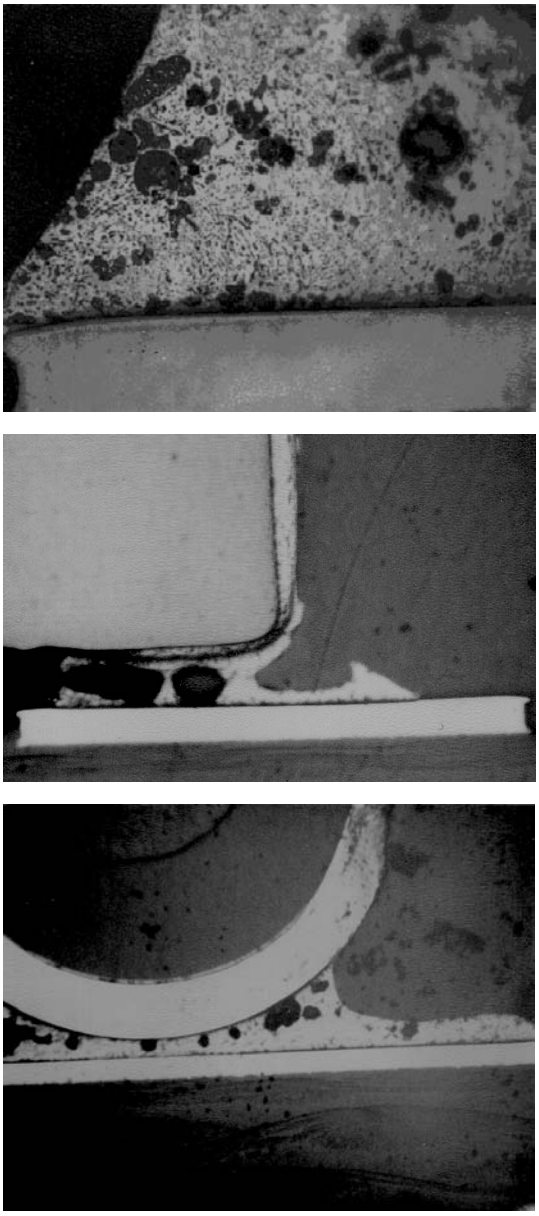

Figure 6.20 Reflowed solder joint formed on Cu-Ni-Au pad with 1.63 μ Au layer printed with 7 mils (175 μ) 63Sn/37Pb no-clean solder paste at 91 percent metal content: (**a**) Au−Sn intermetallics dispersed as particulates in the solder joint, (**b**) solder joint of chip capacitor, (**c**) solder joint of melf

reflow soldering, while a thick Au layer is desired for wire bonding. For a high throughput process, a photo imaging step may be needed to provide differential Au thickness on the same board surface. However, for a low throughput process, a shortcut can be taken to provide differential Au thickness on the same board surface. Here a thick layer of Au can be plated onto all the pads. Prior to the SMT assembly process, a solder paste such as 63Sn/37Pb can be printed onto the pads used for SMT solder joints. The paste is then reflowed on either a hot plate or under hot air, followed by removal of molten solder through either vacuum or scraping. The board with all of the Au on SMT pads being scavenged by the first reflow process is then ready to undergo a regular SMT process for components attachment.

Besides selecting the proper solder alloys or regulating the Au layer thickness, modifying the Au-containing base metal composition may also reduce intermetallic formation. For instance, 60Sn/40Pb can solder onto Au85Ni15 without Au embrittlement problems [21].

6.6 Tombstoning

Tombstoning is the lifting of one end of a leadless component, such as a capacitor or a resistor, and standing on another of its ends, as shown in Figure 6.24. Tombstoning is also known as the Manhattan effect, Drawbridging effect, or Stonehenge effect. It is caused by an unbalanced wetting of the two ends of the component at reflow and accordingly the unbalanced surface tension pulling force of the molten solder exerted onto the two ends, as illustrated in Figure 6.25. Here there are three forces exerted onto the chip: (1) the weight F_1 of the chip; (2) the surface tension vertical vector F_2 of the molten solder surface beneath the chip; (3) the surface tension vertical vector F_3 of the molten solder surface on the right side of the chip. Forces F_1 and F_2 are pulling downward and tend to keep the component in place, whereas force F_3 presses onto the chip corner and tends to tilt the component to a vertical position. Tombstoning occurs when force F_3 overrides the sum of forces F_1 and F_2.

The pad spacing, pad size, chip termination dimension, and thermal mass distribution play an important role in affecting tombstoning. Inadequate spacing between the two pads of the chips can cause tombstoning. Too small a spacing will cause floating of chips over the molten solder caps. Too large a spacing will cause easy detachment of either end from the pad. In Lee and Evans's [22] study, it was found that for the 0805 resistor tested, the optimum gap to produce the lowest tombstoning rate is approximately 43 mil (0.043 in.). Reduction of this gap resulted in more tombstoning, presumably due to the increased flotation of the light chips on the larger molten solder bump. On the other hand, a marginal overlap between the chip and the pad also yielded more tombstoning due to easy detachment of either end from the pad. Therefore, simply for the sake of tombstoning, the optimum gap between pads is considered to be slightly shorter than the gap between the two metallizations on the termination of the chips, as shown in Figure 6.26.

Pad size also affects tombstoning. Too short an extension of the solder pad beyond the chip ends will reduce the effective angle, therefore increasing the vertical vector of pulling force at the fillet-side and aggravating the tombstoning rate. If the solder pad is too wide, the chip tends to float and disrupt the balance of the holding forces between the two ends of the chip, hence causing tombstoning. Besides the rectangular pad, other shapes of pads have also been used. There are several observations citing that the circular pads appear to provide a much lower

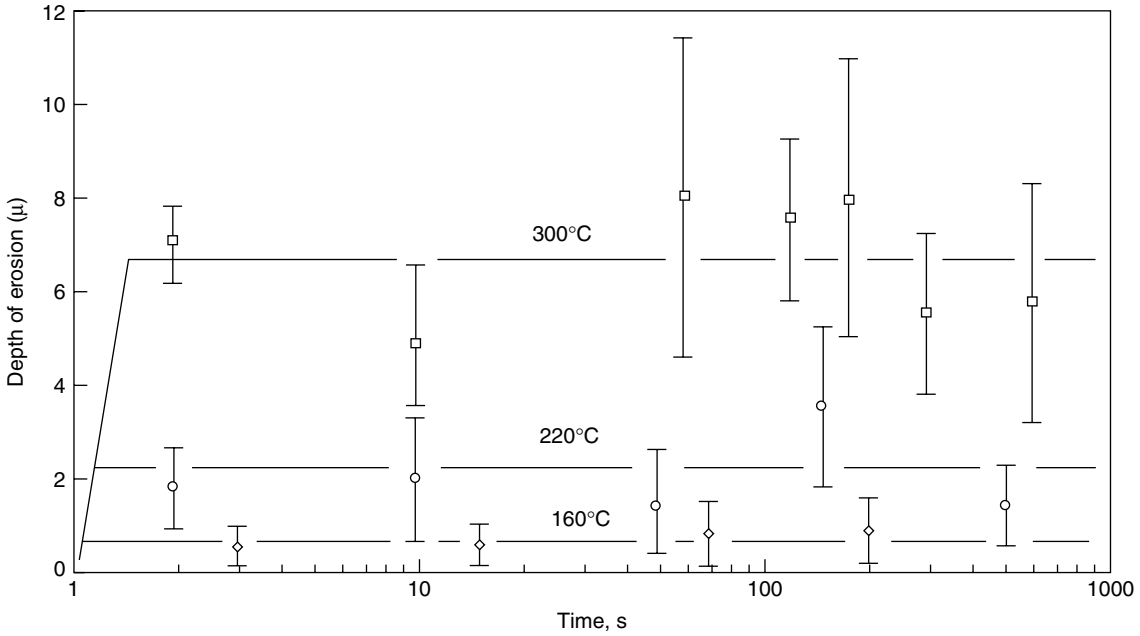

Figure 6.21 Erosion of Au metallization in molten indium [5]

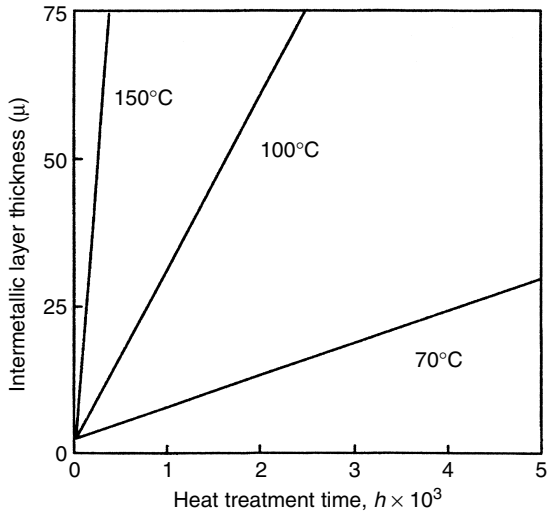

Figure 6.22 Effect of heat treatment time on the growth of Au–In intermetallic phase at the interface between an Au metallization and In–Pb solder at temperature below the solidus temperature of the solder. Source: After Frear, Jones, and Kingsman [1991]

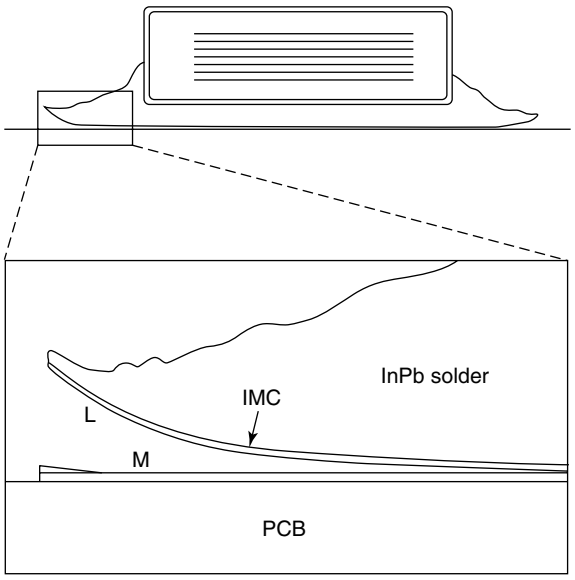

Figure 6.23 The peeling solder joints after temperature cycling. EDX of surface L shows the presence of Au, In and Pb. Surface M is mostly Au with some In. The substrate metallization is 100 μ-in. Au, for both soldering and wire bonding purpose. The solder used is In/Pb alloy. (Source: Hughes Aircraft)

tombstoning rate than either rectangular or square pads. The exact reason for this difference has yet to be identified.

The chip termination metallization dimension is another factor affecting tombstoning. If the width and area of metallization under the chip component are too small, they will reduce the under-chip pulling force which acts against the tombstoning driving force hence, aggravating tombstoning.

The temperature gradient may also be enhanced by uneven thermal mass distribution or by a shadow effect of nearby components. In the former case, one situation which may not be obvious by visual examination is the effect of a heat sink within the PCB on pad temperature. A

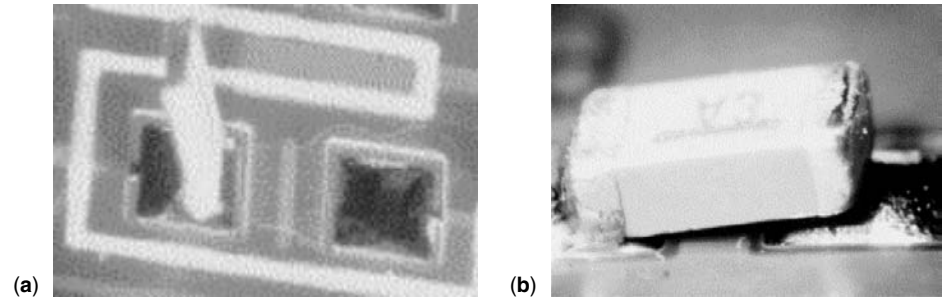

Figure 6.24 Examples of tombstoning: (**a**) chip resistor stands on one of its ends (left), and (**b**) one end of chip capacitor lifted free of contact (right)

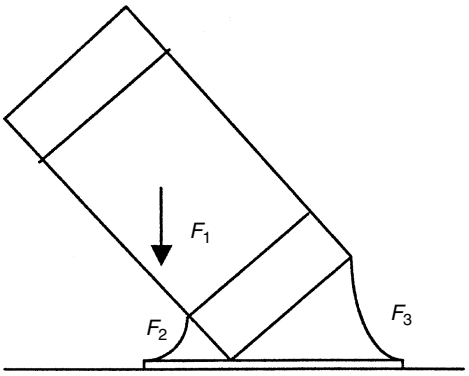

Figure 6.25 Tombstoning model analysis

pad connected to a large heat sink may have a lower temperature than its counterpart pad, and consequently result in tombstoning. The shadow effect is the impedance of heating due to the blocking of flow of a heating medium by nearby components. It can be reduced through adequate PCB circuitry design as well as proper selection of reflow methods. For instance, the short wavelength infrared reflow method is more prone to the shadow effect, while forced air convection is more immune to this effect.

Since the force balance is governed by the location of the molten solder, the solderability of parts and wetting power of the solder paste are expected to be important in tombstoning. Uneven solderability of component termination metallization or PCB pad metallization, due to either contamination or oxidation, is prone to inducing an unbalanced force at both ends of the parts, hence causing tombstoning. On the other hand, if the pad finish is a Sn–Pb coating, wetting onto the pads will be instantaneous once the solder melts. Consequently, it will be more sensitive to a temperature gradient developed across the pads, and will tend to cause more severe tombstoning than pads with plain copper.

Lee and Evans [22] have reported that unbalanced wetting can be aggravated by the use of a flux with a short wetting time. Thus a shorter wetting time is found to result in a greater tombstoning rate, as shown in Figure 6.27. In their study, the wetting time was controlled by adjusting the activator content without changing the wetting force. The data was not conclusive with regard to the cause,

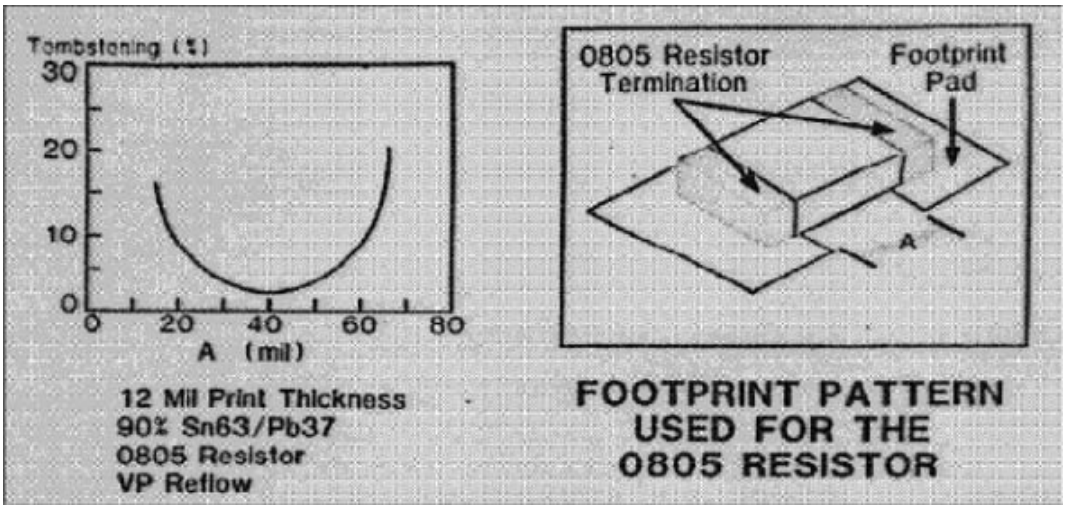

Figure 6.26 Effect of pad spacing on tombstoning [22]

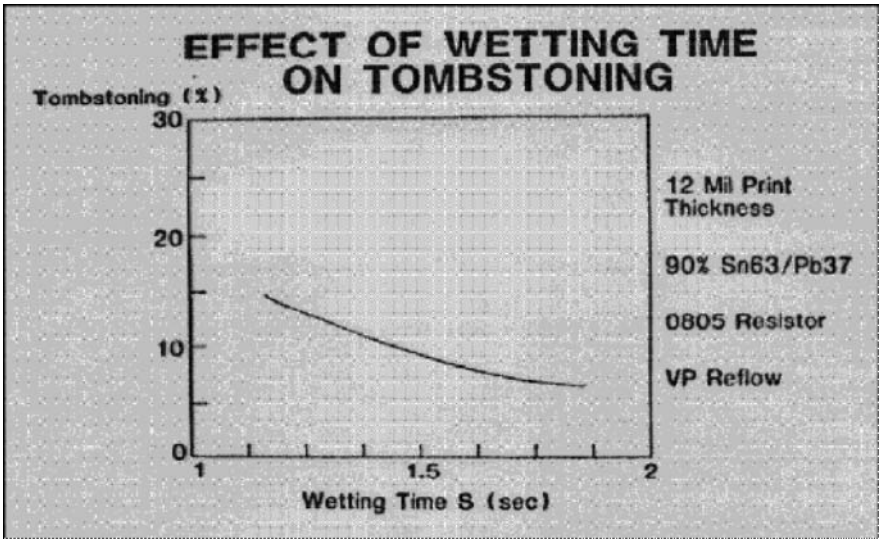

Figure 6.27 Effect of wetting time on tombstoning. The wetting time is regulated through varying the flux activator content [22]

however. The most likely explanation is that one end of the chip is completely wetted before the other end has the chance to start wetting.

The alloy melting speed, hence the wetting speed, of the solder being too fast can also cause tombstoning. Thus, as reported by Klein Wassink and van Gerven [23], using a solder paste with a delayed melting showed no tombstoning while a common solder paste suffered a severe tombstoning rate. In that work, after application of the two solder pastes, the boards were processed simultaneously: placing of components, predrying of the paste at 45 °C for 25 minutes, and soldering in the vapor phase.

The delayed melting can be generated through the use of a solder with a wide pasty range. For instance, use of 62Sn/36Pb/2Ag has been observed by some assembly houses to exhibit less tombstoning than 63Sn/37Pb. The effect can be augmented by addition of Ag and Sb to a eutectic Sn−Pb solder which results in a twin peak solder alloy with a wide solidification range and effectively prevents tombstoning [24]. In the same work, it is noted that if the Ag concentration is less than 0.1 percent or greater than 0.6 percent the extended pasty range will disappear. Delayed solder melting can also be generated by mixing solder powder with different compositions. Thus, a mixture of 63Sn/37Pb and 62Sn/36Pb/2Ag will result in an extended pasty range, which in turn improves the tombstoning defects. A similar effect can also be produced through mixing Sn powder with Pb powder with the final overall composition being equivalent to 63Sn/37Pb.

The temperature gradient across the board can be enlarged by using reflow methods with a fast heating rate. Thus, the vapor phase reflow method tends to result in a high tombstoning rate, compared with other reflow methods such as infrared reflow or hot air convection reflow [22]. This is one of the main reasons that vapor phase reflow technology, once prevailing in 1980s, gradually faded out as the main-stream reflow technology in the 1990s.

The balance in wetting force between the two ends of chips can also be interrupted by the rigorous outgassing of the flux. This outgassing can be a result of flux solvent volatility, or the rapid heating rate of the reflow methods adopted, such as vapor phase reflow. Employment of a predry step before reflow or using a profile with a long soaking zone will help in minimizing the volatile content of the flux and accordingly the outgassing rate at the solder reflow stage. Since tombstoning occurs only when the solder starts to melt, use of a profile with a very slow ramp-up rate through the melting temperature range will provide the best chance to minimize the temperature gradient, as reported by Lee [25], and consequently result in a minimal tombstoning rate. For instance, a profile ramping up from 175 °C to 190 °C in one minute is often very effective in reducing the tombstoning rate.

Too thick a solder paste print thickness can also be an issue. Greater print thicknesses cause more tombstoning, primarily through "walking" of parts over the large molten solder bump, as shown in Figure 6.28 [22]. Poor component placement accuracy will directly result in unbalanced wetting on both ends of chip, hence aggravating tombstoning as well.

In summary, tombstoning can be reduced or eliminated by the following measures.

Processes or designs:

Use a larger width and area of metallization under the chip component.
Use adequate spacing between the two pads of the chips.
Use a proper extension of the solder pad beyond the chip ends. Circular pads appear to be more promising than rectangular or square pads.
Reduce the width of the solder pads.
Minimize the uneven distribution of the thermal mass, including the connection of pads with heat sinks.

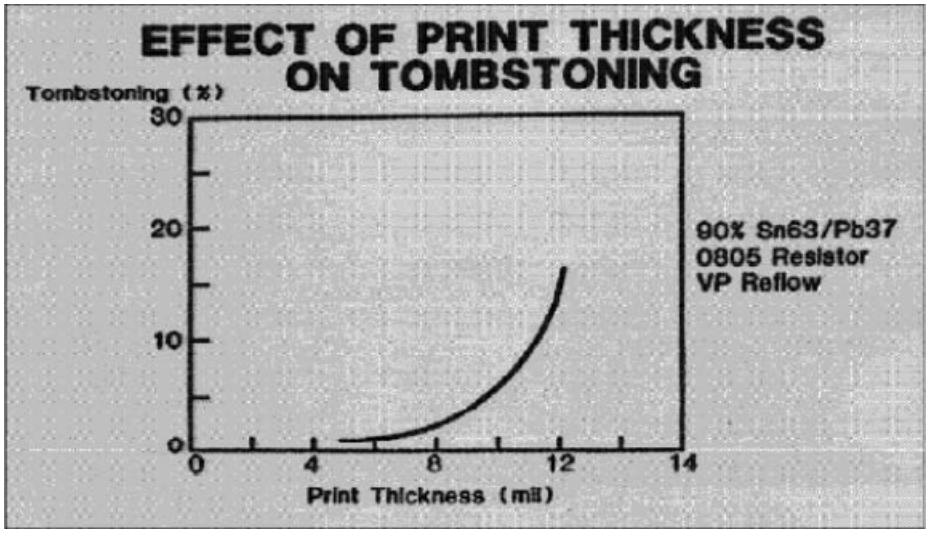

Figure 6.28 Effect of print thickness on tombstoning rate [22]

Minimize the shadow effect through adequate design of PCB and selection of reflow methods.
Use organic solderability preservatives or nickel/gold coating or Sn coating instead of a Sn−Pb coating on copper pads.
Reduce the contamination or oxidation level of the component termination metallization or PCB pad metallization.
Use a thinner paste print thickness.
Improve component placement accuracy.
Use a milder heating rate at reflow. Avoid using the vapor phase reflow method.
Predry the paste before reflow or use a profile with a long soaking zone to reduce the outgassing rate of the fluxes.
Use a profile with a very slow ramp rate across the melting temperature of solder.

Materials:

Use a flux with a slower wetting speed.
Use a flux with a lower outgassing rate.
Use solder paste with retarded melting, such as a blend of Sn powder and Pb powder or alloys with a wide pasty range.

6.7 Skewing

Skewing, also known as floating, swimming, or walking, is the movement of component in a horizontal plane and consequently results in misalignment of the component at reflow, as shown in Figure 6.29. It is caused directly by the unbalanced surface tension of molten solder at the two ends of the chip components. It may be considered as an early stage of a version of tombstoning. Factors causing tombstoning, as discussed in the previous section, typically also aggravate skewing. In addition, skewing is also sensitive to other factors, including (1) lifting of components by the high density heating fluid at reflow,

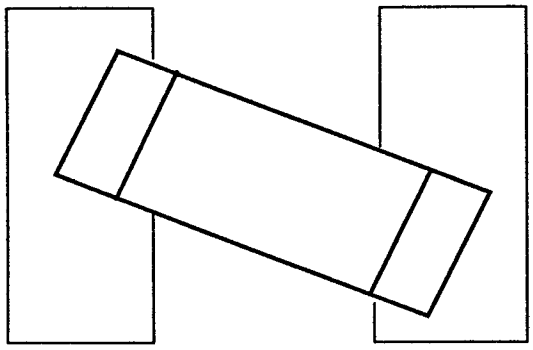

Figure 6.29 Schematic of skewing

(2) solder pad design is not balanced for the two ends of the chips, (3) the width and area of the undermetallization of the components are too small, (4) poor solderability of the component lead metallization, and (5) solder pad is too narrow. Factors (3) and (4) aggravate skewing due to the increasing risk of having the lead floating on top of a molten solder dome.

The effect of solder pad size on skewing has been studied by Klein Wassink *et al*. [23]. They analyzed the effect of pad width on the calculated self-centering forces (expressed in multiples of the surface tension) acting on shifted components, as shown in Figure 6.30. Curve Fw is for a wide solder land, as indicated by the dotted curve; Fs is for narrow solder lands, as indicated by the solid curve. (Dimensions: component width = 1.6 mm; component height = 0.6 mm; solder land width = 2.4 mm and 0.8 mm respectively.) In the case of a wide solder land, the centering force gradually rises when the component is shifted sideways. When one edge of the component reaches the edge of the solder land at a shift of about 400 μ, the self-centering force increases abruptly. In the

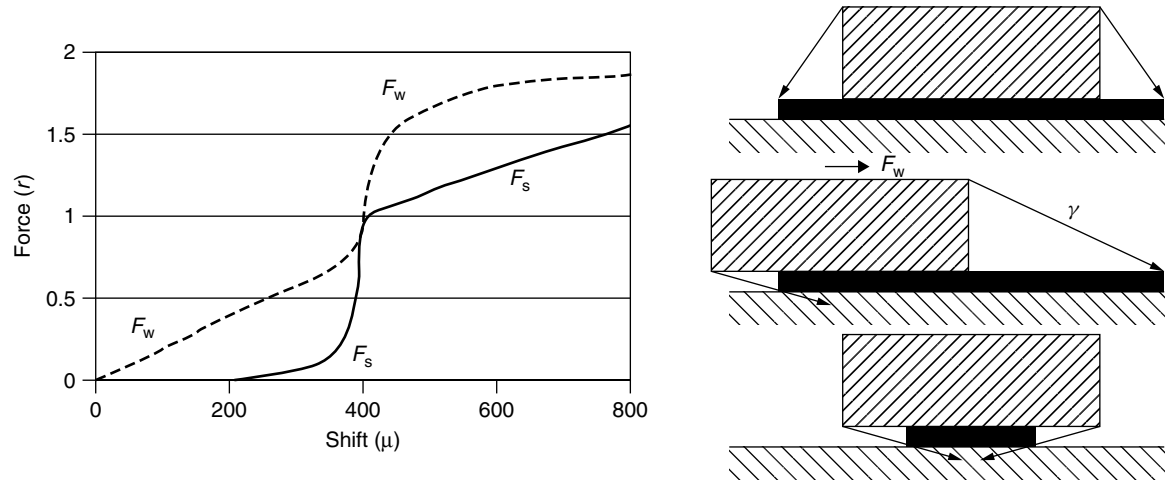

Figure 6.30 Relation between component shift and the self-centering force. Curve F_w is for a wide solder land, as indicated by the dotted curve; F_s is for narrow solder lands, as indicated by the solid curve. (Dimensions: component width = 1.6 mm; component height = 0.6 mm; solder land width = 2.4 mm and 0.8 mm respectively) [23]

case of a narrow solder land, the centering force is negligible initially with increasing shifts. The force then rises sharply at a shift near 400 μ, then gradually rises with further increase in shift. Hence, it can be concluded that a solder land narrower than the width of a component will be more prone to show skewing symptom than a wider solder land [23].

Overall, the solutions for reducing skewing can be summarized as below.

Processes or designs:

Reduce the heating rate at reflow. Avoid using the vapor phase reflow method.
Balance the solder pad design for the two ends of the chips, including pad size, thermal mass distribution, heat sink connection, and shadow effect.
Increase the width and area of the undermetallization of the components.
Increase the width of the solder pads.
Reduce the contamination level of the metallizations of components and boards. Improve the storage conditions.
Reduce the paste print thickness.
Improve the component placement accuracy.
Predry the paste before reflow to reduce the outgassing rate of the fluxes.

Materials:

Use a flux with a lower outgassing rate.
Use a flux with a slower wetting speed.
Use a solder paste with retarded melting behavior. Examples include use of a blend of Sn powder with Pb powder for the solder alloys.

6.8 Wicking

In wicking the molten solder wets the component lead and flows up the lead away from the joint area, to such an extent that a 'starved joint' or an 'open joint' is formed, as shown in Figure 6.31 for J-lead solder joints and in Figure 6.32 for gullwing-lead solder joints [23].

Wicking occurs in three steps, as shown in Figure 6.33. In the first step, the lead is placed in the solder paste. In the second step, the paste in contact with the hot lead melts and wicks up the component lead. In the third step, a starved or open joint is formed once most of the solder has wicked up along the lead. The direct driving forces of wicking are the temperature difference between lead and board as well as surface tension γ of molten solder (see Figure 6.8) [22,26,27]. At reflow, the lead, due to its smaller thermal mass, is often hotter than the board. On the other hand, the internal pressure of a connected molten solder formation may vary from one spot to another. In general, the greater the curvature $(1/R_1 + 1/R_2)$, the greater the internal pressure ΔP, as shown in the Young and Laplace equation. In order to balance this internal pressure, the surface with greater curvature will smooth out and consequently pump molten solder to the area with the smaller curvature. If the balanced new solder formation deviates from the desired "ideal solder formation", this joint formed is then regarded as having a "wicking" problem. Due to this internal pressure effect, leads with greater curvature will tend to entrap more molten solder, thus aggravating wicking.

The wicking phenomena demonstrated in Figures 6.31 and 6.32 are directly caused by the smaller thermal mass of the leads, which tend to heat up faster than the board in many reflow methods. Use of bottom heating will allow the solder to melt and wet to the PCB pads first. Once the pads are wetted, the solder will not usually wick up to the leads when the leads are heated up later. Bottom heating can be achieved through on-contact reflow methods. It can also be obtained by applying more bottom heating in some reflow furnaces such as infrared reflow ovens. If more bottom heating is not allowed due to oven design constraints, use of a slow ramp-up rate will allow the heat

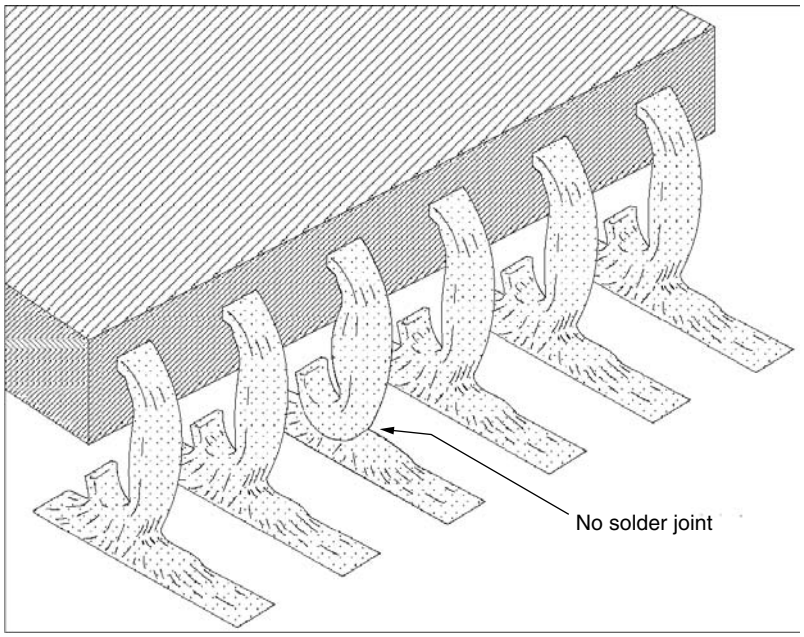

Figure 6.31 Example of solder wicking on a PLCC with J-leads. The third lead from the left has no solder joint, with solder wicked high up on the wide part of the lead [23]

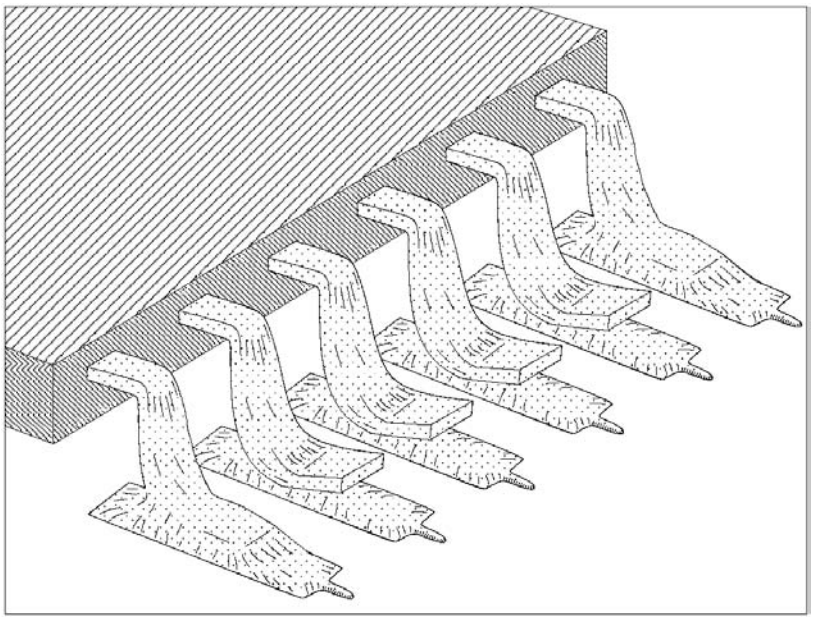

Figure 6.32 Example of wicking on an SO package with gullwing joints. Four leads in the picture showed ''open'' joints, with solder wicked up along the leads [23]

to propagate through the board more evenly, based on the natural heat propagation, and reduce wicking.

The symptom of wicking, such as starved or open solder joints, can be further aggravated by the poor coplanarity of leads. In addition, any situation which allows an easy wetting on leads will tend to aggravate wicking. For instance, use of fusible surface finishes, such as eutectic Sn−Pb, on leads will allow the molten solder from the solder paste to wet easily along the lead. Naturally, this will lead to wicking. Wicking may happen without the removal of surface oxide of fusible surface finishes, as long as the metallization under the oxide film melts during reflow.

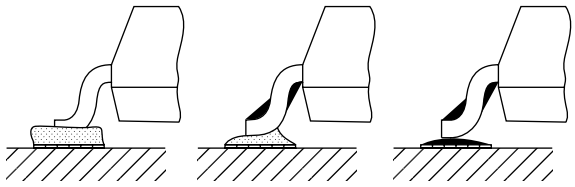

Figure 6.33 Development of solder wicking: (*Left*) The lead is placed in the solder paste. (*Middle*) The solder paste in contact with the hot lead will melt, wet the lead, and flow away from the joint area. (*Right*) When the rest of the solder paste melts, it may form a partial or no joint with the lead [23]

In this case, the molten solder from the solder paste will be pumped through the surface metallization layer underneath the thin oxide film. Use of a flux with a fast wetting speed or of solder alloys which wet easily will also promote wicking. In the latter case, use of solder with a slow melting or a wide pasty range, as described in Section 6.6, will help in reducing the wicking problem. Use of a flux with a high activation temperature will allow more time for the lead and board to reach temperature equilibrium before the flux is activated, and consequently reduce wicking.

Wicking may also be aggravated by slumping. Figure 6.34 shows wicking on a clip-on lead [28]. The symptom is further schematically illustrated in Figure 6.35. Use of solder paste with low viscosity tends to cause slumping more readily, and consequently result in dripping downwards along the lead. In conjunction with the use of a fusible surface finish, the solder inevitably ends up being pumped down the leads.

Use of a fusible Sn−Pb coating as a board finish and having a nearby via connected to the solder pad is another example where wicking will occur easily, as shown in Figure 6.36. Here the solder is pumped into the via, resulting in a gullwing-lead solder joint without a fillet at the toe location. Problems here can be corrected by (1) placing a strip of solder mask or solder dam between pad and via, (2) tenting the via with a solder mask, if the via is small, or (3) using nonfusible surface finishes on PCB.

Solutions for eliminating wicking are summarized as listed below:

Processes or designs:

Use a slower heating rate. Avoid using the vapor phase reflow method.
Use more bottom heating than top heating.
Improve component lead coplanarity.
Use Sn coatings or other nonfusible surface finishes for board and leads.
Apply a solder mask between pad and via prior to application of the Sn−Pb coating for a board finish.
Tent the via.
Reduce the curvature of the leads.

Materials:

Use a paste with less tendency to slump such as a paste with a higher viscosity.
Use a flux with a slower wetting speed.
Use a flux with a higher activation temperature.
Use a solder paste with retarded melting, for example a blend of Sn powder with Pb powder.

6.9 Bridging

Bridging is the solder bridges formed between neighboring solder joints due to the presence of locally excessive solder volume. The solder bridge formed may cross over more than two solder joints. Bridging is of particular

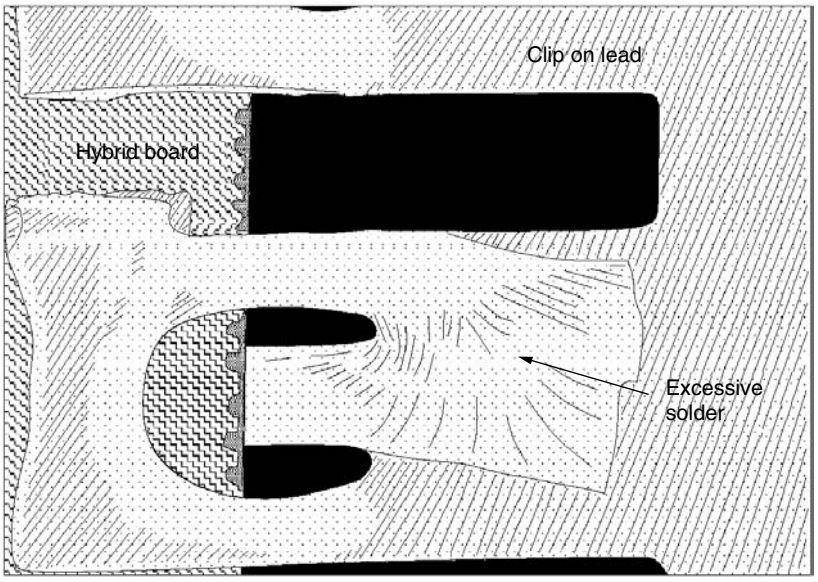

Figure 6.34 Wicking on hybrid board in clip-on leads [28]

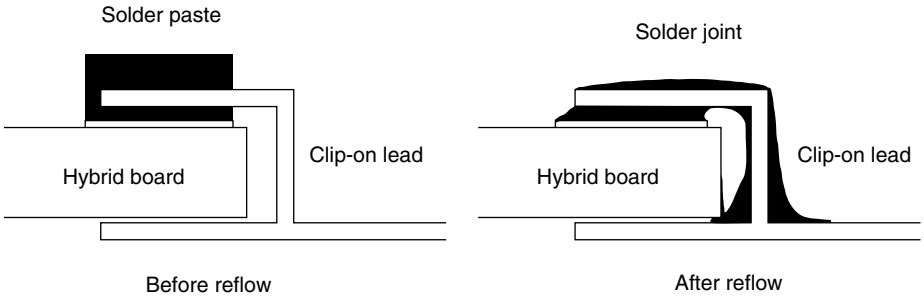

Figure 6.35 Schematic of solder wicking for hybrid board in clip-on leads. Slumping of solder paste increases the wicking problem

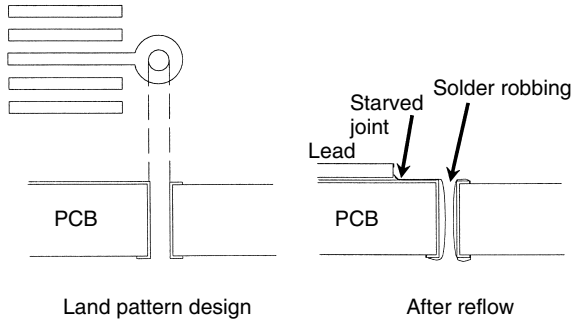

Figure 6.36 Solder wicking due to a nearby via for a pretinned PCB

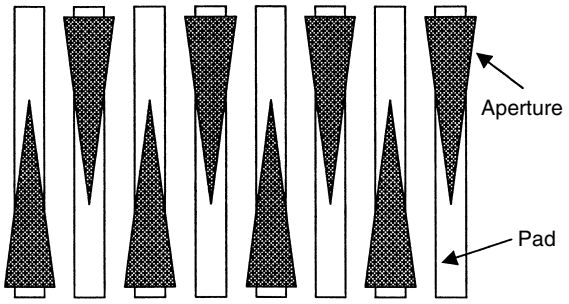

Figure 6.38 Schematic of stencil aperture design with alternate triangles

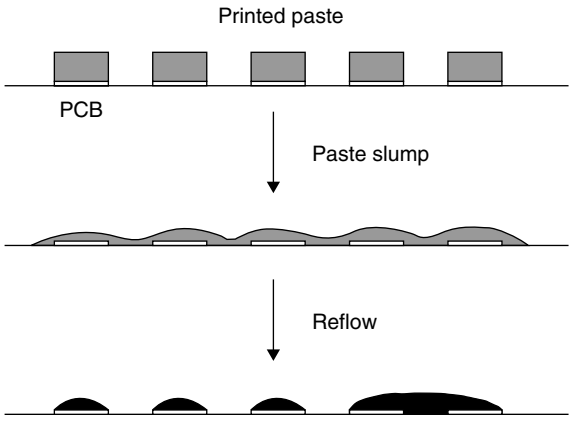

Figure 6.37 Relation between solder robbing and bridging. The solder allocates through the molten solder belt and results in new solder distribution where the curvature formed is smaller than the curvature of solder bumps without solder allocation

concern with gullwing-type leads, although other forms of bridging such as bridging between neighboring chip capacitors or resistors may also happen [22,29,30].

Bridging always occurs first through formation of solder paste bridges. These solder paste bridges may be formed due to (1) excessive solder paste deposited, (2) slumping of paste, (3) excessive component placement pressure, and (4) smearing of paste. Slumping, besides being caused by the factors described in Section 5.10, may also be the result of excessive solder paste deposited, or by excessive component placement pressure. Figure 6.37 illustrates the bridging mechanism. Here the solder paste volume deposited may be adequate for each pad. Upon reflow, if the paste slumps and forms a continuous paste belt across multiple pads, a corresponding molten solder belt will also be formed. This continuous solder belt allows solder robbing where the solder allocates so that the redistributed solder volume will result in either a minimal surface area or a minimal surface curvature (see Figure 6.8).

To reduce bridging through the solder paste volume control, Erdmann [31] has reported that the amount of paste should be reduced by at least one third. This can be achieved by reducing stencil thickness using step-etching, or by reducing aperture length or shape. In addition, bridging can be further contained by using alternate squares, dots, dog bones, triangles, wedges, teardrops, etc., as demonstrated in Figure 6.38.

Bridging rate increases with decreasing pitch. Figure 6.39 indicates that the bridging rate starts from 0 percent for 50 mil center-to-center spacing and climbs up rapidly to 17 percent (bridge/lead) for 30 mil spaced components [22]. This trend is primarily due to the fact that the print thickness reduction rate normally is slower than the pitch dimension reduction rate. For instance, the print thickness for 50 mil pitch typically is 8–10 mils, while that for 25 mil pitch often is 5–6 mils. As a result, the paste is more prone to slump and consequently tends to have a higher bridging rate.

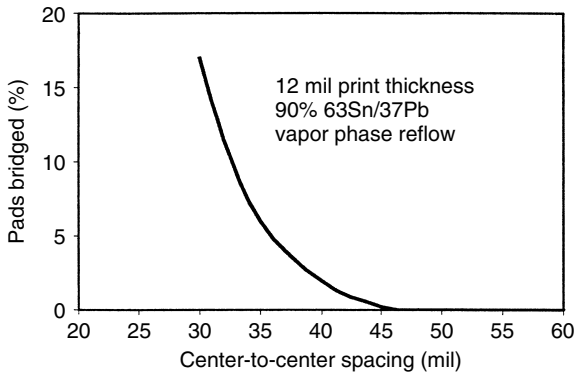

Figure 6.39 Effect of center-to-center spacing on bridging [22]

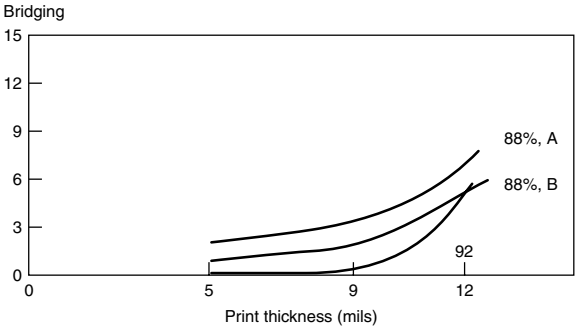

Figure 6.41 Effect of print thickness on bridging rate [32]

The bridging rate increases with increasing reflow temperature. This is reported by Roos-Kozel [32], as shown in Figure 6.40, where the bridging rate is plotted against the reflow temperature setting for soaking and the reflow zone. The sensitivity toward reflow temperature is greater for solder pastes with a lower metal load or lower viscosity. Apparently, this is a direct reflection of the relation between slump and reflow temperature, as discussed in Section 5.11. In fact, this relation should be regarded as a special case between slump and ramp-up rate. In Section 5.11, it was elucidated that a higher ramp-up rate will result in a greater slump, as shown in Figure 5.30 of Chapter 5. Since a higher temperature setting with the same belt speed essentially indicates a higher ramp-up rate, the higher bridging rate associated with higher reflow temperature reported by Roos-Kozel actually can be attributed to a higher ramp-up rate.

Also reported by Roos-Kozel is that the bridging rate increases with (1) increasing print thickness, as shown in Figure 6.41, (2) decreasing metal load (see Figure 6.42), (3) decreasing viscosity (see Figure 6.43), (4) increasing solvent content (see Figure 6.44), (5) decreasing resin softening point (see Figure 6.45), and (6) decreasing solvent vapor pressure (see Figure 6.46) [32]. Except for item (1), all these factors essentially reflect the effect of viscosity on slump.

Lee and Evans [22] have reported that the bridging rate increases with increasing wetting time, as shown in Figure 6.47. The rationale for this phenomenon is: when wetting time is long, solder-robbing (redistribution of solder along neighboring leads) can occur along the belt of molten solder which forms across the leads. This takes place as the molten solder seeks to minimize its surface tension before it has a chance to wet the pads. This will definitely cause bridging. The faster the solder wets the pads, the smaller the chance that solder-robbing will occur, hence the less risk there is of bridging.

Solutions for reducing or eliminating bridging can be summarized as below:

Reduce solder paste volume by using thinner stencil, staggered aperture pattern, or reduced aperture size.
Increase the pitch.
Reduce component placement pressure.
Avoid smearing.
Use cooler reflow profile or slower ramp-up rate.
Heat board sooner than the components. Avoid using vapor phase reflow method.
Use a flux with slower wetting speed.
Use a flux with higher vapor pressure.

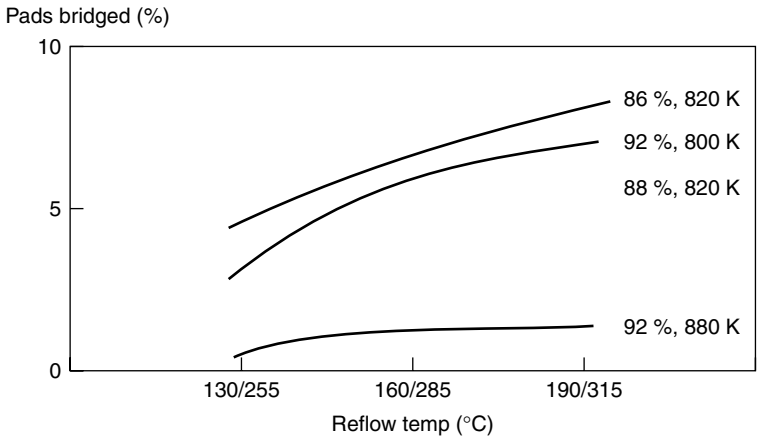

Figure 6.40 Effect of reflow temperature on bridging rate [32]

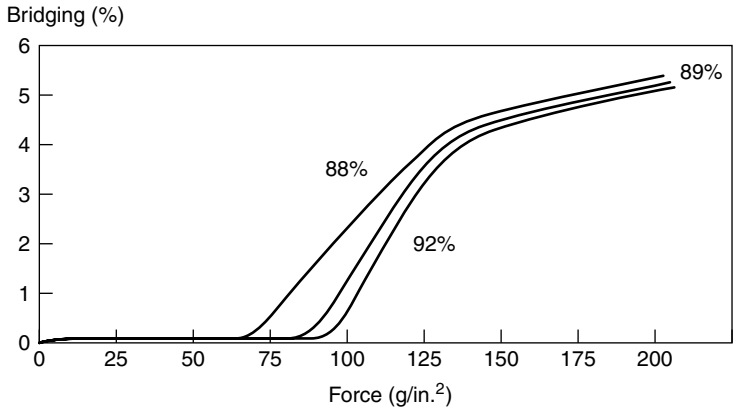

Figure 6.42 Effect of metal load on bridging rate. Here the ''force'' is the pressure exerted on the paste to simulate the weight of the components [32]

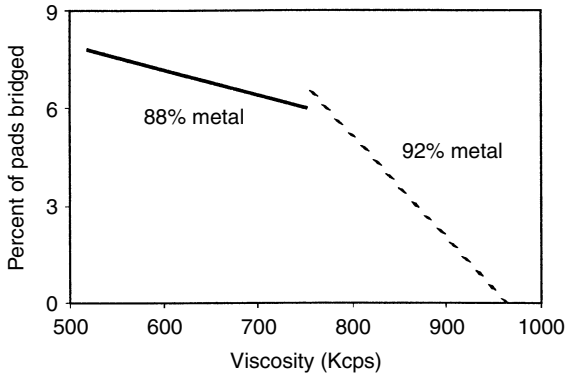

Figure 6.43 Effect of solder paste viscosity on bridging rate [32]

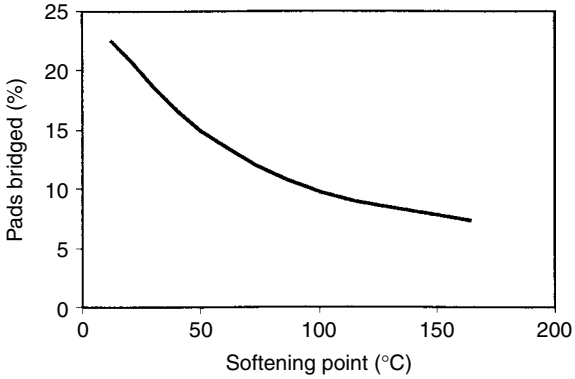

Figure 6.45 Effect of softening point of resin on bridging rate [32]

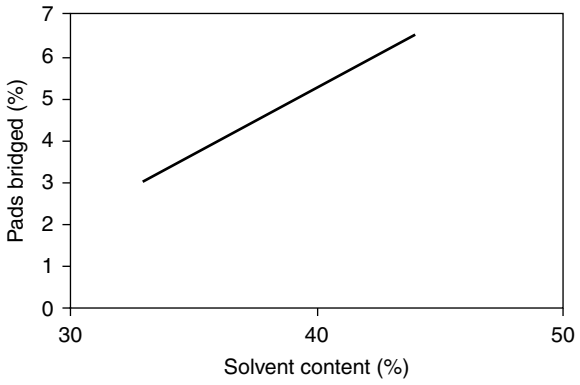

Figure 6.44 Effect of solvent content on bridging rate [32]

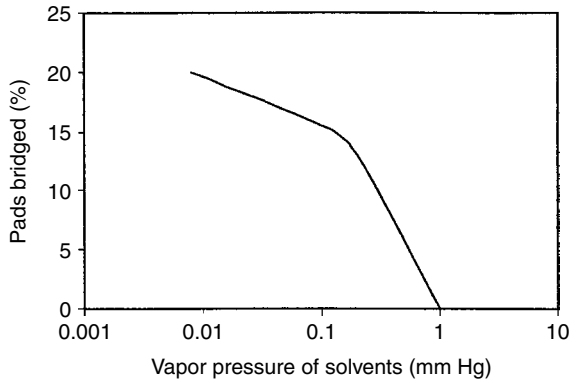

Figure 6.46 Effect of solvent vapor pressure on bridging rate [32]

Use a flux with lower solvent content.
Use a flux with a higher resin softening point.

6.10 Voiding

Voiding is a phenomenon commonly associated with solder joints. This is especially true when reflowing a solder paste in an SMT application, as shown by Figure 6.48. In the case of LCCC, it was found that the overwhelming majority of large (>0.0005 in./0.01 mm) voids were located between the LCCC pads and the PWB solder pads, while the fillets near the LCCC castellations contained very few small voids. The presence of voids will affect the mechanical properties of joints and deteriorate strength,

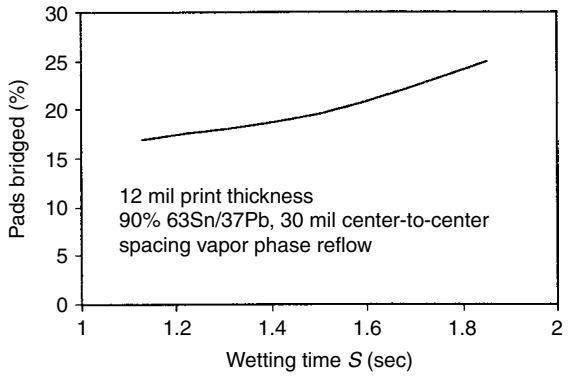

Figure 6.47 Effect of wetting time S on bridging rate [22]

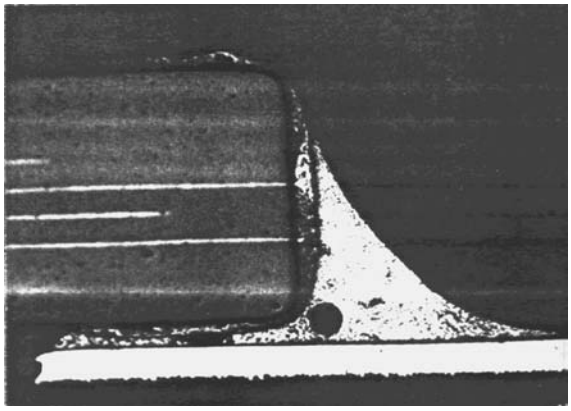

Figure 6.48 Example of voiding in solder joint of SMT component [33]

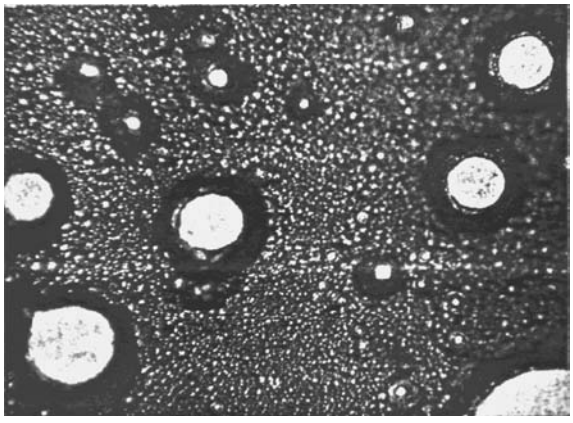

Figure 6.49 Picture of voids examined under optical microscope after the void-sample was peeled apart [33]

ductility, creep and fatigue life, due to the growth in voids which could coalesce to form ductile cracks and consequently lead to failure. The deterioration could also be due to the enhanced magnitude of the stresses and strains of solder caused by voids. In addition, voids could also produce spot overheating, hence lessening the reliability of joints. It is believed that, in general, voiding could be attributed to (1) solder shrinkage during solidification, (2) laminate outgassing during soldering the plated through-holes, and (3) entrapped flux. For solder paste processes, the voiding mechanism is more complicated [22,33,34].

The composition and structure of solder pastes have the most significant effect on void formation [35]. Hance and Lee [33] studied the voiding mechanism by reflowing solder paste sandwiched between two pieces of copper coupons. By examining the void appearance under the optical microscope after the void–sample are peeled apart, it is seen that most of the voids show no entrapped organic residue, and only very few voids exhibit a noticeable amount of residue (see Figure 6.49). This observation is confirmed with the use of reflective infrared spectroscopy. This indicates that most of the voids are formed due to the outgassing of fluxes or fluxing reactions, and therefore upon cooling the vapor condenses and leaves no sign of residue.

The measurement results of the above work indicate that the void content decreases with increasing flux activity, as shown in Figure 6.50 [33]. Here S is the wetting time of the fluxes determined on a wetting balance. Since higher flux activity supposedly will generate more fluxing reaction products, the lower void content associated with higher fluxing activity suggests that fluxing reaction or activator and activator-induced decomposition are not the major sources of outgassing. In other words, the

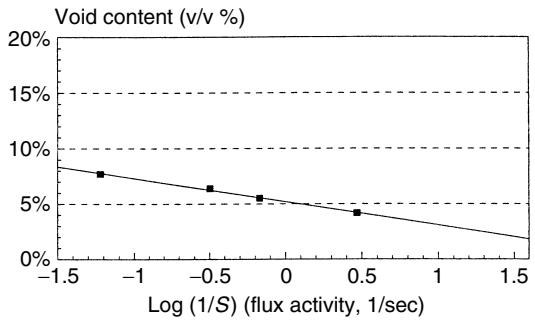

Figure 6.50 Effect of flux activity on voiding [33]

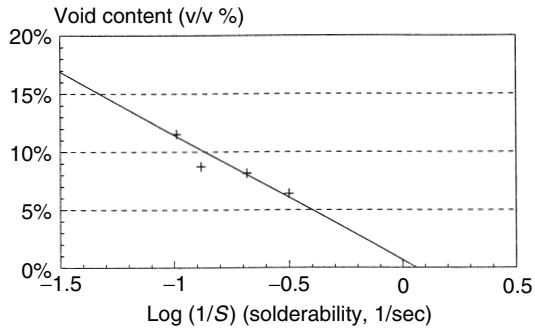

Figure 6.51 Effect of solderability on voiding [33]

outgassing of entrapped flux is directly responsible for the major void formation, and a lower void content means a smaller amount of entrapped flux. When using a solder paste, the flux is in direct contact with the surface oxide of powders and surface-to-be-soldered. Hence at reflow any residual oxide can be expected to be accompanied by some adhered flux. Considering that a higher activity flux usually removes the oxide more rapidly and completely, thereby leaving fewer spots for the flux to adhere to, the relation observed in this figure becomes easily comprehensible.

The void content decreases with increasing solderability, as indicated by Figure 6.51 [33]. This can be explained by the mechanism discussed above. With increasing solderability, the substrate oxide can be cleaned more readily, hence allowing less opportunity for the flux to be entrapped to form voids.

The voiding phenomenon is not a sole function of wetting time, and obviously is more sensitive to the solderability of the substrate (curve B) than to the flux activity (curve A), as indicated in Figure 6.52. This discriminating sensitivity can be attributed to a 'timing factor'. If the paste coalesces much sooner than the substrate oxide removal at reflow, the flux may adhere to the surface of substrate oxide (an immobile phase) and becomes entrapped in the molten solder. Consequently this entrapped flux will serve as an outgassing source and will constantly release vapor which directly contributes to void formation [33].

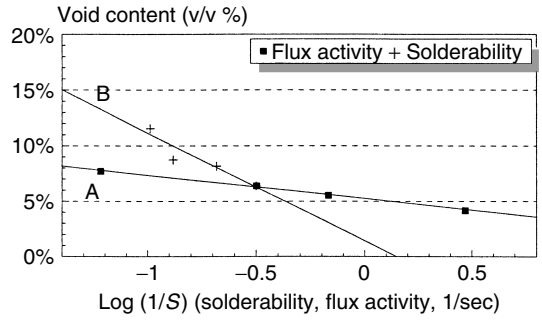

Figure 6.52 Relative impact of solderability and flux activity on voiding – timing factor [33]

In general, the number fraction of voids decreases rapidly with increasing void diameter. This is true in spite of the total void content. The volume fraction of voids versus void diameter relations appear to be more complicated. However, by examining the relations between the accumulated volume fraction of voids and void diameter (see Figure 6.53), it becomes obvious that while the void content increases with decreasing flux activity, as discussed above, so does the fraction of large voids [33]. Here the flux activity increases from A to B to C to D.

The increasing rate of large voids fraction ramps up rapidly with decreasing flux activity, as shown in Figure 6.54 [33]. Similar relationships are also observed on other voiding factors, such as solderability. Therefore it can be summarized that the volume fraction of large voids increases with increasing void content as a result of voiding factor adjustment. Since it is reasonable to speculate that large voids are more harmful than small voids, the results here suggest that factors which cause voiding will have an even greater impact on the solder joint's reliability than is shown by the data of total-void-volume analysis.

Voiding decreases with decreasing coverage area, as shown in Figure 6.55. Since the print thickness and the final joint height remain constant, a reduction in print width means an increase in the ratio of side-opening to total solder volume, and consequently facilitates outgassing and entrapped flux to escape. With advances in ultra-fine pitch technology, the coverage area is expected to be increasingly smaller. This suggests that, on the issue of voiding, the coverage area factor is favoring a shift toward ultra-fine-pitch technology [33].

The above findings on the effect of coverage area on voiding suggests that voiding can be reduced by increasing the ratio of side-opening to total solder volume, such as by raising the lead and splitting the molten solder joint for a very short time during the soldering process. Indeed, later work by Xie *et al.* reported that, for the Sn63Pb37 solder paste with a metal content of 90 percent, the solder joints produced by this method have no detectable

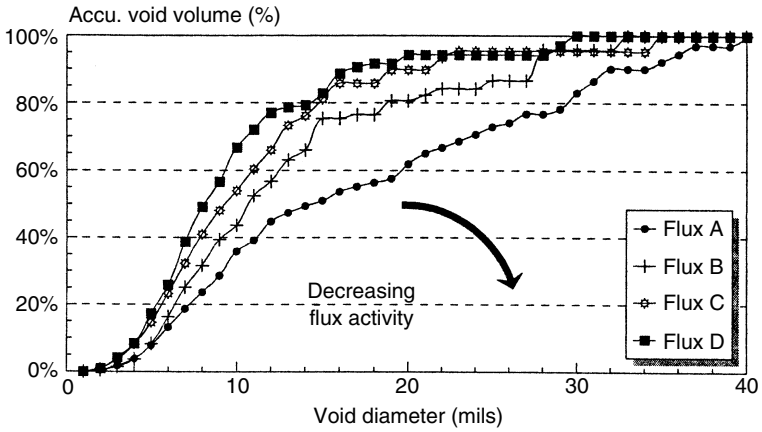

Figure 6.53 Effect of flux activity on void size distribution [33]

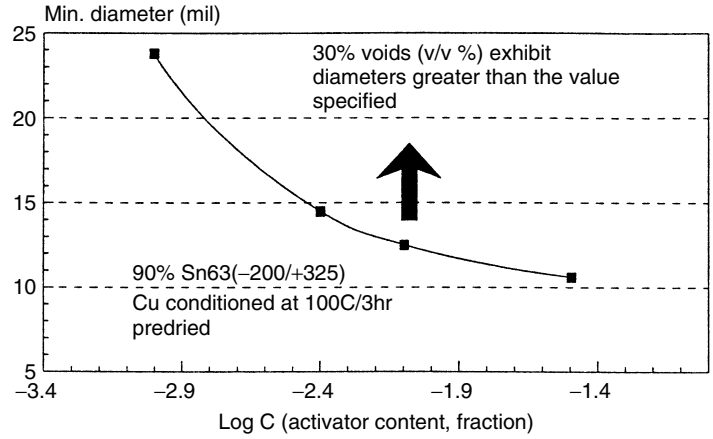

Figure 6.54 Effect of flux activity on tendency of forming large voids [33]

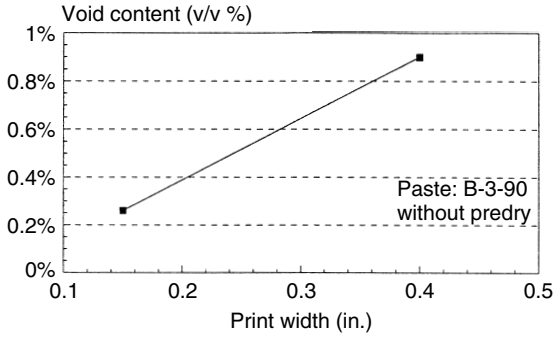

Figure 6.55 Effect of paste coverage area on voiding [33]

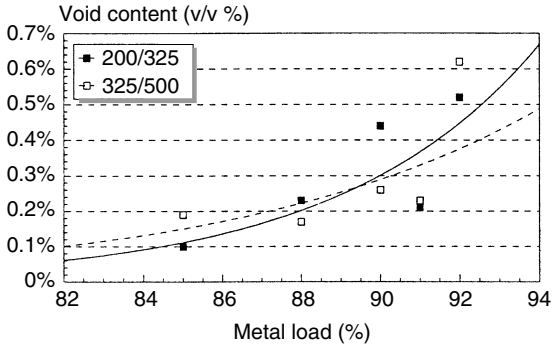

Figure 6.56 Effect of metal load and powder size on voiding [33]

voids compared with 7.5 percent area fraction of pores in normal IR reflow soldering. The joint strength also increases by about 20–40 percent as compared with that of normal solder joints. This method has promising applications, especially in the nitrogen reflow soldering technique, to yield void-free and robust solder joints [35]. The fatigue properties and microstructure of the solder joints are also critically studied by Xie *et al.* [36]. It is found that the method of splitting is effective in eliminating not only void formation (both gas and shrinkage pores), but also inclusions in solder joints. The method is applicable to various solder pastes, including no-clean and water-soluble. Thermal and mechanical fatigue cycling tests show that the fatigue life of the solder joints can be prolonged by more than 60 percent compared to that without splitting. Fractographs illustrate that the fracture in the fatigued joints occurs quite often at the interfaces of printed circuit boards (PCBs) and copper pads when splitting has been applied to the joints. This affirms that the solder joints have been strengthened considerably by splitting. Xie *et al.* consider that the proposed splitting method is particularly suitable for specimens with a large pad area in each joint or when the voids or inclusions are likely to form during solder joint fabrication. Since special fixtures will be required for this splitting process, the potential applications may be limited to rework processes or processes involving only a single component during reflow.

In Hance and Lee's study [33], two series of pastes are used, with metal load ranges from 85% to 92% in both cases. The samples are processed without predrying. In general, both series show an increase in voiding when the metal load increases (see Figure 6.56). Later work by Chan *et al.* [37] also reported that a lower metal load does not necessarily cause higher voiding in solder joints. This can be attributed to (1) an increase in total solder powder oxide, (2) a decrease in flux content for copper oxide removal, and (3) possibly a greater difficulty for flux to escape due to tighter powder packing. The increase in solder oxide not only reduces the flux quantity

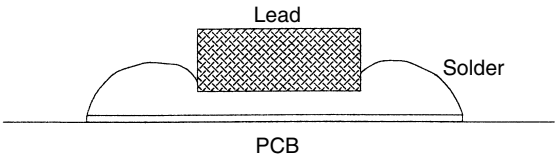

Figure 6.57 Schematic of pillow effect (end view), where the lead is sitting in the solder bump without formation of electrical contact

needed for cleaning substrate oxide, but also increases the chances of leaving some trace of solder oxide entrapped in the molten solder during reflow. However, the effect of this factor should not be overemphasized, as will be discussed in the relation between powder size and voiding. Decreasing the powder size causes only a slight increase on voiding. Being a mobile phase, any residual solder oxide can probably be segregated relatively easily from the interior of molten solder. This may explain, at least partially, why the powder size effect is much milder than that of an immobile substrate oxide.

Results of Chan *et al*. on void formation processes during the whole infrared reflow soldering cycle show that high area fractions of voids in solder joints correspond to the peak temperatures in infrared reflow temperature profiles [35]. Tu and Chan reported that the fatigue lifetime of the solder joints depends on the thickness of the IMCs layer and the voids area fraction, and both are concerned with reflow soldering time. The cracks mainly propagate along the interface between the IMC layer and the solder bulk under long-period reflowing. If the reflow time at the peak temperature of 220 °C is too short, the area fraction of voids will become large so that cracks initiate principally in the large void. Data show that the optimal parameter of soldering is 220 °C for 25 seconds by preheating to 100 °C for 100 seconds when using a three-zone infrared oven [38].

Lai and Hui [39] studied the dimension and stability of voids against thermal excursions in surface mount solder joints fabricated using conventional infrared (IR) reflow soldering. Two major types of specimens are employed in their work: blank pad (with no component) and sandwiched solder joints including a gullwing leaded assembly and shear specimen (i.e. strap specimen). It is found that voids formed in a blank pad have a critical radius which is independent of the reflow time. A void is stable and cannot be annihilated during reheating if its radius is below the critical radius. The critical radius is enlarged and strongly correlated with the maximum radius in the sandwiched solder joints. The void formation in sandwiched solder joints is affected greatly by joint configuration. The maximum principal radius is normally less than 0.2 mm if the joint thickness is greater than 0.20 mm. However, it may be more than 0.3 mm when the joint thickness is less than 0.1 mm. Voids formed in the solder joints cannot be eliminated even by prolonging the reflow time. In contrast, the void radius usually increases with reflow time [39]. Yet, if the reflow time at the peak temperature of 220 °C is too short, the area fraction of voids would become large so that cracks initiate principally in the large void. Data show that the optimal parameter of soldering is 220 °C for 25 seconds by preheating to 100 °C for 100 seconds when using a three-zone infrared oven.

Generally the voids are caused by the outgassing of entrapped flux in the sandwiched solder during reflow. Voiding is mainly dictated by the solderability of metallization, and increases with decreasing solderability of metallization, decreasing flux activity, increasing metal load of powder, and increasing coverage area under the lead of the joint. A decrease in solder particle size causes only a slight increase on voiding. Voiding is also a function of the timing between the coalescing of solder powder and the elimination of immobile metallization oxide. The sooner the coalescing of paste occurs, the worse the voiding will be. An increase in voiding is usually accompanied by an increasing fraction of large voids, suggesting that factors causing voiding will have an even greater impact on joint reliability than is shown by the total-void-volume analysis results. Control of voiding may include (1) improving component/substrate solderability, (2) using fluxes with a higher flux activity, (3) reducing solder powder oxide, (4) using an inert heating atmosphere, (5) minimizing the coverage area of components, (6) splitting the molten joints during soldering, (7) slowing the preheat stage to promote fluxing before reflow, and (8) using adequate time at peak temperature.

6.11 Opening

Opening refers to the presence of a discontinuity in electrical contact with or without a mechanical contact in a solder joint.

6.11.1 Pillowing

Pillowing is a lead sitting on a solder bump, which appears as the lead being laid on a pillow, without formation of electrical contact. It is shown in Figure 6.57, and is caused by nonwetting between lead and solder. Solutions for remedying pillowing are the same as those used for nonwetting, as discussed in Section 6.2.

6.11.2 Other openings

Opening is also often associated with other soldering defects, such as tombstoning and extreme cases of wicking. This can also be corrected by following the solutions described in Sections 6.6 and 6.8. Opening may also be caused by misregistration of component placement. Apparently, this has to be addressed by improving the accuracy of placement registration.

Warpage of components or boards may also cause opens. Examples include soldering of PBGA. Solutions for this cause could include (1) stiffening the components through packaging design and (2) avoiding localized heating. An open may also be a result of cracking induced by stress, such as soldering of PBGA. This can be caused by a mismatch in thermal expansion, and can be remedied by reducing the temperature gradient between the board and components. Excessive intermetallics formation at interfaces of solder joints may also cause opens, such as soldering of CCGA on aged HASL boards, and needs to

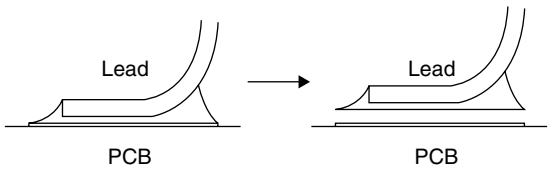

Figure 6.58 Schematic of fillet lifting

be corrected by avoiding formation of excessive IMC in HASL boards. Detailed discussion on these cases involving area array packages will be covered in later chapters.

6.11.3 Fillet lifting

A special form of open is fillet lifting. Figure 6.58 shows a schematic side view of a fillet lifting. Here a fine-pitch gullwing solder fillet of the QFP (quad flat pack) completely lifted at the solder–pad interface after wave soldering. The detached solder fillet maintained the integrity of fillet configuration. A likely cause is the mechanical stress imparted to the leads during a pick test after the reflow process. In pre-wave pick testing, a tweezer is drawn over the leads of QFP components to determine if all the leads had soldered in the reflow oven. This results in a non-alignment of toes when viewed from the top. Fillet lifting may also be caused by mechanical damage imparted during board handling. The mechanical stress induced by the deformed leads behaves like a spring under tension. Once the underside heating of the wave causes a partial secondary reflow or merely weakens significantly the solder strength at the land/fillet interface, this inbuilt stress could be relieved by lifting of the lead and fillet from the board, as reported by Barrett *et al*. [40]

Fillet lifting can be avoided by altering the sequence of the pick test. By conducting the pick test after instead of prior to wave soldering, the solder joints being touched by the tweezers will no longer be heated and hence the fillet lifting problem can be avoided. Barrett *et al*. also reported that in a few instances, fillet lifting may also be observed at some corner solder joints of QFP components where the joints were not pick tested, and attributed it to the excessive internal stress caused by mismatch in TCE of the component and the board. The latter case might have to be corrected by either minimizing the mismatch in TCE or applying more top heating during wave soldering.

6.11.4 Projected solder

Open may also be caused by variation in lead coplanarity and/or variation in paste print thickness. For instance, the leads of QFP often exhibit a variation of $\pm 25\,\mu$ in coplanarity. By using a stencil with $125\,\mu$ thickness and a conventional rectangular pad design, the solder bump height after reflow will typically be around $70\,\mu$, with a variation shown in Figure 6.59. As shown in this graph, the low end of the solder bump height distribution can be lower than the high end of non-coplanarity distribution of leads. This inevitably will result statistically in opens.

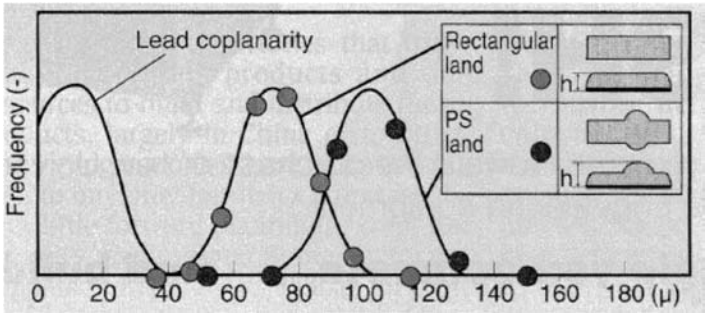

Figure 6.59 Relation between pad design, bump height distribution, and frequency of opens. Projected solder (PS) provides a greater bump height, thus eliminating the opens due to coplanarity variation [41]

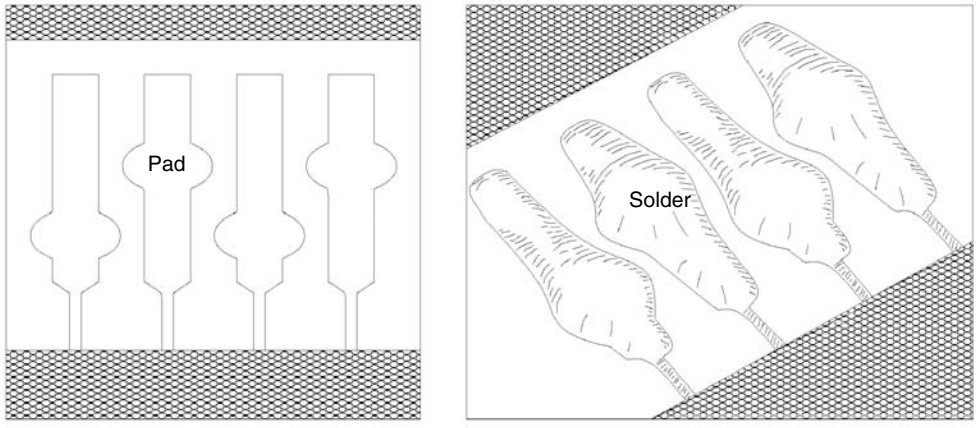

Figure 6.60 Land pattern (*left*) and reflowed solder bumps (*right*) of projected solder system for 12 mil pitch applications [41]

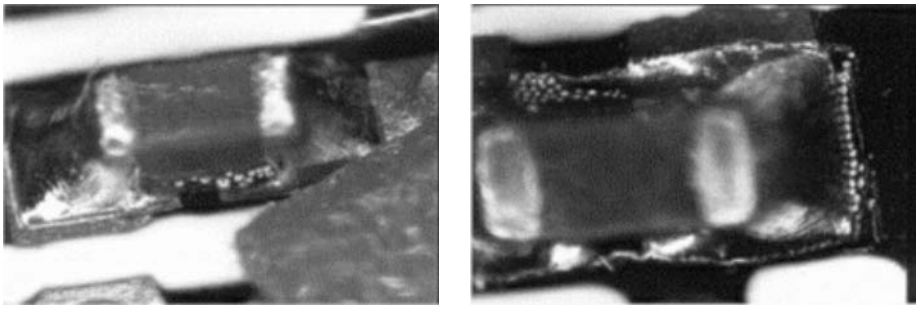

Figure 6.61 Example of solder balling

Opens due to this cause may be corrected by either reducing the non-coplanarity of leads of components or by increasing the paste print thickness. The former approach is limited by the component's manufacturing capability, while the latter approach may introduce bridging due to excessive solder volume.

Wakigawa [41] has reported that this challenge may be addressed with the projected solder (PS) approach, which employs a pad design with an enlarged area in part of the land pattern, as shown in Figures 6.59 and 6.60. Figure 6.59 shows a top view of a typical rectangular pad and a pad with a protrusion. It also illustrates the solder bump shape by showing the side view of solder bumps after reflow. The pad with protrusion (PS land) exhibits a local bump height about 30 μ greater than that of the rectangular pad. As shown in Figure 6.59, the low end of bump height distribution is still about 30 μ higher than the high end of lead coplanarity variation, thus preventing formation of opens. In order to avoid solder bridging, the protrusion is arranged in a zig-zag pattern, as shown in Figure 6.60 for a 12 mil pitch application. Wakigawa has demonstrated this approach with a solder precoating process. This PS approach is expected to be applicable to solder paste process as well.

In summary, opening can be caused by (1) other soldering defects such as poor wetting, tombstoning, and wicking, (2) warpage of components or boards, (3) misregistration, (4) mismatch in thermal expansion, (5) excessive intermetallics at interfaces of solder joints, (6) human factors such as the pick test, and (7) lead coplanarity variation as well as paste print thickness variation. It can be prevented by (1) solutions discussed for improving soldering defects such as for poor wetting, tombstoning and wicking, (2) stiffening components or avoiding localized heating, (3) improving registration, (4) minimizing temperature gradient between board and components, (5) avoiding formation of excessive intermetallics of HASL boards, (6) altering the sequence of the pick test, and (7) employing design adjustment such as the projected solder approach.

6.12 Solder balling

At reflow, small spherical particles with various diameters are formed away from the main solder pool and do not coalesce with the solder pool after solidification, as shown in Figure 6.61. In most instances, the particles are composed of the solder powder used in the solder paste. However, in other cases, the solder balls may be the result of coalescence of several solder powder particles. Solder balling is the most frequently publicized problem associated with the solder paste process. Formation of solder balls causes concern for both circuit shorts or leakage currents as well as the possibility of insufficient solder in the joint. With advances in fine-pitch technology and no-clean approaches, the demand for solder balling free SMT processes is becoming increasingly stringent with time.

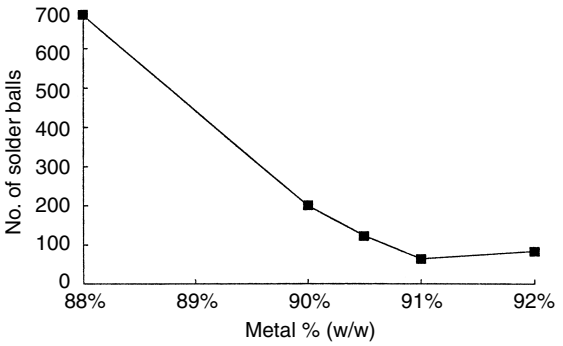

Figure 6.62 Effect of metal load of 63Sn/37Pb (−325/+500 mesh) on solder balling [42]

Solder balling is often caused by smearing due to an inadequate printing process, such as poor gasketing during the printing stage. Too thick a solder coating may result in paste leakage during printing due to the dome-shaped solder bump. Misregisteration during printing can also produce the same results. Excessive slump of solder paste aggravates solder balling as well.

Solder balling may also be caused by poor solderability of component leads and substrate metallization. Excessive tarnish build-up on the metallization will consume some flux and accordingly results in insufficient flux capacity for solder balling control. Extensive exposure of paste to oxidative environment will also aggravate solder balling. This is usually caused by reuse of solder paste beyond the recommended paste handling condition.

Inadequate drying conditions may also result in solder balling. Insufficient drying may leave some volatiles in the paste for some formulations. Those volatiles may result in spattering at reflow.

Thus, solder balling can be reduced by drying the solder paste prior to reflow. Lea [1] has reported that solder balling decreases with increasing drying time up to 90 minutes at 50 °C for RMA solder paste with 90 percent 62Sn/36Pb/2Ag solder powder. In the past, the drying out of the solder paste was often performed in air, at a temperature from 50 °C up to 170 °C, although typically below 120 °C. Lea has indicated that the general guideline times were in the ranges 1–2 hours at 50 °C, 30–60 minutes at 70 °C, 5–20 minutes at 90 °C, and 10 seconds at 170 °C. However, over-drying may oxidize solder powder too much and result in solder balling.

An inadequate reflow profile may also result in solder balling. Too rapid a heating rate may cause spattering. This is particularly true in the case of laser soldering. Also, too long a preheat profile may promote excessive powder oxidation and may result in solder balling. The reflow process now employed rarely utilizes a drying procedure, due to a demand for high throughput and a better reflow furnace and solder paste technology. In the event of having solder balling, the symptom often can be reduced by employing a tent reflow profile with a slow ramp up rate, as reported by Lee [25].

Inappropriate volatiles incorporated into flux for specified reflow processes is another cause of solder balling. Here the reflow technology has a significant effect on solder balling. Some heating methods deliver heat energy to the surface of the solder paste. The volatiles entrapped beneath the hardened surface may erupt causing spattering and solder balling at reflow. Vapor phase reflow does not cause oxidation, but may promote spattering by the volatile-entrapment mechanism. Infrared reflow employs high energy infrared radiation which penetrates the solder paste and reflects throughout the solder powder, thus achieving an even temperature within the solder paste. Forced air convection reflow utilizes hot gas to convey the heat to the parts to be soldered. For air reflow, the hot air can oxidize solder paste thus causing solder balling. This is particularly true for a high gas flow rate setting in the oven. For solder pastes with marginal or insufficient flux capacity, use of a nitrogen reflow atmosphere can effectively reduce solder balling.

Many solder pastes deteriorate in solder balling performance when exposed to humid environments. This is caused by accelerated solder oxide build-up as well as spattering at reflow due to moisture pick-up. Solder pastes with hygroscopic fluxes are often more prone to this problem. Lea [1] has reported that solder balling deteriorates continuously with increasing exposure time below 85 percent RH. At 45 percent RH, solder balling increases initially, then levels off with increasing exposure time. In general, it is recommended to control the humidity level of solder paste process environment at or below 60 percent RH. However, it should be noted that, with advances in flux technology, few current solder pastes are able to withstand exposure under high humidity up to 85 percent RH for 24 hours without solder balling.

The wicking effect can also contribute to solder balling. A tight tolerance between components, such as chip capacitors or chip resistors, and a solder mask may draw the solvent together with the powder under the component and accordingly result in solder balling. Interaction between solder mask and solder paste serves as another cause of solder balling. Some undercured low Tg dry film may release volatiles at the reflow stage. The volatiles can react with the solder paste and cause solder balling.

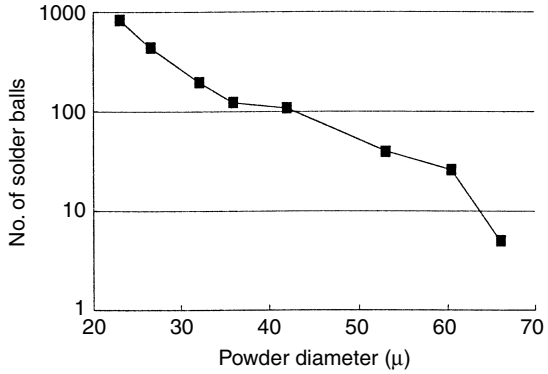

Figure 6.63 Effect of 63Sn/37Pb powder size on solder balling [42]

Solder balling may be affected by metal load. Figure 6.62 shows the effect of metal load on the number of solder balls, as reported by Xiao *et al*. [42]. The powder used in this study is −325/+500 mesh size. The results indicate that the number of solder balls first decreases rapidly, then reaches the minimum value at 91 percent (w/w), followed by a slight increase with increasing metal content. The initial drop in the number of solder balls with increasing metal load is mainly due to the decreasing slump. The slight upswing of solder balling at a metal content beyond 91 percent is attributed to the increasing insufficiency of relative flux capacity. Here the flux capacity is defined as the molar concentration of effective flux functional groups in the flux/vehicle.

Insufficient flux capacity will result in solder balling. This can be due to insufficient flux activity or to excessive solder powder oxides or contaminations. Too much fines will also result in the same phenomenon. The effect of particle size on solder balling is shown in Figure 6.63. With decreasing particle size, the number of solder balls

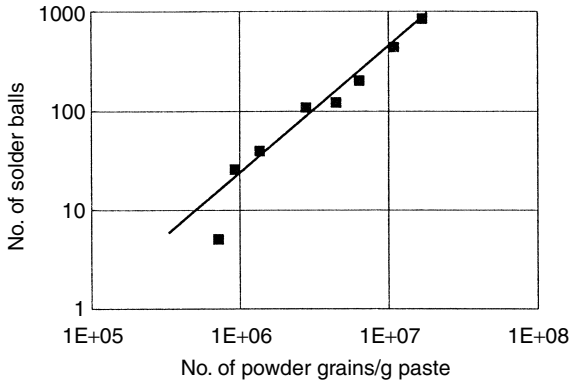

Figure 6.64 Effect of 63Sn/37Pb solder powder concentration on solder balling [42]

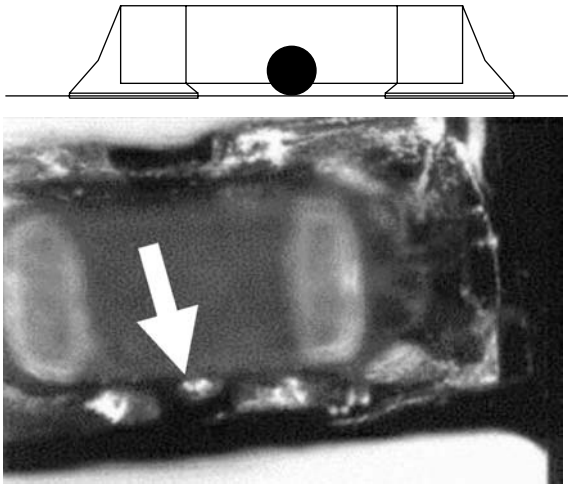

Figure 6.65 Schematic (*top*) and example (*bottom,* with solder bead shown by arrow) of solder beading

increases drastically. Presumably, the more powder grains involved in the coalescence process, the greater the risk of having some particles left behind. Besides the probability mechanism, the high solder oxide content of fine powders may also be responsible for the high frequency to solder balls [42].

Solder balling worsens with increasing solder powder particle concentration in the solder paste, as shown in Figure 6.64. Again, the more powder grains involved in the coalescence process, the greater the risk of having some particles left behind [42].

In summary, the solutions for eliminating solder balling can be categorized as follows:

Processwise:

Adjust the printing process. Wipe the stencil's underside more frequently.
Improve the solderability of components and substrates.
Avoid scavenging leftover paste on the stencil for future use.
Control the humidity of paste processing environment. A relative humidity of no more than 50 percent is preferred for most solder pastes.
Use adequate paste drying conditions. Consult paste vendor for recommendations.
Use an adequate reflow profile. Avoid too long or too short a reflow profile. Also avoid too rapid a heating rate. A tent profile is often desired.
Select the proper reflow method. Bottom or penetrating heating methods will produce a better solder ball performance.
Remove or reduce the solder mask thickness for certain leadless chip component areas to prevent the paste wicking effect.
Select proper solder mask materials to prevent interactions with solder paste.
Use proper registration during printing.
Reduce the aperture dimension. An aperture dimension with 50 μ recession on each end of the opening versus the pad size significantly improves solder balling performance.
Reduce the solder coating thickness or use other thin surface finishes for copper pads.
Use an inert reflow atmosphere.

Materialwise:

Use a paste with sufficient flux activity and capacity.
Reduce the oxide content or contamination level of the solder powder.
Reduce the amount of fines.
Reduce paste slumping and its hygroscopic property through adequate flux formulation.
Use a higher metal load.
Use coarser powder whenever the situation allows.
For specified reflow technologies or reflow profiles, adjust flux volatiles to eliminate spattering.

6.13 Solder beading

Solder beading is a special phenomenon of solder balling when using solder paste in certain SMT applications. In brief, solder beads refer to very large solder balls, with or without the presence of tiny solder balls, formed around components with very low stand-off, such as chip capacitors or chip resistors (see Figure 6.65) [43,44].

The reflow-generated solder beads are secured firmly to the PCB, and only water or solvent cleaning is able to dislodge the balls. For wave-generated solder balls, board handling and vibration testing is able to move the solder balls. For solder beads generated from the reflow process, product vibration testing results in no solder bead movement [45], thus creating no concern on reliability. Solder beads are often not desired mainly due to cosmetic considerations.

Solder beading is caused by flux outgassing which overrides the paste's cohesive force during the preheat stage. The outgassing promotes the formation of isolated paste aggregates underneath the low clearance components. At

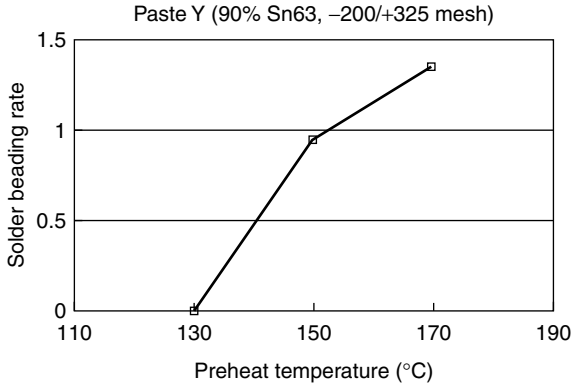

Figure 6.66 Effect of preheat temperature on solder beading rate for solder paste Y with 90 percent 63Sn/37Pb (−200/+325 mesh) [43]

reflow, the isolated paste melts and, once it has emerged from the underside of the components, coalesces into solder beads [43].

Hance *et al*. [43] first reported the solder beading phenomenon and found that the lower the preheat temperature, the lower the solder beading rate, as shown in Figure 6.66. Apparently, the lower preheat temperature allowed the paste to outgas at a slower rate. Therefore, it provided less impetus to expel the paste from the main deposit. In this experiment the preheat time was maintained constant. It is reasonable to expect that with each chosen preheat temperature, the preheat time could also be adjusted in order to achieve the best result. On the other hand, since preheat could also induce further oxidation of the solder powder which in turn would aggravate solder beading, the optimum preheat condition should be a compromise between both effects. Lee has reported that, based on defect mechanism analysis, a linear ramp-up profile (also known as a tent profile) with a ramp-up rate of 0.5.1 °C/sec is an ideal profile for minimizing solder beading [25].

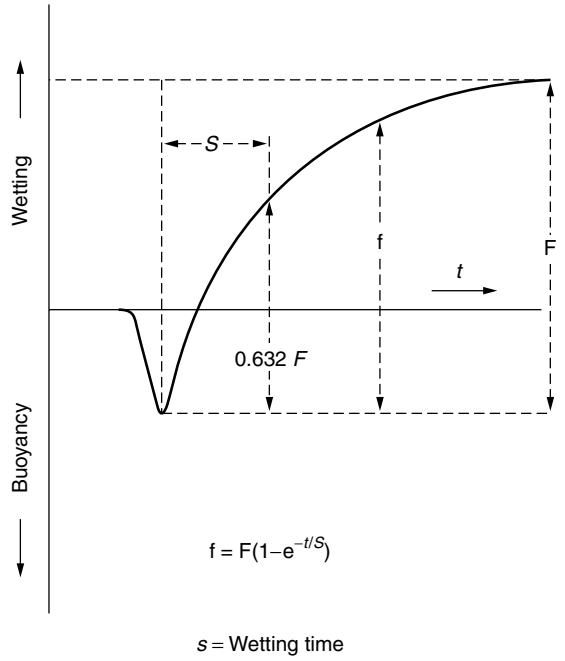

Figure 6.67 Determination of wetting time S with the use of a wetting balance

Solder beading is affected by the activation temperature of fluxes. In a practical sense, the activation temperature can be defined as the minimum temperature needed for a flux to function with a wetting time of no more than a certain value. Since soldering applications could vary considerably, the choice of criteria becomes a relatively subjective decision. Here 20 seconds' wetting time was chosen considering that a solder paste reflow process normally would take several minutes.

In Hance *et al*.'s study [43], the activation temperature of four fluxes was determined with the use of a wetting balance. The substrate material used was a copper coupon that was precleaned and then baked at 100 °C for 3 hours prior to use. Since the wetting behavior of fluxes at a temperature near preheat condition was considered essential for understanding cold welding, a solder alloy 46Bi/34Sn/20Pb with a melting point of 100 °C was then chosen and the wetting test was conducted at 150°, 180°, 210°, and 240 °C. For each flux the wetting time (see Figure 6.67) at each temperature was determined and plotted against temperature, as shown in Figure 6.68. Data here indicate that wetting time S can be expressed as an exponential function of temperature, with S increasing with decreasing temperature.

$$S = K\mathrm{e}^{A/T} \tag{6.1}$$

where K and A are constants (see Table 6.1) and T is temperature in degrees Kelvin.

The activation temperature for the four fluxes A, B, C, and D was then calculated using equation (6.1) and the results listed in Table 6.1. The solder beading rate increases with increasing activation temperature of fluxes, as shown in Figure 6.69. This is due to the fact that fluxes

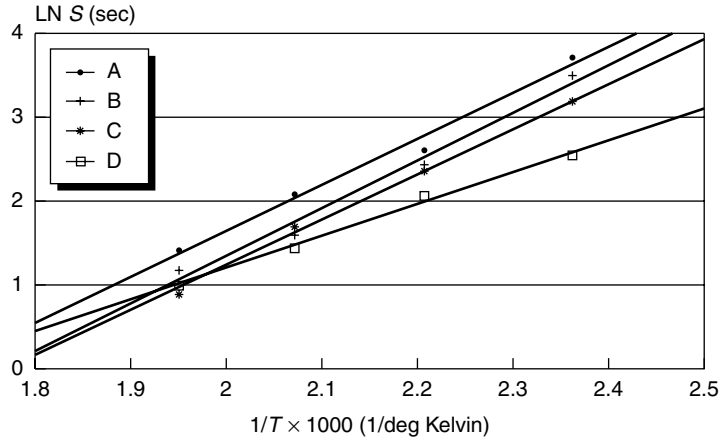

Figure 6.68 Relation between wetting time S and temperature [43]

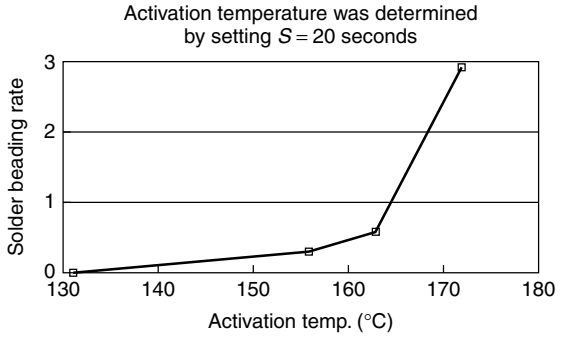

Figure 6.69 Effect of activation temperature of fluxes on solder beading rate [43]

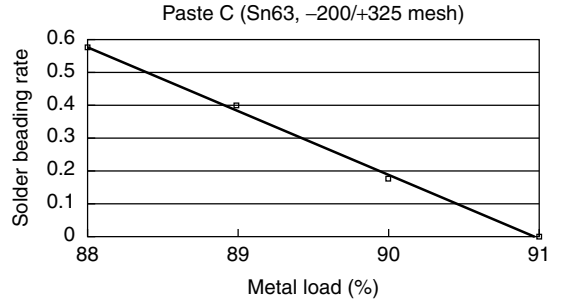

Figure 6.70 Effect of metal load on solder beading rate [43]

Table 6.1 Data for activation temperature study

Parameter	*Flux*			
	A	*B*	*C*	*D*
K	9.64×10^{-5}	4.85×10^{-5}	7.64×10^{-5}	1.00×10^{-3}
A	5.45×10^{3}	5.64×10^{3}	5.36×10^{3}	4.01×10^{3}
Corr. Coef.	0.993	0.992	0.993	9.973
Act. Temp (°C)	172	163	156	131

with a lower activation temperature will promote cold welding of solder powder during the preheat stage thus resulting in a lower solder beading rate.

Clearly the solder beading rate decreases with increasing metal load, as shown in Figure 6.70 [43]. This could be, at least partially, attributed to the cold welding mechanism. When the metal load increases, the powders are packed more densely and therefore have more opportunity to come into contact with each other. This in turn would promote the probability of cold welding. On the other hand, the metal load effect could also be explained by the viscosity factor. In general, paste viscosity increases with increasing metal load. It is reasonable to expect a paste with a higher viscosity would hold its integrity better against outgassing. Also, at a higher metal load, the source of outgassing is reduced. This could contribute to the lower beading rate as well.

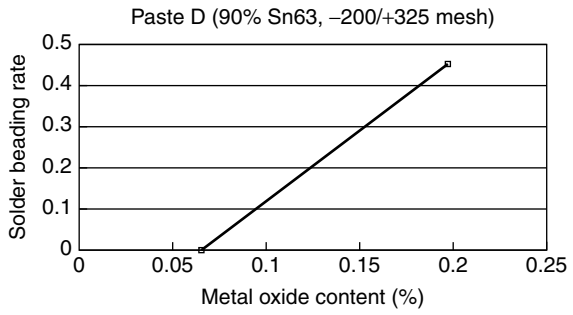

Figure 6.71 Effect of metal oxide content on solder beading rate [43]

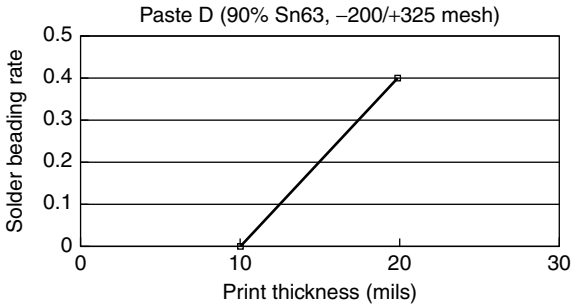

Figure 6.72 Effect of solder paste print thickness on solder beading rate [43]

Paste with higher oxide content exhibited a higher solder beading rate (see Figure 6.71). This is consistent with the cold welding model proposed by Hance *et al*. [43]. With a higher oxide content, the powders would have more barriers to overcome before they could cold weld to each other. Regarding the activation temperature, the flux would require a higher temperature to clean up higher amounts of oxide if the time allowed for fluxing is fixed. In other words, the flux would display a higher apparent activation temperature. Accordingly, a higher solder beading rate would be expected, as verified by the data.

In general, the pastes using coarser powders (−200/+325 mesh) showed lower solder beading rates than those using finer powders (−325/+500 mesh), as shown in Table 6.2 [43]. This can probably be attributed to the oxide content difference. With the same metal load (90 percent), coarser powders, due to their smaller overall

Table 6.2 Effect of solder powder size on solder beading rate [43]

Paste	*Solder beading rate*	
	−200/+325 mesh (45/75 μ)	*−325/+500 mesh (25/45 μ)*
A	2.90	3.43
B	0.60	1.20
C	0.30	0.60
D	0.01	0.03

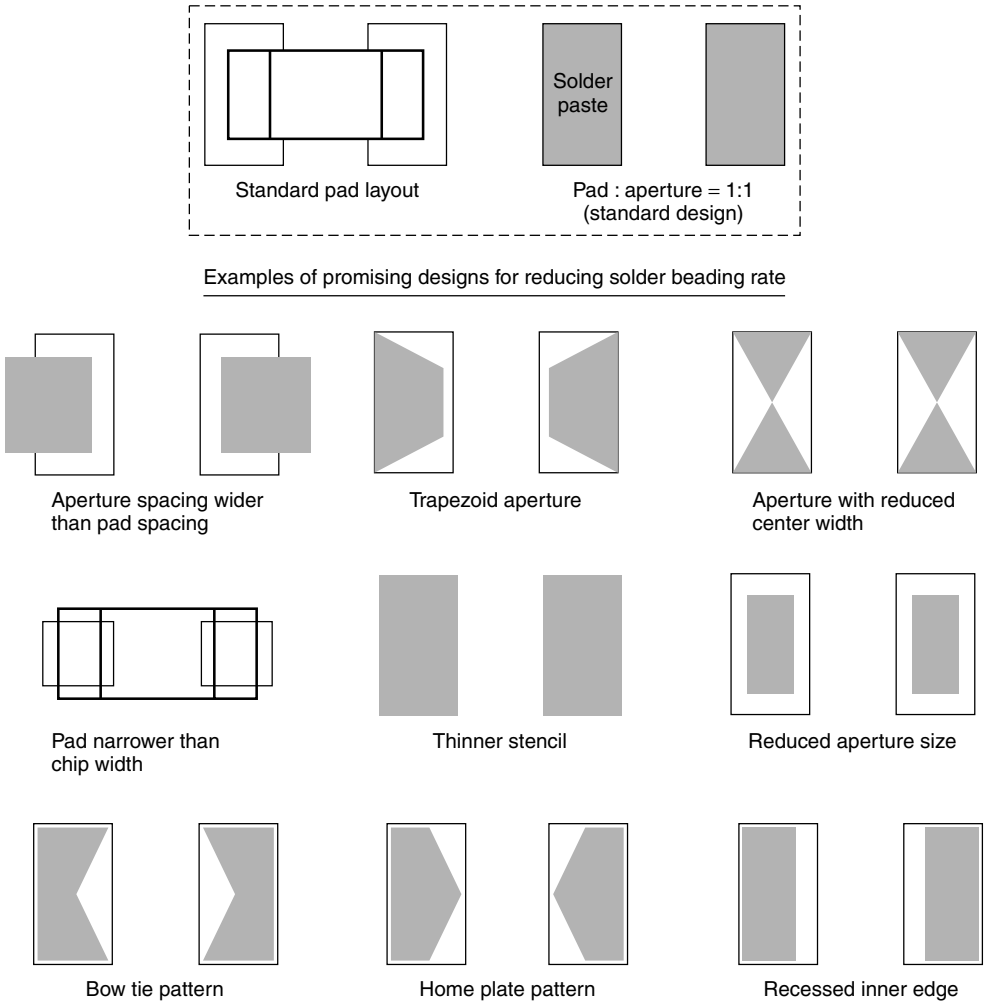
Solder paste
Standard pad layout
Pad : aperture = 1:1 (standard design)
Examples of promising designs for reducing solder beading rate
Aperture spacing wider than pad spacing
Trapezoid aperture
Aperture with reduced center width
Pad narrower than chip width
Thinner stencil
Reduced aperture size
Bow tie pattern
Home plate pattern
Recessed inner edge

Figure 6.73 Pad or stencil design can reduce solder beading rate

powder surface area, normally exhibit less oxide content than finer powders. A lower solder beading rate would then be expected for the coarser powders.

The solder beading rate increases with increasing print thickness, as shown in Figure 6.72. This may be attributed to the higher slump potential and more flux available for outgassing [43].

Perhaps the most commonly used approach for reducing the solder beading rate on assembly lines is by modifying the stencil aperture pattern. Figure 6.73 shows examples of aperture or pad designs which effectively reduce or eliminate solder beading. The guideline of aperture design is reducing the amount of solder paste to be printed underneath the low standoff components. Thus, solder beading can be corrected by changing an aperture from a large rectangle to a smaller trapezoid [46], merely using a smaller aperture [47], or employing a thinner deposit [48].

It should be noted that although all designs shown in Figure 6.73 can effectively reduce solder beading, some of those designs may involve a tradeoff. For instance, a

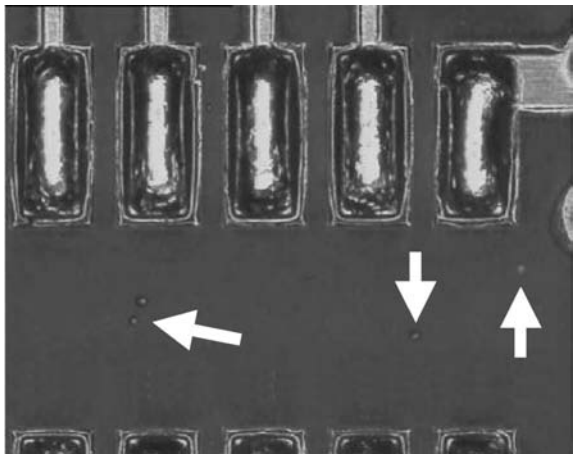

Figure 6.74 Picture of flux spattered at reflow. Note the tiny flux droplets highlighted by arrows on the solder mask (courtesy of Micron)

small pad may aggravate skewing and compromise joint strength, while an aperture spacing wider than the pad spacing may be more prone to tombstoning and solder balling. It is the author's opinion that the bow tie and home plate designs may involve the least tradeoff in overall performance.

Gervascio [49] has reported that IR preheat temperature and dwell time have the largest impact, while stencil thickness has only a minor effect. Obviously, for the assembly house, approaches including reflow technology, reflow profile, and stencil aperture/thickness design should all be employed in order to minimize the possibility of solder beading.

In summary, the solutions for solder beading can be listed as follows:

Processeswise:

Reduce stencil thickness.
Reduce aperture size.
Use aperture design which will allow less paste to be printed underneath the component.
Increase the spacing between printed paste.
Reduce pad width so that it is narrower than the component width.
Reduce preheat ramp-up rate.
Reduce preheat temperature.
Reduce component placement pressure.
Prebake components or boards before use.

Materialwise:

Use fluxes with lower activation temperatures.
Use paste with a higher metal load.
Use paste with a coarser powder.
Use paste with a low oxide solder powder.
Use paste with less slump.
Use solvents with adequate vapor pressure.

6.14 Spattering

Spattering is the spitting of flux or solder around solder joints at reflow and may reach more than several millimeters in distance. If the spattered solder landed on nearby gold fingers, it may form slight "bumps" which may create a disruption of the planar surface of gold fingers and hinder the contact with connector. The solder bumps formed are noncompliable, less electrically conductive and more prone to oxidation than a gold surface finish. In some instances, instead of solder spattering, the flux spatters and results in watermark stains or tiny flux droplets, as shown in Figure 6.74. The watermark stains have no impact on functional performance, and are often referred to as gold discoloration. On the other hand, flux droplets may raise concern on the quality of electrical contact.

Spattering can be caused by moisture pickup of the solder paste. Due to the abundant presence of hydrogen bonding, a water molecule accumulates considerable amounts of thermal energy before it eventually breaks off and vaporizes. This excessive thermal energy associated with water molecules directly contributes to the explosive vaporization action, or spattering. Moisture pickup can be aggravated by exposing the solder paste under humid conditions, or by employing solder pastes with hygroscopic fluxes. Many solder pastes tend to spatter badly when exposed to 90 percent RH for only 20 minutes. Spattering may also be caused by other volatiles with high polarity,

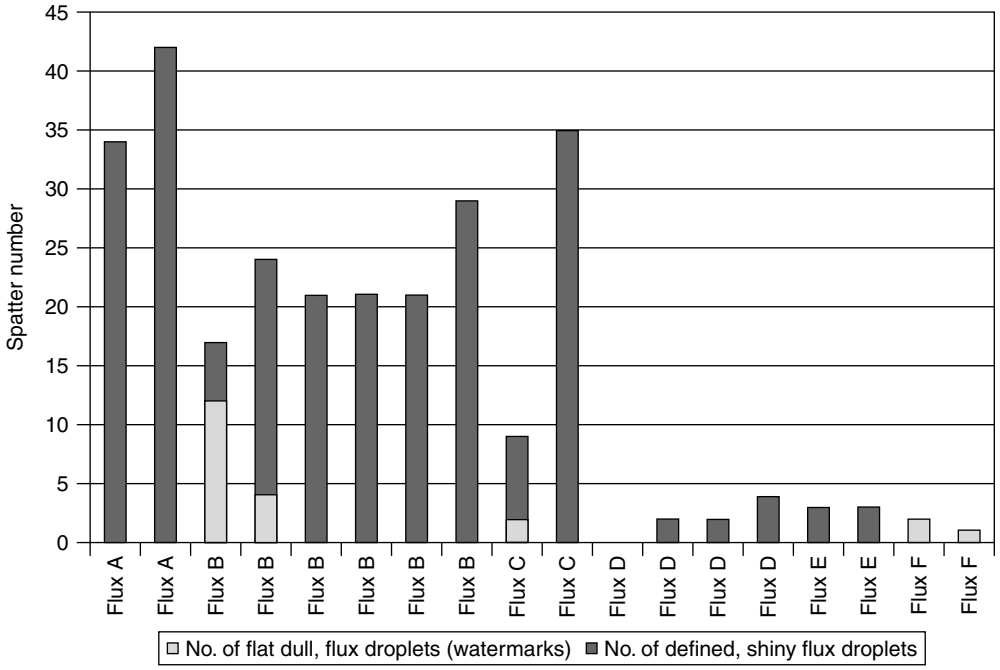

Figure 6.75 Summary of spatter results for each material on a six-up array of memory modules [50]

although cases such as this are considered rare. The spattering phenomenon is considerably more severe in the presence of solder powder, presumably due to the strong adsorption of moisture at the solder powder's surface.

Spattering may also be caused by a solder's coalescence action. At reflow, the interior of solder powder melts. Once the solder powder surface oxide is eliminated by the fluxing reaction, the millions of tiny solder droplets will coalesce and form one integral solder piece. The faster the fluxing reaction rate, the stronger the coalescence driving force, and accordingly the more severe the spattering to be expected.

The effect of fluxing reaction rate, or wetting speed, on flux spattering was studied by Berntson *et al*. [50]. Six solder pastes with varying wetting speeds, solvent contents, reflow atmospheres, and solvent volatilities were examined at a memory module manufacturer's site, as shown in Table 6.3. The flux spattering results are given in Figure 6.75, with defect types categorized as (1) flat, dull flux droplets (watermarks), and (2) defined, shiny flux droplets. Fluxes D–F showed a considerably lower spattering rate than fluxes A–C. By reviewing the parameters involved, wetting speed appears to be the most crucial factor in flux spattering, with a slower wetting speed favoring a lower spattering rate, as mentioned above.

Spattering can be minimized with a drying process, as shown in Table 6.4 [50]. In general, spattering decreases with either increasing drying time or increasing drying temperature. The positive effect of drying on spattering could be attributed to the following reasons: (1) the moisture pickup is dried out, (2) more oxide buildup during drying, thus slowing down the coalescence process, (3) the flux is becoming more viscous due to loss of volatiles, therefore reacting more slowly with solder oxide, and (4) the solder powder coalesces more slowly due to a more viscous flux medium.

Information from the drying study can be used to design a reflow profile for minimizing spattering. A linear ramp profile shown in Figure 6.76 with no plateau soak zone,

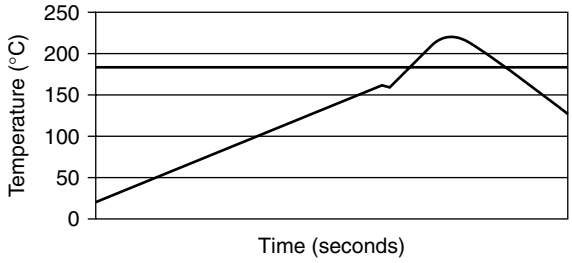

Figure 6.76 Example of linear ramp profile [50]

Table 6.4 Effect of drying on flux spattering with solder paste B at 90 percent, Sn63Pb37 alloy [50]

Drying temperature (°C)	*1 minute*	*2 minutes*	*3 minutes*	*4 minutes*
150	Flux spatter observed	1–2 spatters	No spatter	No spatter
160	1–2 spatters	No spatter	No spatter	No spatter
170	No spatter	No spatter	No spatter	No spatter

although favored for overall minimal reflow defect rate purposes [25], resulted in some spattering for all materials and increased spattering for the base-line production material. To reduce spattering performance, a profile with additional drying will be required, as discussed above.

A more promising basic profile shape included a high temperature soaking zone (dry-out) at 160°C to evaporate all solvents, as demonstrated by Figure 6.77. This soaking zone serves as a drying step, and effectively minimizes spattering. However, the potential problems with such a dry-out are poor wetting and voiding [25].

In summary, the solutions for minimizing spattering are:

Table 6.3 Solder paste materials tested [50]

Flux type used in solder paste	*Description*	*Relative wetting speed*	*Solvent content*	*Reflow atm.*	*Solvent volatility*
A	Current production material at memory module manufacturer. It is a moderate residue RMA based material	Unknown	Moderate	Prefer inert	High
B	Advanced, high performance, long stencil life, moderate residue material	Fast	Moderate	Air or inert	Low
C	Advanced, high performance, long stencil life, moderate residue material	Fast	Moderate	Air or inert	Low
D	High performance, RMA type, long stencil life, moderate residue material	Slow	Moderate	Air or inert	Low
E	Low residue, high solvent content air or nitrogen reflow material (inert atmosphere preferred)	Slow	High	Prefer inert	Moderate
F	Extremely low residue, inert reflow material	Slow	High	inert	Moderate

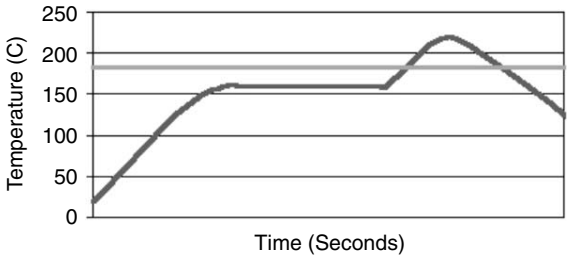

Figure 6.77 Example of high temperature soak profile [50]

Processwise:

Avoid paste processing in a humid environment.
Use a predry step.
Use a profile with long soaking time and/or high soaking temperature.
Use an air reflow atmosphere.

Materialwise:

Use a flux with minimum hygroscopic ingredients.
Use a flux with a slow wetting speed.

6.15 Conclusion

Problems during the SMT reflow process often require rework to correct them. With all the parts already soldered onto the PCB, the rework process itself may compromise the reliability of products, not to mention the increase in costs of manufacturing. Although the problems can be corrected from all three aspects, including materials, designs, and processes, the most frequently used approaches appears to be designs and processes, due to the relatively short turnaround time for change implementation.

References

1. C. Lea, *A Scientific Guide to Surface Mount Technology*, Electrochemical Publications, Isle of Man, UK (1988).
2. J. A. DeVore, ''To Solder Easily: the Mechanisms of Solderability and Solderability-related Failures'', *Circuits Manufacturing*, pp. 62–70 (June 1984).
3. R. J. Klein Wassink and E. E. de Kluizenaar, ''Dewetting of Molten Solder from Copper'', in *Proc. of Deutscher Verlag fur Schweisstechnik Conference on Soldering and Welding in Electronics and Precision Mechanics*, Munich, Germany, Vol. DVS-71, pp. 16–21 (1981).
4. A. W. Adamson, *''Physical Chemistry of Surfaces''*, 3rd edn., John Wiley, New York 1976.
5. G. Humpston and D. M. Jacobson, *Principles of Soldering and Brazing*, ASM International, Materials Park, OH (1993).
6. R. A. Bulwith and C. A. MacKay, ''Silver Scavenging Inhibition of Some Silver-Loaded Solders'', *Welding Journal Research Supplement* (1985).
7. S. F. Dirnfeld and J. J. Ramon, ''Microstructure Investigation of Copper–tin Intermetallics and the Influence of Layer Thickness on Shear Strength'', *Welding Research Supplement*, pp. 373s–377s (October, 1990).
8. P. E. Davis, M. E. Warwick, and P. J. Kay, ''Intermetallic Compound Growth And Solderability'', *Plating & Surface Finishing*, Vol. 69, pp. 72–76 (September, 1982).
9. H. A. H. Steen, ''Aging of Component Leads and Printed Circuit Boards'', Research Report IM-1716, Swedish Institute for Metals Research (1982).
10. Kh. G. Schmitt-Thomas, ''Status and Trends of Soft Soldering Techniques in Research, Development and Industrial Applications'', *Proceedings Deutscher Verlag fur Schweisstechnik Conference on ''Soft Soldering in Research and Practice''*, Munich, Vol. DVS-82, pp. 1–12 (1983).
11. Anon, ''Copper–tin Intermetallics'', *Curcits Manufacturing*, Vol. 20, No. 9, pp. 56–64 (1980).
12. B. G. Le Fevre and R. A. Barczykowski, ''Intermetallic Compound Growth on Tin and Solder Platings on Cu Alloys'', *Wire Journal International*, Vol. 18, No. 1, pp. 66–71 (1985).
13. P. J. Kay and C. A. MacKay, ''Barrier Layers Against Diffusion, Paper 4'', *in Proc. of 3rd Brazing Soldering Conf.*, London (1979).
14. P. J. Kay and C. A. MacKay, ''The Growth of Intermetallic Compounds on Common Basis Materials Coated with Tin and Tin–lead Alloys'', *Transactions of the Institute of Metal Finishing*, Vol. 54, pp. 68–74 (1976).
15. Technical Forum: ''Soft Soldering Gold Coated Surfaces'', *Focus on Tin*, No. 2.
16. J. Glazer, P. A. Kramer and J. W. Morris, Jr, ''Effect of Au on the Reliability of Fine Pitch Surface Mount Solder Joints'', *Journal of SMT*, pp. 15–26 (October, 1991).
17. D. T. Novick and A. R. Kroehs, ''Gold Scavenging Characteristics of Bonding Alloys'', *Solid State Technology*, pp. 43–47 (June 1974).
18. S. J. Muckett, M. E. Warwick and P. E. Davis, ''Thermal Aging Effects between Thick-Film Metallizations and Reflowed Solder Creams'', *Plating & Surface Finishing*, Vol. 73, pp. 44–50 (January, 1986).
19. G. Humpston and D. M. Jacobson, *Principles of Soldering and Brazing*, ASM International, Materials Park, OH (1993).
20. D. R. Frear, W. B. Jones and K. R. Kingsman, ''Solder Mechanics, A state of the Art Assessment'', The Minerals, Metals and Materials Society, Warrendale, PA (1991).
21. Technical Forum: ''Soft Soldering Gold Coated Surfaces'', *Focus on Tin*, No. 2.
22. N. -C. Lee and G. P. Evans, ''Solder Paste – Meeting the SMT Challenge'', *SITE Magazine* (June 1987).
23. R. J. Klein Wassink and J. A. H. van Gerven, ''Displacement of Components and Solder during Reflow Soldering'', *Soldering & Surface Mount Technology*, pp. 5–10 (February, 1989).
24. Senju Metal Industry Co, Ltd. of Tokyo, Japan with US6050480 (Solder paste for chip components) and JP10146690A2 (Solder paste for soldering chip part).
25. N. C. Lee, ''Optimizing Reflow Profile via Defect Mechanisms Analysis'', IPC Printed Circuits Expo '98.
26. R. A. Deighan, III, ''Surface Tension of Solder Alloys'', *ISHM*, Vol. 5, No. 2, pp. 307–313 (November 1982).
27. R. B. Bernston, D. W. Sbiroli and J. J. Anweiler, ''Minimizing solder spatter impact'' *Surface Mount Technology*, pp. 51–58 (April 2000).
28. J. S. Hwang, *Solder Paste in Electronics Packaging*, Van Nostrand Reinhold, New York (1989).
29. Teo Kiat Choon and D. J. Williams, ''Insufficient Solder and Solder Bridges: an Experimental Study of the Interrelations between Assembly Process Faults'', *Journal of Electronics Manufacturing*, Vol. 6, No. 2, pp. 93–9 (June 1996).
30. T. K. Choon, ''The Origin and Prevention of Post Reflow Defects in Surface Mount Assembly'', *Journal of Electronics Manufacturing*, Vol. 6, No. 1, pp. 1–12 (March 1996).
31. G. Erdmann, ''Improved Solder Paste Stenciling Technique'', *Circuits Assembly*, pp. 66–73 (February, 1991).
32. B. L. Roos-Kozel, ''Parameters Affecting the Incidence of Pad Bridging in Surface Mounted Device Attachment'', *ISHM*, Vol. 6(1), pp. 251–255 (October 1983).
33. W. B. Hance and N.-C. Lee, ''Voiding Mechanisms in SMT'', China Lake's 17th Annual Electronics Manufacturing Seminar, China Lake, CA (2–4 February 1993).
34. T. A. Krinke and D. K. Pai, ''Factors Affecting Thermal Fatigue Life of LCCC Solder Joints'', *Welding Journal*, pp. 33–40 (October 1988).
35. D. J. Xie, Y. C. Chan and J. K. L. Lai, ''An Experimental Approach to Pore-free Reflow Soldering'', *IEEE Transactions on Components, Packaging and Manufacturing Technology, Part B: Advanced Packaging*, Vol. 19, No. 1, pp. 148–53 (February 1996).

36. D. J. Xie, Y. C. Chan, J. K. L. Lai and I. K. Hui, ''Fatigue Life Studies on Defect-free Solder Joints Fabricated from Modified Reflow Soldering'', *IEEE Transactions on Components, Packaging and Manufacturing Technology,* Part B: *Advanced Packaging*, Vol. 19, No. 3, pp. 679–84 (August 1996).
37. Y. C. Chan, D. J. Xie and J. K. L. Lai, ''Characteristics of Porosity in Solder Pastes during Infrared Reflow Soldering'', *Journal of Materials Science*, Vol. 30, No. 21, pp. 5543–50 (November 1995).
38. P. L. Tu and Y. C. Chan, ''Optimization of Reflow Soldering Process For The Surface Mounted Assembly'', in *Proc. of The Third International Symposium of Electronic Packaging Technology*, pp. 214–218, 17–21 August 1998, Beijing, China.
39. J. K. L. Lai and I. K. Hui, ''Fatigue Life Studies on Defect-free Solder Joints Fabricated from Modified Reflow Soldering'', *IEEE Transactions on Components, Packaging and Manufacturing Technology,* Part B: *Advanced Packaging*, Vol. 19, No. 3, pp. 679–684 (August 1996).
40. J. Barrett, C. O. Mathuna and R. Doyle, ''Case Studies in Quality and Reliability Analysis of Fine Pitch Solder Joints'', *Soldering & Surface Mount Technology*, No. 13, pp. 4–11 (February 1993).
41. A. Wakigawa, ''Advanced Super Fine Pitch Technology'', *Proceedings of GlobalTronics'94*, Singapore (September 1994).
42. M. Xiao, K. J. Lawless and N. C. Lee, ''Prospects of Solder Paste Applications in Ultra-fine Pitch Era'', *Surface Mount International*, San Jose, CA, August 1993.
43. W. B. Hance, P. A. Jaeger and N.-C. Lee, ''Solder Beading in SMT–Cause and Cure'', *Proc. of Surface Mount International*, San Jose, CA (1990).
44. K. Brown, B. Freitag and S. Jopek,''Inert Soldering of Discrete Components'', *Circuits Assembly*, pp. 50–53 (June 1993).
45. J. Poole, C. Fieselman and R. Noreika, ''Movement of Solder Balls on No-clean Assemblies'', in *Proc. of Surface Mount International*, San Jose, CA, pp. 453–457 (September 1997).
46. S. Gutierrez, R. Komm, C. Tulkoff and G. Rupp, ''Making a Transition from Solvents to Water to no-clean: a roadmap for Success'', in *Proc. of Surface Mount International*, San Jose, CA, pp. 621–625 (29 August–2 September 1993).
47. R. L. Wade, ''No Clean Soldering of Electronic Assemblies'', in *Proc. of Nepcon West,* Anaheim, CA, pp. 574–583 (7–11 February 1993).
48. M. M. F. Verguld and M. C. Seegers, ''Solderballing: Just A Matter of The Right Reflow Environment???'', in *Proc. of Nepcon West*, Anaheim, CA, pp. 980–994 (7–11 February 1993).
49. T. Gervascio, ''Solder Beads: How To Make Them A Vanishing Act'', in *Proc. of Nepcon West*, Anaheim, CA, pp. 1083–1089 (7–11 February 1993).

7 SMT Problems At the Post-reflow Stage

This chapter covers the major problems related to solder paste applications in the SMT post-reflow stage, with a primary emphasis on the impact of flux residue on reliability as well as on subsequent manufacturing operations.

7.1 White residue

White residues are flux residues remaining on the boards after post-soldering cleaning. Here the cleaners used may be aqueous or organic solvent systems. In general, although white residues may also appear to be yellow, gray, or brown, most of them appear as a whitish film or solid tiny organic granules on or around solder joints, as shown in Figure 7.1. In some instances, the white residue may be present as a whitish film on the solder mask around the solder joints, particularly for the region between neighboring fine-pitch QFP solder joints.

The composition of the white residues is fairly complicated. It may be flux itself, or charred flux ingredients, or reaction products of flux with metals, cleaners, board laminates, or solder masks. Lea [1] has summarized the composition of white residues as (1) polymerized rosin, (2) oxidized rosin, (3) hydrolyzed rosin, (4) laminate/flux interaction, (5) solder/activator interaction, (6) metal abietate, (7) solder/solvent interaction, (8) laminate halide/flux interaction, (9) rheological additive, and (10) aqueous cleaning.

One of the reasons for the appearance of the white color for the insoluble flux residue is the "light scattering" effect. Prior to cleaning, the flux residues generally appear as clear or translucent solids. During cleaning, the cleaner may extract and remove only some soluble ingredients of the residue, and may leave behind the insoluble part as a foamy, loose texture. The light scattered from the foamy loose structure often results in a whitish appearance.

Depending on the nature of the white residues, the solutions for eliminating them may also vary. Materialwise, enhancing the thermal and oxidation stability of fluxes will reduce polymerization, charring, and oxidation of flux ingredients, including rosins, resins, activators, and rheological additives. Selecting flux chemistries which do not form insoluble metal salts, such as lead chloride or lead bromide, or employing flux chemistries which promote dissolution of the metal salts into either the flux medium or solvents could eliminate metal salts as a factor in white residues. The chemistry of the laminate or the solder mask should also be selected or cured properly to avoid a chemical reaction with fluxes.

Selecting an adequate cleaner may be the quickest solution for eliminating white residues. The solvency of the cleaner should match that of the flux residues. The flux residue typically comprises multiple ingredients varying widely in polarity. If the cleaner chosen shows a proper solvency for most of the ingredients, all the residues may be completely removed, with the minor insoluble parts being "carried away" by the majority of soluble parts. However, if the cleaner chosen is only adequate for a small portion of the residue ingredients, the "carried away" effect would not be sufficient to result in a total removal of residues.

This "carried away" effect explains why the cleanability of a residue may alter for the same cleaner. A flux residue, originally cleanable with cleaner A, may become uncleanable for the same cleaner if the flux residue has been precleaned with a poorer cleaner B. The "precleaning action" of cleaner B may have extracted some of the soluble parts, and leave only an insignificant number of soluble parts for the better cleaner A. This results in a reduced "carried away" effect for the insoluble parts and consequently the white residue. Thus, it is very crucial to conduct cleaning with the proper cleaner, since any residue left will be more difficult to remove by another cleaner due to a reduced "carried away" effect. Continuous use of a dirty cleaner often results in a white residue, mainly due to the gradually reducing solvency of the cleaner, thus diminishing the "carried away" effect.

The cleaner should not react with the flux residue and form non-soluble reaction products. However, it should be noted that certain reaction between the cleaner, such as saponifiers, and flux actually augments the solubility of flux residue and accordingly improves the cleanability of flux residue. As discussed in Section 3.2.1, the saponification reaction converts the hydrophobic rosin $C_{19}H_{29}COOH$, which is insoluble in water, into water-soluble rosin soap $CH_{19}H_{29}COOCH_2CH_2NH_2$, as shown below:

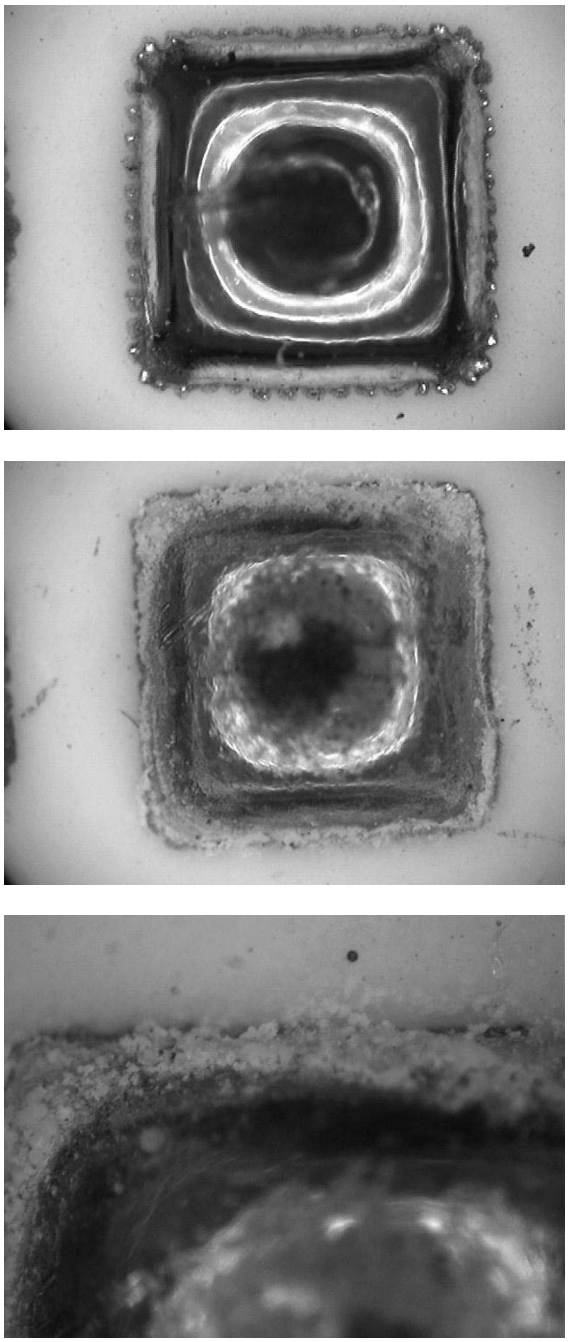

Figure 7.1 63Sn/37Pb solder bumps: (1) clean solder bump (*top*), (2) solder bump with white residue (*center*), and (3) solder bump close-up with white residue (*bottom*)

$$C_{19}H_{29}COOH + HOCH_2CH_2NH_2 \rightarrow CH_{19}H_{29}COOCH_2 \times CH_2NH_2 + H_2O$$

rosin — ethanolamine (saponifier) — water-soluble rosin soap

Enhancing mechanical agitation such as applying ultrasonic agitation or employing a higher spray pressure is also very effective. A higher cleaning temperature often provides a better cleaning efficiency, mainly via a greater extent of residue softening as well as a better solvency of cleaners at elevated temperatures.

The effect of cleaning temperature on cleaning efficiency may be more complicated than the situations described above. In some instances, a higher cleaning temperature may decrease cleaning efficiency, and result in more residues. For example, the fluxes usually react with SnO_2 to form metal salts during the soldering process. Some types of those metal salts may hydrolyze to form insoluble $Sn(OH)_4$ during the hot water cleaning process, and eventually form white residues. Inclusion of other residues such as dusts of oxides may convert the white residue to black residue. Under cold water, those metal salts dissolve and form no residue. This adverse effect of an elevated cleaning temperature on cleaning efficiency has also been observed in other soldering processes, such as soldering with preforms. Figure 7.2 shows some black flux residue after aqueous cleaning for a process using a water-soluble liquid flux in conjunction with a stamped 95Sn/5Ag preform. In the presence of excessive oxide on the surface of preforms, black spots were observed when manually cleaned with water with the water temperature around 77 °C. When the assembly was cleaned with water at room temperature the black spots were not observed.

White residue may also be eliminated by reducing the heat input at reflow. A reduced heat input, through either a reduced temperature or heating time, would reduce the oxidation and cross-linking of flux residues, and consequently a better cleanability of the residue. Use of an inert reflow atmosphere also helps in reducing the oxidation and decreases the white residue.

In summary, white residues can be eliminated by employing the following solutions:

Use of fluxes with thermally stable ingredients.
Use of fluxes with oxidatively stable ingredients.
Use of fluxes which do not form insoluble metal salts.

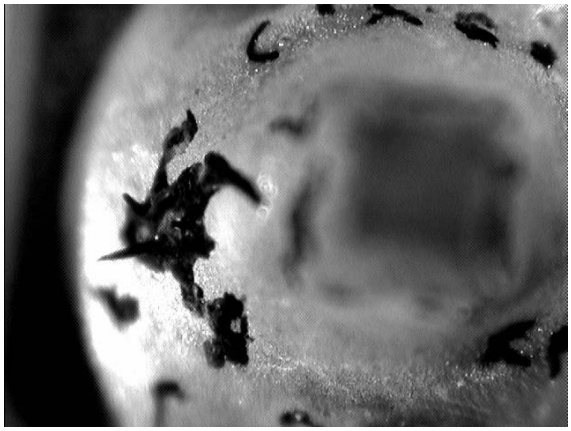

Figure 7.2 Black residue after aqueous cleaning at 77 °C for a process using water-soluble liquid flux in conjunction with a stamped 95Sn/5Ag preform. The residue disappears if cleaning at room temperature

Use of PCBs with properly cured solder masks and laminates.
Use of cleaners with proper solvency toward the flux residues.
Use of a lower reflow temperature.
Use of a shorter reflow time.
Use of mechanical agitation during cleaning.
Employing a proper cleaning temperature.

7.2 Charred residue

Charred residues are caused by overheating, and may or may not be cleanable. Since charring involves excessive heating and oxidation, the thinner the flux film, the worse the charring will be. Figure 7.3 shows a cleaned solder bump with charred residue. The uncleanable charred residue distributed around the perimeter of the flux also spreads on top of the solder bump. The flux film at both locations is thinner than on other areas, thus is more prone to oxidation and charring.

The composition of charred residue is oxidized ingredients, and can be regarded as a special type of white residue. Solutions for elimination of charred residues should address the two causes: heat, and oxygen, and can be listed as below.

Use of fluxes with thermally stable ingredients.
Use of fluxes with oxidatively stable ingredients.
Use of a lower reflow temperature.
Use of a shorter reflow time.
Use of an inert reflow atmosphere.

If the residue is to be cleaned after reflow, then the following three solutions would help to ease the symptom of charred residue:

Use of cleaners with proper solvency toward the flux residues.

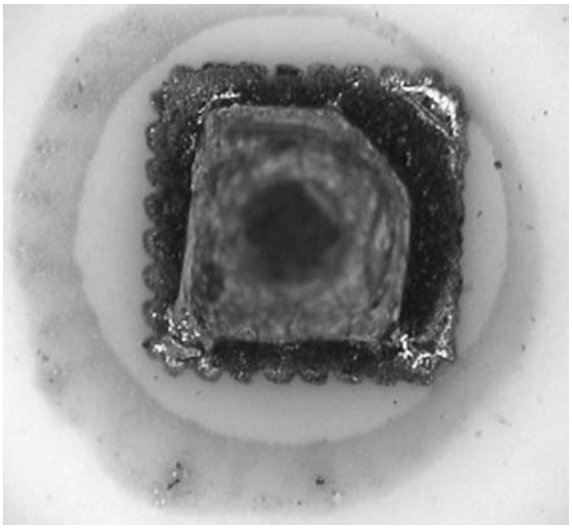

Figure 7.3 Charred residue around a 63Sn/37Pb solder bump after solvent cleaning

Use of mechanical agitation during cleaning.
Employing a proper cleaning temperature.

7.3 Poor probing contact

Poor probing contact is the lack of electrical contact when conducting an in-circuit test, because of the presence of flux residue between the test probe and test pads or solder joints. Due to ozone depletion and environmental concerns as well as cost saving considerations, the no-clean process is rapidly becoming the assembly main stream of the SMT industry. Obviously, abandoning the cleaning process eliminates not only pollution due to the use of the cleaner, but also the whole cleaning step and the costs associated with it. In addition, there is a parallel trend of phasing out the wave soldering process with reflow soldering alone in order to further enhance the benefit of the no-clean process. Interestingly, the major challenge for the industry is not soldering performance or product reliability, but the in-circuit testability issue. With the flux residue remaining on the PCBs, the test probe either cannot penetrate the residue at all or is gummed up quickly by the residue and eventually fails to establish electrical contact. This is particularly true when the test site is the lead tip or pin tip of through-hole components. Apparently, the nature of the flux residue plays a vital role in this issue.

Xiao *et al.* [2] studied the probe testability of a variety of no-clean solder pastes in order to identify the flux parameters which govern the success of testability. Factors examined include flux residue amount, flux residue top-side spread, flux residue hardness, flux rosin content, flux residue bottom-side spread, metal content, and reflow atmosphere. In their study, the probe testability was represented by probeability and penetrability. The probeability (Pr) of the flux residue on PCBs is determined for three types of probing site with the following probing condition (see Table 7.1). A micro-ohm meter is used to determine whether an electrical contact (resistance less than 0.1 ohm) has been established during the probing. Two types of test probe are used: crown probe and spear probe.

7.3.1 Flux residue content

By plotting the solder paste residue content against probeability (Pr) and penetrability (Pe), it is found that the

Table 7.1 Test conditions and definitions for probeability and penetrability study [2]

Test site	*Probe type*	*Probing pressure*	*Probeability or penetrability*
PGA pin-tip	Crown	2–3 g	Percentage of successful electrical contact
Pad	Crown	17 g	Percentage of successful electrical contact
Via	Spear	17, 112, and 190 g	Reciprocal of product of (time taken to establish electrical contact) and (pressure)

Pr value for pads decreases with increasing amounts of residue for air reflowed systems, as shown in Figure 7.4. Obviously, the more flux residue left on the pad, the more likely the test probe will fail to establish an electrical contact. However, a similar trend cannot be assessed for pin-tip *Pr* and via *Pe*. This suggests that properties other than the amount of solder paste residue can override the amount of residue and govern probe testability. Possible properties may include flux residue top-side spread, flux residue bottom-side spread, and flux residue hardness.

7.3.2 Top-side flux spread

Since the further the flux residue spreads, the less flux residue will remain on the pad, it is reasonable to predict that the pad *Pr* will increase with increasing flux spread. However, conversely to what would be expected, the top-side flux spread is found to be inversely proportional to the pad *Pr*, as shown in Figure 7.5 [2]. Perhaps this abnormal behavior can be rationalized with the use of the residue amount factor again. Presumably, a high residue amount of paste is responsible for not only a wide spread in the flux, but also a thick residue deposit on the pads, which in turn results in a lower pad *Pr* value.

7.3.3 Bottom-side flux spread

The bottom-side flux spread turned out to be a very interesting property. Although no trend can be discerned between this and pad *Pr* or via *Pe*, there is indeed a strong relation between it and the pin-tip *Pr*, as demonstrated

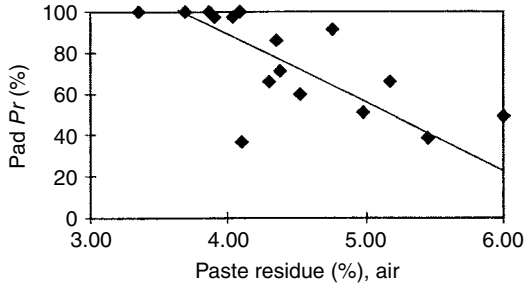

Figure 7.4 Effect of paste residue on pad probeability for air reflowed systems [2]

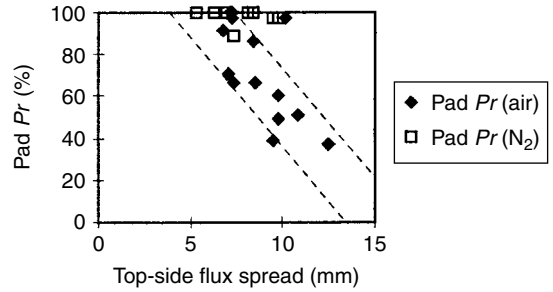

Figure 7.5 Relation between top-side flux spread and pad probeability [2]

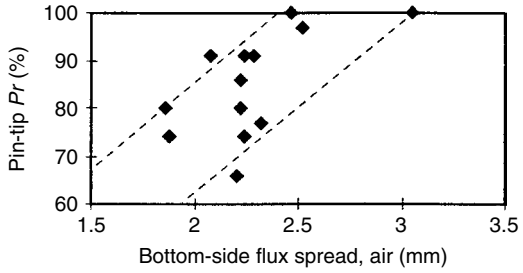

Figure 7.6 Effect of bottom-side flux spread on the pin-tip *Pr* for air reflowed system [2]

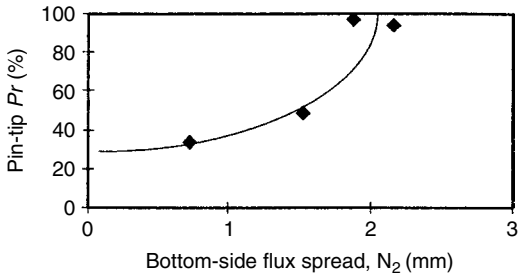

Figure 7.7 Effect of bottom-side flux spread on pin-tip *Pr* for nitrogen reflowed system [2]

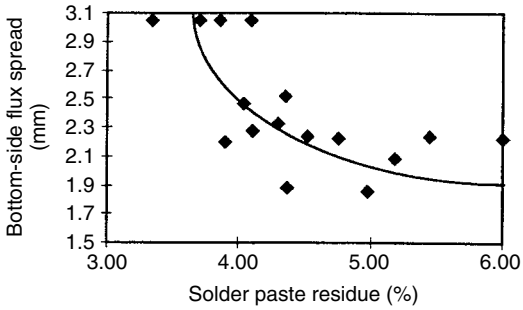

Figure 7.8 Relation between solder paste residue amount (air reflowed) and bottom-side flux spread [2]

by Figure 7.6 for an air reflowed system and Figure 7.7 for a nitrogen reflowed system. In both cases, the pin-tip *Pr* value increases with increasing bottom-side flux spread, which in turn increases with decreasing solder paste residue, as shown in Figure 7.8. The rationale for this lies in the "dripping mechanism". Generally, a paste residue sample will have a low solid content and accordingly a low hot flux viscosity during soldering. This low hot flux viscosity would allow the flux to drip out of the solder paste in the through-hole and spread easily around the bottom-side. The farther the flux spread on the bottom-side, the less flux will accumulate at the pin-tip, and consequently the easier for the test probe to penetrate.

7.3.4 Residue hardness

A soft residue is easier for the probe to penetrate, therefore it should allow a higher *Pr* value. Figure 7.9 [2] illustrates

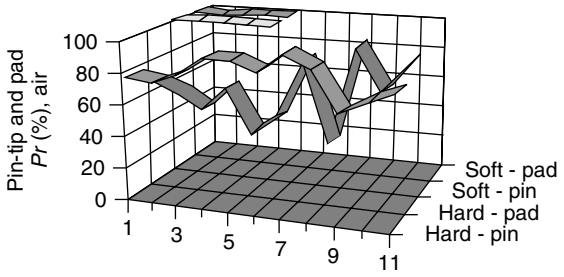

Figure 7.9 Effect of residue hardness on the pin-tip and pad *Pr* value for air reflowed system [2]

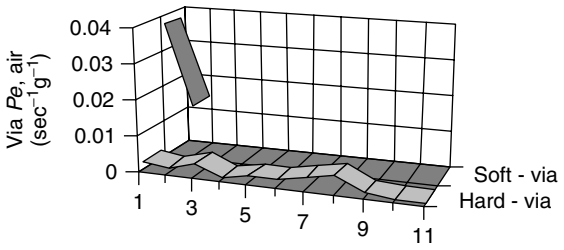

Figure 7.10 Effect of residue hardness on the via *Pe* value for air reflowed system [2]

the effect of flux residue hardness on the pin-tip and pad *Pr* value for air reflowed systems. Clearly, the soft residue systems exhibit a much higher *Pr* value than the hard residue ones. A similar relation also applies to the via *Pe* value, as demonstrated by Figure 7.10 [2].

7.3.5 Reflow atmosphere

A reflow atmosphere can also affect the probing success rate. An inert atmosphere usually produces not only a lower volume of residue, but also a residue with less oxidation and crosslinking which can be penetrated more easily. Figure 7.11 [2] compares the atmosphere effect by examining the *Pr* ratio of nitrogen reflowed systems versus air reflowed systems. A *Pr* ratio greater than one represents a better probing success rate for inert atmosphere

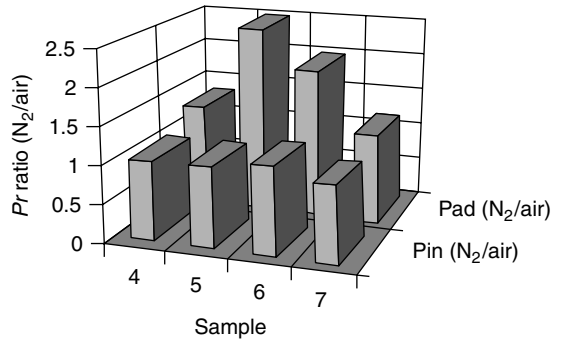

Figure 7.11 Effect of reflow atmosphere on the *Pr* value for pin and pad testing [2]

systems. In the case of pin-tip probing, the success rate for both atmospheres is very high, hence the ratio is only slightly greater than one. In the case of pad probing, the difference becomes much more significant and the ratio is considerably greater than one.

7.3.6 Metal content

Since flux spread plays a vital role in probe testing, it is important to be able to regulate its extent. Besides the flux type discussed above, metal load is also a convenient tool. A solder paste with a higher metal content is expected to have less flux spread. This is shown by the data in Figure 7.12 [2].

7.3.7 Soft-residue versus low-residue

For probe testing, a flux with no residue would be ideal. However, with current flux technology, this is not deliverable for solder paste. The next best option becomes not so obvious. When an inert reflow atmosphere is used, a solder paste with an extremely low paste residue, for instance 0.4 percent, is now available. In Xiao *et al.* [2], the low-residue-no-clean samples all exhibit very promising testability, particularly on the pad probeability. Figure 7.13 [2] shows that all low-residue-no-clean solder pastes displayed a pad *Pr* value of 100 percent while the soft-residue solder pastes also exhibited a pad *Pr* value nearly as good. As to pin-tip probeability, the performance of low-residue-no-clean solder pastes

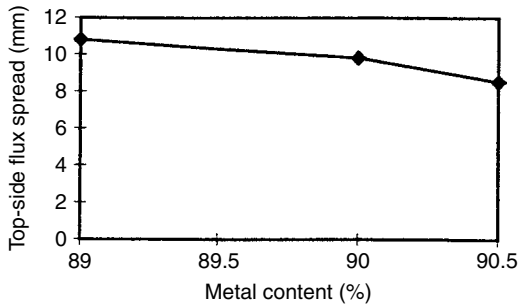

Figure 7.12 Effect of metal content on top-side flux spread [2]

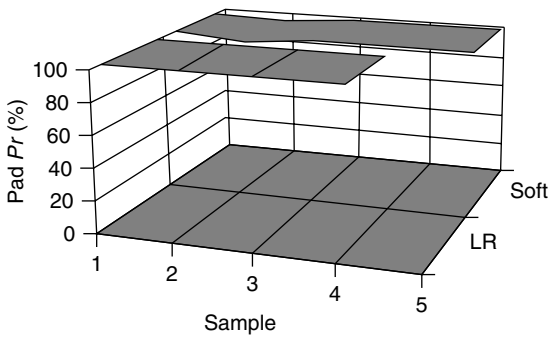

Figure 7.13 Soft residue versus low residue on the pad *Pr* value [2]

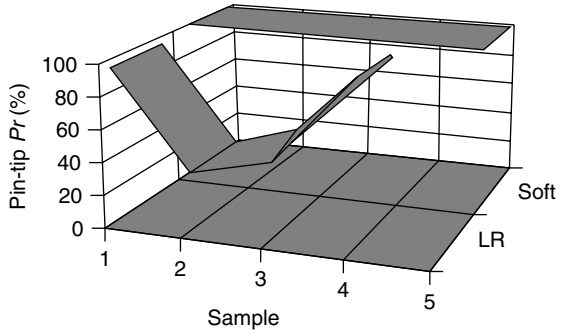

Figure 7.14 Soft residue versus low residue on the pin-tip *Pr* value [2]

may be either good or poor, and is formulation dependent, as demonstrated by Figure 7.14 [2]. On the other hand, the soft-residue solder pastes still performed very well, regardless of their chemistry. The via penetrability appears to be more challenging. Neither low-residue-no-clean nor soft-residue pastes performed consistently well across the various samples. This suggests that design engineers should try to avoid using the via without a through-hole component's lead soldered onto it at the test site when this via is filled with solder from the no-clean reflow process. Overall, the soft-residue solder pastes show a more satisfactory probe testability than the low-residue-no-clean solder pastes. This is especially true when the pin-tip is the test site.

7.3.8 Soft-residue versus RMA residue

When air reflow is the process condition, the use of solder pastes with considerable amount of flux residue is inevitable. Under this condition, soft but nonsticky residue appears to be the only option. Figure 7.15 [2] compares the conventional RMA solder pastes with soft-residue solder pastes on the pad probeability. The soft-residue systems display a superior advantage over the RMA systems on performance. A similar phenomenon is also observed for pin-tip probeability, as shown by Figure 7.16 [2]. As to the via's penetrability, soft-residue systems are still better than RMA systems, as shown in Figure 7.17 [2]. For all three types of probe testing, the success rate for

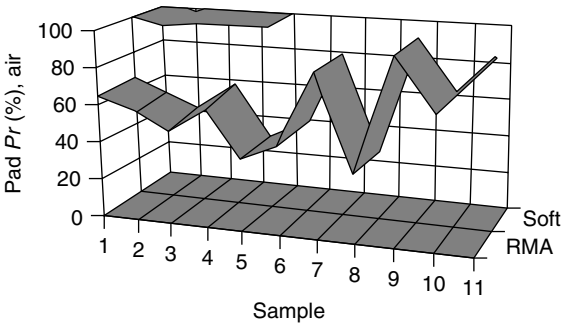

Figure 7.15 Soft-residue versus RMA solder pastes on pad probeability for air reflowed systems [2]

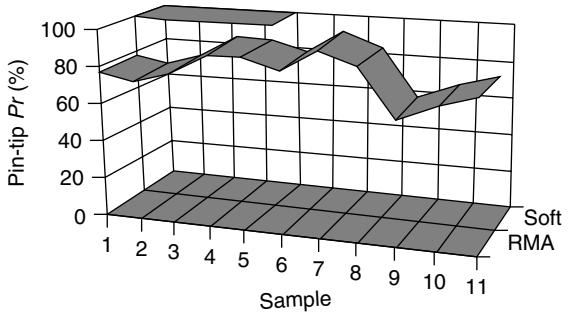

Figure 7.16 Soft-residue versus RMA solder pastes on pin-tip probeability for air reflowed systems [2]

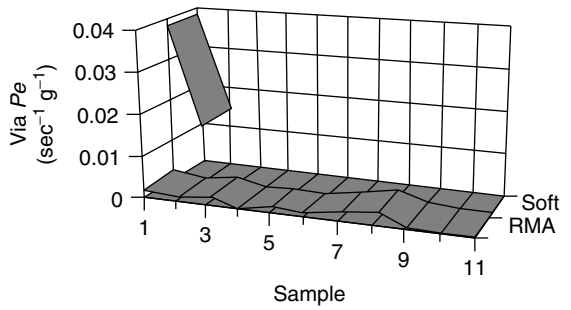

Figure 7.17 Soft-residue versus RMA solder pastes on via penetrability for air reflowed systems [2]

RMA systems is very low and is obviously unacceptable. In contrast, the low-residue systems again demonstrate a superior probe-testability for all conditions. Since the soft-residue systems allow the use of a full residue approach for paste formulation purposes, nitrogen is not required in the use of these soft-residue pastes. The combination of good probe testability with air reflow capability accordingly shows the soft-residue approach as the most promising system for no-clean probe-testing purposes.

7.3.9 Multiple cycles probing testability

The potential of soft-residue solder paste is demonstrated by a multiple cycles probing test using a crown probe. A soft-residue sample is tested against a typical RMA solder paste. The test condition is exacerbated by applying excessive amounts of sample volume. The flux residue of RMA pastes is chiseled away upon probing. Within two hundred cycles, the probe is gummed up by the residue of RMA flux, as shown in Figure 7.18 [2]. However, for the soft-residue sample, the residue opens up upon probing, then self-seals afterwards. The probe remains very clean even after 3200 cycles, as shown in Figure 7.19 [2].

Further tests indicate that the crown probe can last 60 000 cycles without picking up flux residues as well as having no contact problem when tested on the pads that have been soldered with soft-residue solder pastes. This strongly demonstrates the practicality of the soft-residue approach.

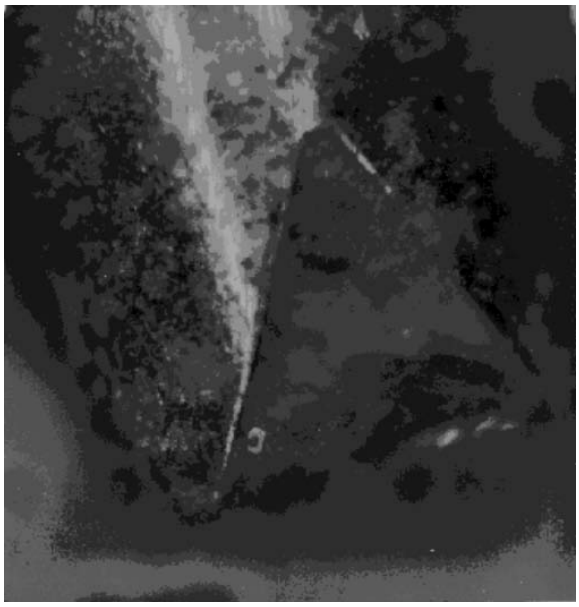

Figure 7.18 The crown probe is gummed up by the residue of RMA flux after 200 testing cycles [2]

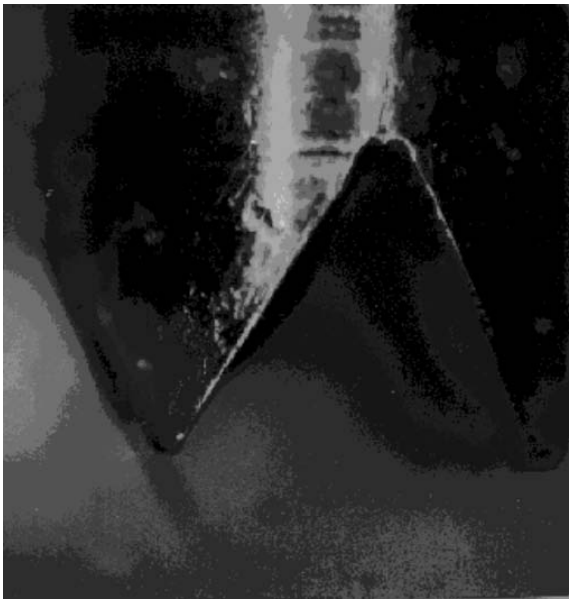

Figure 7.19 The crown probe remains clean after 3200 testing cycles of probing on the soft-residue [2]

The probe-testability of no-clean solder paste flux residue at in-circuit test is determined mainly by the residue's amount, location, and hardness. Testability increases with decreasing amounts of residue and top-side flux spread, and increasing amounts of bottom-side flux spread. The residue amount, top-side flux spread, and bottom-side flux spread affect primarily pad probing, and pin-tip probing, respectively. An inert reflow atmosphere helps probe penetration. A higher metal load effectively reduces flux spreading. Overall, the soft-residue approach appears to be most promising in providing successful probe contact.

7.4 Surface insulation resistance or electrochemical migration failure

7.4.1 Surface insulation resistance (SIR)

SIR is defined by the IPC [3] as "A property of the material and electrode system. It represents the electrical resistance between two electrical conductors separated by some dielectric material(s). This property is loosely based on the concept of sheet resistance, but also contains elements of bulk conductivity, leakage through electrolytic contaminants, multiple dielectric and metallization materials and air."

SIR tests have long been the industry standard as a primary means of assessing the corrosion-related reliability performance of soldering fluxes for electronic applications [4–7]. Some commonly used test methods include J-STD-004 [8] and Bellcore GR-78-CORE [9]. The test conditions typically involve elevated temperature, humidity, bias, and the use of a comb pattern. In general, the pass criteria include a sufficiently high SIR value and negligible signs of corrosion or dendrite formation.

7.4.2 Electrochemical migration (EM)

Electrochemical migration is defined by the IPC [3] as "the growth of conductive metal filaments on a printed wiring board (PWB) under the influence of a DC voltage bias. This may occur at an external surface, an internal interface, or through the bulk material of a composite. Growth of the metal filament is by electro-deposition from a solution containing metal ions which are dissolved from the anode, transported by the electric field and redeposited at the cathode." Electrochemical migration is referred to more widely as "electromigration" in the industry, which will be the term used in the subsequent discussion, and will also be represented by EM.

EM phenomena include surface dendrite formation and conductive anodic filament (CAF) formation. Surface dendrites form from the cathode to the anode under an applied voltage when contamination is present, as shown by Figure 7.20 [10]. For tin–lead solder, the dendrites will be lead needles which form "tree-like" dendrites with a tin coating. CAF is the growth of copper salt filament along the glass–resin interface from the anode to the cathode (see Figures 7.21 and 7.22 [11]). The anions commonly involved in CAF are chlorides and bromides.

The EM test is fairly similar to the SIR test in testing condition, testing vehicle design, and pass criteria. Both tests monitor the insulation resistance (IR). Besides IR, the SIR and the EM test may also monitor dendrite formation. Table 7.2 summarizes the comparison of some SIR and EM tests.

A low IR value for a PCB is developed either immediately after soldering or after the product has been subjected to the field service condition for a period of time.

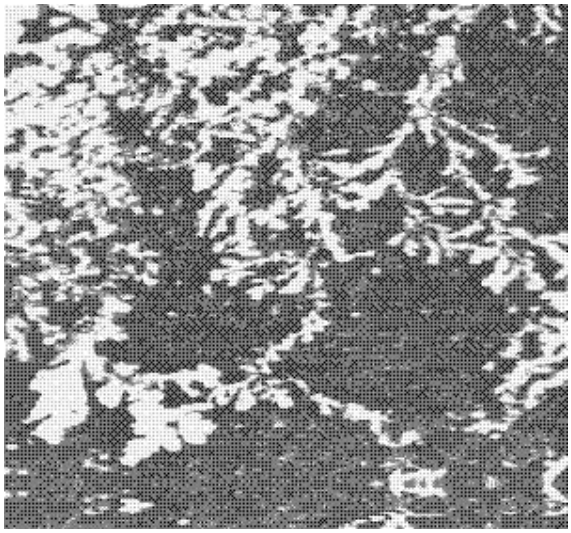

Figure 7.20 Dendrite formation. Source: Phil Wittmer [10]

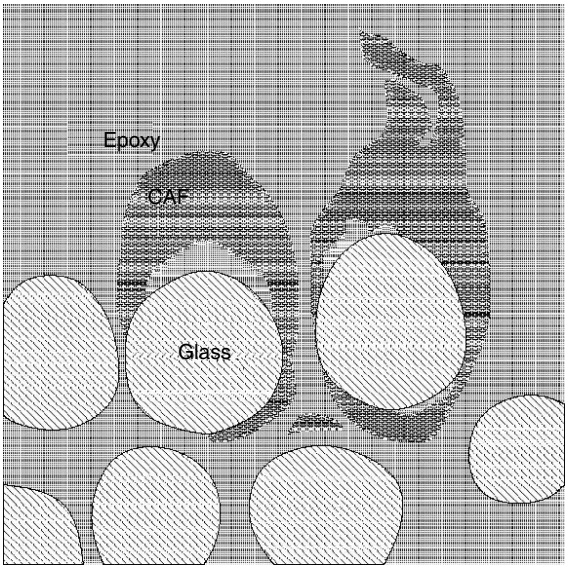

Figure 7.21 Conductive anodic filament formation (CAF) is a failure mode for printed wiring boards (PWBs) in which a conductive filament forms along the epoxy/glass interface growing from anode to cathode. The white region indicates a copper-containing filament growing along the epoxy/glass interface. Source: Turbini *et al.* [11]

Dendrite or CAF formation requires the presence of moisture and often will need some time to develop. Either a low IR value or formation of a metallic filament reflects or easily results in a short circuit or cross-talk, hence is it not desired.

7.4.3 Effect of flux chemistry on IR values

Jozefowicz and Lee [12] investigated extensively the effect of flux chemistry on SIR and EM, therefore their

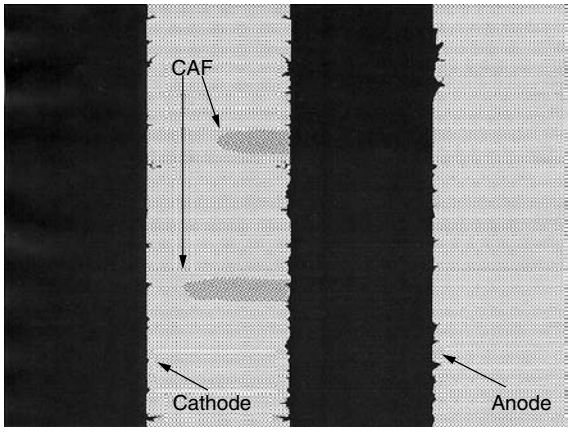

Figure 7.22 Using back lighting CAF appears as dark shadows coming from the copper anode to the cathode. Source: Turbini *et al.* [11]

results will be introduced in more detail here in order to illustrate the effect of flux chemistry on IR value. Their work is confined to the no-clean flux reliability assessment. Therefore, flux samples evaluated on SIR and EM tests are not cleaned with cleaners. Furthermore, all fluxes tested are halide-free. The test specifications used in their study are IPC-SF-818 class 3 SIR test [13] and Bellcore TR-NWT-000078 EM test [14]. In both tests, the test coupons used are B or E of IPC-B-25 comb pattern plated with solder. The major difference between IPC-SF-818 and Bellcore TR-NWT-000078 EM tests is the bias voltage, with the SIR test utilizing a considerably higher voltage than the EM test.

Both SIR and EM tests are believed to reflect the impact of flux corrosivity on the insulation resistance (IR)-related reliability behavior. Therefore, in order to compare the significance of these two tests, their results are analyzed against the flux properties relevant to either corrosivity or resistivity. A total of six flux properties are examined, as summarized in Table 7.3. The bulk flux resistivity and water extract resistivity measurements are intended to simulate the two extremes of the effect of existing ions on resistivity. At 85 °C and 85 percent RH, the flux resistivity at a high level of moisture pickup (MPU) is expected to be proportional to the water extract resistivity. In the case of negligible MPU, the flux resistivity may be proportional to the bulk flux resistivity. Here it is assumed that the effect of reflow may alter the magnitude but not the relative order of the resistivity of fluxes. If flux resistivity plays a vital role in determining the IR value, the relative order of IR of various fluxes will be expected to fit the intrapolated order from the two sets of extreme resistivity data. The pH value is an important chemical property, and is usually closely related to the corrosivity of chemicals. Both pH and water extract resistivity data are taken on 5 percent aqueous solutions of 35 percent flux extracts in isopropanol, i.e. approximately 1.75 percent flux in water. The demineralized water used to prepare the solutions has a pH value of 4.9 and a conductivity of 4.9 μ-mho/cm. The MPU of flux residue is speculated to be inversely

Table 7.2 Comparison of several SIR and EM tests

Test	*SIR* *J-STD-004*	*SIR* *Bellcore* *GR-78-CORE*	*EM* *Bellcore* *GR-78-CORE*
Test condition	85 °C/85%RH	35 °C/85%RH	65 °C/85%RH
Bias/test voltage (V)	−50/100	−50/100	10/100
Duration	1d no bias, measure at 1,4,7d	1d no bias, measure at 4d	4d no bias, measure at 4, 21d
Test vehicle	IPC-B-24	Bellcore IPC-B-25	IPC-B-25
Line spacing (mil)	20	50 12.5	12.5
IR pass criteria (ohms)	4, 7d > 10^8	$>10^{11}$ $>2 \times 10^{10}$	IR (21d) > 0.1 × IR (4d)
Other pass criteria	Dendrites <25% spacing	No green/blue discoloration	Dendrites <20% spacing

Note: d – day, V – volt.

Table 7.3 Flux characterization

Flux properties	*Test conditions*
Bulk flux resistivity	Resistivity of flux paste at room temperature
Flux water extract resistivity	Resistivity of 1.75% flux in aqueous solution
pH	pH of 1.75% flux in aqueous solution
Flux residue MPU	Reflow 1 gm flux in aluminum dish through infrared furnace, then measure the stabilized MPU of residue under 20 °C, 90% RH via gravimetric method
Flux corrosivity on Cu	Measure the thickness reduction rate of Cu ribbon immersed in flux at 60 °C
Flux corrosivity on Sn63	Measure the thickness reduction rate of Sn63 ribbon immersed in flux at 60 °C

proportional to the IR value of fluxes. The corrosivity of fluxes is determined on both copper and Sn63 solder metals at 60 °C without bias and humidity, and is suspected to be inversely proportional to the IR value as well.

7.4.3.1 Halide-free rosin fluxes

Initially, the comparison of EM data versus SIR data is conducted on a series of halide-free rosin fluxes. The chemistry of the fluxes is regulated with the use of organic acids (OA) and organic bases (OB), as shown in Table 7.4. Also shown are the characteristics of those fluxes. The negative value of corrosivity data represents a reduction in metal thickness. Figure 7.23 shows EM data for representative rosin fluxes, while Figure 7.24 gives the SIR data of those fluxes.

In general, the IR shows an initial drop, then a slow increase with increasing time for both SIR and EM tests. Apparently, the initial drop can be attributed to the MPU effect. The gradual increase in IR value presumably can be at least partly attributed to the ion sweeping effect, i.e. the ions are forced by the electrical field to move toward the electrodes with opposite polarity. All four fluxes investigated here pass both SIR and EM tests.

Both SIR and EM show a similar pattern of IR value as a function of flux chemistry, i.e. RA > R > RAB > RB. It is surprising that the RA flux shows a higher IR value than the R flux. With the inclusion of acid activators in the flux, the RA flux was expected to show a lower IR value than the R flux which contains no activators at all. The significance of this will be discussed below.

Bulk flux resistivity and flux water extract resistivity exhibit no correlation with either SIR or EM values. This lack of correlation with either type of resistivity suggests that the IR value is not a simple result of plain migration of existing ions in an electrical field.

Generally a flux with a higher corrosivity is expected to result in a lower IR value. However, an opposite trend is observed. These unexpected results suggest that the flux corrosivity determined without bias and humidity may not reflect the flux corrosivity behavior under SIR or EM test conditions. In addition, it is possible that there are some parameters which are more powerful than corrosivity in affecting the results of both SIR and EM tests.

The pH value of fluxes may be such a parameter, as indicated by Figure 7.25. Here the IR value increases

Table 7.4 Characteristics of rosin flux samples

Sample	*Major flux composition*	*Bulk flux resistivity (Ω-cm)*	*Flux water extract resistivity (Ω-cm)*	*pH*	*Flux residue MPU (%)*	*Cu corrosion (mil/yr)*	*Sn63 corrosion (mil/yr)*
R	Rosin	4.0E+9	5200	3.9	2.0	−0.029	−0.159
RA	Rosin + OA	6.3E+8	1950	3.5	1.9	−0.069	−1.471
RB	Rosin + OB	2.8E+8	6000	5.6	2.2	0	0
RAB	Rosin + OA + OB	4.8E+7	1080	4.4	2.1	−0.037	−0.037

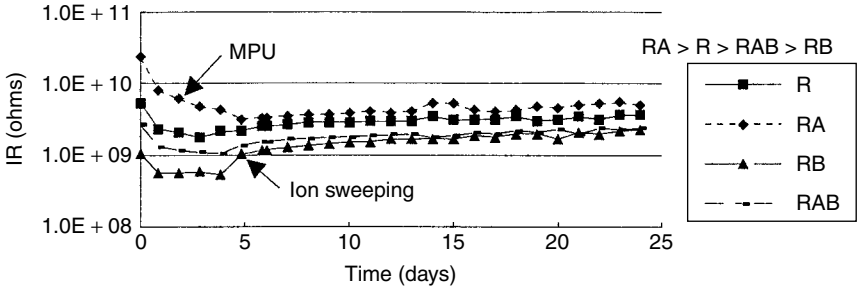

Figure 7.23 EM data for representative rosin fluxes [12]

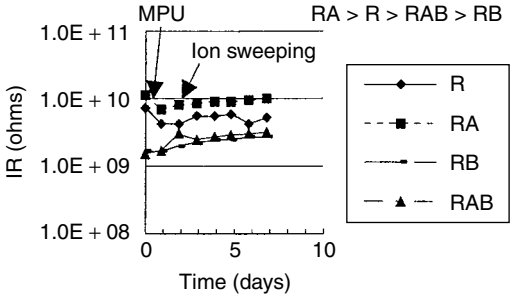

Figure 7.24 SIR data for representative rosin fluxes [12]

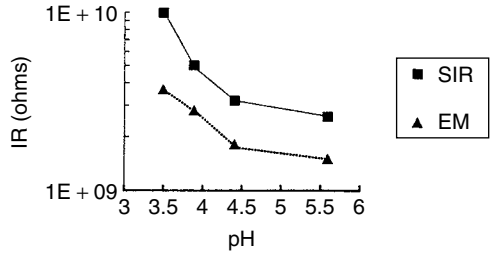

Figure 7.25 Effect of pH on SIR and EM for rosin fluxes [12]

rapidly with decreasing pH value. The effect of pH on the IR value may explain the unexpected IR order (RA > R) described previously. As expected from the fluxes' composition, the pH value of fluxes increases in the following order: RA < R < RAB < RB. The order of IR values observed is exactly the opposite. The meaning of this unusual pH effect will be discussed in the next subsection.

Figure 7.26 shows the effect of MPU of rosin flux residues on SIR and EM. In general, the IR value decreases with increasing MPU for both SIR and EM tests. This appears to be a reasonable trend, considering that presence of moisture usually reduces the resistivity of materials.

7.4.3.2 Low residue no-clean fluxes:

Due to public concern about CFCs, a new family of fluxes, low residue no-clean (LRNC), is rapidly growing and playing a very significant role in the SMT industries. In order to reduce the residue, many LRNC fluxes contain very little or no rosin at all. Accordingly, in general, the flux residue lacks the rosin-encapsulation effect for the possible residual activators, and therefore is normally required to be halide-free. To understand the impact of this new flux family on SIR and EM tests, a series of

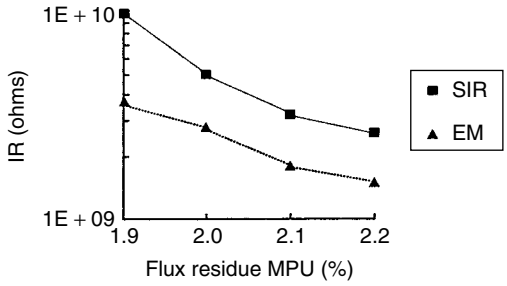

Figure 7.26 Effect of rosin fluxes residue MPU on SIR and EM [12]

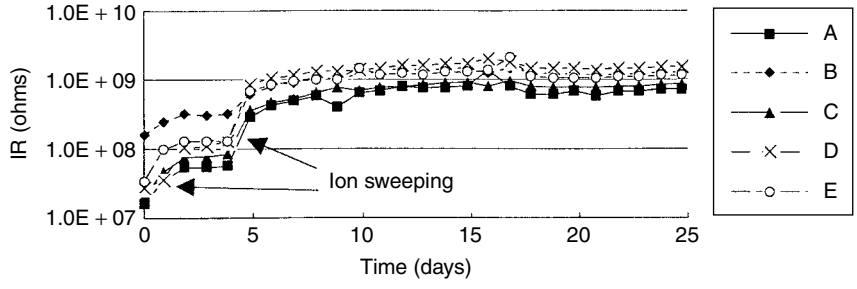

Figure 7.27 EM data for representative LRNC fluxes [12]

Table 7.5 Characteristics of low residue no-clean fluxes

Sample	*Bulk Flux Resistivity (Ω-cm)*	*Flux water extract resistivity (Ω-cm)*	*pH*	*Flux residue MPU (%)*	*Cu corrosion (mil/yr)*	*Sn63 corrosion (mil/yr)*
A	7.7E+7	885	3.8	1.3	−0.201	−0.110
B	2.2E+7	425	4.4	2.1	−0.123	−0.047
C	1.9E+7	746	3.5	1.3	−2.738	−0.041
D	3.7E+8	758	3.6	1.6	−0.061	−0.043
E	2.9E+8	30600	4.8	1.4	−0.034	−0.015
F	3.7E+8	31600	5.2	1.7	−0.026	0
G	7.1E+7	26200	4.9	4.8	0.013	0
H	3.7E+8	31100	5.4	1.6	−0.025	−0.042
I	4.0E+9	38300	6.0	1.3	0.004	0.055
J	2.9E+8	35700	5.5	2.1	−0.026	−0.051
K	2.9E+8	50800	5.4	1.5	−0.007	−0.082
L	3.7E+8	1020	3.6	1.6	−0.032	−0.164
M	6.3E+7	15400	7.0	1.6	−0.135	0.025
N	1.6E+7	990	4.1	2.0	−0.311	−0.091

LRNC fluxes is examined, as shown in Table 7.5. None of the fluxes listed contain rosin. The flux chemistry is regulated by varying the type and amount of OA and OB as activators. Also listed in Table 7.5 are the results of supplementary tests on those fluxes.

Typical examples of EM and SIR results for LRNC fluxes are shown in Figures 7.27 and 7.28, respectively. In general, the IR value is lower than that of rosin fluxes. This can be attributed to the lack of the rosin-encapsulation effect in the LRNC flux system. It is interesting to note that both SIR and EM data show an increase in IR values with increasing time from the very beginning. The absence of the initial dip in the IR curves, which is observed in the rosin flux system, suggests that the MPU of the LRNC flux residue establishes equilibrium very rapidly. Obviously this can be attributed to the very low residue level of the LRNC flux system. Therefore the ion sweeping mechanism dominates almost immediately.

In the case of the EM test, there are two ramp-up stages. The first is ion sweeping due to the test voltage. The second is ion sweeping due to the combined effect of test voltage and bias. After the second ramp-up stage, the IR levels off very quickly, suggesting completion of the ion sweeping mechanism and the absence of other IR-related activity.

In the SIR test, however, it is interesting to note that the IR curves show a continuously rising trend. Considering the higher bias voltage (−50 volts) used in the SIR test, the SIR curves are actually expected to ramp-up very quickly then level off. The rising trend observed here indicates that the IR behavior is not simply a result of the ion sweeping effect. The continuously rising SIR curves strongly suggest that there may be an electrolysis mechanism involved, as shown in Figure 7.29. In this electrolysis model, it is postulated that there are some electrolyzable polar chemicals in the system. These may originate from the flux residue or even from the printed circuit board itself, and constantly generate new ions due to electrolysis under the test conditions. At first the existing ions are quickly removed by the ion sweeping mechanism, thus forming the initial IR ramp-up. Although continuously releasing new ions due to electrolysis since the beginning, the electrolyzable materials are gradually depleted, thus resulting in a slowly increasing IR value. Apparently this electrolysis mechanism does not occur in the EM test for LRNC fluxes. Since electrolysis promotes generation of more ions, hence a lower IR value, it also explains the generally lower IR values observed in the SIR test when compared with EM test results. Considering that

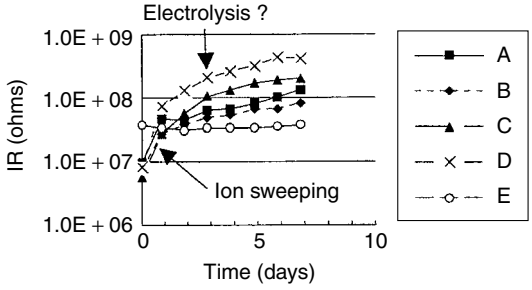

Figure 7.28 SIR data for representative LRNC fluxes [12]

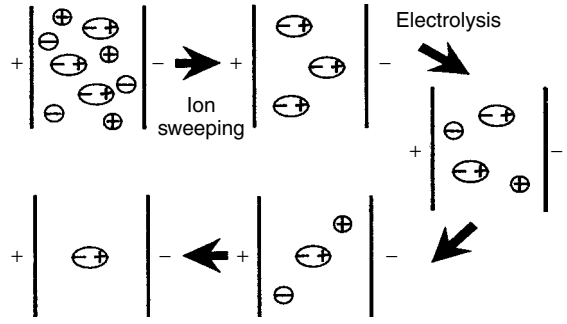

Figure 7.29 Scheme of electrolysis model [12]

the bias voltage is the only essential difference between SIR and EM tests (50 V versus 10 V, respectively), it can be concluded that the electrolysis mechanism is mainly caused by the high bias voltage used in the SIR test. The threshold bias voltage for this mechanism to commence is higher than 10 volts but no more than 50 volts.

As in the case of rosin fluxes, the IR behavior of both SIR and EM tests is independent of the fluxes' resistivity. This indicates, again, the IR is not a simple result of migration of existing ions under an electrical field. Neither LRNC fluxes residue MPU nor flux corrosivity show any effect on SIR and EM. The latter case indicates that, similar to the rosin fluxes, the flux corrosivity determined without bias and humidity does not reflect the flux corrosivity observed under SIR and EM test conditions.

Figure 7.30 shows the effect of pH on SIR and EM results. Although data scattering is quite noticeable, two trends can be easily discerned. First, the EM data appear to be independent of pH values. Second, the SIR values decrease with increasing pH values. Combining these trends with the previous conclusion that only SIR displays electrolysis in LRNC systems, it is logical to deduce that the observed SIR–pH relation is actually a reflection of the electrolysis–pH relation. Since electrolysis will ionize the electrolyzable chemicals and consequently result in a lower IR value, a lower SIR value for a higher pH flux suggests a greater extent of electrolysis in a higher pH environment. Therefore, it can be summarized that, under a high bias voltage, a higher pH will promote a more extensive electrolysis and result in a lower IR value. The nature of pH dependence on the electrolysis reaction is still not quite clear.

The SIR results appear to be more sensitive to variation of flux chemistry than the EM results. This can be explained by the electrolysis model and the pH effect. In this work, the LRNC fluxes with different chemistries usually varied in pH values as well. Accordingly, in the SIR test, these fluxes will undergo electrolysis to various extents and end up with a wider split of IR curves. In the EM test, the IR values of various fluxes are more comparable since there is no electrolysis factor involved.

7.4.3.3 Effect of flux chemistry

It appears that rosin fluxes and LRNC fluxes respond to bias-related electrolysis differently. For rosin flux systems, both SIR and EM tests seem to show the electrolysis phenomenon, and both tests appears to be equally informative.

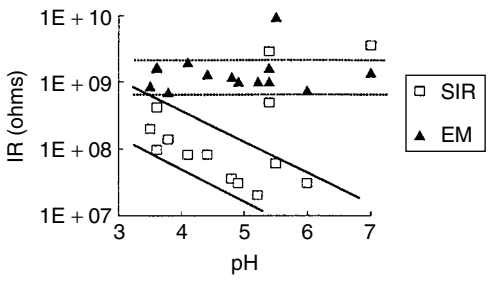

Figure 7.30 Effect of LRNC fluxes pH on SIR and EM [12]

However, in the case of LRNC systems, only the SIR test displays electrolysis. This flux chemistry-dependent relationship strongly suggests that one needs to be very careful in deciding which reliability test to use when moving into LRNC technologies.

In this study, generally the fluxes with a lower pH value display a higher IR value, except in the case of LRNC fluxes in the EM test. Since all the no-clean fluxes used in this study are relatively benign and nonpolar, the positive effect of acidity on SIR and certain EM performance observed here may be a conditional phenomenon, and it is reasonable to expect that fluxes containing highly aggressive acids are not going to perform well in either test. Similarly, the insignificant effects of corrosivity, flux conductivity, and MPU on the IR value of either test may also be observed only in mild fluxes. Presumably the conditions for this behavior are a combination of relatively low corrosivity and low polarity of the fluxes. In addition, absence of halides may also play a role.

By reviewing the test data in Figure 7.30, it can be seen that eight of the fourteen LRNC fluxes show failure in the SIR test, and most of those fluxes exhibit a higher pH value. On the other hand, all the fluxes, including the eight that failed the SIR test, pass the EM test. Hence it can be concluded that the SIR test appears to be more stringent than the EM test. However, in reality, most of the electronic components are operated at around 5 to 6 volts. In other words, compared with the EM test, the SIR test is susceptible to a failure mechanism mainly due to the use of a high bias voltage which will not be encountered by real-life application. Accordingly, the greater stringency of the SIR test is a result not of higher criteria in reliability, but of introducing a new failure mechanism which may never occur in a real application environment.

7.4.3.4 Summary on effect of flux chemistry

The effect of flux chemistry variations on SIR and EM is briefly summarized in Table 7.6.

Although fluxes with a high corrosivity are considered harmful, for fluxes with a relatively low corrosivity neither the SIR nor the EM test results show correlation with bulk flux resistivity, flux water extract resistivity, flux residue moisture pickup, and flux corrosivity without bias. However, in the case of rosin fluxes, the IR behavior of both SIR and EM tests is a function of the pH value of the fluxes. This phenomenon is more noticeable in the SIR test. In the case of LRNC fluxes, only the SIR test displays such a pH-dependent relationship. Data suggest that the 50 volts bias voltage used in the SIR test may be responsible for this, and can be explained with a high-bias-voltage-induced electrolysis mechanism which is more significant for fluxes with a higher pH value. For LRNC fluxes, this failure mechanism is absent in the EM test which utilizes 10 volts bias voltage, and probably will not occur in normal 5 volts application conditions.

7.4.4 Effect of soldering temperature

Soldering temperature has a great impact on SIR and EM performance. It is commonly known that too low a soldering temperature will result in a low IR value, and possibly

Table 7.6 Summary of effect of flux chemistry variation on EM and SIR test results

Flux properties	*Rosin fluxes*	*LRNC fluxes*	*Remarks*
Flux resistivity	SIR ≈ EM, no correlation	SIR≈ EM, no correlation	Indicates IR not simply due to migration of existing ions
Flux residue MPU	SIR ≈ EM, IR decreases with increasing MPU	SIR ≈ EM, no correlation	Relation observed may be due to pH effect
Flux corrosivity	SIR ≈ EM, IR increases with increasing corrosivity?	SIR ≈ EM, no correlation	In rosin fluxes, pH effect overrides corrosivity effect
pH	SIR ≈ EM, IR decreases with increasing pH	EM no correlation, SIR decreases with increasing pH	50 V bias needed for electrolysis of LRNC fluxes, 10 V bias sufficient for electrolysis of rosin fluxes

dendrite formation. In general, the lower the soldering temperature, the less flux will be burnt off, thus the more residual flux activity will remain on the board. In addition, some solvents may still remain in the flux residue and cause reduction in the moisture barrier capability of the residue. At elevated temperature, humidity, and in bias conditions, this residual flux activity often will react with electrodes, undergo electrolysis, or migrate under bias, thus causing problems such as a low IR value or dendrite formation.

On the other hand, too high a soldering temperature can also cause failure. Turbini *et al*. [11] have reported that a higher board process temperature resulted in an increased number of CAF for most of the water-soluble fluxes tested, as shown in Table 7.7. The higher process temperature may have promoted penetration of hygroscopic ingredients of fluxes at the interface of epoxy and glass fiber of PCB, thus stimulating the formation of CAF.

Table 7.7 Comparison of number of CAF associated with two different reflow temperatures [11]

Fluxes	*No. of CAF at 201 °C reflow*	*No. of CAF at 241 °C reflow*
Polyethylene glycol-600 (PEG)	90	55
PEG/HCl	None	None
PEG/HBr	None	None
Polypropyl glycol-1200 (PPG)	None	455
PPG/HCl	None	379
PPG/HBr	1	423
Polyethylene propylene glycol 1800 (PEPG 18)	1	406
PEPG 18/HCl	10	135
PEPG 18/HBr	9	279
Polyethylene propylene glycol 2600 (PEPG 26)	None	91
PEPG 26/HCl	6	218
PEPG 26/HBr	None	51
Glycerine (GLY)	None	56
GLY/HCl	None	583
GLY/HBr	3	104
Ocyl phenol ethoxylate (OPE)	None	83
OPE/HCl	14	62
OPE/HBr	2	599
Linear aliphatic polyether (LAP)	None	Not tested
LAP/HCl	15	203
LAP/HBr	None	272

7.4.5 Effect of cleanliness of incoming parts

Today, the no-clean process is the prevailing choice of assembly process. It is understood that materials such as solder pastes and wave fluxes introduced during assembly should meet no-clean, high reliability criteria. However, a high quality no-clean material can only assure that the cleanliness of the parts will not be reduced by those no-clean materials. If the incoming parts are not clean, a subsequent no-clean process will not eliminate pre-existing contaminants, and the reliability of the assembled parts will be greatly jeopardized. For PCBs, if the substrates used have contaminants, the performance of assembled boards on SIR and EM will often be compromised. Contamination introduced during handling has a similar adverse effect.

For parts or boards with poor cleanliness, employment of the cleaning process becomes essential in order to prevent SIR or EM problems. Also, use of parts with adequate quality is crucial. PCB substrates with improperly cured resin or substrates with some porosity often result in low IR value or the EM phenomenon.

7.4.6 Effect of conformal coating/encapsulation

Conformal coating or encapsulation is widely used on products to be used in a harsh environment. It not only protects the assembled board from mechanical damage, but also reduces the impact of moisture and airborne contaminants, thus minimizing SIR or EM problems.

7.4.7 Effect of interaction between flux and solder mask

Interaction between the solder mask and flux may also pose problems. This is particularly true for water-washable flux system. The interaction may result in a hygroscopic surface coating thus a lower IR value.

7.4.8 Effect of interaction between solder paste flux residue and wave flux

Like the interaction between flux and the solder mask, the interaction between the solder paste flux residue and the wave flux can also result in undesirable reactions and cause SIR or EM problems. Since in general the detailed chemistry of all fluxes remains proprietary information, it is important to run a compatibility test before implementing any combination of fluxes.

In summary, problems associated with SIR or EM can be minimized by the following solutions:

Use of fluxes with low corrosivity.
Use of fluxes with relatively low pH value and MPU.
Use of adequate soldering temperature.
Use of conformal coating.
Use of property clean parts.
Use of cleaning process when necessary.
Use of conformal coating or encapsulation.
Use of boards with adequate quality.
Use of boards that will not have an unacceptable reaction with fluxes.
Use of a flux combination that will not have unacceptable interaction.

7.5 Delamination/voiding/non-curing of conformal coating/encapsulants

For many products, conformal coating or an encapsulation process, such as potting or underfilling, should follow the soldering process. Although these polymer-based processes do not involve soldering, their yield and the quality of finished products are highly dependent on the flux characteristics used in the soldering process, particularly in the case of no-clean soldering. Examples of problems commonly encountered include (1) voiding of underfill, (2) delamination of the polymer coating, including conformal coating, potting compound, and underfill, and (3) incomplete curing of polymer coating.

7.5.1 Voiding

Voiding of the underfill in the flip chip assembly process, as illustrated schematically in Figure 7.31 [15], can be caused by many factors such as high volatility of underfill ingredients, moisture pickup of substrate surface, inadequate flip chip placement speed in a no-flow underfilling process, and uneven surface topology. Voiding can also be caused by a blocked flow in the underfilling process. Here only the voiding mechanism related to soldering will be discussed. For the no-clean soldering process, voiding often increases with increasing flux residue, presumably due to the physical blocking factor. However, the flow of underfill may also be obstructed by the poor wettability of the flux residue, even if the residue quantity is very low. For instance, flux residue with a low surface tension is expected to have poorer wettability, hence more MSK of voiding of the underfill.

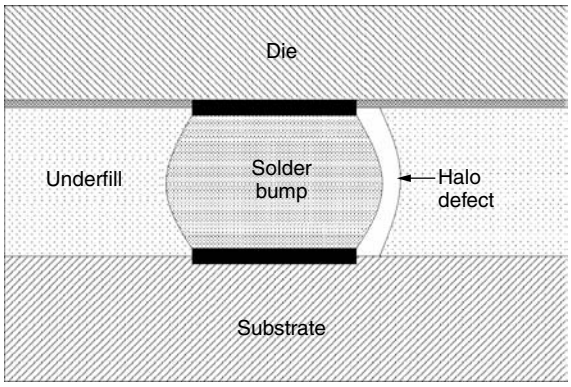

Figure 7.31 Halo defect is a special type of voiding during the underfilling process. It is often caused by the poor wettability of flux residue [15]

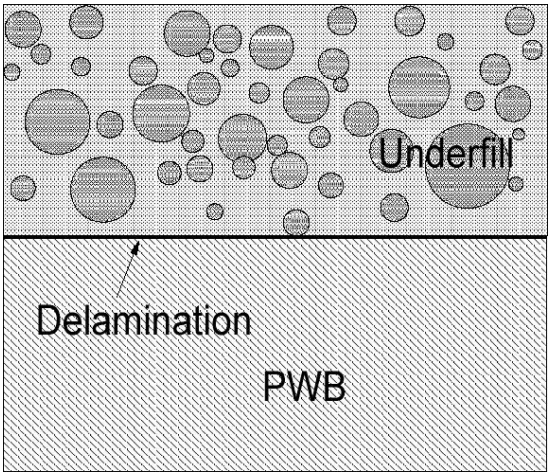

Figure 7.32 Delamination near the board side (eutectic bump–stencil solder paste print process) [16]

7.5.2 Delamination

Delamination of the underfill is shown in Figure 7.32 [16] as a cross-sectional view and in Figure 7.33 as a CSAM view. Often delamination occurs after humidity treatment followed by an additional reflow process. Delamination is considered a more serious threat to flip chip reliability than underfill voiding, and is caused directly by poor adhesion between the underfill and the base materials, such as the chip carrier substrate or the silicon die. This poor adhesion in turn is caused by the presence of flux film between the underfill and the base materials. Certain fluxes appear to be more compatible with some underfills. Although the actual mechanism is still not well understood, it is possible that the solubility of flux residue may play an important role. Fluxes with a residue that readily dissolves in the underfill, and can thus be removed from the interface, are considered to be harmless to the adhesion of underfill. Of course, the amount of flux residue should still be low. For a conformal coating, a similar mechanism may also apply.

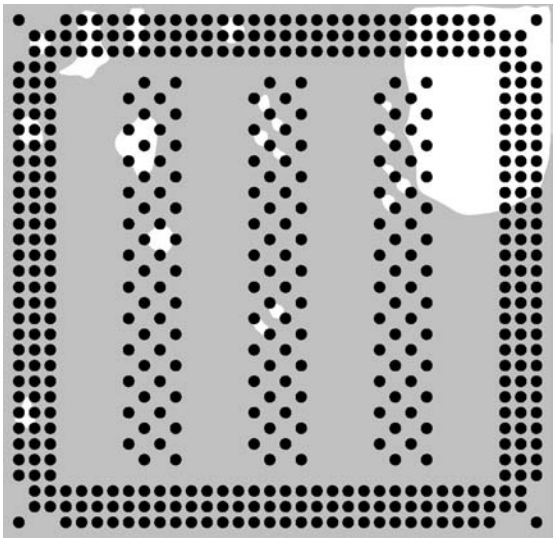

Figure 7.33 CSAM picture illustrating delamination of underfill (note the light colored area near the upper-right corner)

7.5.3 Incomplete curing

The curing of a thermoset encapsulant system, such as a potting compound, has been observed to be retarded by a certain flux chemistry for the no-clean process. For some systems, the curing becomes incomplete when coated on some flux residues. Presumably this can be attributed to the poisoning effect. To eliminate this incomplete curing problem, either a system with a compatible flux and a thermoset should be used, or a cleaning process should be implemented.

In summary, solutions for preventing voiding, incomplete curing, or delamination of a polymeric coating are as follows:

Reduce the flux residue quantity.
Use a flux of which the residue dissolves readily into the polymeric coating.
Select thermoset and flux carefully to assure compatibility.
Use the cleaning process if necessary.

7.6 Conclusion

A number of defects can occur at the post-soldering stage, mainly due to the presence of flux residues. Examples of defects include white residue, charred residue, poor probing contact, poor SIR or dendrite or CAF formation, voiding of underfill, delamination, and incomplete curing. Most of those defects can be minimized through properly selecting fluxes. Post-soldering cleaning is also an effective means of improving performance.

References

1. C. Lea, *After CFCs?* Electrochemical Publications, Isle of Man, UK (1992).
2. M. Xiao, P. A. Jaeger, and N.-C. Lee, ''Probe Testability of No-Clean Solder Pastes'', *Proc. Nepcon West*, Anaheim, CA (1997).
3. IPC-9201, *Surface Insulation Resistance Handbook*, (1996).
4. E. J. Gorondy, ''Surface Insulation Resistance – Part I: The Development of an Automated SIR Measurement Technique'', IPC-TP-518, IPC Fall Meeting, San Francisco, California, September (1984).
5. E. J. Gorondy, ''Surface Insulation Resistance – Part II: Exploring The Correlation Between Standard Industry and Military 'SIR' Test Patterns – A Status Report'', IPC Spring Conference, New Orleans, LA, April (1985).
6. E. J. Gorondy, ''Surface/Moisture Insulation Resistance (SIR/MIR): Part III: Analysis of The Effect of Test Parameters and Environmental Conditions on Test Results'', IPC Conference, Anehaim, California, 24–28 October 1988.
7. J. Brous, D. Culver, R. Lamoureux, B. Hall, and T. Giversen, ''Surface Insulation Resistance Testing: What is it? How Should It Be Done? What Does It Mean?'', IPC-TP-992 panel discussion, International Conference on Solder Fluxes and Pastes, Atlanta, Georgia, 27–29 May 1992.
8. ANSI/J-STD-004, ''Requirements for Soldering Fluxes'', January 1995.
9. Bellcore Technical Reference GR-78-CORE, Issue 1, September 1997, ''Generic Requirements for the Physical Design and Manufacture of Telecommunications Products and Equipment''.
10. P. Wittmer, ''Assembly Materials Interaction Study'', in *Proc. of SMTA/IPC Electronics Assembly Expo*, Providence, RI, p. S23–29, 24–29 October 1998.
11. L. J. Turbini, W. R. Bent, W. J. Ready, ''Impact of Higher Melting Lead-free Solders on the Reliability of Printed Wiring Assemblies'', SMTA International, Chicago, IL, 20–24 September 2000.
12. M. E. Jozefowicz and N.-C. Lee, *'Electromigration vs SIR'*, ISHM (1993).
13. ANSI/IPC-SF-818, ''General Requirements for Electronic Soldering Fluxes''.
14. Bellcore Technical Reference TR-NWT-000078, Issue 3, December 1991, ''Generic Physical Design Requirements for Telecommunications Products and Equipment''.
15. ''Lab Finds Halo Defects in Flip Chips'', *EP&P*, p. 12 (November 1997).
16. S. Yegnasubramanian, R. Deshmukh, J. Fulton, R. Fanucci, J. Gannon, A. Serafino, J. R. Morris and K. Nikmanesh, ''Flip-Chip-on-Board (FCOB) Assembly and Reliability'', in *Proc. of SMTA/IPC Electronics Assembly Expo*, Providence, RI, p. S4–3, 24–29 October 1998.

8 Solder Bumping for Area Array Packages

Packaging trends throughout the history of electronics manufacturing have moved progressively toward the characteristics of being smaller, faster, lighter, and cheaper, as discussed in Chapter 1. In surface mount technology (SMT), packages evolved further to the peripheral fine-pitch lead approach. This development ran into limitations quickly at approximately 12–16 mil pitch applications. To address this challenge, the area array packaging technology emerged, offering almost a quantum leap over the peripheral packaging technology. From flip chips and chip scale packages to ball grid arrays, area array packaging now provides great benefits at both the IC and component levels. Figure 8.1 shows the increasingly wide variety of chip scale packages utilizing area array technologies [1].

Solder and soldering are by far the preferred approaches to interconnecting area array packages [2]. This is especially true for the second-level assembly stage. Consequently, it is important to understand the nature, options, and limitation of both solders and soldering categories in order to successfully implement area array packaging technology.

8.1 Solder criteria

The choice of solder alloys is determined by the requirements of both process and reliability. Initially, besides meeting the solder wetting requirement, the solder chosen should be able to maintain its physical and mechanical integrity during subsequent processing. In this manner, at the end of the packaging and assembly processes, the solder joints formed initially will not be altered or damaged. The second criterion for choosing a solder alloy is reliability. Since solder joints need to survive the challenges of service life, the alloy should have sufficient fatigue resistance as well as sufficient standoff to absorb the thermal expansion coefficient (CTE) differences between parts. The former dictates that the solder should have appropriate mechanical properties in terms of shear, tensile, creep, and fatigue. The latter requires that solder joint height should be maintained above a certain value. This can be achieved through either solder surface tension (in the case of light components), or (in the case of heavy components) when high melting point solder functions as a spacer during the soldering process.

For area array packaging, interconnecting solder materials are usually introduced in two stages. The first is a predeposit of solder onto the packaging, usually accomplished through solder bumping. The solder bumped package is then mounted onto the next level of packaging through soldering. The soldering process here may or may not need the introduction of additional solder materials which may or may not be the same solder alloy as the solder bump on the packaging. When additional solder materials are needed, they are often introduced through either solder coating onto the next level of packaging or through solder paste deposition as a bonding medium.

8.1.1 Alloys used in flip chip solder bumping and soldering

For Flip Chip in Package (FCIP), the solders utilized for flip chip solder bumping and joining normally must have high melting points, such as 97Pb/3Sn or 95Pb/5Sn. This ensures that the solder joints will not remelt during subsequent packaging and assembly processes using eutectic 63Sn/37Pb solders. For direct chip attachment (DCA) or flip chip on board (FCOB) applications, the solders utilized for flip chip bumping as well as solder coating on the next level packaging often are eutectic or near-eutectic tin–lead solders. In some instances, In–Pb solders, such as 81Pb/19In, are chosen for either better fatigue performance or better compatibility with a Ni/Au substrate finish. An Au–Sn alloy system is also used for some fluxless flip chip assembly applications, with a eutectic 80Au/20Sn cap on top of an Au bump or Ni bump base. In the case of wire-bumping applications, the 97.5Sn/2.5Ag alloy has been used as an option.

8.1.2 Alloys used in BGA and CSP solder bumping and soldering

For heavy components such as ceramic column grid array (CCGA) or ceramic ball grid array (CBGA) devices, the solder used for either column or ball is typically 90Pb/10Sn. The column is mounted onto the area array package via either casting or 63Sn/37Pb solder joining. For CBGA, the 90Pb10Sn solder ball is typically mounted

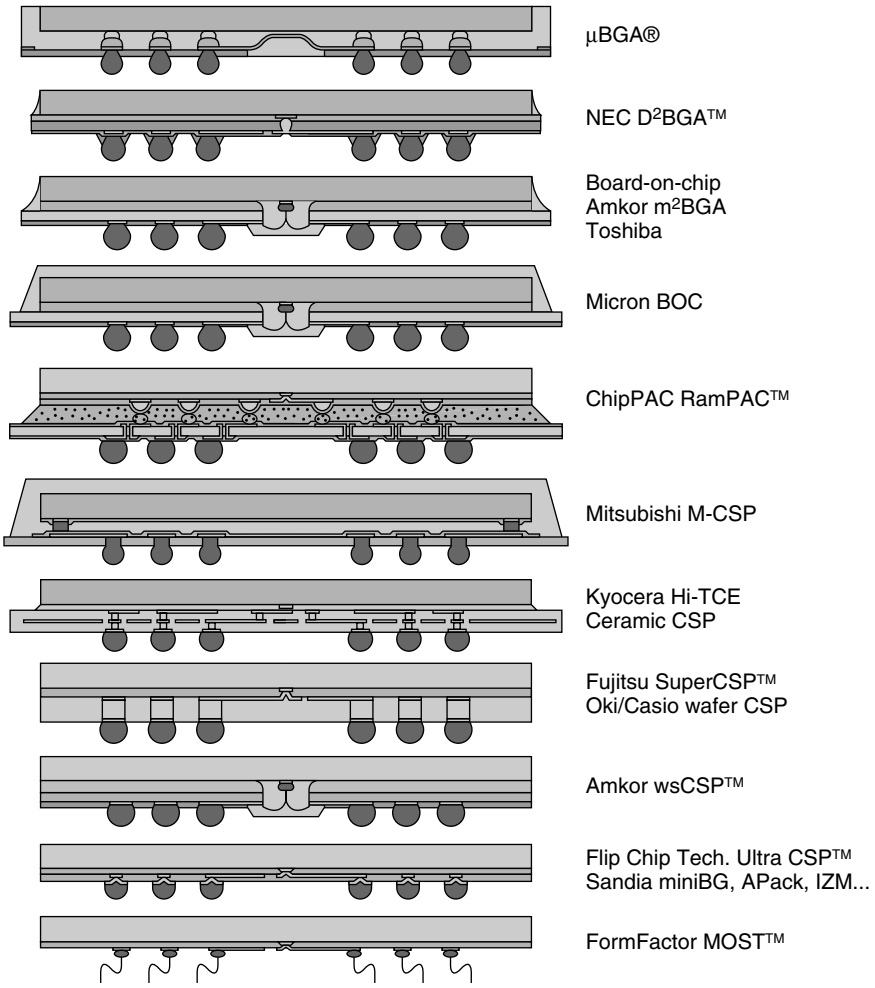

Figure 8.1 Various area array packages [1]

via 63Sn/37Pb solder paste soldering. The high melting point of 90Pb/10Sn solder ensures the required standoff of CCGA or CBGA on PCBs during board level soldering assembly using eutectic 63Sn/37Pb or 62Sn/36Pb/2Ag solders. For light components such as plastic ball grid array (PBGA) devices, the components are bumped with 63Sn/37Pb or 62Sn/36Pb/2Ag, and soldered onto the PCB either with flux alone or with solder pastes using similar alloy systems. In the instance of chip scale packages (CSPs), the alloys used are similar to that of PBGAs. However, the use of solder paste rather than flux alone, for board level assembly, is recommended.

8.1.3 Lead-free solders

Due to the toxicity of Pb, there has been an effort to eliminate it from solders. Through various concerted efforts worldwide, some good Pb-free alternatives have been identified, although none can serve as a 100% drop-in replacement for existing solders. The favorable Pb-free solder systems comprise primarily alloys of Sn with Ag, Bi, Cu, Sb, In, or Zn, as shown in Table 8.1.

These alloys may serve as substitutes for eutectic Sn–Pb solders in area array packages. As to the substitutes for high melting temperature solders, nothing has been developed. However, it should be kept in mind that most of the data generated are either material properties or performance in typical SMT applications. Direct data for Pb-free solders used in area array packaging still needs to be generated.

8.2 Solder bumping and challenges

Solder bumping techniques for area array packaging can be categorized into four major groups, as shown below. Since the defects and challenges are fairly specific to each individual technique, whenever possible, the problems encountered will be discussed and commented on immediately after the description of each technique.

Table 8.1 Examples of lead-free solders

Melting temperature range (°C)	*Alloy*
227	99.3Sn/0.7Cu
221	96.5Sn/3.5Ag
221–226	98Sn/2Ag
205–213	93.5Sn/3.5Ag/3Bi
207–212	90.5Sn/7.5Bi/2Ag
200–216	91.8Sn/3.4Ag/4.8Bi
226–228	97Sn/2Cu/0.8Sb/0.2Ag
213–218	96.2Sn/2.5Ag/0.8Cu/0.5Sb
232–240	95Sn/5Sb
189–199	89Sn/8Zn/3Bi
175–186	77.2Sn/20In/2.8Ag
138	58Bi/42Sn
217–219	95.5Sn/4Ag/0.5Cu
216–218	93.6Sn/4.7Ag/1.7Cu
217–219	95.5Sn/3.8Ag/0.7Cu
217–218	96.3Sn/3.2Ag/0.5Cu
217–219	95Sn/4Ag/1Cu

8.2.1 Build-up process

The solder bump is built up by depositing solder gradually through either a dry process, such as evaporation, or a wet process, such as electroplating.

8.2.1.1 Evaporation bumping

This is a dry solder build-up process, typically used for wafer bumping. In the case of the IBM C4 (controlled collapse chip connection) process as shown in Figure 8.2

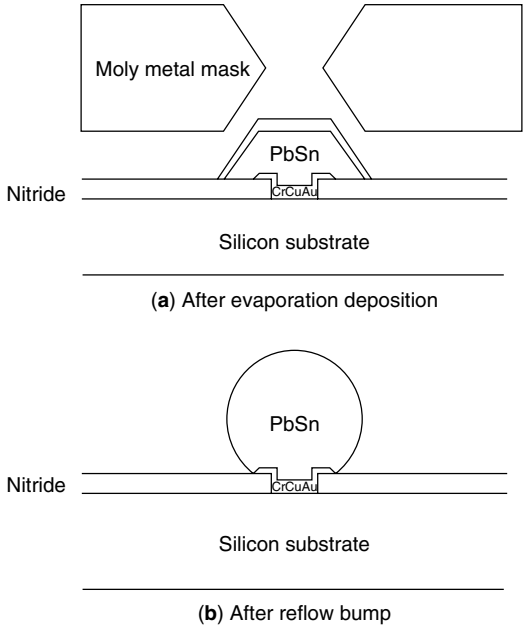

Figure 8.2 Evaporation solder bumping process on wafer: **(a)** solder bump after evaporation deposition, **(b)** solder bump after reflow [1]

[1], the solder materials used are 97Pb/3Sn or 95Pb/5Sn. At first, a molybdenum metal mask is aligned to the bond pads on the wafer and clamped. The under bump metal (UBM) is deposited through evaporation onto Al pads by (1) depositing a 0.15 μ Cr and 0.15 μ phased 50/50 CrCu layer as an adhesion/barrier layer, (2) depositing 1 μ Cu as a wetting layer, (3) depositing 0.15 μ Au as oxidation barrier. The solder with a known composition and volume is then also deposited through evaporation onto the UBM surface. The molybdenum metal mask is then removed, and the solder bump formed is often reflowed in order to fuse the solder.

Motorola has developed an evaporated extended eutectic (E-3) wafer bumping process (see Figure 8.3). Here E-3 bumps are formed by evaporative methods, producing a bump with a pure Pb column and a pure Sn tip. It is not reflowed prior to the die attachment [3].

In general, the evaporation process is adequate for coarse pitch and low I/O devices, due to the constraints of metal mask technology, although 100 μ diameter bumps

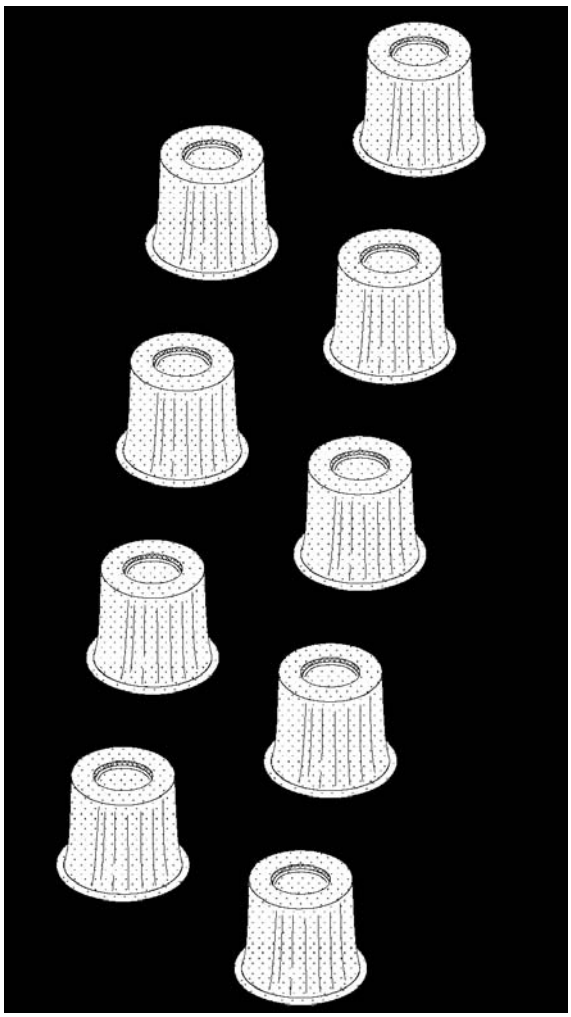

Figure 8.3 E-3 solder bumps [3]

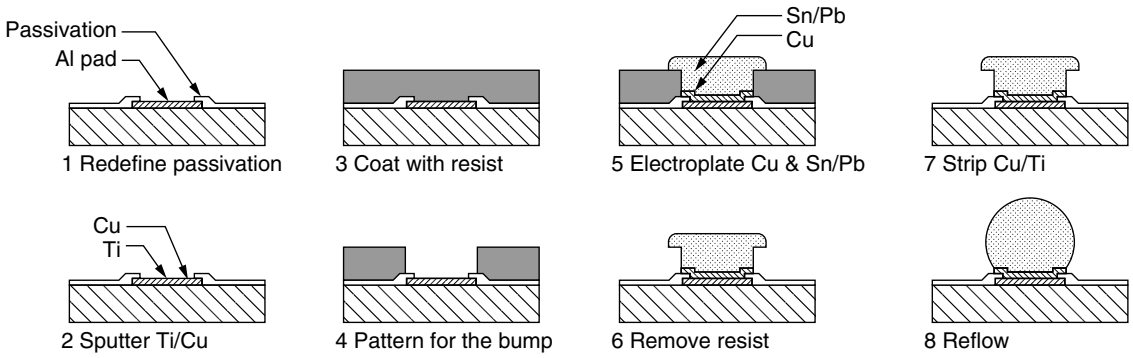

Figure 8.4 Electroplated wafer bumping process flow [5]

on a 250 μ pitch have been demonstrated. The quality of the solder composition and volume is very high. However, the cost of the evaporation process is of some concern.

8.2.1.2 Electroplating bumping

Electroplating bumping can be regarded as a wet solder build-up process. At this stage, electroplating may be the most commonly used process for wafer bumping. Again, the solder alloys deposited are typically Sn–Pb systems. First, the whole wafer is metallized with a seed metal [4]. It is then patterned with photoresist with the desired bumping location exposed. A static or pulsed current is then applied through the plating bath with the wafer as the cathode. After plating, the photoresist is stripped and the seed metal etched away. The solder deposited is then reflowed with the use of flux to form solder bumps. Figure 8.4 shows the process flow for electroplated wafer bumping [5].

Wafer bump size variation However, some bump size variation has been experienced. After reflow, the top view of some neighboring solder bumps varies in diameter, even though the plated solder bumps are dimensional even prior to reflow. The pattern is generally a large bump accompanied by a small bump, as shown in Figure 8.5. The small bumps appear to be more grainy, with more porosity between the grain structures of the bumps, particularly near the interface between solder and pad. No obvious round voids can be discerned. The symptom appears to be more serious when reflowed at 270 °C or higher, and improves at the minimal process peak of temperature 265 °C. Also, the symptom is uneven along the wafer. One side of a wafer may indicate a serious problem, while other side may not.

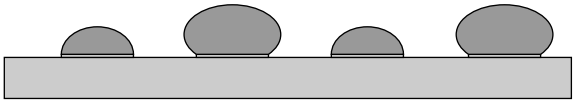

Figure 8.5 Schematic of solder bumping size consistency problem encountered in electroplated solder bumping for wafers

Although the mechanism responsible for this phenomenon is not clear, it is reasonable to speculate that this variation in solder volume from bump to bump may be caused by an impurity. Upon reflow, the rigorous outgassing of impurities in the plated solder or UBM may have caused splashing of the molten solder domes, and consequently resulted in contact between neighboring solder deposits. This transit contact between deformed molten solder domes can easily result in solder robbing, hence forming uneven solder volumes in neighboring bumps. A higher process temperature enhances the outgassing hence aggravating the problem. The impurity outgassing model is also consistent with porosity observations, since an impurity often will prevent proper coalescence of molten solder and result in microvoids between grain structures. The high occurrence of microvoids near the interface between solder and pad suggests that the impurity may come from UBM materials. The grainy appearance associated with small bumps may reflect the presence of an impurity in the bumps that splashed hence a reduced solder volume. The proposed solutions for this problem include (1) improving the plating quality of solder or the UBM quality in order to reduce the impurity introduced, and (2) reducing the reflow temperature.

8.2.2 Liquid solder transfer process

In this process, the solder bump is formed by transferring liquid solder onto the wafer metal base either by solder dipping, such as meniscus bumping, or by liquid solder dispensing, such as solder jetting.

8.2.2.1 Meniscus bumping

This is a solder dipping process [6] developed by the Fraunhofer-Institute as a low cost alternative to conventional processes in cases where–as for flip chip on flex–only a relatively thin solder layer is needed. The wafer level bumping is based on the deposition of electroless Ni as a wettable UBM. Besides the possible cost advantage of this process, a very high uniformity of the layer and a near hermetic sealing of the Al-pad is claimed. Then, a solder layer–80Au/20Sn is chosen in this case for its high reliability and its high melting point–and is applied by a well-controlled dipping technique. A mean

bump height of 32 μ with a variation of ±5 μ (Ni bump: 15 μ) is desired. This is reported to be sufficient for the bonding process (laser based fiber push connection technology, FPC) on the flexible substrate applied here.

The solder bumps formed through this process can be soldered onto the flex through FPC technology. In this instance, an adhesive is dispensed onto the flip chip bump side, followed by placing a three-layer flexible substrate (a copper layer sandwiched between polyimide layers) on top of the flip chip bump. During the FPC process, the fiber maintains bond strength while the laser pulse guided through the fiber heats the contact zone. The temperature generated results in the emission of IR radiation, which is measured by a detector for *in situ* temperature control, thus avoiding overheating the flex. The FPC method allows bonding through the polymer film due to the low absorption of the flex at the wavelength provided by the Nd : YAG laser (1064 nm). The copper leads are thus selectively heated close to the interconnection area. Since FPC technology utilizes sequential soldering instead of mass soldering process, the inherent low rate of throughput can be of concern.

8.2.2.2 Solder jet bumping

Solder jetting is a process whereby a molten solder droplet is ejected from an orifice with the use of a driving force. At this stage, the most commonly used and also the most successful driving mechanism is piezoelectric force, as shown in Figure 8.6.

Solder jetting used for BGA solder bumping has been demonstrated by Sandia National Laboratories (see Figure 8.7) [7]. As mentioned earlier, the driving mechanism used is piezoelectric force. Using a graphite plate with 20 × 20 apertures matching that of a BGA pads, as shown in Figure 8.8, the bumping of 400 pads can be accomplished with a single shot. The BGA substrate is positioned at 0.100-in. under the orifice plate, aligned with the holes, and heated to 180 °C to aid wetting. The most consistent solder droplet with a diameter 30 mil (see Figure 8.9) was produced at 205 °C with a 14 mil orifice. A higher temperature results in a larger solder droplet, due to a lower solder viscosity.

Other mechanisms have also been attempted, such as electromagnetic driving force reported by IBM [8], as shown in Figure 8.10. This IBM design, known as the micro dynamic solder pump (MDSP), utilizes electric current pulse and magnetic field to induce a driving force exerted onto the molten solder and results in controlled solder droplets with dimension down to 0.004 in. This driving mechanism involves no mechanical movement, hence eliminating any mechanical wear.

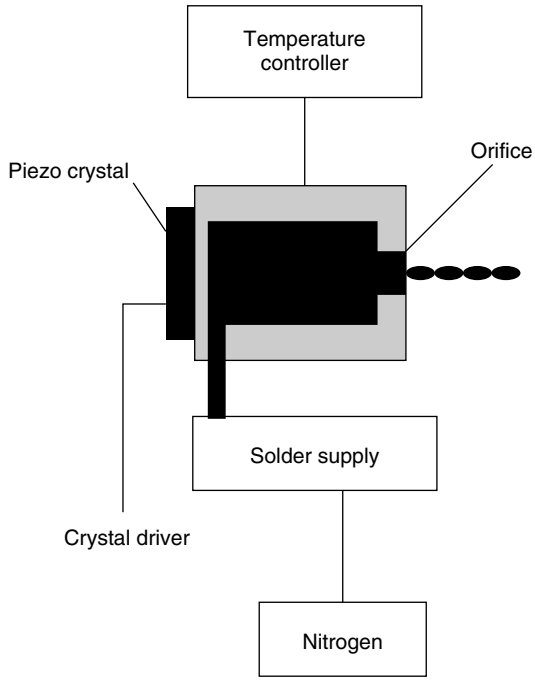

Figure 8.6 The piezoelectric crystal exerts a pulsing mechanical force to break up the solder jet stream to form solder droplets

For a drop-on-demand wafer bumping process developed by MPM and Microfab [9], the molten solder droplet is directly ejected onto a wafer pad with an Au surface finish. The machine can deposit Sn63 solder droplets ($100 - 150 \pm 10$ μ). During jetting, the wafer stage moves around, with the jetting area flooded with nitrogen. The solder solidifies immediately upon landing. Microfab has commented that the technique is limited to small solder droplet sizes. When trying to produce large solder droplets, the machine control burnt down.

The solder jetting process converts molten solder directly into a solder bump, thereby eliminating all other interim steps, such as electroplating, preform punching, cleaning, etc., needed by other bumping techniques. It may be one of the processes with the greatest potential as a low cost wafer bumping process. It has been claimed that this process may cost $16/wafer for solder bumping, versus $50–100/wafer for some plating bumping processes.

The limitation of this jetting technology on wafer bumping is at approximately 3 mil spacing. The solder bump formed has no metallurgical bonding formation with the

Figure 8.7 Picture of solder jetting process taken at 1000 frames per second, 30 microsecond exposure time from left to right at the edge of a 20 × 20 array of orifices. (From D. R. Frear, F. G. Yost, D. T. Schmale, and M. Essien, ''Area Array Jetting Device for Ball Grid Arrays'', in *Proc. Of Surface Mount International*, San Jose, CA, pp. 41–46, (7–11 September 1997): reprinted by permission.)

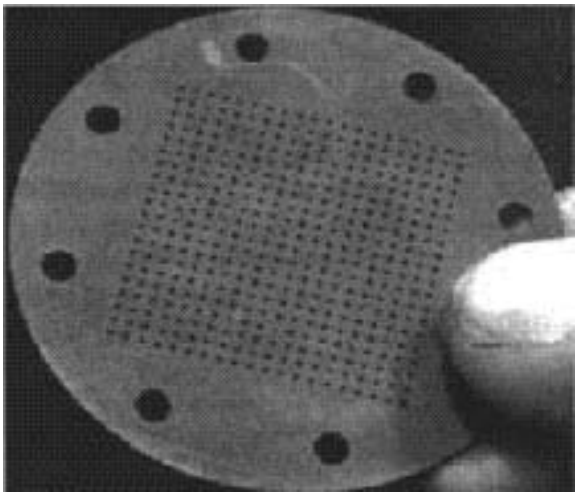

Figure 8.8 Graphite orifice plate with a 20×20 array of 0.20-in. holes. (From D. R. Frear, F. G. Yost, D. T. Schmale, and M. Essien, "Area Array Jetting Device for Ball Grid Arrays", in *Proc. Of Surface Mount International*, San Jose, CA, pp. 41–46, (7–11 September 1997): reprinted by permission.)

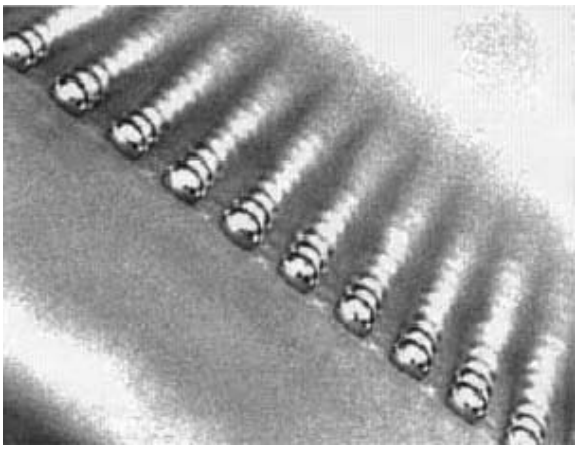

Figure 8.9 Solder bumps formed with Sandia solder jetting process. (From D. R. Frear, F. G. Yost, D. T. Schmale, and M. Essien, "Area Array Jetting Device for Ball Grid Arrays", in *Proc. Of Surface Mount International*, San Jose, CA, pp. 41–46, (7–11 September 1997): reprinted by permission.)

pad, as shown by the lack of intermetallics, and apparently adheres to the pad mainly by physical force. However, true solder wetting can be developed by reflowing the bumped wafer. If the quality of metallurgical bonding after reflow can meet the reliability requirement, this reflow process can be implemented following the jetting process at the bumping house, or may also be conducted at the assembly house, if the solder bump will remelt again in the flip chip attachment process.

One of the major concerns is that the throughput of this process is still fairly low, as reflected by the maximum jetting speed of 250 drops/sec. The most important issue may be the questionable consistency of bump size.

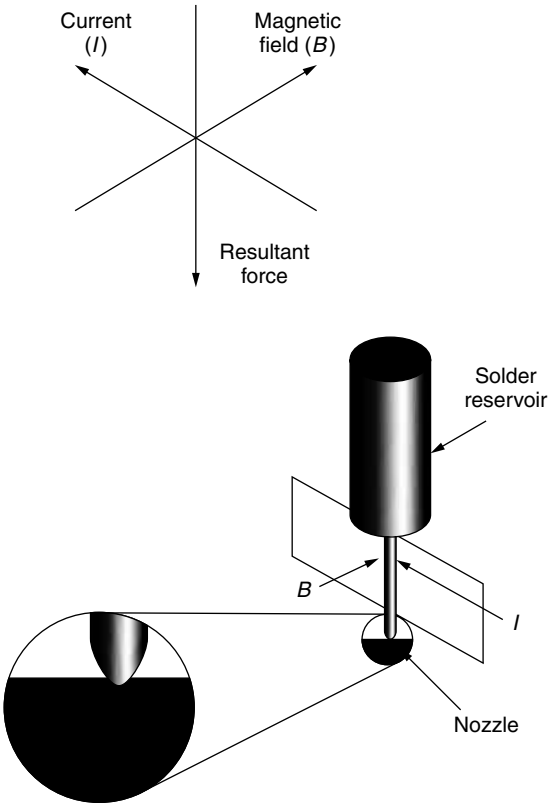

Figure 8.10 Schematic of micro dynamic solder pump [7]

For the wafer bumping process, selectively reworking the individual off-size bumps is cost prohibitive, and technically difficult. The jetting process is also sensitive to the quality of solder used. Without an additional purification step, the molten solder tends to clog the orifice very quickly. Perhaps due to those challenging issues, recently some further developmental work on this wafer bumping approach has been discontinued.

This reduction in developmental activity does not apply to only MPM-Microfab wafer bumping applications. It is also interesting to learn that, although the MDSP process is considered very ingenious, this technology was said to be shelved at IBM. Today, solder jet bumping seems to have disappeared from industry news or conferences. However, solder jetting has been adopted by several sphere manufacturers for high throughput solder sphere manufacturing, which is much less demanding in aiming precision and size consistency. The success in sphere manufacturing but not in bumping indicates that, although throughput is not an issue, the major challenges in achieving accuracy and/or size consistency have not been fully resolved.

8.2.3 Solid solder transfer processes

The transferring of a solid solder mass to the pad area forms the defined solder bumps. This process can be wire bumping, sphere welding, decal solder transfer, tacky dot

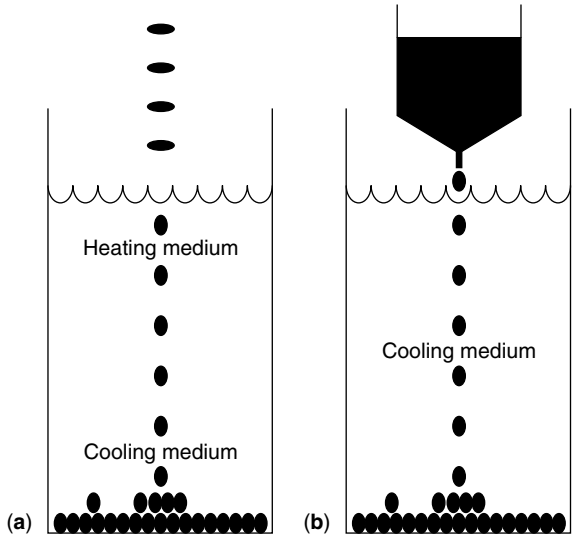

Figure 8.11 Solder sphere manufacturing process: **(a)** dropping solder preforms or short solder wire segments into a heating medium, following by solidifying in the cooling medium, **(b)** dripping molten solder into cooling medium

solder transfer, pick-and-place solder transfer, fluxless solder sphere bumping, or integrated preform, as described below.

Since normally the solder sphere is the solid solder mass to be transferred, it will be useful to review briefly the manufacturing technology for solder spheres. There are several methods for making solder spheres. The first type is by remelting solid solder tailored to the right solder mass in a heating medium, followed by solidifying in a cooling medium. This solid solder can be preforms punched from solder ribbon, or a short piece of solder wire cut from a long spool, as shown in Figure 8.11(a). The second type is by dripping molten solder into a cooling liquid medium via gravity as shown in Figure 8.11(b). The third type is by the solder jetting process, as discussed in the previous section. This molten solder droplet may solidify in an inert gas, or in a cooling liquid medium. The fourth type is by remelting solder paste prints and resolidifying the coalesced solder piece. The sphere size is regulated by the size of the solder paste deposit.

8.2.3.1 Wire bumping

Wire bumping is similar to wire bonding in that a solder wire, such as 97.5Sn/2.5Ag, can be bonded directly onto the aluminum bond pad using thermosonic energy. The solder stud formed then can be reflowed to form a solder ball. Ball size and pitch limitations are determined by the diameter of the solder wire and the thermosonic bonder's capability.

8.2.3.2 Sphere welding

For TBGA, IBM Endicott has developed a solder bumping process using a fluxless welding approach, as shown in Figure 8.12. The 25 mil diameter 90Pb/10Sn sphere is

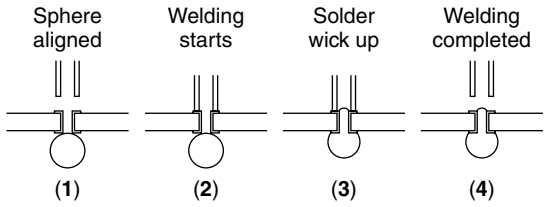

Figure 8.12 Sphere welding process for TBGA

Figure 8.13 Top view of TBGA, where the impression of vertically aligned welding tips on the surfaced solder can be noticed easily

placed onto a thin nest with a cup to hold the sphere in place. The TBGA tape with an Au-plated via is then placed on top of the spheres on the nest, followed by placing the setup under a welding machine. The welding tip is then lowered onto the tape via, and presses the via against the sphere underneath. If the welding tip traveling depth falls within the required specification, a current is then passed through the tip. This current will heat up the via Cu within a few milliseconds to 600–700 °C on the top side. The bottom side of the via is cooler, but is hot enough to melt the top of the 90Pb/10Sn sphere. The pressure on the via is maintained during the solder sphere melting stage to force the molten solder not only to wet the bottom side of the pad (including the pad side edge, by forming $AuSn_4$ intermetallics), but also to wick up the via and emerge slightly from the top of it. Once the depth has increased a pre-specified distance from the point before solder melting, the power is then cut off. The solder cools rapidly, and resolidifies. During the welding process, the device holding stage moves around while the welding tip fixture remains stationary. The welding process throughput is approximately 7.5 bumps/sec. Figure 8.13 shows the top view of TBGA where the impression of two vertically aligned welding tips on the surfaced solder can be

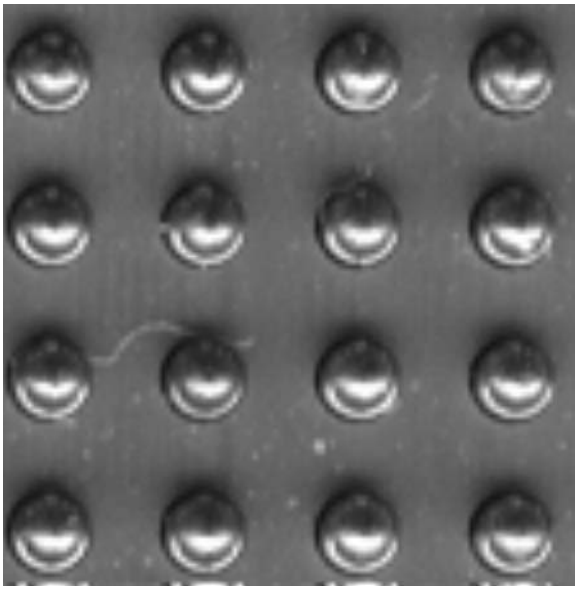

Figure 8.14 Bottom view of TBGA

noticed easily for each solder site. Figure 8.14 shows the bottom view of TBGA.

This TBGA process can rework unwelded vias or underwelded vias. However, it cannot rework an overwelded via. If there is an overwelded via, the whole TBGA tape has to be scrapped.

8.2.3.3 Laser attachment

Laser solder reflow and attachment provides excellent results for CSP and extremely fine-pitch devices, as shown in Figure 8.15. The method utilizes a specialized placement/reflow head which drops a single preformed sphere onto the desired placement site. The patented placement head as seen in Figure 8.16 simultaneously holds the ball in the exact position. A small ND : YAG laser simply heats each individual solder ball to reflow temperature in an inert environment typically of nitrogen thereby eliminating the need for flux or flux processes. This produces excellent results but the throughput is fairly low and therefore it may not be adequate for high volume applications [1].

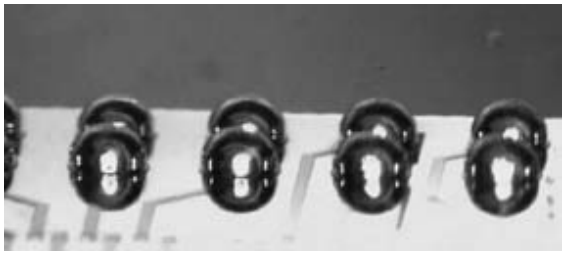

Figure 8.15 Spheres attached to distributed array utilizing laser attach method

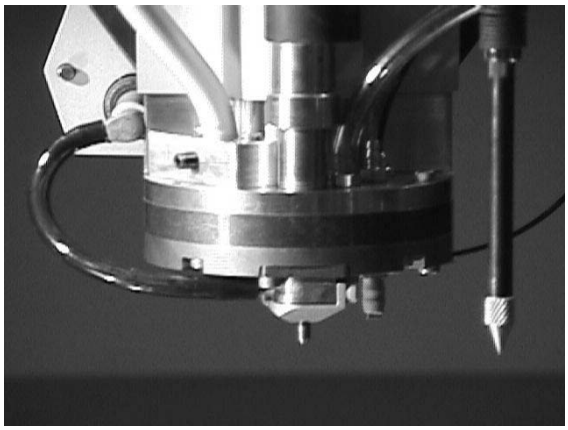

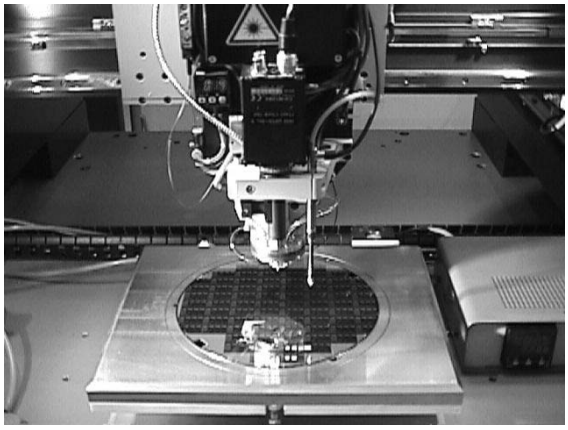

Figure 8.16 Laser attachment head (courtesy Pac-Tech Industries)

8.2.3.4 Decal solder transfer

Decal solder transfer is a method reported to be simple as well as effective for the addition of controlled amounts of eutectic solder to flip chip attach (FCA) carrier pads or BGA pads (see Figure 8.17). In this process developed by IBM-Endicott [10,11], solder is plated onto a nonwettable decal substrate such as aluminum, and forms solder studs with a pattern matching that of a flip chip or BGA footprint. This decal substrate, loaded with solder studs, is then placed on a fluxed wafer or BGA substrate, with each solder stud registered onto a metallized pad such as copper. This sandwiched assembly is then reflowed, followed by removal of the decal. The solder studs wet to the pad metallization and are detached from the decal substrate. The method, based on electroplated "nonwettable" substrates or decals, is a viable technique for chip attach and chip rework processes for card-on-board (COB) or BGA mounting applications.

Two important characteristics of the "nonwettable" substrate are the degree of wetting to the molten solder and its planarity. If the substrate is wetted by the solder, the solder bumps often become ruptured upon removal of the decal, as shown in Figure 8.18. On the other hand, if the decal is warped, some of the solder studs may not

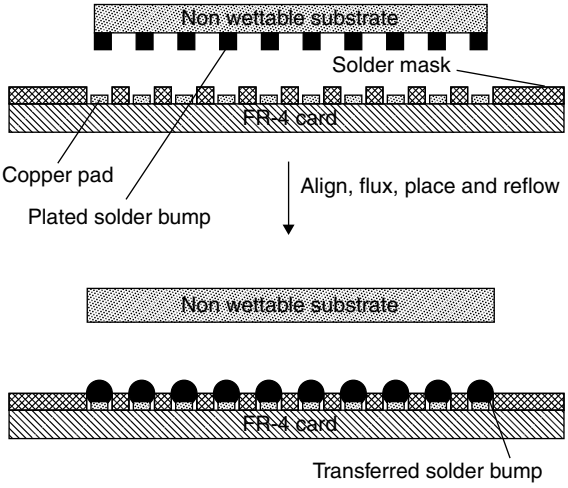

Figure 8.17 Schematic of decal solder transfer process [10,11]

contact the area array substrate pads, and hence may not be transferred to the pads (see Figure 8.19). For instance, for an 8-in. wafer bumping process with a target bump size 5 mil, a non-coplanarity of more than 2–3 mils out of 8-in. decal plate is sufficient to result in missing bumps. This stringent requirement may be a serious challenge for wafer bumping. For BGA or CSP bumping, the coplanarity requirement is much less stringent due to the larger size of solder bumps. However, the large size of solder bumps associated with BGA or CSP also requires a lengthy electroplating time, hence reducing the throughput.

8.2.3.5 Tacky dot solder transfer

Du Pont has developed an approach using tacky dots on polyimide film to transfer solder spheres for bumping CSP and flip chip [12,13]. The process involves the following steps: (1) preparing polyimide film with an adhesive coating, and covering the adhesive coating with a Mylar cover sheet; (2) photoimaging the film to form the desired tacky dot pattern to match the CSP or flip chip pattern, with the tacky dot diameter being 20% to 30% of the sphere diameter; (3) peeling off the Mylar cover sheet; (4) pulling the polyimide film through a solder sphere bath to populate the tacky dots with spheres followed by a full inspection; (5) placing the bumped film onto a flex stage typically used in the wafer dicing process; (6) cutting off the individual sheet; (7) mounting the bumped sheet onto a wafer printed with flux; and (8) either reflowing the solder so that the solder sphere wets to the wafer and detaches from the tape, followed by removal of the film, or UV curing the tacky dot to release the sphere, followed by inspecting the sphere on flux and then reflowing. The whole process may produce 1 wafer per minute, and has been demonstrated with wafers containing 29 000 bumps.

The target application is solder bumping the CSP or flip chip using small spheres. The spheres investigated range from 5 to 20 mil diameter, primarily of eutectic SnPb solder. However, peeling off the Mylar cover sheet from the

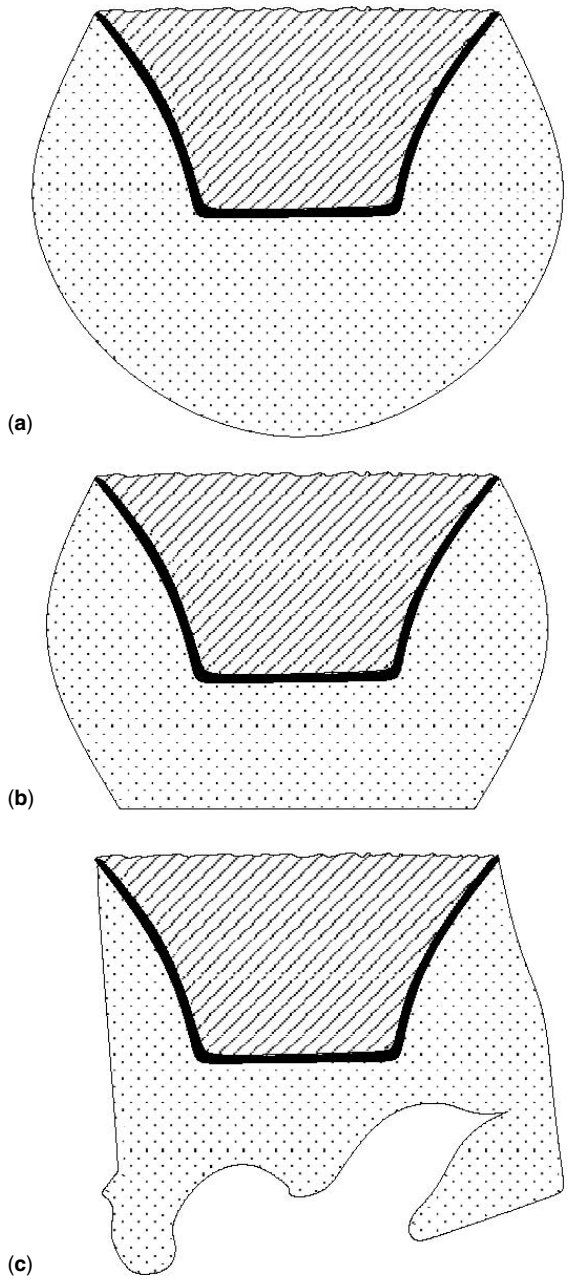

Figure 8.18 Flip chip solder bumps from decal transfer process. **(a)** The molten solder completely dewets the decal surface, **(b)** some wetting has occurred, leading to a flattening of the top of the solder bump, and **(c)** the wetting is so high that the excessive force required to separate the decal substrate leads to separation within the solder joint [10]

adhesive layer tends to generate a static charge, and the static becomes a factor in handling these tiny spheres. In addition, an agitated solder sphere bath tends to oxidize the solder sphere surface, which further increases the sensitivity toward static. Therefore, the bottleneck is attaching the sphere to a tacky dot on polyimide film

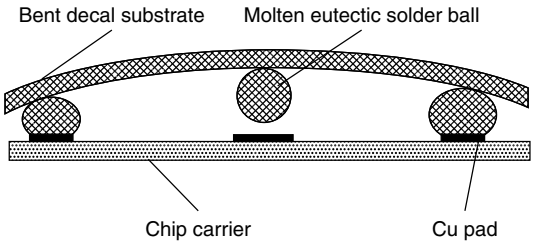

Figure 8.19 Poor coplanarity of decal substrate can result in missing bumps due to lack of contact [10]

carrying a static charge while at the same time achieving a high yield.

8.2.3.6 Pick-and-place solder transfer

For BGA solder bumping, the most common process involves using a pick-and-place machine to transfer solder spheres to a BGA substrate pre-deposited with flux or solder paste, followed by reflow. The pick-and-place mechanisms utilized include (1) vacuum pick-and-place, and (2) gravity pick-and-place [14].

Figure 8.20 shows the process flow for the vacuum pick-and-place solder bumping approach. Here a sphere tray with a cavity pattern matching that of the BGA is connected to a sphere reservoir. The vacuum-regulated tray cavity is first loaded with spheres through a cycled-tilting process. Another vacuum fixture with a mirror cavity pattern is then placed near the top of the tray to pick up the spheres through gas-blow-ejection plus a vacuum-pick mechanism. The sphere is then ejected onto a BGA substrate pre-deposited with either tacky flux or solder paste. The solder paste is often deposited via the stencil printing process, while the tacky flux is deposited through either stencil printing or a pin-transfer process. The BGA substrate loaded with spheres is then reflowed to complete the solder bumping process.

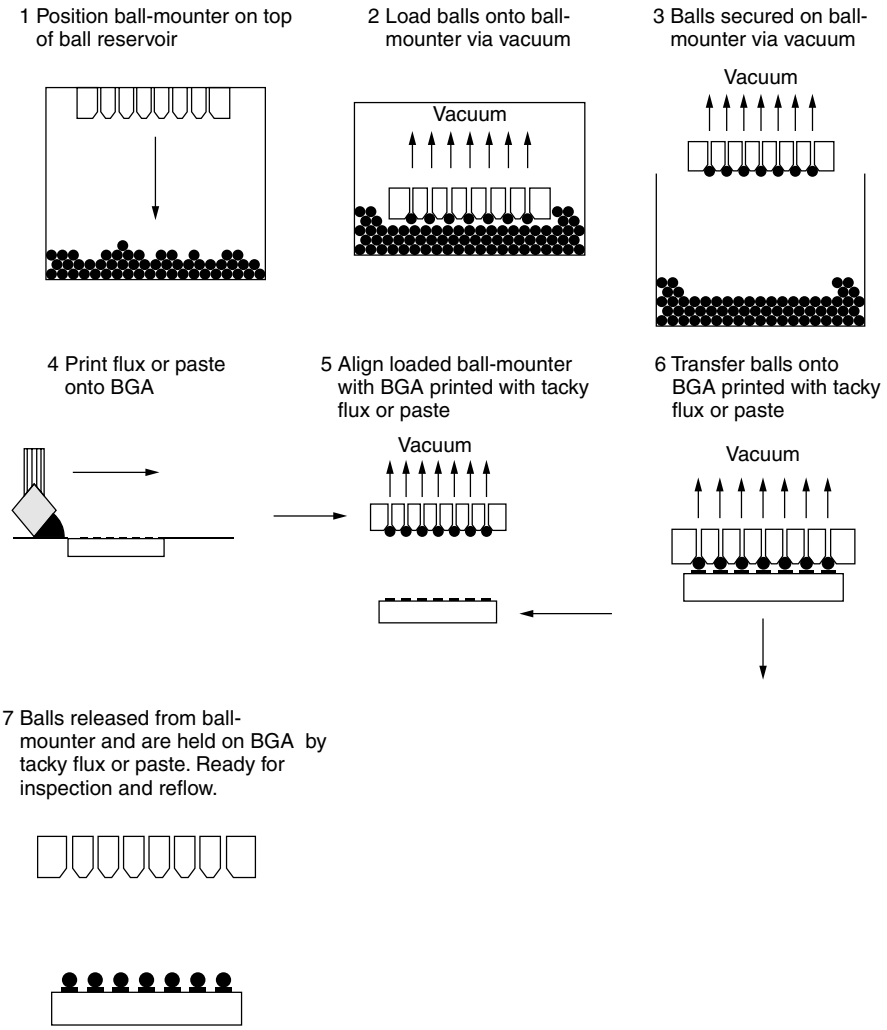
1 Position ball-mounter on top of ball reservoir
2 Load balls onto ball-mounter via vacuum
Vacuum
3 Balls secured on ball-mounter via vacuum
Vacuum
4 Print flux or paste onto BGA
5 Align loaded ball-mounter with BGA printed with tacky flux or paste
Vacuum
6 Transfer balls onto BGA printed with tacky flux or paste
Vacuum
7 Balls released from ball-mounter and are held on BGA by tacky flux or paste. Ready for inspection and reflow.

Figure 8.20 Process flow for vacuum-solder-sphere-placement for BGA solder bumping

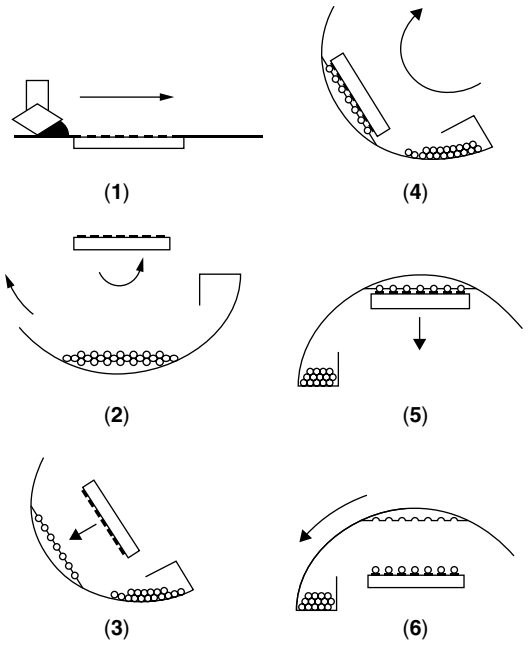

Figure 8.21 Gravity pick-and-place process. **(1)** Print solder paste or flux onto BGA strip, **(2)** rotate BGA strip and sphere loader for proper alignment, excessive spheres being drained from sphere securing tray, **(3)** attach BGA strip to sphere on sphere securing tray, **(4)** rotate loader/BGA strip to allow BGA strip to face upward, **(5)** detach sphere-loaded BGA strip from loader, **(6)** rotate sphere loader to reload sphere securing tray with spheres

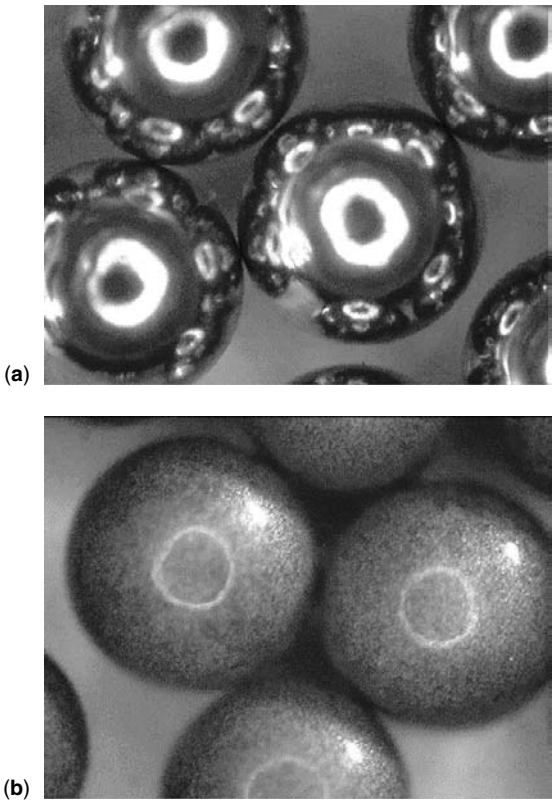

Figure 8.22 (**a**) 63Sn37Pb solder spheres with 30 mil diameter turn into dark after 12 hours' use. **(b)** Solder spheres with improved quality exhibit much higher oxidation resistance, as reflected by the shiny appearance after 12 hours' use

In the gravity pick-and-place approach, no vacuum is involved. A revolving process is used to first load spheres onto a sphere tray, and subsequently transfer them onto a BGA substrate pre-deposited with either tacky flux or solder paste, as shown in Figure 8.21. All sphere transferring processes rely on gravity alone. This is possible through the proper positioning of both tray and BGA substrate via the revolving process. The populated BGA substrate is then reflowed to complete the solder bumping process. In wafer bumping, a prototype pick-and-place unit has been built, and it is reported that a vacuum is not needed to pick up and transfer the tiny solder spheres.

Both pick-and-place designs for BGA solder bumping involves rolling the solder spheres back and forth between the sphere tray and the reservoir. This inevitably oxidizes the solder spheres and may pose a soldering quality issue at a later stage. Earlier, almost all the solder spheres available tended to turn dark within several hours on the pick-and-place machine, as shown in Figure 8.22(a). Considerable improvements have now been achieved, and solder spheres which can easily last for more than 24 hours on the machine are available, as shown in Figure 8.22(b). These darkened spheres exhibit a heavy oxide on the surface, which often persists after the sphere mounting process. Figure 8.23(a) shows solder bumps produced with dark sphere. Notice the wrinkled bump surface due to the presence of heavy oxide film. This heavily oxidized solder bump surface may compromise solder joint quality at a subsequent second level assembly. In extreme cases, the sphere can be rendered completely unwettable, as shown in Figure 8.24. Here the highly oxidized 90Pb/10Sn spheres are not wettable at all by 63Sn/37Pb solder paste, and merely remain around the 63Sn/37Pb solder domes formed by reflowing the solder paste. Figure 8.23(b) shows the bumps produced with a shiny, oxidation resistant sphere. The bump surface also appears smooth. In general, improvement in oxidation resistance is obtained mainly with a layer of surface coating which may be extremely thin and undiscernible, as demonstrated by Figure 8.25.

As for wafer bumping, there are at least two challenges facing the sphere placement approach. First, at sphere size of smaller than 4–5 mils, precision sphere dimension control, such as ± 5 percent in diameter, becomes very difficult. Second, static becomes a factor in handling such tiny spheres. The type of defects encountered in BGA/CSP bumping via sphere placement include (1) missing, (2) misalignment, (3) double/bridging, (4) wrinkled, dull, or high oxide surface, and (5) voiding.

An example of a missing ball on BGA is shown in Figure 8.26, while Figure 8.27 shows misalignment of 90Pb/10Sn bumps mounted with 63Sn/37Pb solder paste. Double/bridging is shown in Figure 8.28, and the oxidized

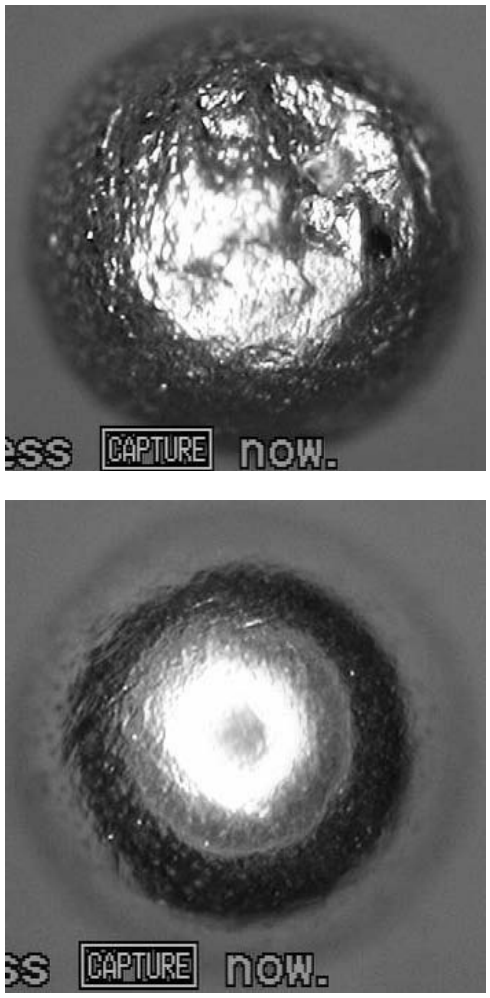

(**a**)

(**b**)

Figure 8.23 Top view of 63Sn/37Pb solder bump **(a)** with the use of heavily oxidized 30 mil diameter dark solder sphere, and **(b)** with the use of oxidation resistant shiny solder sphere

surface was demonstrated in Figure 8.23, while that of voiding is shown in Figure 8.29.

Missing, misalignment, bridging A systematic study of the reflow bumping process has been conducted by Chiu and Lee [17]. The defect rate considered including missing, bridging, and misalignment. For a bumping process involving Sn62 or Sn63 spheres, the use of solder paste for sphere attachment produces excellent alignment results. When using fluxes for Sn62 or Sn63 sphere attachment, the defect rate increases with decreasing flux viscosity (see Figure 8.30). Presumably this can be attributed to the possibility that it is more difficult for a sphere to roll across a high viscosity flux during reflow. The defect rate also decreases with increasing solvent volatility, as shown in Figure 8.31. Perhaps this can be attributed to the hot viscosity effect of the fluxes. A solvent with a lower boiling point will dry out more readily during reflow, and

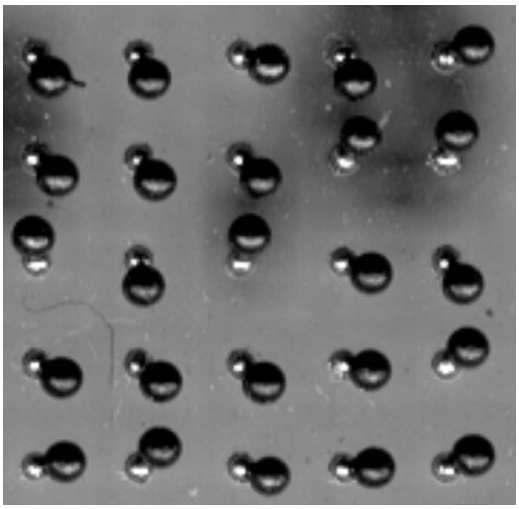

Figure 8.24 90Pb/10Sn solder spheres are heavily oxidized and are not wettable by 63Sn/37Pb solder paste. [17]

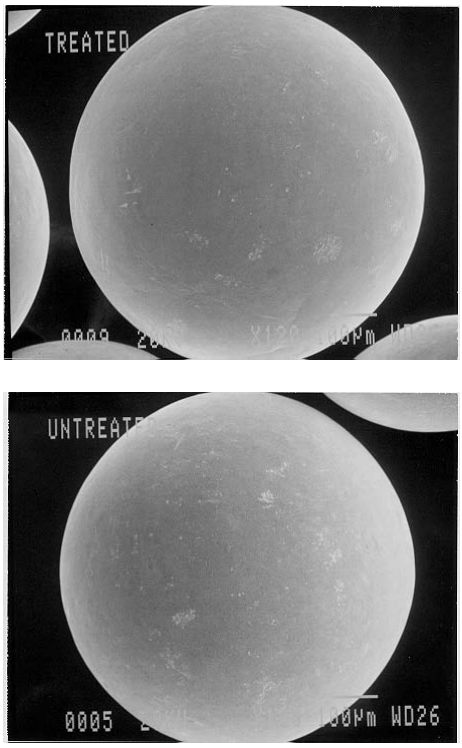

(**a**)

(**b**)

Figure 8.25 30 mil diameter 63Sn37Pb solder sphere **(a)** treated with surface coating, and **(b)** without surface coating. Virtually no surface appearance difference can be discernible between the two spheres

accordingly will develop a higher viscosity and exert a greater restraint on the rolling of the spheres.

Increasing the pitch dimension results in a decreasing defect rate, as demonstrated in Figure 8.32. Apparently, a large pitch reduces the risk of solder coalescence that

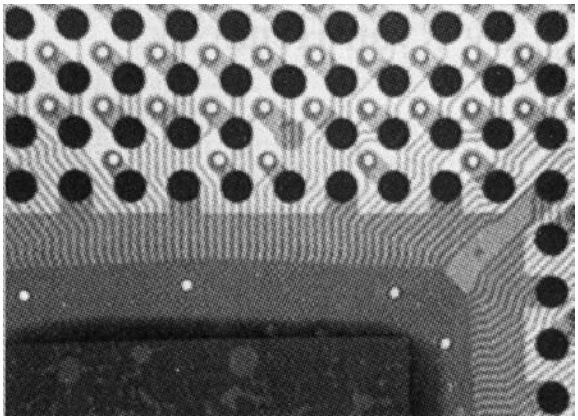

Figure 8.26 Missing solder bump in BGA

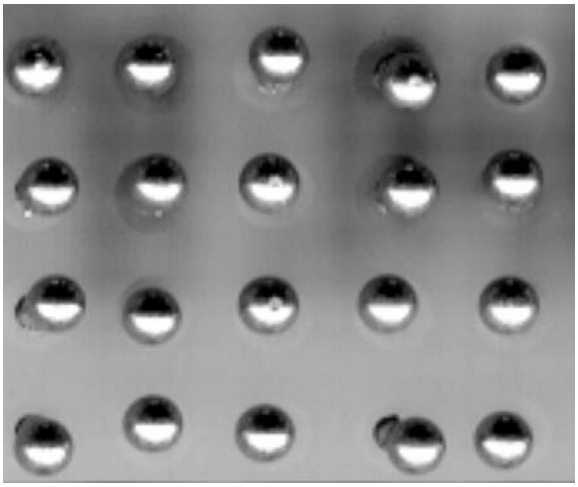

Figure 8.27 Misalignment of 90Pb/10Sn solder bumps soldered to pads with 63Sn/37Pb solder paste

occurs when the neighboring Sn63 spheres roll into each other. Figure 8.33 indicates that a thicker flux deposition results in a higher defect rate. This is attributed to the flux barrier effect. Upon reflow, the flux stays between the sphere and the pad. The greater the flux deposition thickness, the longer it will take for the sphere to sink through the flux and make contact with the pad, and consequently the more risk of the sphere rolling away before any solder wetting can occur. As to the flux activity, results indicate that the missing rate increases with increasing activator content in a semi-log scale relationship, as shown in Figure 8.34. A stronger flux will react more rigorously with the sphere oxide, and accordingly will outgas more rigorously at reflow. This outgassing very likely will affect the sphere's rolling action. In addition, fluxes with higher activity remove the sphere oxide film sooner. This allows the sphere to have more time and therefore more opportunity to coalesce with neighboring spheres when the spheres roll into each other.

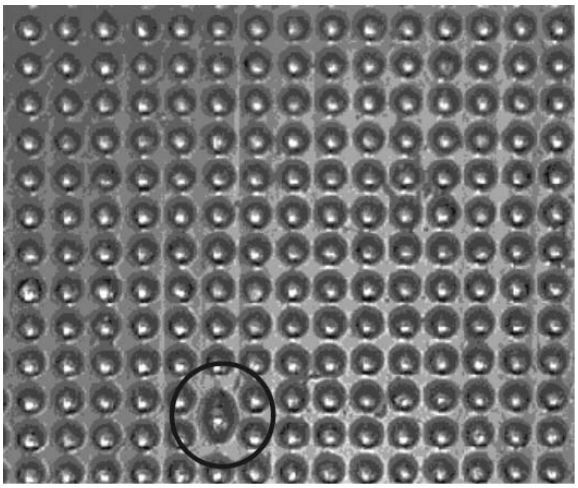

Figure 8.28 Example of double/bridging of 63Sn/37Pb solder bumps as marked by circle

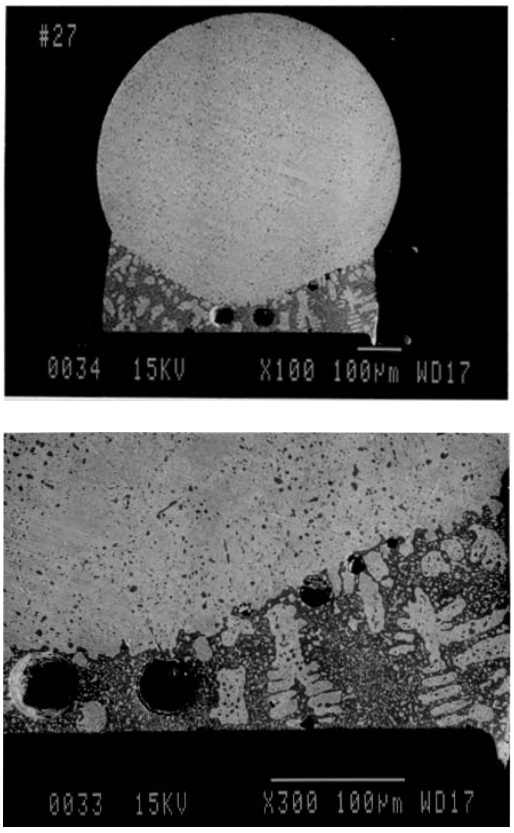

(**a**)

(**b**)

Figure 8.29 Large voids in the cross-sectioned sample of 90Pb/10Sn solder bump, mounted with Sn63 solder paste and examined with SEM

The missing rate of the balling process using Sn63 spheres and printed fluxes is found to increase with increasing pad dimension, as displayed in Figure 8.35. Here the pitch dimension studied is 50 mil. The trend observed

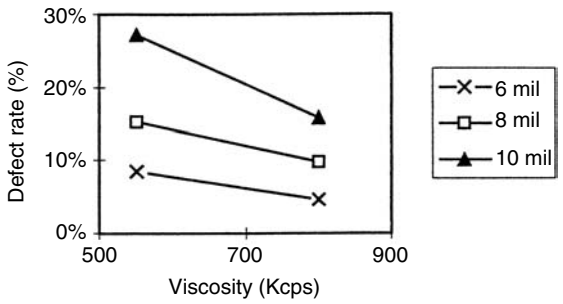

Figure 8.30 Effect of flux viscosity on the defect rate of balling process using Sn63 sphere and printed flux

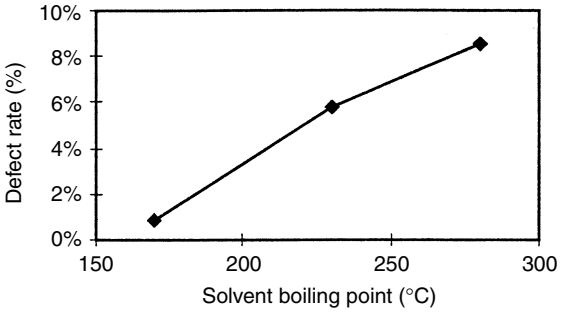

Figure 8.31 Effect of flux solvent boiling point on the defect rate of balling process using Sn63 sphere and printed flux

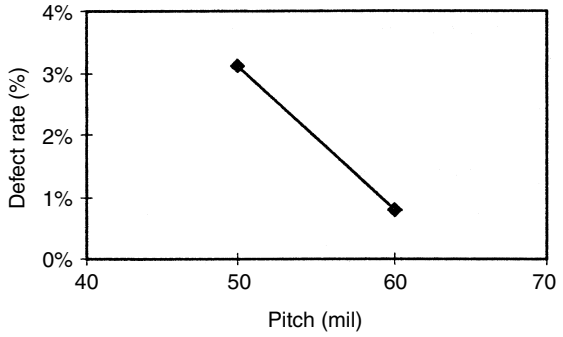

Figure 8.32 Effect of pitch dimension on the defect rate of balling process using Sn63 spheres and printed fluxes, with a pad diameter of 20 mil

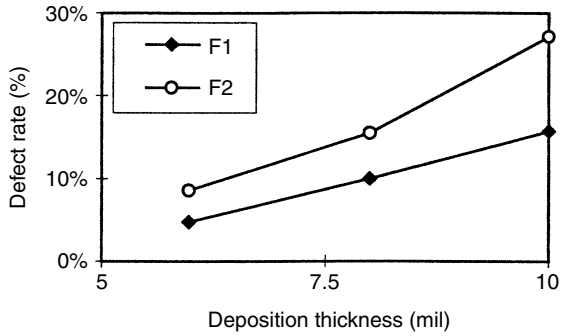

Figure 8.33 Effect of flux deposition thickness on solder bumping defect rate using Sn63 sphere

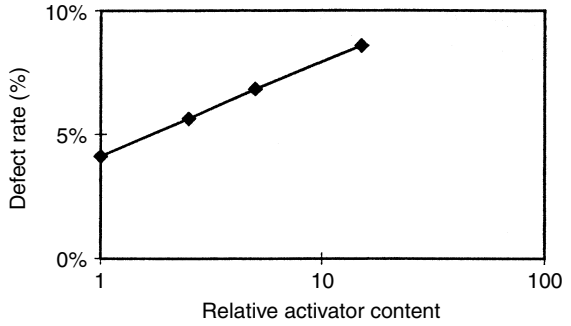

Figure 8.34 Effect of activator content in the flux on the defect of balling using Sn63 sphere

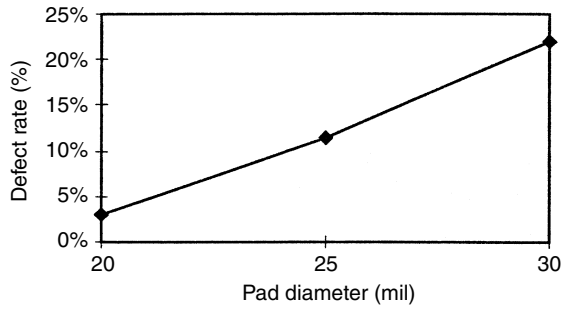

Figure 8.35 Effect of pad dimension on the missing rate of balling process using Sn63 spheres and printed fluxes, with a pitch dimension of 50 mil

can be explained by the surface tension driven, capillary force enhanced barrier effect. The surface tension here refers to that of organic liquid. At reflow, the liquid flux typically wicks and accumulates around the bottom of the sphere through the capillary force. Since the amount of flux printed increases with increasing pad dimension, more flux will accumulate on the bottom of the sphere for large pads. As a result, the barrier effect, which is also observed in the flux deposition thickness experiment mentioned above, for the large pad will be more significant and consequently will result in a higher missing rate.

For systems using pastes for 90Pb/10Sn sphere attachment, no missing rate has been observed, and alignment improves with decreasing paste deposition thickness, as shown in Figure 8.36. This is explained by the solder dome effect. The coalescence of Sn63 solder paste typically occurs sooner than any wetting which is to be developed on other solid metal surface, such as a 90Pb/10Sn sphere. Accordingly, upon reflow, the Sn63 liquid solder dome developed first, followed by wetting between the Sn63 solder and the 90Pb/10Sn sphere. The thicker the paste deposition thickness, the taller the solder dome will be, and the more opportunity the 90Pb/10Sn sphere will

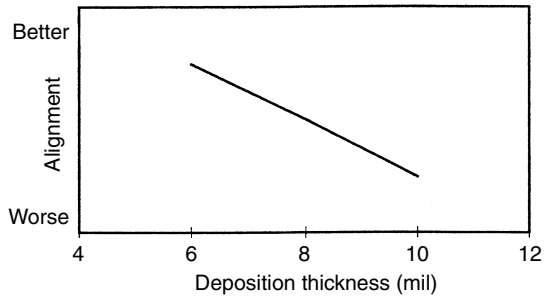

Figure 8.36 Effect of Sn63 solder paste deposition thickness on the 90Pb/10Sn solder ball alignment

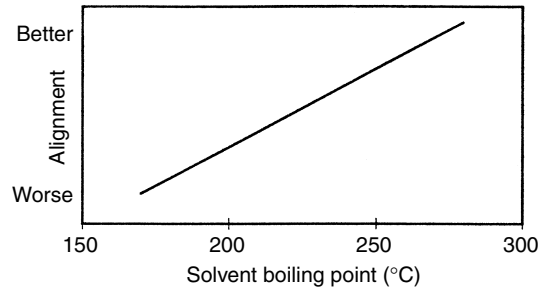

Figure 8.37 Effect of solvent boiling point on the alignment of 90Pb/10Sn spheres soldered with Sn63 solder pastes

have to roll away from the center of the top of the liquid solder dome. The extent of sphere rolling is not enough to cause sphere missing, but will result in misalignment of spheres. Figure 8.27 showed an example of misaligned 90Pb/10Sn spheres attached with Sn63 solder paste.

In contrast to the effect of flux volatility on the Sn63 sphere's missing rate when using flux for sphere mounting, the alignment of a 90Pb/10Sn sphere attachment using Sn63 solder paste is found to improve with increasing solvent boiling point. This relation is demonstrated in Figure 8.37, and can be explained by the viscosity-related wicking effect. Presumably, the higher boiling point of the solvent will allow the flux to remain low in viscosity during reflow. This low viscosity characteristic of flux will facilitate better spreading and a better wicking ability. As a result, the paste will wet better to the 90Pb/10Sn sphere and allow a better self-centering effect on the sphere.

As expected, the defect rate increases with decreasing solderability of 90Pb/10Sn spheres. On the other hand, as shown in Figure 8.38, the alignment of 90Pb/10Sn spheres soldered with Sn63 solder paste increases with increasing flux activity, expressed as a relative activator content. Again, this can be explained by the oxide film removal rate. Fluxes with higher activity remove the 90Pb/10Sn sphere oxide film more quickly. This allows the sphere to be wetted sooner by the molten Sn63 solder, and consequently less chance for the sphere to roll away. Furthermore, a good wetting developed on the 90Pb/10Sn sphere surface is expected to help self-centering of the sphere due to the surface tension driving force of the molten Sn63 solder.

Figure 8.39 shows that large pads display a better Sn10 sphere alignment than small pads. Although the trend is opposite to that of systems using Sn63 spheres and printed fluxes, it can also be explained by a surface tension driven, self-centering force effect. However, the surface tension here refers to that of molten solder. For larger pads, more paste is printed for each sphere attachment. Upon reflow, this results in a larger volume of molten solder which wicks and accumulates around the bottom of the Sn10 sphere. This larger molten solder volume will contribute to a greater surface tension driven, self-centering force, and accordingly result in a better alignment. The alignment of a 90Pb/10Sn sphere is also found to improve with increasing metal load, as shown in Figure 8.40. This similar trend can be explained with the mechanisms described above.

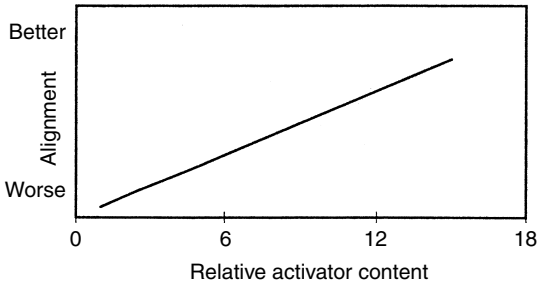

Figure 8.38 Effect of relative activator content on the alignment of 90Pb/10Sn spheres using Sn63 solder paste

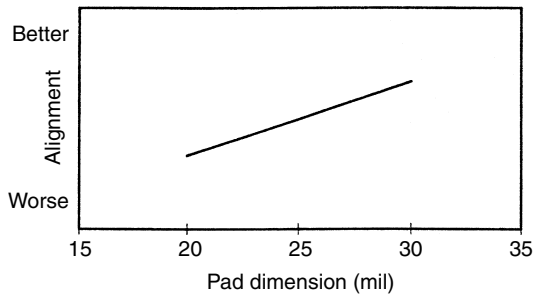

Figure 8.39 Effect of pad dimension on the alignment of 90Pb/10Sn spheres attached with Sn63 solder pastes in the case of 50 mil pitch BGA land pattern design

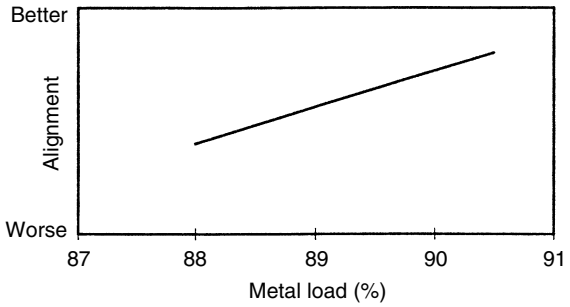

Figure 8.40 Effect of metal load on the alignment of 90Pb/10Sn spheres using Sn63 solder paste for balling process

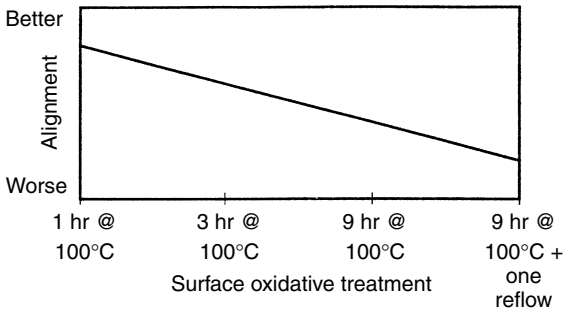

Figure 8.41 Effect of BGA pad solderability on the alignment of 90Pb/10Sn spheres using Sn63 solder paste for the balling process

The pad's solderability can be considered as inversely proportional to the extent of pad surface oxidative treatment. First, no missing rate can be detected during attachment of 90Pb/10Sn spheres. Second, Figure 8.41 shows that the alignment of 90Pb/10Sn spheres attached with a Sn63 solder paste is inversely proportional to the extent of oxidative treatment, or is proportional to the solderability of the BGA pads. Again, this relation can be attributed to the solder dome effect. A poorer pad solderability will result in a taller solder dome initially during the paste coalescence stage. Undoubtedly, this temporary tall solder dome will increase the misalignment of 90Pb/10Sn spheres. Paste viscosity, pitch, and reflow profile have negligible effect on the 90Pb/10Sn bumping yield using Sn63 solder paste. The factors affecting the performance of sphere attachment are summarized in Table 8.2.

Although Chiu and Lee concluded that BGA sphere placement with the use of solder paste produces a higher yield, many packaging houses still use tacky fluxes for BGA ball mounting, mainly due to the more forgiving nature of fluxes on handling, and the difficulty in finding a robust solder paste with very long open time. The tacky fluxes are deposited via pin-transfer process instead of stencil printing process. This is mainly due to sphere drifting problems associated with smeared fluxes caused by the printing process. However, the pin-transfer process becomes questionable when ball size becomes increasingly smaller, due to the fragility of the very fine pins needed for delivering tiny flux dots.

Table 8.2 Effect of various parameters on sphere attachment using fluxes or solder pastes

Parameters	*Defect rate changing trend with increasing parameter value*	
	Sn63 sphere attachment using flux	*Sn10 sphere attachment using Sn63 paste*
Print thickness	Higher	Higher
Flux activity	Higher	Lower
Viscosity	Lower	No effect
Sphere solderability	N/A	Lower
Flux volatility	Lower	Higher
Pitch dimension	Lower	No effect
Pad dimension	Higher	Lower
Pad solderability	No effect	Lower
Reflow profile	No effect	No effect

Voiding Lee and Randle studied voiding mechanisms in BGA at the solder bumping stage using solder sphere placement [29]. Their study includes spheres for both eutectic Sn–Pb and a high temperature 90Pb/10Sn system with the use of real-time X-ray equipment. Figure 8.42 shows examples of voiding in both solder systems.

In the first place, the cross-sectioned solder bumps show that virtually all the voids observed exist at or near the interface of solder and substrate. This is particularly pronounced for systems with Sn62 or Sn63 solder bumps, as shown by the eight pictures displayed in Figure 8.43. The initiation of fume bubbles at the solder/substrate interface is attributed to the fact that the fume comes from the entrapped flux located at the non-wetted spots on the substrate metallization surface. The dominant interface-location for almost all the voids indicates that this is a metastable location for the fume bubbles at reflow. Apparently the buoyancy of the fume bubble is not sufficient to overcome the attachment force between the bubble and the interface. It appears that the bubble needs to grow to a size large enough in

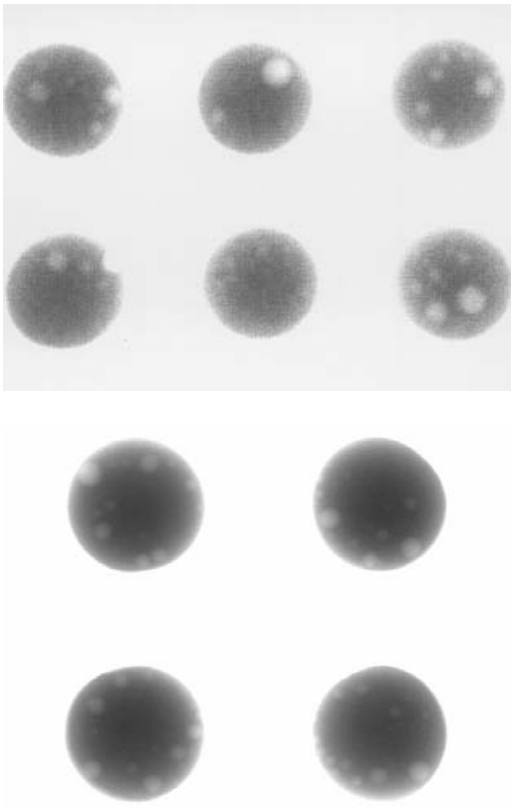

Figure 8.42 Thermal printout of X-ray image of 50 mil pitch solder bumps of BGA: **(a)** Sn63 bumps with voids, **(b)** 90Pb/10Sn bumps with voids

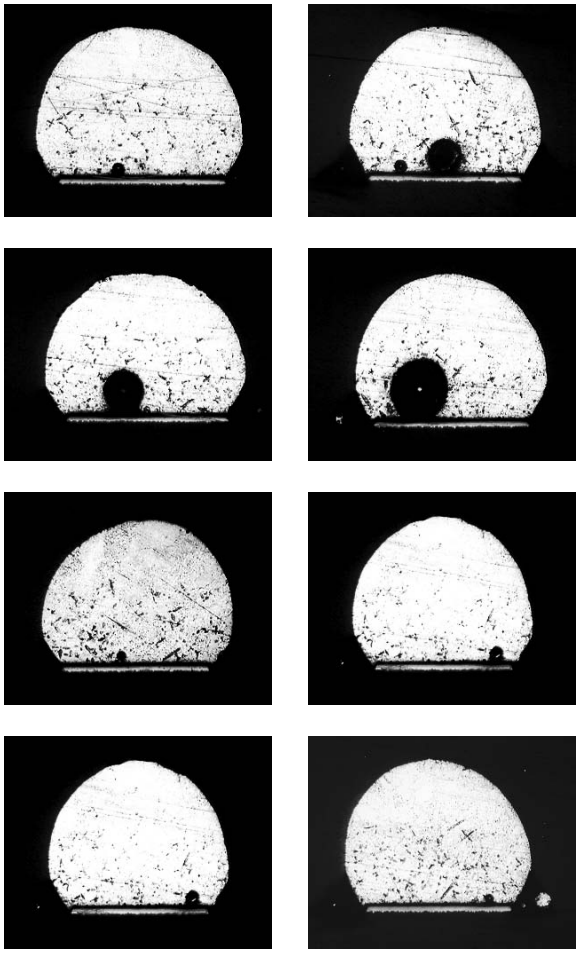

Figure 8.43 Eight examples of cross-sectioned Sn63 solder bump examined with optical microscope. All voids observed located at the solder/substrate interface

order to develop sufficient buoyancy to break away from the solder/substrate interface. Lack of voids observed between the solder/substrate interface and the bump surface indicates that, once the bubble is detached from the interface, it surfaces very quickly and accordingly leaves virtually no voids along the surfacing path.

Forming minimal liquid surface area at bubble surface The attachment force is attributed to the tendency to form a minimal liquid surface area on the bubble's surface. This tendency is driven by surface tension force. With the bubble anchored at the solder/substrate interface, part of the bubble's surface will be formed by the substrate surface, as illustrated in Figure 8.44. The contribution of the substrate surface to the medium/bubble interface reduces the total surface area of molten solder needed for forming the bubble's surface. If the bubble is to be detached from the substrate/bubble interface, more energy will be required in order to generate the additional molten solder surface area to complete the whole bubble surface. This additional energy required serves as an energy barrier and

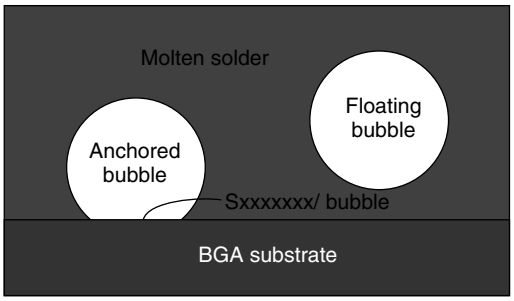

Figure 8.44 Schematic of flux fume bubbles in the molten solder bump during reflow

prohibits the bubble from detachment. The bubble stays at the substrate surface until it grows so large that the buoyancy factor eventually overrides the surface tension factor.

Effect of flux activity The voiding tendency at the solder bumping stage is found to be inversely proportional to the flux activator content. This relationship holds true for BGA systems bumped with either a Sn63 sphere or a 90Pb/10Sn sphere, as shown in Figure 8.45. It has been reported [30–32] that, within the composition range studied, flux activity is proportional to the activator content. By applying that relationship to the results obtained here it can be concluded that voiding decreases with increasing flux activity. This is consistent with the previous study [1,2] and is attributed to the fact that a higher flux activity reduces the possibility of having non-wetted spots on the substrate metallization at soldering. This consequently allows less risk of having flux entrapped at the solder/substrate interface, which in turn results in less risk of voiding.

Effect of sphere alloy type The effect of sphere alloy type on voiding at the bumping stage is studied by comparing the two curves shown in Figure 8.45. Obviously, the Sn63 sphere system is more sensitive to the impact of voiding factors, such as flux activator content, than the 90Pb/10Sn sphere system. Hence, by decreasing the flux activator content, voiding increases rapidly from almost zero to about 5 percent. For the same flux activator content

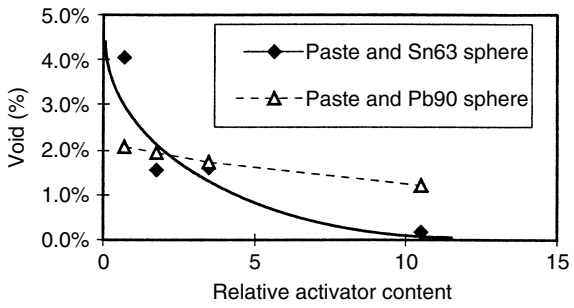

Figure 8.45 Effect of relative activator content on voiding at solder bumping stage for both Sn63 and 90Pb/10Sn sphere systems

reduction conditions, the voiding of a 90Pb/10Sn sphere system increases only moderately from 1.5% to 2.1%. It is interesting to note that, at low voiding (such as systems with a high activator content), a 90Pb/10Sn sphere results in higher voiding than an eutectic Sn–Pb sphere. However, at high voiding (such as systems with a low activator content), the eutectic Sn–Pb sphere results in higher voiding than a 90Pb/10Sn sphere.

These X-ray image analysis data are consistent with observations on the cross-sectioned samples, as demonstrated by the high voiding rate systems. In these systems, both the 90Pb/10Sn and the Sn63 spheres are mounted with Sn63 solder paste using a very low flux activator content. Figure 8.29 showed the scanning electron microscope picture of a 90Pb/10Sn solder bump with large voids. Comparing this with the large voids found in a Sn63 bump system (see Figure 8.43), the voids in a 90Pb/10Sn bump are considerably smaller. The complicated relationship between alloy type and voiding rate can be attributed to the results of two major effects: (1) sandwich, and (2) radius of curvature.

Sandwich effect For Sn63 bump systems, the bubbles can escape easily from the molten solder by surfacing through the top. For 90Pb/10Sn bump systems, as shown in Figure 8.29, the molten solder Sn63 is sandwiched between the solid 90Pb/10Sn sphere and the BGA pad at the bumping stage. In this figure, the light color phase is the Pb-rich phase, and the dark color phase is the Sn-rich phase. Any bubbles generated during reflow have to travel to the side edge in order to escape from the molten solder. This limited escape path naturally results in a higher voiding rate for 90Pb/10Sn bump systems. This is consistent with the previous findings that the larger the coverage area for a sandwiched joint, the more voiding there will be [30]. Furthermore, for 90Pb/10Sn bump systems, some Pb dissolves in the molten solder Sn63 and forms many solid, discrete Pb-rich particulates, especially around the surface of a 90Pb/10Sn sphere. These Pb-rich particulates hinder the traveling of bubbles and serve as traps for the bubbles, hence enhancing the sandwich effect, as shown in Figure 8.29(b).

The sandwich effect explains the phenomenon that the 90Pb/10Sn systems exhibit more voiding than eutectic Sn–Pb systems when the voiding rate is low and voids are small. However, when the voiding rate is high and voids are large, 90Pb/10Sn systems exhibit less voiding than eutectic Sn–Pb systems. This can be explained by the radius of curvature effect, as discussed below.

Radius of curvature effect For a curved surface, any point on the surface can be specified by two principal radii of curvature, as shown in Figure 8.46. R_1 is the radius of curvature in the plane of the paper and R_2 is the radius of curvature perpendicular to the plane of the paper.

For eutectic sphere systems (see Figure 8.43), the sphere and solder paste melt and coalesce to form one large integral piece of molten solder bump during reflow (see Figure 8.47(a)). For 90Pb/10Sn sphere systems (see Figure 8.29(a)), the sphere remains solid and only the small amount of Sn63 solder from the solder paste melts during reflow (see Figure 8.47(c)). The almost vertical contour line of the Sn63 solder indicates that the molten solder has a very large radius of curvature.

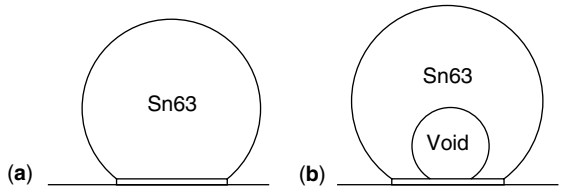

Figure 8.46 Schematic drawing for the effect of bubble on the shape of molten solder for **(a)** Sn63 bump, and **(b)** Sn63 bump with void

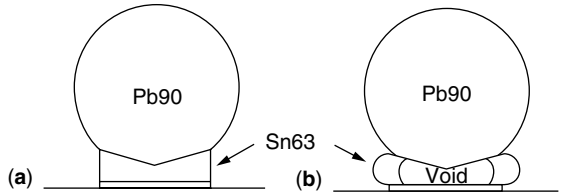

Figure 8.47 Schematic drawing for the effect of bubble on the shape of molten solder for **(a)** 90Pb/10Sn bump, and **(b)** 90Pb/10Sn bump with the same size of void as Figure 8.46(b)

For systems with a large volume of molten solder (see Figure 8.47(a)), forming a large void within the molten solder (Figure 8.47(b)) has a negligible effect on the radius of curvature. However, for a sandwiched system with a small volume of molten solder (Figure 8.47(c)), forming a large void within the molten solder will force the solder to bulge out to accommodate the void inside the solder (see Figure 8.47(d)). This will result in a small radius of curvature.

The effect of radius of curvature on the void stability can be revealed by

$$\Delta P = \gamma \left(\frac{1}{R_1} + \frac{1}{R_2} \right) \tag{8.1}$$

Equation (8.1) describes the pressure difference across a curved interface (ΔP) in terms of the surface tension of the interface (γ) and the two principal radii of curvature at a point on the surface [33]. Therefore, a smaller radius of curvature (see Figure 8.47(d)) represents a greater hydraulic pressure exerted on the void within the molten solder, and accordingly will compress the void to a smaller size until a new pressure equilibrium is established. In other words, in the same outgassing rate condition, the systems with a sandwiched small volume molten solder will have a small stable void.

The radius of curvature effect is negligible when the void is small. However, when the void is large, as shown in Figures 8.47(b) and 8.47(d), the effect becomes the dominant factor, and Figure 8.47(d) shows a much greater pressure resistance against large void formation and accordingly explains the lower voiding rate observed in 90Pb/10Sn systems than in Sn63 systems.

The sandwich effect is reported to be proportional to the coverage area [30]. Since the coverage area in 90Pb/10Sn bump systems is determined by the size of a 90Pb/10Sn sphere, this effect is expected to be constant in this study, regardless of void size. On the other hand, the radius of curvature effect is expected to be a strong function of void size. The larger the potential void, the greater the difference in radius of curvature between the two alloy systems, and consequently the greater the difference in the stable void size resulting from the two alloy systems. This means a more rapidly increasing voiding rate and void size for eutectic Sn–Pb bump systems than for 90Pb/10Sn bump systems. The relative contribution of the two effects versus void size can be qualitatively expressed by Figure 8.48.

Effect of pad dimension The effect of pad dimension on voiding is reflected in Figure 8.49 for systems using Sn63 sphere and paste for bumping. Results indicate that the voiding increases with increasing pad dimension. Presumably, this can be attributed to two factors. The first is the radius of curvature effect. Since the sphere used is constant in diameter, the resultant bump will have an increasing radius of curvature with an increase in pad dimension, as shown in Figure 8.50. This increase results in a larger void size due to a smaller hydraulic pressure exerted on the void, as discussed above. The second is the probability factor. Assuming the outgassing rate per unit area of pad is constant at soldering, the larger the pad dimension, the higher the outgassing frequency per pad will be, and the greater number of voids can be obtained per pad.

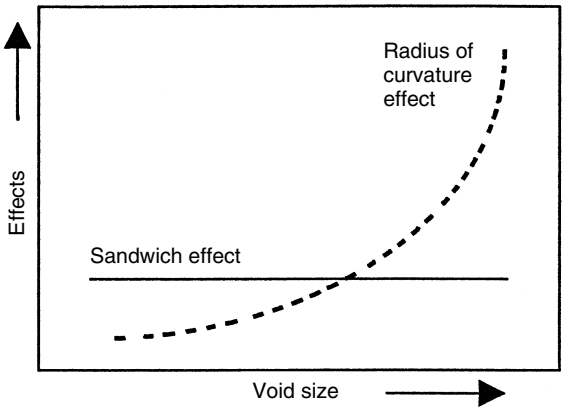

Figure 8.48 Relative contribution of sandwich effect and radius of curvature effect versus void size

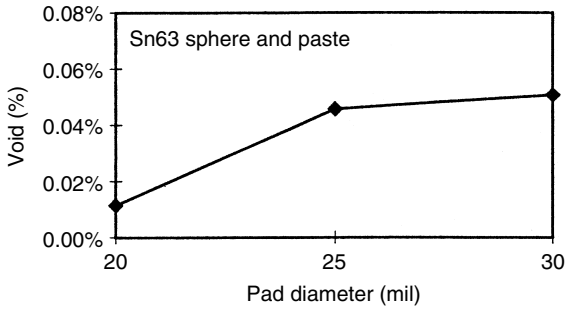

Figure 8.49 Effect of pad dimension on void content

Effect of deposition thickness The effect of deposition thickness on voiding is investigated for systems using flux and a Sn63 sphere for bumping, with results shown in Figure 8.51. Data indicate that the thicker the print deposition, the less the voiding will be. This can be explained by the fact that the thicker print provides a higher flux capacity to eliminate oxides, and consequently results in less voiding.

Effect of viscosity Two systems are studied for the effect of viscosity: Sn63 sphere bumping with flux (see Figure 8.52) and Sn63 sphere bumping with a Sn63 solder paste (see Figure 8.53). The results indicate that a higher viscosity provides a lower voiding rate. The higher viscosity is a result of higher rosin content in the flux. Since systems with a higher rosin content normally provide a better wetting, it is believed that the lower voiding is actually a result of better wetting [30],

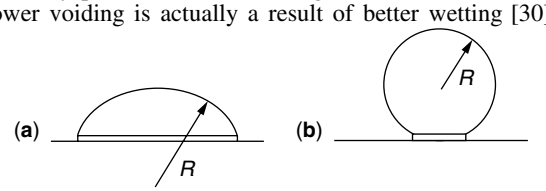

Figure 8.50 Schematic of solder bumps with the same bump volume but various pad dimension. Larger pad **(a)** results in a solder bump with a greater radius of curvature *R*

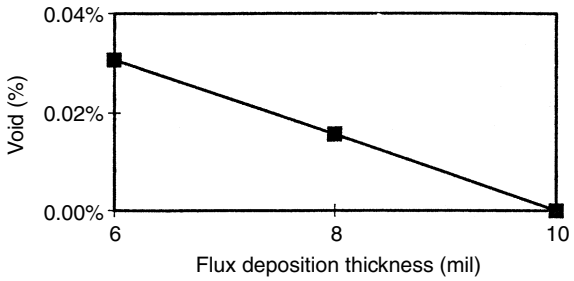

Figure 8.51 Effect of flux deposition thickness on voiding

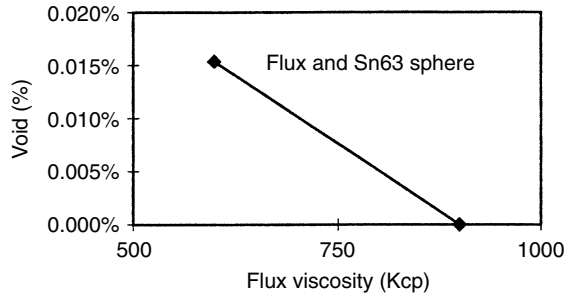

Figure 8.52 Relation between flux viscosity and voiding

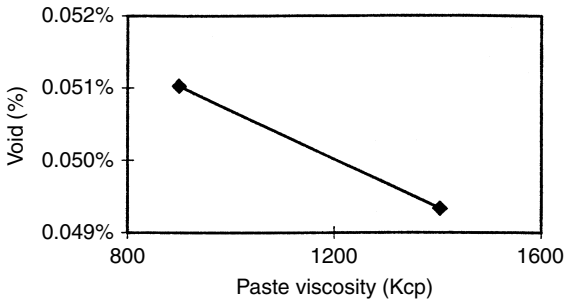

Figure 8.53 Relation between paste viscosity and voiding

as discussed in the previous section, instead of higher viscosity.

Effect of sphere oxide level The oxidation treatment of a sphere is conducted by tumbling the spheres in a semi-open container in an ambient environment for a specified period. The surfaces of the spheres darken with increasing tumbling, reflecting an increase in the oxide level. These oxidized spheres are then used for solder bumping. Results show that, in general, voiding increases with increasing sphere oxide level, or increasing amounts of oxidation time (tumbling time), as shown in Figure 8.54. This is attributed to the increasing risk of having flux entrapped in the molten solder and serving as an outgassing source, which directly results in voiding. The larger the amount of oxide on the sphere, the more risk of having some oxide remaining uncleaned by the flux during soldering, and accordingly of having some flux anchored to the oxide surface and serving as an outgassing source.

This effect is very pronounced for the 90Pb/10Sn bump systems, but is only barely discernible for the Sn63 bump systems. This is attributed to the effect of mobility of sphere oxide during reflow. For the low melting point Sn63 sphere systems, the oxide on the sphere's surface is mobilized during reflow and can be excluded from the interior of molten solder due to surface tension driving force. This will greatly reduce the risk of having some anchored flux entrapped in the molten solder and contributing to voiding. In other words, the oxide level for the Sn63 sphere has a negligible effect on voiding. However, for the high melting point 90Pb/10Sn sphere systems, the oxide on the sphere's surface is immobilized. Therefore, any uncleaned sphere oxide will serve as an anchoring site for the flux and will result in more outgassing from the entrapped flux. The impact of this immobilized 90Pb/10Sn sphere oxide is further enhanced by the sandwich effect, as discussed above.

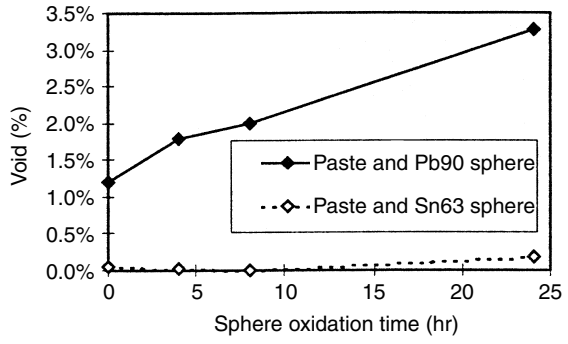

Figure 8.54 Effect of sphere oxide level on voiding

Effect of pad oxide level The pad oxide level is regulated by subjecting the BGA substrates to (1) OSP coating stripping, followed by (2) various heat treatments, as shown in Table 8.3. The effect of pad oxidation level on voiding is demonstrated by systems bumped with Sn63 solder paste and 90Pb/10Sn spheres, as illustrated in Figure 8.55. Voiding increases with increasing pad oxidation level. The mechanism of this has been discussed in the previous section, and is attributed to the increasing risk of having some flux entrapped on the non-wetted pad surface, and accordingly an increased possibility of outgassing.

Effect of metal load The voiding rate is found to increase with increasing metal load, as shown in Figure 8.56. This is attributed to the higher metal oxide content associated with the larger powder surface area. This oxide factor has been discussed in the previous sections, and is consistent with previously reported studies of voiding in SMT [30] and BGA assembly [31].

Effect of reflow profile The impact of reflow profile on voiding is investigated by varying the reflow profile length for systems bumped with Sn63 sphere and solder paste. Results (see Figure 8.57) indicate that voiding increases with increasing reflow profile length. This can probably be attributed to two factors. The first is the viscosity-dictated-flux-exclusion-rate-factor, which has been reported previously [31]. A longer reflow profile dries out the flux

Table 8.3 Heat history for various pad oxidation levels

Pad oxidation level	*Heat treatment*
1	100 °C/1 hr
2	100 °C/3 hr
3	100 °C/9 hr
4	100 °C/9 hr + 1 reflow

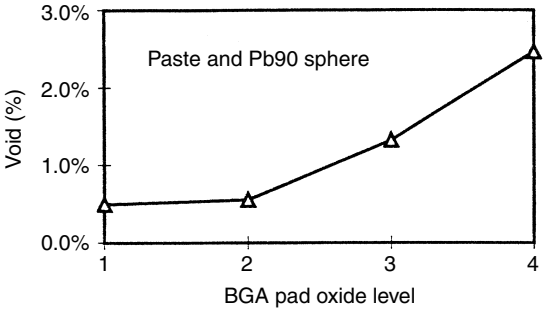

Figure 8.55 Effect of pad oxide level on voiding

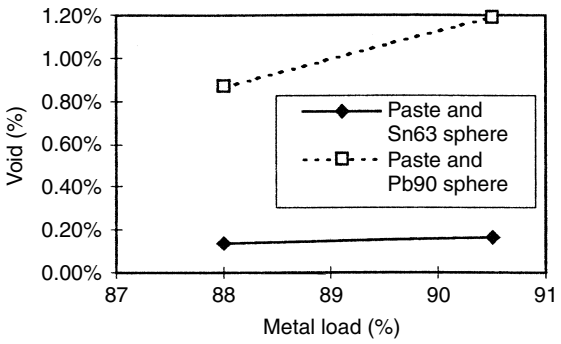

Figure 8.56 Effect of metal load on voiding

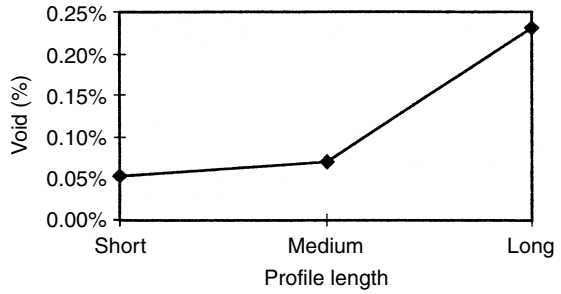

Figure 8.57 Effect of reflow profile length on voiding

volatiles more thoroughly during the reflow stage. This leaves a flux remnant with higher viscosity which is more difficult to be excluded from the interior of the molten solder. As a result, a higher voiding rate is observed. The second factor is oxidation. Reflow under air with a longer profile typically results in a greater extent of oxidation of the materials. This is expected to result in more voiding, as discussed in the previous sections.

Effect of flux volatility The effect of flux volatility is regulated by varying the solvent boiling point of the fluxes. The impact of the volatility is studied by comparing the average of the voiding rate of all the samples using the same solvent type. Results indicate that there is virtually no correlation between the flux volatility and voiding, as shown in Figure 8.58.

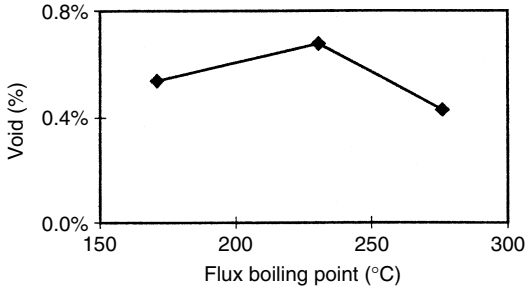

Figure 8.58 Averaged effect of flux volatility on voiding for all samples

Voiding summary Voiding in BGA at the 63Sn/37Pb solder bumping stage typically occurs at the interface of eutectic solder and the BGA pad, due to the tendency to form a minimal molten solder surface area at bubble surface. At low voiding levels, 90Pb/10Sn bump systems exhibit more voiding than eutectic Sn−Pb bump systems, due primarily to the sandwich effect which entraps fume bubbles for 90Pb/10Sn systems. However, at high voiding level, 90Pb/10Sn bump systems exhibit less voiding than eutectic Sn−Pb bump systems, due to the radius of curvature effect which compresses the bubble size of 90Pb/10Sn bump systems. In general, voiding in BGA at solder bumping stage increases with decreasing flux activity, decreasing flux or paste deposition thickness, increasing oxide level of spheres or pads, increasing pad dimension, increasing reflow profile length, and increasing metal content. The sphere oxide effect is more pronounced for 90Pb/10Sn bump systems than for eutectic Sn−Pb bump systems, due to the immobilized oxide for the former systems as well as the sandwich effect. Voiding also increases with decreasing flux/paste viscosity, presumably due to a decrease in the flux capacity. No correlation can be identified between voiding and flux volatility [29].

8.2.3.7 Fluxless solder sphere bumping

Ramos [16] has reported a fluxless solder sphere bumping process. Here, the BGA package is placed between a graphite carrier plate and a graphite alignment plate. After the spheres have been loaded into the cavity of alignment plate, the setup is secured with a handling frame, as shown in Figure 8.59. Then an electrical current is passed through the graphite, to heat up the device and to make the solder balls reflowed and wetted onto the BGA pads. The captured solder balls are aligned with the pads of the BGA package and the walls of the alignment plate holes prevent the balls from moving during processing.

8.2.3.8 Integrated preform

The integrated preform is a patterned solder preform, as shown in Figure 8.60. The patterned preform has a sub-preform corresponding to each pad of the BGA land pattern, and all neighboring sub-preforms are interconnected by a thin solder link. Bumping with an integrated preform can be achieved by placing the integrated preform on top of either flux or solder paste printed onto the BGA substrates. This approach has been reported by the Indium Corporation of America [17] to be promising. Reducing the thickness and width of the solder link is considered essential for achieving a high bumping success rate. In addition to alloy link matrices other preform designs include designs such as the SolderQuick™ paper matrix which has 63Sn/37Pb spheres integrated into a paper matrix placed on the top of the designated BGA component, as shown in Figure 8.61. The entire design is then reflowed. The final stages include the removal of the paper matrix by utilizing a DI water bath to both dissolve and remove the unwanted paper fixture. The method has been successful for components with I/Os exceeding 700 [18].

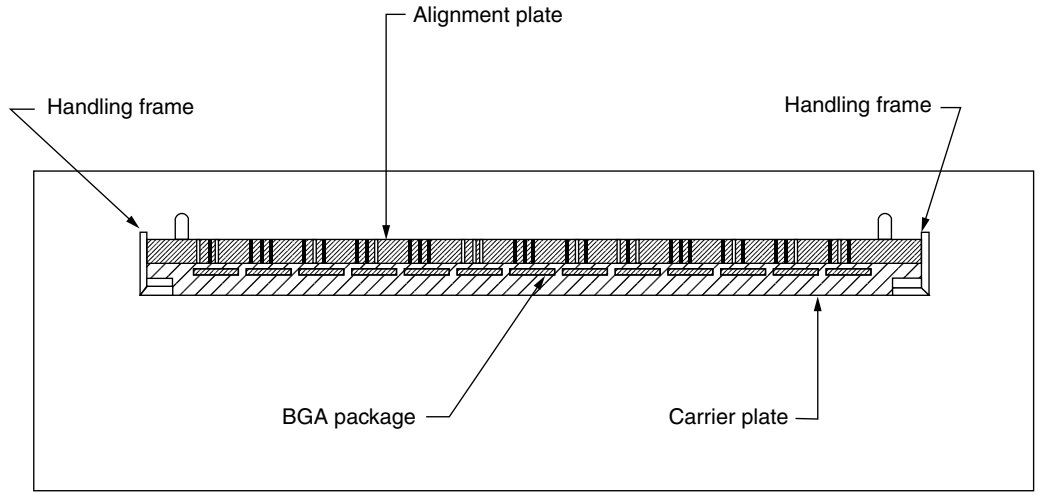

Figure 8.59 Loaded handling frame cross-sectioned in the plane for a fluxless solder sphere bumping process. The captured solder balls are perfectly aligned with the pads of the BGA package. The walls of the alignment plate holes prevent the balls from moving during processing [16]

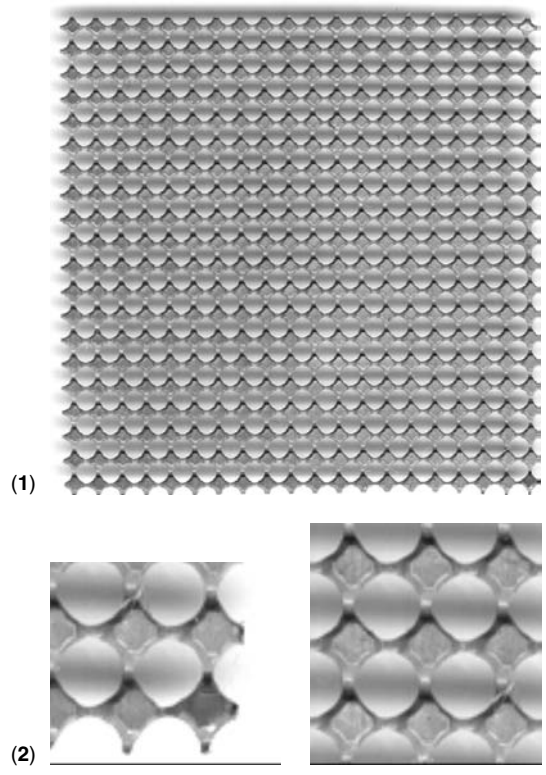

Figure 8.60 Integrated preform: **(1)** overall view, **(2)** close-up of corner (*left)* and center (*right*) of integrated preform

8.2.4 Solder paste bumping

Solder bumping can also be accomplished with the use of solder paste alone. This approach becomes increasingly attractive when the area array packaging becomes further miniaturized, therefore the solder bumps become increasingly smaller. This is due mainly to both cost and throughput considerations.

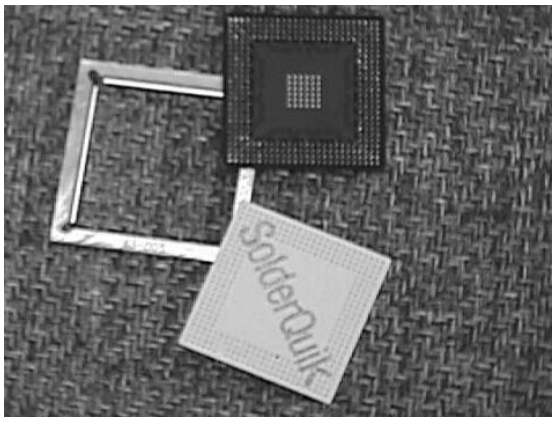

Figure 8.61 SolderQuick^{TM} Integrated preform system

With the use of the sphere transfer approach, since the cost of the sphere remains the same regardless of sphere size, the cost per bump is accordingly constant, regardless of bump size. Conversely, the cost of solder paste is determined by its volume. Therefore, with decreasing bump size, the cost per solder bump will reduce significantly when employing the solder paste bumping approach. Figure 8.62 shows a comparison of solder materials cost for processes using sphere placement versus paste bumping. At bump sizes below 30 mils (0.75 mm) diameter, the paste bumping cost becomes increasingly favorable with further decrease in bump size.

In the case of wafer bumping, with the use of the solder evaporation or plating process, the cost per bump is even higher. As mentioned in section 8.2.2.2, the cost of the electroplating process is about $50–100/wafer, or

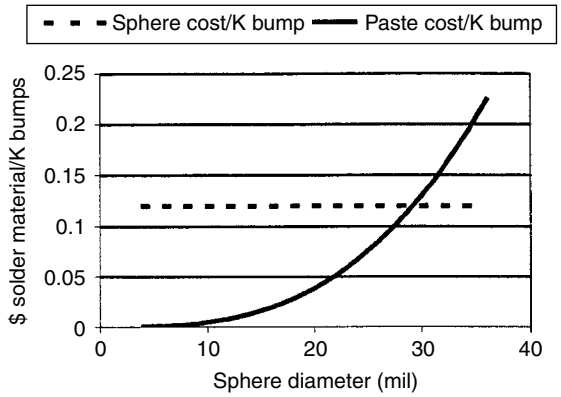

Figure 8.62 Comparison of solder materials cost using solder paste versus sphere placement for producing 1000 solder bumps. The solder paste bumping process becomes advantageous at bump sizes below 30 mil diameter

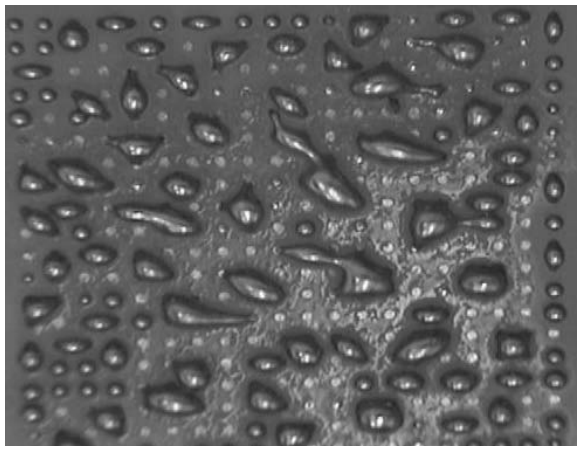

Figure 8.63 Massive bridging caused by slumping and the resultant solder robbing during the 63Sn/37Pb paste bumping process. The procedure used is print-detach stencil-reflow

$75/wafer on average. Assuming a wafer size of 8 in. diameter, patterned with full area array dies each loaded with 10 mil pitch bumps, the cost of electroplating solder bumping is about $0.26/1000 bumps. For the solder paste bumping process, the cost of solder paste for 10 mil pitch bumps will be less than $0.001/1000 bumps. Obviously this is more than two orders of magnitude lower than the electroplating process.

Throughput is another major consideration. The sphere placement process is sequential and is typically limited to one chip per placement. The electroplating process involves multiple time-consuming steps, as depicted in Figure 8.4, therefore it is even lower in throughput. On the other hand, solder paste bumping is a very high throughput process. With one printing stroke, it is possible to deposit solder pastes onto hundreds of BGA or CSP packages or multiple wafers. Although the exact throughput of paste bumping depends on the detailed approaches chosen, the overall throughput is considered to be much higher than all other processes. Processes of solder paste bumping include print-detach-reflow, print-reflow-detach, and dispense.

8.2.4.1 Print-detach-reflow

Solder paste printing is considered a viable low cost bumping process [15,19–26]. The most desirable procedure is similar to the conventional surface mount process: print, detach the stencil, then reflow. It offers the greatest potential to cut bumping costs markedly. However, in order to deliver sufficient solder volume to form an adequate bump height, the stencil aperture must be much larger than the pad dimension. This will be fine for peripheral pad design or staggered pad patterning. In both cases, an overprint can be tolerated without causing problems.

However, for full area array designs, the slumping of the overprinted solder paste will result in solder robbing at reflow, and consequently uneven solder bump size. Figure 8.63 shows an example of massive bridging due to slump and solder robbing when using the print-detach-reflow process. The appropriate solder volume can also be achieved using a thick stencil instead of a large aperture. The potential problem here is typically poor paste release from the stencil aperture. Therefore, an easily releasable solder paste is crucial for area-array BGA processes if a regular print-release process is desired for bumping with solder paste alone. In addition, the paste has to have minimal slump performance in order to avoid solder robbing.

Furthermore, the solder should wet to the pad quickly during coalescence so that the molten solder bead will not drift away from the pad. In general, it has been found that a pre-bake treatment, for instance, 100 °C for 10 minutes in a forced air convection oven prior to reflow, is very helpful in reducing the bumping defect rate. After pre-bake, running the paste through a profile with a long and hot soaking zone, for example, 175 °C for 2.5 minutes, also helps reduce the defect rate. Presumably this can promote diffusion between the base metal and solder powder, and consequently allow the solder paste glob to anchor to the pad better, minimizing drift of the paste glob during spiking. BGA solder bumping with this process has been reported to be successful for pitches of 1.0 and 1.5 mm [26].

Reducing pitch will necessitate the use of a finer solder powder. Although 25–45 μ powder size is adequate for BGA solder bumping, a powder size less than 25 μ is desired for wafer bumping. The excessive oxide caused by the large surface area of solder powder requires a flux with a high capacity to prevent void formation. Results from the Fraunhofer Institute [25] for wafer bumping using solder paste with a powder size 15–25 μ showed a bump height of 125–150 μ (standard deviation 4.5–5 μ) achieved for 300 μ pitch device, and 80–115 μ (standard deviation 5–5.5 μ) bump height for 200 μ pitch devices.

Figure 8.64 shows the four stages of the solder paste bumping process for wafer [24]. Figure 8.65 shows the solder bump height distribution for a 4-in. wafer bumped with the solder paste reflow process [24]. The bumping process has been advanced to the level that the quality and consistency are virtually ready for production applications. Thus, Huang and Lee [23] have reported successful solder

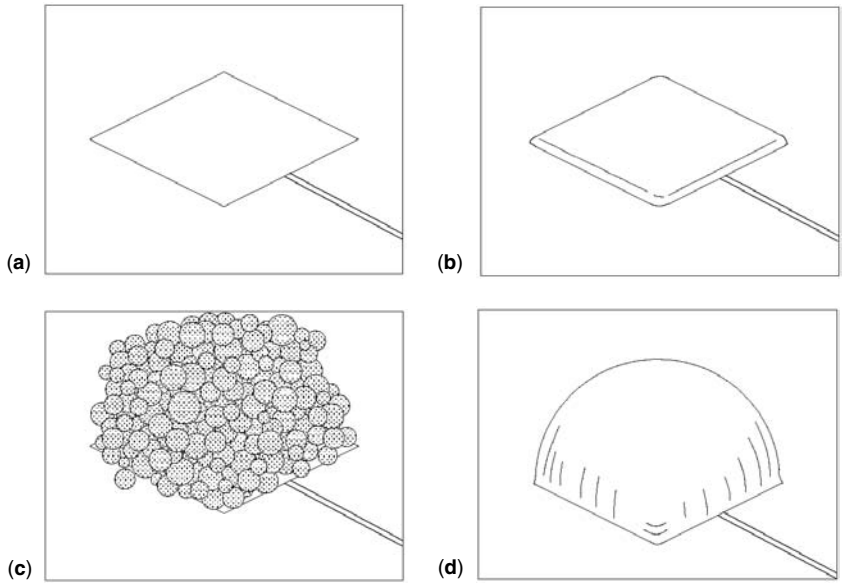

Figure 8.64 SEM pictures of solder bumping steps: **(a)** bond pad in initial state, **(b)** with Ni/Au UBM, **(c)** with printed solder paste and **(d)** after solder reflow [24]

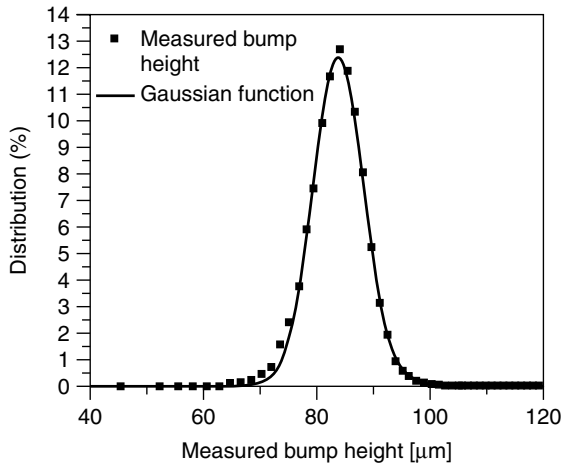

Figure 8.65 Solder bump height distribution when using solder paste for 4-in. wafer bumping process [24]

paste bumping results for BGA, CSP, and wafer. The first critical factor in this success is the satisfactory release of solder paste during the printing stage. Figure 8.66 demonstrate the print quality for solder paste using a 16 mil stencil with a 50 mil pitch BGA pattern. The aperture is 47 mil square. Figure 8.66(a) shows the overall view of the print, while Figure 8.66(b) is a close-up view of the print quality. A similar print quality is also achieved for CSP and wafer bumping applications, as demonstrated in Figures 8.67 and 8.68, respectively.

The second critical factor is good wetting and non-slumping. The Indium Corporation of America has reported the first successful development of paste bumping

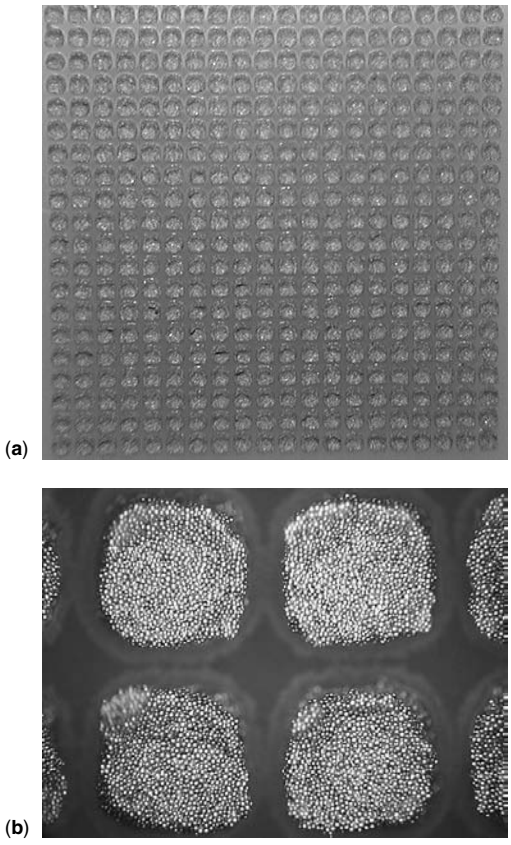

Figure 8.66 63Sn/37Pb solder paste with 25–45 μ particle size printed using a 16 mil stencil with a 50 mil pitch BGA pattern. The aperture is 47 mil square. **(a)** The overall view of the print, **(b)** a close-up of the print quality

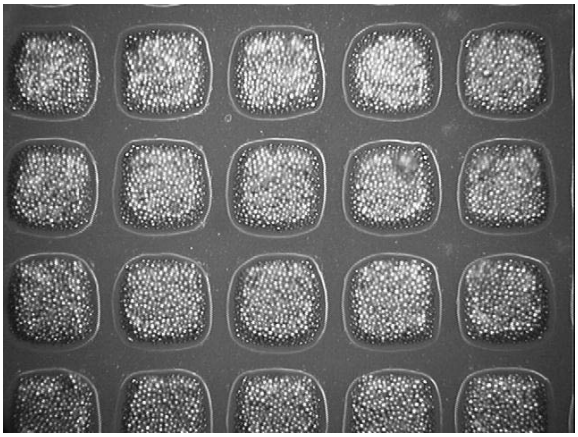

Figure 8.67 A close-up view of 63Sn/37Pb solder paste with particle size 25–45 μ printed for CSP solder bumping. The stencil used is 9 mil thick with 20 mil pitch pattern. The tapered aperture is 12 mil and 15 mil for the squeegee side and board side, respectively

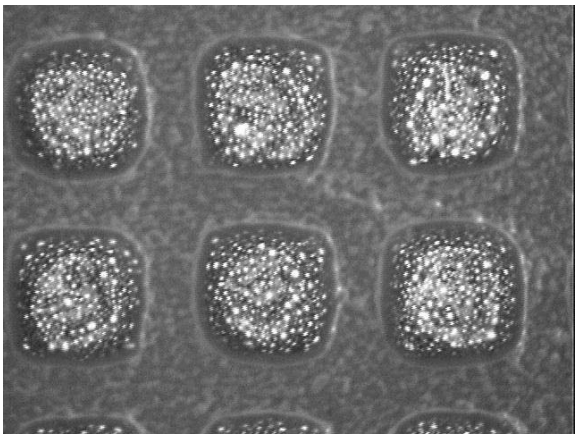

Figure 8.68 A close-up view of 63Sn/37Pb solder paste with a particle size smaller than 20 μ printed for wafer solder bumping. The stencil used is 3 mil thick with 10 mil pitch pattern. The tapered aperture is 5.5 mil and 7 mil for the squeegee side and board side, respectively

materials and processes via the print-detach-reflow process for area array packages including BGA, CSP, and wafer [23]. Figure 8.69 shows an array of 63Sn/37Pb solder bumps processed with solder paste print-detach-reflow for a 50 mil pitch BGA and bump height distribution. Figure 8.70 illustrates the SEM of an array of 63Sn/37Pb solder bumps processed with solder paste print-detach-reflow for a 20 mil pitch CSP and bump height distribution. Figure 8.71 shows the SEM of an array of 63Sn/37Pb solder bumps processed with solder paste print-detach-reflow for a 10 mil pitch wafer and bump height distribution [23]. Cross-sectional views of those solder bumps are shown in Figures 8.72–8.74 for BGA, CSP, and wafer, respectively [23]. In general, those bumps present a fairly normal microstructure compared with bumps produced

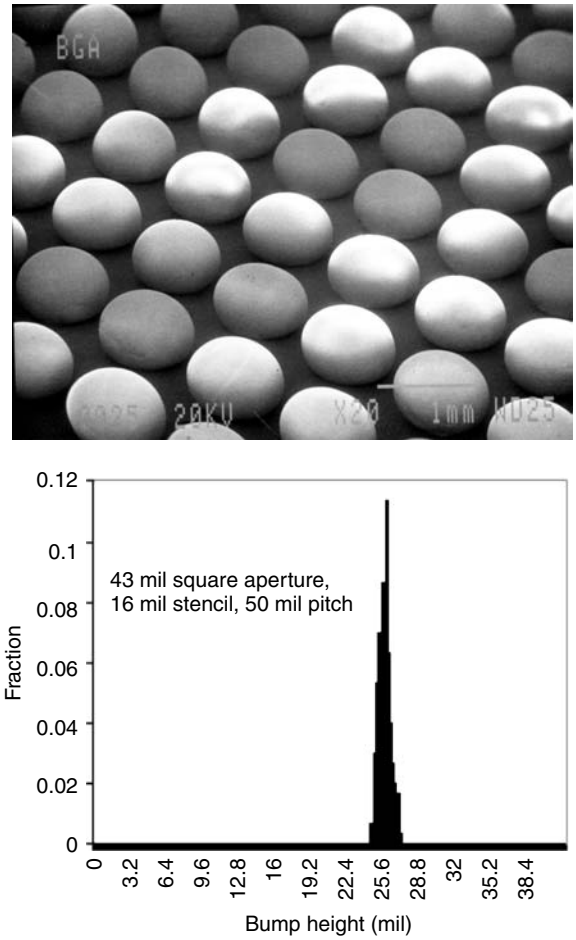

Figure 8.69 SEM of array of 63Sn/37Pb solder bump processed with solder paste print-detach-reflow for a 50 mil pitch BGA. Also shown is the bump height distribution [23]

by sphere placement or other existing wafer bumping processes.

If not formulated and processed properly, voiding may still be an issue with the solder paste bumping process. Figure 8.75(top) shows a cross-section of a void in a 63Sn/37Pb solder bump on CSP. The bump is formed with a solder paste print-detach-reflow process. For wafer bumping applications, extra attention should be paid to the voiding issue due to the extremely fine solder powder used. Figure 8.75(bottom) is an example of voiding in a wafer solder bump formed with solder paste.

Stencil design is a very critical part of the paste bumping process. Always maximizing the opening and minimizing the stencil thickness should be the rule to be applied to stencil pattern design for paste bumping purposes. Figure 8.76 shows an example of a stencil used in a successful 50 mil pitch BGA paste bumping process [23]. This electroformed stencil has an aperture width of 47 mil, with 3 mil spacing and 16 mil thickness.

Overall, solder paste bumping via the print-detach-reflow process is considered the most attractive low cost

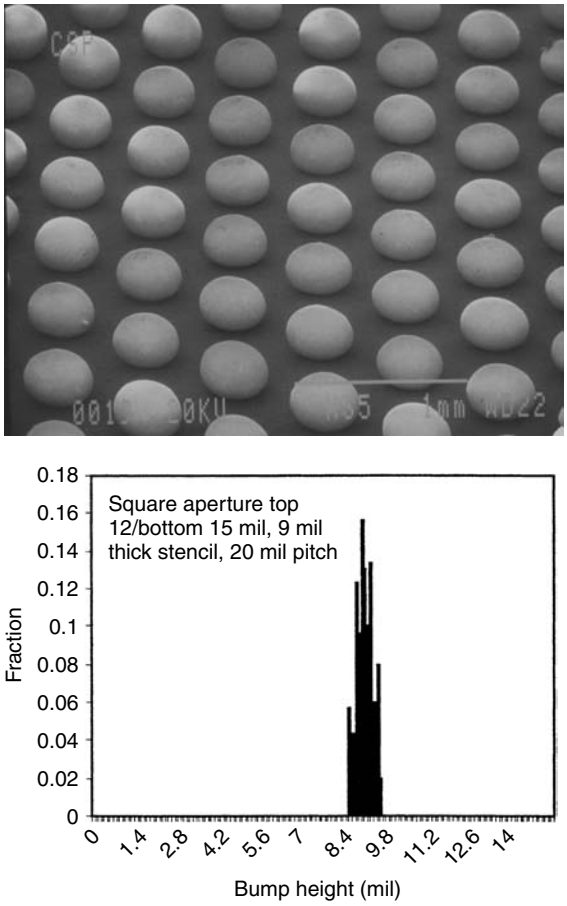

Figure 8.70 SEM of array of 63Sn/37Pb solder bump processed with solder paste print-detach-reflow for a 20 mil pitch CSP. Also shown is the bump height distribution [23]

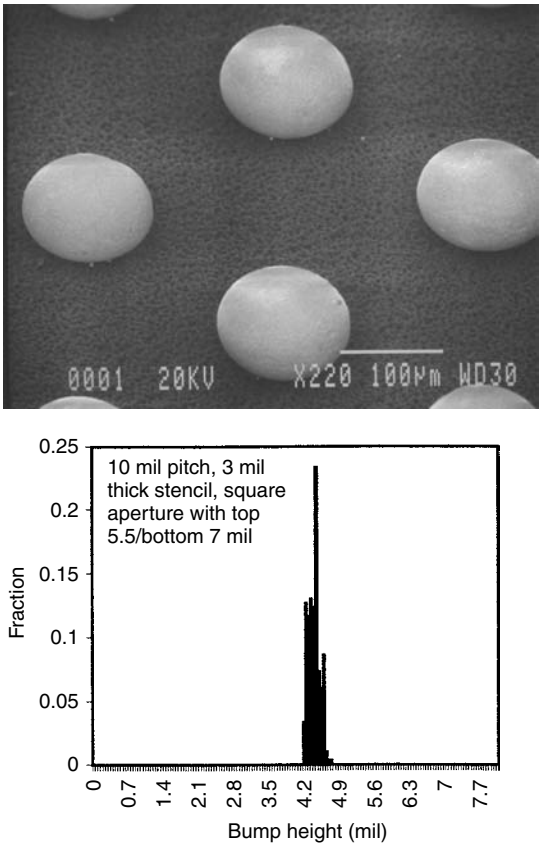

Figure 8.71 SEM of array of 63Sn/37Pb solder bump processed with solder paste print-detach-reflow for a 10 mil pitch wafer. Also shown is the bump height distribution [23]

and high throughput option for area array packages. Today, this process is almost ready for production implementation.

8.2.4.2 Print-reflow-detach

The second alternative involves printing the paste onto the area array packaging with the use of a metal stencil, then reflowing the solder paste with the stencil left on, and then the removal of the stencil, followed by cleaning. This process does not require very stringent stencil release and non-slump performance of the solder paste. However, additional sets of stencils as well as stencil-securing fixtures and stencil cleaning steps add to the cost of this process. In addition, the solder bumps formed may tilt toward one side in some cases. Tilted solder bumps are caused by surface tension. At reflow, the flux may wick up one corner between the aperture wall and the molten solder bump, due to its tendency to form a minimal exposed surface area. Meanwhile, the molten solder attempts to minimize the exposed surface area by maximizing the interface area between flux and solder. As a result, the molten solder dome will tilt toward the flux-rich corner

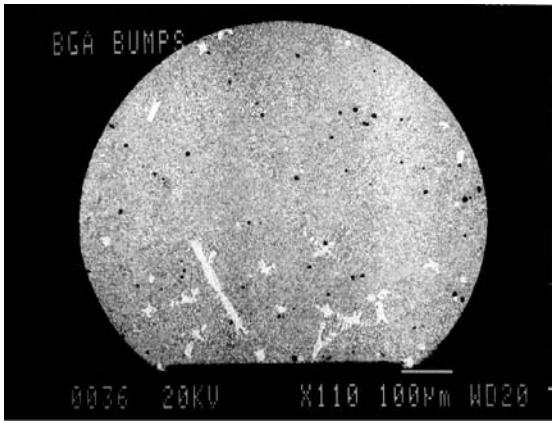

Figure 8.72 SEM of cross-section of BGA solder bump manufactured with 63Sn/37Pb solder paste via the print-detach-reflow process [23]

in the aperture well, and consequently solidify into a tilted solder bump. This bump can be corrected by reflowing the solder again with the presence of flux after removal of the stencil.

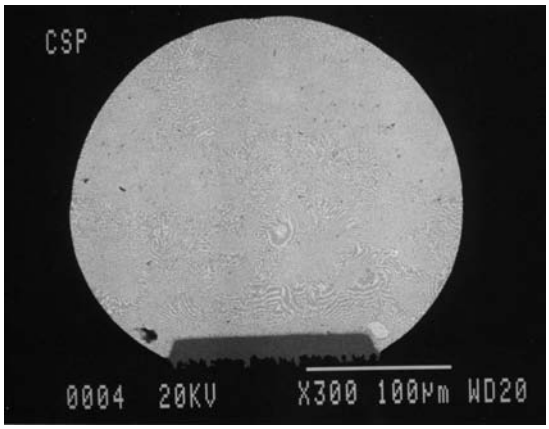

Figure 8.73 SEM of cross-section of CSP solder bump manufactured with 63Sn/37Pb solder paste via the print-detach-reflow process [23]

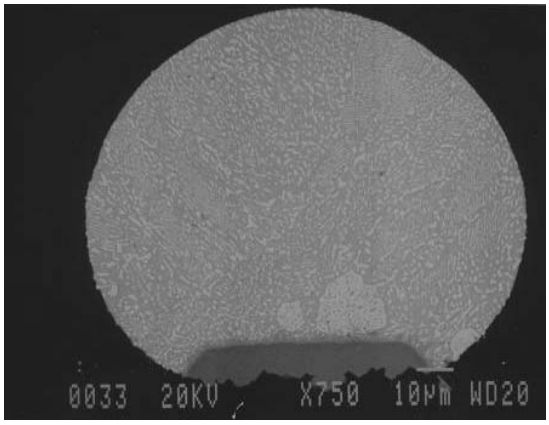

Figure 8.74 SEM of cross-section of wafer solder bump manufactured with 63Sn/37Pb solder paste via the print-detach-reflow process [23]

IBM-Charlotte has developed a process combining both print-detach-reflow and print-reflow-detach techniques, as shown in Figure 8.77 [27]. Here a metal mask is mounted onto a BGA substrate and secured with magnets. This temporary mask–BGA package is then sent through a conventional solder paste printing process, using a printer equipped with a stationary stencil. Thus, the paste is printed through the stationary stencil onto the mask–BGA package, which is then reflowed, followed by mask-removal, and cleaning. This design allows the solder paste volume control at the deposition stage to be split between the stationary stencil and the metal mask, therefore avoiding the challenge of paste release using a single thick stencil for solder paste volume delivery. In addition, it also avoids the challenge of reflowing solder paste in the presence of a large thermal mass due to the use of a thick metal mask when using the print-reflow-detach process. This screen printing method was applied to the bump forming of a chip size/scale package (CSP) with a pitch from 0.3 to 0.8 mm

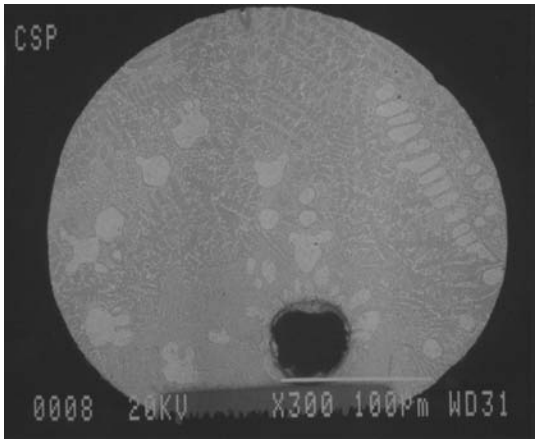

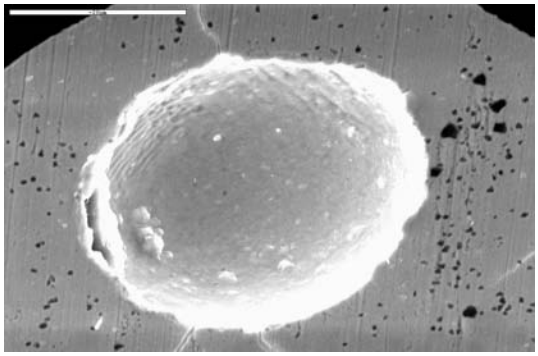

Figure 8.75 SEM view of voiding in cross-sectioned solder bump on a CSP (*top*) and wafer (*bottom*). The solder bump is formed through a 63Sn/37Pb solder paste print-detach-reflow process

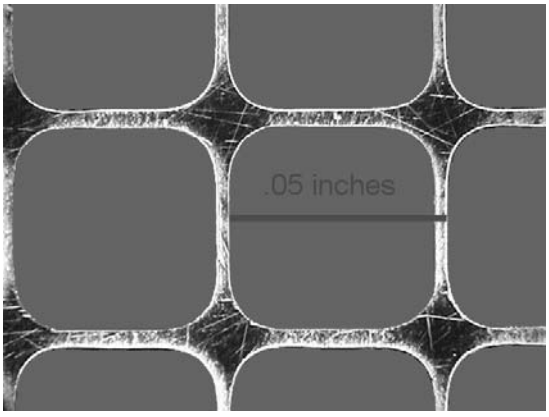

Figure 8.76 An electroformed stencil with 47 mil aperture width and 16 mil thickness. This stencil is used for BGA paste bumping process

[28]. However, it should be pointed out that attempts in the industry to duplicate these results have been unsuccessful.

The print-reflow-detach process costs more than the print-detach-reflow process. However, it is still considered cheaper than existing bumping approaches, and is

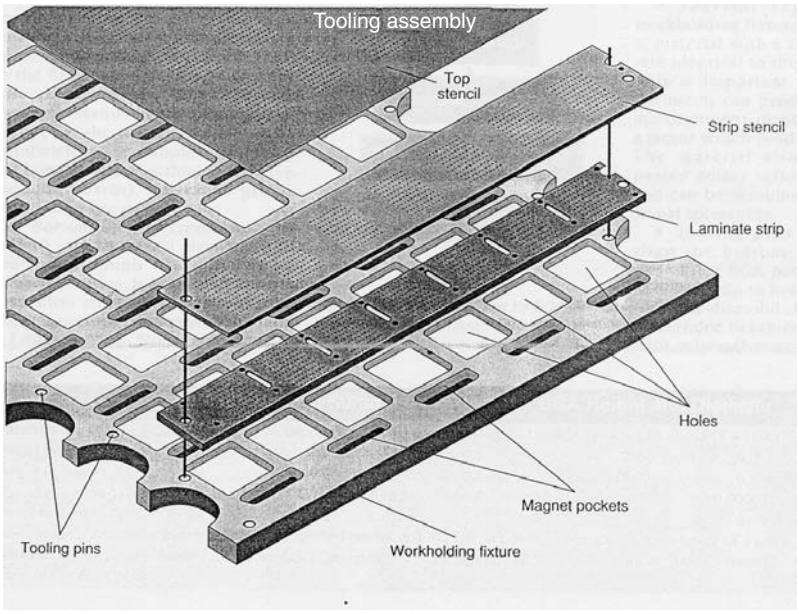

Figure 8.77 Solder bumping with solder paste alone, using a combined print-detach-reflow and print-reflow-detach process [27]

regarded as an interim process before the print-detach-reflow process is mature enough for implementation.

8.2.4.3 Dispensing

BGA solder bumping may also be achieved with a solder paste dispensing approach. Although non-slump performance is still a required paste property, there is no issue related to an aperture non-clogging requirement. However, this approach may be more challenging than the printing approach. In order to deliver sufficient solder volume without slump, the paste volume dispensed should be low and the paste metal content should be high. The high metal content requirement directly conflicts with the low metal content requirement for a good dispensable paste. In addition, the paste volume control for a dispensing process is generally more difficult than that for a printing process. The dispensing approach also faces challenges on throughput. Being a linear sequential process in nature, dispensing is expected to be low in throughput.

The attractive feature of dispensing is in its indifference in the coplanarity of substrate during the deposition stage. Since area array packages are flat in general, the strength of the dispensing technique is not able to contribute to the performance in paste bumping. At this time, the dispensing approach remains of interest, but its feasibility remains to be proven.

8.3 Conclusion

Soldering is the primary interconnection technology for area array packages. Methods for solder bumping for area array packages can be categorized as follows: (1) build-up process, (2) liquid solder transfer, (3) solid solder transfer, and (4) solder paste bumping. The first group includes both evaporation and electroplating processes, while the second includes meniscus bumping and solder jetting. The third group includes wire bumping, sphere welding, decal solder transfer, tacky dot solder transfer, integrated preform, and pick-and-place solder transfer processes, with the last being the current prevailing option. Solder paste bumping has the greatest potential to reduce bumping costs dramatically, and includes the print-detach-reflow, print-reflow-detach, and dispense approaches, with the first option being the lowest in cost. At this stage, print-detach-reflow is ready almost for production implementation.

References

1. Pack Tech, ''Packaging Technologies'', SB2 technology interface, http://www.pactech.de (1999).
2. N.-C. Lee and W. Casey, *''Soldering Technology for Area Array Packages''*, SMTA International, San Jose, CA, September (1999).
3. W. Chen, ''FCOB Reliability Evaluation Simulating Multiple Rework/Reflow Process'', *IEEE Transactions on Components, Packaging, and Manufacturing Technology-Part C*, Vol. 19, No. 4 (October 1996).
4. J. H. Lau (ed.), *''Flip Chip Technologies''*, McGraw-Hill, New York (1996).
5. M. Kelly and J. Lau, ''Low Cost Solder Bumped Flip Chip MCM-L Demonstration'', *Circuit World*, Vol. 21, No. 4 (1995).
6. R. Aschenbrenner, Ch. Kallmayer, R. Miebner and H. Reichl, ''High Density Assembly on Flexible Substrates'', in *Proc. of The Third International Symposium of Electronic Packaging Technology*, pp. 371–379, 17–21 August 1998, Beijing, China.
7. D. R. Frear, F. G. Yost, D. T. Schmale, and M. Essien, ''Area Array Jetting Device for Ball Grid Arrays'', *Proc. of Surface Mount International*, San Jose, CA, 41–46, 7–11 September 1997.
8. T. Schiesser, E. Menard, T. Smith, and J. Akin, ''Micro Dynamic Solder Pump: An Innovative Liquid Solder Dispense

Solution to FCA and BGA Challenges'', *Proceedings NEPCON West 95*, p. 3, vol. 1994, 1680–7 vol.3, Anaheim, CA, USA; 26 February-2 March 1995.
9. D. J. Hayes, D. B. Wallace, M. T. Boldman, R. E. Marusak, ''Picoliter Solder Droplet Dispensing'', *International Journal of Microcircuits and Electronic Packaging*, Vol. 16, No. 3, pp. 173–180 (1993).
10. R. Venkatraman, M. Jimarez, and K. Fallon, ''Decal Solder Bumping Process for Direct Flip Chip Attach Applications'', *Proceedings 1995 International Flip Chip, Ball Grid Array, TAB and Advanced Packaging Symposium*, ITAP '95, p. 299, 88–95, San Jose, CA, USA; 14–17 February 1995.
11. G. B. Hotchkiss, ''Aluminum Decal for Transferring Solder Spheres During Electronic Package Assembly'', in *Proc. of 47th Electronic Components and Technology Conference*, p. 1294, 1008–14, San Jose, CA, 18–21, May 1997.
12. A. Beikmohamadi, A. Cairncross, J. E. Gantzhorn, Jr., B. R. Quinn, M. A. Saltzberg, G. Hotchkiss, G. Amador, L. Jacobs, R. Stierman, S. Dunford, and AP. Hundt, ''Tacky Dots Technology for Flip Chip and BGA Solder Bumping'', in *Proc. of 1998 Electronic Components and Technology Conference*, pp. 448–453.
13. G. Hotchkiss, G. Amador, L. Jacobs, R. Stierman, S. Dunford, P. Hundt, A. Beikmohamadi, A. Cairncross, J. Gantzhorn, B. Quinn, and M. Saltzberg, ''Tacky Dots Transfer of Solder Spheres for Flip Chip and Electronic Package Applications'', in *Proc. of 1998 Electronic Components and Technology Conference*, pp. 434–447.
14. N. C. Lee, ''Solder Ball Manufacturing and Attachment for BGA's'', in Symposium of BGA, Nepcon West, Anaheim, CA, February 1997.
15. J. Kloeser, R. Aschenbrenner and H. Reichl, ''Low Cost Flip-chip Assembly: a Challenge for Future Market'', in *Proc. of The Third International Symposium of Electronic Packaging Technology*, pp. 487–494, 17–21, August 1998, Beijing, China.
16. R. Ramos, ''Flux-Free Process for Placement and Attach of Solder Balls to Wafers, Flip Chips and All BGA Packages'', in *Proc. of IMAPS '98*, San Diego, CA, pp. 345–355, 1–4 November 1998.
17. C. S. Chiu and N. C. Lee, ''Options and Concerns of BGA solder bumping'', in *Proc. of The Third International Symposium of Electronic Packaging Technology*, pp. 395–404, 17–21 August 1998, Beijing, China.
18. Winslow Automation, *BGA Re-Balling instruction Manual* San Jose, CA, (1998). SolderQuick is a registered Trade mark of Winslow Automation.
19. T. Oppert, T. Teutsch, E. Zakel, and D. Tovar, ''A Low Cost Bumping Process for 300 mm Wafers'', in *Proceedings of IMAPS*, pp. 34–38, 1999.
20. A. J. G. Strandjord, S. F. Popelar, and C. A. Erickson, ''Low Cost Wafer Bumping Processes for Flip Chip Applications (Electroless Nickel-Gold/Stencil printing)'', in *Proceedings of IMAPS*, pp. 18–33, 1999.
21. J. Kloeser, P. Coskina, E. Jung, A. Ostmann, R. Aschenbrenner, and H. Reichl, ''A Low Cost Bumping Process for Flip Chip and CSP Applications'', in *Proceedings of IMAPS*, pp. 1–7, 1999.
22. J. D. Schake, ''Stencil Printing for Wafer Bumping'', *Semiconductor International*, pp. 133–144 (October 2000).
23. B. Huang and N.-C. Lee, ''Low Cost Solder Bumping Via Paste Reflow For Area Array Packages'', in *Proceedings of Etronix*, Anaheim, CA, 2001.
24. J. Kloeser, K. Kutzner, E. Jung, K. Heinricht, L. Lauter, M. Töpper, E. Ochi, R. Aschenbrenner, and H. Reichl, ''Experience with a Fully Automatic Flip-chip Assembly Line Integrating Smt'', in *Proc. of Nepcon West*, Anaheim, CA, 1–5 March 1998.
25. J. Kloeser, R. Aschenbrenner, and H. Reichl, ''Low Cost Flip-chip Assembly: a Challenge for Future Market'', in *Proc. of The Third International Symposium of Electronic Packaging Technology*, pp. 487–494, 17–21, August 1998, Beijing, China.
26. N.-C. Lee, ''Troubleshooting BGA Assembly'', in Symposium of BGA, in Nepcon West, Anaheim, CA, February, 1998.
27. C. Brutovsky, C. Eieselman, and K. Slesinger, ''Forming BGAs with Solder Paste'', *Electronic Packaging & Production*, p. 57 (May 1997).
28. S. Greathouse, ''Critical Issues with Chip Scale Packages (CSPs)'', *Proceedings of Surface Mount International Advanced Electronic Manufacturing Technologies*, p. 2 Vol. 826, 203–15, Vol. 1, San Jose, CA, USA (10–12 September 1996).
29. N.-C. Lee and K. Randle ''Voiding in BGA at Solder Bumping Stage'', *ISHM* (1997).
30. W. B. Hance and N.-C. Lee, ''Formation and Control of Voiding in SMT'', in *Proc. of 1992 ISHM*, San Francisco, CA, pp. 535 (1992).
31. W.B. O'Hara and N.-C. Lee, ''Voiding in BGA'', in *Proc. of 1995 ISHM*, Los Angeles, CA (1992).
32. W. O'Hara and N.-C Lee, ''Solder Beading in SMT – Cause and Cure'', in *Proc. of SMI*, San Jose, CA, 1991.
33. A. W. Adamson, *Physical Chemistry of Surfaces*, 3rd edn., John Wiley, NewYork (1976).

9 BGA and CSP Assembly and Rework

One of the major advantages of BGA is its robustness in handling. Unlike fine-pitch QFPs which use densely lined-up flimmy leads for interconnect, the leadless BGA is fairly easy to handle. Assembly and rework of BGA typically result in high yield if processed properly. The downside of BGA is the difficulty in inspecting the interior solder joints. CSP behaves similar to BGA, except in being more sensitive to mis-handling. In this chapter, the assembly and rework procedure for BGA and CSP will be briefly reviewed, with the challenges discussed in more detail.

9.1 Assembly process

Assembly of BGA and CSP follows a typical SMT process: print solder paste, place components, reflow, and inspection. Figure 9.1 [1] depicts the process flow from paste printing to reflow. Due to the crucial role of solder volume of the joints in reliability, particularly in the case of CSP, the stencil design guideline should be followed.

9.1.1 General stencil design guideline

Since solder joint reliability is a strong function of the solder volume as well as the package type, the stencil design should be tailored for each type of package, as discussed below.

9.1.1.1 CBGA and CCGA

CCGA and CBGA utilize high melting temperature solders such as 90Pb/10Sn or 95Pb/5Sn. The solder ball or column does not melt during reflow, and the solder joint with the PCB depends solely on the bonding of eutectic

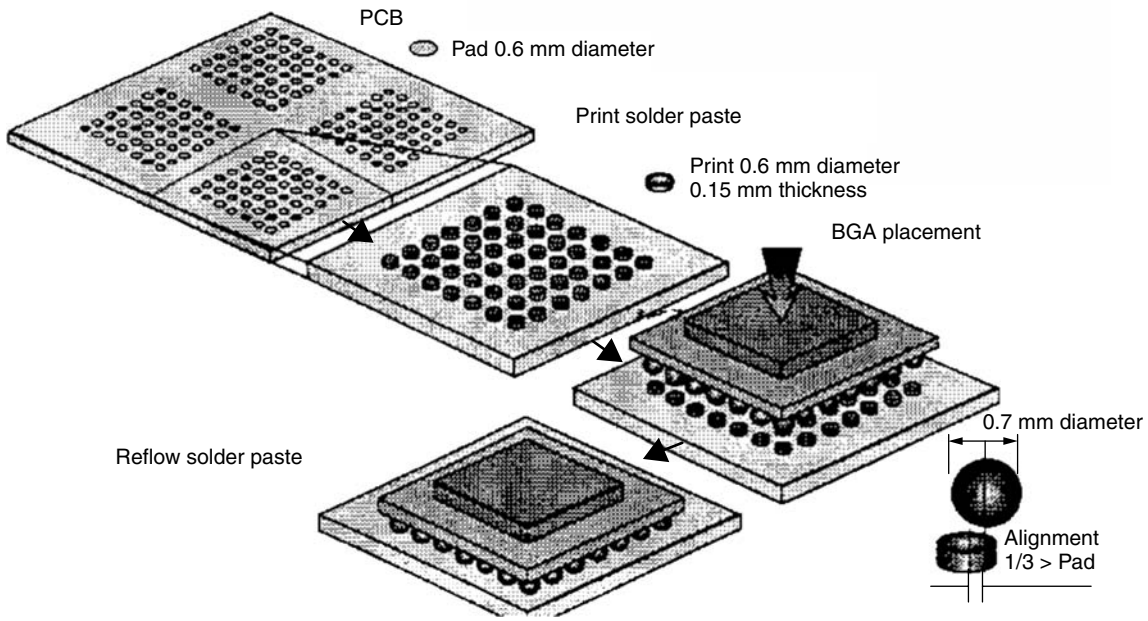

Figure 9.1 Process flow of BGA assembly. (Source: Kyocera [1])

Table 9.1 Recommended stencil design guideline for CBGA [2]

Package type	*Pitch (mils)*	*Paste volume requirement (mil^3)*	*Stencil pattern recommended*
CBGA	50	Min. 4800; nominal 7000	0.034 or 0.035-in. diameter opening in a 0.008-in. thick stencil
	40	Range 2500 to 4600	0.027-in. opening in a 0.0075-in. thick stencil
CCGA	50	Min. 3000; nominal 5000	0.032-in. diameter opening in a 0.008-in. thick stencil
	40	Min. 2000; max. 5000	0.029-in. diameter opening in a 0.008-in. thick stencil

Sn−Pb between the PCB pads and the high temperature balls or columns. Accordingly, it is critical to meet the minimal solder paste volume requirement in order to form an adequate bonding. In general, CBGA requires slightly more minimal solder paste volume than CCGA in order to meet the minimal reliability requirement, as shown in Table 9.1. This reflects the difference in the shape of ball and column. In the former case, more paste volume is needed to form an adequate solder fillet around the ball.

9.1.1.2 PBGA

With PBGA, the solder alloy for the ball is typically eutectic Sn−Pb solder. Upon reflow, the ball collapses and wets to the pad, in the presence of flux. The contribution of solder paste to the solder volume of joint depends on the metal content of solder paste, print diameter, and print thickness. In general, the solder ball provides about 80–100 percent of final solder joint volume. For instance, for PBGA with bumps made with a 30 mil diameter ball, if the solder paste is 90 percent w/w in metal content, or 52 percent v/v, with a print 35 mil in diameter and 8 mil in thickness, the solder volume provided by solder ball comprises 78 percent of the final solder joint volume. However, if only flux is used for PBGA mounting, the solder volume of solder ball will be 100 percent of the final volume. The large solder joint size plus the dominant solder volume contribution of the solder ball indicates the paste volume control at PBGA assembly is not as critical as for CCGA and CBGA. For 50–60 mil pitch PBGAs, the stencil design is typically 0.026–0.034-in. diameter opening in a 0.006–0.008-in. stencil. For 40 mil pitch PBGAs, a 0.020-in. diameter aperture in a 0.004-in. stencil is adequate to deliver the nominal solder volume of 1200 mil^3 recommended [2].

9.1.1.3 CSP

The solder volume of a CSP solder ball is considerably smaller than that of a BGA. As a result, the solder joint of CSP will be quite vulnerable if insufficient additional solder volume is added through the solder paste printed.

Table 9.2 Stencil aperture shapes and sizes and paste printed for CSP [3]

CSP	*PCB*		*Stencil 5 mil thick*		
	Pad size (mm)	*Pitch (mm)*	*Aperture (mm)*	*Aspect ratio*	*Shape*
Type A, 188 I/O	0.305 dia.	0.5	0.305 sq.	2.4	Square
Type A, 46 I/O	0.305 dia.	0.75	0.305 sq.	2.4	Square
Type B, 48 I/O	0.450 dia.	0.8	0.450 dia.	3.6	Round
Type C, 324 I/O	0.500 dia.	0.8	0.500 dia.	4.0	Round
Type D, 144 I/O	0.200 dia.	0.5	0.275 sq.	2.2	Square

Table 9.3 A list of selected CSP components [3]

	Type	*Size (mm)*	*I/O*	*Pitch (mm)*
Type A 46	Flexible interposer	6 × 8	46	0.75
Type A 188	Flexible interposer	13 × 13	188	0.5
Type B 48		6 × 8	48	0.8
Type C 324	Rigid interposer	15 × 15	324	0.8
Type D 144	Wafer-level assembly	7 × 7.5	144	0.5

Critical solder volume for the CSP joint is a strong function of CSP type, ball size, CSP pad size, pitch, and PCB pad size. For instance, Nakajima *et al.* [3] have reported that the following stencil design (see Table 9.2) has been applied to several types of CSP, as shown in Table 9.3. The results are satisfactory in reliability except for Type C, a ceramic rigid base CSP. On the other hand, Cole has suggested [2] that, for CSP with 0.5 mm pitch and 0.008-in. pad, the min–max paste volume is 100–500 mil^3. As a rule of thumb, the solder paste volume for CSP should be as high as possible in order to have better reliability. The upper limit for paste volume should be the volume where the bridging becomes a concern.

There are several approaches to deliver a high print volume, including an increase in stencil thickness and aperture diameter, and a change in aperture shape. The most effective is employing a square aperture pattern, as shown in Figure 9.2. In order to allow a better paste release, a round corner is preferred, with a corner radius being 1× stencil thickness. With the use of a square aperture, a maximum overprint becomes possible with a minimal compromise in non-bridging performance, as shown in Figure 9.3. Use of trapezoidal aperture would help a better release, as illustrated in Figure 9.4 [5,6].

9.1.2 BGA/CSP placement

The self-centering capability of BGA due to the surface tension of solder, as illustrated in Figure 9.5, allows

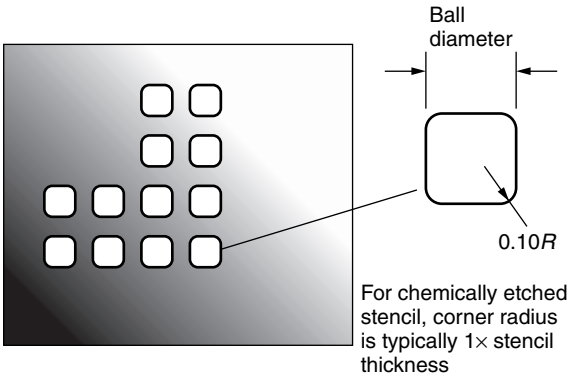

Figure 9.2 Recommended stencil aperture design for CSP attachment [4]

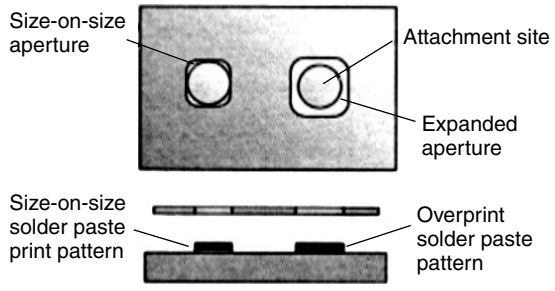

Figure 9.3 Overprint is desirable for CSP stencil design [4]

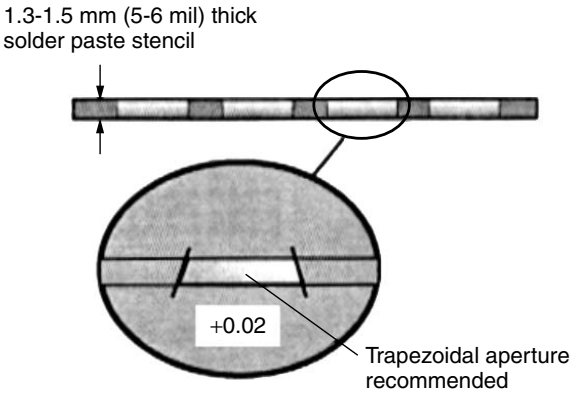

Figure 9.4 Trapezoidal aperture recommended for CSP stencil [4]

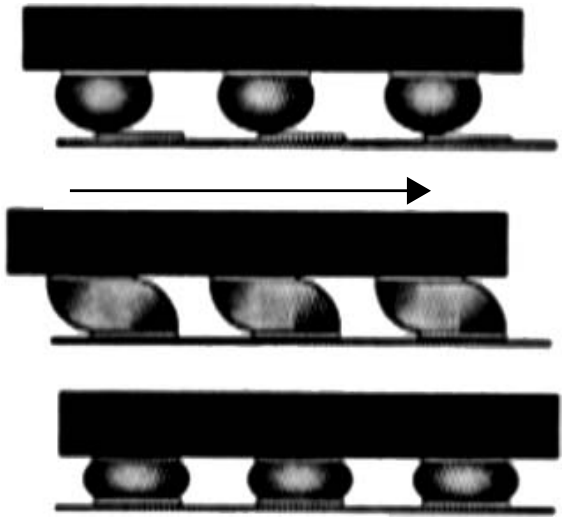

Figure 9.5 BGA will self-align to PCB land pads due to surface tension of solder. (Source: Intel.)

significant misregistration at BGA placement. For 50 mil pitch BGA, 50 percent of misregistration is acceptable, while 40 percent off is acceptable for 40 mil pitch BGA.

For CSP, these devices exhibited significantly different results from the other BGA packages. Failure occurred with much less linear offset, while rotational skew produced no failures through 2° of theta. One factor that contributed to the limitation of linear misplacement was a reduced pad-to-pad spacing [7].

The equipment for BGA placement includes blackbody/binary vision and array vision systems. The first system registers on the edge of the package. While the accuracy is adequate, it is limited by array to body edge registration. The array vision system defines the package location with the use of a solder ball array. It is the fastest option, and the best in accuracy, although it may suffer false rejects caused by lighting contrast requirements and ball surface variations [2].

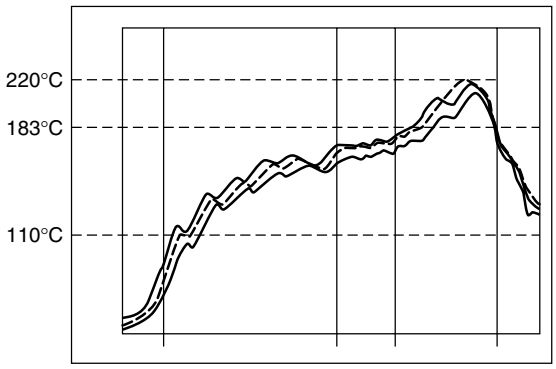

Figure 9.6 Conventional reflow profile with a soaking plateau

9.1.3 Reflow

As with other surface mount components, reflow of BGA/CSP can be carried our with forced air convection, infrared furnace, and vapor phase, with the first option being the preferred method. Although a conventional profile with a ramp, soak, reflow, and cool profile, as shown in Figure 9.6, is fairly acceptable, a "Tent profile" utilizing a gradual linear ramp-up, spike, and cool profile (see Figure 9.7) is now being adopted [8,9]. In general, the slower ramp rate (<0.7°C/sec below 100°C) found with the Tent profile has been associated with lower defect rates. Figure 9.8 shows an example of a Tent profile used for 32.5 mm 1.27 mm pitch CCGA [2].

Components with peripheral interconnections such as QFP, where all leads have a fairly comparable thermal environment, normally display fairly comparable temperatures for all these leads. This is no longer true for BGA, where the thermal mass around the center balls is larger than that of the peripheral balls. As a result, it is crucial to establish a profile so that all joints will reach minimum reflow temperature but do not exceed maximum reflow temperature.

For CBGA and CCGA, both high thermal mass and high Pb solder impose a challenge for establishing a profile. On the one hand, all joints should reach the minimum reflow temperature, as discussed above. On the other, the maximum reflow temperature should not exceed 220°C in order to minimize the dissolution of Pb into the eutectic Sn−Pb solder joint. In the presence of a large thermal mass, achieving this tight temperature control becomes fairly difficult. In principle, a very slow ramp-up profile with an elongated heating time could be promising.

9.1.4 Inspection

The criteria for a BGA solder joint inspection are similar to those for other SMT solder joints. An ideal solder joint should have a smooth transition between the ball or column and the edge of shiny solder. In addition, the fillet shapes for CBGA should not be highly concave [2].

One of the biggest challenges in implementing BGA is inspection. Although visual inspection of external row joints allows verification of good wetting and alignment, with the majority of solder joints concealed behind the external row joints, a full inspection can only be carried out with the use of X-ray equipment.

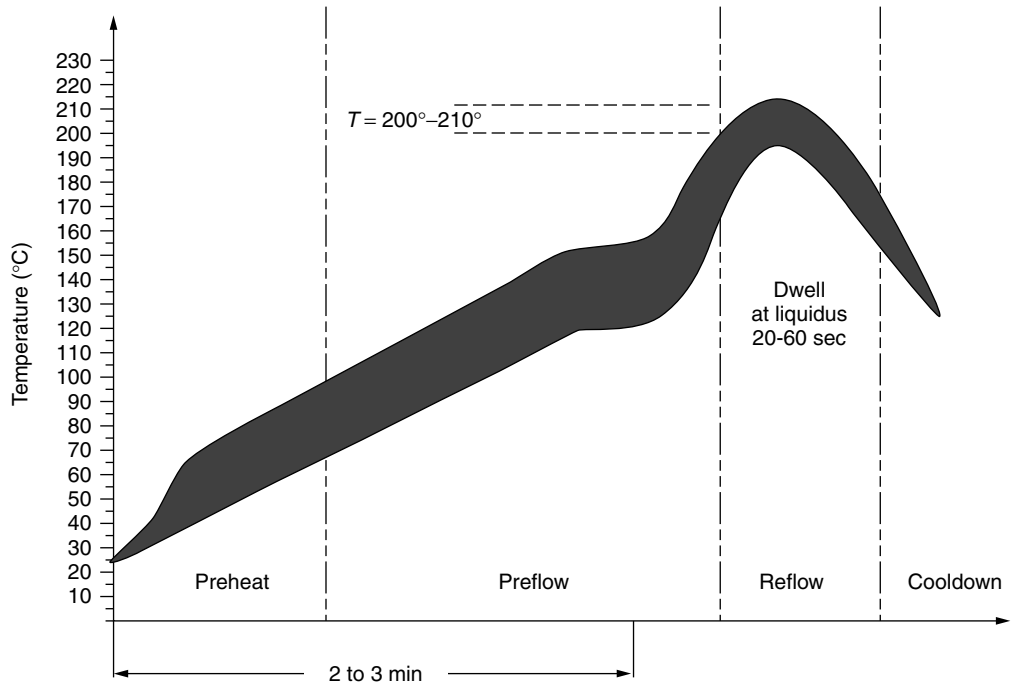

Figure 9.7 "Tent" profile [8,9]. (Source: Heller Industries)

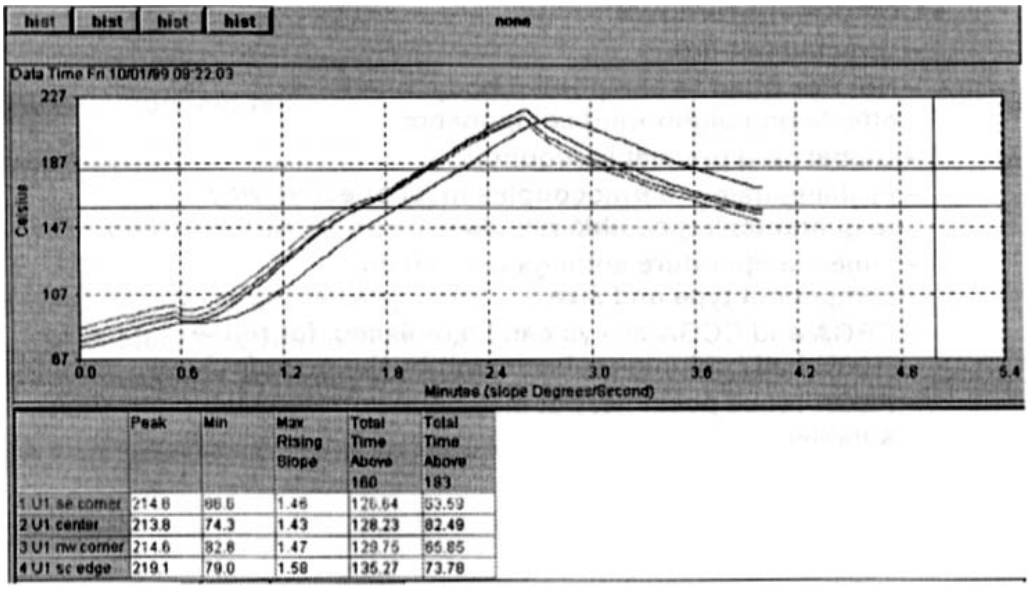

Figure 9.8 Reflow profile with a linear ramp up for 32.5 mm 1.27 mm pitch CCGA [2]

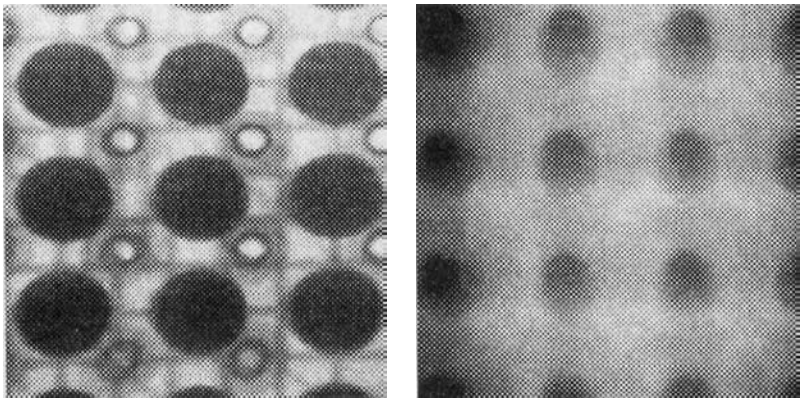

Figure 9.9 Transmission versus cross-sectional X-ray systems. Transmission X-ray systems often cannot detect open solder joints (*left*). The cross-sectional X-ray image clearly identifies the open non-collapsible BGA joints (*right*). (From S. Rooks, "Controlling BGA Assembly using X-ray Laminography", *EP & P,* pp. 24–30 (January 1997): reprinted by permission)

Transmission X-ray can detect voiding, bridging, misalignment, and gross opens. Cases with marginal opens are not easily detectable, as shown in Figure 9.9 [10]. Better wetting assessment may be provided with the use of a teardrop pad design. Alternatively, tilting the PCB against the X-ray path could also provide a side view of solder joints hence wetting information. However, the latter approach is limited by the relative size of the PCB versus the X-ray sample chamber. Laminography X-ray provides more graphical analysis of joint geometries. Thus, by taking three image slices, a non-collapsible BGA joint can be characterized by conducting four measurements: (1) location of the joint centroid, (2) joint radius, (3) solder thickness in each of five annular rings concentric with the joint centroid, and (4) error of the joint shape relative to a circle (circularity) (see Figure 9.10 [10]).

9.2 Rework

Due to the sensitivity toward moisture and warp, rework of BGA and CSP requires extra caution. The process is different from that of conventional peripheral components, and has been studied extensively [11–39]. The key features will be discussed below.

9.2.1 Process flow

Described below is a general process for BGA rework using a semi-automated rework system with special consideration of micro-BGA devices [13,40,42]. Procedure: (1) board preparation for rework: apply low solid liquid flux along one edge of the components, then tip the board slightly; (2) component removal: preheat board from both

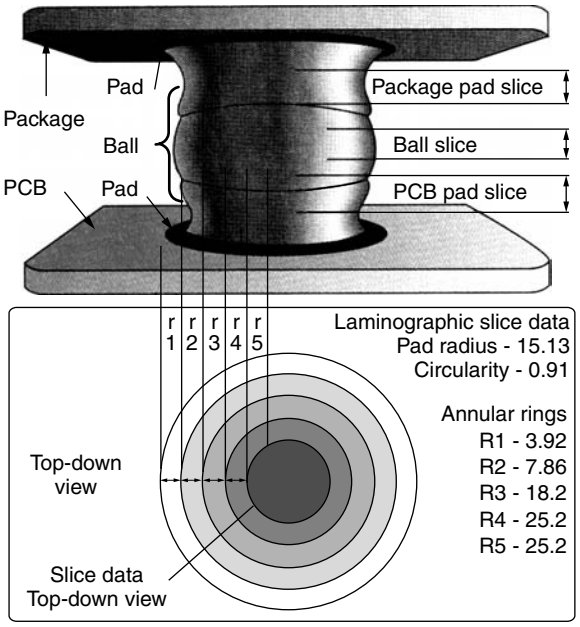

Figure 9.10 X-ray laminographic analysis on a non-collapsible BGA joint [10]

top and bottom side to 100–120°C to prevent board warp, then heat the board to 205–220°C; (3) site preparation for installation: remove excessive solder from the pad, level the pads, clean the site thoroughly, inspect for damage to solder mask or pads, apply flux (a slightly tacky low solid flux) or solder paste (square aperture helps release for 20 mil pitch and 12 mil diameter pad print); (4) component installation: use a vacuum nozzle pick-up and a beam-splitting prism for alignment, preheat the board to prevent warp, peak temperature 205–230°C, at least 60 sec above 183°C; (5) cleaning and inspection. In a production environment, the rework procedure can be simplified as: (1) prepare the board for rework; (2) select and run the component removal profile; (3) remove excess solder from pads; (4) clean the sites; (5) inspect under microscope for pad or trace damage; (6) apply flux or solder paste; (7) inspect under microscope for proper flux or paste application; (8) select and run the component installation profile; (9) clean the assembly; (10) visually inspect and X-ray for voiding and solder bridges; (11) perform functional test when possible.

9.2.2 Pre-baking

Due to the sensitivity of PBGA toward moisture, PBGAs should be used within 8 hours after removal from the dry-pack. Detailed handling conditions are shown in Table 9.4. All BGAs either needing or undergoing repair should be stored in a 5 percent RH drying box. If the BGA has been exposed to the room environment for more than 48 hours, it should be kept in the drying box for a minimum of 48 hours or baked in an oven at 125°C for 24 hours to remove the moisture absorbed by the plastic PBGA body [38]. As a general precaution, it is recommended to pre-bake the board and component prior to component removal, particularly if the component is to be reused.

9.2.3 Component removal

In general, the heating profile for component removal is the same as for component mounting. However, if the component is not to be reused, and if the board does not become thermally stressed excessively, a rapidly jumped up profile can be used. Preheat should always be employed in order to avoid warp.

9.2.4 Reflow equipment

During rework, the surrounding components should be kept as cool as possible. Figure 9.11 shows a heat delivery system with the hot air exhausting through the top opening, hence minimizing thermal damage to the adjacent SMD.

9.2.5 Site preparation

Site preparation is needed after component removal, since all components leave behind variable amounts and types of solders and flux residues. For instance, CBGA and CCGA leave some 90Pb/10Sn balls/columns, besides

Table 9.4 IPC/JEDEC moisture sensitivity levels or MSL [41]

MSL	*Floor life after opening bag and storing at ≤30°C/60%RH*	*Pre-conditioning soak requirement*	
		Standard (duration, ambient)	*60°C/60% RH accelerated equivalent*
1	Unlimited	168 hr, 85°C/85% RH	NA
2	One year	168 hr, 85°C/85% RH	NA
2a	Four weeks	696 hr, 30°C/60% RH	120 hr
3	One week	192 hr, 30°C/60% RH	40 hr
4	Three days	96 hr, 30°C/60% RH	20 hr
5	Two days	72 hr, 30°C/60% RH	15 hr
5a	One day	48 hr, 30°C/60% RH	10 hr
6	Time on label	TOL, 30°C/60% RH	

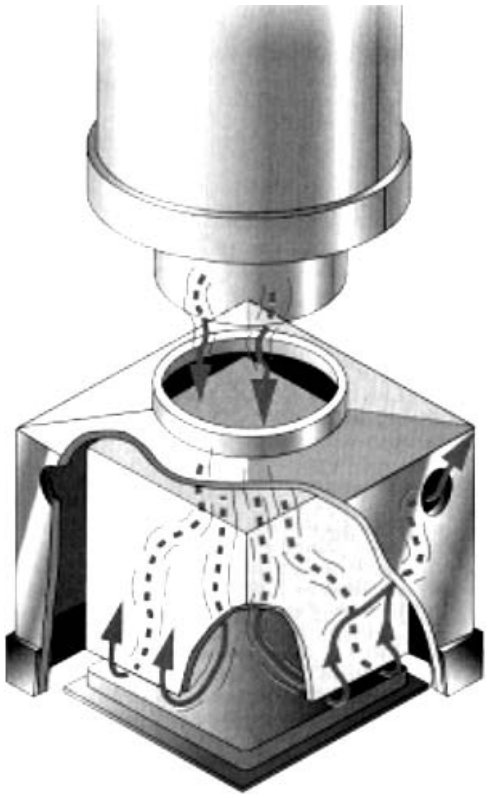

Figure 9.11 BGA reflow heat delivery system. (Source: OK Industries)

63Sn/37Pb solder, on PCB pads. A preparation step will allow the site to be returned to an even mountable surface. In addition, the warped board can also be flattened at this step.

9.2.6 Solder replenishment

Solder can be replenished with the following approaches: (1) printing solder paste to either the site or the component, (2) adding solid solder through the use of individual or integrated preform, (3) adding liquid solder through tooling such as a roller. For PBGA, replenishing solder on the site may not be needed. Applying flux to site is sufficient to form a well-wetted solder joint. However, eliminating the solder addition step may compromise solder joint reliability due to reduced solder joint size.

A reballing process is applied to CCGA and CBGA through stencil printing eutectic Sn−Pb solder paste followed by populating with high lead balls/columns and then reflowing the eutectic Sn−Pb paste. For PBGA, a new component is often used instead of reballing the used component.

9.2.7 Placement of component

Placement of component can be done manually by registering the component between the diagonal marks on the PCB. However, the best way is to use the split-beam prism system. Overlaying the image of balls on the pads allows the component to be placed most accurately.

9.2.8 Reflow of BGA and CSP

As a rule of thumb, the reflow profile should duplicate the production profile. Preheat is crucial, particularly in the case of CBGA. The package is more sensitive to planarity variation between itself and the site on the board, thus requiring more precise bottom-side preheat to minimize board warpage and planarity variations. Reflow of the high temperature solder (302°C) should be avoided. Mixing of this high temperature solder with that on the pads will result in a high-temperature alloy that will make any future site rework very difficult. Due to the high thermal mass of the ceramic body, heating the component body along with the joints is necessary [24,26].

9.3 Challenges at assembly and rework stages

Due to the robust package body design, the defect rate of BGA/CSP processing is much lower than that of QFP. Table 9.5 shows the BGA/QFP yield comparison for 304-pin devices [43]. However, if the process is not properly handled, problems still can occur to a significant extent, as will be discussed below.

9.3.1 Starved solder joint

A starved solder joint is a solder joint where the solder volume is insufficient to form a reliable joint. The most common cause is insufficient solder paste printed, as shown by Figure 9.12 which illustrates the solder joints

Table 9.5 BGA/QFP yield comparison for 304-pin devices (source: IBM)

Feature	*BGA*	*QFP*
Package size (mm^2)	525	1600
Lead/ball pitch (mm)	1.27	0.5
Assembly defect rate (ppm/lead)	0.6	100
Component reject rate*	0%	7%
Chip carrier signal noise	1.0X	2.25X

*Due to bent leads; 2100 QFPs and 20000 BGAs tested.

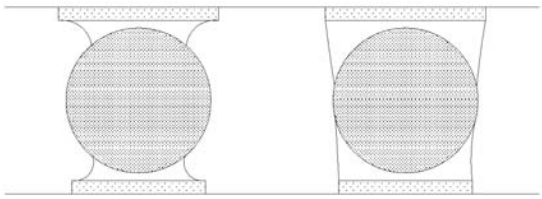

Figure 9.12 Starved solder joint (*left*) versus normal solder joint (*right*) for CBGA [2]

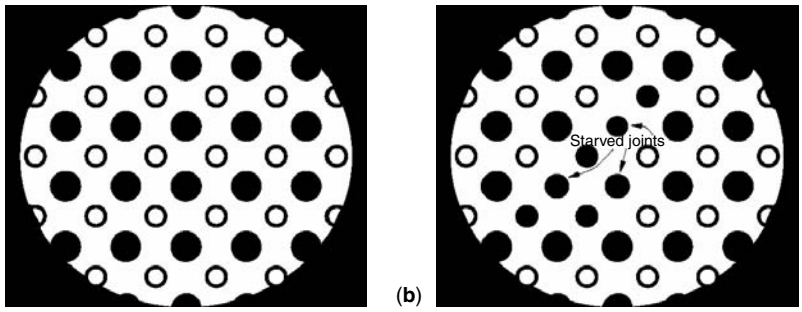

Figure 9.13 X-ray of PBGA solder joints, (**a**) normal BGA solder joints, (**b**) a starved solder joint caused by wicking into the via [44]

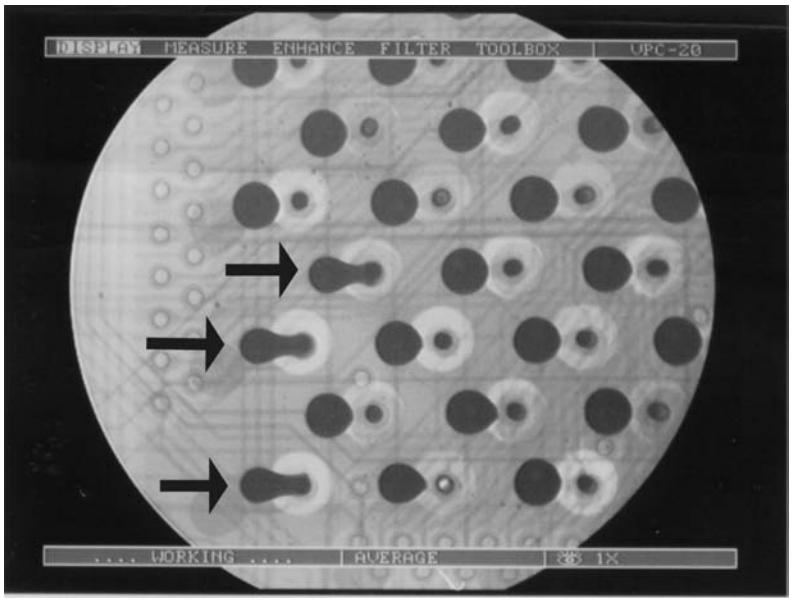

Figure 9.14 X-ray picture of starved solder joints, as marked by arrows, of a PBGA. The solder wicked along the trace into the via through damaged solder mask coverage

of a CBGA. The picture on the left shows a starved, concaved bottom fillet shape. This is in contrast to the picture on the right where the high-Pb ball is well wrapped by the eutectic Sn−Pb fillet hence displaying a straight contour line.

Starved joints may also be caused by solder wicking. Figure 9.13(a) shows PBGA normal solder joints, while Figure 9.13(b) shows some starved solder joints plus some plugged via holes [44]. The solder of BGA bumps wicked into the via holes, presumably caused by misregistration or a poor solder paste print coverage. It should be noted that improper rework procedures or improper handling of BGA components during rework may also promote wicking and consequently starved joints. Figure 9.14 shows starved solder joints caused by wicking along the trace line into the via holes. Here the solder mask on top of the trace line was damaged during an earlier rework process.

Starved joints may also be caused by poor design. For instance, Figure 9.15 shows a low stand-off solder joint on top of a "via in pad" on the PCB. Apparently, a significant part of the solder from the solder ball drained into the via and resulted in a short standoff. One way to compensate for this is to deposit extra amounts of solder paste at the via in the pad area through the use of a thick stencil and an enlarged aperture. Another solution to reduce solder drainage is using microvia technology instead of a via in pad design.

Another factor that also contributes to starved solder joint is poor coplanarity. Even if the solder paste volume deposited is accurate, the solder joint may appear starved if the clearance between the BGA and the PCB is too large. This is especially true in the case of CBGA.

In summary, the starved solder joint can be eliminated by the following solutions.

Deposit a sufficient amount of solder paste.
Tent the via with a solder mask.
Avoid damaging the solder mask during rework.
Register properly during paste printing.

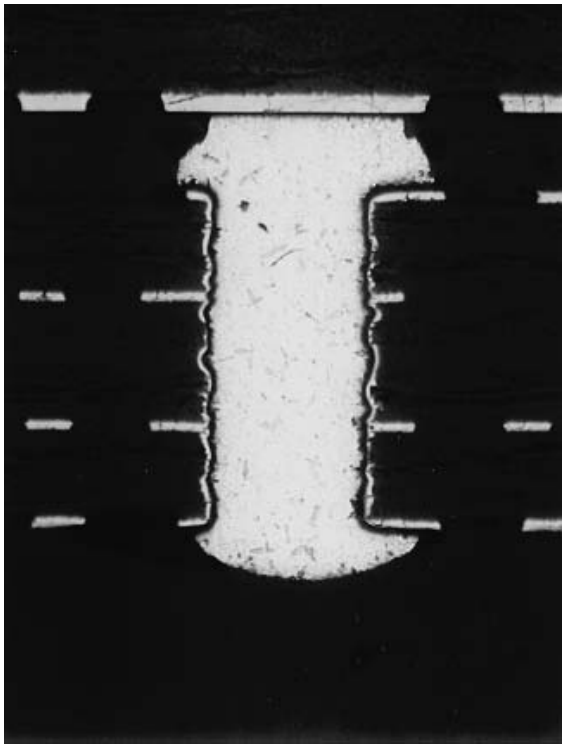

Figure 9.15 Starved solder joint of PBGA driven by solder filling up the ''via in pad''

Register properly during BGA placement.
Handle component properly during rework.
Maintain high coplanarity of PCB, such as by employing proper preheat during rework.
Use a microvia instead of a via in pad design to reduce solder drainage.

9.3.2 Poor self-alignment

Before discussing poor self-alignment, as shown in Figure 9.16 [44], it will be beneficial to review the limitations of self-alignment capability. As discussed in section 9.1.2, self-centering capability allows 50 percent misregistration at 50 mil pitch BGA placement. Noreika *et al*. [7] have reported that BGA packages exhibited varied self-centering attributes, with ball metallurgy and the ball-to-carrier interface appearing to be the most significant factors. It was further concluded that the 50 percent linear offset prior to reflow is conservative for mainstream array packages. This linear offset tolerance seems to gradually diminish with decreasing pitch dimension. Hence, for 40 mil pitch BGA, the tolerance is 40 percent, while for CSP, it becomes much less. Although it was postulated that the reduced pad-to-pad spacing contributed to the limitation of linear misplacement [7], results on a flip chip in the same study indicate that self-alignment occurs at up to 60 percent misplacement. Since a flip chip is typically fairly light, the conflicting results suggest that the dominant factor might rely on fundamental physics and reside in the relative component weight per unit solder joint contour length.

With the above understanding on the limitations of self-alignment, "poor self-alignment" can be categorized as insufficient self-alignment associated with (1) misregistration beyond nominal tolerance range and (2) misregistration within a nominal tolerance range.

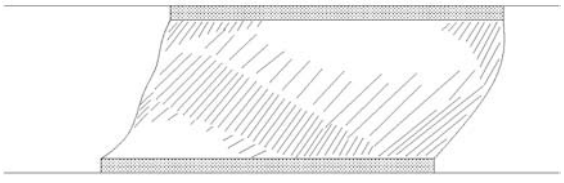

Figure 9.16 A poor self-aligned PBGA solder joint [44]

9.3.2.1 Excessive misregistration

The first category is a simple result of placement accuracy, and can only be corrected by improving the placement equipment capability or programming accuracy. The second category is a result of interference with the self-alignment process, which may be caused by the following factors.

9.3.2.2 Insufficient solder volume

A common phenomenon is insufficient solder paste deposited. With a reduced solder volume, the surface tension driving force will often be reduced as well.

9.3.2.3 Poor spreading

If the solder cannot spread properly due to either poor flux activity or poor pad solderability, as illustrated by Figure 9.17(a), a compromised self-centering certainly will result. Figure 9.17(b) shows a properly wetted solder joint. The surface tension pulling force is exerted by both sides of the joint surface.

9.3.2.4 Reduced surface tension

The apparent surface tension of solder can be affected by the reflow environment. In an oxidizing reflow atmosphere, if the flux is not active enough, the surface of the molten solder will oxidize and form an oxide film and result in a lower apparent surface tension. Consequently,

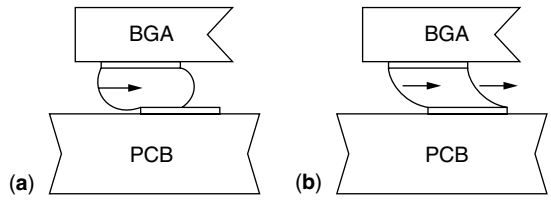

Figure 9.17 BGA solder spread at reflow: **(a)** partial spread due to either poor flux activity or poor pad solderability, **(b)** full spread. The self-alignment driving force of **(b)** is stronger than that of **(a)** due to contribution from both sides of joint for **(b)**

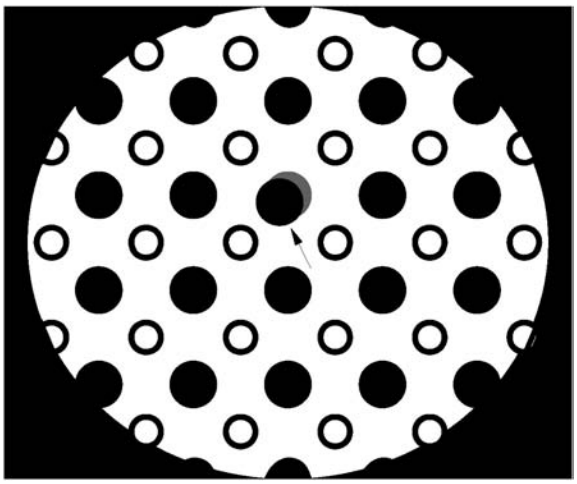

Figure 9.18 X-ray photograph of a ball that did not self-align to within 50 percent of the board pad [7]

the self-alignment driving force will be reduced. Use of an inert atmosphere can eliminate this factor.

9.3.2.5 Changing solder composition

For CBGA assembly, if the solder bumping process is conducted at 240°C instead of 220°C when using high temperature sphere and eutectic solder paste, the bumping process will be satisfactory. However, component alignment for later PCB attachment will be poor due to the dissolved Pb in the solder joint between the ball and the BGA component. This high Pb particulate, as demonstrated by Figure 8.29(b) will make a eutectic solder joint increase in melting point and become sluggish at later board level assembly [45]. This high Pb particulate formation may also cause an individual ball to fail to self-align to within 50 percent of the board pad, as shown in Figure 9.18. In general, TBGA was reported to have a tendency to have incomplete self-alignment [7], presumably also attributable to this reason.

9.3.2.6 High inertia of momentum of component

For CCGA, where the 90Pb/10Sn column is soldered onto the package with 63Sn/37Pb, the self-alignment action during CCGA assembly may pull the bottom of the column toward the pad center, but fail to pull the whole heavy ceramic package with it. The column may tilt within the 63Sn/37Pb joints to accommodate the shifted column base, as shown in Figure 9.19. A similar phenomenon may also occur to CBGA, but to a lesser extent.

9.3.2.7 Solder mask misregistration

Misregistration of the solder mask may result in partial coverage of the BGA pads by the mask, and consequently cause an incorrect center after self-alignment.

9.3.2.8 Large corner pads and overprint

The self-alignment of BGA or CSP can be improved through a design change. By utilizing a large board pad for the corners, the package will have a greater tolerance to misregistration, as illustrated in Figure 9.20. This large pad approach can be enhanced by over printing the large pads with solder paste so that more solder volume will be available to facilitate the self-centering process.

In summary, poor self-alignment of BGA and CSP can be improved through the following approaches:

Improve accuracy of placement.
Increase solder paste volume deposited.
Improve pad or ball solderability.
Use fluxes with a higher activity.
Use an inert reflow atmosphere.
Reduce the soldering temperature for both CBGA bumping and mounting processes.
For CCGA, cast the 90Pb/10Sn column onto the package instead of soldering onto it with 63Sn/37Pb.
Improve solder mask registration accuracy.
Use large corner pads for the board footprint design.
Overprint the large corner pads with solder paste.

9.3.3 Poor wetting

The wetting here refers to the wetting of bump or column with either a solder paste or a board pad. Although wetting is usually not a problem for eutectic Sn–Pb solder bumps, a highly oxidized bump surface may cause wetting problems. Oxidation of the bump often occurs at the ball shipping or ball placement stage and appears as a dull ball. Although the metallurgical phase structure was

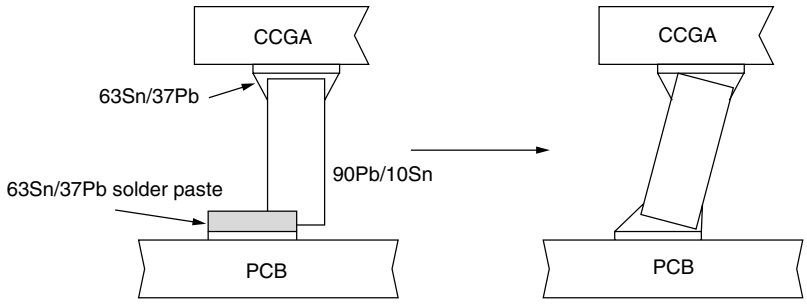

Figure 9.19 Schematic view of partial self-alignment of CCGA. The heavy mass of ceramic package prevented it from movement, and the column tilted to adopt the offset in anchoring sites

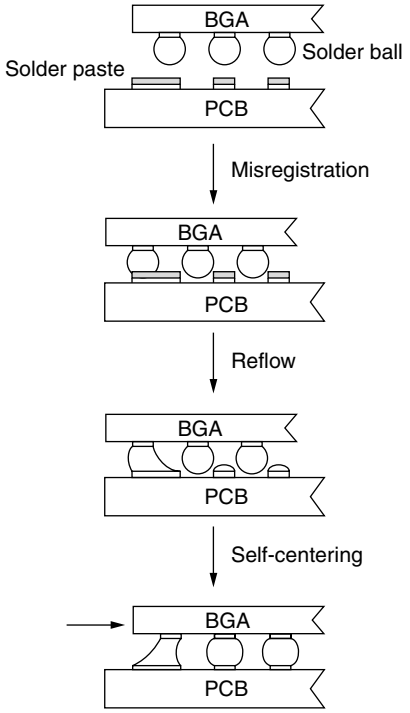

Figure 9.20 Enlarged corner pads allow the BGA to have more opportunity to be pulled back after a misregistered placement. An overprint of solder paste on the corner pads provides more solder volume, hence may enhance the self-centering force

found to have some correlation with the oxidation rate, the presence and type of surface coating appears to be the dominant factor in determining how fast a ball will turn into a dull ball. The chemistry and process of those coatings are typically proprietary information. Alternatively, a dull bump can be avoided by using a "first come, first go" ball placement mechanism so that perturbation of the balls can be minimized.

Upon solder bumping, if the flux activity and flux coverage is not sufficient, the oxide film may remain on the surface of the bump and maintain its dull ball appearance, as shown in Figure 9.21(b), in contrast to a shiny ball (see Figure 9.21(a)). Figure 9.22 shows a half-shiny, half-dull solder bump or "two tone" bump caused by partial coverage of the bump surface with flux. Obviously, use of a more active and better wicking flux will improve both coverage and oxide removal. In addition, a more active flux will allow a higher tolerance for the solderability of board pads. In the case of a no-clean BGA mounting process where use of an aggressive flux may raise concern about reliability, improving the solderability of board pads then becomes the preferred option.

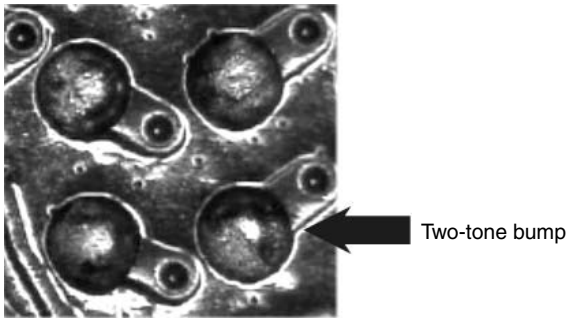

Figure 9.22 A "two-tone" solder bump

For high Pb balls or columns, an oxidized surface often poses difficulties in wetting, since wetting cannot be facilitated by coalescence of a high Pb solder with an eutectic Sn−Pb solder. The relative ease of oxidation for high lead solder further increases the problem.

Unlike leaded components, the wettability of solder bumps on BGA and CSP is not easily measurable. Reynolds and Romm [46] have suggested modifying ANSI/EIA-638, a procedure for solderability testing of fine-pitch SMDs, for testing BGA and CSP. The modified procedure can be described as follows.

Deposition of solder paste on to a ceramic plate (0.035-in. thick) via a stencil in the pattern of the BGA balls to be tested.

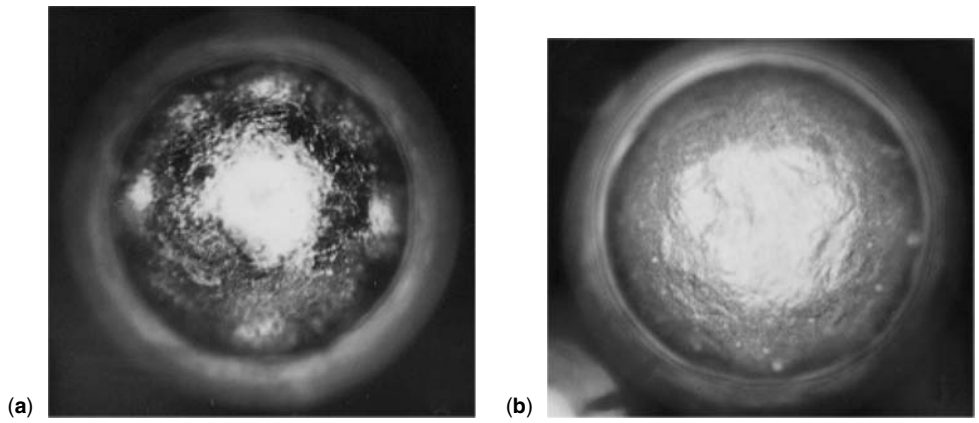

Figure 9.21 62Sn/36Pb/2Ag solder bump: **(a)** shiny bump, **(b)** dull bump

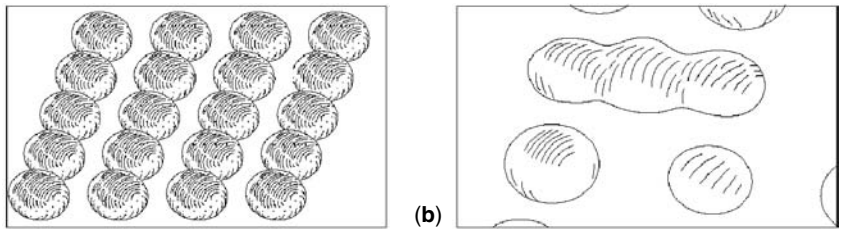

Figure 9.23 BGAs after reflow in the solderability test. **(a)** BGA with a good solderability, where solder paste evenly wets to each bump with no bridge formed, **(b)** BGA with a poor solderability, where solder paste bridges instead of evenly wets to each bump [46]

The devices are then placed on the solder paste print.
The substrate is processed through a reflow cycle and allowed to cool before the units are removed from the ceramic and inspected.

Figure 9.23 shows BGAs after reflow in the solderability test and Figure 9.23(a) shows BGA with a good solderability. Here the solder paste evenly wets each bump with no bridge formed. Figure 9.23(b) shows BGA with a poor solderability. Here the solder paste bridges due to excessive solder paste volume caused by poor wettability of the solder bumps [46].

In summary, poor wetting can be reduced by the following approaches:

Avoid shaking the balls by using a "first come, first go" ball placement mechanism.
Use balls with better oxidation resistance.
Use a more active and better wicking flux.
Improve the solderability of board pads.

9.3.4 Voiding

Voiding in BGA (see Figure 9.24) has been a controversial issue for many years. On the one hand, a void is considered a stress concentrator. The presence of voids is expected to affect the mechanical properties of joints [47] and reduce strength, ductility, creep and fatigue life [48,49]. It can also produce spot overheating [50], hence reducing the reliability of joints. On the other hand, a void is also considered a crack terminator. It may slow crack propagation by forcing re-initiation of the crack, thus having crack arresting properties [51].

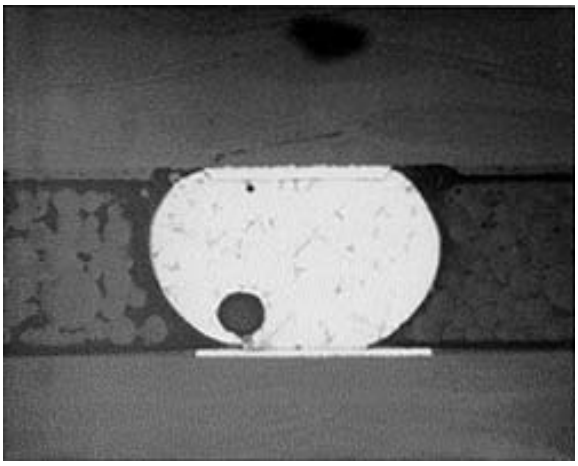

Figure 9.24 Cross-section of a PBGA solder joint showing the presence of a void

Since both schools of thought have valid arguments, perhaps the best way to understand the impact of voiding on reliability is by reviewing the correlation between voiding and reliability. Unfortunately, there are few data published on this issue. In order to establish a preliminary consensus on voiding, the author would like to cite a few statements on voiding learned through either conference conversations or private communications:

IBM: Considers 20 percent voiding (area/area) in BGA joints would be a considerable threat to reliability, and sets 15 percent as a maximum allowable voiding extent.
Solectron: Considers 25 percent (area/area) as a maximum allowable voiding extent.
Delco: Has carried out a voiding study on flip chip applications and examined the void size effect. Six or seven large voids (at 20 percent solder joint diameter) result in 50 percent reduction in performance in a temperature cycling failure test. Four voids were set as a criterion (16 percent area/area) and three were found to be maximum in production conditions.
HP: A small amount of voiding is not a concern.
Motorola: A voiding content up to 24 percent (area/area) is still acceptable for reliability.
General Instruments: The upper control limit for void area is set at 15 percent.

The statements cited above suggest that:

Voiding is acceptable at low contents.
Too much voiding is unacceptable.
An acceptable maximum void area could be about 15–25 percent.

Since the consensus appears to be that excessive voiding is harmful, it becomes clear that it is crucial to understand the factors governing voiding behavior in order to control voiding level.

O'Hara and Lee [52] have studied voiding mechanisms in BGA assembly and their findings will be briefly introduced below. The first observation they have made is that voiding is negligible at solder ball and BGA component

stage. Voiding is introduced mainly at the BGA assembly stage.

9.3.4.1 Effect of solvent volatility

The effect of the solvent's boiling point on voiding for both flux soldering and solder paste soldering is shown in Figure 9.25 [52]. Here the tack fluxes used vary in solvent boiling point and the solder pastes used are composed of the same series of tack fluxes and are 90 percent (w/w) in Sn63 (−325/+500 mesh) metal content. Results indicate that the void content increases with decreasing boiling point. This trend holds true for either type of soldering material. Primavera *et al*. [53] have reported that the lowest void producing paste has the highest weight loss during flux activation dwell time. In their study, the flux chemistry was not maintained constant, therefore it is difficult to attribute the voiding trend to the weight loss factor instead of flux chemistry.

Voiding in a typical SMT process has been reported [54] to be directly caused by the outgassing of an entrapped flux in the molten solder during reflow. In this study, both flux and paste samples which display the highest void content in the corresponding series utilize a solvent with the lowest boiling point (137°C) in the series. Since this boiling point is much lower than the peak temperature (226°C) at reflow, the solvent is expected to dry out at a fairly early stage during reflow. In other words, the remaining solvent content during reflow should not be the dictating factor of outgassing which is responsible for voiding. Other sources such as the flux chemical itself or the released product from a fluxing reaction could be equally important.

9.3.4.2 Flux-exclusion-rate model

The voiding trend observed above can be explained by a viscosity-dictated flux-exclusion-rate model. The fluxes drying out more readily will result in a flux remnant with a higher viscosity. This higher viscosity remnant will be difficult to exclude from the interior of the molten solder, therefore there will be more risk of its being entrapped in the molten solder and serving as an outgassing source, hence contributing to more voiding. In other words, the solvent volatility affects voiding through the viscosity factor instead of direct solvent outgassing. The higher the solvent volatility, the more risk of the flux remnant being entrapped, therefore the stronger the tendency to form voids.

9.3.4.3 Effect of reflow profile

Figure 9.26 shows the effect of reflow temperature on the voiding of BGA joints [52]. Obviously, the cool reflow profile (peak temperature 205°C) results in less voiding than the typical profile (peak temperature 226°C). The difference in voiding between the two reflow profiles decreases with increasing solvent boiling point. The relations observed above can also be explained by the viscosity-dictated flux-exclusion-rate model. Presumably, the cool reflow temperature dries out the volatile solvent less readily than does the typical profile. The remaining undried solvent effectively reduces the viscosity of the flux remnant, hence facilitating exclusion of the flux from the molten solder, and resulting in less voiding.

With an increasing solvent boiling point, it becomes increasingly difficult to dry out the solvent, and the amount of remaining solvent becomes increasingly less sensitive to the reflow temperature employed. As a result, the difference in voiding between the two profiles also diminishes.

Besides the simple time–temperature variation studies discussed above, Lee[8] has reported that, based on defect mechanisms analysis, a linear ramp-up profile (Tent profile) will result in less oxidation and better wetting, therefore less voiding. Heller [9] later concurred that BGA components can be successfully reflowed with a traditional ramp, soak, reflow, and cool profile or with a gradual ramp-up, spike, and cool or Tent profile. In general, the

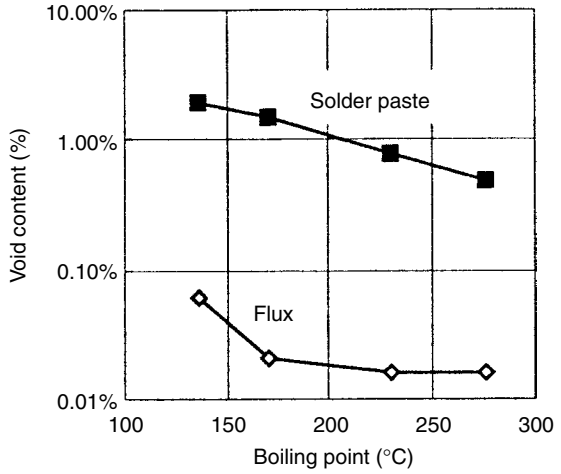

Figure 9.25 Effect of solvent boiling point on the voiding of BGA joints using 63Sn/37Pb solder pastes or fluxes [52]

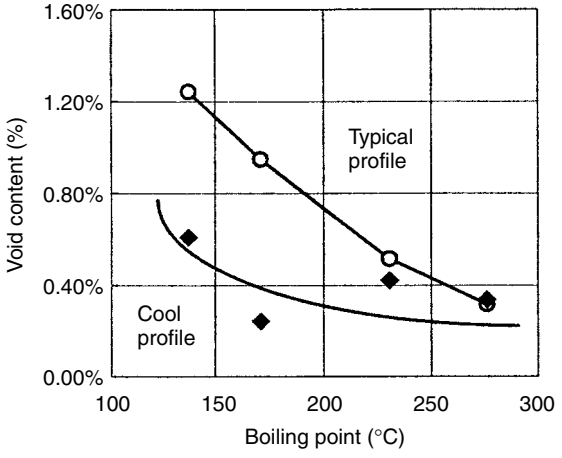

Figure 9.26 Effect of reflow temperature on the voiding of BGA joints soldered with 63Sn/37Pb solder paste in an air atmosphere [52]

slower ramp rate (<0.7°C/sec below 100°C) found with the Tent profile has been associated with lower defect rates. Similar findings have also been reported by Shina *et al*. [55]. However, the two later studies did not specifically focus on voiding performance.

Primavera *et al*. [53] have also studied the effect of profile on voiding. They reported that the variable soak temperature seems to have only a negligible effect when the soak time is at the upper value of 2.5 min and the peak temperature is at the lower value of 205°C. Of the reflow parameters, the soak time is the primary factor that affects voiding. The peak temperature also shows a slightly smaller significant effect as does time above liquidus.

9.3.4.4 Effect of metal content

The effect of metal content was studied with metal content varying from 0% to 91% (w/w), under a typical profile and air reflow atmosphere. The results shown in Figure 9.27 indicate that the void content increases with increasing metal content [52]. A similar trend was also observed by Primavera *et al*. [53]. This can be attributed partly to an increase in solder powder oxide, therefore an increase in outgassing due to an increasing fluxing reaction. It can also be due to an increasing difficulty for flux to escape due to tighter powder packing and the formation of a greater amount of high viscosity metal salt. This is consistent with the flux-exclusion-rate model postulated above.

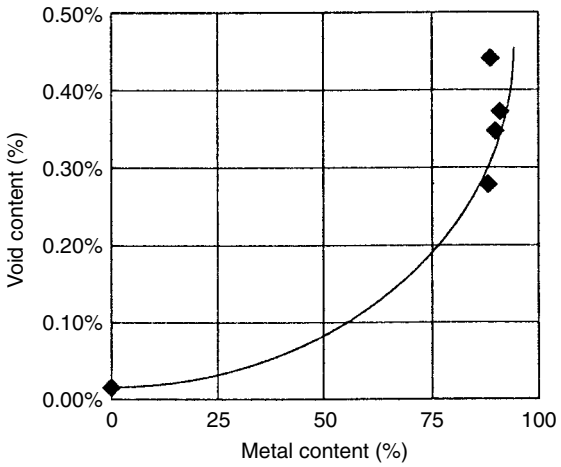

Figure 9.27 Effect of Sn63 (−325/+500 mesh) metal content on voiding of BGA joints [52]

Table 9.6 Correlation between mesh number and size

Mesh number	*Size (μ)*
200	74
325	44
400	38
500	25

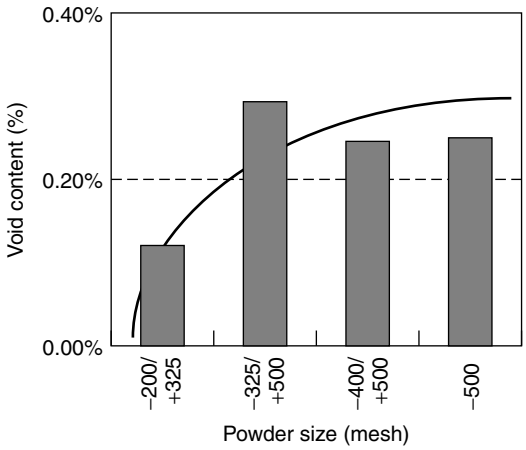

Figure 9.28 Relation between powder size and voiding of BGA joints [52]

9.3.4.5 Effect of solder powder size

Four mesh ranges of Sn63 solder powder are used in this study, with mesh-dimension correlation shown in Table 9.6. As indicated in Figure 9.28, there is a slight trend showing that voiding increases with increasing mesh number (or decreasing powder size) [52]. This trend was also reported in a later study [53]. This relation can be attributed to the increasing oxide content of the powder associated with decreasing powder size. As discussed in sub-section 9.3.4.4, section, the increasing oxide content will result in greater outgassing and also more high viscosity metal salt formation, and consequently more voiding.

9.3.4.6 Effect of reflow atmosphere

The presence of oxygen during reflow usually promotes metal oxidation and results in poorer solderability [56]. This can be fairly significant when trying to solder onto an immobile metallization, such as copper or nickel. As discussed in Chapter 6, section 6.10, poor wetting directly contributes to more voiding due to entrapped flux at non-wetted sites. Primavera *et al*. [53] have confirmed that the voiding frequency for joints reflowed in a nitrogen atmosphere of less than 50 ppm O_2, was one half as much as joints reflowed in air. In their study, the substrates are primarily immobilized surface finishes. With the metallization being solder itself, the solderability of both BGA bumps and PCB pads is very good and should not be sensitive to the reflow atmosphere. This is found to be true, as demonstrated in Figure 9.29. Within experimental error, the reflow atmosphere basically shows no effect on the voiding of BGA joints [52].

9.3.4.7 Effect of surface finishes

In general, the Ni/Au attachment pads showed the fewest voids, followed by HASL, OSP with one reflow, Ni/Pd, and Ni/Pd with an Au flash. A significant increase in voiding was observed when OSP coated attachment pads were

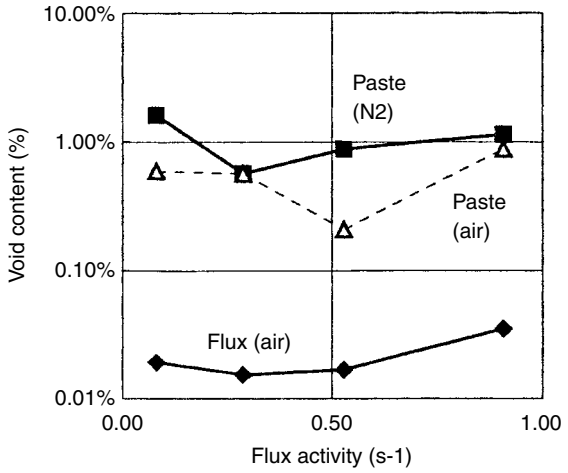

Figure 9.29 Relation between flux activity and voiding in BGA joints [52]

printed after cleaning in acetone or isopropanol. Minimal differences were noted on other finishes studied. PCBs covered with human fingerprints showed more voids [53].

9.3.4.8 Effect of paste exposure time

Voiding increases with increasing paste exposure time [53]. Presumably increasing exposure time will result in more oxidation and more moisture pickup, hence more voiding.

9.3.4.9 Effect of board pad design

Board pad design has a considerable effect on voiding and several examples are given below.

Via in Pad Via in pad is a design where the via is positioned within the pad instead of laying next to the pad and forming a dumbbell. It allows more space between pads for trace routing, thus enabling a higher I/O density design. For BGA attached onto a via in the pad land pattern with the use of solder paste, large voids tend to form next to the base of the BGA package, as shown in Figure 9.30. Air reflow yielded less voiding, associated with higher standoff. If a tacky flux is used instead of solder paste for a BGA attachment, then the voiding problem is eliminated.

At first, it is interesting to note the large voids being retained in the joints instead of escaping. This is attributed to the surface tension effect. The buoyancy effect is able to bring the void up to the top of joint. However, to further escape from the joint the large void will have to flatten its round shape in order to pass through the small standoff between the BGA and PCB. Since a flattened void has more surface area than a round one, this flattening requirement is unfavorable due to the additional surface energy needed in order to provide this extra surface area. In other words, the dictating factor here for large voiding is the low standoff.

Air reflow usually produces more voiding due to poorer wetting, as discussed in section 9.3.4.6. In this case, the poorer wetting results in less spreading on the board pad and consequently a higher standoff for the joint. A higher standoff would allow the large void to escape much more easily, thus explaining the positive effect of air reflow on reducing voiding.

Voiding is caused by outgassing which in turn is the result of fluxing reactions or flux volatiles. When a solder paste is used for BGA attachment onto the card with a via in the pad, the paste filled within the via hole will melt, coalesce, and wet to the parts at the same time. During this coalescence process, some flux will inevitably be temporarily entrapped within the molten solder. At this stage, any outgassing from the entrapped flux will result in voiding. Coalescence of small voids plus the effect of buoyancy plus the low standoff eventually result in a large void stuck at the top of the solder joint.

On the other hand, if a tacky flux is used instead of a solder paste, the solder joint will be progressively formed through the meltdown and spreading of the solder bump. The molten solder from the solder bump will progressively advance down through the via hole, with flux staying in front of the solder front. Any outgassing during this process can be easily emitted into the air and cause no voiding, since all flux is located at the outside of the molten solder.

Although the use of a tacky flux will alleviate the voiding problem here, it will also eliminate the additional solder volume introduced by solder paste and result in an unacceptably low standoff for meeting reliability requirements. Presumably, this problem can be resolved by prefilling the via hole with solder or another filler. It

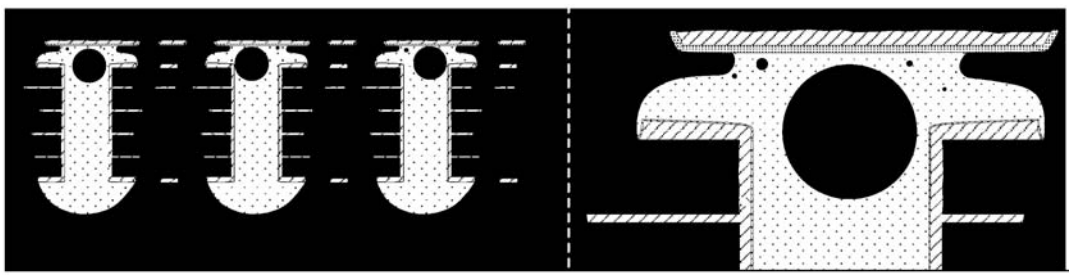

Figure 9.30 Cross-section of BGA attached to via in pad with solder paste. **(a)** Fairly large voids are found next to the base of the BGA package. **(b)** Close-up of a large void. (Courtesy Motorola)

may also be overcome with the use of a BGA loaded with extra large bumps.

Microvia Similar to via in pad, microvia also positions the via within the pad. The difference is that microvia uses build-up technology, and the via typically is smaller, and is a blind via. Figure 9.31 shows a schematic view of microvia with penetration down to layers 1 and 2 [57].

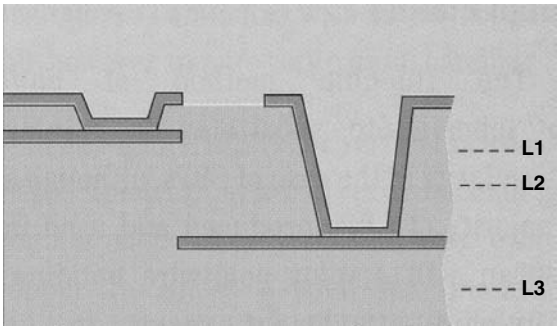

Figure 9.31 Schematic of microvia with penetration down to layer 1 and layer 2 [57]

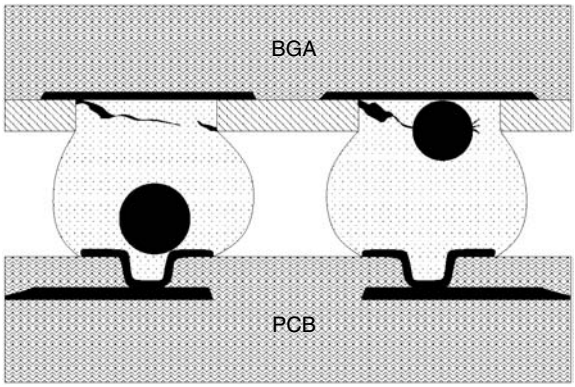

Figure 9.32 Cross-section of BGA solder joints formed on microvia. Voids tend to form at the opening of microvia, but can also form at the upper side of the joint. (Source: Ericsson)

With the increasing adoption of microvia technology, it becomes apparent that BGA or CSP solder joints on microvia tend to have more voids [58] than joints on a flat pad. The typical symptom is a void sitting on the opening end of microvia, as shown by the left-side joint in Figure 9.32. However, sometimes the voids may be located on the upper side of the joint, as shown by the right-side joint.

The voiding problem associated with microvia can probably be primarily attributed to the semi-sealed via structure. Due to the confined opening, the following effects can be expected:

- *Greater difficulty in via plating quality control and subsequent cleaning efficiency*.

  Figure 9.33 shows an example of uneven plating thickness at a microvia cavity site. This implies that the solderability may also be uneven. In addition, the confined opening will very likely hamper post-plating cleaning efficiency. As a result of both factors, the solderability within the microvia cavity will very likely be compromised. As shown by the earlier discussion, voiding is caused by outgassing, which in turn is caused by flux volatiles or fluxing reactions. Any spot on the pad being unsolderable will serve as a source for entrapped flux and consequent outgassing. Apparently, the compromised solderability of a microvia cavity will contribute to voiding. Although using flux with a higher activity will help in compensating the reduced solderability, concerns on corrosion and SIR will limit this approach for no-clean applications.

- *Greater difficulty in releasing the void formed at the via opening*.

  By examining microvia voiding closely (see Figures 9.32 and 9.33), the voids typically stick to the opening rim of the microvia, as schematically illustrated in Figure 9.34. As a result, the surface of the rim contributes to part of the void surface. To dislodge the anchored void from the via opening, additional energy will be needed in order to create the extra solder surface area, S, originally provided by the rim of the microvia.

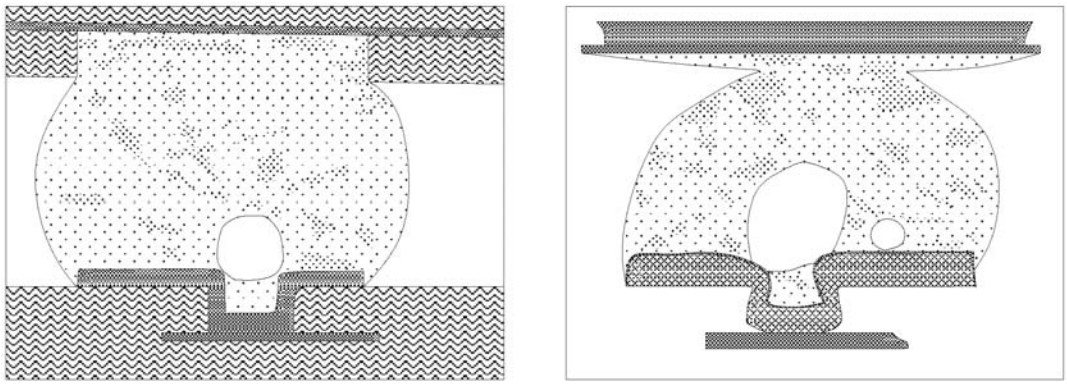

Figure 9.33 Examples of BA solder joints on microvia with voids formed on microvia opening [58]

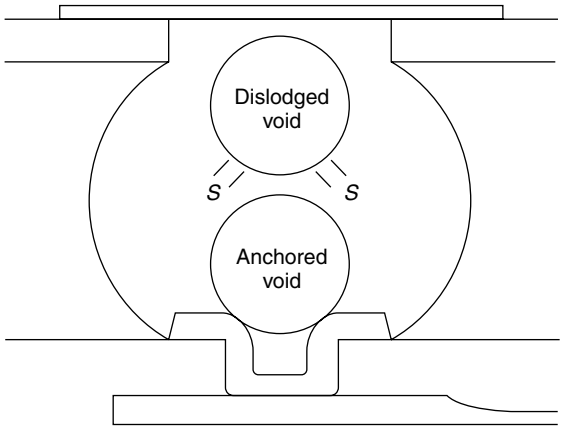

Figure 9.34 Schematic of voiding in a BGA solder joint. To dislodge the anchored void from the via opening, additional energy will be needed in order to create the extra solder surface area *S* originally provided by the rim of the microvia

This is unacceptable, therefore the void tends to stay until the buoyancy overrides the surface energy factor.

- *Greater difficulty in expelling the flux entrapped within the via cavity.*

  The semi-sealed cavity structure dictates that the entrapped flux will have greater difficulty in escaping. As long as the flux is still entrapped within the cavity, it will continuously outgas and contribute to voiding.

Based on the voiding mechanisms discussed above, the following directions are considered promising in reducing or eliminating the voids:

Increase the solderability of the microvia.
Fill the cavity prior to BGA attachment.
Use flux with minimum outgassing, at least at a temperature above the melting point of solders.
Use a reflow profile which provides better wetting and burns off the volatiles.

One attempt to pre-fill the cavity was carried out by printing solder paste onto the pads, followed by reflow. The board was then sent through a normal BGA attachment process. Unfortunately, the results showed no improvement in voiding [59]. The failure experienced here can probably be explained by the untouched root cause. If poor solderability within the cavity is the root cause, it cannot be corrected by pre-filling the cavity with reflowed solder paste, and the entrapped flux at non-solderable sites will still outgas during the subsequent BGA attachment process.

Perhaps the problem can be corrected by electroplating solder onto the microvia, followed by applying flux and reflow. Figure 9.35 shows a cross-section of laser-ablated holes after electrolytic Cu and SnPb plating and reflow [60]. Since flux can only stay on the top of the electroplated solder layer, the flux entrapment problem is accordingly eliminated for the solder filling process. In Figure 9.35, although the top microvia is not completely

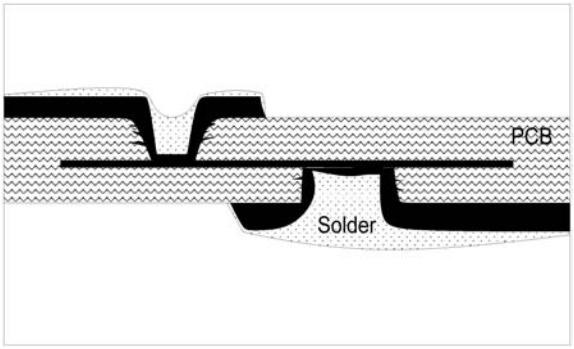

Figure 9.35 Cross-section of laser-ablated holes after electrolytic Cu and SnPb plating and reflow [60]

filled by the solder, this can be easily improved by electroplating more solder onto the microvia. Once the microvia is leveled with the solder, the root cause for microvia voiding is then eliminated.

9.3.4.10 Effect of quality of parts

Voiding in BGA can also be affected by the quality of parts. For instance, some unacceptable voiding has been experienced when attaching BGA to via in pad. Figure 9.36 shows cross-sectioned samples with such joints. In Figures 9.36(d), 9.36(e), and 9.36(f), the voids are so large that little solder is left in the via. The solder paste used for this assembly was found to be normal when tested.

The cause resides in the barrel quality. After investigation, it was found that the barrel was not properly plated, and exhibited very high porosity. Upon reflow, the volatiles from a PCB escaped through the porous barrel and blew the solder out of its way.

Although the problem was eventually eliminated by straightening the barrel plating process, those problematic PCBs were scavenged by pre-baking them prior to solder paste deposition. Without volatiles from the board, a solid, well-filled joint was produced again, as shown in Figure 9.15.

The case described above serves as a very good example of troubleshooting. As mentioned earlier, almost all the problems can be attributed to material, process, and design. If the cause of a problem is beyond the control of the manufacturer, the problem still can be solved or minimized through tempering with other factors. Here the plating quality of via is the cause. However, the problem was solved by pre-baking the boards long before the plating process was straightened out.

9.3.4.11 Effect of process orientation

Depending on the location of a void, a void can cause more damage to the joint if little solder can be found around the void. Figure 9.37 shows a cross-section of BGA 63Sn/37Pb solder joints after a temperature cycling test. The solder joint has an asymmetrical shape, with package side being smaller than the PCB side. Both

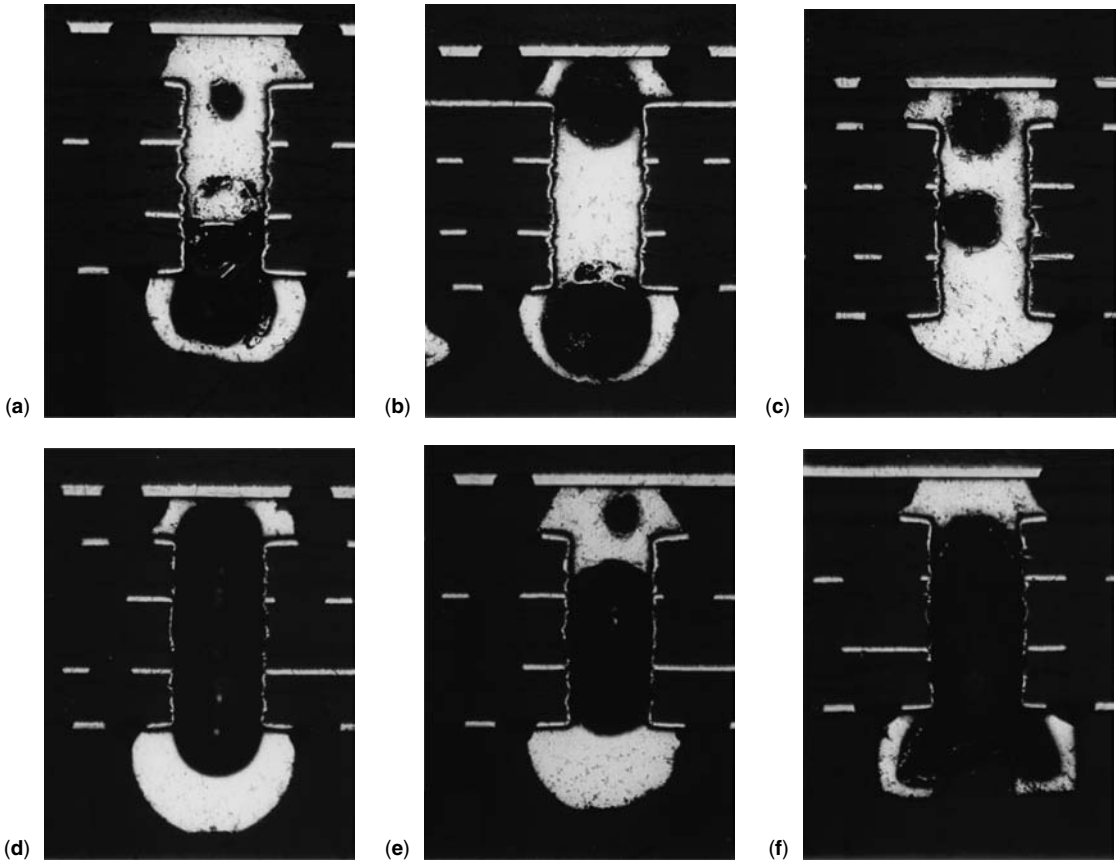

Figure 9.36 62Sn/36Pb/2Ag solder joints of BGA mounted on via in pad. The joints exhibit extremely bad voiding behavior

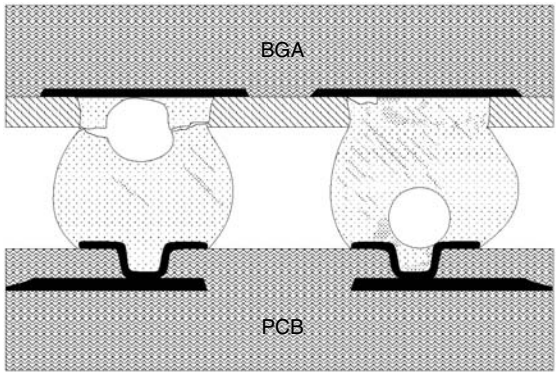

Figure 9.37 Cross-section of BGA 63Sn/37Pb solder joints after temperature cycling test. Both joints have voids of comparable size. The joint on the left cracked due to a smaller solder volume around the void. The joint on the right held well due to a larger solder volume around the void [59]

joints have voids of comparable size. The joint on the left cracked due to a smaller solder volume around the void but the joint on the right held well due to a larger solder volume around the void [59]. The results here indicate that if the void location can be controlled, better reliability may be achieved by locating the voids at the least vulnerable location within the solder joint.

Location control can be accomplished through process orientation. Although voids in BGA joints may appear at either top or bottom sides [61], buoyancy does drive more voids toward the top sides of the joints [59, 62]. Hence, for a double-sided PCB containing BGAs or CSPs with an asymmetrical solder joint configuration, better reliability can be achieved if the wider side of the solder joint is in the upper position during the second reflow step, as shown in Figure 9.38.

9.3.5 Bridging

Bridging (see Figure 9.39) constitutes one of the major defect types of BGA [15]. Poor solderability of solder balls can be the cause of bridging, as demonstrated by Figure 9.23 [46]. In general this occurs on CBGA and CCGA. Fauser *et al.*[63] have reported that bridging can result from excessive solder paste deposited. The same study also reported that bridges can also be caused by a manual tweaking device to correct misalignment after machine placement. Long, thin, uni-axial bridges, encompassing two or more joints, characterized this occurrence

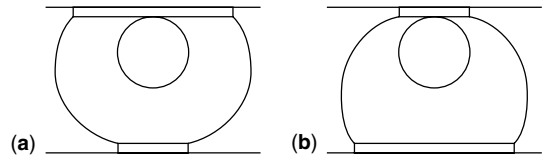

Figure 9.38 BGA joint **(a)** is expected to have better reliability than joint **(b)**

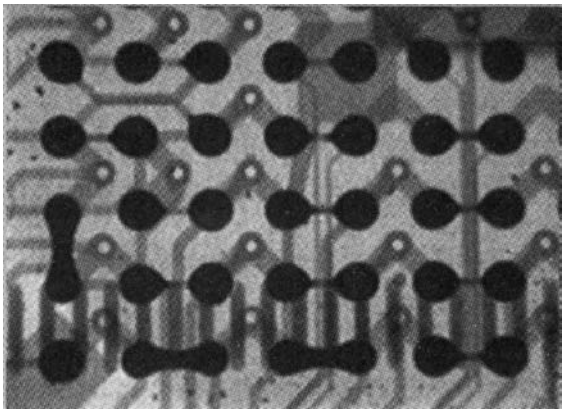

Figure 9.39 X-ray photograph of BGA joints with bridges

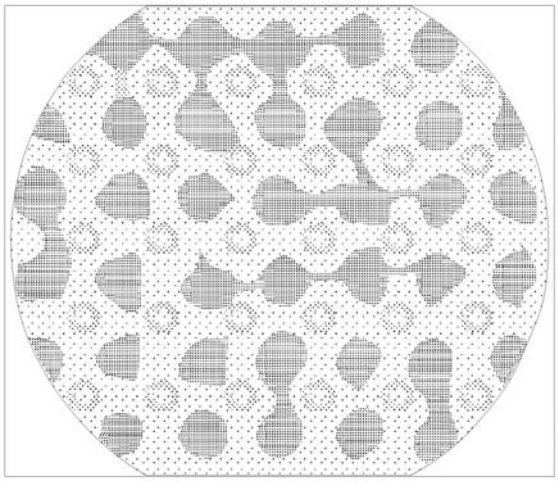

Figure 9.40 X-ray photograph of BGA joints with bridges caused by manually tweaking device to correct misalignment after machine placement [63]

(see Figure 9.40). In addition, bridges may also occur due to popcorn or delamination of PBGA. The joints flatten out and form bridges, as shown in Figure 9.41. Foreign material under the device may also cause shorts [63].

Bridging is often aggravated by misregistration of component placement, including both linear offset and rotational skew. CBGA appears to be limited to 1° of

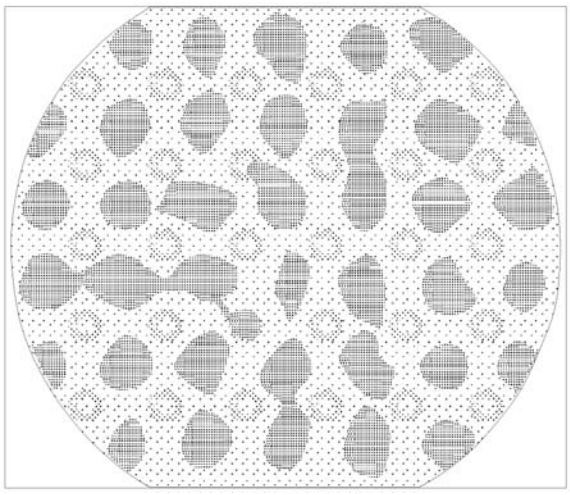

Figure 9.41 X-ray photograph of PBGA solder joints. Bridges may occur due to popcorn or delamination of PBGA. The joints flatten out and form bridges [63]

rotational skew, evidenced when one device in four resulted in solder bridges. Figure 9.42 shows the bridging condition that was observed during a linear misplacement of 80 percent [7]. The "flattened" eutectic ball of PBGA caused by collapse of the ball at reflow minimizes spacing between balls and contributes to solder bridging when misplaced more than 62 percent off the pad. This device has the same 1° rotational limitation as CBGA, with solder bridging as the failure mechanism (see Figure 9.43). For CSP, due to the smaller pitch plus the overprint area of solder paste commonly used for CSP paste deposition, CSP is more sensitive to linear misplacement.

In summary, bridging can be eliminated by the following solutions:

Improve the solderability of packages.
Control the solder paste volume deposited.
Avoid manually mishandling devices after placement.

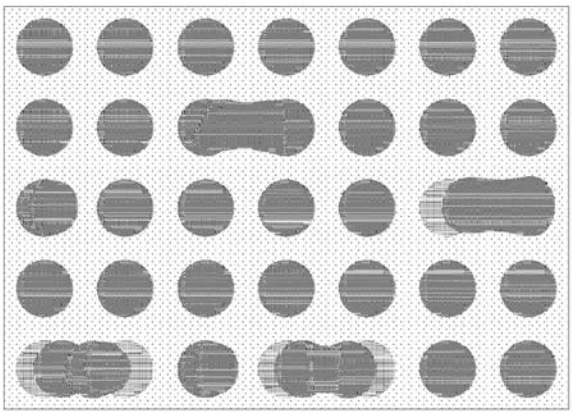

Figure 9.42 X-ray photograph of CBGA ball-to-ball bridging at 80 percent offset [7]

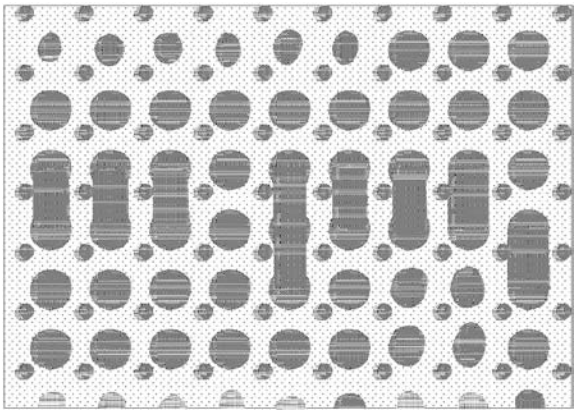

Figure 9.43 X-ray photograph of PBGA bridging at 1° rotation [7]

Pre-bake PBGA when necessary to avoid the popcorn effect.
Avoid leaving foreign materials under the device.
Avoid misregistration at device placement.

9.3.6 Open

Open can be caused by several factors, including insufficient solder volume, poor solderability, non-coplanarity, misregistration at placement, mismatch in thermal expansion, and outgassing through the solder mask, and will be discussed below.

9.3.6.1 Insufficient solder volume

Insufficient solder paste deposited, mostly caused by clogging, can result in open. This is more likely when CBGA or CCGA is being attached, since both types of device do not collapse during reflow.

9.3.6.2 Poor solderability

Pad contamination or oxidation often cause wetting problems. In Figure 9.44, the open (left) is caused by pad contamination. Since the solder cannot wet to the PCB pad, it wicks up the solder ball to the component interface [10]. A similar defect has also been observed for DBGA [64]. In addition, this poor solderability of the pad can also cause open in collapsible PBGA, as shown in Figure 9.45 [44] .

9.3.6.3 Non-coplanarity

Non-coplanarity often contributes to or directly causes open. Therefore, PCB variation in coplanarity should not exceed max 5 mils local or 1 percent overall per IPC-600A, acceptability D, class 2&3 [15]. During the rework process, ensuring a preheat procedure will minimize the warp and reduce the problem.

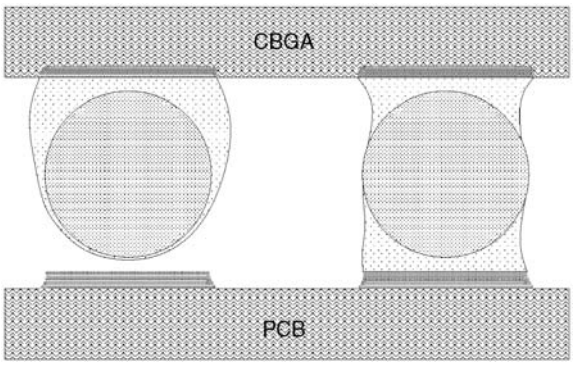

Figure 9.44 Cross-section of CBGA solder joints showing opens caused by pad contamination [10]

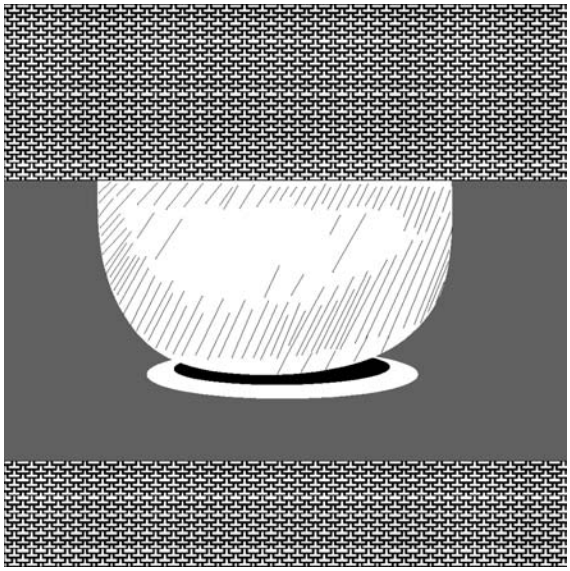

Figure 9.45 PBGA solder joints showing an open [44]

9.3.6.4 Misregistration at placement

Excessive misregistration at placement often causes open. Figure 9.46 shows opens in a CSP caused by misplacement. The picture on the right shows jumping a row caused by 50 percent linear misplacement [7], that on the left suggests that the problem is further aggravated by skewing at placement.

9.3.6.5 Mismatch in thermal expansion

Solder joint open can be caused by a shearing force generated by internal stress. This can be due to the excessive temperature gradient developed across the board in certain process conditions. For instance, for a SMT reflow process followed by wave soldering, the PBGA corner joints formed in the reflow process can crack open at the interface of the solder joint and the package at the wave soldering stage, as shown in Figure 9.47. In some

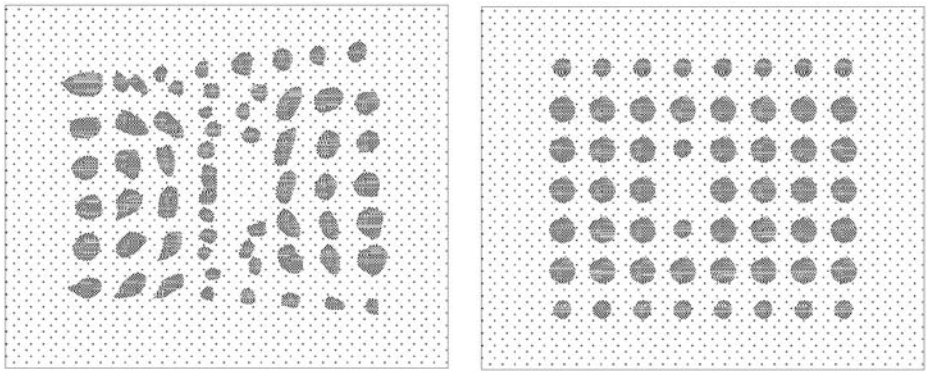

Figure 9.46 X-ray photographs of CSP showing jumping a row caused by 50 percent linear misplacement [7]. Picture at left suggests a problem further aggravated by skewing at placement

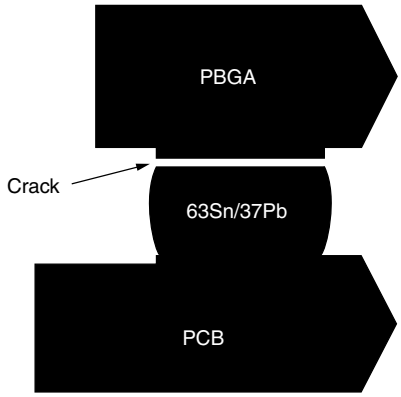

Figure 9.47 Schematic of PBGA 63Sn/37Pb solder cracked between joint and PBGA package during wave soldering

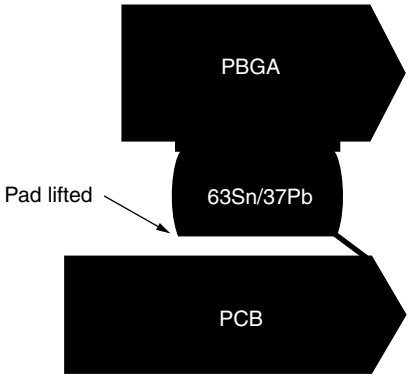

Figure 9.48 Schematic of PBGA solder joint with corner pad lifted from the board during wave soldering

instances, at corners of PBGA, the solder ball remains in contact with both the PBGA component and the PCB pad. However, the pad is peeled away from the PCB and is barely connected to the PCB through the traces, as shown in Figure 9.48. In both instances, the PBGA solder joints are close to vias.

The direct cause is the high temperature gradient from the board to the package. During wave soldering, the hot solder emerges through the via to the topside of PCB, and causes the PCB's topside surface to rise quickly in temperature. As solder is a good thermal conductor, the joint temperature accordingly also quickly rises. However, the package itself does not have as good a thermal conductivity, and accordingly warms up much more slowly. Since a hot solder is fairly weak in mechanical strength, the stress developed between the hot PCB and the cold PBGA due to mismatch in thermal expansion consequently results in rupture between the solder and the package pad. In some instances, adhesion between pad and board may be weaker than the bond strength between solder and package pad. This conversely results in the pad lifting from the board instead. Corner joints suffer most due to a larger distance to a neutral point, therefore a greater mismatch in thermal expansion.

The problem can be solved by covering the vias with a solder mask. The opens then become much fewer than in cases with uncovered vias. If the volume is not high, manually applying a tape at the vias prior to wave soldering can also eliminate the problem.

9.3.6.6 Outgassing from beneath the solder mask

For a BGA with solder mask defined pad, an open has also been observed as a result of outgassing. Here the volatiles vigorously emitted from the interface between solder mask and package pad may blow the solder away from the package pad and cause an open, as shown in Figure 9.49. This problem can be minimized by prebaking the PBGA prior to attachment.

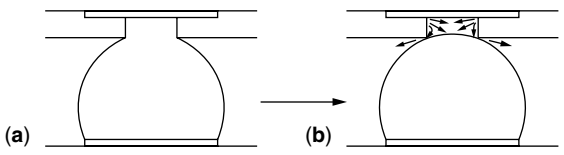

Figure 9.49 Schematic of BGA joint with open caused by outgassing from underneath the solder mask on the package side

In summary, an open can be eliminated by the following approaches.

Deposit sufficient solder paste.
Improve the solderability of the board pad.
Maintain coplanarity of the board.
Place component accurately.
Avoid development of temperature gradient. Cover the via prior to wave soldering.
Pre-bake the components.

9.3.7 Uneven joint height

The solder joint of BGA and CSP typically is a round convex shape, with joint height determined by surface tension of solder, pad dimension, solder mask layout around the pad, and component weight. For a double-sided PCB, the joint height of the bottom-side components may be elongated depending on the weight of the package. In most instances, the joint still remains a convex shape. However, if the component is heavy, the joint may be stretched to a slim concave shape. In general, the joint height is even and all these solder joint configurations are considered acceptable, with the elongated joints preferred under certain conditions due to a higher standoff, therefore a better capability in absorbing mismatch in thermal expansion.

However, there are occasions where the joint height is not even and the elongated solder joint is not acceptable. It has been observed that during assembly of some PBGA types, the outer joints were stretched to about 27 mils in height, while the inner joints were around 19 mils in height. A closer look revealed that the outer joints surfaces appeared rough, with some orange peel texture showing some signs of rupture or micro-cracks. A cross-section of those joints showed irregularly shaped micro-voids ($<25\,\mu$) formed near the interface of solder and board pad. Those micro-voids were deeper around some voids near the interface [65]. Since either a micro-crack at the surface or a micro-void within the solder joint often serve as crack initiators, these elongated solder joints are considered not acceptable, regardless of the higher standoff associated with them. Further investigation indicated that the PBGA molding compound and PBGA substrate exhibited a mismatch in TCE, with the molding compound displaying a higher TCE. The structure of the assembled PBGA is illustrated in Figure 9.50.

Obviously, the uneven joint height is caused by the warp of the PBGA package which in turn is caused by the mismatch in TCE of the molding compound and the PBGA substrate. When the package begins to cool, the package starts to warp, with the edge being pulled upward. The warp continues to increase with decreasing temperature, even at a temperature below the solidification temperature of solder, causing the outer joints to be longer than the inner joints.

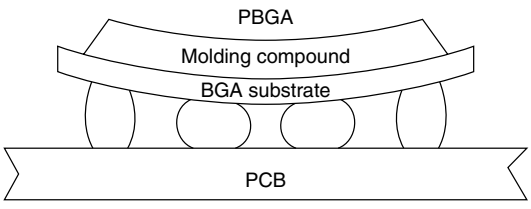

Figure 9.50 Schematic of BGA with uneven joint heights

The microvoiding and surface fracture phenomena are attributed to the cold-drawing of solder. At a temperature just below solidification temperature, the solder is soft and weak. Under warp tension, the soft solder starts to deform and microvoids start to develop, presumably between grain boundaries. Meanwhile, the surface also starts to show a rupture texture. Since the PCB has a larger thermal mass than PBGA, thus cooling more slowly, these effects are expected to be more serious near the board's surface where the solder temperature is higher and the solder is weaker.

The cause of the problem is a mismatch in TCE within PBGA. Adjusting the reflow profile will not alter this mismatch, therefore it will not be helpful in correcting the problem. The ideal way to eliminate the problem is employing packaging materials with a matching TCE. Another way to fix the problem, which has been attempted and successful, is stiffening the BGA substrate with one more copper layer so that the BGA substrate will not bend.

9.3.8 Solder webbing

Solder webbing is a continuous film of solder parallel to but not necessarily adhering to surfaces between separate conductive patterns [15]. It is caused by temporary bridging followed by incomplete breaking apart of the solder. This temporary bridging can be caused by a smeared solder paste, a misplacement, or a tweaking action. Upon reflow, if the solder volume is not sufficient to sustain a stable solder bridge, the solder will snap open and form individual joints. However, if the flux activity

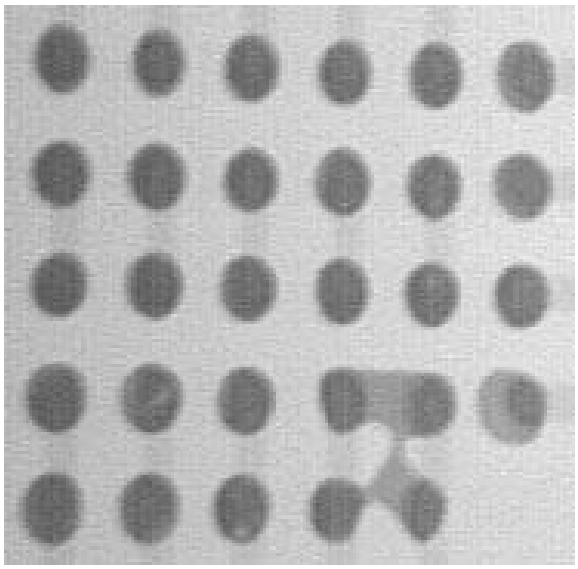

Figure 9.51 X-ray photograph of underfilled 63Sn/37Pb solder joints showing solder webbing

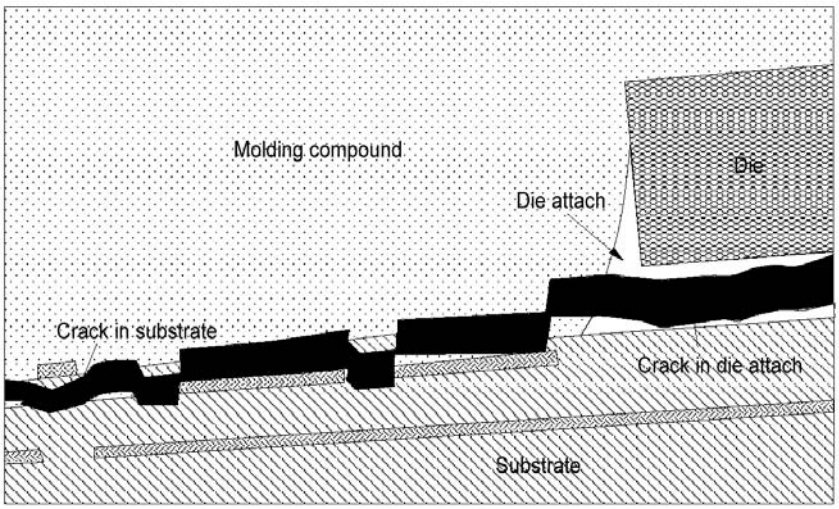

Figure 9.52 Cross-section of the 2-layer PBGA package after level 2a/260°C stressing indicating delamination within the die attach layer and internal/substrate layers [41]

is not sufficient to remove the surface oxide film of the solder, this surface oxide film, or dross, will remain as solder webbing. In general, most of the fluxes available should be active enough to prevent the formation of solder webbing.

Solder webbing may also occur in the presence of underfill. For certain CSP assembly processes, underfill is used between CSP and PCB to enhance the reliability of CSP solder joint. Upon curing of the underfill, or upon a subsequent reflow process after underfilling the CSP, the underfilled CSP solder joints may remelt or be malleable enough to be squeezed by the internal pressure of underfill. The leaked solder forms a thin film along any path with a weak flow resistance, such as the interface between underfill and substrate. Figure 9.51 shows 63Sn/37Pb solder webbing caused by underfill.

Besides selecting an underfill with adequate adhesion and curing behavior, use of a lower curing temperature or avoiding reflowing underfilled solder joints should help in eliminating solder webbing.

9.3.9 Solder balling

Perhaps the most common problem encountered in any SMT solder paste reflow process is solder balling. Attachment of BGA and CSP may also have this problem. This is particularly true if a manual printing solder paste is required during the rework stage. Generally, the causes and cures of solder balling for BGA/CSP are fairly comparable to those for a typical SMT process, as discussed in Chapter 6.

9.3.10 Popcorn and delamination

Due to moisture absorption, plastic BGA is prone to have popcorn or delamination problems if not handled properly. Figure 9.52 shows a two-layer PBGA package after being conditioned at IPC/JEDEC moisture sensitivity level 2a (see Table 9.4) then reflowed with a peak temperature of 260°C. A delamination is found within the die attach layer and internal substrate layers [41]. Solutions for preventing those problems have been discussed in section 9.2.2.

9.4 Conclusion

BGA and CSP are taking center stage now for producing miniaturized high density electronic devices. Although the leadless feature allows them to be processed easily without the need of ultra-fine pitch equipment capability, the two-dimensional area array I/O feature imposes a great challenge on the assembly and rework due to the temperature gradient factor and the hidden joint formation process. In addition, the high density substrate technology needed for area array assembly further complicates the process control needed. The challenges discussed in this chapter show that additional considerations should be given in order to have a high yield process.

References

1. ''Kyocera Dimpled BGA'', *RDP-TB-0102-2*. Kyocera Corp. (1995).
2. M. Cole, ''BGA Design and Assembly Considerations'', short course in SMTA International, Chicago, IL, 24–28 September 2000.
3. K. Nakajima, A. Lewis, and N. Brathwaite, ''Implementation and Qualification of Chip Scale Package On-Board Assembly Process'', in *Proc. of Nepcon West 1999*, Anaheim, CA, 21–25 February 1999.
4. V. Solberg, ''Assembly Process Development for Chip-Scale and Chip-Size uBGA®'', In *Proc. of SMTA/IPC Electronics Assembly Expo*, Providence, RI, p. S12–4, 24–29, October 1998.
5. M. Xiao, K. J. Lawless, and N. C. Lee, ''Prospects of Solder Paste Applications in Ultra-fine Pitch Era'', in *Proc. of Surface Mount International*, San Jose, CA, (August 1993).
6. N. C. Lee, ''How to Make Solder Paste Work in Ultra-fine-pitch and Non-CFC Era'', short course at Surface Mount International, San Jose, CA, September, 1994.

7. R. Noreika, C. Fieselman, K. Slesinger, and M. Wells, ''SMT Component Self-centering Properties during Solder Reflow'', in *Proc. of Surface Mount International*, San Jose, CA, pp. 338–346 September 1997.
8. N. C. Lee, ''Optimizing Reflow Profile via Defect Mechanisms Analysis'', IPC Printed Circuits Expo '98.
9. D. Heller, ''CSP and uBGA Reflow'', in *Proc. of Nepcon West 1999*, Anaheim, CA, 21–25 February 1999.
10. S. Rooks, ''Controlling BGA Assembly Using X-ray Laminography'', *EP&P*, pp. 24–30 (January 1997).
11. M. Deley and C. C. Ramsey, ''Accurate Placement of Ball Grid Array Packages'', *EP&P*, pp. 36–42 (April 1996).
12. E. Zamborsky, ''BGAs in the Assembly Process'', *Circuits Assembly*, pp. 68–70 (May 1996).
13. E. J. Vardaman, ''Rework and Repairs: Still Issues for the '90s'', *Circuits Assembly*, pp. 22–25 (May 1996).
14. V. Solberg, ''Ball Grid Array Assembly'', *SMT*, pp. 124–134 (August 1995).
15. J. Kratz, ''BGA Removal & Replacement'', short course in IMAPS/ISHM'97, Philadelphia, PA, 12, October 1997.
16. J. Chen, private communication on reworking BGA experience at Solectron, Austin, TX, 14 October 1997.
17. J. Nash, ''Sharing the Knowledge: Close Encounters During BGA Rework'', *SMTA Newsletter*, p. 2 (October 1997).
18. L. K. Bergman and M. Tazi, ''The Critical Steps of BGA Rework and Repair'', *Surface Mount Technology*, Vol. 11, No. 8, pp. 50, 52–3 (August 1997).
19. D. L. Foster, ''BGA Repair – a Review of the Fundamentals'', *Proc. of SMTA National Symposium Emerging Packaging Technologies*, pp. 138, 95–106, 18–21 November 1996.
20. J. G. Davis, C. R. LeCoz, and J. J. Tomaine, ''Circuit Board Repair and Engineering Change for BGA'' in *Proc. of SMI*, San Jose, CA. p. 2, Vol. 826, 181–7, Vol. 1, September 1996.
21. L. Abbagnaro, ''Reparing BGA components'', in *Proc. of Nepcon West 95*, p. 3, Vol. 1994, 1017–34, vol. 2, Anaheim, CA, February 1995.
22. L. K. Bergman and M. Tazi, ''The Critical Steps of BGA Rework and Repair'', *Surface Mount Technology*, Vol. 11, No. 8, pp. 50, 52–3 (August, 1997).
23. B. Mullins, ''Reworking Ball Grid Array Assemblies'', *Electronic Packaging and Production*, Vol. 36, No. 9, pp. 35–6, 38, 40 (August 1996).
24. D. J. Peck and T. Lee, ''Successful BGA Rework'', *Circuits Assembly*, Vol. 7, No. 4, pp. 36–8, 53, (April 1996).
25. M. J. Jones, ''Increasing BGA Manufacturing Yields'', *Electronic Packaging and Production*, Vol. 36, No. 2, pp. 38–40, 42, 44, 46 (February 1996).
26. T. C. Chung and P. A. Mescher, ''Rework of Ball Grid Array Assemblies'', in *Proc.of Nepcon West 95*, p. 3, Vol. 1994, 334–45, Vol. 1, Anaheim, CA, February 1995.
27. J. G. Spadafora, ''A Rework Process for Ball Grid Array Packages Containing Flip-chip Silicon-on-silicon Multi-chip Modules'', *Proc. of SMI*, pp. 723, 219–24, San Jose, CA, USA, 28 August-1 September 1994.
28. L. K. Bergman and M. Tazi, ''The Critical Steps of BGA Rework and Repair'', *Surface Mount Technology*, Vol. 11, No. 8, pp. 50, 52–3, August 1997.
29. B. Mullins, ''Reworking Ball Grid Array Assemblies'', *Electronic Packaging and Production*, Vol. 36, No. 9, pp. 35–36, 38, 40 (August 1996).
30. G. Dody, and T. Burnette, ''BGA Assembly Process and Rework'', *Proceedings of Surface Mount International Conference*, pp. 1082, 361–6, San Jose, CA, USA, 29–31 August 1995.
31. W. Goers, ''Reworking BGAs – a Joint Concern'', *Surface Mount Technology*, Vol. 10, No. 3, pp. 42, 45, (March 1996).
32. M. J. Jones, ''Increasing BGA Manufacturing Yields'', *Electronic Packaging and Production*, Vol. 36, No. 2, pp. 38–40, 42, 44, 46, (February 1996).
33. R. C. Lasky, A. Primavera, P. Borgesen, and C. Lassen, ''Critical Issues in Electronic Packaging. II'', *Circuits Assembly*, Vol. 7, No. 1, pp. 50, 52, 54, (January 1996).
34. W. Goers, ''Rework of BGAs – A Comparative study'', *Proceedings Nepcon West 95*, p. 3, Vol. 1994, 360-4 Vol. 1, Anaheim, CA, USA, 26 February-2 March 1995.
35. T. C. Chung and P. A. Mescher, ''Rework of Ball Grid Array Assemblies'', *Proceedings Nepcon West 95*, p. 3, Vol. 1994, 334-45 Vol. 1, Anaheim, CA, USA, 26 February-2 March 1995.
36. M. Economou, L. Repellin, G. Vial-David, R. Braude, and S. Sato, ''Reworking Area Array Components'', *Surface Mount Technology*, Vol. 8, No. 8, pp. 113–14, 116, 118, (August 1994)
37. L. Abbagnaro, ''Repairing BGA Components'', *Proceedings Nepcon West 95*, p. 3, Vol. 1994, 1017-34 Vol. 2, Anaheim, CA, USA, 26 February-2 March 1995.
38. J. Tien, T. Kao, M. Duh, and R. Davis, ''Implementation of a PBGA Into a High Volume Digital Set-Top Box Application'', In *Proc. of SMTA/IPC Electronics Assembly Expo*, Providence, RI, p. S2-1, 24–29, October 1998.
39. D. J. Peck, ''BGA Rework in Perspective'', In *Proc. of SMTA/IPC Electronics Assembly Expo*, Providence, RI, p. S5–1, 24–29, October 1998.
40. Conceptronics report (1996).
41. B. T. Vaccaro, R. L. Shook, and D. L. Gerlach, *''The Impact of Lead-free Reflow Temperatures on the Moisture Sensitivity Performance of Plastic Surface Mount Packages''*, SMTA International, Chicago, IL, 24–28, September 2000.
42. S. F. Kench, ''Rework Process for Chip Scale Components'', in *Proc. of Surface Mount International*, p. 2, Vol. 826, 260–4, Vol. 1, San Jose, CA, 10–12, September 1996.
43. E. Zamborsky, ''BGA and CSP Rework: Theory, Methods, and Applications'', short course at SMTA International, Chicago, IL, 24–28 September 2000.
44. B. Farrell, B. Clark, and D. DePalma, ''Process Control for Assembly and Rework of High Pin Count PBGA's'', In *Proc. of SMTA/IPC Electronics Assembly Expo*, Providence, RI, p. S2–3, 24–29, October 1998.
45. R Master, private communication regarding AMD's internal data, 17 October 1997.
46. W. R. Reynolds and D. W. Romm, ''Testing BGA Solderability'', *SMT*, pp. 64–65, (June 1997).
47. D. T. Novick, ''A Metallurgical Approach to Cracked Joints,'' *Welding J. Res. Suppl.* Vol. 52, No. 4, pp. 154S–158S (1973).
48. A. der Marderosian and V. Gionet, ''The Effects of Entrapped Bubbles in Solder for the Attachment of Leadless Ceramic Chip Carriers,'' in *Proc. 21st IEEE International Reliability Physics Symposium*, Phoenix, Arizona, pp. 235–241 (1983).
49. V. Tvergaard, ''Material Failure by Void Growth to Coalescence,'' in *Advances in Applied Mechanics*, Vol. 27, pp. 83–149, Pergamon Press (1989).
50. M. Mahalingham, M. Nagarkar, L. Lofgran, J. Andrews, D. R. Olsen, and H. M. Berg, ''Thermal Effects of Die Bond Voids in Metal, Ceramics and Plastic Packages,'' in *Proc. 34th IEEE Electronic Components Conference*, New Orleans, Louisiana, pp. 469–477 (1984).
51. D. R. Banks, T. E. Burnette, Y. C. Cho, W. T. DeMarco, and A. J. Mawer, ''The Effect of Solder Joint Voiding on Plastic Ball Grid Array Reliability'', in *Proc. of SMI 96*, San Jose, CA, pp. 121–126, August 1996.
52. W. O'Hara and N.-C. Lee, ''Voiding Mechanism in BGA Assembly'', *ISHM*, (1995).
53. A. A. Primavera, R. Sturm, S. Prasad, and K. Srihari, ''Factors that Affect Void Formation in BGA Assembly'', in *Proc. of IPC/SMTA Electronics Assembly Expo 1998*, S2–2-1, Providence, RI, October 1998.
54. W. B. Hance and N.-C. Lee, ''Formation and Control of Voiding in SMT'', in *Proc. of 1992 ISHM*, San Francisco, CA, p. 535 (1992).
55. S. Shina, H. Belbase, K. Walters, T. Bresnan, P. Biocca, T. Skidmore, D. Pinsky, P. Provencal, and D. Abbott, ''Design of Experiments for Lead Free Materials, Surface Finishes and Manufacturing Processes of Printed Wiring Boards'', SMTA International, Chicago, IL, 20–24 September 2000.
56. P. A. Jaeger and N.-C. Lee, ''A Model Study of Low Residue No Clean Solder Paste'', in *Proc. of 1992 Nepcon West*, Anaheim, CA, pp. 394–404 (1992).
57. H. Nakahara, ''Fabrication Technologies for IC Packages and High-density PWBs Are Merging'', *Chip Scale Review*, Vol. 1, No. 3, pp. 26–35 (September 1997).
58. L. Gopalakrishnan, V. Sion, and R. Srivastava, ''Reliability Experiments for Different Microvia Constructions'', *Journal of SMT*, Vol. 12, Issue 4, pp. 22–27 (October 1999).

59. T. Castello, R. Lund, and W. Oden, private communication, 11, December 2000.
60. D. J. Powell and M. Weinhold, ''Laser Ablation of Microvia Holes in Nonwoven Aramid-reinforced PWBs'', *Chip Scale Review*, Vol. 1, No. 3, pp. 38–45 (September 1997).
61. S. Chiu and N.-C. Lee, ''Voiding in BGA at Solder Bumping stage'', ISHM, 1997.
62. D. Bell, Private communication, October 1997.
63. S. Fauser, C. Ramirez, and L. Hollinger, ''High Pin-Count PBGA Assembly'', *Circuits Assembly*, pp. 36–40 (February 1995).
64. T. Scheler, P. Viswanadham, M. A. Garza, S. Dunford, and B. Thomas, ''Ceramic Ball Grid Array Assembly Reliability in Military Applications'', in *Proc. of SMTA/IPC Electronics Assembly Expo*, Providence, RI, p. S8–4, 24–29, October 1998.
65. Hewlett-Packard, private communication, 1993.

10 Flip Chip Reflow Attachment

A flip chip is a chip mounted on the substrate with the chip's active surface facing the substrate. The bonding feature on the flip chip includes metal (Au, NiAu, Cu, solders) bumping or studding, polymer bumping (compliant bumps, isotropic conductive polymer bumps), a combination of metal and polymer bumping, and metal pads. The interconnecting methods can be thermosonic or thermocompression (VIS), anisotropic conductive adhesive bonding (OKI's Au on plastic ball, Microconnector, MCA, Samsung & Zymet method, Double Layer), isotropic conductive adhesive bonding (Mitsubishi's method, Seiko Epson's pad particles), and soldering (PADS, C4, solder paste reflow) (see Figure 1.31, Chapter 1). At this stage, the reflow soldering process is the prevailing method. Therefore, its process and troubleshooting will be the emphasis of this chapter. In addition, since underfilling is an integral part of flip chip attachment, it will also be covered in the discussion.

10.1 Flip chip attachment

Flip chip attachment involves mounting a silicon die onto substrate. Ceramic substrates have been used for the C4 process for about 30 years. However, the high cost of multiplayer ceramic substrate prevents flip chip technology from being adopted widely, hence the practice of mounting a flip chip on a polymeric substrate. Although a polymeric substrate can be much cheaper, its high thermal expansion coefficient also poses a TCE mismatch problem, as shown in Figure 10.1. Underfilling a flip chip with materials that bond strongly to both a silicon die and a substrate can help to constrain the CTE mismatch locally and to couple the die and substrate mechanically, thus significantly alleviating stress on solder joints and extending the fatigue life of a flip chip. In addition, the underfill materials can enhance heat dissipation, thus further increasing the reliability of a flip chip. The introduction of the underfill layer results in a paradigm shift in reliability mechanics wherein the focus changes from the familiar fatigue damage (creep, stress history, joint profile etc.) of the solder interconnect to the mechanical integrity of the die–substrate structure [1]. Furthermore, use of underfill not only enables the use of cheap polymeric substrates, but also benefits ceramic substrate applications. Accordingly, a flip chip attachment via a reflow process almost always involves both soldering and underfilling.

The conventional flip chip attachment process starts with soldering and is then followed by cleaning and underfilling. With increasing demands for lower cost and a higher throughput, many new materials and processes have emerged. The representative approaches will be introduced in the following sections.

10.1.1 Conventional flip chip attachment

Depending on the alloys used for flip chip solder bumps and the type of substrate to be mounted, the soldering process can be categorized as four major types, as shown in Figure 10.2. Figure 10.2(a) represents the collapse of a high melting solder bump, 10.2(b) represents bonding of

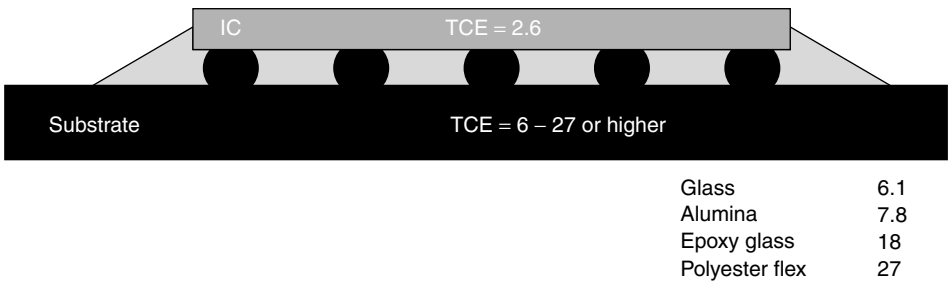

Figure 10.1 Flip chip mounted on a substrate. The significant mismatch in TCE between silicon die and polymeric substrate causes stress in solder joints. Use of underfill forms strong bonding with both die and substrate, thus greatly reducing the stress on solder joints

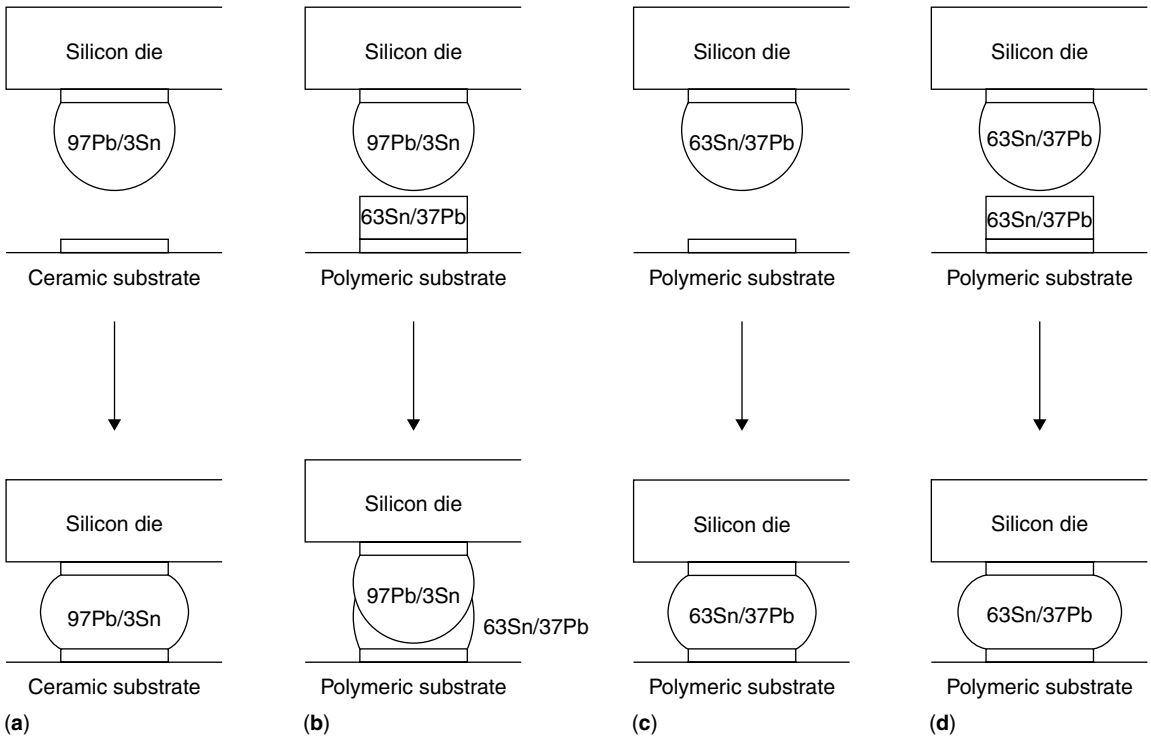

Figure 10.2 Types of flip chip assembly materials match

a high melting bump with eutectic Sn–Pb solder, 10.2(c) depicts the collapse of an eutectic Sn–Pb bump, and 10.2(d) shows the collapse of an eutectic Sn–Pb bump with additional solder volume from the board side.

In Figures 10.2(b) and 10.2(d) the eutectic solder on the board side may be solder paste printed, which will be discussed later. It may also be provided by a coating process [1,2]. In Motorola manufacturing, eutectic solder is plated and fused on the PCB Cu pads, followed by mechanical flattening [2]. The addition of the 63Sn/Pb solder to the substrate typically increased the cost of the board by 20–35 percent. Often board solder deposition costs more than the expense of bumping the flip chip used [3].

10.1.1.1 Fluxing

Where solder paste is not used for flip chip attachment purposes, the use of flux becomes necessary, as reflected by the "flip chip fluxing and placement" step in the simplified flip chip attachment process flow chart (see Figure 10.3). This fluxing step can be used for each combination depicted in Figure 10.2. The detailed processes and options are described below.

Dip A schematic of dip-flux process flow is shown in Figure 10.4. At first, a creamy flux is applied to a rotating disk equipped with a doctor blade. The thickness of flux film, e.g. 50 μ, is controlled by the clearance of the doctor blade (see Figure 10.4(a)). The board now enters the placement tool. Depending on the design, the board may already have SMDs placed on the printed solder paste. The die is picked from a feeder medium, such as waffle pack feeders, tape and reel, surf tape or a direct wafer feeder, and is then imaged and centered by a stationary flip chip camera or an on-board camera in the placement head chassis. Afterwards, the chip is brought to the dip flux module (see Figure 10.4(a)) and dipped into the flux film for a preset amount of time (see Figure 10.4(b)). Once dipped, the chip with the bottoms of solder bumps covered by flux is brought to the board (see Figure 10.4(c) and 10.4(d)) and placed onto the corresponding pads (Figure 10.4(e)). The assembled device is then reflowed in an oven, typically in an inert atmosphere. The solder wets to the pad to form the joint and self-aligns (see Figure 10.4(f)). Figure 10.5 shows a dip-flux device [4].

Imaging the flip chip prior to dip fluxing has the disadvantage that the mechanical contact of the flip chip bumps with the flux carrier can have a negative impact on placement accuracy. Alternatively, the flip chip imaging step may be carried out after the dip fluxing step. There is a very slight risk that the optical bump image can be adversely influenced by the flux material. Dipping prior to imaging seems to be the preferable sequence [4].

To avoid the possibility of placing flip chips in the wrong orientation, the programming bump pattern used for recognition should be asymmetric. The minimum flux film thickness depends on the bump height variations within a die. To ensure good soldering of the solder bumps

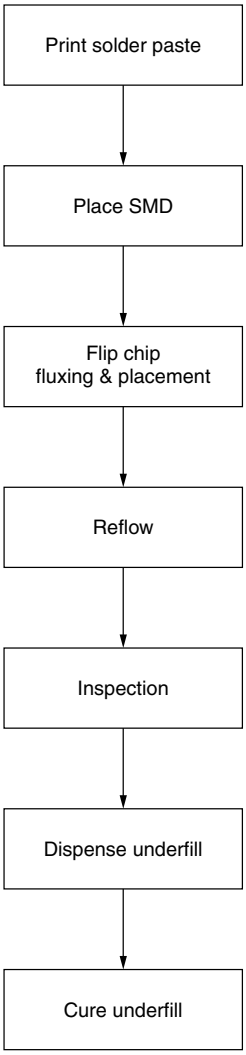

Figure 10.3 Flip chip attachment process flow

on the die, all the bumps have to be dipped in the flux. This principle of dip flux is most suitable for high viscosity fluxes. The amount of flux involved in the process is brought to a minimum by fluxing only the bump's underside. This is particularly important for the no-clean process. Dip fluxing is not adequate for fluxes with a high evaporation rate [4–6].

Spray The process flow for spray fluxing is shown in Figure 10.6. The PCB is placed in the sprayer sample stage, then sprayed with flux. After spraying, the flip chip is placed on the pads. Depending on the flux solvent system, a period of time is allowed for the volatile solvent to evaporate at ambient or slightly elevated temperature. The assembled board is then sent through the reflow oven for soldering.

Like dip fluxing, spray fluxing is one of the two most commonly used methods. This sprays a mist of flux over the footprint area. Figure 10.7 shows a flux jetting system for spray applications [7]. This system can apply a flux quantity of 1–2 µg per mm^2, with 5 percent volume consistency. The throughput is 1500 units per hour.

Figure 10.8 shows a coaxial flux jetting system. This employs a coaxial air column to further force the flux droplets landed on the board to spread out and form a uniform film [7]. It prefers fluxes with a viscosity of 7–30 cps and applies 4 µg per mm^2 flux on board. Surface tension of the substrate surface is important for control of spray quality.

Most fluxes used for spray fluxing are low solid content fluxes with an alcohol content of 95–98 percent. The fluxes are sprayed on to the substrate before placement and the alcohol evaporates rapidly at room temperature. The remaining flux, when properly formulated, can provide sufficient tackiness to hold the flip chip in place during board handling and reflow.

Brush The process flow for brush fluxing is almost identical to spray fluxing. The only difference is that the spray action is replaced by brushing.

Figure 10.9 shows a brush fluxing setup. A low viscosity flux, such as 80 cps, is stored in a reservoir. The brush

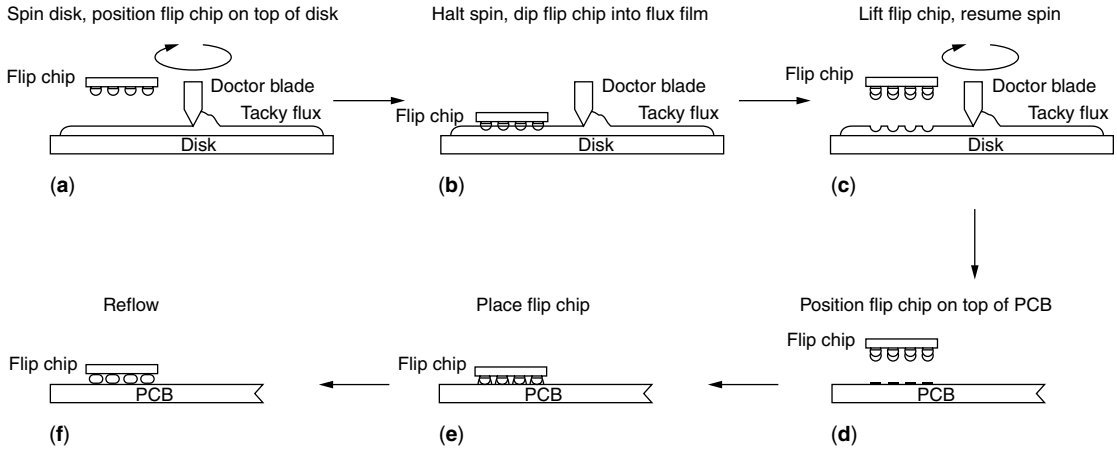

Figure 10.4 Dip-flux process flow

Figure 10.5 A dip fluxing device [4]

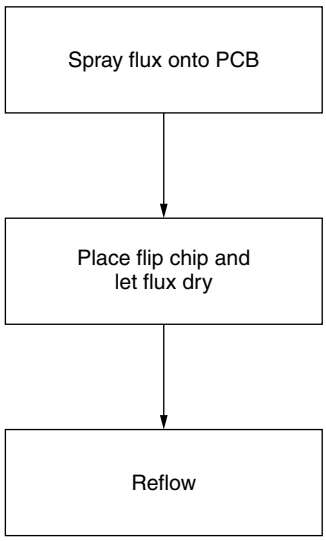

Figure 10.6 Spray fluxing process flow

is wetted by the flux fed through a small tubing with an outlet hidden in the interior of the brush. Upon brushing, the brush sweeps through the flip chip footprint area along a programmed path and deposits a layer of flux. In general, the flux quantity applied is greater than that by spray fluxing.

Dispense Again, the process flow is identical to spray fluxing. Figure 10.10 shows an example of dispense fluxing setup [7]. Dispense fluxing utilizes the same principle as spray, except that control of volume and flux film formation is poorer.

Stamp Stamp fluxing is more similar to brush fluxing in principle. The stamp is made of a spongy rigid material and is wetted by the flux fed through the back of the stamp. Figure 10.11 shows a pad/stamp headset.

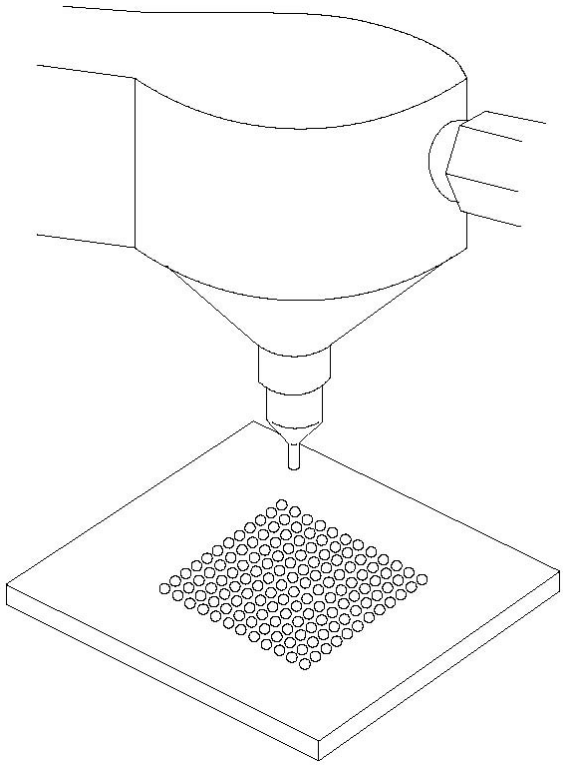

Figure 10.7 Accujet Flux Jetting system for spray flux applications [7]

10.1.1.2 Underfilling

Once the reflow cycle is complete, the board is inspected, and cleaned if necessary, followed with an underfill cycle. The cleaning process can be a tedious and difficult process. The cleaner used may be hazardous, such as xylene, although some non-hazardous cleaners have also been identified as effective [8]. The cleaning process is expected to run into more problems with increasing die size and decreasing die standoff, and may eventually be ruled out as an acceptable process.

The underfill is dispensed around the die, and allowed to flow and fill the gap between the flip chip and the PCB. Once a proper fillet is formed around the flip chip, it is then placed in an isothermal oven to cure. For most conventional filled underfills this curing cycle can take up to 1.5 hours at 165 °C.

The underfill dispensing pattern commonly used includes straight line, L shape, and U shape, as shown in Figure 10.12 [9]. The needle of the valve should be positioned as close to the die edge as possible in order to avoid contamination around the die perimeter. In general, a distance of 0.003–0.005 in. should be sufficient (see Figure 10.13). The needle tip should be positioned just below the lower surface of the die in order to maximize the flow underneath the die [11].

Usually a dispensing underfill cannot be completed in one pass. For a die smaller than 3 mm^2, one pass may

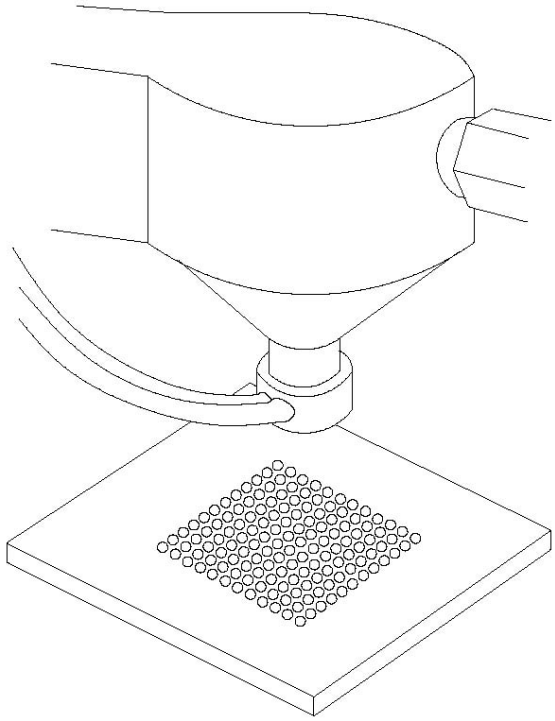

Figure 10.8 Accujet Coaxial Flux Jetting system for spray flux applications. A coaxial air column forces the landed flux droplets to spread out uniformly [7]

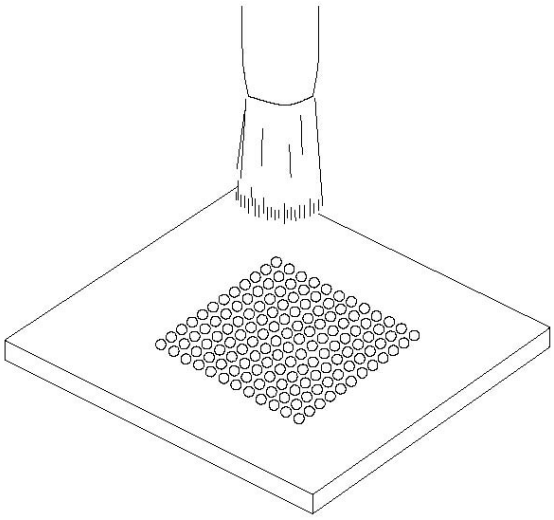

Figure 10.9 A brush fluxing setup [7]

be sufficient. For dies larger than 3 mm^2 and smaller than 6 mm^2 a two-sided pass may be preferred in an "L" shape. These special "L" shaped passes may be performed in different ways as shown in Figure 10.14. For dies larger than 6 mm^2 repetitive passes along the same edge of the die

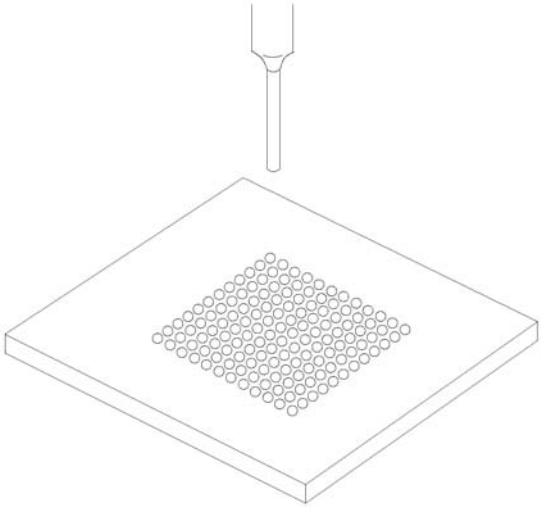

Figure 10.10 A dispense fluxing setup [7]

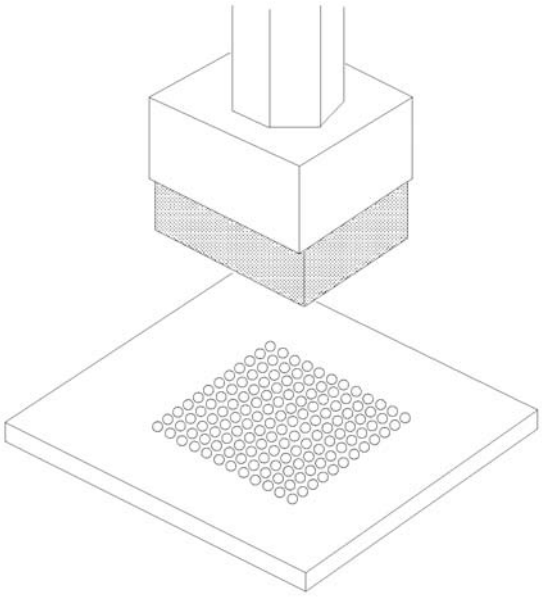

Figure 10.11 A pad/stamp headset [7]

may be needed in order to fill the flip chip properly and minimize the spread of fillet at the same time. The time interval between passes should be long enough to allow the materials previously deposited to flow underneath the die, and also should be short enough so that the throughput does not suffer. The second, third, and even fourth passes should be made at heights slightly more than the previous passes in order to maximize flow and reduce contamination around edges where the material is being dispensed.

At the sides of the die where the underfill emerges through capillary flow, one more pass is preferred in order to optimize the underfill fillet shape, as shown in

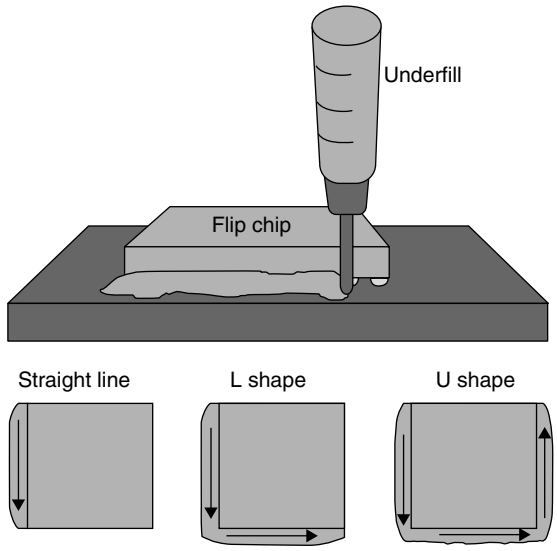

Figure 10.12 Three common patterns used in underfill dispensing [9]

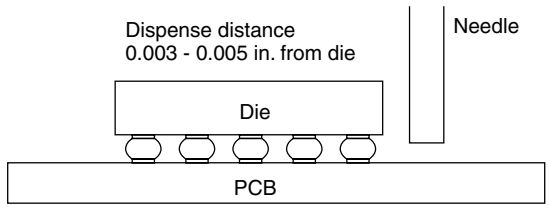

Figure 10.13 Desired needle-to-die distance before underfilling

Figure 10.14 [10]. If not, the dispense side has a much larger fillet. It has been seen that during curing the underfill material, the die may be subjected to uneven stresses that in some cases have lifted up the die and caused a fracture of the interconnections on one side of the die [11]. Too much material can be unacceptable not only from a cosmetic point of view but also because of concern on contaminating SMD components around the die, making it difficult to rework them. Relatively, an excessive dispense is better than an insufficient one [11]. Figure 10.15 illustrates three dispense volume statuses, (1) excessive dispense, (2) insufficient dispense, and (3) complete fillet dispense [11].

The available space around the dies may not allow a close-up dispense in all cases, as demonstrated by Figure 10.16 [4]. Here dispensing is only possible on one side of the die. An underfill material that forms fillets by itself is then required.

10.1.2 Snap cure

Conventional underfilling takes a long time to cure the underfill. In order to reduce the cycle time and increase the throughput, the cure time has to be shortened. A snap cure underfill fills the gap and offers a considerably shorter cure time. The snap cure underfill process is exactly the same as that of conventional underfill, except that the cure cycle is much shorter. Table 10.1 shows cycle time comparisons of different flip chip underfill materials, including normal, snap cure, and no-flow, which will be discussed later.

Studies indicate that a snap cure underfill appears to be the most attractive option, due to its high throughput performance while still retaining the reliability of normal underfill [1,12].

10.1.3 Epoxy flux

Epoxy flux is an epoxy-based flux. It is a viscous, honey-like material, and is used in dip fluxing as a flux. The epoxy flux process is exactly the same as the dip fluxing process. Epoxy flux will remove metal oxide upon heating, thus allowing solder to wet to board pads. It

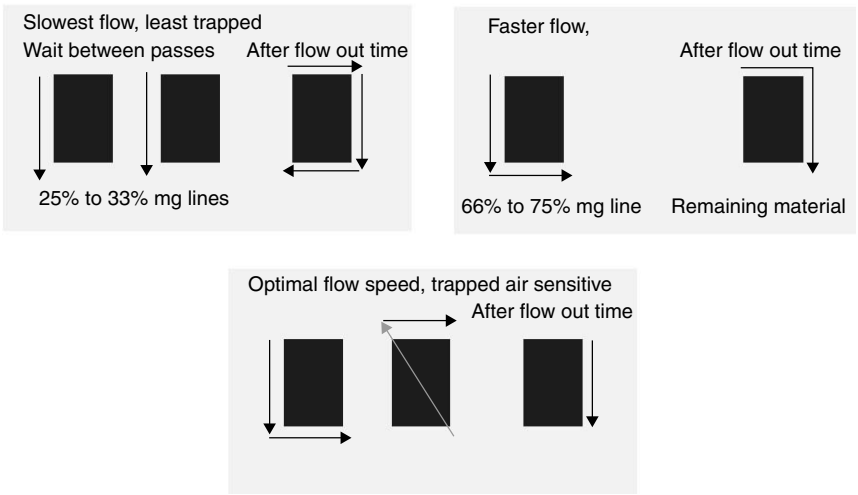

Figure 10.14 Design of underfill dispense pattern [10]

Figure 10.15 Examples of underfilling filling results [11]

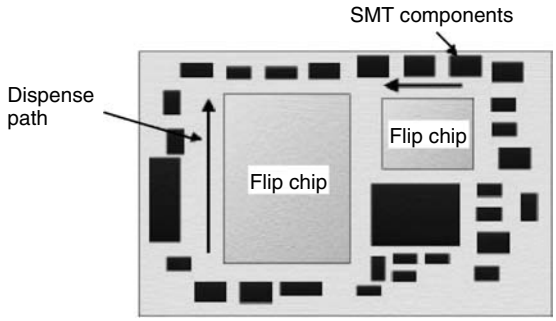

Figure 10.16 Cluttered spacing between components allows only one side dispense [4]

Table 10.1 Cycle time comparisons of different flip chip underfill options [12]

Feature	*Flip chip underfill options*		
	Normal	*Snap cure*	*No-flow*
IC fluxing	4–15	4–15	6
Reflow	300	300	300
Underfilling	8–15	8–15	0
Curing	900	180–300	300–900
Total time	1212–1230 sec	492–630 sec	606–1206 sec

also cures and forms a thermoset flux residue, thus it is not cleanable. Since this flux residue is expected to bond strongly to any surface, and since it is an epoxy-based thermoset material, it is expected to be compatible with the subsequent epoxy underfilling process and to form an integral part of the underfiller system.

Lewis [6] has reported that placement force and dwell time when placing on board are not important on the yield. However, placement offset, dip flux height, and dip time exert a significant impact on the process yield and will be discussed later.

10.1.4 No-flow

No-flow is a process which provides fluxing and underfilling, or encapsulation, at the same time. Depending on the type of materials used, no-flow can be categorized as a "liquid no-flow" process (see Figure 10.17, left, [13]) and "film no-flow" process (see Figure 10.17, right). The first process starts with a dispense liquid no-flow underfill, followed by pick and place flip chip, and ends with the reflow/cure step. The second process starts with heating up the PCB, then placing of the no-flow underfill film, allowing the underfill film to melt, followed by pick and place flip chip, and ends with the reflow/cure step. In both processes, at the reflow/cure stage, the underfill removes metal oxides and allows solder to wet to the board pads. The underfill also wets to the surface of substrate, die, and solder joint, and cures as an encapsulant.

The major advantage of no-flow is that it is a highly simplified process. It consolidates fluxing, soldering, cleaning, underfilling, and curing into deposition and heating, thus eliminating many steps associated with the conventional fluxing and underfilling process. It is an intrinsic no-clean process. Since the flux and underfill are the same, it eliminates issues of incompatibility between flux residues and underfill.

Lau *et al.* [14] have compared several underfill technologies. Their results indicate that liquid no-flow is SMT compatible, while film no-flow is not. The latter is much more complicated, and much higher in production cost than the former. Although the adhesion of both systems is excellent, both liquid and film no-flow suffer serious voiding problems [14].

Besides a tendency to form voids, no-flow underfill suffers one more major constraint. Since a filler normally does not give way for molten solder bumps to contact board pads, the presence of filler greatly restricts formation of solder joints. As a result, no filler can be used in no-flow underfill materials. This results in an increase in thermal expansion coefficients and a decrease in thermal conductivity and modulus, hence a compromised performance in reliability enhancement. Lau [14] has also reported that the solder bump thermal reliability of the flip chip assemblies with the epoxy-based no-flow underfill materials is not as good as that with the conventional underfill.

10.1.5 SMT

A flip chip may also be attached with the use of solder paste. The process flow can be described as shown in Figure 10.18. Due to the extremely fine pitch involved, the solder powder used also has to be very small. In general, type 5 or type 6 is considered acceptable for this process. Figure 10.19 shows solder paste prints for

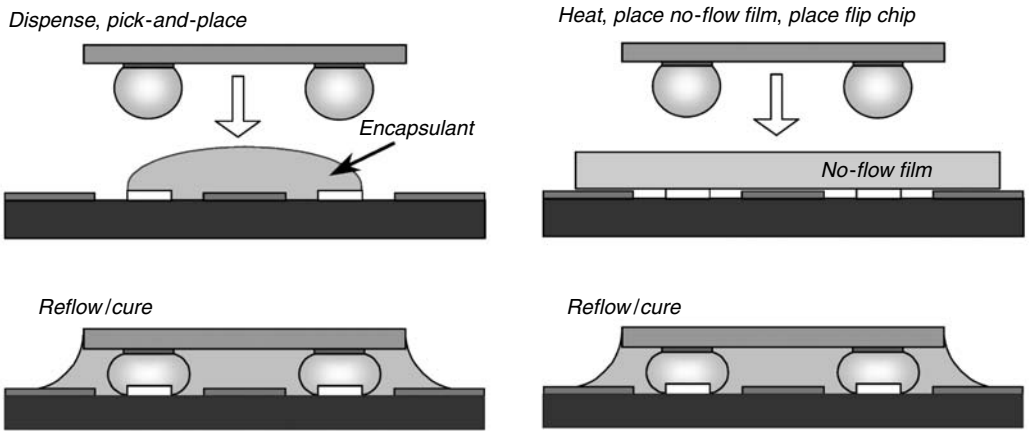

Figure 10.17 No-flow process flow using liquid (*left*) and film (*right*) no-flow underfill [13]

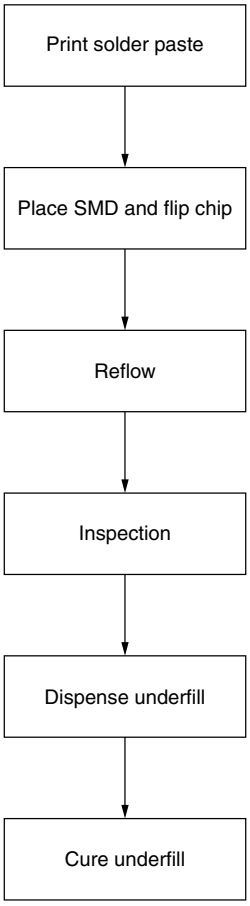

Figure 10.18 Flip chip attachment process via conventional SMT solder paste process

10 mil pitch peripheral and area array bumped flip chip attachment, with the use of a 3 mil thickness stencil. The solder paste used is 63Sn/37Pb, with 5–15 μ powder size distribution.

The SMT process described above is attractive due to the elimination of an additional flip chip fluxing step. In addition, solder paste deposition adds more solder volume to the flip chip joints, hence it should provide higher reliability. The requirement of using type 5 or 6 powder will result in a higher cost in paste material. Compared with the benefits, however, this is considered a trivial factor.

Alternatively, since other SMDs attached at the same time do not require the use of such fine powder, the paste material cost can be reduced by employing a sequential printing process, with a fine powder paste printed for flip chip first, followed by a printing type 3 powder paste for the remaining SMDs. For the second print, use of a stencil with a recessed bottom-side cavity covering the preprinted flip chip paste should retain the print quality of the first print. However, the cost of the double-print process very likely will override that of paste.

Perhaps the real challenge is: will the underfill be compatible with the flux residue of solder paste? Solder paste in general yields a higher flux residue than using flux alone. This is due to the higher solid content in the solder paste flux needed for paste rheology control and for removing oxides of solder powder. With advances in flux technology, this issue is gradually diminishing.

10.1.6 Fluxless soldering

MCNC has developed a fluxless, no-clean process which has been successful with assembly of a variety of flip chip configurations. The process, called plasma assisted fluxless soldering (PADS) relies on a pretreatment which enables the subsequent solder reflow in inert ambients. Conventional mass production soldering tools can be used, eliminating the flux dispense and flux cleaning steps, and adding the pretreatment step. Examples include high lead (97Pb/3Sn) bumped flip chips joined to multilayer ceramic substrates with Mo/Ni/Au microsockets at 350 °C in nitrogen, eutectic Sn–Pb solder bumped flip chips joined at 250 °C to bare copper, 95Pb/5Sn bumped flip chips joined to eutectic dipped FR4 printed circuit boards, joining of 90Pb/10Sn bumps to each other at 350 °C, and solder bumped flip chips joined to flexible circuits [15].

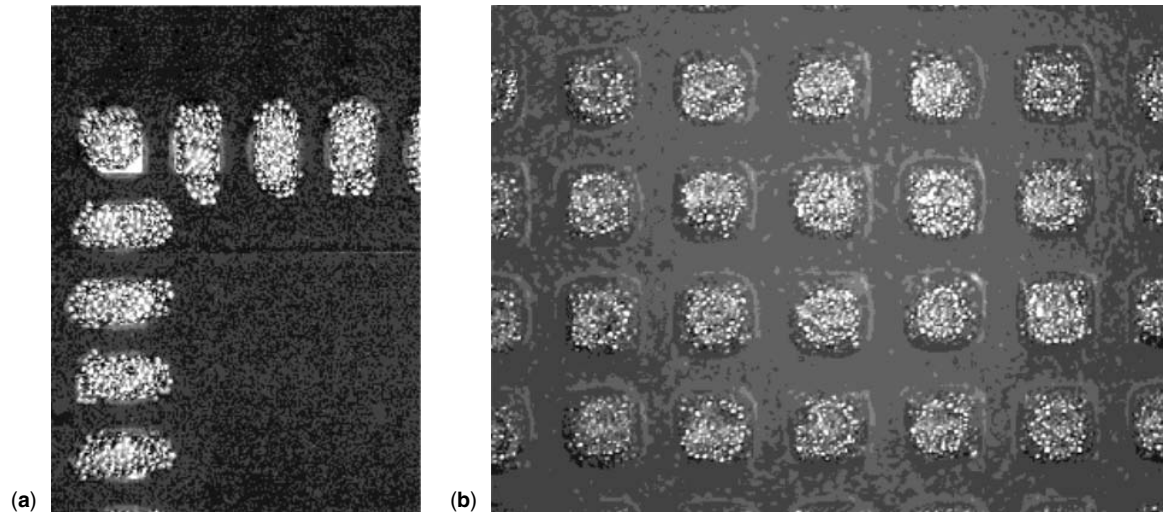

Figure 10.19 Solder paste prints for 10 mil pitch flip chip attachment using 3 mil stencil and 63Sn/37Pb solder paste with 5–15 μ particle size: **(a)** peripheral footprint, **(b)** area array footprint

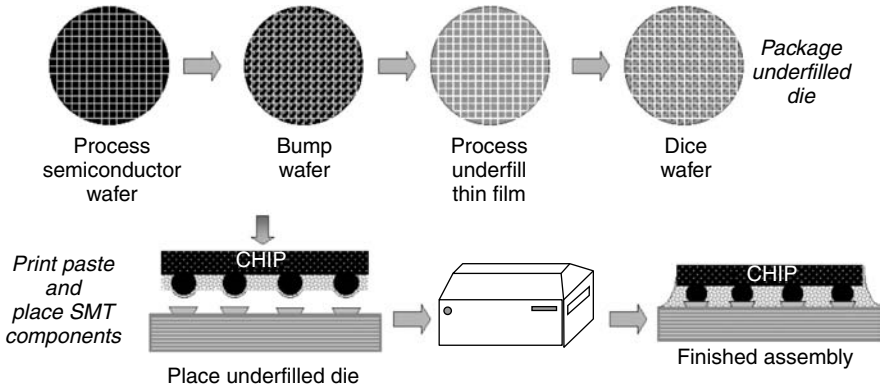

Figure 10.20 Low-cost flip chip processing based on wafer-applied underfill systems. (Source: Georgia Institute of Technology.)

Another fluxless process is based on soldering techniques using Au–Sn metallurgy. Soldering is performed with a thermode and a laser-based system. For these FC-joining processes, alternative bump metallurgies based on electroplated gold, electroplated gold–tin, mechanical gold and electroless nickel gold bumps are also applied [16].

Although both fluxless soldering techniques have been demonstrated to be feasible, lack of a chip-securing mechanism during the soldering process is a major concern for high-volume applications.

10.1.7 Wafer-applied underfill

One process under development at Georgia Tech is the wafer-applied underfill system, as shown in Figure 10.20. This process follows the approach of no-flow underfill technology. However, it allocates the flux/underfill deposition step to wafer level, thus streamlining the process of a SMT line to a simple placement step for a flip chip. At wafer level, after the solder bumping step, a thin layer of flux/underfill is formed by processes such as spin coating. This wafer level single deposition step virtually replaces the multiple deposition steps needed for placing multiple flip chips at a SMT line, thus it is considered a potentially lower defect process. The underfill coated wafer is then diced, and packed for a later SMT assembly process.

Although the process is fairly simple, the possibility of void formation within the underfill still exists. In addition, a heated stage for flip chip placement may be needed in order to activate the tack of flux/underfill.

10.1.8 Wafer level compressive-flow underfill (WLCFU)

Another process also under development at Georgia Tech is wafer level compressive flow underfill (WLCFU), as illustrated in Figure 10.21 This process addresses the lack of tack issue associated with a wafer-applied underfill by

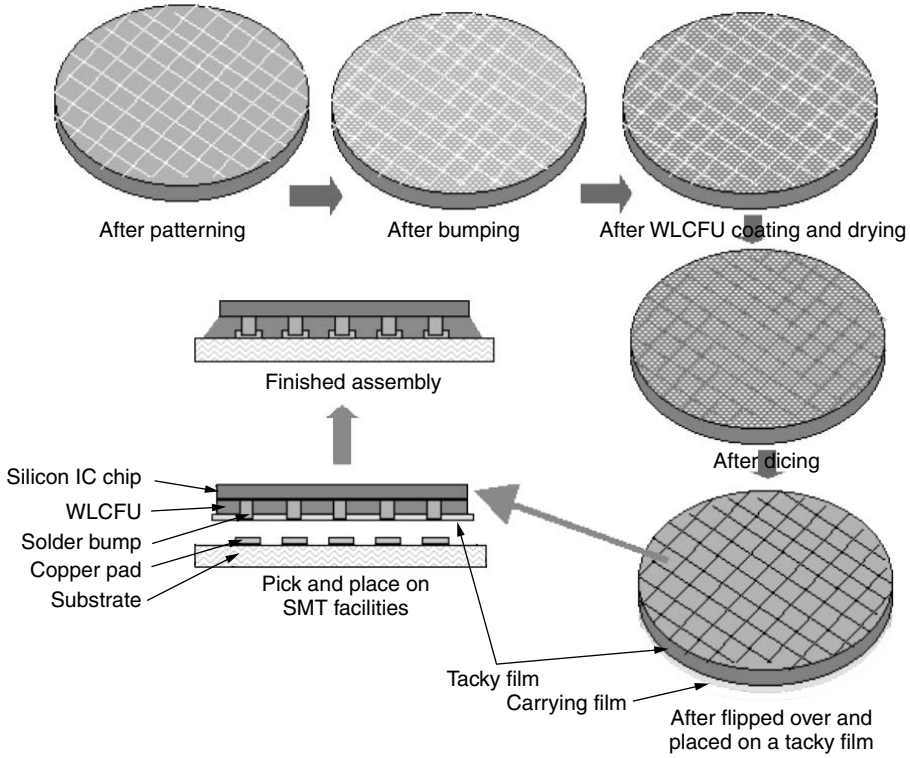

Figure 10.21 Wafer level compressive-flow underfill (WLCFU) process and materials. (Source: Georgia Institute of Technology.)

attaching a tacky film on top of the underfill layer, thus allowing flip chip placement to be conducted at ambient environment.

10.2 Problems during flip chip reflow attachment

Flip chip reflow attachment is a process involving both soldering and underfilling. Therefore, the problems encountered are much more diverse than other surface mount reflow processes, even including BGAs and CSPs reflow attachment. For the problems to be discussed below, emphasis will be placed on the conventional flip chip attachment process. However, other processes such as no-flow or epoxy flux will also be discussed in more detail.

10.2.1 Misalignment

Misalignment in flip chip, as shown in Figure 10.22 [6], will compromise reliability and will thus have to be minimized. Noreika *et al*. [17] have reported that flip chip self-centering capability is impressive, given the minimal initial chip-to-board contact area prior to reflow. The study suggests that self-alignment occurs at up to 60 percent misplacement, validating the accepted rule of 50 percent minimum bump-to-pad overlap. However, defect rates increased rapidly at linear misplacements beyond this range. The array configuration of flip chips appears to tolerate large amounts of rotational skew. This is because the relative shift of bumps near the centroid is far less than those bumps near the perimeter, providing more bump-to-pad contact area, thus a greater associated self-centering force.

10.2.1.1 Causes of misalignment

Misalignment can be caused by: (1) excessive misregistration, (2) low flux tackiness, (3) conveyer is not flat and stable, (4) unbalanced gas flow in oven, (5) poor support of PCB during reflow, (6) reflow profile [2],

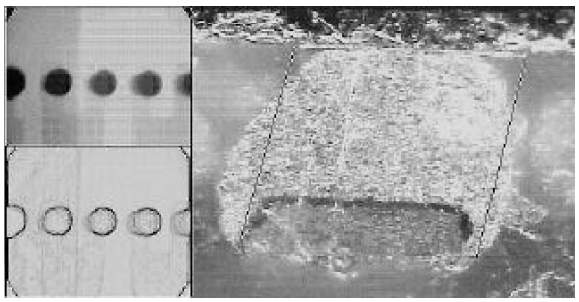

Figure 10.22 X-ray image and cross-section of misaligned die. (From B. J. Lewis, ''Process Characterization and the Effect of Process Defects on Flip-Chip Reliability'', APEX, Long Beach, CA, 14–16 March 2000: reprinted by permission.)

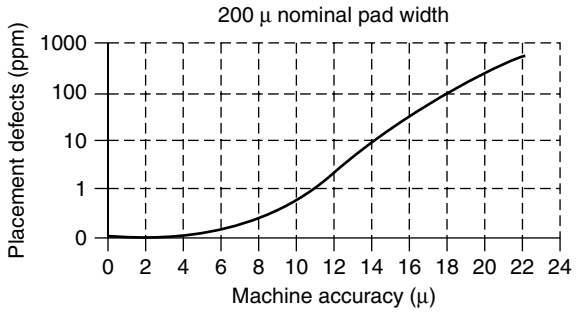

Figure 10.23 Effect of machine placement accuracy on placement defect rate [4]

(7) insufficient fluxing activity, (8) oxidative reflow atmosphere, or (9) inadequate solder mask opening. The first five causes belong to mechanical perturbation and are self-evident. Figure 10.23 shows the effect of placement accuracy on placement defect rate [4] for 200 μ nominal pad width. A placement accuracy of 11 μ is sufficient to render a 1 ppm defect rate, indicating the demand on machine accuracy is not extremely high. Due to the light mass of a flip chip, a high gas flow rate in the oven may blow the chip away from its site. If a flux with a higher tack value is not available, reducing the gas flow rate will be mandatory.

Cause (6) is related partially to mechanical perturbation and partially to a fluxing reaction. For a reflow profile with a fairly high ramp rate, the flux may outgas rigorously and cause shifting of the flip chip. On the other hand, if the ramp rate is too slow, the flux may burn off prematurely before self-alignment is complete. Without flux, the oxide on the molten solder and board pad will prevent a full wetting. It will also cause a lower apparent surface tension of solder, hence resulting in a weaker driving force for self-alignment. Causes (7) and (8) are related to fluxing reaction. A compromised fluxing, due either to insufficient fluxing reaction or to excessive oxide formation, will result in incomplete oxide removal and accordingly obstruct self-centering. It has been seen that, although flip chip attachment onto a PCB can be processed together with SMT components in an air atmosphere, self-centering has suffered. Use of a nitrogen atmosphere eliminated this problem.

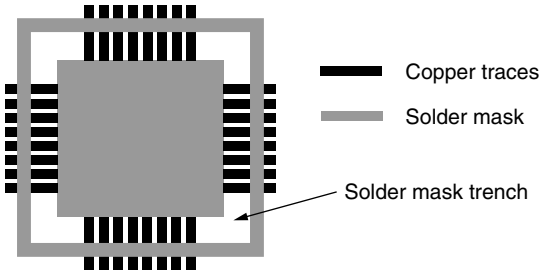

Figure 10.24 Pad design showing copper pad defined by solder mask trench [4]

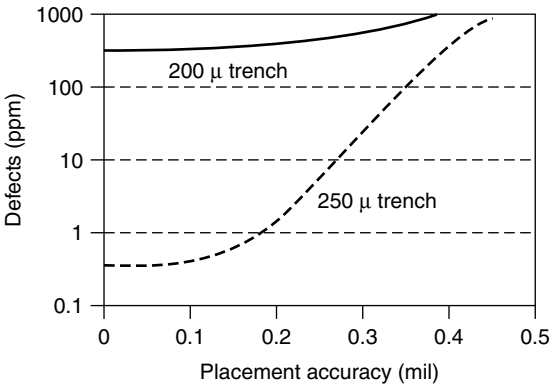

Figure 10.25 Effect of trench size on defect rate [4]

Cause (9) relates to physical constraints caused by too small a solder mask opening [17]. The flip chip bumps mate to corresponding board pads, with pad dimensions typically defined by the solder mask openings on the board surface, as shown in Figure 10.24. These solder mask openings are usually slightly larger than the bump diameter. Chip placement outside this tolerance results in mechanical interference between bumps and the wall of the opening, tilting the chip and preventing proper contact with the board during solder joint formation. By widening the solder mask opening, the defect rate will reduce significantly, as shown in Figure 10.25 [4]. However, it should be kept in mind that while a wider opening results in a higher self-centering success rate, it also causes a lower standoff for the solder joints thereby compromising reliability. Solder mask registration accuracy is also an integral part of flip chip attachment placement requirements, and can be critical to chip attach yield.

10.2.1.2 Epoxy flux

Epoxy fluxe appears to have a similar behavior to the true fluxes. Lewis [6] studied the effect of five placement variables on the process yield when using epoxy flux for flip chip attachment. Of all the dies that were offset in the study, 93 percent self-aligned fully onto the corresponding pads, 5 percent of the offset dies did not align completely and 2 percent did not recover from the extreme offsets to which they were exposed. Dip flux height was clearly the largest factor in the yield and self-alignment of the die studied, with alignment yield rising with increasing dip height, as shown in Figure 10.26. Placement offset and dip time were also important factors while placement force and dwell time on board were not, as shown in Figure 10.27. Self-alignment occurred for dies placed 40 percent off the center of the pad. Lewis's data show that for the larger dip heights, solder self-alignment occurs even when 40 percent off the center of the pad.

10.2.2 Poor wetting

Poor wetting can be detected with X-rays based on the lack of joint image distortion, as shown in Figure 10.28.

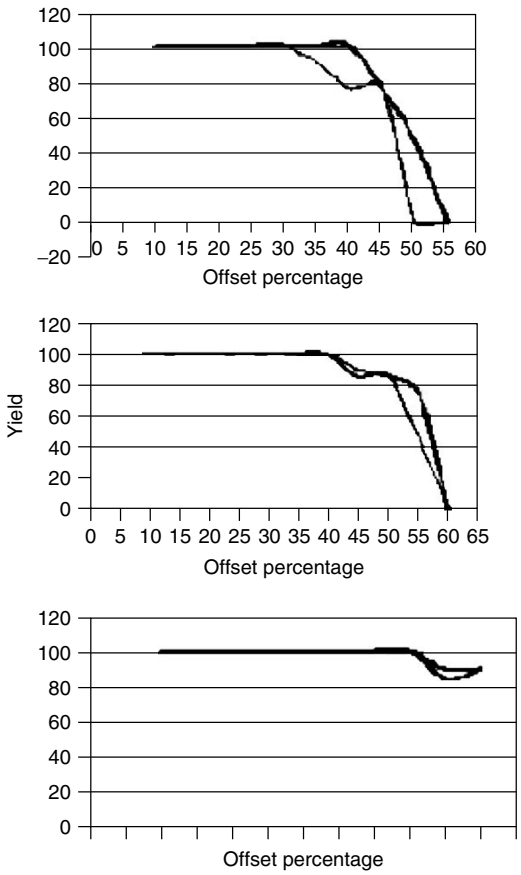

Figure 10.26 Effect of epoxy flux dip height on yield when the die was placed off center. Top plot is for 25 μ dip height, middle for 45 μ dip height, and bottom for 65 μ dip height [6]

Discussion in previous chapters has concluded that poor wetting can be caused by either insufficient flux activity or an oxidative reflow atmosphere. Hessen reported that no significant sensitivity to the amount of flux used on the dip fluxer could be seen at any given oxygen level [4]. Perhaps this can be interpreted by the existence of an amount of threshold flux and the flux quantities used in Hessen's study exceeding this threshold value. He also reported that all the fluxes used showed a need for an inert atmosphere during reflow. The oxygen level must be less then 1000 ppm to achieve good soldering results [4]. The author considers that, to assure solder joint quality for a flip chip attachment, an oxygen level no higher than 200 ppm is recommended. This is particularly true for applications using low residue fluxes due to the need to have better subsequent underfilling results. A low residue flux must be processed under a high purity reflow atmosphere, since there is only a minimal oxygen barrier ingredient included in the flux. If possible, the oxygen concentration must be maintained below 50 ppm.

Poor wetting is also observed when using epoxy flux [6], as shown in Figure 10.29 and no-flow underfills [13], as in Figure 10.30. In both instances, the poor wetting could be caused by either a weak fluxing of epoxy materials or an early onset of gelling of epoxy. In general, epoxy flux or no-flow underfill does not employ aggressive flux activators, thus exhibiting only a marginal wetting ability. This weak fluxing characteristic plus the gelling interference are the most common causes of poor wetting for epoxy fluxing systems.

10.2.3 Solder voiding

As discussed in section 9.3.4, voiding in solder joints can result in significant reductions in performance in a temperature cycling failure test. Figure 10.31 shows a cross-section of a large void in a flip chip solder joint. Voiding in flip chip joints can be detected by X-ray and scanning acoustic microscopy. The former is shown in Figure 10.32 together with an optical image of a column-shaped void in a solder joint [6]. The latter is demonstrated in Figure 10.33 [18]. Solder voiding behavior will be discussed separately for flux and epoxy flux applications.

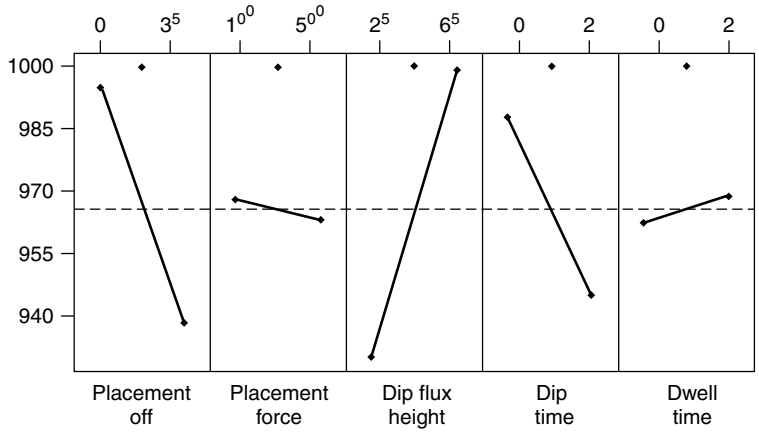

Figure 10.27 Effect of placement variables on process yield of flip chip attachment with epoxy flux [6]

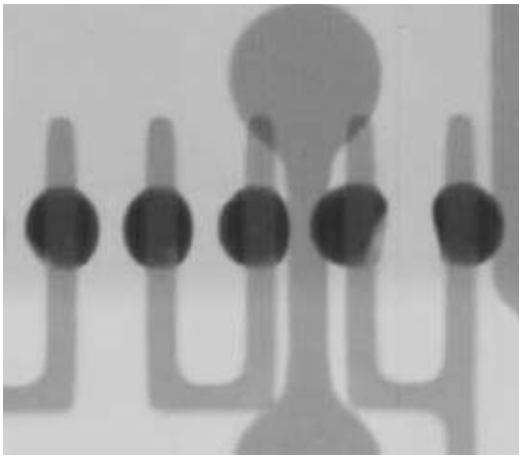

Figure 10.28 X-ray of flip chip shows the visible joint formation due to the pad geometry. Poorly wetted pads on the substrate are easy to detect, since the bumps will not deform during reflow [4]

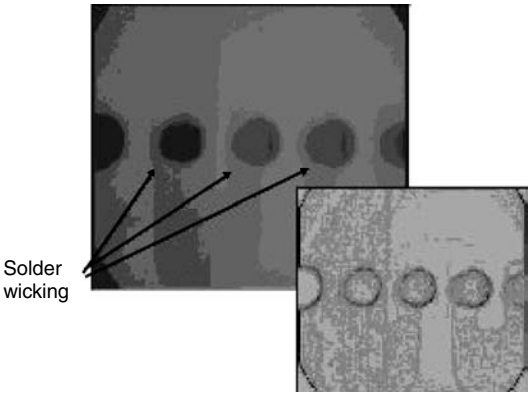

Figure 10.29 C-SAM images of inadequate wetting of solder joints. While the rear picture shows sign of wicking, the front picture shows virtually no wetting. Epoxy flux is used for this flip chip attachment [6]

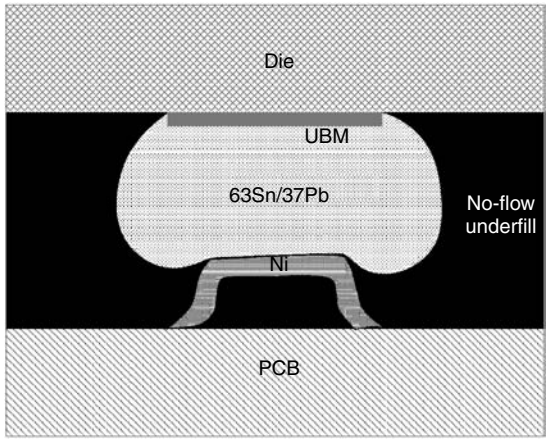

Figure 10.30 A joint that fails to form due to early onset of the gelling of the encapsulant [13]

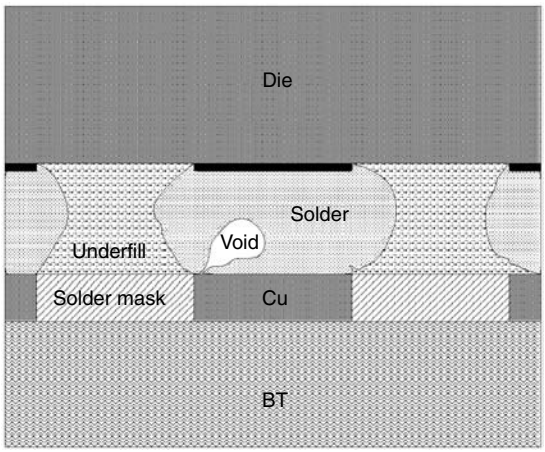

Figure 10.31 Close-up view of one solder bump with a large void [14]

10.2.3.1 Flux

Poor wetting is the primary cause of solder voiding. This can be attributed to (1) weak flux, (2) poor solderability of board pad, or (3) oxidative reflow atmosphere. The mechanism is similar to that of a typical surface mount process. In the case of solder mask defined board pad, voiding is a processing-induced failure mode. The emission of moisture in the solder mask and bulk board contribute to void formation [2]. Using solder paste for attachment often displays more voiding than using flux alone. The cause for this has been discussed in the section on BGA/CSP.

A flux which works well for BGA or CSP may not work for a flip chip attachment. This is attributed to the relative volume factor. For instance, while the linear dimension reduces ten times from BGA to flip chip, the oxidized surface area of flip chip bump and pad is reduced to 1/100; meanwhile the flux volume deposited for a flip chip attachment is reduced to 1/1000. Since the oxide thickness often does not reduce with decreasing feature size, the more rapid reduction rate of relative flux volume will inevitably result in more difficult fluxing. A study by Xiao *et al*. [22] has found that the oxide layer thickness increases at very small feature size. This is interpreted by the higher energy state associated with a surface with a smaller radius of curvature, and this higher energy state is more prone to oxidize under oxygen. Therefore, both relative flux quantity factor and absolute oxide layer thickness are becoming more unfavorable for a good wetting with decreasing feature size. As a result, a flux which works for BGA may no longer be good enough for flip chip.

10.2.3.2 Epoxy flux

Solder voiding behavior in the use of epoxy flux complies with the rules of normal fluxes. However, there is one additional solder voiding behavior associated with epoxy flux. While use of more epoxy flux through a higher dip

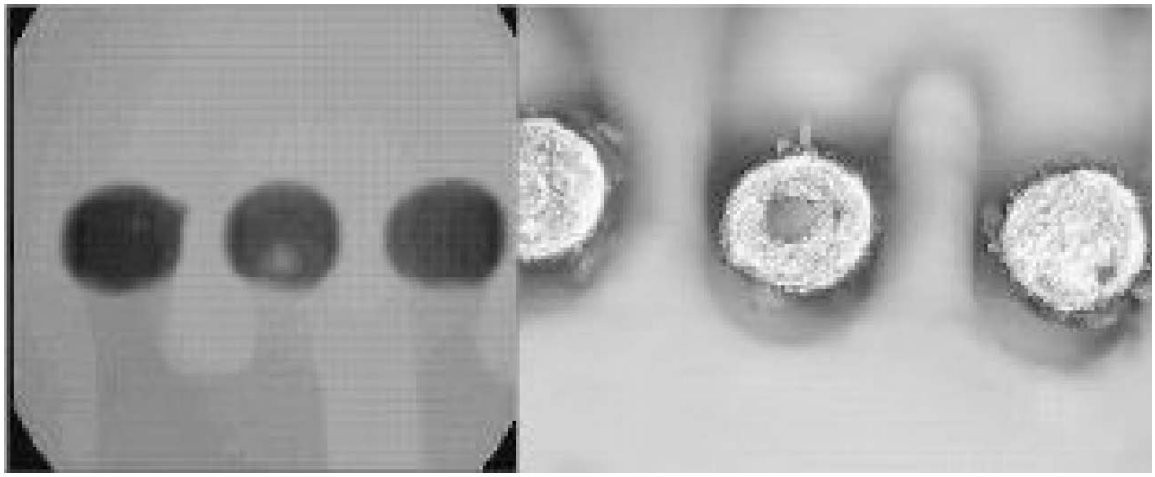

Figure 10.32 X-ray of a gross solder void and optical image of a column void [6]

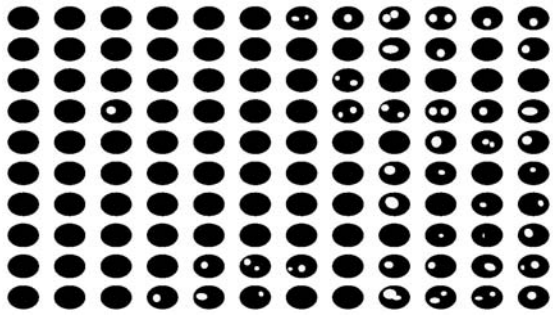

Figure 10.33 Each solder bump has a length of 0.25 mm in this 230-MHz acoustic image. White areas are voids in the chip-to-bump bond [18]

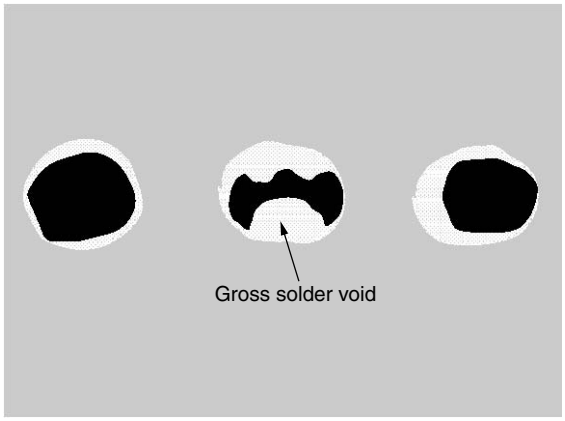

Figure 10.34 C-SAM image of solder voiding associated with a dip height of 65 μ when using epoxy flux [6]

height yielded a better self-alignment, larger voids were also observed with higher dip height, as demonstrated in Figure 10.34, where the dip height was 65 μ [6]. This intriguing phenomenon is also reflected by the thermal shock reliability and self-alignment yield results as a function of epoxy flux dip height, as shown in Figure 10.35 [6]. Here a higher dip height results in a higher self-alignment yield, but poorer thermal shock reliability.

Perhaps this perplexing behavior can be explained by an "encapsulation effect". A higher dip height provides a higher flux capacity, therefore promoting better wetting and better self-alignment. However, a higher dip height also means a greater coverage of the solder bump by the epoxy flux. At reflow, the epoxy flux will cure and form a partial or full coverage around the solder joint. The greater the dip height, the better the coverage of the solder joint. Figure 10.36 shows a flip chip solder joint fully encapsulated by the unfilled epoxy flux, indicating the encapsulation effect can be very significant.

As discussed above, voiding is caused by outgassing of any entrapped flux within the molten solder. Outgassing often continues during the course of reflow until the solder solidifies. Upon reflow, a lower dip height results in poorer wetting, therefore there may be more non-wetted sites within the solder joints which serve as anchoring sites for entrapped flux. Since for a lower dip height encapsulation is also lower, the volatiles produced can easily escape, thus not fully contributing to the final voiding. However, in the case of a higher dip height, even though the outgassing may be lower due to a better wetting, the vapor generated will have greater difficulty in escaping since the solder joint is wrapped around by a cured epoxy encapsulant. Consequently, a higher voiding results for a dip height which provides better wetting and self-alignment. A similar encapsulation effect is also expected for no-flow underfill systems, since both utilize the same fluxed epoxy approach.

10.2.4 Underfill voiding

Voiding in underfill may appear as a halo around the solder joint, or as small or large voids within the underfill, as shown in Figure 10.37. Here the halo defects are

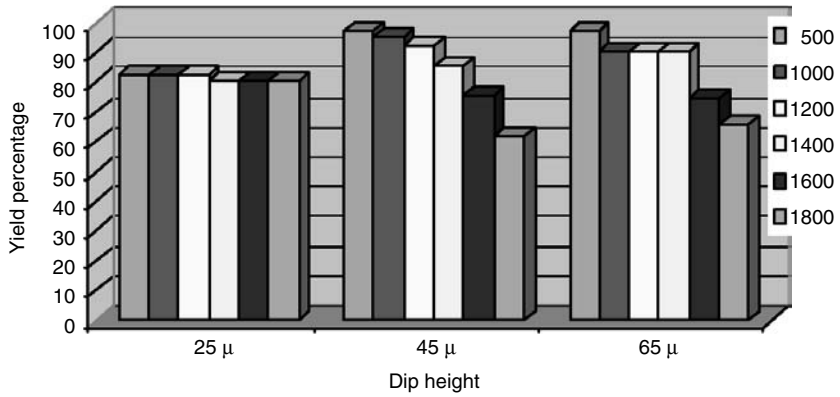

Figure 10.35 Thermal shock reliability and alignment yield results as a function of epoxy flux dip height [6]

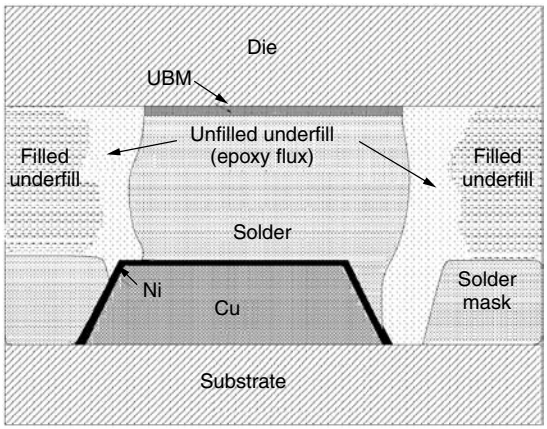

Figure 10.36 Cross-sectional view of a flip chip solder joint formed with epoxy flux followed by conventional underfilling. Note the solder joint on the left is fully encapsulated by the unfilled epoxy flux. The righthand side shows more detail. The amount of flux is related directly to the reliability of these devices. Results showed that from 1000 to 2000 thermal shock cycles, the 25 μ dip height only showed a 4 percent failure rate compared to 35 percent for the 45 and 65 μ heights [19]

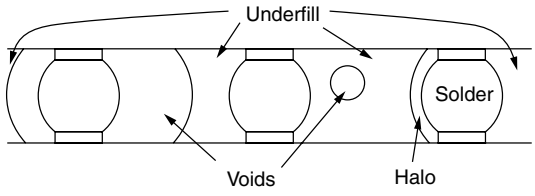

Figure 10.37 Voiding in underfill

delamination-like vertical spacings between underfill and solder joint. Voiding phenomena will be discussed based on regular underfill and no-flow underfill.

10.2.4.1 Regular underfill

For filled underfill systems, voids in underfill can be caused by (1) air or volatiles in the underfill, (2) moisture in the solder mask and board, (3) fingering of underfill flow, (4) an inadequate dispense path, (5) solder mask geometry, and (6) flux residue.

Air or volatiles in the underfill During curing, the volatiles in the underfill will vaporize, and accordingly may form voids. Air bubbles pre-existing in the underfill can also contribute to voids. Underfill materials on the market in general exhibit a very low content of air bubbles in order to minimize this factor. However, volatiles may still be a problem, particularly in the case of moisture. Predrying the filler will help in eliminating the moisture adsorbed on the filler surface.

Moisture in the solder mask and board Liu *et al.* [20] have reported that voiding is a processing-induced failure mode. The emission of moisture in the solder mask and bulk board contributes to void formation. Although for filled underfills this is not a major factor, it is still good practice to prebake the board prior to underfilling if the boards have been stored in humid conditions.

Fingering of underfill flow Certain underfill chemistries display uneven flow characteristics, and result in a finger-like flow front, as shown in Figure 10.38. Upon closure of these fingers, some air can be entrapped and form voids. Voids such as these can occur at the very beginning of a flow as well as at a later stage. The cause of this is often inhomogeneous material composition of the underfills. However, uneven surfaces of the flip chip or board can also aggravate this problem.

Inadequate dispense path Formation of voids can be easily induced via an incorrectly planned dispensing path and timing. For instance, carrying out a final fillet dispensing pass before the underfill emerges from beneath the die will most likely generate voids. In a way, this can be regarded as an artificially created fingering phenomenon. Figure 10.39 shows an acoustic image of voids formed under a large die due to an inadequate dispense pattern [13]. Unfortunately, there is no simple rule about which dispense path is the best choice. Performance is often affected by the underfill material type, the flip chip

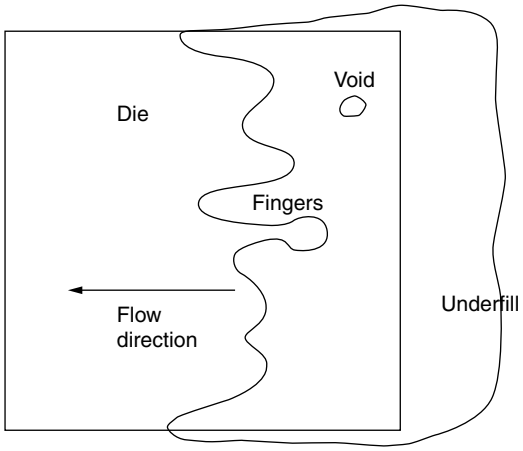

Figure 10.38 Fingering of underfill

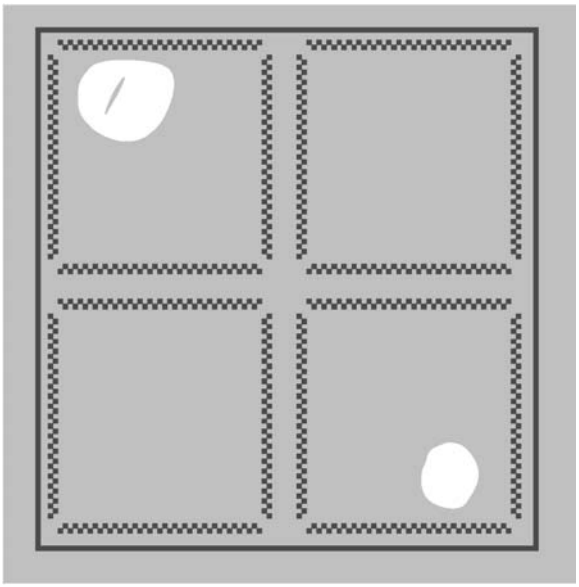

Figure 10.39 Acoustic images of voids under large dies formed because of inadequate dispense pattern [13]

I/O pattern, the surface condition of both die and board, and the standoff. Practice is still the only way to find out which path is adequate.

Solder mask geometry Proper flow of underfill is not usually a concern on a flat surface. However, when the underfill is applied to a flip chip on a PCB, the topology is complicated by solder joints and the solder mask. If the solder mask forms an open trough with the solder joint, as shown in the top two schemes in Figure 10.40 underfill can still fill the cavity without leaving voids. However, if the trough is semi-closed as shown in the bottom scheme in Figure 10.40, air can be entrapped easily and becomes voids [6,19].

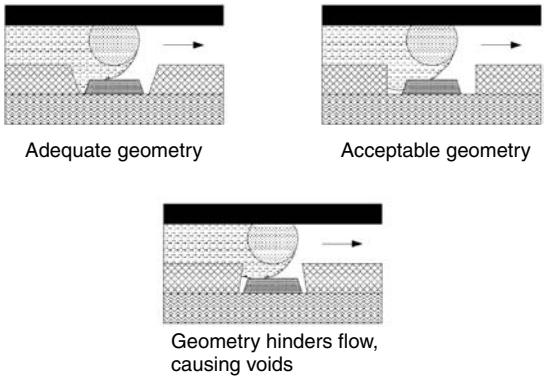

Figure 10.40 Effect of solder mask geometry on underfill voiding [6]

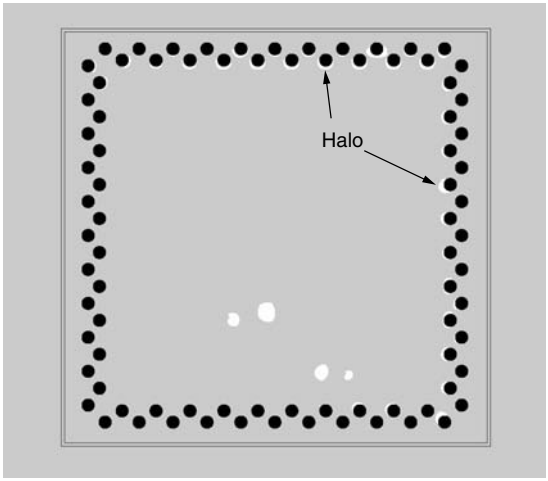

Figure 10.41 White halo defects partly surround the peripheral solder bumps in this acoustic image. Halo defects are a type of vertical delamination, and probably result when flux residue contaminates the bump surface. Solder will probably creep into the delamination [18]

Flux residue Besides restriction of flow, the presence of an organic flux residue can reduce the surface energy of inorganic materials (such as solder) of devices thus causing more difficulty in underfill spread and flow. The flux residue may be responsible for halo defects. Figure 10.41 shows white halo defects partly surrounding the peripheral solder bumps in this acoustic image. Halo defects probably result when flux residue contaminates the bump's surface, causing either poor wetting or easy delamination due to poor adhesion. With air pockets formed on the joints surface, the solder will probably creep into the delamination either under stress or in the subsequent heating process [18]. With the industry moving toward the no-clean process, this flux residue issue poses a challenge to the flip chip attachment process.

No-flow Causes for voiding in no-flow processes are not exactly the same as those for regular underfill systems. In

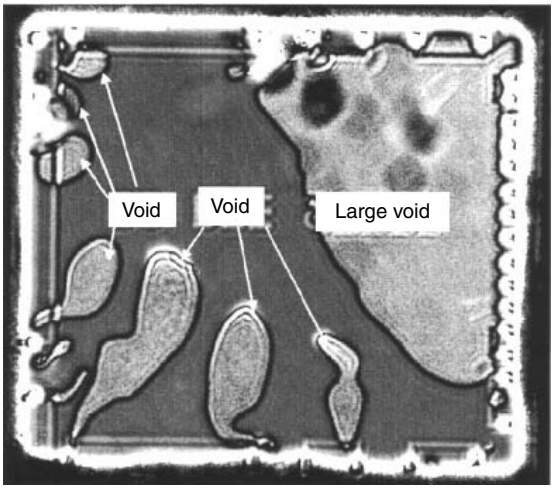

Figure 10.42 TAMI2-D view of the solder bumped flip chip on low-cost substrate with the no-flow (liquid-like) underfill material [14]

general, the voiding problem in a no-flow system is more serious than conventional underfill, as demonstrated by Figure 10.42 [14]. The causes may include the following factors: (1) air or volatiles in the underfill, (2) moisture in the solder mask and board, (3) inadequate dispense path, (4) wrong curing condition, (5) solder mask geometry, and (6) placement speed.

Since no-flow does not contain fillers, the viscosity is lower than that of regular underfill, especially at elevated temperatures. This lower viscosity material allows volatiles or moisture to expand more easily within the underfill to form voids, hence making the no-flow process more sensitive to volatiles and moisture in the solder mask and board. Using an incorrect curing profile can aggravate this voiding problem [2]. As a result, prebaking the board prior to the no-flow process becomes crucial for non-voiding performance. DeBarros *et al*. [21] have studied the effect of prebaking on no-flow voiding. Their results indicate that when the prebaking time and temperature increase, the voiding symptom lessens. At prebaking for 2 hours at 120 °C, no voids can be discerned (see Figure 10.43). Other studies also indicate that a 2-hour board baking at 125 °C before underfill was sufficient to remove any accumulated moisture [3].

The dispense path is also important for a liquid no-flow process. DeBarros *et al*. [21] have compared several dispense patterns (see Figure 10.44) and found that the glob pattern entrapped no air voids while the other two occasionally created a small void around a solder joint and sometimes an elongated void running down the trench. They accordingly concluded that when multiple flow fronts converge during placement they are more likely to trap air voids.

Placement also plays a role in no-flow voiding. Slow placement speed generates much less voiding than fast placement. This is understandable considering that the underfill will need time to wet and wick the underside of the flip chip as well as the board's surface.

10.2.5 Bridging

Bridging behavior in a flip chip (see Figure 10.45) is different from that of BGA or CSP, mainly due to its very low weight and the use of underfill. It can be caused by (1) insufficient flux tack value, (2) improper reflow profile, (3) movement of parts, (4) inadequate underfill system, and (5) inadequate cure profile.

It has been observed that the bridging rate is high (5–10 percent) when reflowed in a belt furnace. Due to either insufficient tack value or excessive outgassing caused by an incorrect reflow profile, the flux is seen to cause frequent random movements of the chips before they are finally drawn back to their normal position by overall self-alignment force [2].

Bridging can also be caused by the underfill. It has been seen in previous sections that voids can be generated in the underfill if not processed correctly. If the void occurs next to a solder joint, as shown in Figure 10.46 [14], solder extrusion may occur where solder creeps or flows into the void under stress, particularly at an elevated temperature. Figure 10.47 shows the evolution of solder extrusion, with a bridge eventually formed [21]. The occurrence of solder extrusion can be fairly extensive and may cover many solder joints. Figure 10.48 shows solder extrusion where, due to the popcorning effect, the solder migrates into the die–underfill interface and into underfill voids.

10.2.6 Open

Open may be caused by too high an oxygen level during reflow [2]. Using fluxes with insufficient activity or using boards with poor pad solderability will have the same effect. Open may also occur due to the inability to make contact as a result of too large a spacing. Figure 10.49 shows a flip chip without a solder connection [17]. This

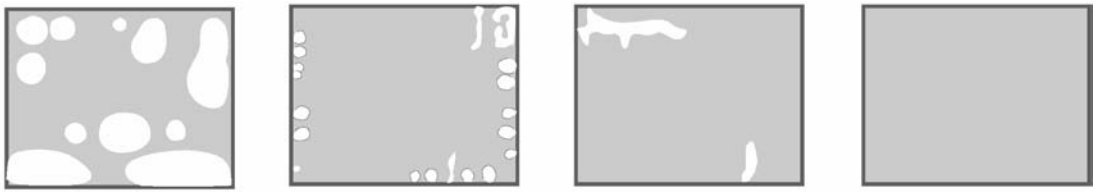

Figure 10.43 Moisture absorbed by the substrate previous to assembly can create voids in the no-flow underfills during reflow processing. To eliminate moisture-induced voids, the substrate must be pre-baked [21]

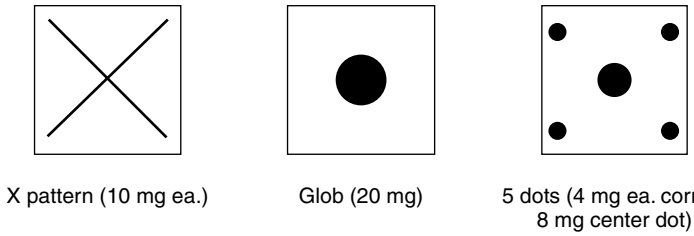

Figure 10.44 Dispense patterns for no-flow underfills. The glob pattern entrapped no air voids while the X pattern and five-dot pattern occasionally created a small void around a solder joint and sometimes an elongated void running down the trench [21]

is due to an increase in clearance due to chip tilting, which in turn can be caused by either too high an oven gas flow rate, a jerky belt movement, or an uneven flux deployment. Apparently, a poor coplanarity on the board or a gross misregistration can also result in the same symptom.

Open may also be caused by a barrier between the bump and the pad. Figure 10.50 shows no solder joint formed in a no-flow process [14]. This open is probably caused by an early onset of gelling of underfill, which prevents solder from contacting the pad.

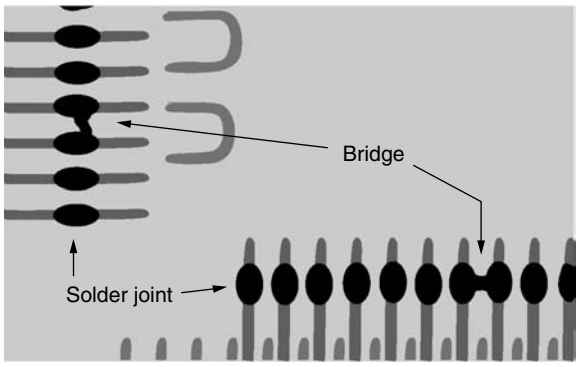

Figure 10.45 X-ray photograph of flip chip showing bridged joints [4]

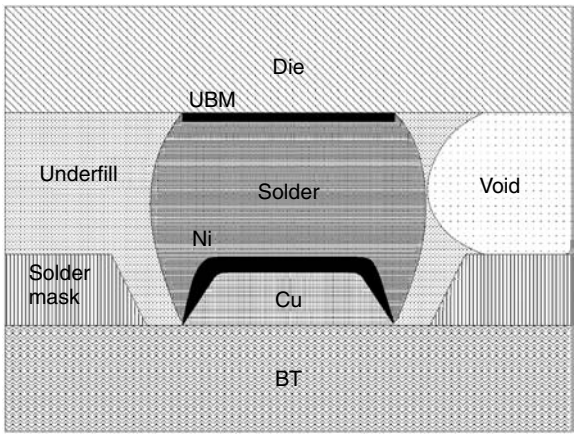

Figure 10.46 Cross-section of flip chip showing a void formed next to the solder bump [14]

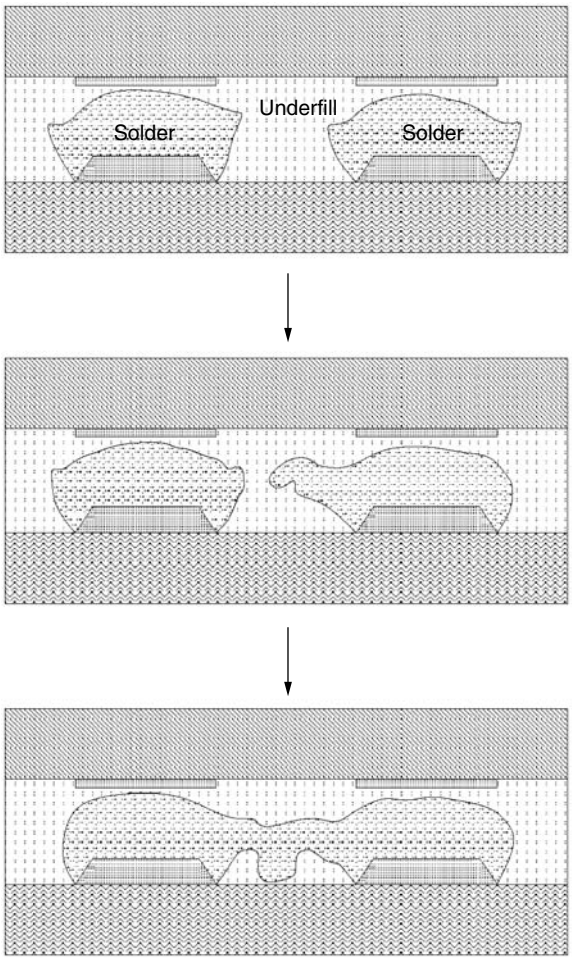

Figure 10.47 Solder migrating into voids between bumps [21]

10.2.7 Underfill crack

Cracks in an underfill fillet may occur immediately after curing. Figure 10.51 shows a schematic corner crack of underfill, while Figure 10-52(a) is an optical photograph of a corner crack, with delamination developed from this corner crack after temperature cycling (see Figure 10.52(b)) [23]. The underfill can also occur at the bottom edge of a die, as shown in Figure 10.53, or

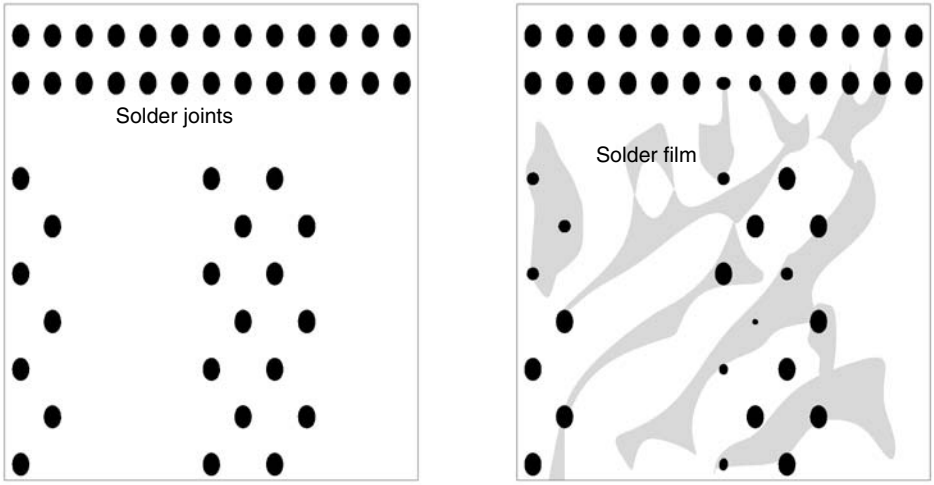

Figure 10.48 Popcorning led to solder-migration into the die–underfill interface and into underfill voids. (Courtesy Universal Instruments Corporation.)

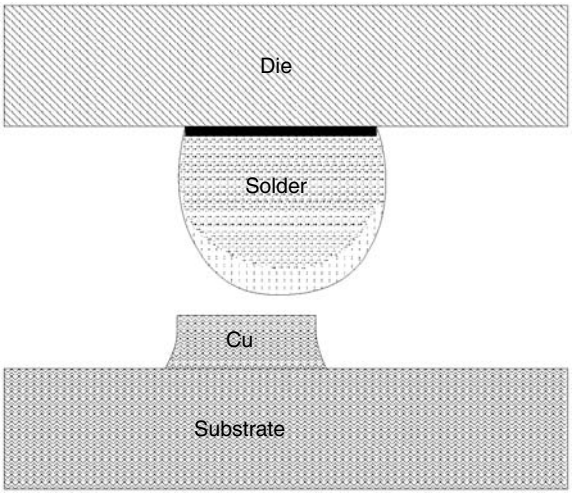

Figure 10.49 Flip chip with no solder connection due to tilt. Chips used in this study contained an optimal volume of eutectic solder to create the joint, delivered as a ''tin cap'' covering the high-melt bumps [17]

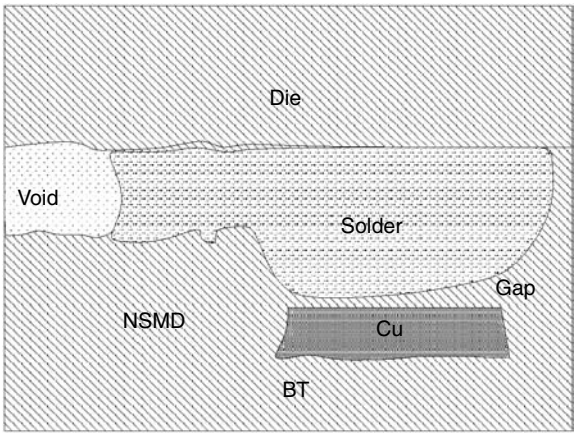

Figure 10.50 Close-up view of one solder bump with solder flows into the nearby void in a no-flow underfilling process. Notice that there is no joint formed between the badly shaped solder bump and copper pad [14]

the edge of fillet, as shown in Figure 10.54(a), which can eventually develop into edge delamination (see Figure 10.54(b)) [23]. The fillet edge crack or fillet corner crack are caused by mismatch in TCE, as can be seen easily in Figure 10.55. The crack developed at the bottom edge of the die is caused by unbalanced shear stress and normal stress (compression), as shown in Figure 10.56. Borgesen *et al*. [23] have indicated that whether the compression is sufficient to suppress the initiation of shear driven delamination depends, among other things, on the adhesive strength as well as on the thicknesses of chip, substrate and edge fillet. It has been observed that an underfill with a lower modulus, thus being less brittle, can effectively eliminate crack formation.

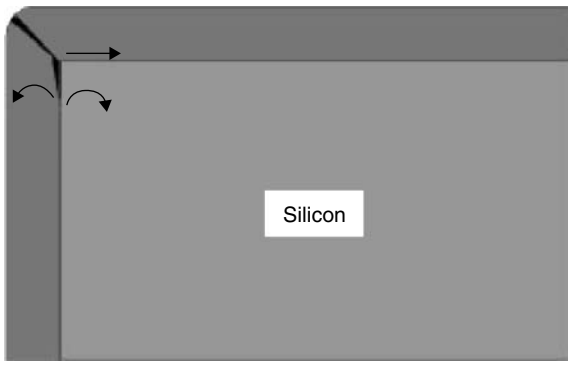

Figure 10.51 Schematic of underfill corner crack [23]

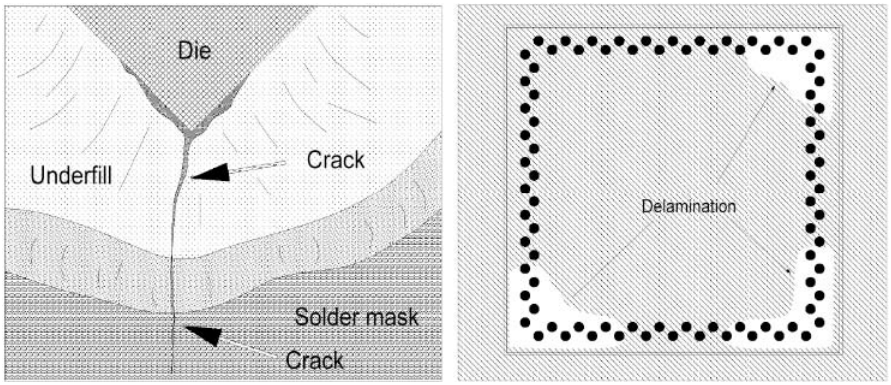

Figure 10.52 Optical micrograph of flip chip assembly with corner crack extending into solder mask **(a)**. This corner crack further developed into delamination after temperature cycling **(b)** [23]

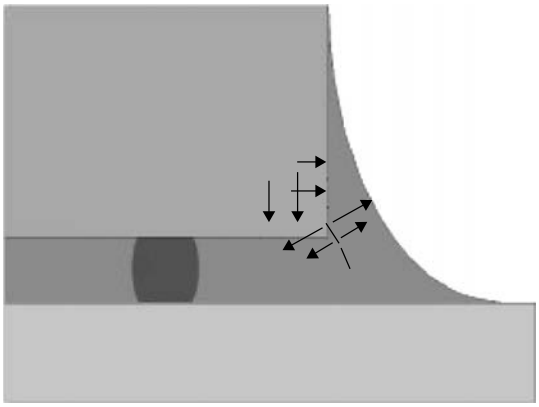

Figure 10.53 Crack opening forces outward and downward from bottom of vertical chip edge [23]

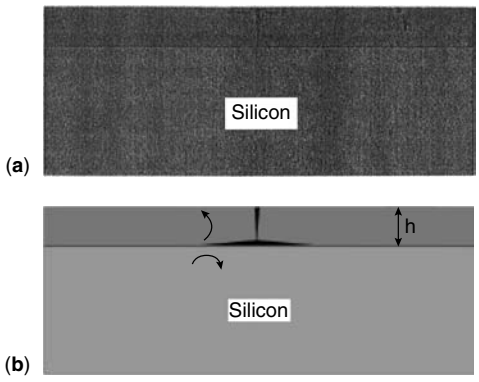

Figure 10.54 Schematic of underfill: **(a)** edge crack and **(b)** the delamination developed from the edge crack [23]

10.2.8 Delamination

Although voids are considered undesirable for an underfill, delamination may be an even greater threat to the reliability of a flip chip. Yegnasubramanian *et al*. [1] have

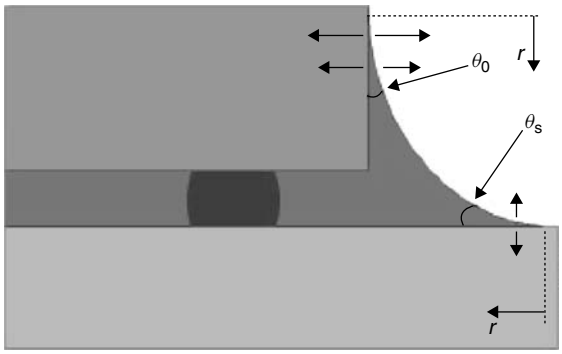

Figure 10.55 Stress distribution at end of underfill fillet [23]

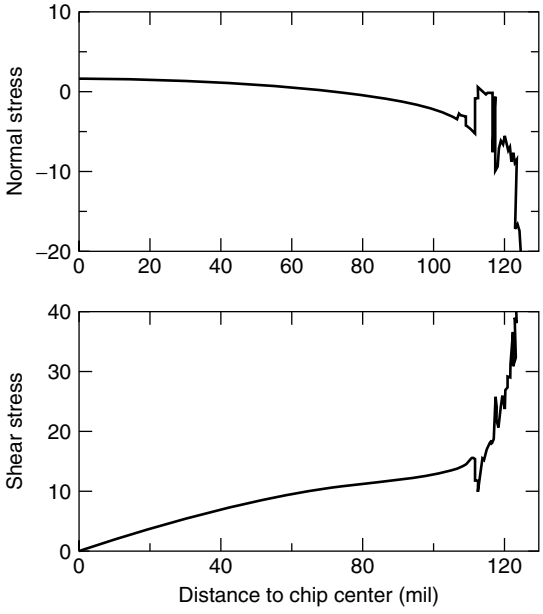

Figure 10.56 Stresses at chip passivation/underfill (solder) interface from center to chip edge shows singularity in shear stress at edge. Here a perfect adhesion everywhere is assumed [23]

reported that, in the case of high lead bumps, the most common failure mechanism is delamination of the underfill from the chip interface followed by a fatigue crack of the solder joint near the chip side. In the case of eutectic solder bumps, a fatigue crack was found near the board side and in some instances, near both the chip and board sides. Also delamination of the underfill from the board interface was seen in some instances, as shown in Figure 10.57.

Liu *et al*. [20] have reported that, due to the numerous interfaces, the first important failure mode of flip chip packaging is delamination. Cracking is the second important failure mode, including die cracking, underbump cracking, underfill cracking, and substrate PTH/microvia cracking. For a traditional underfilled (highly filled with filler) flip chip package, delamination between the passivation and underfill is more critical. For the reflowable underfills (having very low or no filler content), the fracture occurs through the solder interconnect near the substrate surface.

Delamination usually occurs after temperature cycling [1] or humidity treatment. This failure is often a result of the combined effects of insufficient adhesion, mismatch in thermal expansion coefficients with parts, and moisture pickup. Figure 10.52(b) shows delamination caused by a corner fillet crack, while Figure 10.54(b) illustrates a delamination caused by a fillet edge crack. Delamination can be increased by poor adhesion between underfill and solder joints. Borgesen *et al*. [23] showed that the compression stress varies with distance to the center while shear stress increases considerably in the absence of adhesion between underfill and solder, as illustrated in Figure 10.58. The increase in shear stress plus local reduction of compression inevitably enhances the probability of delamination.

For a no-clean process, the most important factor is probably the compatibility between underfill and flux residue. A lower flux residue usually provides a better result, although this is not always true. For a conventional underfill process, carefully selecting and testing the flux and underfill appears to be the only way to prevent delamination.

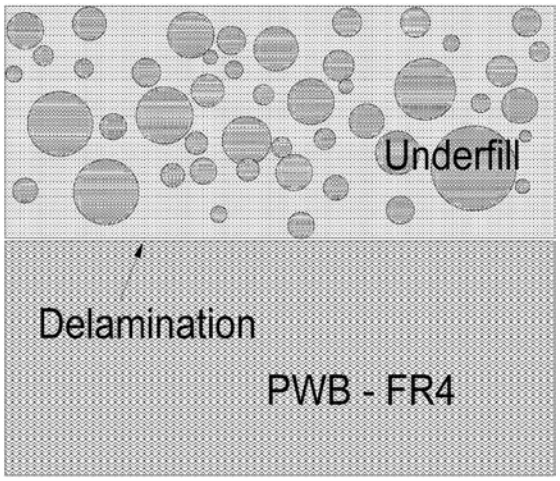

Figure 10.57 Delamination near the board side for a flip chip bumped with eutectic Sn–Pb solder [1]

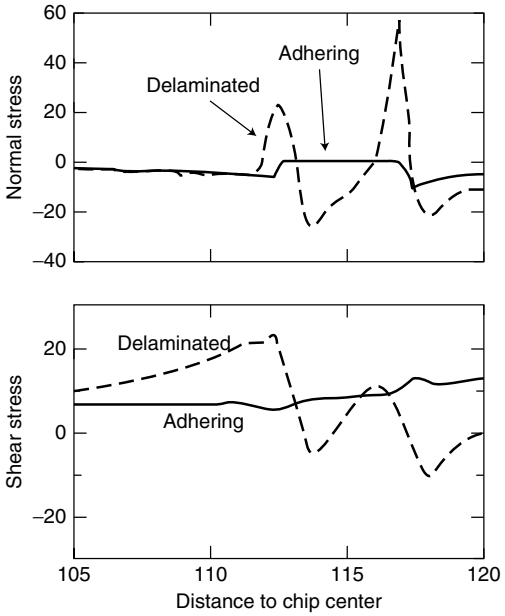

Figure 10.58 Normal and shear stresses across chip/underfill and chip/solder interfaces with and without adhesion at underfill/solder interface. Here a solder joint of 5 mil diameter centered 10 mil from the chip edge which is 125 mil from the center [23]

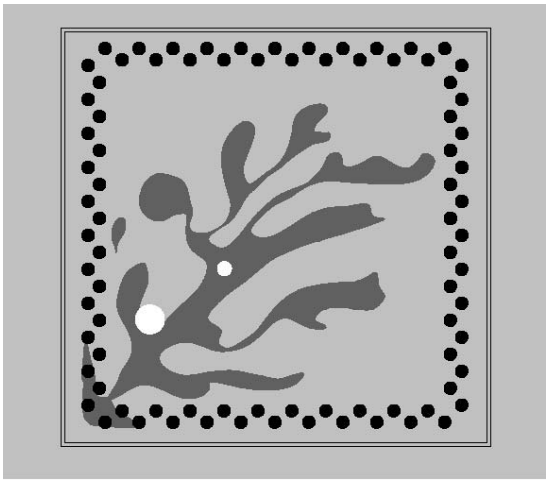

Figure 10.59 Acoustic image shows segregation of filler particles in underfill. Dark areas are concentrations of filler particles. The two white dots are voids, which often formed on the segregated area [18]

10.2.9 Filler segregation

One of the common symptoms encountered during underfilling is filler segregation. This happens when the underfill is flowing through the small clearance between die and board. Two common types of filler segregation are

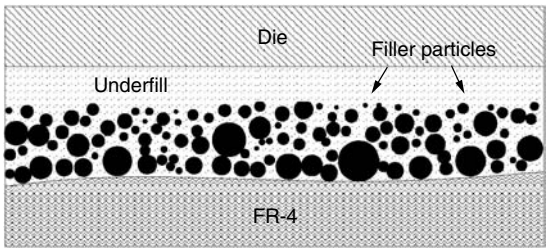

Figure 10.60 SEM micrograph showing a segregation of an underfill after dispensing and curing [12]

(1) striation and (2) particle settlement. The first can be demonstrated by Figure 10.59. The acoustic image shows tree-like segregation of filler particles in the underfill. Dark areas are concentrations of filler particles. These areas are often the sites for formation of voids such as the two shown here [18]. The second type of segregation is illustrated in Figure 10.60 where the SEM micrograph shows segregation of an underfill after dispensing and curing [12]. The segregation can be seen especially if the clearance between a silicon and a PCB is thin, e.g. less than 50 mm.

Segregation results in uneven underfill properties. It will cause uneven stress distribution as well as uneven

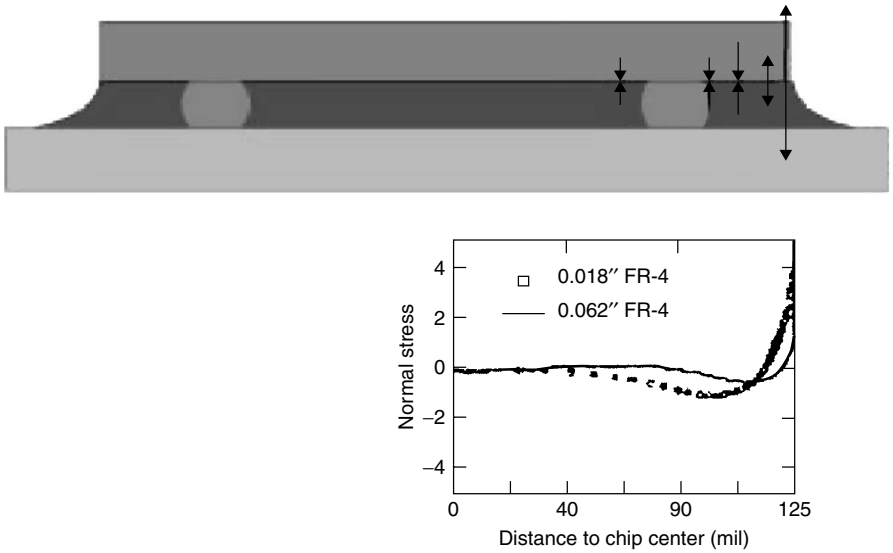

Figure 10.61 Stress analysis indicates a tension stress exists at the edge of die in the absence of edge fillet for a 25 mil thick chip on a thin (18 mil) and a thick (62 mil) FR-4 [23]

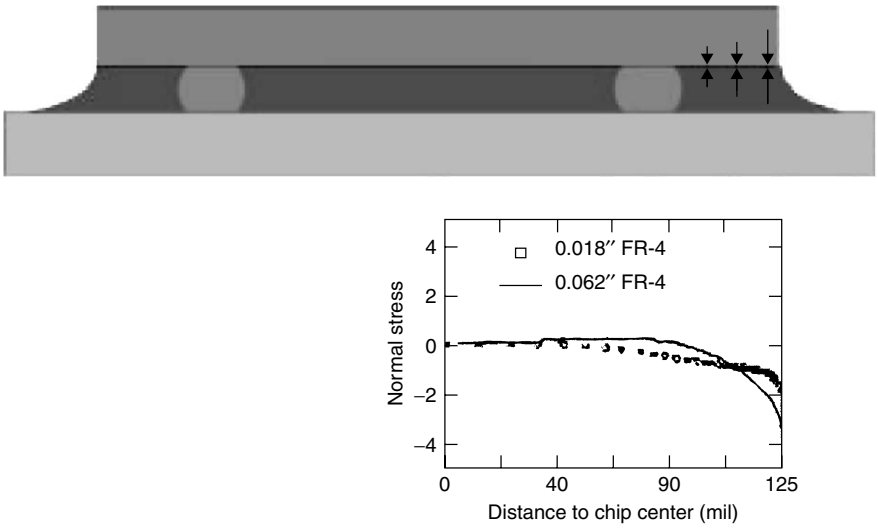

Figure 10.62 Stress analysis indicates a compression stress exists at the edge of die in the presence of edge fillet for a 25 mil thick chip on a thin (18 mil) and a thick (62 mil) FR-4 [23]

thermal conductivity, thus compromising the reliability of a flip chip. Filler segregation is mainly governed by the underfill property. Therefore, care should be taken in selecting an underfill.

10.2.10 Insufficient underfilling

Sometimes underfill may not form a proper fillet, or may not completely fill underneath a flip chip. Insufficient underfill at the bottom of die will cause a premature solder joint crack due to lack of bonding support from the underfill. In addition, lack of fillet formation can also cause delamination initiated from the edge of the die, as reported by Borgensen *et al*. [23]. Figure 10.61 shows a tension stress at the edge of a die in the absence of an edge fillet, while Figure 10.62 illustrates a compression stress in the presence of edge fillet.

Insufficient underfilling can be caused by (1) too fast a cure rate, (2) too high a viscosity, (3) too large a filler particle size, (4) uneven surface smoothness and coplanarity, and (5) improper curing temperature. The first two causes are self-evident. As to filler particle size, too large a particle size may result in staggering or particles, thus restricting the flow of the underfill. As a rule of thumb, the particle size should be no larger than 1/3 of the standoff. In general, the filler size used is no larger than 10 μ in diameter.

10.3 Conclusion

Flip chip reflow attachment is a sophisticated process. The need for underfilling further complicates the subject and differentiates it from BGA and CSP assembly. The process is still evolving rapidly, as reflected by the new underfilling materials under development. The author expects that advances in materials will be the major emphasis in order to achieve a low cost, high yield and high throughput process.

References

1. S. Yegnasubramanian, R. Deshmukh, J. Fulton, R. Fanucci, J. Gannon, A. Serafino, J. R. Morris and Khalil Nikmanesh, ''Flip-Chip-on-Board (FCOB) Assembly and Reliability'', in *Proc. Of SMTA/IPC Electronics Assembly Expo*, Providence, RI, p. S4–3, 24–29 October 1998.
2. Chang Liangbin, Wei Koh, Jay Huang, and Wei Chun, ''Failures in DCA Assembly'', in *Proc. of The Third International Symposium of Electronic Packaging Technology*, pp. 287–290, 17–21 August 1998, Beijing, China.
3. P. Elenius, ''Flip Chip Bumping for IC Packaging Contractors'', in *Proc. of Nepcon West 1998*, pp. 210–205, Anaheim, CA, 1–5 March 1998.
4. W. P. von Hessen, ''Flip Chip – Integrated in a Standard SMT Process'', APEX, Long Beach, CA, 14–16 March 2000.
5. G. Schiebel, ''High-speed Second – Level CSP and Flip Chip Assembly Using Flip Chip Shooters'', SMTA International, San Jose, CA, 12–16 September 1999.
6. B. J. Lewis, ''Process Characterization and the Effect of Process Defects on Flip Chip Reliability'', APEX, Long Beach, CA, 14–16 March 2000.
7. Technical literature from Nordson Corporation.
8. R. N. Master, M. Khan, and M. Guardado, ''Advances in Materials and Processes for Flip Chip Packaging'', APEX 2000, Long Beach, CA, 14–16 March 2000.
9. J. Kloeser, K. Kutzner, E. Jung, K. Heinricht, L. Lauter, M. Töpper, E. Ochi, R. Aschenbrenner and H. Reichl, ''Experience with a Fully Automatic Flip-Chip Assembly Line Integrating SMT'', in *Proc. of Nepcon West 1998*, Anaheim, CA, 1–5 March 1998.
10. J. Newbold and A. Lewis, ''The Effects of New Trends in Flip Chip Packages on Automating the Underfill Processes'', in *Proc. of Nepcon West 1998*, Anaheim, CA, February 1998.
11. M. J. Norris, ''Dispensing Flip Chip Underfill Process Problems and Solutions'', in *Proc of Nepcon West 1998*, Anaheim, CA, February 1998.
12. K. Kulojärvi, ''Flip Chip Processing for Miniaturized Telecommunications Applications'', APEX 2000, Long Beach, CA, 14–16 March 2000.
13. P. A. Kondos and P. Borgesen, ''Flip Chip Assembly with Reflow Encapsulants'', SMTA International, Chicago, IL, September 2000.
14. J. H. Lau, C. Chang, and C. Ouyang, ''No-Flow Underfill for Solder Bumped Flip Chip on Low-Cost Substrates'', in *Proc. of Nepcon West 1999*, Anaheim, CA, February 1999.
15. N. Koopman, S. Nangalia, and V. Rogers, ''Fluxless No-clean Assembly of Solder Bumped Flip Chips'', *Proceedings, 46th Electronic Components and Technology Conference*, p. 1311, 552–8, Orlando, FL, USA, 28–31 May 1996.
16. R. Aschenbrenner, E. Zakel, G. Azdasht, A. Kloeser, and H. Reichl, ''Fluxless Flip-chip Bonding on Flexible Substrates: A Comparison between Adhesive Bonding and Soldering'', *Soldering & Surface Mount Technology*, No.23, pp. 5–11 (June 1996).
17. R. Noreika, C. Fieselman, K. Slesinger, and M. Wells, SMT Component Self-centering Properties During Solder Reflow'', in *Proc. of Surface Mount International*, San Jose, CA, pp. 338–346 (September 1997).
18. J. E. Semmens and T. Adams, ''Flip Chip Package Failure Mechanisms'', *Solid State Technology*, pp. 59–64 (April, 1998).
19. P. N. Houston, B. A. Smith, D. F. Baldwin, and B. J. Lewis, ''Failure Mode Analysis of Advanced Electronics Packaging'', Apex 2000, Long Beach, CA, March 2000.
20. Sheng Liu, Jianjun Wang, and Zhengfang Qian, ''Several Reliability Related Issues For Flip-Chip Packaging'', in *Proc. of The Third International Symposium of Electronic Packaging Technology*, pp. 349–356, 17–21 August 1998, Beijing, China.
21. T. DeBarros and D. Katze, ''Achieving SMT Compatible Flip Chip Assembly with No-flow Fluxing Underfills'', in *Proc. of Nepcon West 2000*, Anaheim, CA, February 2000.
22. M. Xiao, K. J. Lawless, and N. C. Lee, ''Prospects of Solder Paste Applications in Ultra-fine Pitch Era'', *Proc. of Surface Mount International*, San Jose, CA (August 1993).
23. P. Borgesen, D. Blass, and K. Srihari, ''Flip Chip Reliability'', Apex, Long Beach, CA, 14–16 March 2000.
24. S. Wang and N.-C. Lee, Indium Corporation of America, unpublished data.

11

Optimizing a Reflow Profile Via Defect Mechanisms Analysis

Reflow solder paste is the primary method of forming solder joints at board level assembly in SMT industries. In general, when correctly performed, the reflow process provides a high yield, high reliability, and low cost advantages. Among all the process considerations, reflow profile is one of the most important factors in determining the soldering defect rate. The types of defects [1] affected by a reflow profile include component cracking, tombstoning, wicking, solder balling, bridging, solder beading, cold joints, excessive intermetallics formation, poor wetting, voiding, skewing, charring, delamination, leaching, dewetting, solder or pad detachment. Therefore, it is extremely important to have the reflow profile engineered properly in order to achieve both high yield and high reliability.

In general, a reflow profile can be roughly divided into three major elements: the peak temperature, the heating stage, and the cooling stage. Each element has its impact on the reflow results. Based on an understanding of defect formation mechanisms, the discussion in this chapter will focus on how each part of the profile can be engineered to minimize the defect rate and to maximize reliability.

11.1 Flux reaction

In the SMT industries, soldering normally starts with fluxing to clean up the metal oxides, then solder wetting to form the solder joints. Therefore, before discussing any profile setting, it is essential to understand the time and temperature requirements for the fluxing reaction.

11.1.1 Time/temperature requirement for the fluxing reaction

The fluxing reaction usually can be monitored by determining the wetting time S with the use of a wetting balance, as illustrated by Figure 11.1. A short wetting time normally reflects a fast fluxing reaction. It can also be investigated by examining the coalescence, or reflow, behavior of solder paste. Again, a fast solder paste coalescence process indicates a fast fluxing reaction.

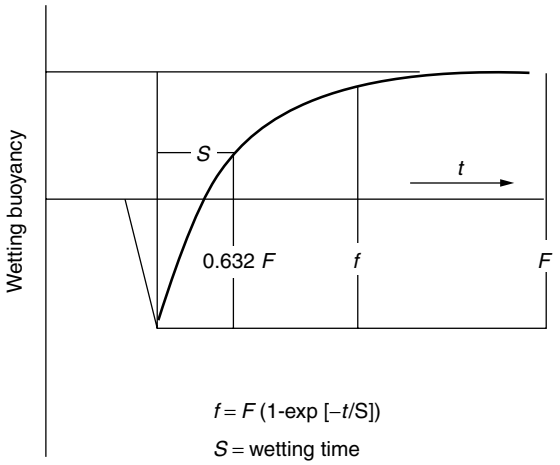

Figure 11.1 Kinetics of wetting

Reflow of solder pastes can usually be completed in a very short time. This can be demonstrated easily by printing a small dot of 63Sn/37Pb solder paste onto a copper coupon, followed by reflowing this sample on a hot plate with a reasonable surface temperature. The paste reflow and solder spreading processes can usually be completed in a few seconds.

This rapid reflow, or fluxing, behavior of solder paste can also be confirmed by examining the wetting time of fluxes with the use of a wetting balance. Table 11.1 shows the wetting time of four fluxes A, B, C, and D, from several commercially available 63Sn/37Pb solder pastes at 200° and 240°C, respectively. The copper coupons tested have been prebaked in a forced air convection oven at 100°C for 3 hours to simulate the "difficult to solder situation". The solders used in this study are 63Sn/37Pb and 62Sn/36Pb/2Ag. Results indicate that the wetting time is around several seconds at the designated temperatures. Therefore, it can be concluded that the fluxing reaction does not require more than a few seconds as long as the temperature can be raised to about 200°C or higher. A simple, extremely rapid heating profile is sufficient to complete the fluxing and yield a good reflow and wetting result.

Table 11.1 Wetting time of several fluxes tested at 200° and 240°C using 63Sn/37Pb and 62Sn/36Pb/2Ag

Fluxes	*Wetting time (seconds)*			
	63Sn/37Pb		*62Sn/36Pb/2Ag*	
	200° C	*240° C*	*200° C*	*240° C*
A	2.87	1.48	4.68	2.52
B	1.03	0.50	1.44	0.63
C	1.65	1.00	2.60	1.03
D	2.50	1.44	3.48	2.10

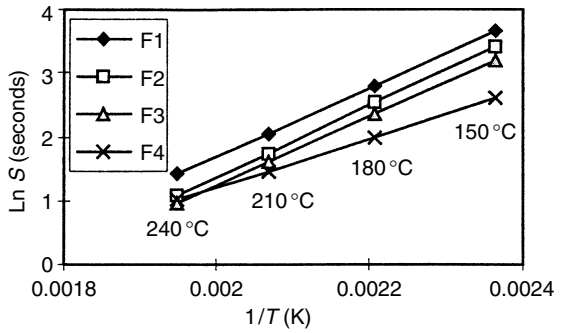

Figure 11.2 Wetting time *S* of fluxes as a function of temperature

11.1.2 Fluxing contribution below the melting temperature

In order to understand the contribution of the fluxing reaction below the melting temperature, the wetting times of fluxes F1, F2, F3, and F4 from four RMA solder pastes are measured with the use of a low melting temperature solder (46Bi/34Sn/20Pb, with a melting point of 95–108°C). Although this low melting temperature solder in general shows a slower wetting behavior than eutectic Sn–Pb solder, the wetting time measured at various temperatures is expected to reflect the relative fluxing reaction rate at the corresponding temperature. Results shown in Figure 11.2 indicate that the wetting time is proportional to the reciprocal of absolute temperature. This is true at least for the temperature ranging from 150° to 240°C. At 150°C, the wetting time is about one or two orders of magnitude longer than the wetting time at 210–240°C. Hence, it can be concluded that (1) temperature is the dominant factor in the fluxing reaction, and (2) with equal dwell time, the contribution of the fluxing reaction at lower temperatures is negligible when compared with that at higher temperatures.

11.2 Peak temperature

11.2.1 Cold joint and poor wetting

The peak temperature of a reflow profile is usually determined by the solder melting temperature and the temperature tolerance of the board and parts to be assembled. Being heterogeneous in nature, solder pastes typically take longer to coalesce than is shown by wetting balance test. Accordingly, the minimal peak temperature should be about 25–30°C above the solder melting temperature. A reflow with a peak temperature lower than this will have more risk of yielding cold joints as well as insufficient wetting. In the case of eutectic Sn–Pb solder, this minimum peak temperature is approximately 210°C.

11.2.2 Charring, delamination, and intermetallics

The maximum peak temperature required is about 235°C. Beyond this, the charring and delamination of epoxy boards and plastic parts may become a problem. Furthermore, an excessive amount of intermetallic compound may also be formed and result in a brittle solder joint.

11.2.3 Leaching

Leaching [2] is a problem in hybrid applications when excessive amounts of base metal appear in the solder. The extent of leaching is dictated by the peak temperature, and can be reduced by using a lower peak temperature. Using a shorter time at a temperature above the liquidus would also help to reduce leaching.

11.3 Cooling stage

11.3.1 Intermetallics

The optimum cooling stage is also relatively easy to determine. A slow cooling rate at a temperature above the melting temperature of solder will result in excessive intermetallics. To minimize intermetallics, a fast cooling rate is required.

11.3.2 Grain size

A slow cooling rate often results in solder joints with a large grain structure due to the annealing effect. This mainly refers to the temperature range between the melting temperature and a temperature below this. This large grain structure typically exhibits a poor fatigue resistance and thus it is not desired. Solder joints with a fine grain structure can be produced with the use of a fast cooling rate. However, the cooling rate effect diminishes with an increasing temperature gap. A 50°C temperature gap is believed to be sufficient to have a negligible annealing effect.

11.3.3 Internal stress-component cracking

The maximum cooling rate allowed is often determined by the tolerance of the components against thermal shock. For components such as chip capacitors, the maximum cooling rate tolerable is approximately 4°C/min.

11.3.4 Deformation of joints

The cooling mechanism of a reflow oven is typically operated by using forced cold air. A very fast cooling rate

will require the use of a very fast cold air blown onto the molten solder joints, which may result in deformed solder joints. In general, solder joint deformation is negligible at a cooling rate no higher than 4°C/min.

11.3.5 Internal stress solder or pad detachment

The cooling rate may also affect the delamination of pads from the board or detachment of solder joints from the pads. A fast cooling rate may result in too high a temperature gradient between components and board, and accordingly yield a mismatch in thermal expansion. This in turn will create internal stress around the solder joints, and consequently result in detachment of solder joints from the pads, or delamination of pads from the board. Examples include detachment of the corner solder joints of BGAs in some instances.

11.4 Heating stage

Perhaps the heating stage can be regarded as the most complicated part of a reflow profile. As in the cooling stage, the parameters involved here are both time and temperature.

11.4.1 Slumping and bridging

Bridging is a direct result of slumping. Therefore, the discussion here will focus on the slumping of solder paste. Since slumping only occurs at the paste stage, the temperature in our discussion will be at or below the melting point of the solder.

In general, the viscosity of materials with a fixed composition and chemical structure decreases with increasing temperature, due to increasing thermal agitation at the molecular level. This decrease in viscosity at a higher temperature will yield a greater slump. On the other hand, the increase in temperature usually dries out more solvent of the flux and results in an increase in solid content, thus an increase in the viscosity. These two opposite effects, thermal agitation effect and solvent loss effect, are shown in Figure 11.3.

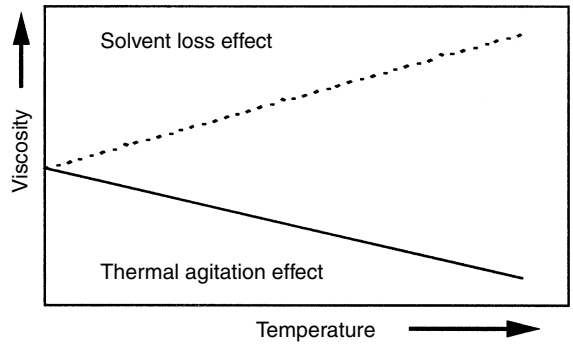

Figure 11.3 The effect of thermal agitation and solvent loss on viscosity as a function of temperature

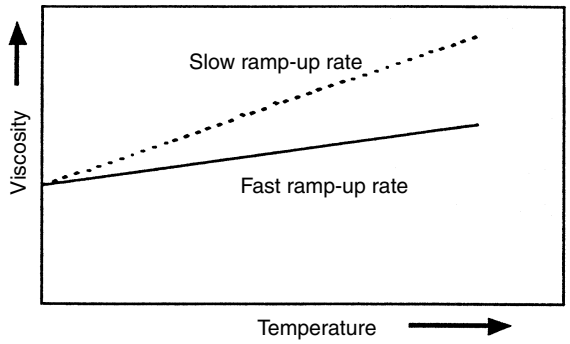

Figure 11.4 Relation between ramp-up rate and viscosity due to solvent loss effect

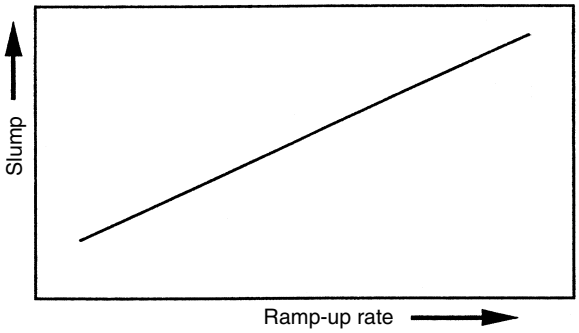

Figure 11.5 Relation between slump and ramp-up rate

The thermal agitation effect is an intrinsic material property. It is a function of temperature only and is independent of time. Therefore, the ramp-up rate has no effect on it. However, the solvent loss effect is a kinetic phenomenon and will be affected by the ramp-up rate. The solvent vaporization rate is proportional to the thermal energy, or temperature, of the solvent. The solvent loss quantity is proportional to the product of the vaporization rate and the time allowed for vaporization. In other words, the total solvent loss is a function of both time and temperature, hence it can be regulated by varying the reflow ramp-up rate. At a slow ramp-up rate, the viscosity of solder paste is higher than that of the fast ramp-up rate at any given elevated temperature due to the greater amount of solvent loss, as shown in Figure 11.4.

Therefore, by applying a fairly slow ramp-up rate, the solvent loss effect can be enhanced and can override the thermal agitation effect. This will result in either a viscosity decrease or even a net viscosity increase with increasing temperature. Consequently, slumping decreases with decreasing ramp-up rate, as shown in Figure 11.5. In general, a ramp-up rate of 0.5–1°C/sec from room temperature to melting temperature is recommended.

11.4.2 Solder beading

Solder beading [3] is caused by flux outgassing which overrides the paste's cohesive force during the preheat

stage. The outgassing promotes the formation of isolated paste aggregates underneath the low-clearance components. At reflow, the isolated paste melts and, once it has emerged from the underside of the components, coalesces into solder beads. The outgassing rate can be controlled by controlling the ramp-up rate at the heating stage prior to melting of solder. At a very slow ramp-up rate, the outgassing of flux can occur via the diffusion process instead of rigorous vaporization, hence preventing the formation of isolated paste aggregates caused by the erupting outgassing force, and consequently avoiding formation of solder beading.

11.4.3 Wicking

In wicking [4] the molten solder wets the component lead and flows up the lead away from the joint area, to such an extent that a starved or an open joint is formed. It is a result of the lead being hotter than the pad of the PCB at the solder melting stage. This can be prevented by using more bottom-side heating or a very slow ramp-up rate at a temperature around the melting point of solder. By doing so, it will allow the temperature of leads and pads to reach equilibrium before any solder wetting occurs. Once the solder wets onto the pads, the solder fillet shape will remain stable and will no longer be sensitive to the ramp-up rate.

11.4.4 Tombstoning and skewing

Tombstoning [1] and skewing [2] are caused by uneven wetting occurring at the two ends of the chip. As with the wicking defect, these can be minimized by using a very slow ramp-up rate profile around the melting point of solder to allow the temperatures of the two ends of the chip to reach equilibrium. Below the melting temperature, the ramp-up rate has no impact on these two defects at all. Above the melting point, wetting has usually occurred therefore the ramp-up rate also has no impact.

11.4.5 Solder balling

Solder balling can be caused by spattering. In many instances, this can happen at a ramp-up rate greater than about 2°C/sec prior to solder coalescence. A slow ramp-up rate is a very effective means of preventing spattering. However, too slow a ramp-up rate can also introduce excessive oxidation and also deplete the flux capacity.

Solder balling can also be caused by excessive oxidation at a temperature prior to the solder's coalescence. To minimize this oxidation, the heat energy input prior to solder melting should be minimized. Therefore, when both spattering and oxidation factors are considered, the optimal heating process to minimize overall solder balling would be a profile with a linear ramp-up until the solder's melting temperature is reached.

11.4.6 Poor wetting

Poor wetting can result from excessive oxidation at a temperature prior to the solder's coalescence. As with the solder balling discussed above, the heat energy input prior to solder melting should be minimized in order to minimize this oxidation. The required profile is a heating time as brief as possible. If the heating time cannot be shortened due to other considerations, then a linear ramp-up profile from ambient temperature to solder melting temperature is crucial for minimizing oxidation.

11.4.7 Voiding

Voiding [5] is primarily caused by outgassing of flux entrapped at the unwetted sites at the interface of solder–substrate or solder–lead. The unwetted sites can be reduced by lowering the oxidation, as described in the previous section, that is, either a heating time as short as possible or a linear ramp-up profile from ambient temperature to solder melting temperature. If the solderability is very good, such as a HASL board, then wetting is not an issue, and voiding can be further improved by reducing the viscosity of the flux remnant. This can be accomplished with the use of a cooler profile [6].

11.4.8 Opens

Opens can be caused by either wicking or non-wetting. Wicking can be reduced by using the profile described in section 11.4.3, that is, using either more bottom-side heating or a very slow ramp-up rate at a temperature around the melting point of solder. In the non-wetting case, it is often observed as the "pillow effect". Here the lead sags into the solder bump without formation of a real bonding or wetting. Problems such as this can be minimized by reducing the oxidation, as discussed in section 11.4.6. Again, a linear ramp-up profile from ambient temperature to solder melting temperature is desired.

11.5 Timing considerations

11.5.1 Ramp-up stage

For the heating stage, it has been suggested in previous sections that, to minimize most defects (such as slumping, bridging, solder beading, solder balling, etc.), a slow ramp-up rate is required for the temperature range between ambient and the melting temperature of solder. It is recommended that a linear ramp-up rate be applied between room temperature and slightly below the melting temperature.

11.5.2 Soaking zone

Although mass reflow technology is improving in heating efficiency, a small temperature gradient may still exist across the board. In order to minimize defects (such as tombstoning, skewing, and wicking) caused by a temperature gradient across the melting temperature of

solder, a short plateau is recommended as a soaking zone. In general, the less efficient the heating, the longer the soaking zone should be. However, adapting a soaking zone may imply a compromise in a slow ramp-up rate prior to solder melting. With a constant overall profile length, the longer the soaking zone, the higher the ramp-up rate prior to the soaking zone will be. A soaking period of 30 seconds is considered adequate for a heating-efficient reflow technology.

11.5.3 Onset temperature of spike zone

The profile section around the peak temperature with both a fast ramp-up rate and a fast cooling rate is often referred to as spike zone. Considering the possibility of internal-stress-related component cracking, the ramp-up and cooling rates used are normally between 2.5–3.5°C/sec, with the maximum change rate no higher than 4°C/sec. This onset temperature of spike zone is adequate for a reflow technology that is able to maintain the temperature gradient on the board to within about 5°C.

11.6 Optimization of profile

11.6.1 Summary of desired profile feature

Listed in Table 11.2 are the major reflow-related defect types, mechanisms of defect formation, and the desired profile features, as well as a breakdown of the desired profile elements for each of these subjects discussed here.

11.6.2 Engineering the optimized profile

The desired profile features are also shown in Table 11.2. An optimized profile should minimize most of the defects,

Table 11.2 Desired profile features for minimizing defects

Subjects	*Defect mechanisms*	*Desired profile feature*	*Ramp-up rate*	*Peak temp.*	*Cooling rate*
Parts cracking	Too high an internal stress due to fast temperature change rate	Slow temperature change rate	Slow		Slow
Tombstoning	Uneven wetting at both ends of chip	Use slow ramp-up rate at temperature near and above solder mp to minimize the temperature gradients across the chip	Slow		
Skewing	Uneven wetting at both ends of chip	Use slow ramp-up rate at temperature near and above solder mp to minimize the temperature gradients across the chip	Slow		
Wicking	Leads hotter than PCB	Slow ramp-up rate to allow the board and components reaching temperature equilibrium before solder melts; more bottom side heating	Slow		
Solder balling	Spattering	Slow ramp-up rate to dry out paste solvents or moisture gradually	Slow		
Solder balling	Excessive oxidation before solder melting	Minimize heat input prior to reflow (slow ramp-up rate, no plateau at soaking zone) to reduce oxidation	Slow		
Hot slump	Viscosity drops with increasing temperature	Slow ramp-up rate to dry out paste solvent gradually before viscosity decreases too much	Slow		
Bridging	Hot slump	Slow ramp-up rate to dry out paste solvent gradually before viscosity decreases too much	Slow		
Solder beading	Rapid outgassing under low standoff components	Slow ramp-up rate prior to reflow to slow down the outgassing rate of paste	Slow		
Opens	Wicking	Slow ramp-up rate to allow the board and components reaching temperature equilibrium before solder melts; more bottom-side heating	Slow		
	Non-wetting	Minimize heat input prior to reflow (minimize soaking zone, or use linear ramp-up from ambient to solder melting temperature) to reduce oxidation	Slow		

(*continued overleaf*)

Table 11.2 (*Continued*)

Subjects	*Defect mechanisms*	*Desired profile feature*	*Ramp-up rate*	*Peak temp.*	*Cooling rate*
Poor wetting	Excessive oxidation	Minimize heat input prior to reflow (minimize soaking zone, or use linear ramp-up from ambient to solder melting temperature) to reduce oxidation	Slow		
Voiding	Excessive oxidation	Minimize heat input prior to reflow (minimize soaking zone, or use linear ramp-up from ambient to solder melting temperature) to reduce oxidation	Slow		
	Flux remnant too high in viscosity	Cooler reflow profile to allow more solvents in flux remnant		Low	
Charring	Overheat	Lower temperature, shorter time		Low	Fast
Leaching	Overheat at temperature above solder mp	Minimize heat input at temperature above solder mp by using lower temperature or shorter time		Low	Fast
Dewetting	Overheat at temperature above solder mp	Minimize heat input at temperature above solder mp by using lower temperature or shorter time		Low	Fast
Cold joints	Insufficient coalescence	Use high enough peak temperature		Medium	
Excessive intermetallics	Too much heat input above solder mp	Lower peak temperature and use shorter time		Low	Fast
Large grain size	Annealing effect due to slow cooling rate	Fast cooling rate			Fast
Solder or pad detachment	High stress due to mismatch in thermal expansion	Slow cooling rate			Slow

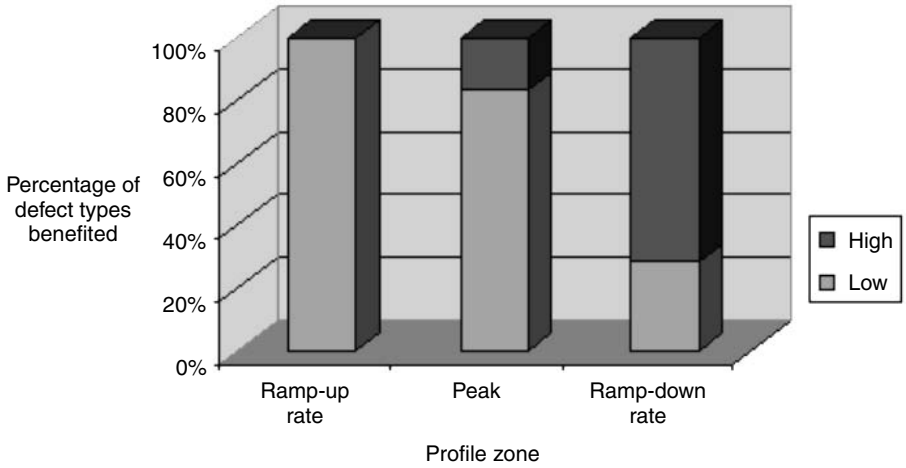

Figure 11.6 Summary of relative preference on profile characteristics based on percentage of defect types benefited

even if it may not be the best choice for reducing certain defects. For a heating zone, thirteen defects require a low ramp-up rate, and none require high one. In other words, 100 percent of all defect types will benefit from a low ramp-up rate. For a cooling zone, two defects require a low ramp-down rate, and five a high one, or 71 percent of defect types relevant needing a high ramp-down rate. For a peak temperature, five require a low temperature, and one a high one. These results are summarized in Figure 11.6. Therefore, the dominant trend can be summarized as a slow ramp-up rate to a low peak temperature, followed by a fast cooling rate. Combined with the tim-

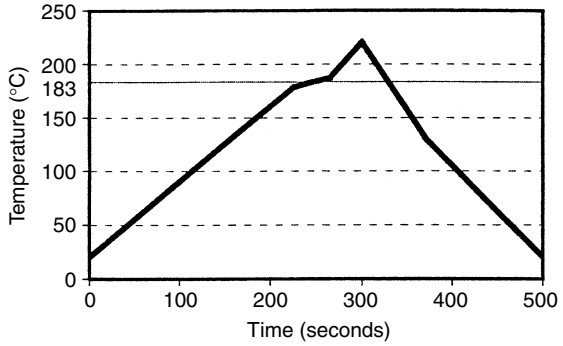

Figure 11.7 Optimized profile via defect mechanisms analysis

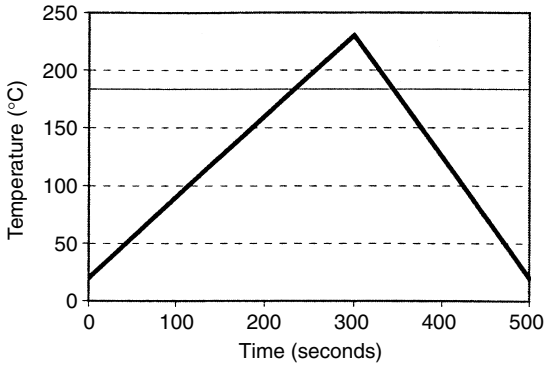

Figure 11.8 "Tent" profile with linear ramp-up to peak, then cooling down rapidly

ing considerations discussed above, the optimized profile can be represented by Figure 11.7. Here the temperature ramps up slowly with a ramp-up rate of 0.5–1°C/sec until reaching about 180°C. The temperature is then gradually raised further to 186°C within about 30 seconds, then raised quickly at about 2.5–3.5°C/sec until reaching 220°C. Then, the temperature is reduced with a rapid cooling rate which is no higher than 4°C/sec.

By examining Figure 11.7, it can be noticed that the small soaking shoulder causes only a ripple in the ramp-up path. The effect of that small shoulder may not be significant, and a linear ramp-up path may be preferred due to the ease of setting up on the oven. Figure 11.8 represent a profile with such a linear ramp-up to peak temperature, then cooling down quickly. As the shape of this profile resembles that of a tent, it can also be called a "Tent" profile.

11.7 Comparison with conventional profiles

11.7.1 Conventional profiles

It is interesting to compare the optimized profile with the conventional "textbook profiles" prevailing in the past, as shown in Figure 11.9. The conventional profiles typically are composed of an initial rapid ramp-up as preheat

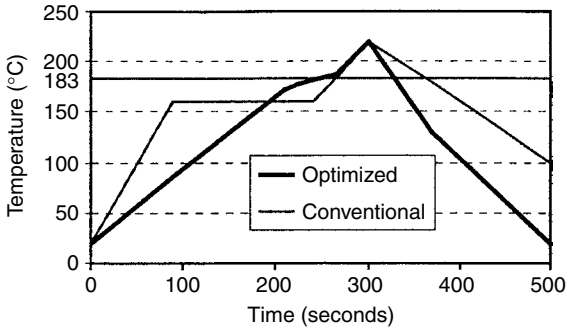

Figure 11.9 Optimized profile versus conventional profile

until about 150–160°C, then leveling off for a couple of minutes as a soaking zone. This is then followed by the spike zone with a relatively slow cooling rate after reaching the peak temperature. The primary difference between the optimized profile and the conventional profiles is that the former has a negligible plateau structure in the curve.

11.7.2 Background of conventional profiles

Conventional profiles were generated due to the constraint of reflow technologies used in the past. Before the emergence of modern forced air convection reflow technology, an infrared mass reflow oven was the mainstream reflow technology. Although this has provided relatively satisfactory reflow results, infrared reflow technology suffers several major constraints, including sensitivity toward uneven thermal mass distribution, difference in color and material type of board or parts, and component shadow effect. As a result, a considerable temperature gradient can be developed quickly across the board. With a linear ramp-up profile, such as that shown in Figure 11.7, the temperature gradient can become so significant that the hot spots may be just right but the cold spots may still be under-reflowed, or the cold spots may be just right but the hot spots may already be burned, as shown in Figure 11.10.

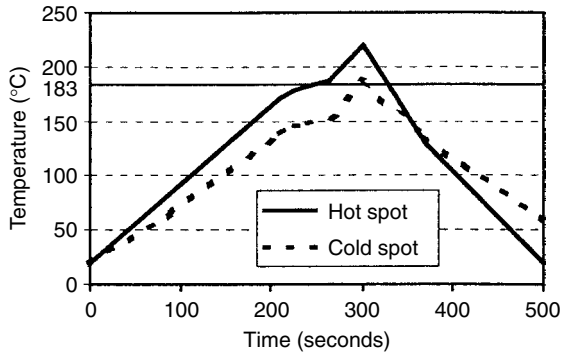

Figure 11.10 Typical temperature gradient developed using linear ramp-up profile on an infrared reflow

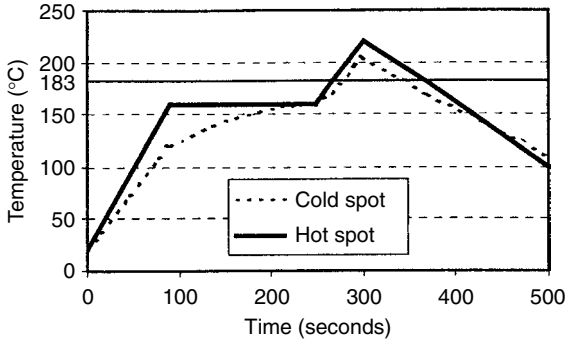

Figure 11.11 Typical temperature gradient developed using conventional profile on an infrared reflow oven

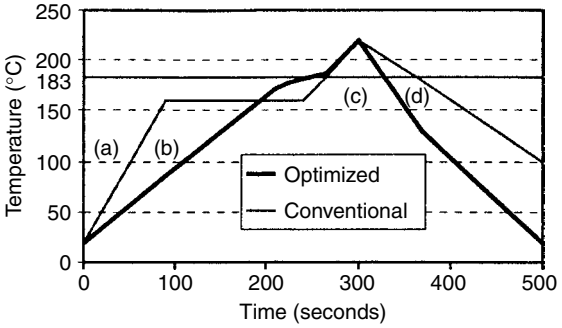

Figure 11.12 Unfavorable attributes of the conventional profiles when compared with the optimized profile

11.7.3 Approach of conventional profiles

In order to minimize the temperature gradient, a plateau-shaped equilibrating zone then becomes necessary, as shown in Figure 11.11. By bringing the temperature of the hot spots to below the melting temperature of solder and holding it there for a couple of minutes, the temperature of the cold spots will be able to catch up with it. After all parts have reached the same temperature, another rapid ramp-up process will bring them to the peak temperature. Since all parts start at a temperature near the melting point, the new temperature gradient developed becomes much smaller hence it is much more tolerable.

11.7.4 Compromise of conventional profiles

The rapid ramp-up from room temperature needed to form the plateau is not the desired due to the reasons discussed in the previous sections. However, without the plateau, or equilibrating zone, the board will encounter an even more serious problem. Besides the defects caused by the temperature gradient, the board may also be either charred or under-reflowed. Therefore, the conventional profiles with the plateau structure yield relatively better performances than a profile without it.

11.7.5 Earlier mass reflow technologies

Implementation of the optimized profile (Figure 11.7) requires the support of a heating-efficient mass reflow technology with a controllable heating rate. Vapor phase reflow can provide rapid heating, but has difficulty in controlling the heating rate. The high defect rate caused by the significant temperature gradient developed eventually results in the phasing out of this mass reflow technology. Infrared reflow can regulate the heating rate, therefore it is more competitive than the vapor phase reflow. However, it is sensitive to variation in features of the parts, as described above.

11.7.6 Forced air convection reflow technology

Forced air convection reflow also provides a controllable heating rate. In addition, it has a better heating efficiency than the infrared reflow and is not sensitive to the difference in material type, color, and thermal mass of components or boards, as is its infrared counterpart. As a result, the temperature gradient across the board becomes much less significant and the justification for the equilibrating zone is no longer valid. Consequently, the plateau structure can be minimized, and the rapid initial ramp-up rate can be slowed to allow realization of the optimized profile.

Table 11.3 Defects associated with conventional profile characteristics

Attributes	*Defects*
a	Solder balling, hot slump, bridging, solder beading
b	Voiding, poor wetting, solder balling, opens
c	Tombstoning, wicking, skewing, parts cracking, opens
d	Intermetallics, large grain size, charring, leaching, dewetting

11.7.7 Defect potential associated with conventional profiles

The unfavorable attributes of the conventional profiles can be categorized as (a) rapid initial ramp-up, (b) long soaking time at about 150–160°C, therefore excessive heat energy input and oxidation, (c) rapid ramp-up when passing through the melting point, and (d) slow cooling, therefore excessive heat input, as noted in Figure 11.12. The types of defect potential associated with each of those attributes are summarized in Table 11.3.

11.8 Discussion

The profile discussed here relates to eutectic Sn–Pb solder pastes with the use of typical flux systems. For solder pastes with other solder alloys or with flux systems with more constraints, although the defect mechanisms and the principles of optimization are still the same, the emphasis

can be different and accordingly the resultant optimized profiles can also be different. Several examples are discussed below.

11.8.1 Profiles for low temperature solder pastes

When dealing with low melting solder alloys such as 58Bi/42Sn (mp 138°C) using a low temperature profile, the dominant factor is usually the heat energy input. In general, the higher the temperature and the longer dwell time allowed for the peak temperature, the better the reflow results will be. This is attributed to the fact that (1) oxidation of metallization is not an issue at a low heating temperature, and (2) most current flux technologies developed for solder pastes often exhibit a relatively high activation temperature. The latter is particularly true for no-clean solder paste systems. Therefore, under low temperature reflow process conditions, poor wetting and solder balling are usually the main defect types, and consequently the additional heat energy input becomes the most crucial approach for reducing defect rates. As a result, the optimum profile may resemble a bell shape, as shown in Figure 11.13. Here the temperature is quickly brought up to the peak temperature, then held there as long as possible before cooling.

11.8.2 Profiles for high temperature solder pastes

For high temperature solder paste systems such as 90Pb/10Sn (mp 275–302°C), flux residue charring often is one of the main problems. Hence, the preferred profile may exhibit minimal exposure to high temperature in order to avoid flux-charring. As a result, the optimized profile usually has a higher ramp-up rate than that of an eutectic Sn–Pb reflow profile, as demonstrated in Figure 11.14.

11.8.3 Limited oxidation tolerance

Some solder paste systems may have very limited oxidation tolerance. For instance, most of the low residue no-clean solder pastes belong to this category [7]. If exposed

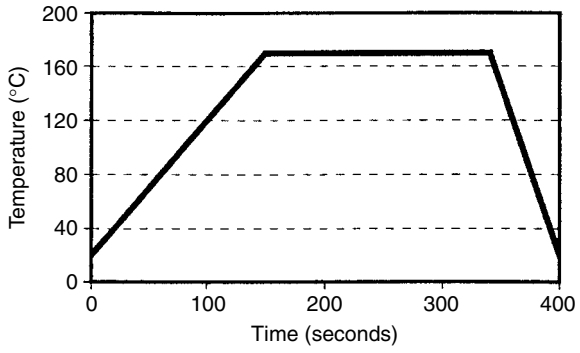

Figure 11.13 Profile for low temperature solder pastes

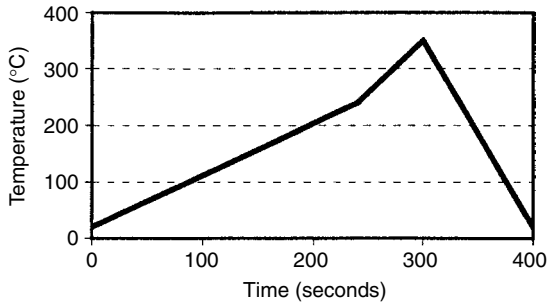

Figure 11.14 Example of reflow profile for high temperature solder paste

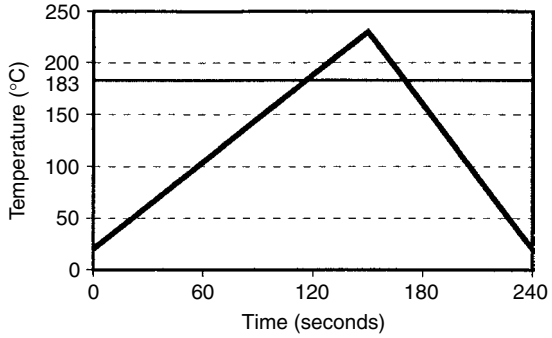

Figure 11.15 Profile for solder pastes with limited oxidation tolerance

to heat in air beyond the tolerance limit prior to solder melting, the solder paste may not even reflow. Accordingly, the optimum profile often is a short one with a linear ramp-up all the way to the peak temperature, as shown in Figure 11.15. This short and linear ramp-up profile minimizes oxidation of metallization prior to solder melting. By eliminating the rapid ramp-up spike zone, it also maximizes the dwell time above the melting temperature allowed by this short profile. The trade-off of this type of profile is limited in utilizing the advantage of a slow ramp-up rate.

11.8.4 Unevenly distributed high thermal mass systems

For a system where the thermal mass of some components is very large and is fairly unevenly distributed on the topside of the board, the profile needs to be lengthened. In addition, more bottom-side heating plus a very long dwell time above the solder melting temperature should be utilized to allow establishment of temperature equilibrium. In order to minimize intermetallics formation and charring, the peak temperature should be lowered considerably, as shown in Figure 11.16.

11.8.5 Nitrogen reflow atmosphere

The oxidation problem associated with an extended soaking dwell time is caused by oxygen in the air. When

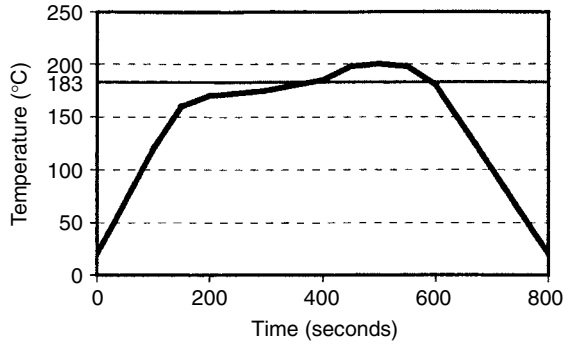

Figure 11.16 Profile for an unevenly distributed high thermal mass system

the reflow is performed in a nitrogen atmosphere, the oxidation factor is minimized and can be ignored when considering optimization.

11.8.6 Air flow rate

Some forced air convection oven designs utilize fairly high air flow rates to deliver heating efficiency. This often increases oxidation and results in wetting and poor solder balling. If the air flow rate cannot be reduced, a profile with shorter heating time will usually help lessen the symptoms.

11.8.7 Adjustment of optimal profile

The optimal profile characteristics are a function of reflow technology. When the heating-efficiency or control of the heating rate differs from that of an efficient forced air convection reflow system, the timing requirements for the ramp-up rate, soaking zone dwell time, and the total heating time should also be adjusted accordingly. It is recommended that the optimized reflow profile described in this chapter should be used as a starting point. Its adaptability should be checked by monitoring the temperature gradient and the type and extent of soldering defects developed. For instance, if too large a temperature gradient is reached, the heating efficiency of the reflow oven used is not high enough and the profile should be adjusted to have a longer dwell time for the soaking zone.

Another example is tombstoning. If there is no other issues except that the tombstoning rate is particularly high, whether this is due to component, solder alloy type, or board design issues, the profile can be tailored to further minimize the possibility of tombstoning. Figure 11.17 demonstrates such a profile, where the soaking shoulder (see Figure 11.7) has been extended for considerably longer time than the standard optimized profile. This extended soaking zone, again, crosses over the melting temperature of solder with a slow-ramp rate. Here the ramp-up rate from room temperature up to the onset of the soaking zone has been increased in order to minimize

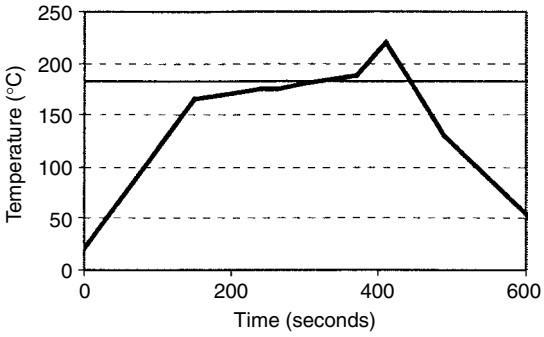

Figure 11.17 Reflow profile with emphasis on suppressing tombstoning

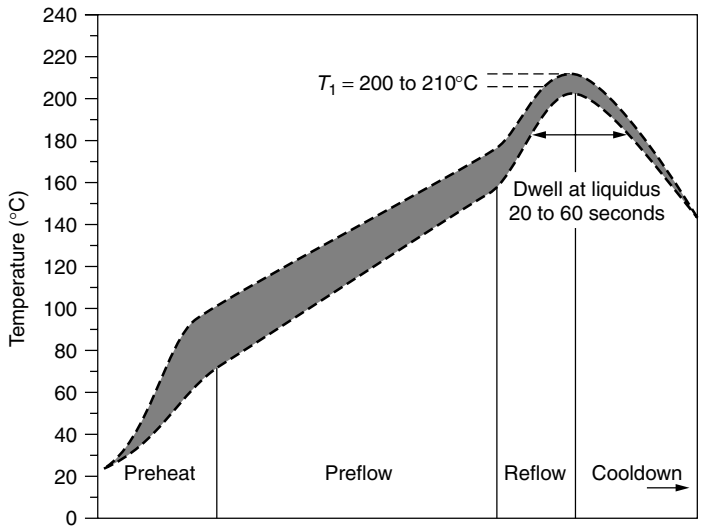

Figure 11.18 Reflow profile with linear ramp-up [9]

the increase in reflow cycle time due to a longer soaking time. This extended soaking time allows better temperature equilibration across the board. In addition, it dries out the solvent more thoroughly and renders the flux stickier at elevated temperatures, and hence can hold the chip better to prevent tombstoning.

11.9 Implementing linear ramp-up profile

The optimized reflow profile with a linear ramp-up based on defect mechanisms analysis was first reported in 1998 by Lee [8]. Since then, it has been adopted and echoed by industry [9,10]. Figure 11.18 and 11.19 represents

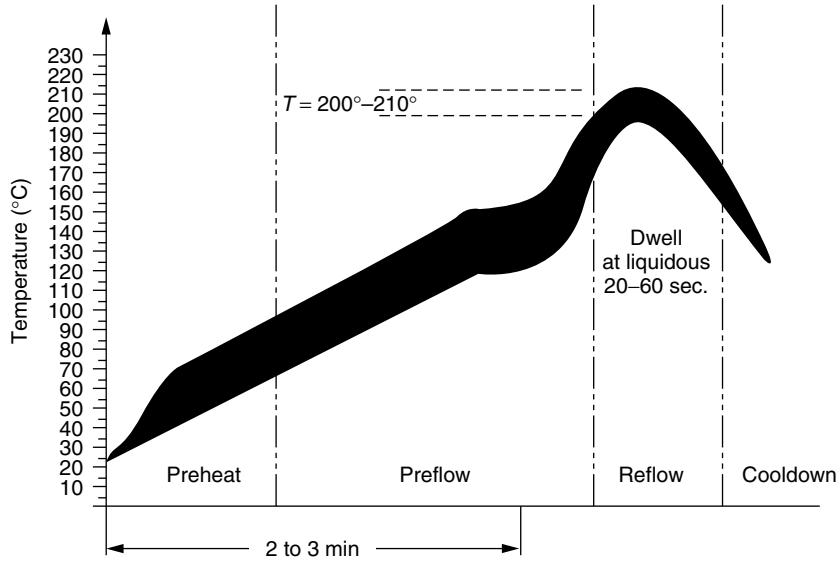

Figure 11.19 ''Tent'' profile [10]. (Source: Heller Industries)

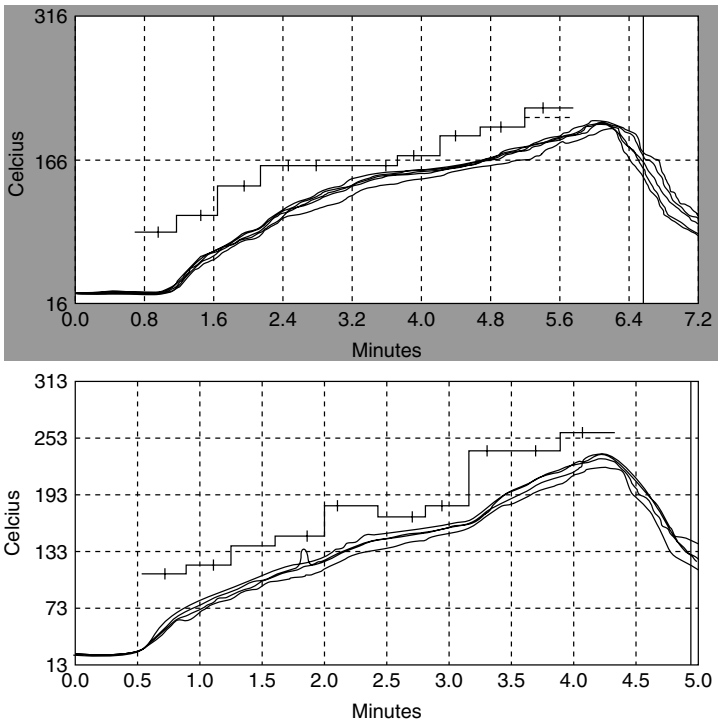

Figure 11.20 Linear ramp-up profile (*top*) 63Sn/37Pb paste (220°C peak), (*bottom*) 95.5Sn/3.9Ag/0.6Cu (249°C peak) [11]

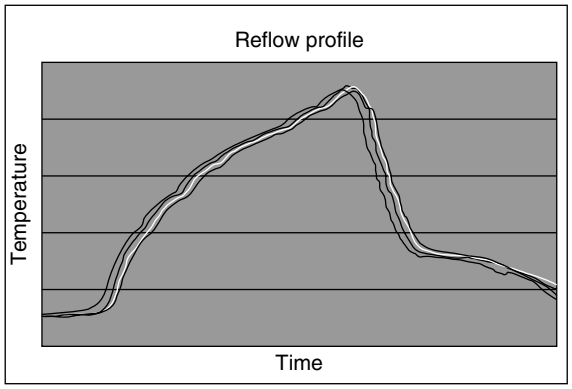

Figure 11.21 Profile used for 95.5Sn/3.8Ag/0.7Cu solder paste reflow process [12]

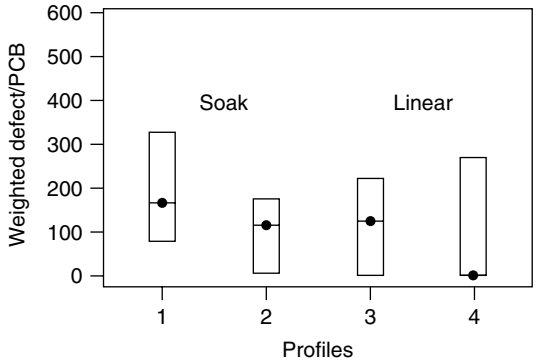

Figure 11.22 Linear ramp-up profiles (3,4) show a lower defect rate then conventional profile with a profound soaking zone (1,2) [13]

different versions of recommended profiles reflecting the approaches of linear ramp-up. In Figure 11.20 the top profile shows an example used for processing 63Sn/37Pb solder paste [11].

The linear ramp-up profile is recommended not only for eutectic Sn–Pb reflow but also for Pb-free reflow. Figure 11.20 (bottom profile) and Figure 11.21 are examples used for Pb-free solders. Practice indicates the linear ramp-up profile provides better yield not only for Sn–Pb solders [10] but also for Pb-free solders, as shown in Figure 11.22 [13]. This is expected, since in defect mechanisms analysis, the failure mode is applicable for both Sn–Pb and Pb-free solders.

11.10 Conclusion

The reflow profile is engineered to optimize soldering performance based on defect mechanisms analysis. In general, a slow ramp-up rate is desired in order to minimize hot slump, bridging, tombstoning, skewing, wicking, opens, solder beading, solder balling, and component cracking. A minimized soaking zone reduces voiding, poor wetting, solder balling, and opens. Use of low peak temperature lessens charring, delamination, intermetallics, leaching, dewetting, and voiding. A rapid cooling rate helps reduce intermetallics, charring, leaching, dewetting, and grain size. However, a slow cooling rate reduces solder or pad detachment. The optimized profile requires the temperature to ramp-up slowly until reaching about 180°C. It is then gradually raised further to 186°C within about 30 seconds, then rapidly until reaching about 220°C. Then, the temperature is brought down with a rapid cooling rate.

The conventional profile was developed due to the limitations of previous reflow technologies. Implementation of the optimized profile requires the support of a heating-efficient reflow technology with a controllable heating rate. Vapor phase reflow can provide rapid heating, but has difficulty in controlling the heating rate. Infrared reflow can regulate the heating rate, but is sensitive to variations in component geometry. Emergence of forced air convection reflow provides a controllable heating rate. In addition, it is not sensitive to variation in components thus allowing realization of the optimized profile.

References

1. N.-C. Lee, ''Reflow Soldering: Meeting the SMT Challenge'', in *Proc. of Nepcon West*, Anaheim, CA, (February 1997).
2. N.-C. Lee, ''How to Make Solder Paste Work in Ultra-fine-pitch and Non-CFC Era'', Short course at Nepcon West, Anaheim, CA, (February 1994).
3. W. Hance and N.-C. Lee, ''Solder Beading in SMT–Cause and Cure'', in *Proc. of SMI*, San Jose, CA, (1991).
4. N.-C. Lee and G. Evans, ''Solder Paste: Meeting the SMT Challenge'', *SITE Magazine* (1987).
5. W. Hance and N.-C. Lee, ''Voiding Mechanisms in SMT'', in *Proc. of China Lake's 17th Annual Electronics Manufacturing Seminar*, (1993).
6. W. Hance and N.-C. Lee, ''Voiding Mechanism in BGA Assembly'', in *Proc. of ISHM* (1995).
7. P. Jaeger and N.-C. Lee, ''A Model Study of Low Residue No-Clean Solder Paste'', in *Proc. of Nepcon West*, Anaheim, CA, (1992).
8. N.-C. Lee, ''Optimizing Reflow Profile Via Defect Mechanisms Analysis'', IPC Printed Circuits Expo'98.
9. P. Zarrow, ''Reflow Profiling: Revisited, Rethought and Revamped'', *Circuits Assembly*, pp.28–30 (February 2000).
10. D. Heller, ''CSP and uBGA Reflow'', in *Proc. of Nepcon West 1999*, Anaheim, CA, 21–25 (February 1999).
11. S. Prasad, F. Carson, G.S. Kim, J.S. Lee, P. Roubaud, G. Henshall, S. Kamath, A. Garcia, R. Herber and R. Bulwith, ''Board Level Reliability of Lead-Free Packages'', SMTA International, Chicago, IL, 24–28 (September 2000).
12. A. Butterfield, V. Visintainer, and V. Goudarzi, ''Lead Free Solder Flux Vehicle Selection Process'', SMTA International, Chicago, IL, 20–24 (September 2000).
13. S. Shina, H. Belbase, K. Walters, T. Bresnan, P. Biocca, T. Skidmore, D. Pinsky, P. Provencal, and D. Abbott, ''Design of Experiments for Lead Free Materials, Surface Finishes and Manufacturing Processes of Printed Wiring Boards'', SMTA International, Chicago, IL, 20–24 (September 2000).

12 Lead-free Soldering

Lead (Pb) has been widely used in the industry for a long time. Of the approximately 5 million tons of lead consumed globally every year, 81 percent is used in storage batteries, with ammunition and lead oxides together accounting for about 10 percent, as shown in Table 12.1 [1]. However, despite the long-term acceptance of lead by human society, lead poisoning is now well recognized as a health threat. The common types of lead poisoning may be classified according to (a) alimentary; (b) neuromotor; and (c) encephalic [2]. Lead poisoning commonly occurs following prolonged exposure to lead or lead compounds. The damage is often induced slowly. Some historians even speculate that the fall of the Roman Empire could be related to the use of lead in pipelines for their drinking water.

With obvious evidence of toxicity, use of lead chemicals in paint and gasoline applications has been prohibited for many years. Storage batteries, due to almost 100 percent recycling, do not contribute to pollution or contamination hence pose no immediate threats. On the other hand, although solder is only a small percentage by weight of electronic products (TVs, refrigerators, PCs, phones etc.), these often end up in landfill sites after disposal, and lead could be leached out into the water supply. For instance, in Japan the lead elution environmental standard in landfills is set at 0.3 mg/l. In the toxic materials detection tests recently performed by the Japanese Environmental Agency it was confirmed that the amount of lead leaching from the pulverized remains of TV tubes and printed substrates for PCs and pachinko machines far exceeds the environmental standard [3]. In the USA, the regulatory limit for lead in drinking water is set at 0.015 mg/l per EPA40 CFR141. The limit is set at 5 mg/l if the test follows the Toxicity Characteristics Leaching Procedure (TCLP) per EPA40 CFR261. A recent study [4] demonstrates that the lead leached out from solder can be several hundred times higher than the limit.

Table 12.1 Lead Consumption by Product [1]

Product	*Consumption (%)*
Storage batteries	80.81
Other oxides (paint, glass and ceramic products, pigments, and chemicals)	4.78
Ammunition	4.69
Sheet lead	1.79
Cable covering	1.40
Casting metals	1.13
Brass and bronze billets and ingots	0.72
Pipes, traps, other extruded products	0.72
Solder (excluding electronic solder)	0.70
Electronic solder	0.49
Miscellaneous	2.77

12.1 Initial activities

The attempt to ban lead from electronic solder was initiated in the US Congress. In 1990, Reid S2638, which was subsequently modified to S729, proposed to ban all lead-bearing alloys, including electronic solders, and a tax of $1.69/kg on primary lead and $0.83/kg on secondary lead used in industry. However, lead solders were removed from the bills after intense lobbying by the US electronics industry.

In 1994, Denmark, Sweden, Norway, Finland and Iceland signed a statement to phase out Pb in the long run. On 16 June 1997, a press release from the Swedish government identified lead as one of the elements to be eliminated from products over the following 10 years. The Sweden Environmental Quality Objectives direct that any new products, including batteries, introduced to Sweden should be largely free of lead by 2020. Swedish manufacturers are also under a voluntary ban effective from 2000 [5].

At about the same time, recycling laws were proposed in various Asian countries. The Japanese Ministry of Trade (MITI) has drafted a recycling law (approved on February 1998) requiring consumers and business users of electrical appliances to return end-of-life goods to retailers or local authorities for recycling. This will come into force in April 2001 and mainly targets TVs, refrigerators, washing machines and air conditioning units. Manufacturers are expected to recycle parts made from copper, aluminium,

iron, zinc, tin and glass. An extension to cover other product types such as PCs, audio equipment and game machines is also expected at a later date. Consumers are required to return goods to retailers and pay recycling costs. Retailers are then obliged to return the goods to the manufacturer who must recycle them [7].

Many companies are setting up recycling plants to deal with waste electronic equipment and are also voluntarily reducing the amount of hazardous materials used in their products. Also in 1996, the Japanese Automobile Industrial Association set up a self-managed environmental program. The Pb used in new automobiles is to be cut by half by 2000 (excluding Pb used in batteries), and to one third by 2005 (versus 1996). Most of the Pb usage in Japanese vehicles now is in paint and radiators.

12.2 Recent activities

There are impending producer responsibility laws for electronic and electrical equipment for a number of European countries. Laws were passed in Holland and Switzerland before 1999 involving producer responsibility. Norway followed in 1999 and Sweden in 2000. In some cases producer responsibility may involve the manufacturer, importer or reseller taking responsibility for the return of products and proper end-of-life treatment. Threshold limits for recycling of specified materials types may also be included. Denmark has its own lead ban proposed, but CRTs and electronics are not included [8].

In 1998 the European Union (EU) introduced a draft directive (law) called the WEEE (Waste from Electrical and Electronic Equipment) Directive. This calls for a ban on lead in all electronics (except automotive) by 1 January 2004. The WEEE Directive intends to ban the selling and/or import of electrical/electronic equipment containing lead interconnect, and encountered objections from many European electronics trade bodies including EUROBIT (IT), ECTEL (telecommunications), PCIF (Printed Circuit Industry Federation), and FEI (Federation of Electronics Industries). The move toward Pb-free attracted the attention of some major manufacturers. Nortel Network is one of the lead-free pioneers in Europe. They initiated a lead-free program in 1991, selected Sn99.3/Cu0.7 in 1994, built 500 lead-free phones in 1998, and targeted meeting the second WEEE Directive in 2001 [9]. Ericsson also set a goal in 2000 to use lead-free solder in 80 percent of their new products by the end of 2001.

On 13 June, 2000 the European Commission adopted two proposals:

(1) Directive on Waste of Electrical and Electronic Equipment (WEEE): requires Member States to set up return centers for end-of-life recovery at no cost to the consumer.
(2) Directive on the restriction of the use of certain hazardous substances in electrical and electronic equipment: requires lead-free electronics by 2008, but exempts lead in cathode ray tubes, (CRTs), light bulbs and fluorescent tubes, and lead as an alloying agent in steel (< 0.3 wt%), aluminum (< 0.4 wt%), and copper (< 4.0 wt%) [9].

Table 12.2 JEIDA's roadmap for introduction of lead-free solders [9]

Year	*Activity*
1999	First mass production using lead-free solders
2000	Adoption of lead-free components
2000	Adoption of lead-free in wave soldering
2001	Expansion of lead-free components
2001	Expansion of lead-free products
2002	General use of lead-free solders in new products
2003	Full use of lead-free solders in all new products
2005	Lead-containing solders used only exceptionally

In Asia, since 1998, recycling laws have been enacted in various countries including Japan and Taiwan. In Japan, the recycling law applies only to TVs, refrigerators and similar items. On 30 January, 1998, the Japanese Electronic Industry Development Association JEIDA and the Japanese Institute of Electronics Packaging (JIEP) presented a lead-free roadmap, as shown in Table 12.2 [10].

Some major Japanese OEMs have begun jointly to develop recycling processes for electronic products. A number of major Japanese companies (e.g. Sony, Toshiba, Matsushita, Hitachi, and NEC) have made commitments to be lead-free in their products by 2001. This is in advance of Japanese legislation on "take-back" due to come into force in April 2001. The lead-free advances of these companies are described below.

Matsushita (Panasonic) have shipped 40 000 MiniDisc players/month with lead-free solder since 1 October, 1998 and will eliminate all lead interconnect for four products by April 2001. Matsushita's market share of its lead-free MiniDisc player jumped from 4.6 percent to 15 percent in 6 months in Japan. This lead-free product was reported to be introduced into Europe in March 1999. Matsushita is using Sn/Ag/Bi for reflow soldering. Currently only disk, and TVs are using lead-free solder, and Matsushita had no plan to roll out products in the summer of 1999.

Sony proposed using Sn93.4/Ag2/Bi4/Cu0.5/Ge0.1 solder for assembly. By 2001, all lead will be eliminated except for high density electronics packaging. Akikazu Shibata of Sony 1999 predicts 50 percent lead-free in 1–2 years and more than 75 percent in 5 years. Toshiba plans to eliminate Pb solder in mobile phones by 2000. Hitachi plans to cut lead usage 50 percent by 1999 from the 1997 level and will eliminate Pb interconnect by April, 2001. NEC will reduce lead use by 50 percent by 2002 (versus 1997). NTT announced no Pb or Cd in newly purchased equipment. Many other announcements were expected from OEMs in 1999.

12.3 Impact of Japanese activities

By 2001 the leading Japanese OEMs will have introduced products that contain no lead in interconnect systems. This will allow them to be positioned to exclude products from Japan that do not meet these environmental standards. Furthermore, Japanese products will justify European legislation requiring lead reduction and highly recyclable

electronic products by 2004 [11] and therefore will further increase pressure on the rest of the world to convert to lead-free.

12.4 US reactions

Since the initial attempt in Congress in the early 1990s, very little activity was seen in the USA until recently. The automotive industry is probably the only segment with a sustained interest and there is no legislation pending. The Lead Industry Association (LIA), EIA, IPC, and NEMA all have been active in lobbying against lead-free legislation.

Obviously, the message from offshore is clear and loud. You either work on lead-free soldering now, or you can forget about doing business. Hence, NEMI called for a "Lead Free Initiative Meeting" in February 1999 at Anaheim, CA, to review the situation, and since then has rolled out a series of action items to establish a lead-free direction for the US electronics industry. The second NEMI Meeting was held on 26–27 May, 1999 at Northbrook, IL. This meeting effectively motivated many manufacturers to become involved in lead-free development. Then IPC announced that they are not lobbying against lead-restrictions, but feel they can better serve the industry by helping with lead-free. The IPC statement probably fairly reflects the opinion of most US industry: "Pb in electronics is not perceived as a health issue, but government and commercial drivers will push for its adoption anyway. Thus IPC will facilitate activities to enable it to happen." [12] IPC also organized a conference, IPC Works'99, to be held in October 1999 at Minneapolis with a major emphasis on lead-free issues. The HAL User Group (HUG), an organization composed of manufacturers of PCBs, OEMs, CMs, chemical suppliers, and equipment, also held a meeting in August 1999 to address lead-free surface finishes issue as a response to the pressure on lead-free soldering. NEMI considers that North American OEMs/CEMs need to prepare processes to deliver lead-free products by 2001 with an "eye" to total elimination of lead by 2004.

12.5 What is lead-free interconnect?

Lead may be present in metals, such as tin, as an impurity at a level of <0.1 percent by weight. Obviously this impurity is going to carry over into lead-free alloys. In addition, it is difficult to have all components converted to lead-free finishes in a given amount of time. It was therefore proposed by the High Density Packages User Group (HDPUG, a UK organization) that a target lead content of 1 percent by weight in the interconnect now would be reasonable with a level of <0.1 percent in several years. When considering the presence of lead per weight of product, the concentration may be around 100 ppm [5].

12.6 Criteria of lead-free solder

The criteria used for screening candidate lead-free alloys can be categorized as follows:

Nontoxic
Available and affordable
Narrow plastic range
Acceptable wetting
Material manufacturable
Acceptable processing temperature
Form reliable joints

12.7 Viable lead-free alloys

The following alloys are considered representative of viable candidates for replacing eutectic Sn/Pb systems. Many of the systems are based on adding small quantities of third or fourth elements to binary alloy systems in order to lower the melting point and increase wetting and reliability. It is reported that with increasing amount of additive elements, (1) the melting point of system decreases, (2) the bond strength first rapidly decreases, then almost levels off, then decreases again, and (3) the wettability increases rapidly first, reaching the maximum at composition corresponding to mid-point of plateau of bond strength, then decreases [12].

12.7.1 Sn96.5/Ag3.5

Sn96.5/Ag3.5 (221 °C) is one of the most promising by NCMS, Ford, Motorola, and TI Japan. A German study has suggested it to be one of the most suitable alloys. There is long experience of using this alloy and the Indium Corporation reported it to have the poorest wetting for reflow soldering among high Sn alloys [13].

12.7.2 Sn99.3/Cu0.7

Sn99.3/Cu0.7 (227 °C) is reported by Nortel to have a soldering quality equal to eutectic Sn/Pb in telephone manufacturing. In air reflow the wettability reduced and the fillet exhibits a rough and textured appearance. It is probably the "poorest" in mechanical properties available from all lead-free solders but is preferred for wave soldering due to its low material cost and inerting of waves.

12.7.3 Sn/Ag/Cu

This is ternary eutectic at 217 °C, although the exact composition is to be clarified. Cu is added to Sn/Ag in order to slow Cu dissolution, lower the melting temperature, and improve wettability, creep and thermal fatigue characteristics. Nokia and Multicore found yields and reliability comparable or better than eutectic Sn/Pb alloy. A Brite-Euram project reported better reliability and solderability than Sn/Ag and Sn/Cu, and recommended this alloy for general-purpose use. The following compositions are examples:

Sn93.6/Ag4.7/Cu1.7 (216–218 °C, AMES Labs, covers any alloy containing 3.5–7.7 percent Ag and 1–4 percent Cu)
Sn95/Ag4.0/Cu1 (217–219 °C, AMES Labs)
96.5Sn/3.0Ag/0.5Cu (Harris Brazing Co.)

Sn95.5/Ag4.0/Cu0.5 (217–219 °C, published 50 years ago: unpatentable)
Sn95.5/Ag3.8/Cu0.7 (217–219 °C, unpatented)
Sn96.3/Ag3.2/Cu0.5 (217–218 °C, unpatented)
Sn95.75/Ag3.5/Cu0.75 (Senju)

12.7.4 Sn/Ag/Cu/X

Sn96.2/Ag2.5/Cu0.8/Sb0.5 (213–218 °C, AIM, Castin Alloy) is reported by the International Tin Research Institute, Lucent, Ford, and Sandia Labs to have greater fatigue performance than eutectic Sn/Pb alloy. A Brite-Euram Project reported 0.5 percent Sb addition may strengthen the alloy further. Sn97/Cu2/Sb0.8/Ag0.2 (226–228 °C, Kester, SAF-A-LLOY) may be considered for wave and hand soldering applications. Sn/Ag/Cu/In (Tamura) may also be promising.

12.7.5 Sn/Ag/Bi/X

Addition of ≤5 percent Bi lowers the melting point and improves wettability of Sn/Ag systems. Solderability is the best among a range of lead-free alloys, confirmed by the Indium Corporation [13] and Matsushita. NCMS observed fillet lifting at through-hole joints as a concern for wave soldering, and other alloys such as Sn96.5/Ag3.5 also suffer fillet lifting although to a lesser extent. Fillet lift is caused by mismatch in TCE between solder and PCB materials, and aggravated by solders with a pasty range. It can be altered by addition of other elements. Addition of Cu and/or Ge results in improvements in strength and possibly wettability. Adding Pb to Sn/Bi alloys can cause a 96 °C ternary eutectic Bi52/Pb32/Sn16 to form. Calculations predict that at a fixed 6 percent Pb, even alloys with ≤4.8 percent Bi can have this eutectic liquid form, hence Sn/Pb surface finishes should be avoided. The Japan Electronic Industry Promotion Association recommended both Sn/Ag/Cu and Sn/Ag/Bi. Some examples are shown below. There are no unpatented compositions.

Sn91.8/Ag3.4/Bi4.8 (202–215 °C, Sandia Labs): NCMS considered these, along with eutectic Sn/Ag and eutectic Sn/Bi the most promising alloys.
Sn93.5/Ag3.5/Bi3 (210–217 °C, Nihon Handa)
Sn90.5/Bi7.5/Ag2 (191–210 °C, Tamura Kaken)
Sn/Ag/Bi (Matsushita)
Sn94/Ag3/Bi3 (213 °C)
Sn92/Ag3/Bi5 (210 °C)
Sn92.7/Ag3.2/Bi3/Cu1.1/Ge (Japan Solder)
Sn93/Ag3.5/Bi0.5/In3 (Harima, Mitsui Metals)

Addition of a large amount (~5–20 percent) of Bi lowers the melting point of eutectic Sn/Pb solders but loses the beneficial properties of eutectic Sn/Ag systems. Moreover, a low temperature eutectic Bi58/Sn42 which has a low partial melting point (138 °C) is formed. Also there are reliability problems such as interfacial problems with plating containing Pb on the electrodes of electronic components. It is attractive for low cost manufacturing. Examples are shown below.

Sn/Ag2/Bi7.5/Cu0.5 (Alloy H, Alpha Metals, developed at ITRI)
Sn/Ag2.0–2.8/Bi13–17/Cu0-1 (Hitachi)
Sn/Ag2.8/Bi10/Cu0.6 (Ono)
Sn/Ag/Bi3 (210 °C, Matsushita)
Sn/Ag/Bi6 (220 °C, Matsushita)
Sn/Ag/Bi10 (205 °C, Matsushita)
Sn/Ag/Bi15 (209 °C, Matsushita)

12.7.6 Sn/Sb

Sn95/Sb5 (232–240 °C) has poor wetting, although it is better than Sn96.5/Ag3.5, but the liquidus temperature is too high.

12.7.7 Sn/Zn/X

Sn91/Zn9 (eutectic 199 °C) is fairly reactive, since Zn causes oxidation and corrosion, and reacts with flux to form a hardend paste. Japanese home electronics manufacturers are interested in Sn89/Zn8/Bi3. Bi replaces Zn to reduce Zn corrosion in humid conditions. Sn/Zn/Bi alloys can have a melting point close to that of eutectic Sn/Pb. Developed primarily by home electronics manufacturers targeting low cost products.

Sn90/Zn9/In1 (AT&T)
Sn89/Zn8/Bi3 (191–195°, Matsushita, Senju)
Sn/Zn/Bi/X (Hitachi Harima, Tamura)

12.7.8 Sn/Bi

Bi58/Sn42 (138 °C) is recommended by NCMS as a promising replacement. Eutectic Bi58/Sn42 is unusually resistant to coarsening. It is reported by HP to have properties better/equivalent to eutectic Sn/Pb and it is promising for low temperature applications or some consumer products. Addition of 1 percent Cu dramatically slows coarsening of eutectic Sn/Bi. Problems are (1) eutectic Bi52/Pb32/Sn16 (96 °C) formed on lead surface finishes, (2) Bi is a byproduct of lead mining.

12.8 Cost

The cost of a solder bar is dictated by the raw materials cost (see Table 12.3). However, for fabricated products such as solder pastes, the processing cost of manufacturing this material can become a dominant factor, and the difference between Sn/Pb and Pb-free materials becomes very small.

12.9 PCB finishes

Lead-free surface finishes for PCBs are readily available, some of which have a long history of use, such as Ni/Au and Organic Solderability Preservative (OSP). Shown below are some more promising options.

- OSP – such as benzotriazole or benzimidazole. However, the low temperature process may not remove OSP,

Table 12.3 Relative cost of lead free solder materials [14]

Solder alloy	*Relative bar cost ($/kg)*	*Relative paste cost ($/kg)*
Sn63/Pb37	1	1
Sn96.5/Ag3.5	2.29	1.07
Sn95/Ag3/Bi2	2.17	1.06
Sn96.1/Ag2.6/Cu0.8/Sb0.5	2.06	1.05
Sn91.8/Ag3.4/Bi4.8	2.26	1.06
Sn95/Ag3.5/Cu0.5/Zn1	2.27	1.06
Sn93.6/Ag4.7/Cu1.7	2.56	1.08
Sn96.1/Ag3.2/Cu0.7	2.21	1.06
Sn95.2/Ag3.5/Cu1.3	2.28	1.06

Note: Relative cost of selected metals: Pb – 1, Zn – 1.7, Cu – 3, Sb – 3.9, Bi – 8.6, Sn – 11, Ag – 260, Au – 15000

but the high temperature process may remove OSP and allow oxidation, particularly for multiple passes.
- Immersion Ag (organic Ag, Alpha Level)
- Immersion Au/Electroless Ni
- HASL Sn/Cu
- Sn/Bi
- Electroless Pd/Electroless Ni
- Electroless Pd/Cu
- Sn – pure whiskerless varieties.

12.10 Components

Lead can exist in components in three different forms. Among the following, the second and the third categories are related to soldering:

Lead used in functional materials in piezoelectric elements, capacitors, glass, fuses, etc.
Lead in solder used in internal connections within the components
Lead in solder-plating surface finishes on the leads of components

In general, it is relatively easy to eliminate lead from surface finishes of the leads of components. Examples of alternatives include Sn, Pd/Ni, Au, Ag, Ni/Pd, Ni/Au, Ag/Pt, Ag/Pd, Pt/Pd/Ag, Ni/Au/Cu, Pd, and Ni. However, Pd plating is difficult when the leads are made out of iron Alloy 42 [3,5]. Also, Ag/Pd can cause voids due to Ag diffusion into the solder. As to the Pb in solder used in internal connections within the components, such as flip chip in package, the first level interconnection solder melting temperature (around 300 °C) is normally considerably higher than the second (about 180 °C).

If the melting temperature for the latter interconnection is set around 220 °C, then the first level interconnection needs to have a melting point at least above 260–270 °C in order to avoid remelt during subsequent reflow processes. There are only few alloys identified into that category, including Au80/Sn20 (280 °C) and Sn65/Ag25/Sb10 (365 °C). The former is very expensive, while the latter, known as J alloy, exhibits very low ductility and unacceptable thermal and mechanical fatigue life for die attach [3]. For the lead used in functional materials in components, technologically it will be even more difficult to substitute.

12.11 Thermal damage

There is more to consider besides finding solder alloy alternatives to phase out lead. Since most of the promising alloy alternatives require a higher processing temperature, whether the components or substrates used can sustain the process becomes a large question [5]. For instance, electrolytic capacitors are highly susceptible to high temperature damage as are wound components, such as relays. It is also considered likely to have an increased tendency to have popcorn effect from plastic-encapsulated ICs close to their expiry date. In addition, a parametric damage to memory ICs processed around 250 °C is possible. As mentioned above, PCB and BGA polymeric substrates and solder masks may also suffer from higher processing temperatures and the plastic insulation of connectors may also distort. All those pose a great challenge to material scientists and design engineers.

12.12 Other problems

The corrosion and electromigration tendencies of the new alloys need to be measured as well as Rework studies – lead-free solder on lead solder, lead-free solder on lead-free solder, etc. Pastes, fluxes need to be evaluated. Since solder without lead is different in appearance and is more difficult to monitor via X-rays, new standards for visual and X-ray inspections are needed.

12.13 Consortia activity

There are many coordinated efforts addressing the lead-free challenge. In North America, the National Center for Manufacturing Sciences (NCMS) has invested $10 million over four years, with reports released in August 1997. The National Institute of Standards and Technology (NIST) is also active in participating in lead-free programs. Currently, National Electronics Manufacturing Initiative, Inc. (NEMI) is most active in leading the industry in finalizing the options for lead-free soldering processes.

In Japan, NEDO has committed 350 million yen over two years to find answers, while in Europe, Improved Design Life and Environmentally Aware Manufacture of Electronic Assemblies by Lead-Free Soldering (IDEALS, an European collaboration supported by the Brite/EuRam program of the European Commission, six partners) project is scheduled for 3 years (May 1996 to April 1999). The International Tin Research Institute (ITRI) has been involved in developing lead-free solder options since the early 1990s.

12.14 Opinions of consortia

In the USA, NCMS recommends three alloys: Sn96.5/Ag3.5, Sn91.7/Ag3.5/Bi4.8, Bi58/Sn42. NEMI maintains that Sn/Ag/Cu without Bi (217–221 °C) is the best

in reliability in the presence of lead contamination. The highest melt alloy with Bi is more manufacturable but the 96 °C Pb/Sn/Bi phase is a problem. NEMI recommends 95.5Sn/3.9Ag/0.6Cu for reflow, 99.3Sn/0.7Cu for wave. The Brite-Euram Project recommends Sn95.5/Ag3.8/Cu0.7 for general-purpose soldering. Other alloys with potential are Sn99.3/Cu0.7, Sn96.5/Ag3.5 and Sn/Ag/Bi. In the UK, The Department of Trade and Industry (DTI) notes that the favored options vary depending on applications: high professional group (automotive, military) – Sn/Ag/Cu(Sb); medium professional group (industrial, telecoms) – Sn/Ag/Cu, Sn/Ag, general consumer & low professional group (TV, audio-video, office equipment) – Sn/Ag/Cu(Sb), Sn/Ag, Sn/Cu, Sn/Ag/Bi. JEIDA favors Sn/Ag/Cu (before lead-free components were available) and Sn/Ag/Bi alloys (after lead-free components were available). In January 1999, JEIDA standardized the lead-free solder alloys as follows: (1) wave soldering: Sn−3.5Ag, Sn−(2–4)Ag−(0.5–1)Cu, or Sn−0.7Cu with small amounts of other elements (Ag, Au, Ni, Ge, In); (2) reflow soldering: (a) low temperature: Sn−57Bi−1Ag, (b) medium/high temperature: Sn−3.5Ag, Sn−(2–4)Ag−(0.5–1)Cu, Sn−(2–4)Ag−(1–6)Bi including some with 1–2 percent In, and Sn−8Zn−(0–3)Bi, (c) high temperature (chip attachment): not available [9]. In Germany, the favored alloys appear to be Sn96.5/Ag3.5 and Sn99/Cu1.

12.15 The selections of pioneers

The following is a list of the selections or seriously considered candidates of some lead-free pioneering companies. Since new data are being generated rapidly, the favored options may change with time.

Nortel – Sn99.3/Cu0.7 (N_2) wave and reflow
Motorola – Sn95.5/Ag3.8/Cu0.7 and Sn96.5/Ag3.5 (most likely)
Ford – Sn96.5/Ag3.5
Texas Instruments – Sn/Ag/Cu/Sb (Ni/Pd finish)
Delco – Sn/Ag/Cu (probably)
Nokia – Sn95.5/Ag3.8/Cu0.7
Ericsson – Sn95.5/Ag3.8/Cu0.7
Hitachi – Sn91.75/Ag3.5/Bi5/Cu0.7
NEC – Sn94.25/Ag2/Bi3/Cu0.75 and Sn97.25/Ag2/Cu0.75
Matsushita – Sn90.5/Ag3.5/Bi6 and Sn/Ag/Bi/X series
Fujitsu – Sn42.9/Bi57/Ag0.1
Toshiba – Sn/Ag/Cu
Sony – Sn93.4/Ag2/Bi4/Cu0.5/Ge0.1 (claimed to have 5× reliability of Sn/Pb)
Solectron – may end up with a high and low temperature alloy but would prefer only one for bar, paste and rework.

12.16 Possible path

According to NEMI [7], the possible path to lead-free soldering can be a sequence as shown below. However, this sequence may vary between manufacturers.

SMT solder pastes and rework
Board finishes
Component metallizations
Wave solders
Internal component interconnects

As reported in a NEMI meeting [10], the Japanese appear to be taking a cautious step, as shown below:

Initial implementation of Sn/Ag/Bi/X in low tier products.
Convert high tier products when lead-free components available or utilize Sn/Ag/X alloys.
Lower temperature components useable versus Sn/Ag/X (5–10 °C).

12.17 Is lead-free safe?

While the industry is moving quickly toward lead-free soldering processes, and while everything seems to fall into place on supporting a green world, an odd question is asked: "Is lead-free solder environmentally safe?" According to a recent study [4], five lead-free solders – Sn96.3/Ag3.2/Cu0.5, Sn96.5/Ag3.5, Sn98/Ag2, Sn99.3/Cu0.7, and Sn95/Sb5 – were leached using EPA methods, which were designed to simulate waste disposal and groundwater contact. The results indicate that Sb and Ag alloys failed every test. Sn/Cu has the least environmental impact. Sn did not leach significantly, due to the low solubility of Sn salt in water. Since both Sb and Ag elements, particularly Ag, are very likely to be included in the lead-free alloy alternatives, the data above demonstrates that the road to a lead-free soldering world may be more bumpy than anticipated.

12.18 Summary of lead-free adoption

Lead-free soldering for the electronics industry is part of a global trend toward a lead-free environment. Although initiated in the USA in the early 1990s, it developed much more rapidly in Japan and Europe. This differentiation in lead-free progress triggered great concerns of users of lead-containing solders about maintaining business opportunity, thereby further expedites the advances of lead-free soldering programs. The favored lead-free solder alternatives vary from region to region. However, in general, high tin alloys are preferred, including Sn/Ag, Sn/Cu, Sn/Ag/Cu, Sn/Ag/Bi, and various versions of those alloys with small amounts of other elements, such as Sb. Sn/Ag/Bi systems are already used in some Japanese products. However, Sn/Ag/Cu systems are more tolerant toward lead contamination than Bi-containing systems, therefore are more compatible with existing infrastructures for the transition stage. Lead-free surface finishes for PCBs include OSP, immersion Ag, immersion Au/electroless Ni, HASL Sn/Cu, Sn/Bi, electroless Pd/electroless Ni, electroless Pd/Cu, and Sn. The challenge for components is greater than for solder materials or PCBs. Although some lead-free surface finishes for components do exist, such as Sn, Pd/Ni, Au, Ag, Ni/Pd, Ni/Au, Ag/Pt, Ag/Pd, Pt/Pd/Ag, Ni/Au/Cu, Pd, and Ni, their performance remains to be verified. In addition, options for

higher melting temperature solder are still not available for high temperature applications, including first level interconnect within the components. Thermal damage can be a concern for both PCBs and components.

12.19 Troubleshooting lead-free soldering

Implementing lead-free soldering encounters a series of challenges, as discussed above. The first is overall compatibility with reflow process. The challenges then can be further broken down to performances such as fillet lifting, grainy solder surface, poor wetting, etc.

12.19.1 Compatibility with reflow process

In a study conducted by Huang and Lee [13], a group of representative lead-free solders were evaluated for their compatibility with the reflow process. The materials tested include ten lead-free solders and ten flux chemistries. The latter include (1) no-clean, and water-wash; (2) medium temperature flux and high-temperature flux; (3) halide-containing, and halide-free; (4) air-reflow, and nitrogen-reflow; (5) probe testable, and non-probe testable. The performance evaluated includes: wetting, solder balling, joint appearance, shelf life, and tack time. Their results showed that the lead-free alloys are not as compatible as eutectic Sn−Pb with the reflow process. Figure 12.1 shows the rankings in compatibility, with a grade 30 being full score.

By reviewing the data in Figure 12.1, it becomes obvious that the Sn/Ag/Bi group is the best in compatibility with the reflow process, followed by a large group of alloys including Sn/Ag/Cu, Sn/Bi, Sn/Cu, Sn/Ag/Cu/Sb, and Sn/Sb. Sn/Ag eutectic is measurably poorer than this large group, while Sn/Zn/Bi is way below all the groups.

A better compatibility in process with reflow suggests a higher process yield. Therefore, from a process point of view, the Sn/Ag/Bi family is expected to be the main choice for improving yield.

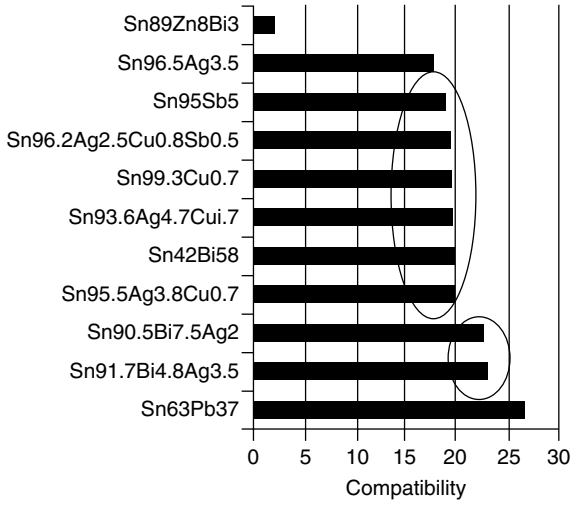

Figure 12.1 Ranking of lead-free alloys on compatibility in process with reflow process [13]

12.19.2 Fillet lifting

Fillet lifting is a solder cracking phenomenon where the solder fillet lifted from the edge, as shown in Figure 12.2 [16]. This symptom occurs mostly at wave soldering, and occasionally at reflow soldering. Separation usually occurs between intermetallic and solder, and the crack stops at the knee on the land side. Sometimes cracking also occurs between component lead and solder. It is seen in high-Sn alloys, including Sn−3.5Ag, but not observed in eutectic Sn−Pb and Sn−Bi. It is also more frequently observed with pasty alloys, Bi-containing alloys, and Pb contamination [17]. It should be noted that lead-free solders are sensitive to lead contamination, and 1 percent lead will lower the solidus by 40–50 °C: for instance, (1) Sn99.3/Cu0.7: 227 °C to 183 °C; (2) Sn96.5/Ag3.5: 221 °C to 179 °C, (3) Sn42/Bi58: 138 °C to 96 °C.

The direct cause of fillet lifting can be attributed to mismatch in TCE, as shown in Figure 12.3. Upon cooling from the liquid state, solder generates a tearing shearing force in the $x-y$ direction due to its higher TCE than PCB, while PCB generates a tearing tension force in the z-direction due to its higher TCE than solder. Altogether, the tearing forces result in fillet lifting.

It is caused by thermal expansion mismatch. Cooling from a stress-free state generates lifting forces, and alloys with a larger pasty range are more susceptible to fillet lift, thus Sn96.5/3.5Ag shows lowest tendency and

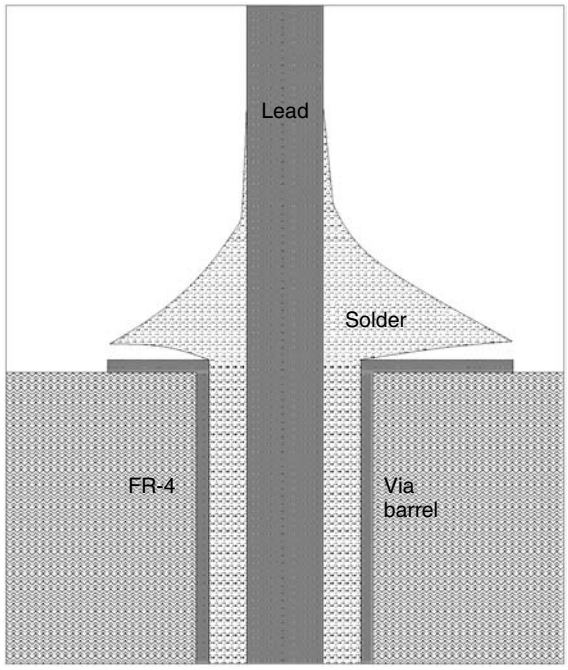

Figure 12.2 Cross-section of solder joint showing fillet lifting phenomenon [15]

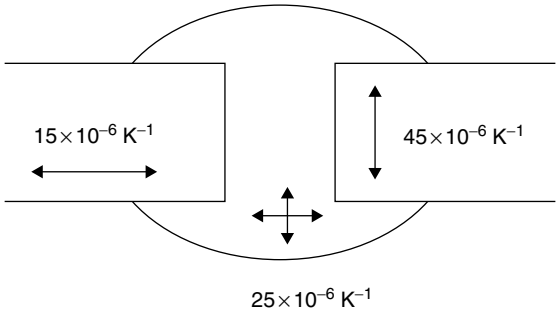

Figure 12.3 Mechanism of fillet lifting. This is caused by thermal expansion mismatch. Cooling from a stress-free state generates lifting forces, and alloys with larger pasty ranges are more susceptible to fillet lift. Thus Sn96.5/3.5Ag shows the lowest tendency and Sn91.9/Ag3.4/Bi4.7 shows a severe tendency [14]

Sn91.9/Ag3.4/Bi4.7 shows a severe tendency [14]. However, this mechanism is applicable to all alloys, and does not explain why certain alloys are more susceptible to fillet lifting than others.

The lifting problem associated with a pasty range is easy to understand. Upon cooling, the alloy solidifies gradually instead of instantaneously like eutectic solder. In the liquid state, no stress can be accumulated, thus there is no problem. When the solder is partially solidified, the pasty nature causes the alloy to be fairly weak and prone to tearing. Upon further cooling, the stress can be too high for the pasty alloy to tolerate and this results in tearing. Since the solder temperature is higher at the board interface due to a larger thermal mass of the PCB, and since the fillet tip exhibits the highest stress due to mismatch in TCE, it becomes understandable that tearing occurs first at the fillet tip.

The fillet lifting problem associated with some Bi-containing alloys is not so easy to explain. Suganuma [17] studied the Bi-bearing alloy systems by examining the cross-section of 97Sn/3Bi fillet and Bi mapping. Bi segregation is apparent near the Cu–solder interface, as shown in Figure 12.4.

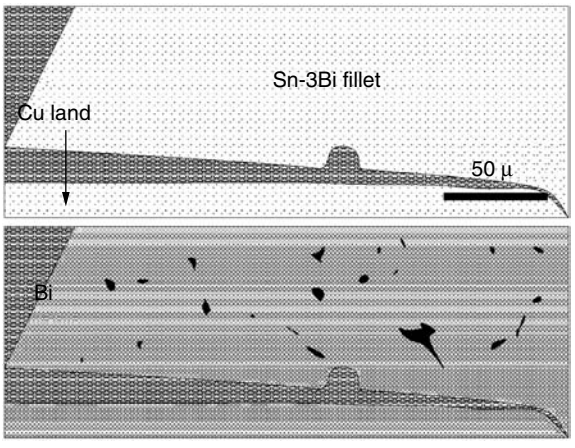

Figure 12.4 Cross-section of 97Sn/3Bi fillet and Bi mapping [17]

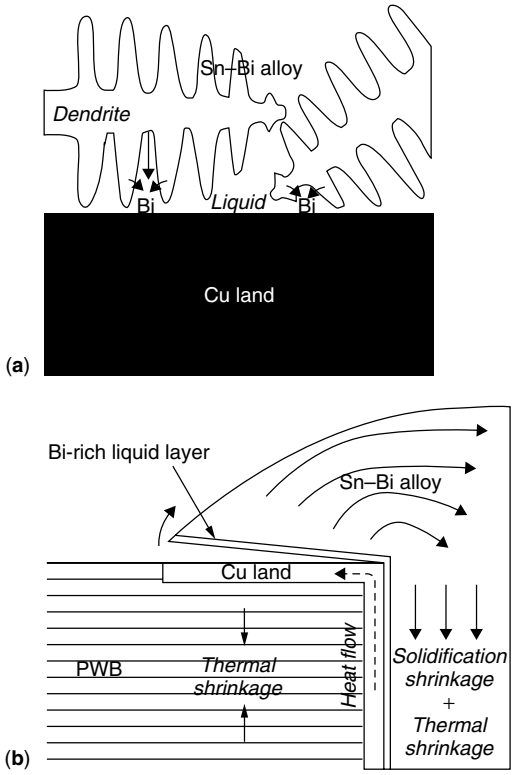

Figure 12.5 Fillet lifting mechanism associated with Bi-bearing alloys [17]

Even for solder with 2 percent Bi, fillet lifting results from the presence of a low melting temperature phase along the Cu–solder interface. Long distance of Bi diffusion in solder fillet is not a necessary condition for fillet lifting, but rather the Bi micro-segregation accompanied by dendrite formation. Suganuma proposed the fillet lifting mechanism as follows [17].

Upon solidification, Bi is enriched into the liquid interface region between a solder fillet and a Cu land by dendrite formation (see Figure 12.5(a)). The diffusion distance is only a few microns. A substantial amount of Bi along the interface remains in a liquid state.

Heat flow through the Cu land retards cooling of the interface region (see Figure 12.5(b)).
Mismatch in TCE between solder and substrate results in fillet lifting.
Dendrite skeleton formation may absorb residual liquid and aggravate the lifting process.

Suganuma [17] further investigated the fillet-lifting observed on the top side only for Sn–Pb finished components wave soldered with 99.3Sn/0.7Cu, as shown in Figure 12.6. He concluded that Sn–Cu solder touches the lead wire of the bottom of a PCB and flows up to the topside by means of the through-hole (see Figure 12.7). The surface Sn–Pb coating dissolved by the Sn–Cu liquid flow is conveyed to the topside. Sn–Cu with Pb exhibit a lower solidus temperature.

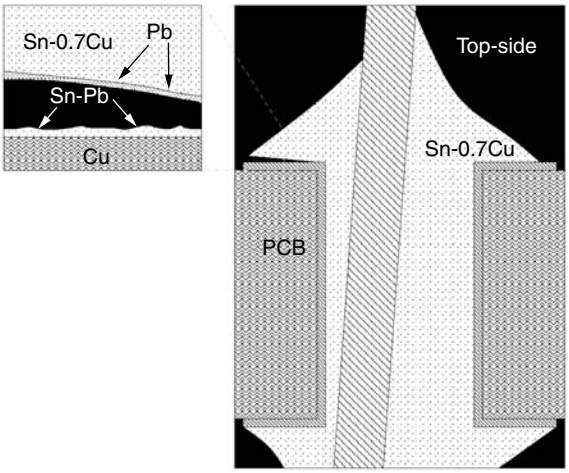

Figure 12.6 Fillet lifting observed on top side only for Sn–Pb finished components wave soldered with 99.3Sn/0.7Cu [17]

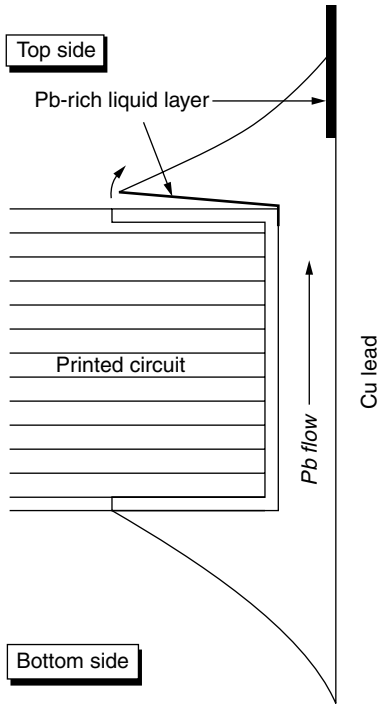

Figure 12.7 Fillet lifting mechanism on top side only for Sn–Pb finished components wave soldered with 99.3Sn/0.7Cu [17]

Suganuma proposed that fillet lifting can be prevented by stopping micro-segregation of Bi along the solder/Cu land interface on solidification. Micro-segregation is accompanied by the formation of dendrites and suppressing the formation of dendrites can stop the Bi segregation. Rapid cooling and adding third elements, both of which are typical refining treatments for an alloy microstructure, are expected to reduce Bi segregation, retaining Bi deep inside the solder.

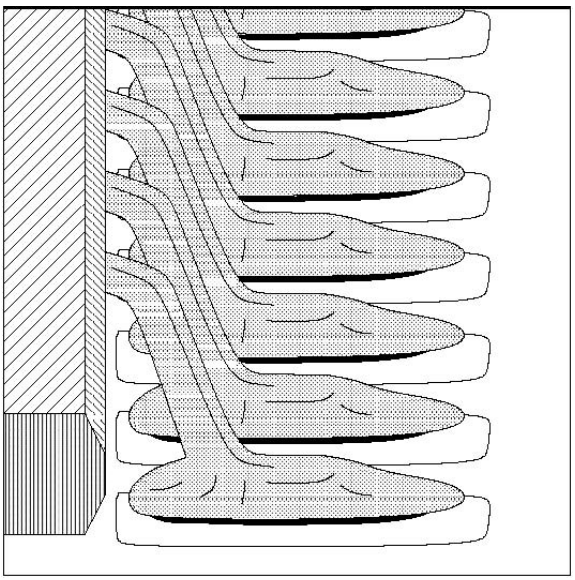

Figure 12.8 Ruptures in the vicinity of Sn–Ag–Bi–Cu solder/Cu pad interface formed with the reflow process [18]

Nakatsuka *et al*. [18] studied ruptures in the vicinity of a Sn–Ag–Bi–Cu solder/Cu pad interface formed with a reflow process, as shown in Figure 12.8. Their findings indicate that the nature of the rupture is similar to fillet lifting. Ruptures of SMCs are caused by warps of PCBs and constituent, particularly Bi, redistribution in joints. They can be avoided by prevention of warps in PCBs. Constituent redistribution generates a vicinity of eutectic Bi–Sn composition with a low melting point. A higher thermal capacity of a SMC results in a greater temperature gradient, thus more constituent redistribution. Most importantly, temperature equalization in joints reduces ruptures. Nakasuka *et al*. applied heating on the top side of a PCB at the cooling zone of a wave soldering process in order to eliminate the temperature gradient from board to component, and found the rupture was significantly reduced. The joint strength also increased.

12.19.3 Conductive anode filament

Conductive anodic filament formation (CAF) is a failure mode for printed wiring boards (PWBs) in which a conductive filament forms along the epoxy/glass interface growing from anode to cathode. In Figure 12.9, the white region indicates a copper-containing filament growing along the epoxy/glass interface. In Figure 7.22, the CAF appears as dark shadows coming from anode to cathode.

Turbini *et al*. [9] studied the effect of reflow temperature on CAF, and found that a higher board processing temperature results in increased numbers of CAF for most of the water-washable fluxes tested. Since lead-free solders typically have a higher melting temperature, therefore a higher process temperature, the CAF problem may become a major issue if a water-cleanable flux is used.

To prevent this CAF problem, the following approaches are recommended:

Use a no-clean or solvent cleanable flux system. Do not use water-soluble fluxes.
Use a lower reflow temperature whenever possible.
Use a board material with better thermal stability.

12.19.4 Grainy surface

Lead-free solders typically yield a grainy, dull surface texture instead of a shiny, smooth one, as shown in Figure 12.9. This grainy appearance can be attributed to the crystalline structure of the high tin alloys. It poses a great challenge to inspection. Lee [19] studied the effect of process condition, and found that the surface texture is fairly sensitive to reflow cooling rate. With a high cooling rate, the surface can be shiny and smooth. With a low cooling rate, the surface becomes fairly grainy and rough. Figures 12.10 and 12.11 show the effect of cooling rate on surface texture for alloy 95.5Sn/3.8Ag/0.7Cu and 91.5Sn/3.7Ag/4.8Cu alloys, respectively. Apparently, the effect of cooling rate on surface texture is much stronger for lead-free solders than for eutectic Sn−Pb solders. The surface appearance of the latter is often insensitive to the cooling rate.

Although a large grainy structure is associated with a poorer fatigue life for an eutectic Sn−Pb system, it is to

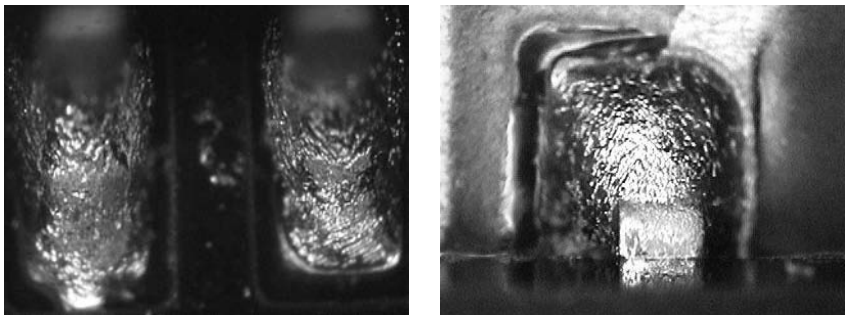

Figure 12.9 95.5Sn/3.8Ag/0.7Cu solder joints

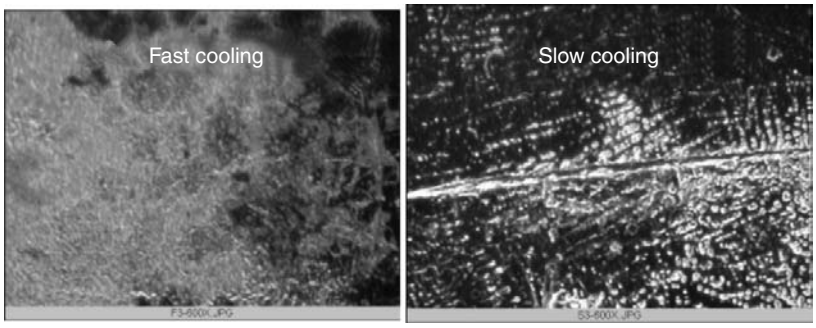

Figure 12.10 Effect of reflow cooling rate on the surface texture of 95.5Sn/3.5Ag/0.7Cu

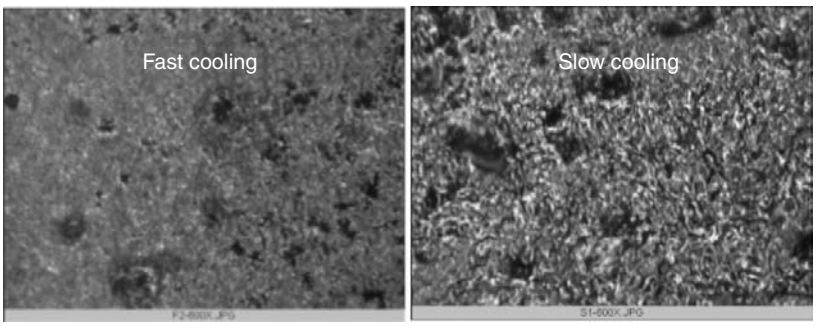

Figure 12.11 Effect of reflow cooling rate on the surface texture of 91.5Sn/3.7Ag/4.8Cu

be verified for lead-free solders. To prevent formation of this grainy surface texture, a reflow furnace with a very high cooling rate will be needed.

12.19.5 Sn/Pb/Bi ternary low melting eutectic phase

Mei *et al*. [20] studied the effect of lead contamination on a Sn−Bi eutectic, and found the formation of a Sn−Pb−Bi ternary eutectic phase results in drastic failure of the solder, as shown in Figure 12.12. Figure 12.12(a) shows the as-solidified microstructure of 58Bi/42Sn solder joints between a hot air leveled (HAL) 63Sn/37Pb pad and an 80Sn/20Pb coated component lead. The microstructure appears normal. Figure 12.12(b) shows the microstructure after 400 cycles between −45 °C and +100 °C over 16 days. The lead dissolves into molten Bi−Sn during the soldering process, resulting in the formation of a 52Bi/30Pb/18Sn ternary eutectic structure in the solidified solder joint. The solder joints became weak in mechanical strength when subjected to thermal cycling with a temperature above 96 °C because the low melting ternary eutectic phase accelerated grain growth and phase agglomeration. A small addition of indium (such as 2–3 percent) to 58Bi/42Sn solder may eliminate the formation of the ternary eutectic phase, indicated by the disappearance of a ternary phase peak in differential scanning calorimeter measurements.

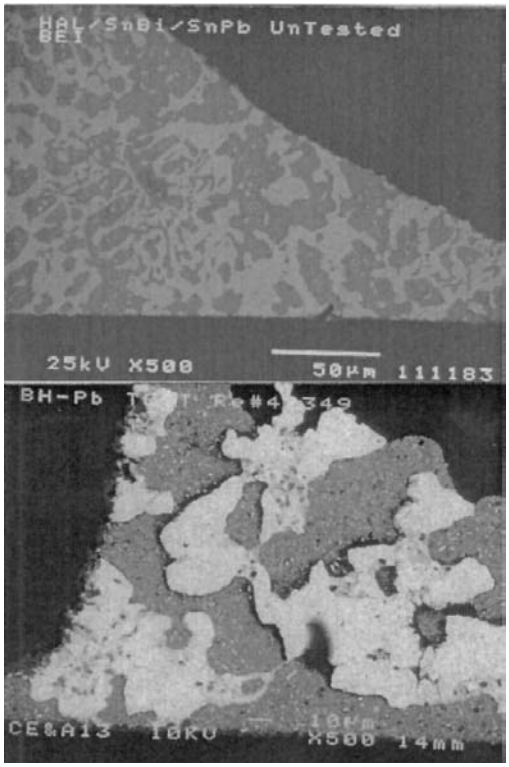

(**a**)

(**b**)

Figure 12.12 Microstructure of eutectic Bi/Sn solder which has been contaminated by Pb before (**a**) and after (**b**) temperature cycling [20]

The adverse effect of lead contamination is not confined to an eutectic Sn−Bi system. Other findings indicate that SnBiX alloys such as SnAgBi systems are also vulnerable to lead contamination. Although the SnAgBi system has been demonstrated to be a very high reliability solder [21], its vulnerability to lead contamination virtually rules out this alloy system as a primary lead-free alternative, at least in phase one where lead contamination may still be prevailing. It is the author's opinion that SnAgBi may become the logical choice once the lead contamination problem has been solved. This is mainly due to the very high reliability demonstrated [21], plus its superior processability for reflow applications [13].

12.20 Conclusion

Lead-free soldering is an unstoppable global trend, due to both environmental concern and business considerations. At this stage, consensus gradually developed on the mainstream options and eutectic Sn−Ag−Cu appears to be the most popular choice for reflow applications. Sn−Ag−Bi systems also receive great attention, due to their high reliability, in the absence of lead, and processability. Perhaps the logical choice will be using Sn−Ag−Cu in phase one, but Sn−Ag−Bi−X system in phase two, when lead contamination is no longer an issue. Challenges for using lead-free alloys are inevitable. Fortunately, the failure modes of those problems are being gradually identified, and troubleshooting strategies are also being developed. It is expected that the lead-free soldering movement will drive the industry into a world which is greener and better in product reliability.

References

1. National Center for Manufacturing Sciences, ''Lead and the Electronic Industry: A Proactive Approach'', May 1995.
2. N. Ir. Sax, *Dangerous Properties of Industrial Materials*, 6th edn, Van Nostrand Reinhold Company, New York (1984).
3. ''Lead-Free Solder Roadmap – A Scenario for Commercial Application'', http:\\www.jeida.or.jp/document/geppou/etc/9802namari.html, JEIDA, 3 February 1998.
4. E. B. Smith III and L. K. Swanger, ''Are Lead-free Solders Really Environmental Friendly?'' *SMT*, pp. 64–66 (March 1999).
5. ''Lead-Free Soldering 1'', HDP User Group International, Inc, Doc Number Proj032, Rev A, June 1999.
6. K. Ninmo, ''Environmental Issues in Electronics and the Transition to Lead-free Soldering'', SMTA International, San Jose, CA, 13–17 (September 1999).
7. NEMI, Lead Free Task Meeting, Northbrook, IL, 26 May 1999.
8. F. Gibbs, ''Pb Free Interconnect'', NEMI Lead Free Meeting, Chicago, 25 May 1999.
9. L. J. Turbini, W. R. Bent, and W. J. Ready, ''Impact of Higher Melting Lead-free Solders on the Reliability of Printed Wiring Assemblies'', SMTA International, Chicago, IL, 20–24 September 2000.
10. E. Bradley, ''Overview of No-lead Solder Issue'', NEMI meeting, Anaheim, 23 February 1999.
11. M. Buetow, ''The Latest on the Lead-Free Issue'', Technical Source, IPC 1999 Spring/Summer Catalog.
12. A. Furusawa, K. Suetsugu, A. Yamaguchi, and H. Taketomo, ''Thermoset Pb-Free Solder Using Heat-Resistant Sn−Ag Paste'', National Technical Report, Vol. 43, No. 1, February 1997.
13. B. L. Huang and N. C. Lee, ''Prospects of Lead Free Alternatives For Reflow Soldering'', in *Proc. of IMAPS'99*, Chicago, 28 October 1999.

14. C. Handwerker, ''NCMS Lead Free Solder Project: A National Program'', NEMI Lead Free Solder Meeting, Chicago, 25 May 1999.
15. ''Lead-Free Solder Project Final Report'', NCMS Report 0401RE96, August 1997.
16. K. Nimmo, ''Worldwide Environmental Issues in Electronics and the Transition to Lead-free'', IPCWorks '99, Minneapolis, MN, 27 October 1999.
17. K. Suganuma, ''Mechanism and Prevention of Lift-off in Lead-free Soldering'', IMAPS, pp. 325–329, Boston, MA, 20–22 September 2000.
18. T. Nakatsuka, K. Serizawa, T. Soga, H. Shimokawa, and A. Nishimura, ''Reliability of Pb-free Solder Joints of Surface-mounted LSI Packages after Flow-soldering'', IMAPS, pp. 330–335, Boston, MA, 20–22, September 2000.
19. N. -C. Lee, unpublished information.
20. Z. Mei, F. Hua, and J. Glazer, ''SN-BI-X SOLDERS'', SMTA International, San Jose, CA, 13–17 September 1999.
21. P. T. Vianco, J. A. Rejent, I. Artaki, and U. Ray, ''An Evaluation of Prototype Circuit Boards Assembled with a Sn–Ag–Bi Solder'', IPCWorks, Minneapolis, MN, 22 October 1999.

Index

Acid–base reactions 37–8
Acoustic microscope inspection 85, 86, 228, 229–30, 235–6
Activators 40–2, 170, 171, 175
Air reflowed systems 146, 147, 148, 203, 246, 248
Alignment 169–70, 171, 173, 174, 197–8, 224–5
Amine activators 41
Antonow's rule 20, 34
Aperture patterns 5, 67–9, 96–9, 138–9, 183, 184, 190–1
Application-specific integrated circuits (ASIC) 9
Aqueous cleaning 87, 144
Archimedes screw dispenser 59, 60
Area array packages 11–17, 159–87
Arrhenius relationship 21
Assembly processes 4–5, 6, 7, 57–89
  ball grid arrays 189–93, 195–211
  chip scale packages 189–93, 195–211
  no-clean process 145, 147–9, 152–4, 155, 156, 222, 235, 247
  process flow 189
Atomization 43–4, 45
Auger type dispensers 59, 60
Auto-oxidation reactions 40
Automotive industry applications 14, 17

Ball grid arrays (BGA) 3, 4, 12–14, 15
  assembly 189–93, 195–211
  bridging 206–8
  joint height 210
  joint inspection 192–3, 194
  openings 209
  pick-and-place solder transfer 168–79
  placement 191
  reflow profile 192, 195, 201
  rework 193–211
  self-alignment 197–8
  solder balling 211
  solder bumping 159–60, 163, 164, 166, 179–86, 199–200
  starved solder joints 196
  voiding 179, 200–6
  wettability 199–200
Band etching 65
Base metal dissolution 21–2, 23–5, 110–11
Boiling points, solvents 173, 179, 201
Bonding 15, 16, 31–2
Brass–tin system 114, 115
Bridging 124–7, 128, 241, 243
  area array packages 170, 171, 181
  ball grid arrays 200, 206–8, 210–11
  flip chips 231, 232
Brookfield viscometer 50–1, 52
Brush fluxing 217–18, 219
Bubbles 175, 176, 229
Build-up process 161–2, 204
Bumping technologies 16
Butt-leads 4

C-SAM imaging 156–7, 228
Capacitor cracking 76, 243, 255
Carboxylic acid activators 41, 42
Castor oil derivatives 43
Cavitation 29
Cellular phone applications 14
Ceramic ball grid arrays (CBGA) 13
  bridging 206–7
  joint inspection 192
  reflow profile 192, 195
  solder bumping 159–60
  solder composition 198
  solder replenishment 195
  starved solder joints 195–6
  stencil design 189–90
Ceramic chips 3, 10–11, 12
Ceramic column grid arrays (CCGA) 13
  bridging 206
  reflow profile 192
  solder bumping 159
  solder replenishment 195
  stencil design 189–90
Ceramic substrates 215
Chamber-print designs 73
Charred residues 145, 240, 244
Chemical etch technology 63–5
Chip capacitors 3, 10–11, 12, 119
Chip inductors 3
Chip resistors 1–2, 119
Chip scale packages (CSP) 14–15
  assembly 189–93, 195–211
  joint height 210
  placement 191
  reflow profile 192, 195

Chip scale packages (CSP) (*Continued*)
rework 193–211
solder balling 211
solder bumping 159, 160, 166–7, 183, 185, 199–200
solder webbing 211
stencil design 190–1
wettability 199–200
Chip shooters 75–7
Chlorofluorocarbons (CFC) 86–7
Clam-shell opening mechanism 74
Cleaning:
aqueous 87, 144
printed circuit boards 85–7
surface mount boards 5
white residues 143–5
Clip-on leads 124, 125
Clogging 52, 99–101
Coating:
conformal 155, 156
polymer 71–3, 156
roller 59, 61, 62
Cohesion properties 52
Cold-drawing 210
Cold joints 107–8, 240, 244
Cold slump 101
Complexity 9–10
Compliance 51–2, 73
Components:
chip size 10–11
lead-containing 255
momentum inertia 198
pick-and-place 75–7, 104
placement 75, 191, 195, 197–8, 207, 208, 209, 225, 226
removal 194
skewing 121–2, 207, 224, 242, 243
surface mount technology 1–4
warpage 131, 194, 210, 259
Computer processing speed 8–9
Conduction reflow 80–1, 82
Conductive adhesive curing 4
Conductive anodic filaments (CAF) 149–50, 155, 259–60
Conformal coating 155, 156
Contact angle 19, 34–5
Contacts:
openings 131–3, 208–10
probe testing 145–9
Contamination:
base metal 110
cold joints 107
lead–bismuth solders 261
pads 208
printed circuit boards 86–7
Convection reflow 80, 81, 246
Coplanarity 132–3, 167, 168, 196, 208, 232
Copper–nickel–gold system 115, 117
Copper–tin system 22–5, 30, 113, 114, 115, 116
Corner pads 198, 199, 209
Corrosivity 150–1, 255
Cracking:
capacitors 76, 240, 243, 255
underfill fillets 232–4, 235, 257
Creep 28–30
Cross-sectional X-ray inspection 193
Crown probes 148–9
Crusting 91, 92
Cuprous oxide 37
Curing 157, 220
Curvature effect 109–10, 176–7
Decal solder transfer 166–7, 168
Defects:
print 51–2, 95, 99
reflow profile optimization 243–5, 248–50
solder powder 45, 46–7
stencils 63, 64, 68–9, 97–8
Deformation mechanisms 28–30
Delamination 67, 156–7, 211, 229, 232–3, 234–5, 240, 241
Dendrite formation 149, 150, 258–9
Deposition, solder paste 57–61
Dewetting 109–10, 244
Dilatant fluids 50
Dip-flux process 216–17, 218, 220, 226, 229
Direct chip attachment (DCA) 159
Discontinuities 131
Discrete semiconductors 3, 4
Dislocation climb 28–9
Dislocations 28–9
Dispense fluxing 218, 219
Dispensing 58–9, 186, 218–20, 229–30, 231, 232
needle clogging 100–1
rate 53
Dissolution:
barrier 23–5
rates 21–2, 110–11
Doctor blade 216–17
Double-print process 70, 71
Downstop 98
Drawbridging effect 117–21
Drop-on-demand wafer bumping 163
Drying 140–1

Elastic properties 51–2
Electrochemical migration (EM) 149–56, 255
Electroforming 66, 67, 183, 185
Electroless nickel plating 66–7
Electrolysis model 153–4
Electroplating:
electroless 66–7
microvia 204–5
solder bumping 162, 180–1
Electropolishing 65–6
Encapsulation 155, 157, 221
Enthalpy of reaction 38
Epoxy flux 220–1, 225, 226, 227–8
Equiaxed grain structure 30
Etching 63–5
European legislation 252
Eutectic binary alloys 25–7, 159–60
Evaporative bumping 161–2, 180
Exposure time 203

Failure 29–30
Fatigue resistance 29–30, 130, 159, 215, 235, 240
FC-joining 223
Feature size 10
Fillets:
formation 20, 236, 237
lifting 27–8, 131, 132, 257–9
segregation 235–7, 259
Film no-flow process 221, 222
Fine-pitch applications
flip chip attachment 221–2, 223
stencil design 67–70
Finger-like flow front 229, 230

Flip chip on board (FCOB) 159, 160, 166–7
Flip chip in package (FCIP) 16, 159
Flip chips 15–17
  assembly processes 156, 159, 160
  bonding processes 15, 16
  global production 16, 17
  reflow attachment 215–37
  solder bumping 166, 167, 215–16
Floating components 121–2
Flow rate 53
Fluid flow 20–1, 53
Flux-exclusion-rate model 201
Flux jetting 217, 218, 219
Fluxes:
  activation temperature 136–7
  chemistry 39–43, 53, 143, 150–4, 155
  deposition thickness 171, 172–3, 177
  flip chip attachment 216–18
  mask interactions 155
  reflow soldering 39
  residues 143–9, 152–4, 156, 230
  separation 91, 100
  spattering 138, 139–41, 242, 243
  spreading 146
  surface tension 20, 30, 32, 34–5, 102, 172, 173
  tackiness 103, 201, 203
  viscosity 170, 172, 173, 177–8, 201, 231
  voiding 128, 129, 130, 171, 174–8
  volatility 173, 179
Fluxing reactions 37–9, 82, 217–19, 225, 239–40
Fluxless soldering 39, 179, 180, 222–3
Fluxless welding 165
Forced convection reflow 80, 81, 246
Formic acid 38–9

Gas evolution 110
Gasketing effect 98–9, 103
Gate delay 9
Gibbs free energy 38
Glycol systems 42, 43
Gold–indium system 115, 118
Gold–tin system 114–15, 117, 159, 162–3, 165, 223
Grain boundary sliding 29
Grain structure 30, 240, 244, 260–1
Gravity pick-and-place solder bumping 169
Grittiness 32, 33
Gullwing leads 4, 122, 123, 124, 125, 131, 132

Hagen and Poiseuille relation 53
Halide salt activators 41, 42
Halo defect 156, 228–9, 230
Harada operating window 52–3, 54
Hardness:
  residues 146–7
  solder paste 91–2
  squeegee 72–3, 96
Heat input 77–9, 107–8, 110, 144, 194, 195, 240–6, 248
Hot-bar reflow 81
Hot slump 101, 241, 243
Hourglass profile problem 63–4
Humidity 102, 134, 156
Hydrochlorofluorocarbons (HCFC) 86–7

Impurity effects 30–3, 108
In-circuit-testing 87, 145, 149
In-line conduction reflow 80–1, 82
In-line placement 75
Indium–lead system 83–4
  gold erosion 115, 118
Inert atmospheres 147
Infrared reflow 77, 79, 80, 130, 131, 134, 246
Input/output density 13
Inspection:
  printing 73–5
  solder joints 84–5, 192–3, 194
Integrated circuits (IC) 3–4
  solder joint configurations 3, 4
  transistor integration 9–10
Integrated preform 179, 180
Intel 9
Interfacial tension 19–20, 34–5
Intergranular creep 28–9
Intermetallic compounds 22–5, 110, 111–17, 118, 240, 244
International Interconnection Intelligence 12
Intrusive reflow process 69–70
Ion sweeping 153

J-lead configuration 4, 122, 123
Japan 8, 251–3, 255, 256
Joints:
  bond strength 31–2
  bridging 124–7, 128, 206–8, 241, 243
  cold 107–8, 240, 244
  configurations 3, 4
  copper–nickel–gold 115, 117
  deformation 240–1
  flip chip attachment 225–7
  grain structure 240, 244
  height 210
  inspection 84–5, 192–3, 194
  mechanical properties 28
  peeling 115, 118
  reliability 28, 159, 189, 200, 206, 215
  starved 195–7
  strength 130
  voiding 127–31, 226–31

KEPOCH stencil system 63

Lamellar microstructure 25, 30
Laminography 193, 194
Land patterns 132, 133
Laser attachment 81, 166
Laser-based sensors 74–5
Laser cut stencil process 63, 65, 66
Laser-infrared inspection 85, 86
Laser reflow 81, 166
Leaching 22, 110–11, 240, 244
Lead:
  in components 255
  consortia activity 255–6
  global consumption 251
  particulates 198
  phasing out 251–2, 255–7
Lead-free solders 160, 251–62
Lead–tin system
  fluxless soldering 222
  intermetallic compounds 25
  missing rate 172–3

Lead–tin system (*Continued*)
solder bumping 159–60, 161, 165, 172–3, 175–8
voiding 174
Leadless ceramic chip carriers (LCCC) 2, 3
Leads:
configurations 3, 4
pillowing 130, 131
wicking 122–4, 125, 242, 243
Legislation 251–3
Light scattering effects 143
Linear dicarboxylic acid activators 41, 42
Liquid no-flow process 221, 222, 231
Liquid solder transfer process 162–4
Low residue no-clean fluxes (LRNC) 152–4, 247

Manhattan effect 117–21
Manufacture, solder paste 45, 48–9
Masks:
flux interactions 155
geometry 230
misregistration 198, 199, 225
print–reflow–detach process 185
Mass reflow process 6–7, 246
Melting points, solder 31–2, 159, 198, 240, 255
Meniscus bumping 162–3
Meta-rigidity 51–2
Metal blade squeegee 71–3, 74
Metal electrode face resistors (MELF) 2–3
Metal filaments 149–50, 155, 259–60
Metal load effects 53–4, 147
alignment 173
bridging 126, 127
slump 101–2
solder balling 133, 134
solder beading 137
tack 103, 104
voiding 130–1, 178, 179, 202
Metallization:
intermetallic compound formation 113–14, 115
solderability 128, 129, 131, 133
tombstoning 118
wettability 21, 108
Micro dynamic solder pump (MDSP) 163, 164
Micromodification 65, 67–8
Microstructure 25, 28–33, 30, 260, 261
Microvia 204
Miniaturization 9, 10, 12, 14, 180
Minimal liquid surface area 175
Misalignment 169–70, 171, 173, 174, 197–8, 224–5
Mismatch in thermal expansion 27–8, 159, 208–9, 210, 215, 257–8
Misregistration 197, 207, 208, 209
masks 198, 199, 225
phototools 64, 65
Missing solder bumping 169–70, 171–3, 174
Moisture 139–40, 155, 194, 211, 229
Molybdenum stencils 62, 63
Morphology, intermetallic compounds 112
Multilayer ceramic chip capacitors 10–11, 12

Needle clogging 100–1
Newtonian fluids 49–50
Nickel plated stencils 66–7
Nitrogen reflowed systems 146, 147, 225, 247–8
No-clean process 145, 147–9, 152–4, 155, 156, 222, 235, 247
No-flow process 221, 222, 223, 230–1, 232, 233
Nonwetting 107–9, 131, 166, 242

Off-contact mode 73–4
On-contact mode 74
Opens 131–3, 208–10, 231–2, 233, 242, 243
Optical inspection 85, 232, 234
Organic solderability preservative (OSP) 245–6
Outgassing 128–9, 131, 135–6, 162, 171, 203, 204, 209–10, 228
Overetching 64
Overheating 145
Oxidation:
charred residues 145
defect mechanisms 242, 243–5, 246
solder bumping 169, 170, 173, 178, 197–8
Oxidation–reduction reactions 38–9
Oxidative atmosphere 110, 197, 202
Oxides 37–9, 137, 169, 170, 173, 178, 197–8

Pads:
corner 198, 199, 209
design 138–9, 203–5
detachment 241, 244
oxide level 178
rounded openings 64, 65
size 117–18, 121–2, 171–2, 173, 177
spacing 117–18, 119
Particle size and shape 44–5, 48
defect effects 98, 99
needle clogging 100–1
print thickness 95
rheology 54
slump 102
solder balling 134–5, 137
tack 103–5
voiding 200
Paste *see* Solder paste
Paste-in-hole process 69–70, 84
Patents 12
Peeling 115, 118
Permalex edge coating 71–3
pH values 150–2, 154
Phase diagrams 26–8, 83
Photoresists 63, 66
Phototools 63, 64, 65
Pick-and-place 75–7, 104, 168–79
Pick test sequence 132
Piezoelectric force 163
Pillowing 130, 131
Pin count number 10, 11
Pin-transferring 59, 174
Piston positive displacement dispensers 59, 61
Pitch 67–70, 98, 125, 170–1, 171–2, 181
Placement 75, 191, 195, 197–8, 207, 208, 209, 225, 226
Plasma assisted fluxless soldering (PADS) 39, 222
Plastic ball grid arrays (PBGA) 13
bridging 207–8
delamination 211
joint height 210
openings 208, 209
pre-baking 194
solder replenishment 195
starved solder joints 196, 197
stencil design 190
Plastic leaded chip carriers (PLCC) 3

Pneumatic dispensers 58–9, 100
Poiseuille flow 53
Polyimide film 167–8
Polymer coating 71–3, 156, 167–8
Polymeric substrate 215
Polymerization 40
Polyurethane rubber 70–3
Popcorning effect 211, 231, 233
Positive displacement dispensers 59, 60, 61, 100
Potting 157
Powder *see* Solder powder
Pre-baking 109, 194, 205, 231
Preforms 179, 180
Printed circuit boards (PCB)
  cleaning 85–7, 155
  component alignment 198
  contamination 86–7
  lead-free surface finish 254–5
  site preparation 194–5
  surface insulation resistance 149
Printed wiring boards (PWB) 149–56, 259–60
Printing:
  defects 51–2, 95, 99
  Harada operating window 52–3, 54
  head design 73
  inspection process 73–5
  performance 61–75
  quality 182, 183
  solder paste thickness 73, 92, 95–7, 120–1, 126, 132, 137, 138
  see also Stencil printing
Print–detach–reflow process 181–4, 185, 186
Print–reflow–detach process 184–6
Probing testing 145–9
  crown probes 148–9
Projected solder approach 132–3
Pseudoplastic fluids 49–50

Quad flat packs (QFP) 3, 192, 195

Ramp-up rate 102–3, 153, 201–2, 225, 241, 242, 243–6, 248–50
Reballing process 195
Recycling 251–2
Reduced oxide soldering activation (ROSA) 39
Reduction reactions 38–9
Reflow-alloying 82–3
Reflow attachment, flip chips 215–37
Reflow profile 78–9, 192, 195
  conventional profiles 245–6
  cooling stage 240–1
  defect mechanisms analysis 239–50
  dewetting 110, 244
  heating stage 241–2, 243–4
  misalignment 225
  optimization 243–5, 248–50
  peak temperature 240, 247
  ramp-up rate 102–3, 153, 201–2, 225, 241, 242, 243–6, 248–50
  solder balling 134, 242
  spattering 140, 242, 243
  spike zone 243
  voiding 178–9, 201–2, 242, 244
Reflow soldering 5, 6
  atmosphere effects 82, 140–1, 147, 202
  flip chips 215–37
  fluxes 39
  intrusive process 69–70
  methods 77–82
  special processes 82–4
  troubleshooting 87–8, 205, 257–61
Reliability, solder joints 28, 159, 189, 200, 206, 215
Residues 143–9, 152–4, 156, 230
Resins 39–40
Rework:
  ball grid arrays 193–211
  chip scale packages 193–211
  lead-free solders 255
  process flow 193–4
Rheological additives 42–3
Rheology 49–54, 53–4
RMA solder pastes 148–9
Roller coating 59, 61, 62
Rosin fluxes 39–40, 41, 143–4, 151–2, 154, 177
Rounded pad openings 64, 65
Rupture 259

Sandwich effect 176, 177
Screen printing 57
Segregation 235–7, 259
Self-alignment 191, 197–8, 224–5
Self-centering force effect 173, 225, 226
Semiconductor Industry Association Roadmap 9–10, 252
Semiconductors, discrete 3, 4
Sensors, laser-based 74–5
Sequential placement 75
Shear bands 29–30
Shear rate 49–50
Shear strength, intermetallic compounds 112
Shear stress 233, 234, 235, 236, 258
Shearing, solder paste 92–3
Sieve number 44–5
Silicon dies 215
Simultaneous placement 75
Skewing 121–2, 207, 224, 242, 243
Slump 101–3, 181, 182–3, 241, 243
  resistance 51–2
  wicking 124, 125
Small-outline integrated circuits (SOIC) 3
Smearing 52, 68–70, 97–9
Snap cure 220
Snap-off value 73, 96
Soaking 78, 140–1, 242–4, 248–9
Soft-residue systems 147–9
Softening point 126, 127
Solder balling 133–9, 195, 211, 242, 243
Solder beading 135–9, 241–2, 243
Solder bumping:
  area array packages 159–87
  build-up process 161–2
  liquid solder transfer process 162–4
  misalignment 169–70, 171, 173, 174, 224–5
  missing rate 169–70, 171–3, 174
  oxidation 169, 170, 173, 178, 197–8, 242, 243–4
  print–detach–reflow process 181–4
  print–reflow–detach process 184–6
  solder composition 198
  solder paste bumping 180–6
  solid solder transfer processes 164–80
Solder jet bumping 163–4
Solder paste technology 37–55
  advantages 6–8
  during reflow 107–42
  flip chip attachment 221–2, 223

Solder paste technology (*Continued*)
post-reflow stage 143–57
prior to reflow 91–105
Solder pastes:
composition 45, 47–9, 198
costs 254, 255
crusting 91, 92
deposition 57–61
dewetting 109–10
dispensing 53, 58–9, 100–1, 186, 218–20, 229–30, 231, 232
exposure time 203
handling and storage 57
hardening 91–2
height 75–6, 159
high temperature 247
insufficiency 98, 99–100, 195–7, 208
low temperature 247
manufacture 45, 48–9
materials 57–61, 139–41, 180, 181
nonwetting 107–9, 131, 166
reflow 4, 5, 239
replenishment 195
residues 143–9, 152–4, 156, 230
rheology 49–54
RMA 148–9
shearing 92–3
smearing 52, 68–70, 97–9
solder bumping 180–6
spattering 138–41, 242, 243
squeegee release 93–5
tack value 51–2, 103–5
thickening 92
thixotropy 50–1, 52–3, 54, 101
viscosity 49–54, 92, 101–5, 231
volume fraction 47–8, 53, 125
wave flux interaction 156
Solder powder 43–5
defects 45, 46–7
mixing 48, 49
rheology effects 54
see also Particle size and shape
Solder webbing 210–11
Solderability 128, 129, 131, 133, 173, 174, 200, 204–5, 208
Soldering theory 19–25
SolderQuick^{TM} integrated preform 179, 180
Solders:
area array packages 159–60
cold-drawing 210
lead-free 160, 251–62
melting point 31–2, 159, 198
replenishment 195
spattering 138, 139–41, 242, 243
sphere manufacturing 165
spreading 19–20, 25, 31–2, 34–5, 197
surface tension 197–8
tin–lead system 21–2, 23–5
wetting 19, 21, 22–3, 25–6, 31–2, 159, 240
wicking 122–4, 125, 131, 133, 134, 173, 196
Solid solder transfer processes 164–80
Solvents 42, 86–7
boiling points 173, 179, 201
bridging 126, 127, 241, 243
solder bumping 170, 172
solvent loss effect 103, 241
spattering 140
stencil wiping 99
Spattering 138, 139–41, 242, 243
Sphere welding 165–6
Split-beam prism system 195
Spray fluxing 217, 218
Spreading 19–20, 197
bottom-side flux spread 146
elemental constituent effects 25
impurity effects 31–2
surface tension effects 34–5, 197
top-side flux spread 146
Squeegee 66, 70–3
downstop 98
hardness 72–3, 96
holders 94–5
materials 70–3
paste release 93–5
pressure 74, 95–6
print thickness 95–7
speed 74, 95
Staggered patterns 67
Stamp fluxing 218, 219
Starved solder joints 195–7
Stencil printing 51–2, 57–8, 92–3
Stencils 63–70
aperture patterns 5, 67–9, 96–9, 138–9, 183, 184, 190–1
defects 63, 64, 68–9, 97–9
design 67–70, 183, 184, 189–91
forming technology 63–7
life 92–3
materials 63
print–reflow–detach process 184
thickness 97, 99, 181
wiping 99
Step-down patterns 69–70
Step soldering 7, 82
Step-stencils 73, 74
Stonehenge effect 117–21
Strain rate 28
Structure–property correlation 53
Substrates 215
Surface finish 202, 254–5, 260–1
Surface insulation resistance (SIR) 149–56
Surface mount boards
cleaning 5, 143–5, 155
site preparation 194–5
type I 5, 6, 7
type II 5, 6
type III 5, 7
warpage 131, 194, 210, 259
Surface mount technology
assembly processes 4–5, 57–89
components 1–4
during reflow 107–42
flip chip attachment 221–2, 223
history 1
introduction 1–18
post-reflow stage 143–57
prior to reflow 91–105
soldering process 5–8
trends 8–17

Surface tension 20, 30, 32, 102
  solder bumping 159, 172, 173, 175
  solder spreading 34–5, 197
  tombstoning 117–21
Swimming components 121–2

Tack value 51–2, 103–5
Tacky dot solder transfer 167–8, 174
Tacky film 224
Tapered apertures 67–9, 97–9
Tearing 258
Temperature:
  bridging 126
  electrochemical migration 154–5, 255
  solder beading 135–7
  solder paste materials 57
  surface insulation resistance 154–5
  thermal damage 255
  tombstoning 118–20, 248–9
  see also Heat input; Reflow profile
Testing:
  electrochemical migration 149, 150, 151
  in-circuit 87, 145, 149
  multiple cycles 148–9
  pick sequence 132
  probing contact 145–9
  surface insulation resistance 149, 150, 151
Texture 260–1
Thermal agitation effect 102–3, 241
Thermal expansion mismatch 27–8, 159, 208–9, 210, 215, 257–8
Thermal mass 247, 248
Thermoset encapsulant systems 157
Thickness:
  flux deposition thickness 171, 172–3, 177
  solder paste 73, 92, 95–7, 120–1, 126, 132, 137, 138
  stencils 97, 99, 181
Thin small-outline packages (TSOP) 3
Thixotropy 50–1, 52–3, 54, 101
  thixotropic index (TI) 52–3, 54
Through-hole applications 69–70
Throughput 181
Tin oxides 38, 144
Tin–antimony systems 254, 256, 257
Tin–bismuth system 254, 255–6, 257, 258, 261
Tin–copper system 253, 256, 258–9
Tin–lead system:
  base metal dissolution 21–2, 23–5, 110–11
  creep 29
  dendrite formation 149, 150
  flip chip attachment 222, 223
  fluxless soldering 222
  intermetallic compound formation 114, 115
  metal content 45, 47
  phase diagrams 26–7
  pick-and-place solder transfer 169, 170
  reflow profiles 245–7
  replacement 253, 255–6
  solder balling 133–4
  solder bumping 159–62, 177, 179, 185
  surface tension 30–2
  tack 103–4
  voiding 174–9, 183
  wetting 199, 239–40
  white residues 144
  wicking 124, 125
Tin–lead–bismuth system 261
Tin–lead–gold system 114–15, 117
Tin–lead–silver system 21–2, 25, 32, 33, 111, 159, 199, 239–40
Tin–silver system 253, 255–6, 257
Tin–silver–bismuth systems 254, 255–61, 257, 259
Tin–silver–copper systems 160, 253–4, 255–6, 257, 259
Tin–zinc systems 254, 256, 257
Tombstoning 117–21, 131, 242, 243, 248–9
Toshiba Corporation 10, 11
Transistors 9–10
Transmission X-ray inspection 193
Trapezoidal apertures 191
Triangulation 75
Troubleshooting 87–8, 205, 257–61
Tubing-squeezing positive displacement dispensers 59, 60

Ultra-fine-pitch applications 98, 129
Ultrathin packages 8
Underetching 64
Underfilling 156, 211, 215, 218–24, 222–34, 228–37
USA 8, 251, 253, 255–6

Vacuum pick-and-place solder bumping 168
Vapor phase reflow 77, 79–80, 246
Via in pad design 203–4
Viscometers 50–1, 52
Viscosity:
  bridging 126, 127, 241, 243
  fluid flow 20
  flux-exclusion-rate model 201
  fluxes 170, 172, 173, 177–8, 231
  measurement 50–1, 52
  solder paste 49–54, 92, 101–5, 231
Visual inspection 84, 192
Voiding 127–31, 242, 244
  ball grid arrays 200–6
  flip chip attachment 156, 226–31
  solder bumping 171, 174–9, 183, 185
Volatile organic chemicals emission 69
Volume fraction, solder paste 47–8, 53, 125

Wafer-applied underfill system 223
Wafer bumping 162, 163–4, 167, 169, 180–3, 185
Wafer level compressive-flow underfill (WLCFU) 223–4
Walking components 121–2
Water-washable flux system 155
Wave soldering 4, 5–6, 8, 145, 208–9
  flux–residue interaction 156
Waxes 43
Wetting 19, 159, 242, 244
  bridging 126, 128, 200
  dewetting 109–10, 244
  elemental constituent effects 25–6
  enhancement 22–3
  impurity effects 31–2, 108
  kinetics 239–40
  metallization 21, 108

Wetting (*Continued*)
nonwetting 107–9, 131, 166, 242
solder beading 136
solder bumping 182–3, 198–200
spattering 140
tombstoning 117–21, 242, 243
voiding 177, 227, 242
wicking 122–4, 125
X-ray detection 225–6, 227
White residues 143–5
Wicking 122–4, 125, 131, 133, 134, 242, 243
area array packages 173
ball grid arrays 196
Wire bonding 115
Wire bumping 165
X86 microprocessors 9

X-ray image analysis 174, 176
X-ray inspection 84–5, 192–3, 194, 225–7, 228
X-ray laminographic analysis 193, 194

Yield stress 51–2

Zipper patterns 67